1127.21
146

JOURNAL OF COLLOID SCIENCE

Editor-in-Chief
Victor K. La Mer, Columbia University, New York

Editors:

F. E. Bartell
T. R. Bolam
R. M. Fuoss
H. R. Kruyt
J. W. McBain

E. K. Rideal
William Seifriz
A. W. Thomas
Arne Tiselius
Robert D. Vold

Consulting Committee:

W. T. Astbury
J. J. Bikerman
W. Clayton
P. Debye
W. Feitknecht
Alexander Frumkin
William D. Harkins
Ernst A. Hauser
Wilfried Heller

Hans Jenny
S. S. Kistler
Herman Mark
J. N. Mukherjee
F. F. Nord
J. Th. G. Overbeek
R. Ruyssen
Robert Simha
The Svedberg

VOLUME 5

1950
ACADEMIC PRESS INC., PUBLISHERS
NEW YORK, N.Y.

Copyright 1950, by Academic Press Inc.
Made in United States of America

JOURNAL OF COLLOID SCIENCE

Editor-in-Chief
Victor K. La Mer, Columbia University, New York

Editors:

F. E. Bartell
T. R. Bolam
R. M. Fuoss
H. R. Kruyt
J. W. McBain
E. K. Rideal
William Seifriz
A. W. Thomas
Arne Tiselius
Robert D. Vold

Consulting Committee:

W. T. Astbury
J. J. Bikerman
W. Clayton
P. Debye
W. Feitknecht
Alexander Frumkin
William D. Harkins
Ernst A. Hauser
Wilfried Heller
Hans Jenny
S. S. Kistler
Herman Mark
J. N. Mukherjee
F. F. Nord
J. Th. G. Overbeek
R. Ruyssen
Robert Simha
The Svedberg

VOLUME 5

1950

ACADEMIC PRESS INC., PUBLISHERS
NEW YORK, N. Y.

Second Printing, 1968

Copyright 1950, by Academic Press Inc.
Made in United States of America

CONTENTS OF VOLUME 5

No. 1, February, 1950

Marjorie J. Vold and Robert D. Vold. The Phase Behavior of Lithium Stearate in Cetane and in Decalin 1
Nils Gralén and Mariänne Karrholm...The Physicochemical Properties of Solutions of Gum Tragacanth 21
Bernard Vonnegut. Techniques for Generating Silver Iodide Smoke 37
M. Joly. General Theory of the Structure, Transformations and Mechanical Properties of Monolayers 49
Lannes E. Davis. Ionic Exchange and Statistical Thermodynamics. I. Equilibria in Simple Exchange Systems 71
Lannes E. Davis and John M. Rible. Monolayers Containing Polyvalent Ions 81
Carl Wagner. Mathematical Analysis of the Formation of Periodic Precipitations 85

Letters to the Editors:

Robert Ginell. Association Phenomena II. Theories of Chain Molecules and their Application to Hydrogen Bonding in Gaseous Hydrogen Fluoride: *A Correction* 99
Todd M. Doscher. The Electrophoretic Mobility in Relation to Suspendability and Detergency 100
Benjamin Carroll. Solubilization in Aqueous Solutions of Bovine Serum Albumin 103

No. 2, April, 1950

Lannes E. Davis. Ionic Exchange and Statistical Thermodynamics. II. Equilibria in Irregular Systems 107
Hershel Markowitz and George E. Kimball. The Effect of Salts on the Viscosity of Solutions of Polyacrylic Acid 115
O. Beeck, J. W. Givens and A. W. Ritchie. The Adsorption of Hydrogen on Nickel Catalysts. II. Sorption Isobars from 20°K. to Room Temperature 141
Noburo Kamiya and Shigemi Abe. Bioelectric Phenomena in the Myxomycete Plasmodium and their Relation to Protoplasmic Flow 149
Milton Kerker. The Use of White Light in Determining Particle Radius by the Polarization Ratio of the Scattered Light 165
W. Philippoff. Micelles and X-Rays 169

Book Reviews:

V. A. Gordieyeff. Electron Microscopy, Technique and Applications 193
C. Neuberg. Chemistry of Specific, Selective, and Sensitive Reactions 193
George Goldfinger. Elastomers and Plastomers, Their Chemistry, Physics and Technology. Volume II. Manufacture, Properties and Applications 195

No. 3, June, 1950

Hugh S. Taylor. Introduction of Henry Eyring 197
Henry Eyring. Acceptance of the Bingham Medal 200

A. J. Guzzetti, G. J. Dienes and Turner Alfrey, Jr. Rheological Properties of Phenolic Resins. Effect of Reaction with Hexamethylenetetramine on Properties of a Phenol-Formaldehyde Novolak..... 202
Leif Hougen and N. J. Hipp. Plastic Flow Properties of Casein...... 218
F. D. Dexter and G. J. Dienes. Extrusion Behavior of Viscoelastic Materials........ 228
F. D. Stockton and D. C. Drucker. Fitting Mathematical Theories of Plasticity to Experimental Results........ 239
Turner Alfrey, Jr., A. I. Goldberg and John A. Price. Dilute-Solution Viscosity of Polymethyl Methacrylate and a Methyl Methacrylate-Styrene Copolymer........ 251
Welker G. Bechtel. Measurements of Properties of Corn Starch Gels.. 260
Earl K. Fischer. Rheological Properties of Commercial Paints....... 271
Lawrence E. Nielsen and Rolf Buchdahl. Viscoelastic and Photoelastic Properties of Polystyrene above its Softening Temperature.. 282
R. N. Weltmann. Instruments for the Determination of Rheological Parameters of Liquid Bodies........ 295
A. B. Bestul and H. V. Belcher. Flow Behavior of Concentrated GR-S Rubber Solutions........ 303

No. 4, August, 1950

C. F. Turner and Andrew Van Hook. The Effect of Ultrasonic Irradiation on the Formation of Colloidal Sulfur and Ice........ 315
M. van der Waarden. Stabilization of Carbon-Black Dispersions in Hydrocarbons........ 317
Jett C. Arthur, Jr., and Barbara H. Saik. Intrinsic Viscosity of Cottonseed Globulin Solutions........ 326
Hans Kuhn. Viscosity, Sedimentation, and Diffusion of Long-Chain Molecules in Solution as Determined by Experiments on Large-Scale Models........ 331
J. J. Bikerman. Sliding of Drops from Surfaces of Different Roughnesses. 349
D. D. Lord. The Action of Polyoxyethylene Monostearate Upon Starch with Reference to its Softening Action in Bread........ 360
Jack Schubert and John W. Richter. The Use of Ion Exchangers for the Determination of Physicochemical Properties of Substances, Particularly Radiotracers, in Solution. III. The Radiocolloids of Zirconium and Niobium........ 376
Robert Simha. The Concentration Dependence of Viscosities in Dilute Solutions........ 386
M. D. Schoenberg, J. Riseman and F. R. Eirich. Extinction Angles, Intrinsic Viscosities, and Molecular Weights of Polystyrene in Solution.. 393
E. G. Richardson. The Formation and Flow of Emulsion........ 404

No. 5, October, 1950

Emil J. Burcik. The Rate of Surface Tension Lowering and its Role in Foaming........ 421
Teru Hayashi and George R. Edison. Enzyme-Substrate Stabilization with Surface-Denatured Pepsin-Albumin........ 437
M. van der Waarden. Micelle Formation of Sulfonates in Hydrocarbons 448
A. Bondi. Solubility and Swelling of Alkali Soaps in Organic Solvents.. 458
Victor K. La Mer, Edward C. Y. Inn and Irwin B. Wilson. The Methods of Forming, Detecting, and Measuring the Size and Concentration of Liquid Aerosols in the Size Range of 0.01 to 0.25 Microns Diameter........ 471

BOOK REVIEWS:

GEORGE GOLDFINGER. Elastomers and Plastomers Vol. I. General Theory . . . 497
VICTOR K. LA MER. Structure of Molecules and the Chemical Bond . 498
VICTOR K. LA MER. Physical Chemistry of High Polymeric Systems. High Polymers. Volume II . . . 498

No. 6, DECEMBER, 1950

FRANK C. COLLINS. Diffusion in Chemical Reaction Processes and in the Growth of Colloid Particles . . . 499
MARJORIE J. VOLD. The Application of the Mass Law to the Aggregation of Colloidal Electrolytes . . . 506
H. W. FOX AND W. A. ZISMAN. The Spreading of Liquids on Low Energy Surfaces. I. Polytetrafluoroethylene . . . 514
J. FRED HAZEL AND EDGAR SCHIPPER. Low Temperature Studies with Colloidal Silicic Acid . . . 532
S. NEWMAN AND F. EIRICH. Particle Shape and the Concentration Dependence of Sedimentation and Diffusion . . . 541
J. H. WILSON AND T. R. BOLAM. Chemisorbed Oxygen on Charcoal and the Sorption of Strong Inorganic Bases and Acids . . . 550
HARRY SOBOTKA, SHIRLEY ROSENBERG AND AINA BIRNBAUM. Films of Omega-Branched Fatty Acids . . . 567
HARRY SOBOTKA AND SHIRLEY ROSENBERG. Films of Hydrocarbon-Stearic Acid Mixtures . . . 581

LETTER TO THE EDITORS:

ROBERT D. VOLD, HENRY F. COFFER AND RICHARD F. BAKER. Direct Observation of Gel Structure with the Electron Microscope . . . 586
AUTHOR INDEX . . . 589
SUBJECT INDEX . . . 592
INDEX OF BOOK REVIEWS . . . 595

THE PHASE BEHAVIOR OF LITHIUM STEARATE IN CETANE AND IN DECALIN[1]

Marjorie J. Vold and Robert D. Vold

From the Department of Chemistry, University of Southern California

Received August 15, 1949

INTRODUCTION

The determination of the phase behavior of soaps in hydrocarbon solvents is of both fundamental and practical importance. Soap-thickened oils (greases) appear to consist of a mesh of crystalline fibers incorporating free solvent in a sponge-like structure (5,6,13,15). However, greases may be employed as lubricants at temperatures such that the original fibers swell and dissolve in oil with the formation of various types of liquid or liquid crystalline phases. Likewise, the phase state of the grease at various stages of its manufacture may influence the physical texture of the fiber network ultimately formed. Understanding of the general features of the phase behavior of soaps in oils can be of assistance in meeting the practical problems associated with these phenomena.

Various investigators have advanced hypotheses concerning the molecular structure of mesomorphic phases (1,2,8,19). Most of this work is concerned with the stepwise melting of single substances rather than with liquid crystalline solutions. However, Marsden and McBain (9) have proposed a structure for an aqueous middle soap based on X-ray diffraction studies and Doscher and Vold (4) have advanced some speculation as to the structure of mesomorphic phases of sodium stearate in both water and cetane. It is of interest to see to what extent the compositions and temperatures at which such solutions form with one soap and solvents of different molecular geometry are compatible with these speculations.

EXPERIMENTAL

Materials

Lithium stearate was prepared from stearic acid by neutralization of a hot carbon dioxide-free solution of the acid to phenolphthalein with Merck lithium hydroxide (No. S4589) dissolved in distilled water. The acid (Armour Neo-fat No. 1–65) was twice recrystallized from acetonitrile, and then had the following characteristics: I.V. (Wijs) 0.35; m.p. 69–

---

[1] This work is part of a project "Phase Studies of Greases" sponsored by the Office of Naval Research, Contract No. N6-onr-238-TO2, NR 057057.

70°C.; equiv. wt. 285.5. The soap was dried to constant weight at 110°C. to remove alcohol and water. Du Pont cetane was used after sweeping with nitrogen. It had $n_D^{20} = 1.4345$ comparing with the literature value, $n_D^{20} = 1.43449$. Eastman Kodak decalin (No. P1905) was used directly. It is presumably a mixture of the cis and trans isomers and may also contain small amounts of both tetralin and naphthalene.

For comparison with reasonably pure materials, parallel observations were made on a technical lithium stearate (from the Metasap Chemical Co.) probably consisting of a mixture of palmitate and stearate with about 5–10% unsaturates, calculated as oleate. This soap was studied in three petroleum oils X, S, and R. Oil X is an SAE 20, approx. 30 V. I. solvent-refined California oil, commonly employed by a major oil company as a grease base. Oil S is a 56 V. I. oil, viscosity 108 cs. at 100°F. also commonly used as a grease base. Oil R is a special sample for which the following data are available: A. P. I. gravity 29.3, viscosity at 100°F., 434 S. S. U., viscosity at 210°F., 58.4, V. I. 88, mol. wt. 475. Waterman Type analysis: 1.4% aromatic rings, 25.6% naphthenic rings, 73% paraffinic side chains.

Four commercial lithium greases were also examined visually. These are from the group of greases previously subjected to X-ray diffraction and differential thermal analysis (15). Their characteristics are given in Table IV.

Techniques

Differential thermal analysis was carried out in the apparatus described elsewhere (14), at a rate of 0.5 deg./min. using white mineral oil (Nujol) as a reference material.

Samples were made by intimate admixture of the required amounts of solvent and finely powdered soap. The resultant pastes remained homogeneous on standing for long periods. A few visual observations were made of samples sealed in glass tubes and suspended in an air oven provided with windows. Most of the visual observations, however, were carried out in the following way: Forty-nine ⅝-in. holes were drilled in a square array in a 5 × 8 × 8-in. aluminum block. Numbering these by row and column, holes 22, 26, 62, and 66 contained 100-watt cartridge type heaters and hole 44 a "Fenwal" thermoswitch. The block was insulated with 1½-in. thick magnesia fiber blocks. Samples were sealed in glass tubes and allowed to remain at a given temperature a minimum of 12 hr. Their phase state was then observed. This required removal of each tube from the block. An insulated "viewing box" with crossed polaroid windows was constructed for this purpose. With practice, salient features of the appearance of each tube could be noted in less than 30 sec. so that cooling of the tube during observations did not prove a serious obstacle.

X-ray diffraction patterns of a few samples were obtained using a North American Philips X-ray spectrometer; as described elsewhere (17).

DATA AND RESULTS

Differential Heating Curves

Figs. 1 and 2 show differential heating curves for lithium stearate in cetane and lithium stearate in decalin. A qualitative discussion of the interpretation of such curves has already been presented (16). It is useful to extend the quantitative theory of differential thermal analysis (14) to some of these concepts in order to facilitate use of the present data in establishing phase diagrams for the systems.

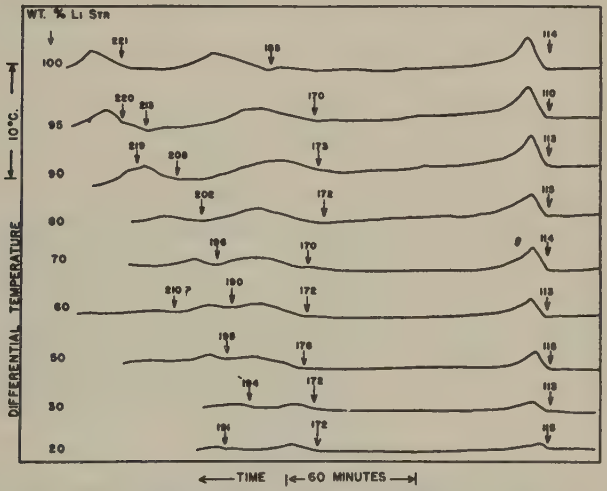

FIG. 1. Differential heating curves for lithium stearate in cetane. Numbers on the curves are the temperatures (°C). of the samples at the times indicated by the arrows. Phase transformations accompanied by absorption of heat begin in the sample at these temperatures.

The fundamental equation of differential calorimetry is

$$\frac{dy}{dt} = \frac{\Delta H}{C_s}\frac{dS}{dt} - A\,(y - y_0), \tag{1}$$

where y is the differential temperature and y_0 is its steady state value. A is a constant dependent on the thermal characteristics of both the sample and the apparatus. ΔH is the change in heat content of the sample during a transformation and is positive when heat is absorbed. S represents the phase change and may refer to a melting process involving the whole sample, or solution of part of the solid present in the solvent, or change in the compositions of two phases in equilibrium, etc.; and dS/dt is the time rate of occurrence of this change. C_s is the heat capacity of the sample and its container.

It can be seen from Eq. 1 and also by qualitative reasoning that the differential temperature begins to rise when the sample begins to undergo transformation. No further development is necessary when only a single transition temperature is being sought. However, in a binary system, a phase change may occur at a single temperature (*i.e.*, a eutectoid) or over a range of temperature, as in crossing a two-phase region. It becomes of interest to investigate whether the shape of the peak produced can be used to derive or infer which of these two alternative types of change is responsible for a particular peak.

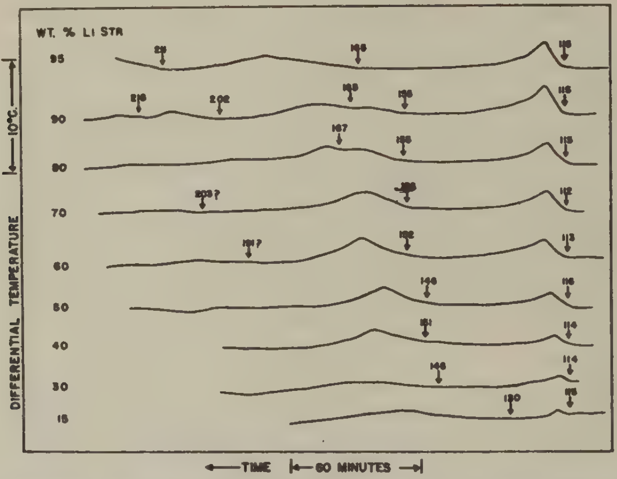

FIG. 2. Differential heating curves for lithium stearate in decalin. Numbers on the curves are the temperatures (°C.) of the samples at the times indicated by the arrows. At these temperatures the rate of heat abosrption by the sample, due to the occurrence of phase transformation, first becomes detectable. In most cases, this is equivalent to the temperatures at which phase transformation begins, but in 15–60% systems the gradual rises beginning at 130–152° are due to continuously increasing solubility of soap in solvent.

1. If the rate of occurrence of a transformation is small, the corresponding peak in the differential heating curve is broad. The rate of rise due to the transformation (first term of Eq. 1) may become balanced by the second term, or even over-balanced, so that the differential temperature begins to decline again towards its steady state value before the sample is completely transformed. This is likely to be the case in crossing a two-phase region. If the heating rate were sufficiently small so that equilibrium is maintained, one could write

$$dS/dt = (dS/dT)(dT/dt), \tag{2}$$

and equate the temperature range within which heat is being absorbed with the temperature extent of the corresponding two-phase region. In real systems no finite heating rate is low enough to ensure the validity of Eq. 2 so that only qualitative inferences can be drawn from the shapes of the peaks, *i.e.*, when a series of peaks corresponding to the same phase change occur in adjacent compositions over increasingly wide temperature ranges it can be inferred that that change corresponds to crossing a two-phase region of increasing width.

2. In a one-component system, $dy/dt = 0$ up to a transition temperature and then suddenly assumes a positive value; but in a binary system, the slope of the differential heating curve may gradually increase without there being any associated phase boundary which is being crossed at that sample composition. This can be seen by differentiating Eq. 1 and incorporating Eq. 2 in the result. One obtains

$$\frac{d^2y}{dt^2} = \frac{\Delta H}{C_s}\left(\frac{dT}{dt}\right)^2 \frac{d^2S}{dT^2} - A\,\frac{dy}{dt}. \tag{3}$$

Eq. 3 shows that the rate at which the slope of the heating curve increases depends on the curvature of the phase boundaries (d^2S/dT^2). If the slope of the solubility curve changes rapidly with increasing temperature, this fact will be reflected in the changing slope of the differential heating curve, and it is necessary to consider this possibility before attempting to associate each change of slope with an actual point on a phase boundary of the system being studied.

Visual Observations

At room temperature all samples are suspensions of crystalline soap in mobile solvent, the solubility of the soap being negligibly small. In systems containing more than about 25% soap, the free liquid is absorbed into interstices between the particles to yield a paste, and in still more concentrated systems (about 70%) the paste becomes quite crumbly. On heating very dilute samples the soap simply dissolves to yield a mobile isotropic solution. On heating more concentrated systems the soap swells and takes on a waxy appearance. Next it increases in translucence and gradually becomes entirely transparent. Observation between crossed polaroids shows that samples which are transparent may be composed entirely of isotropic solution, or entirely of liquid crystalline solution, or a mixture of the two. As heating is continued all samples eventually melt to isotropic liquid. The temperature at which the last trace of opacity disappears, and the temperature at which the system becomes isotropic, may be determined quite precisely. Traces of liquid crystal in a waxy matrix, and traces of isotropic solution in a liquid crystalline matrix, are not easy to identify positively. Tables I and II record the results of visual observations for samples of lithium stearate in cetane and in decalin.

The Phase Diagram for Lithium Stearate in Cetane

A phase diagram for this system is given in Fig. 3. So far as can be seen visually, samples assume the same phase state after standing sufficiently long at a given temperature whether the initial temperature was higher or lower. Fig. 3 is thus probably an equilibrium diagram. The two crystal forms of lithium stearate (II, stable at room temperature and up to 114°C. and I, stable from 114°–185°C.) apparently dissolve negligible amounts of cetane. The mesomorphic form (waxy lithium stearate), stable betweeen 185° and 224°C., can dissolve nearly one mole of cetane per mole of soap. Above 224°C. liquid lithium stearate and cetane are miscible in all proportions. A fifth homogeneous phase, designated nonaqueous middle soap because of its similarity to this form in the sodium stearate–cetane system (3), occurs between 41.5 and 78 mole % soap and 190°–222°C. The composition and temperature limits of stability of these phases and the associated two-phase equilibria were derived from the data of Table I and Fig. 1 in the following way:

TABLE I

Lithium Stearate-Cetane

(Temperatures, °C., of visible phase changes)[a]

Soap content		A[b]	B[c]	Soap content		A[b]	B[c]
Wt. %	Mol %			Wt. %	Mol %		
5	3.9	185–191	185–191	55[e]	48.7	191–198	223
10	8.0	185–191	185–191	60	54.0	191–198	223
15	12.0	185–191	185–191	65	60.1	198–206	224
20[d]	16.3	185–191	191–198	70	64.6	198–206	222
25[d]	20.6	185–191	213–217	75	70.0	206–211	222
30[d]	25.0	185–191	220	80	75.8	211–213	221
35[d]	29.5	—	222	85	81.6	213–217	218
40[d]	34.2	185–191	223	90	87.6	—	220
45[e]	39.0	185–191	222	95	93.6	—	226
50[e]	43.8	191–198	222				

[a] Where a range is given, the specified change had not occurred at the lower and was complete at the higher temperature.

[b] Temperature at which sample becomes transparent.

[c] Temperature at which sample becomes isotropic.

[d] In these samples liquid and liquid crystal can be seen to coexist between 191° and the given *B* temperature.

[e] In these samples liquid and liquid crystal can be seen to coexist between 198° and the given *B* temperature.

1. That lithium stearate II does not interact with cetane is established by the fact that all samples undergo transformation to lithium stearate I at the same temperature (114°C.) as does the solvent-free soap.

2. That lithium stearate I does not interact with cetane is inferred from the fact that even the most concentrated samples next absorb heat at a temperature (172°) which is independent of composition. This eutectoid involves lithium stearate II, waxy lithium stearate, and isotropic liquid. The approximate eutectoid composition of the waxy phase (80 wt. % soap, 76 mole %) is fixed by the fact that the size of the peaks in the differential heating curves reaches a maximum at this composition.

TABLE II

Lithium Stearate-Decalin

(Temperatures, °C., of visible phase changes)[a]

Soap content		*A*[b]	*B*[d]	*C*[e]
Wt. %	Mol %			
5	2.44	151–157	151–157	—
10	4.94	151–157	151–157	—
15	7.73	151–157	162–172	151–157
20	10.6	151–157	172–174	151–157
25	13.7	151–157	174–182	151–157
30	16.9	151–157	191–198	172–174
40	24.1	151–157	213–217	172–182
45	28.1	151–157	217–224	211–213
50	32.2	151–157	224–228	224–228
55[c]	36.7	162–182	228–230	224–228
60[c]	41.7	182–185	230–233	224–228
70[c]	52.6	to 185	224–230	217–224
75[c]	58.6	to 217	224–230	217–224
80[c]	65.5	to 217	224–230	217–224
85[c]	73.2	to 217	224–230	217–224
90[c]	80.8	to 217	224–230	217–224
95[c]	90.0	to 224	217–224	—

[a] The temperature range given has the meaning that the observed change was complete at the higher temperature but not at the lower.

[b] Temperatures at which white, opaque material disappears, leaving the samples substantially transparent.

[c] In these samples a slight opacity persisted to the temperature given. However above 60% they appeared nearly transparent from about 170–180°C. Some transparent, anisotropic material was seen at 157–162°.

[d] Temperatures at which formation of isotropic liquid is complete.

[e] Temperature at which isotropic liquid is first seen coexisting with liquid crystal.

3. The temperature of coexistence of waxy soap, nonaqueous middle soap and liquid is fixed at 190° both by visual observations (samples containing up to 45 wt. % soap become transparent at 190°) and by differential thermal analysis. Samples containing 20–60 wt. % soap show peaks at or near this temperature.

4. The temperatures at which waxy soap begins to transform on further heating are fixed by differential thermal analysis of samples containing 70 wt. % soap (196°), 80 wt. % (202°), 90 wt. % (208°), and 95 wt. % (213°). The temperature at which transformation to middle soap is complete is determined by visual observation (the samples become transparent).

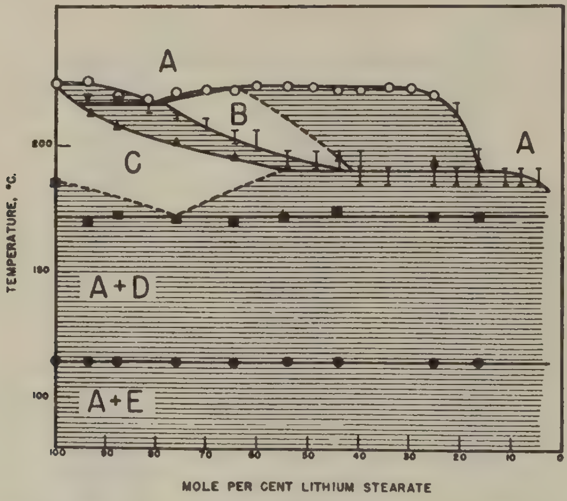

FIG. 3. A phase diagram for the system lithium stearate-cetane. ○, Visually determined m.p.; *I*, temperature range within which visible phase change occurs. ●, ■, ▲, ▼ points obtained from differential heating curves (first, second, third, and fourth peaks, respectively). *A*, isotropic liquid; *B*, nonaqueous middle soap; *C*, waxy lithium stearate; *D*, crystalline lithium stearate I; *E*, crystalline lithium stearate II.

5. The temperatures at which melting is complete, determined visually, display a minimum, a maximum, and a further inflection point as a function of composition, corresponding to changes in the phase coexisting with the liquid just below its final melting point.

6. The remaining phase boundary, that giving the composition of the nonaqueous middle soap in equilibrium with liquid, is tentatively established by visual observation of whether or not any free liquid is present with the nonaqueous middle soap at various compositions and temperatures. The two phases have so nearly the same density that stratification into layers does not occur readily so that small amounts of liquid may

escape detection. Further confidence in the validity of the boundary as drawn, however, is engendered by the existence of a small peak at 210° in a sample containing 60 wt. % soap, which could correspond to transformation from nonaqueous middle soap to liquid.

The Phase Diagram for Lithium Stearate in Decalin

A phase diagram for this system is given in Fig. 4. It was derived from the data of Fig. 2 and Table II in the way described in detail for lithium stearate in cetane. Although the same five homogeneous phases occur in the two systems, the binary equilibria differ somewhat in the following respects.

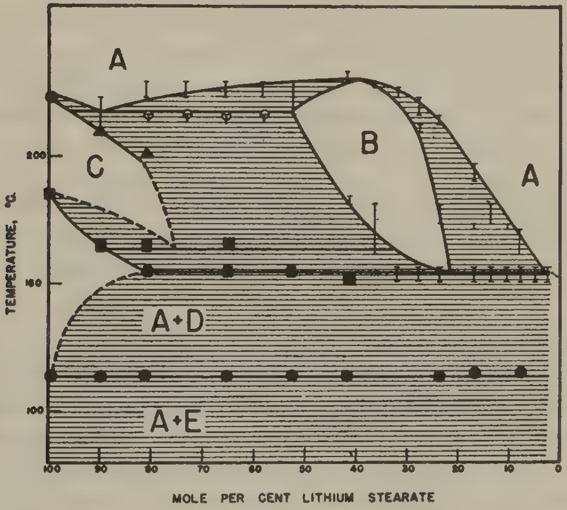

Fig. 4. A phase diagram for the system lithium stearate-decalin. *I*, temperature range within which visible phase change occurs; *T*, lower limit of range within which change occurs not definable visually; o, isotropic liquid appears on heating, coexisting with nonaqueous middle soap; filled points obtained from differential heating curves. *A*, isotropic liquid; *B*, nonaqueous middle soap; *C*, waxy lithium stearate; *D*, crystalline lithium stearate I; *E*, crystalline lithium stearate II.

1. Nonaqueous middle soap forms in the decalin system at a lower temperature than does waxy soap so that the three-phase equilibrium, lithium stearate I–nonaqueous middle soap–liquid (155°), replaces the equilibrium lithium stearate I–waxy lithium stearate–liquid (172°) found in the cetane system.

2. Lithium stearate I appears able to dissolve some decalin. This conclusion is based on the fact that the eutectoid temperature of 155° is not found in samples more concentrated than 90 wt. % (81 mole %) soap.

3. Although still very low, the solubility of lithium stearate I in decalin appears to be greater than in cetane. This follows from the fact

that peaks in the differential heating curve begin in samples containing 15, 30 ,40, 50, and 60 wt. % soap in decalin at temperatures substantially below the eutectoid at 155°, the more so the more dilute the sample, whereas no such effect is encountered with cetane. As samples which are mixtures of solid and liquid are heated, some of the solid dissolves, the more so the more rapidly its solubility changes with temperature. Eq. 3 may be used to predict the type of differential heating curve to expect. Curvature (*i.e.*, a change in slope) of the curve will develop at a temperature such that the first term on the right hand side of Eq. 3 is large enough to detect, considering the sensitivity of the apparatus. ΔH of this term refers in the present connection to the heat of formation of as much saturated solution as can be formed, considering the liquid content of the one-gram total sample employed. Thus it is larger for more dilute systems. The term d^2S/dT^2 refers to the curvature of the solubility curve. It is increasing very rapidly with increasing temperature in the range 130–150°C. The temperature at which the product $\Delta H \, d^2S/dT^2$ becomes large enough to produce curvature in the differential heating curve is thus lower as ΔH is higher (*i.e.*, in more dilute systems).

Possible Phase Change of the Second Order

In both the decalin system and the cetane system, the differential heating curves of concentrated samples (80–100 wt. % soap) are not entirely smooth. The very slight irregularity which occurs at about 140° can be seen on the curves of Figs. 1 and 2. It appears to correspond to a very small decrease in heat capacity or increase in thermal conductivity of the sample. Usually phase changes of the second kind are accompanied by an increased heat capacity at higher temperatures.

When samples containing soap and solvent are cooled, crystallization of lithium stearate I from either the waxy form or nonaqueous middle soap begins at temperatures lower than the equilibrium values and clustering around 140°C. This suggests that perhaps the unproved higher order transition occurring near this temperature may act as a trigger to initiate crystallization.

The Phase Behavior of Lithium Stearate-Cetane during Cooling

A glance at the differential cooling curves of Fig. 5 shows that the transformations occurring as the melted samples are cooled (mean rate 1°min.) are not the same as those found on heating so far as temperatures of occurrence are concerned, although the number and relative magnitudes of the dips are not greatly different from those found on heating.

Formation of lithium stearate II from lithium stearate I occurs in all samples with about the same extent of undercooling (5–10°C.). Formation of lithium stearate I from waxy lithium stearate occurs at the same tem-

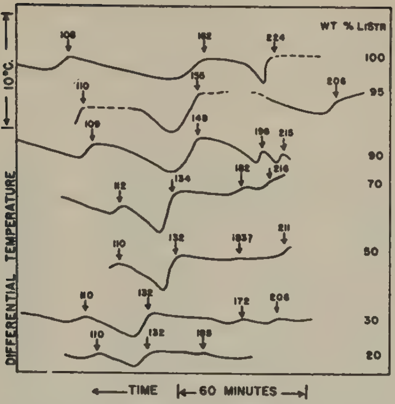

Fig. 5. Differential cooling curves for lithium stearate in cetane. Numbers on the curves are temperatures of the samples at the times indicated by the arrows. Heat is evolved by the sample at the beginning of each dip.

perature (132°) in all samples in which, at equilibrium, the waxy soap would have a fixed composition (80 wt. % soap), and at higher temperatures in samples (90, 95, 100 wt. %) in which solvent-free soap crystallizes leaving a residue of more dilute waxy soap.

The Phase Behavior of Lithium Stearate–Decalin during Cooling

Differential cooling curves for this sytem are given in Fig. 6. It is interesting to observe that in 90 and 95% systems the behavior of the

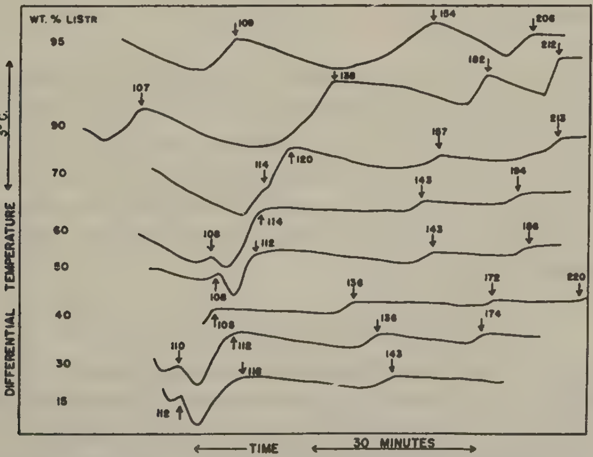

Fig. 6. Differential cooling curves for lithium stearate in decalin. Numbers on the curves are temperatures of the samples at the times indicated by the arrows. Heat is evolved by the sample at the beginning of each dip.

decalin and cetane systems are qualitatively similar, as are the equilibrium phase diagrams, even though equilibrium is not maintained during the cooling process. The formation of lithium stearate I from waxy lithium stearate appears to proceed in the same way whether the solvent is cetane or decalin.

Although the data are not complete since the 15% system was not observed at high enough temperatures and the 40% system was not observed at low enough temperatues, it appears that cooling curve for all samples from 15–70 wt. % lithium stearate in decalin contain the same number of dips (four) whereas the sequence of changes suggested by the phase diagram would yield but three for the 15%, 30%, and 40% systems. A possible explanation of this behavior is that the middle soap first formed thereafter transforms independently, and with a different extent of undercooling than the residual phase (liquid for 15–40% systems, waxy soap for the 50–70% systems). Formation of lithium stearate I in all the systems thus occurs in two steps, at 136–157° from liquid or from waxy soap, and 112–120° from nonaqueous middle soap. Formation of lithium stearate II from lithium stearate appears to occur as readily in the decalin system as in the cetane system with but little undercooling.

X-Ray Diffraction Results

Data for the two systems are given in Figs. 7 and 8. Despite the fact that the various phases stable at high temperatures undercool markedly, none of them appear to be realized at room temperature in significant amount, regardless of the speed of cooling. This conclusion is based on the fact that the diffraction patterns obtained at room temperature are substantially the same as those of a mechanical mixture of lithium stearate II and liquid.

With decalin, the soap crystallites appear to have retained liquid. Although the pattern contains four principal short spacings (between 3.7 and 4.3 A) at approximately the same positions as for solvent-free soap, their values are all shifted towards smaller diffraction angles (larger values of d/n) indicating swelling of the soap lattice. The long spacing (40.5 A) is of very low intensity indicating gross imperfection in the regularity of lattice of the swollen crystallites.

The Phase Behavior of Technical Samples

It seems likely that the phase diagrams for technical lithium stearate in petroleum oil are qualitatively like that of lithium stearate in cetane rather than in decalin in that nonaqueous middle soap is not formed on heating until a temperature is reached which is well above that required to convert the crystalline lithium stearate I to waxy soap. Visual observations for three such systems are presented in Table III. Nonaqueous

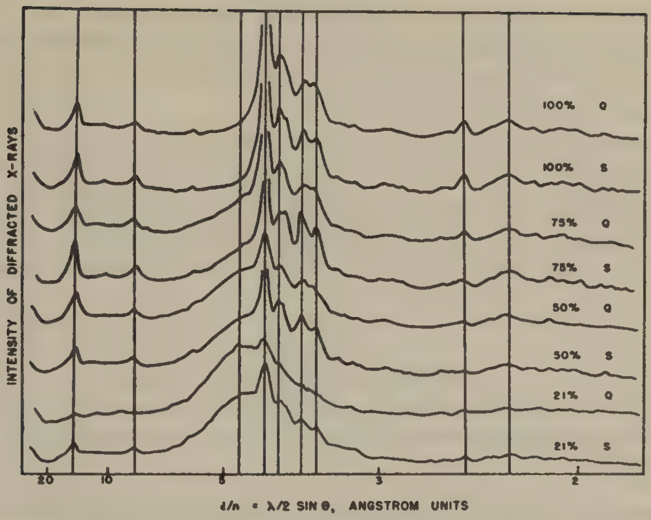

FIG. 7. X-ray diffraction patterns of lithium stearate in cetane. *Q*, quenched from 250°C.; *S*, cooled at a mean rate of 0.5 deg./min. from 250°C. The vertical lines have been drawn through the principal peaks of the solvent-free soap. The precision with which they pass through the peaks on the remaining curves is a measure of the validity of the generalization that crystalline lithium stearate (II) is inert towards cetane at room temperature.

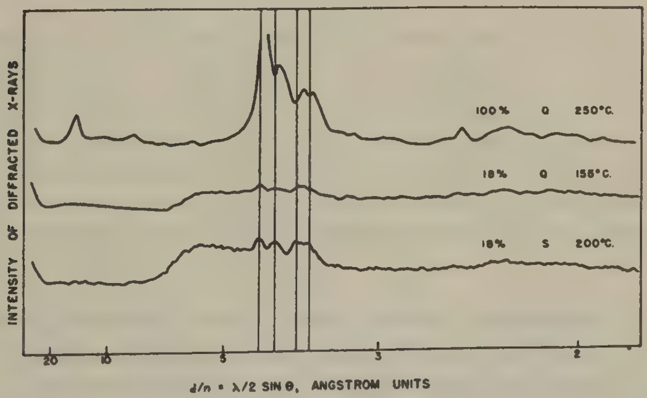

FIG. 8. X-ray diffraction patterns of lithium stearate in decalin. *Q*, quenched from the given temperature; *S*, cooled from the given temperature at a mean rate of 0.5 deg./min. The vertical lines have been drawn through the principal peaks of the grease pattern. They fall at longer values of d/n than corresponding peaks for the solvent-free soap, supporting the hypothesis that expulsion of decalin from the soap lattice during crystallization is incomplete.

middle soap does not form even in the most dilute samples examined until a temperature of 173–176° is reached. In this technical sample, waxy soap forms in the oil-free soap at 177°, and presumably at substantially lower temperatures in samples containing oil.

Data for four commercial lithium greases are presented in Table IV. On heating, these greases appear to pass through exactly the same sequence of phase changes as do laboratory samples of similar gross chemical composition. (Lithium soap II → lithium soap I, at 80–90°, determined by differential thermal analysis; lithium soap I→waxy soap, at 139–162°, determined by differential thermal analysis; formation of nonaqueous middle soap, at 170–186°, determined both by visual observations and differential thermal analysis, and true melting, observed visually.)

TABLE III

Lithium Stearate-Petroleum Oils

(Temperatures, °C., of visible phase change)

Oil / Wt. % soap	*X*	*S*	*R*
A. Temperatures at which sample becomes transparent			
10[a]	173–176	173–176	174–178
20[a]	173–176	173–176	174–178
40[a]	173–176	173–176	174–178
60	195–205	195–205	195–205
80	205–208	208–213	208–213
B. Temperatures at which the sample becomes isotropic			
10	195–205	195–205	205–208
20	195–205	205–208	208–213
40	205–208	208–213	208–213
60	208–213	208–213	208–213
80	208–213	208–213	213–218

[a] Nonaqueous middle soap is formed. In 10% systems it coexists with liquid at first, but 40% systems appear to be all anisotropic. In 20% systems, the amount of liquid is very small.

It is noteworthy that technical lithium soaps of different fatty acids behave similarly. Even lithium 12-hydroxy stearate for which crystal form I does not exist, displays similar transformations between the remaining phases. Also apparent is the gross difference between technical "stearates," since the 4% difference in soap content between the second

TABLE IV

Temperatures of Phase Change in Commercial Lithium Greases

Composition of soap[a]	Wt. %	Oil	A[b]	B[c]	C[d]	D[e]
Palmitate	14	— —	90	139	170, ?	208
Stearate	10	—	81	148	168, 165	195
Stearate	14	59 S. S. U. at 100°F.	91	162	186, ?	205
12-Hydroxy stearate	10	56 V. I.; 108 cs. at 100°F.	—	159	?, 195	205

[a] Data supplied by the manufacturers.

[b] Temperature of the change from crystalline lithium soap II to crystalline lithium soap I obtained from differential heating curves (15).

[c] Temperature of the eutectoid waxy lithium soap, liquid and crystalline lithium soap I, obtained from differential heating curves. (For the grease containing lithium palmitate, this point, though apparent on the differential heating curve, was overlooked in the earlier publication.)

[d] Temperature of the eutectoid waxy lithium soap, liquid and nonaqueous middle soap, obtained either from differential heating curves (first figure) or visually (second figure.) Visually, this transformation is hard to see in greases made from dark oils or those whose fineness of fiber makes them nearly transparent even at room temperature.

[e] Temperature at which the sample becomes isotropic, obtained by visual observation.

and third greases of Table IV is entirely insufficient to account for the much lower transition temperatures of the former.

DISCUSSION

Inferences as to the Structure of the Mesomorphic Phases

Speculations as to the structure of the waxy type of mesomorphic soap phase and of nonaqueous middle soap (4,11) are apparently adequate to account semiquantitatively for the differing amounts of cetane and decalin involved in their formation in lithium stearate systems. Moreover, comparison of the behavior of lithium stearate in cetane with sodium stearate in cetane (3) leads to a correlation between the mesomorphic forms of the solvent-free soaps.

Waxy Phases of Solvent-Free Lithium and Sodium Soaps

Lithium stearate exhibits only a single mesomorphic phase, which is of the "waxy" type while sodium stearate forms three such phases in succession as the temperature is raised. The phase behavior of the two soaps in cetane suggests that waxy lithium stearate is isomorphous with super waxy sodium stearate. The phase diagram for sodium stearate in cetane by Doscher and Vold (4) indicates very little penetration of cetane into either the subwaxy or waxy lattice of sodium stearate, but the superwaxy form can dissolve about one mole of cetane per mole of soap just as can waxy lithium stearate. This correlation serves as a justification for attributing to waxy lithium stearate the structure which has been postulated (4) for superwaxy sodium stearate.

Waxy Soap

The proposed structure for waxy soap is that of a loose hexagonal packing of rods which are roughly elliptic cylinders so that there is an average distance of closest approach of the parallel hydrocarbon chains and also a preferred orientation of adjacent molecules. Solvent is thought to be incorporated into this structure by substitution of solvent molecules for soap molecules, possibly in a nonrandom manner.

Each substitution creates a weak spot in the lattice since the binding together of the soap molecules occurs partly as a result of interactions between their polar "heads." Dissolution of the lattice occurs when there are enough such weak spots to form continuous breaks. This occurs in the cetane system at various compositions depending upon the temperature, but the maximum amount of cetane which can be incorporated at any temperature is approximately one molecule per molecule of soap. For decalin, the limiting amount is one molecule per three molecules of soap.

Since the *trans*-decalin molecule is twice as wide as the cetane molecule and of the same thickness, its insertion between parallel chains in the waxy lattice creates a break between two and four times as extensive as does insertion of cetane, depending on whether the packing is mobile enough to permit rotation of the decalin about its longest axis. *Cis*-decalin, with its "chair" structure is less regular in shape, but can be shown to form a break only slightly larger than does *trans*-decalin. Thus the limiting molal composition in the decalin system would be expected to involve between one-half and one-fourth as many solvent molecules as in the cetane system compared to the one-third found.

Nonaqueous Middle Soap

This phase is interesting because it is not produced by direct incorporation of solvent into any form of solvent-free soap, but nevertheless has sufficient structure to exhibit double refraction. It can be regarded either as a disintegration product of waxy soap as the amount of solvent increases beyond that which can be incorporated in the waxy lattice, or as an aggregation product of the colloidal micelles present in the isotropic solution as the soap concentration increases. It has been suggested on the basis of optical properties (4) that this phase consists of sheetlike aggregates of clusters of commonly oriented soap and solvent molecules.

If the phase diagrams of lithium stearate in cetane and in decalin are compared at points where similar phase changes occur rather than at fixed soap contents or equal temperatures, it is seen that at all such points nonaqueous middle soap contains more decalin than cetane, and forms dilute solutions containing less soap in decalin than in cetane.

The hypothesis of Oster (12) advanced to account for the separation of dilute solutions of tobacco mosaic virus into an isotropic and an anisotropic phase seems to offer the possibility of accounting for these differences. According to this hypothesis, aggregation of anisometric particles present in isotropic solution to a liquid crystalline phase occurs when the average free space between adjacent particles becomes small enough for each such particle to induce a parallel orientation of its neighbors. Solvation of the particles, and an increase in their effective volume due to thermal motions other than simple translation, are mentioned as factors decreasing the free space between particles over that which would be calculated from a uniform mechanical dispersion of rigid unsolvated particles.

Although such a hypothesis offers scope for fairly elaborate calculations of the probable "effective" volume of the colloidal particles, these are not necessary to derive the qualitative prediction that a solution of lithium stearate in decalin should separate nonaqueous middle soap at a lower soap content than a solution of lithium stearate in cetane.

The "sheets of commonly oriented soap and solvent molecules" described as constituting nonaqueous middle soap (4) are considered to be formed as aggregates of platelike micelles which are thought of for simplicity as discs of a diameter (d) depending on the number of molecules in the aggregate and a thickness (t) dependent on the length of the molecules, their inclination to the surface of the disc or sheet, and possibly the number of layers of molecules involved. The largest volume that such a disc could fill is that of the sphere swept out by its rotation about a diameter, and is larger than the volume of the disc itself in the ratio $1/6\ \pi d^3/\pi d^2 t = d/6t$.

All of the factors affecting the shape of a micelle in a solution of lithium stearate in hydrocarbon solvents appear to suggest a larger ratio of $d/6t$ for decalin than for cetane. Thus, a single decalin molecule with its length parallel to the long axis of the soap molecule forced into a preexisting group of soap molecules (*i.e.*, a crystallite) expands the crystallite from two to four times as much in the direction contributing to d as does a cetane molecule because of the greater physical thickness of the decalin molecule. Further, decalin molecules, being shorter than cetane molecules, produce a greater distortion of the mutual parallelism of the hydrocarbon chains leading to a larger average inclination and thus reduced thickness. This same factor reduces the likelihood of many layers being stacked together, again operating to reduce the average thickness of a micelle.

Phase Considerations Affecting Commercial Lithium Greases

As with other greases, a considerable body of semiempirical information exists concerning the relationship between process variables and the performance characteristics of lithium greases. At least two of these, taken from the early summaries of Fisher and Meyer (7,10) are explicable in terms of the general features of the phase behavior of lithium stearate in oils and serve to illustrate the potential practical utility of this type of study.

That a temperature of 210–220°C. is required to disperse lithium soaps in oil, even though the achieved dispersion is not durable as a grease above about 150–180°C. follows from the fact that temperatures of this order (195–230° for the oils studied in this investigation) are required to melt nonaqueous middle soap.

Explanation of the assertion (7) that greases formed by working oil into a preformed concentrate containing more than about 40% soap are prone to extensive bleeding on storage is less straightforward because it involves the assumptions that the colloidal nature of the final dispersion of crystallites in oil controls the syneretic properties and that this in turn is partly dependent on the phase history of the grease (*i.e.*, the phases which were present at various stages in the processing). Although deductions based on an equilibrium phase diagram might be invalidated by undercooling, it is reasonable to suppose that cooling samples containing more than 40% soap will result in initial formation of waxy soap and nonaqueous middle soap, while cooling more dilute systems from the same temperature results in initial separation of nonaqueous middle soap alone from the liquid.

ACKNOWLEDGMENTS

The authors wish to thank Mrs. Helen S. Davis for the determination of the melting point curve of lithium stearate in cetane and Dr. Gopal S. Hattiangdi for the X-ray data.

SUMMARY

Phase diagrams for the two systems lithium stearate–cetane and lithium stearate–decalin have been established by means of differential thermal analysis and visual observations. In both systems, five single phases are possible (two crystal forms of lithium stearate, one waxy phase, isotropic liquid, and nonaqueous middle soap), together with associated two- and three-phase equilibria.

The similarities and differences between cetane and decalin as a solvent for lithium stearate are explicable in terms of existing theories of the structure of the various phases.

Some of the phenomena associated with the manufacture of lithium greases can be interpreted in terms of their phase behavior, which appears to resemble that of lithium stearate in cetane.

REFERENCES

1. BERNAL, J. D., AND CROWFOOT, D., *Trans. Faraday Soc.* **29**, 1032 (1933).
2. BRAGG, W., *Nature* **133**, 445 (1934).
3. DOSCHER, T. M., AND VOLD, R. D., *J. Colloid Sci.* **1**, 299 (1946).
4. DOSCHER, T. M., AND VOLD, R. D., *J. Phys. Colloid Chem.* **52**, 97 (1948).
5. FARRINGTON, B. B., AND BIRDSALL, D. H., *Oil Gas J.* **45**, No. 46, 268 (1947).
6. FARRINGTON, B. B., AND DAVIS, W. N., *Ind Eng. Chem.* **28**, 414 (1936).
7. FISHER, H. M., AND MEYER, H. C., JR., *Foote Prints* **19**, No. 1, 9 (1948).
8. HERMANN, K., *Trans. Faraday Soc.* **29**, 972 (1933).
9. MARSDEN, S. S., JR., AND MCBAIN, J. W., *J. Chem. Phys.* **16**, 633 (1948).
10. MEYER, H. C., JR., *Foote Prints* **16**, No. 1, 3 (1944).
11. NORDSIECK, H., ROSEVEAR, F. B., AND FERGUSON, R. H., *J. Chem. Phys.* **16**, 175 (1948).
12. OSTER, G., European Scientific Notes, Office of Naval Research London Branch, **3**, No. 5, 82 (1949).
13. SMITH, G. H., *J. Am. Oil Chemists' Soc.* **24**, 353 (1947).
14. VOLD, M. J., *Anal. Chem.* **21**, 683 (1949).
15. VOLD, M. J., HATTIANGDI, G. S., AND VOLD, R. D., *Ind. Eng. Chem.* (accepted for publication).
16. VOLD, R. D., *J. Phys. Colloid Chem.* **51**, 797 (1947).
17. VOLD, R. D., GRANDINE, J. D., 2nd, AND VOLD, M. J., *J. Colloid Sci.* **3**, 339 (1948).
18. VOLD, R. D., AND VOLD, M. J., *J. Phys. Chem.* **49**, 32 (1945).
19. VORLÄNDER, D., *Ber.* **70**, 1202 (1937).

THE PHYSICOCHEMICAL PROPERTIES OF SOLUTIONS OF GUM TRAGACANTH

Nils Gralén and Marianne Kärrholm

From the Swedish Institute for Textile Research, Gothenburg, Sweden

Received September 22, 1949

INTRODUCTION

Gum tragacanth is obtained as exudations from various species of shrubs belonging to the genus *Astragalus* (of the order Leguminosae), occurring in southeastern Europe and parts of Asia. The gum is produced spontaneously, but the formation is artificially stimulated by incisions in the plant. The gum is formed mainly in the bottom portions of the shrubs and in the older branches. The younger parts of the plant contain only small amounts of gum. This is considered to be transformed cells from the pith portion of the wood and not simply the dried juice (Mantell, 1947).

Gum tragacanth is sold in the form of hard flakes of white to brown color (depending on the purity) or as a powder.

About 30–40% of the gum is soluble in water while the rest forms a highly swollen, insoluble gel. The water-soluble part is called "tragacanthin" and the insoluble gel "bassorin." Hydrolysis of the water-soluble portion gives arabinose and uronic acids (Norman, 1937). James and Smith (1945) have made an extensive investigation of the chemical composition of gum tragacanth. They state that the gum contains 3.8% ether-bonded methoxy groups. The exhaustively methylated gum has been separated into three parts: An acid polysaccharide, tragacanthic acid; a neutral polysaccharide; and a small quantity of a third component which is supposed to be a glycoside. These parts have been hydrolyzed and the constituents isolated and identified. The arrangement of the molecules of tragacanthic acid is of a branched chain character containing uronic acids with fucose and xylose as terminal units. Tragacanthic acid also contains galacturonic acid residues; this is an uncommon constituent of plant gums.

The neutral polysaccharide contains arabinose mainly of the furanose type. Hexoses have also been isolated. For details the reader is referred to the papers by James and Smith. Water solutions of tragacanth are slightly acid. A solution containing 1 g./100 ml. shows a pH value of 5.7–6.0. After boiling for about 5 hr. the pH value is decreased to 5.0. The equivalent weight of the gum is 442 according to James and Smith.

EXPERIMENTAL METHODS AND RESULTS

Purification of the Gum and Preparation of Solutions for Molecular-Weight Determination

As raw material we have used a high grade of the gum in the form of faintly yellow flakes. The ash content was 2.6%. On purifying the gum we have tried to avoid decomposition of the molecules as much as possible. The following procedure was used. Ten grams tragacanth was allowed to swell on stirring in 1 l. distilled water during 2 days at 4°C. A rather homogeneous highly viscous solution was formed. After filtration through a glass filter, which allows the mucilage to pass through, the inorganic compounds were removed by dialysis for 2 days against distilled water at 4°C. The gum was precipitated by addition of twice the volume of ethyl alcohol. The precipitate was washed with alcohol and dried in a vacuum desiccator at room temperature. In this way we obtained a white gum with an ash content of 1.9%. This rather high value depends on Ca-, Mg-, and K-salts of uronic acids, which are constituents of the gum (Mantell, 1947). These salts can be decomposed by hydrochloric acid, but we avoided addition of acid as it might cause a degradation of the gum. The determinations of the molecular weight were made in 0.2 *N* sodium chloride solutions. These solutions were made in the following way. One gram of the purified gum was dissolved in 100 ml. 0.2 *N* NaCl on stirring for 16 hr. (overnight) at room temperature. A highly viscous solution was obtained. The dissolved part was separated from the swollen part by centrifuging in a laboratory centrifuge. The solutions thus obtained were slightly turbid as it was not possible to get a quantitative separation of the swollen part. After dialysis against 0.2 *N* NaCl, the solutions were diluted with 0.2 *N* NaCl to proper concentrations. Centrifuging and dialysis were performed at 4°C. The prepared solutions could be stored at 4°C. for one month without degradation.

This investigation also included tragacanth degraded by boiling water solutions for 30 min. and for 5½ hr. The degradation experiments were performed in a three-necked flask connected to a reflux condenser and stirring equipment through ground-glass joints (rubber stoppers were affected, the solution becoming red-colored by the rubber). After boiling for 30 min., or for 5½ hr., the heating was interrupted and the solution was cooled rapidly with water (30-min. experiment) or allowed to cool to room temperature (5½-hr. experiment) while the stirring was continued. The solutions were then centrifuged and dialyzed in the usual manner.

TO*a* symbolizes nondegraded tragacanth;
TO*b* symbolizes nondegraded tragacanth, new sample for control;
T30 symbolizes tragacanth degraded by boiling for 30 min.; and
T330 symbolizes tragacanth degraded by boiling for 330 min.

Determination of the Refractive Index Increment

The concentration of the tragacanth solutions was determined by measurement of the refractive index. For this purpose the refractive index increment dn/dc must be known. The measurements were made with a dipping Zeiss refractometer in sodium light. The refractometer permits an accuracy in determining the refractive index of $\pm 1 \times 10^{-5}$. For the determination of dn/dc, the concentrations were found by evaporation of a weighed amount of the solution and drying at 100–105°C. to constant weight. An accurate measurement of the volume of tragacanth solutions is difficult because of the high viscosity even at low concentrations and the consequent tendency to retain air bubbles. The concentration therefore is given as g./100 g. solution. dn/dc was also determined for T330 because it is possible to obtain solutions of higher concentrations with the degraded material. No difference was found in dn/dc of the nondegraded and degraded gum. Figure 1 gives $(n - n_0)$ as a function of c, where n is the refractive index of the solution, n_0 is the refractive index of the solvent, and c denotes the concentration in g./100 g. solution. The function is linear, thus indicating that dn/dc is independent of the concentration in the observed interval within experimental errors. dn/dc has the value 147×10^{-5}. Kubal (1948) has obtained the value 148×10^{-5} of dn/dc for karaya and locust bean gums.

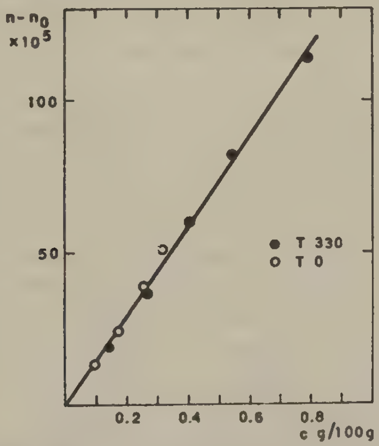

FIG. 1. Difference between the refractive index of solution and solvent, $n - n_0$, as a function of the concentration, c. The diagram shows the values of undegraded (TO) and degraded (T330) tragacanth in 0.2 N NaCl as solvent. $dn/dc = 147 \times 10^{-5}$.

Sedimentation Experiments

The sedimentation experiments were made with a Svedberg ultracentrifuge at a velocity of 60,000 r.p.m. corresponding to a centrifugal force of about 260,000 × g. (Svedberg and Pedersen, 1940). The sedimentation constants were determined with Lamm's scale method (Lamm, 1937), 0.2 N NaCl being used as a solvent to eliminate charge effects. The sedimentation constants are given in Svedberg units (1 $S.$ = 10^{-13} cm./sec. dyne) and their value reduced to 20°C. and pure water as solvent, by ordinary corrections for the viscosity and density of the sodium chloride solution.

The determined sedimentation constants were extrapolated to zero concentration by the empirical formula

$$s = \frac{s_0}{1 + kc} \tag{1}$$

given by Gralén (1944),

where s_0 = sedimentation constant at conc. = 0,
s = sedimentation constant at conc. = c, and
k = constant for each substance.

By plotting s as function of $s \times c$, a straight line is obtained, which gives s_0 after graphical extrapolation to $c = 0$. The degree of polydispersity of the substance can be characterized by the value of dB/dx at zero concentration. $B = A/H$, where A is the area under the sedimentation curve and H is the maximum height of the same curve. B is called the width of the curve. B is an almost linear function of x, where x denotes the distance from the peak to the centre of rotation (Kinell, 1947). dB/dx is calculated for each concentration and plotted as a function of c. The extrapolation of this function is facilitated by the linear relationship between dB/dx and $c/1 + kc$, where k has the same value as in Eq. 1. For detailed information refer to Gralén (1944) and Gralén and Lagermalm (1948).

When the refractive index increment is known, the concentration of the sedimenting substance can be calculated from the area between the sedimentation cuve and the x-axis (Svedberg and Pedersen, 1940, p. 293).

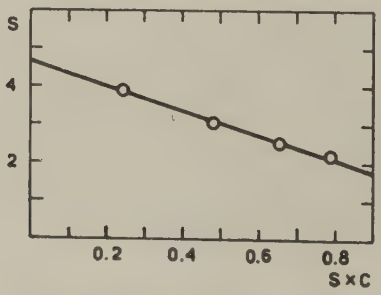

FIG. 2a. The sedimentation constant, s, as a function of $s \times c$ for T330 (tragacanth degraded by boiling for 330 min.). Extrapolation of the straight line to zero concentration gives s_0 = 4.65; k, the slope of this line = 3.2.

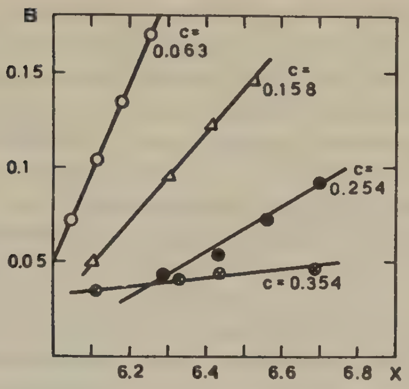

FIG. 2*b*. The width of the sedimentation curves, *B*, as a function of the distance to the center of rotation, *x*, for different concentrations of T330.

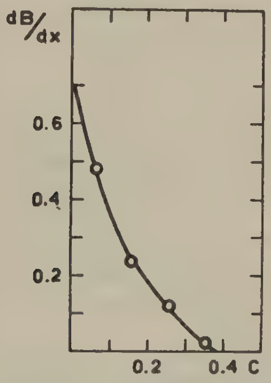

FIG. 2*c*. The widening value, *dB/dx*, as a function of the concentration, *c*, for T330.

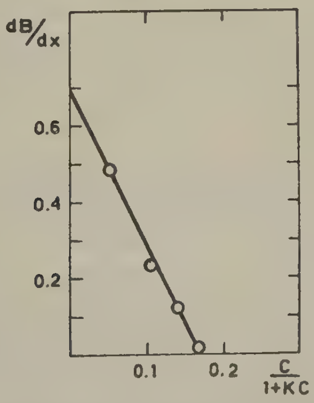

FIG. 2*d*. The widening value, *dB/dx*, as a function of $c/(1 + kc)$ for T330. Extrapolation of the straight line to zero concentration gives $(dB/dx)_0 = 0.70$.

The concentration determined in this way, however, was only 60–70% of the initial concentration. This is due to the fact that heavier aggregates of molecules settle to the bottom of the cell in the strong centrifuge field of the ultracentrifuge before the full speed is reached. These aggregates could not be removed from the solution by an ordinary laboratory centrifuge.

The following procedure gives the most reliable value of the concentration during the sedimentation. The base lines of the curves were drawn to

TABLE I

A. Sedimentation Constants and Polydispersity of TOa

$c = 0.6 \times c_0$ g./100 g.	s	$s \times c$	dB/dx	$\frac{c}{1+kc}$
0.104	3.37	0.350	0.092	0.0431
0.079	3.69	0.292	0.113	0.0381
0.055	4.73	0.260	0.242	0.0315
0.027	6.01	0.162	0.405	0.0198
0	8.0	$k = 13.6$	0.68	
	extrapol.		extrapol.	

B. Sedimentation Constants and Polydispersity of TOb

0.128	3.47	0.444	0.106	0.0558
0.084	4.23	0.355	0.200	0.0455
0.067	4.92	0.330	0.322	0.0400
0	8.0	$k = 10.1$	0.72	
	extrapol.		extrapol.	

C. Sedimentation Constants and Polydispersity of T30

0.207	2.84	0.588	0.041	0.104
0.124	3.35	0.415	0.144	0.078
0.077	4.40	0.339	0.368	0.056
0.039	4.76	0.186	0.605	0.033
0	5.7	$k = 4.8$	0.77	
	extrapol.		extrapol.	

D. Sedimentation Constants and Polydispersity of T330[a]

0.354	2.23	0.789	0.022	0.167
0.254	2.57	0.653	0.122	0.141
0.158	3.05	0.482	0.233	0.105
0.063	3.89	0.245	0.484	0.053
0	4.65	$k = 3.16$	0.70	
	extrapol.		extrapol.	

[a] For Table I*D*, $c = 0.7 \times c_0$.

fit the experimental points in the best manner, and the concentration was calculated from the area of the curves and other constants required. A mean value of the part remaining in solution can thus be obtained from several experiments at various concentrations. It is thereby assumed that for different concentrations of one substance the same proportion of the initial concentration remains in solution. No evidence against this assumption was found. The base lines were then adjusted so that the areas corresponded to the calculated concentration. For TO and T30 about 60% of the initial concentration remained in solution. For T330 this portion was 70%. The results from the sedimentation experiments are given in Table I*a*, *b*, *c*, and *d*. Figure 2 shows the method of calculation of s_0, k, and (dB/dx) for $c = 0$ of T330. The values of TO*a* and TO*b* show the reproducibility of the experiments.

Diffusion Experiments

The diffusion constant from an experiment with an originally sharp boundary between solution and solvent can be calculated from Wiener's equation (Wiener, 1893):

$$\frac{dn}{dx} = \frac{n_1 - n_0}{2\sqrt{\pi D t}} e^{-x^2/4Dt}$$

where D = diffusion constant,
t = time after the beginning of the diffusion,
x = distance from the original boundary, and
$n_1 - n_0$ = difference in refractive index between solution and solvent.

The diffusion experiments were made with the aid of Lamm's scale method (Lamm, 1937) in a thermostat at 20°C. Lamm's slide cells of stainless steel were used. This method gives dn/dx as a function of x. The diffusion constant was calculated from the following expressions which represent different averages of D for a polydisperse substance:

$$D_A = A^2/4\pi t H^2 \text{ and } D_m = m_2/2At,$$

where A = area between the diffusion curve, $dn/dx = f(x)$, and the x-axis; H = maximum height of the curve; and m_2 = second moment of the curve around the vertical axis through the arithmetic medium of the curve. D_A is denoted as the diffusion constant according to the "area" method. D_m is denoted as the diffusion constant according to the moment method. For the calculation of D_m and D_A, m_2/A and A^2/H^2, respectively, have been plotted as a function of t. The slope of the straight lines obtained give D_m and D_A, respectively. The intersection with the t-axis is considered as the time of the beginning of the diffusion. This time is usually not the same as the starting time of the experiment. See Fig. 3. Gralén (1944) has treated these relations more fully. For a polydisperse substance, D_m represents a weight average of the diffusion constants of the constituents:

$$D_m = \frac{\Sigma c_i \times D_i}{\Sigma c_i} \qquad \text{(Gralén, 1941)}$$

Theoretically, for a polydisperse substance $D_m > D_A$. The ratio D_m/D_A has sometimes been used as a measure of the polydispersity. A high experimental accuracy is necessary, however, especially in the determination of the position of the base lines. (*Cf.* Gralén, 1947.) These have been drawn to give the same area under the curves for the different exposures of the same experiment.

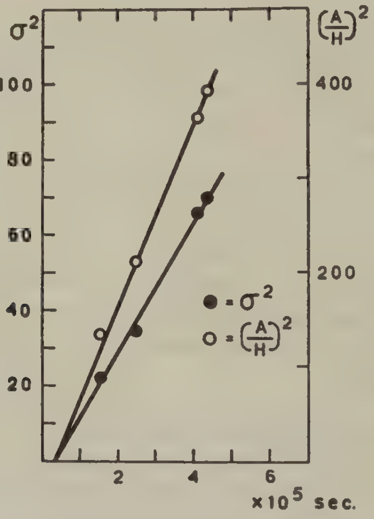

FIG. 3. σ^2 and $\left(\frac{A}{H}\right)^2$ as a function of the time for T330. The slope of these lines gives the diffusion constants, D_m and D_A, resp.

The diffusion curves of tragacanth are skew, thus indicating a concentration dependence of the diffusion constants.

The diffusion constants at zero concentration, D_0, have been calculated from the following expression.

$$D_0 = D_m + \frac{A \times Mo}{4t \times H}$$

where *Mo* (mode) is the difference between the positions of the maximum ordinate and the arithmetic mean of the diffusion curve. *Mo* is negative. Thus, $D_0 < D_m$.

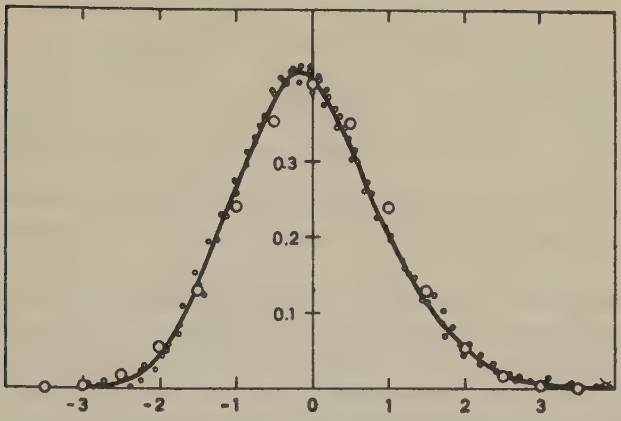

FIG. 4. The diffusion curve of T330 in normal coordinates. The small circles are points obtained from different exposures, the curve connecting the experimental points. The large circles indicate the corresponding normal curve.

The above formula has been used for the individual curves of TO and the mean value calculated. The diffusion curves of T30 and T330 have been transformed into normal coordinates, and the concentration dependence calculated from these curves.

Table II gives the results of the determinations. The diffusion constants are given in units of 10^{-7} cm.^{2}/sec. Figure 4 gives the diffusion curve of T330 in normal coordinates.

All diffusion constants are corrected for the viscosity of the solvent and refer to pure water at 20°C.

TABLE II

Diffusion Constants of Tragacanth Solutions

Solution	Concentration, g./100 g.	D_m	D_0	D_A
TO	0.12	0.67	0.60	0.45
TO	0.20	0.78	0.58	0.42
T30	0.21	0.78	0.64	0.57
T330	0.51	1.08	0.82	0.97

Determination of the Partial Specific Volume

The partial specific volume, V, can be calculated from the following formula (Kraemer, in Svedberg and Pedersen, 1940, p. 57):

$$V = v\left(1 - \frac{(100 - w_1)}{m}\frac{dm}{dw_1}\right)$$

where $v = \frac{v_p}{m}$ = specific volume of the solution,
v_p = volume of the pycnometer,
m = weight of the liquid in the pycnometer, and
w_1 = concentration of the substance in g./100 g. solution.

The values of m and w_1 are determined for different concentrations and m plotted as a function of w_1. The slope of the straight line obtained gives dm/dw_1.

The partial specific volume of undegraded tragacanth was determined both in pure water and in 0.2 *N* NaCl solution. A pycnometer with a volume of about 40 ml. was used. The tare consisted of a similar pycnometer. The weights were corrected for buoyancy (Drucker, 1941).

The greatest experimental accuracy was obtained with water solutions, as the concentration in this case could be measured through evaporation. When 0.2 *N* sodium chloride was used as solvent the concentration was determined by refractive index measurements before filling and also immediately after emptying the pycnometer. The air bubbles were removed from the gum solutions before the determinations by evacuation. Air bubbles were easily formed during the filling of the pycnometer and had to be carefully removed before weighing.

The results are given in Table III*a* and *b*. Figure 5 shows m as a function of w_1, for water solutions of tragacanth.

The difference of the value of V obtained from sodium chloride and water solutions is within the limits of error of the experiments.

The value of V = 0.607 has been used.

TABLE III

A. Partial Specific Volume of Tragacanth in Water Solutions

w_1	m	dm/dw_1	v	V
0.316	38.8267		1.0005	0.6075
0.254	38.8156		1.0008	0.6073
0.173	38.8048	0.153	1.0011	0.6071
0.099	38.7934		1.0014	0.6068
0	38.7779		1.0018	0.6065

B. Partial Specific Volume of Tragacanth in 0.2 N *NaCl*

w_1	m	dm/dw_1	v	V
0.39	39.1538		0.9922	0.6085
0.27	39.1408		0.9925	0.6081
0.185	39.1249	0.152	0.9929	0.6078
0.090	39.1099		0.9933	0.6076
0	39.0969		0.9936	0.6073

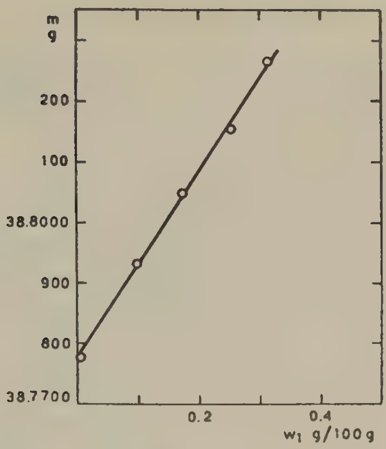

FIG. 5. The weight of the liquid in the pycnometer, m, as a function of the concentration of the substance, w_1 in g./100 g. solution for tragacanth in water solution. The slope of the line gives $dm/dw_1 = 0.153$.

Calculation of the Molecular Weight

The molecular weight has been calculated from Svedberg's formula

$$M = \frac{RTs}{D(1 - Vd)}$$

where M = molecular weight of solute,
R = gas constant = 8.314 joules/mole degree,
T = absolute temperature, and
d = density of the solution.

As s and D refer to zero concentration and pure water at 20°C. as solvent, d is taken as the density of water at 20°C. M represents different averages of the molecular weight of a polydisperse substance, depending on the calculation of s and D. The diffusion constant, D_0, is a weight average (see under *Diffusion Experiments*). s_0 can also be considered as a weight average. These are denoted as D_w and s_w, respectively. The molecular weight obtained is a weight-weight average.

$$M_{ww} = \frac{RT}{(1 - Vd)} \cdot \frac{s_w}{D_w}$$

This is not usually the same as a weight average, M_w, where

$$M_w = \frac{\Sigma c_i M_i}{\Sigma c_i} \qquad \text{(Jullander, 1945)}$$

The following molecular weights were obtained:

TO	840,000
T30	550,000
T330	350,000

The Shape of the Molecules

Sedimentation and diffusion experiments offer certain possibilities for calculating the shape of the molecules. A thread-like molecule has a larger frictional coefficient than a spherical one. The ratio between the frictional coefficients can be calculated from the following formulas:

$$f = \frac{RT}{D} = \frac{M(1 - Vd)}{s}$$

$$f_0 = 6\pi\eta N \left(\frac{3MV}{4\pi N}\right)^{\frac{1}{3}}$$

where f = frictional coefficient of the molecule in question,
f_0 = frictional coefficient of a spherical molecule,
N = Avogadro's number, and
η = viscosity of the solvent.

If the ratio $f/f_0 > 1$, this is caused by either hydration of the molecules, a shape deviating from spherical, or, in general, both. If the shape of the molecules can be approximated to ellipsoids of revolution with the axes, l and d, the ratio l/d can be calculated from the ratio f/f_0 (Herzog, Illig and Kudar, 1933). It is therein assumed that the molecules are not hydrated and that the influence of the Brownian movement is strong enough to prevent orientation of the molecules. Further

$$\frac{\pi l d^2}{6} = \frac{MV}{N}$$

This formula makes the calculation of l and d possible.

These calculations have been made for the tragacanth solutions and the results are given in Table IV.

TABLE IV

The Shape of the Molecules

	f/f_0	l/d	l	d
			A	A
TO	6.15	235	4500	19.0
T30	6.5	265	4200	15.9
T330	5.9	220	3200	14.5

Viscosity Measurements

The viscosity of the tragacanth solutions was measured in an Ostwald viscometer at 20°C. Two-tenths normal NaCl was used as solvent. The intrinsic viscosity $[\eta]$ was calculated from the formula

$$[\eta] = \lim_{c\to 0} \frac{\ln \eta/\eta_0}{c} = \lim_{c\to 0} \frac{\eta_{sp}}{c}$$

where $\eta_{sp} = \eta/\eta_0 - 1$,
η = viscosity of the solution, and
η_0 = viscosity of the solvent.
c = concentration (*g.*/100 *g.*)

The following values of the intrinsic viscosity were obtained:

Solution	Intrinsic viscosity
TO	12.3
T30	12.0
T330	6.4

The viscosity measurements indicate hardly any decomposition of T30 compared with TO. The diffusion constants of these solutions are about the same. The sedimentation constants, however, differ markedly (5.7 *vs.* 8.0, respectively), which indicates that the soluble part of the gum has been degraded. According to a prevoius discussion in this paper, the portion of the gum of highest molecular weight immediately settles to the bottom of the cell. This portion, however, contributes to the high viscosity and the relatively low diffusion constant of T30. The area under the diffusion curves corresponds to the initial concentration. From these findings it must be concluded that some of the swollen material gets into solution, while the part previously dissolved is degraded to some extent during boiling for 30 min. After 5½ hr. boiling, the degradation is evident, as shown both by a lower viscosity and by a lower sedimentation and higher diffusion constant. As the swollen gel dissolves during boiling, the decrease in molecular weight is not so great as could be expected were only the water-soluble material degraded.

Flow Curves

Flow curves for rather highly concentrated solutions of gum tragacanth were measured in the consistometer described by Säverborn (1945) and Jullander (1945). For these experiments, the solutions were prepared by swelling the dry gum in water at room temperature overnight and afterwards boiling the thick solution for 3 hr. While this will mean a certain degradation, for practical use the solutions are generally prepared in this way. The consistometer consists of an outer fixed cylinder and an inner cylinder hanging in a torsional thread. The flow curve (rate of flow, *D*, *vs.*

shearing stress, τ) is obtained from a single experiment. The ratio between the diameters of the inner and outer cylinders is small (in these measurements 0.286), and this fact allows us to use the simple equation

$$D = 2\tau \frac{d\Omega}{d\tau}$$

for the calculation of the flow curve. Here Ω is the negative angular velocity of the rotating inner cylinder, moved by the shearing stress of the liquid, and τ is proportional to the angular deviation from the equilibrium position, the proportionality factor being determined by the dimensions of the instrument. For the complete theory the reader is referred to Jullander's paper (1945). The flow curves obtained at different concentrations are given in Fig. 6.

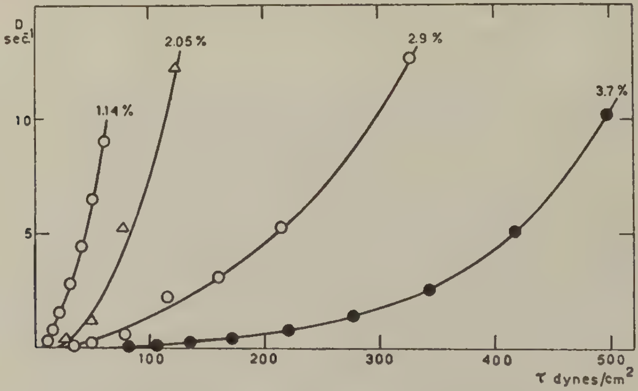

FIG. 6. The rate of flow, D, as a function of the shearing stress, τ, for tragacanth solutions.

The curves are bent, indicating the structural viscosity which increases with the concentration. The yield point is very close to $\tau = 0$, even at high concentrations, which means that the solutions behave as liquids, not as solid gels, even at very low shearing stresses. At low concentrations, the solutions do not deviate much from Newtonian liquids, which should give straight lines through the origin in this diagram.

SUMMARY AND DISCUSSION

Table V gives a summary of the results obtained.

The physicochemical properties of the solutions of gum tragacanth indicate that the molecules have an extended shape. The average lengths and diameters of the molecules, as calculated from the frictional ratios, show this clearly. The figures given in Table IV are calculated under the assumption that the molecules are nonsolvated. The number of hydroxyl groups and other hydrophilic groups available in the gum certainly give rise to a considerable hydration of the molecules. This solvation also increases the frictional ratio, and therefore the values given of l are too high and those of d, too low. However, the effect of the hydration is certainly much smaller than that of the molecular asymmetry. The hydration is probably about the same for all preparations, and this allows a comparison between the figures from the various preparations. This leads to the conclusion that the first degradation during boiling (T30) consists mainly in a decrease of the width of the molecules. This reasoning is also consistent with the viscosity measurements. The prolonged boiling causes a definite shortening of the molecules.

TABLE V

Summary of the Results Obtained

	Tragacanth, nondegraded	Tragacanth degraded by boiling for 30 min.	Tragacanth degraded by boiling for 330 min.
Sedimentation constant at zero concentration, s_0, in Svedberg units	8.0	5.7	4.6
Diffusion constant at zero concentration, D_0, in 10^{-7} cm.^{2}/sec.	0.59	0.64	0.82
Partial specific volume, V	0.607		
Molecular weight from s_0 and D_0	840,000	550,000	350,000
Widening value at zero concentration, $(dB/dx)_0$	0.70	0.77	0.70
Intrinsic viscosity	12.3	12.0	6.4
Frictional ratio, f/f_0	6.2	6.5	5.9
l/d	235	265	220
l = length of molecule in A	4500	4200	3200
d = width of molecule in A	19.0	15.9	14.5

The results show that the molecules of gum tragacanth must be considered to be rather long chain molecules with small adjacent side chains. The hydrolysis first attacks the side chains the bonds of which seem to be split more easily than those of the main chain. The difference in strength is small between the bonds in the side chains (or connecting the side chains to the main chain) and the bonds in the main chain, and this fits well with the chemical analysis of gum tragacanth made by James and Smith, and the picture of the molecule suggested by them.

The solutions are polydisperse. The value of dB/dx (widening value of sedimentation curves) is about 0.7, and no appreciable change in this value could be observed during hydrolytic cleavage. The polydispersity is higher than for native cellulose, but not so high as can sometimes be found for moderately degraded cellulose or for synthetic polymers.

Kubal and Gralén (1948) and Kubal (1948) investigated the behavior of two other plant gums (Karaya gum and Locust bean gum) in the ultracentrifuge. A comparison between their results and ours on gum tragacanth shows that the molecules of gum tragacanth have a much more extended shape than the other plant gums. Its molecules are not so big as those of Karaya gum, but they give rise to a higher viscosity. It is probably because the side chains of Karaya gum are longer. The molecules of Locust bean mucilage do not show as asymmetric a shape as the other two.

Of the three gums investigated, gum tragacanth shows the highest viscosity for a given concentration. The viscosity is really extremely high, but the solutions always behave as liquids, not as solid gels, even at so high a concentration as 3.7%. This property is essential for the practical use of gum tragacanth. It gives highly viscous, stable solutions at a low concentration, and these solutions are liquids and not gels. Certainly these properties depend on the shape of the molecules of the gum. It is obviously difficult for the long molecules with probably irregularly spaced side chains to form a stable gel. Owing to the relatively low concentration, they are rather free to thermal movements in the solution, and there is very little tendency for gelatinization or thixotropy even if the viscosity is comparatively high.

ACKNOWLEDGMENTS

The authors wish to thank Mr. G. Lagermalm for valuable discussions. We are also indebted to Mr. I. Walldén and Miss B. Fehrling for assistance in the numerical calculations and the experimental work.

REFERENCES

DRUCKER, C., *Arkiv Kemi Mineral. Geol.* **14A**, No. 15 (1941).
GRALÉN, N., *Kolloid-Z.* **95**, 188 (1941).
GRALÉN, N., Dissertation. Uppsala, 1944.
GRALÉN, N., *Svensk Papperstidn.* **50**, No. 11B, 96 (1947).
GRALÉN, N., AND LAGERMALM, G., Polydispersity of Polystyrene, p. 215. Festskrift tillägnad J. Arvid Hedvall, Göteborg, 1948.
HERZOG, R. O., AND ILLIG, R., AND KUDAR, H., *Z. physik. Chem.* **167A**, 329 (1933).
JAMES, S. P., AND SMITH, F., *J. Chem. Soc.* **1945**, pp. 739, 746, 749.
JULLANDER, I., *Arkiv Kemi Mineral. Geol.* **21A**, No. 8 (1945).
JULLANDER, I., *Svensk Kem. Tid.* **57**, 148 (1945).
KINELL, P. O., *Acta Chem. Scand.* **1**, 335 (1947).
KUBAL, J. V., *Collection Czechoslov. Chem. Commun.* **13**, 378 (1948).
KUBAL, J. V., AND GRALÉN, N., *J. Colloid Sci.* **3**, 457 (1948).
LAMM, O., Dissertation. Uppsala, 1937.
MANTELL, C. L., The Water-Soluble Gums. New York, 1947.
NORMAN, A. G., The Biochemistry of Cellulose, the Polyuronides, Lignin, etc. Oxford, 1937.
SVEDBERG, T., AND PEDERSEN, K., The Ultracentrifuge. Oxford, 1940.
SÄVERBORN, S., Dissertation. Uppsala, 1945.
WIENER, O., *Ann. Physik Chem.* **49**, 105 (1893).

TECHNIQUES FOR GENERATING SILVER IODIDE SMOKE

Bernard Vonnegut

General Electric Research Laboratory, Schenectady, New York

Received August 4, ,1949

INTRODUCTION

Appreciable numbers of nuclei for the formation of ice crystals at temperatures higher than − 20°C. or − 10°C. are frequently absent from the atmosphere. Because of this, supercooled clouds are a very common occurrence. Schaefer (1,2) has demonstrated that these clouds can be greatly changed by seeding them with the many small ice crystals produced by dropping dry ice particles. Seeding by this technique has been successfully used to change supercooled clouds to ice crystals and, under the proper conditions, to cause them to shed their moisture as snow or rain. The meteorological aspects of dry ice seeding have been treated in a recent paper by Bergeron (3).

It has been observed in the laboratory (4) that silver iodide particles serve as nuclei for the formation of ice crystals. It is believed that silver iodide smoke particles are very good nuclei for ice formation because of the close similarity between the crystal structure of ice and silver iodide. Trillat and Laloeuf (5) have recently reported the results of electron diffraction studies of silver iodide smokes. They have found that all of the silver iodide smokes they examined contain the hexagonal form of silver iodide which closely resembles ice.

The fact that silver iodide particles serve as nuclei for the formation of snow crystals has suggested the possibility that under the proper conditions clouds might be *modified* by the introduction of large numbers of silver iodide particles into the atmosphere, either from the ground or from an airplane. Inasmuch as silver iodide particles should not melt or rapidly evaporate under atmospheric conditions, it is not necessary to introduce them directly into a cloud.

It is obvious that very large numbers of silver iodide particles would be required for any experiments in the natural atmosphere. If a cloud has a water content potentially capable of yielding 1 g. of snow/m.^{3}, and if the ice crystals weigh 2×10^{-5} g. each, an average of 50 nuclei/l. will be required to precipitate this moisture. This is of the order of 10^{14} nuclei/cu. mile. An area such as the state of New York would, therefore, require perhaps 10^{19} nuclei.

It immediately becomes apparent that if this many particles are required for seeding, the particles must be very small or the expense of materials and dispensing equipment would be prohibitively large. For example, if each particle were about 1μ in diameter, which is not generally considered very large, about 50 tons of silver iodide or other nucleating material would be required. Clearly much smaller particles are required. Fortunately, particles of silver iodide less than 100 A in diameter are effective as nuclei. Experiments indicate that 10^{16} nuclei can be produced/g. of silver iodide (4,6). Using particles of this size, only about 2 lb. of silver iodide would be required to give 10^{19} nuclei. It is true that nuclei of this very small size are not quite as effective as the larger size particles. However, this minor sacrifice in effectiveness is well worth the great gain in economy.

Shortly after silver iodide was found to be a good nucleus, a generator was made which produced silver iodide smoke by feeding a silver iodide coated string into an oxyhydrogen flame (4). While this generator produced large numbers of nuclei/g. of silver iodide, the rate of output, approximately 10^{13} nuclei/sec., was somewhat less than that which would be required for large scale seeding operations. In addition, the apparatus was not well adapted to field use as it required both hydrogen and oxygen, as well as a mechanism for feeding the string into the flame. The techniques to be described deal with simpler and more effective silver iodide nuclei generators which have since been developed.

Techniques of Smoke Generation

Silver Iodide Solutions

The problem of generating silver iodide smokes has been greatly simplified by the use of solutions of silver iodide in an acetone-sodium iodide solution. The generators to be described all make use of these solutions.

Although silver iodide is highly insoluble in both water and organic solvents, it is nevertheless quite soluble in water or acetone solutions of a soluble iodide, such as iodides of sodium, potassium, ammonium, etc. Water solutions containing upwards of 20% by weight of silver iodide can be made by dissolving silver iodide in a saturated solution of sodium iodide. However, if these water solutions are diluted by adding water, the silver iodide precipitates out. Therefore, water solutions have the disadvantage that they cannot be readily diluted to any desired concentration. Acetone solutions, on the other hand, can be diluted with acetone to any concentration without precipitation of the silver iodide. Accordingly, acetone solutions are used in all of this work.

These acetone solutions can readily be made by dissolving silver iodide and sodium iodide in acetone using about 4 parts by weight of silver iodide to 1 part by weight of sodium iodide.

The same solutions can very easily be made at about one-half the cost by making the silver iodide directly from metallic silver and elementary iodine. It is the practice in this laboratory to make up a stock solution containing approximately 40% by weight of silver iodide. The solution is then diluted with acetone to any required concentration. This stock solution is usually made in 2-l. quantities as follows: Place an excess of granulated silver (around 2 or 4 lb.) into a 4-l. Pyrex Erlenmeyer flask. Add 200 g. of sodium iodide, 400 g. of iodine crystals, and 2 l. of acetone. (The purity of the chemicals is not important; technical grade is satisfactory.) Following the addition of the acetone, the iodine and sodium iodide go into solution and the chemical reaction which involves the solution of the silver begins. After a few minutes, the solution begins to boil because of the heat of reaction. The acetone which boils off is returned to the solution by placing a reflux condenser on the flask. If the reaction proceeds too rapidly, it can be slowed down by cooling the flask in water or by directing a stream of air on the flask. After a few minutes, the speed of the reaction diminishes even though much of the iodine has not reacted. When this point is reached, the flask is placed on a hot plate and the solution kept at a gentle boil for several hours. This gentle boiling circulates the solution through the silver granules in the bottom of the flask so that the reaction can take place. After several hours, the solution loses most of its dark iodine color indicating that the reaction is completed and that the iodide is completely reacted. In general, the color of the solution at this point may vary from a light yellow to a fairly dark brown. It is not yet known what causes this color, but it seems to have no adverse effect on the solution. When the solution has cooled to room temperature, it is well to filter it to remove any suspended matter. It has been found that this stock solution can be kept indefinitely in stoppered bottles without deterioration.

Silver Iodide Impregnated Charcoal

The production of silver iodide smokes is most easily accomplished by first evaporating silver iodide at a high temperature and then rapidly cooling this silver iodide vapor so that it condenses into many small particles. A very simple method of doing this is to burn silver iodide impregnated charcoal in a stream of air (7). The heat of the burning charcoal evaporates the silver iodide on the surface of the charcoal and the air stream quenches the silver iodide vapor, as well as promoting the combustion of the charcoal.

The impregnated charcoal is made by soaking wood charcoal or charcoal briquettes in a 2% silver iodide solution made by diluting a stock solution. When the acetone is evaporated off, the charcoal contains about 1% by weight of silver iodide. No extensive work has been done on the optimum amount of silver iodide to use in the charcoal, but one per cent seems to be quite satisfactory.

Ground Type Charcoal Burner

Charcoal burners have been developed for generating silver iodide smoke from the ground. Essentially, these burners consist of a simple arrangement for burning the charcoal in a rapidly moving stream of air. It is highly important that the air flow over the charcoal be sufficiently rapid to prevent the formation of a layer of ash over the burning coals. A layer of ash prevents the silver iodide vapor from escaping into the air stream. A good stream of air is also desirable in order to keep the charcoal burning at a high temperature. The air stream should have a velocity of the order of 15 miles/hr. or more. A convenient charcoal burner of this sort is shown in Fig. 1. It consists of a small gasoline-powered blower, which directs a stream of air on a mass of charcoal burning in a wire cage. This cage is made of nickel-chrome wire to withstand the high temperatures. The charcoal automatically feeds by gravity into the cage from a hopper above the burner. The air for burning the charcoal can equally well be supplied by a jet of compressed air.

Several difficulties are associated with this type of generator. Sometimes the charcoal clogs in the tube feeding the burner. Also, a certain amount

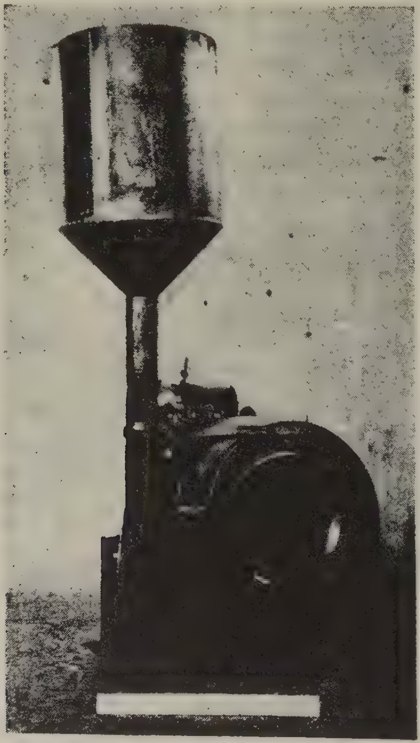

FIG. 1. Gasoline-powered charcoal burner for ground use.

of the charcoal is lost as small buring pieces are blown through the holes of the burner. This makes the apparatus somewhat hazardous to operate near dry leaves or wooden construction.

The apparatus does have the advantage of great simplicity. If the wind velocity is 20 miles/hr. or more, a generator would not require any other air supply. Small pieces of impregnated charcoal are a very convenient source of nuclei for small scale tests. By igniting a piece of charcoal and blowing one's breath over it, one can produce large numbers of nuclei for cold-box experiments. The impregnated charcoal is very useful for experiments in supercooled ground fogs or local regions of atmosphere that are supersaturated with respect to ice.

Airplane Type Charcoal Burner

The charcoal-burning method of nuclei production is particularly well adapted for use in seeding from airplanes. The technique that is used consists of dropping small pieces of burning charcoal from the airplane as it flies along. These charcoal particles burn as they fall until they are entirely consumed, and as they burn, they leave behind a trail of silver iodide smoke. The burner shown in Figs. 2 and 3 is essentially a small stove in which several pounds of impregnated charcoal are ignited. The top of the charcoal is ignited by a burning piece of paper and a strong draft allowed to flow through the burner. The charcoal is stirred by means of the crank at the top of the burner. When all of the charcoal is ignited, it is released by pulling up on the crank handle. This lifts up the perforated steel plate at the bottom of the burner and allows the charcoal to drain out.

The nuclei are dispersed in a curtain beneath the path of flight in a manner analogous to that achieved by dropping dry ice particles. This has the advantage that nuclei are very rapidly distributed through a very large volume of atmosphere.

The method of dropping burning charcoal can be used to introduce very large numbers of nuclei into an air mass in a very short time. The rate at which nuclei can be generated is limited only by the rate at which the charcoal can be ignited and dropped from the airplane. The small burner in Figs. 2 and 3 can be emptied in about 15 to 30 sec. The nuclei yield obtained using the charcoal method has been estimated in the cold-box experiments to be of the order of 10^{16}/g. of silver iodide at a temperature of -20°C. The discharge of the 3 or 4 lb. of charcoal in the burner in 30 sec., therefore, corresponds to a rate of nuclei production of the order of 10^{16}/sec. while the charcoal is being discharged. It is planned to develop an apparatus for continuously igniting and discharging charcoal at about this rate for use in filling large air masses at any altitude with nuclei.

The distance through which the burning charcoal falls before it is completely consumed depends, of course, on the size of the charcoal particles. Estimates of this distance have been obtained from experiments

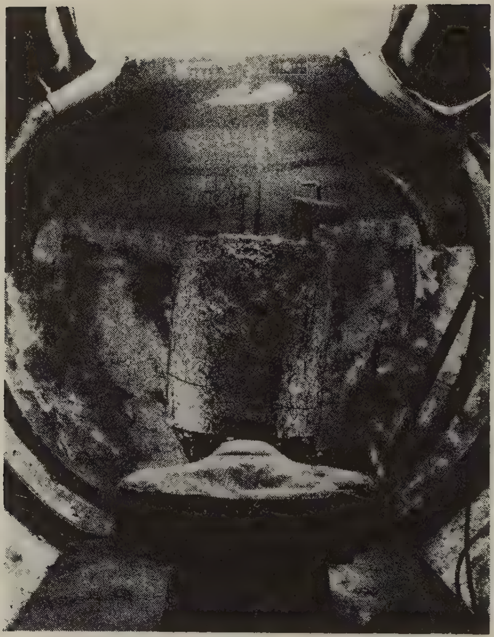

FIG. 2. Charcoal igniter for airplane use.

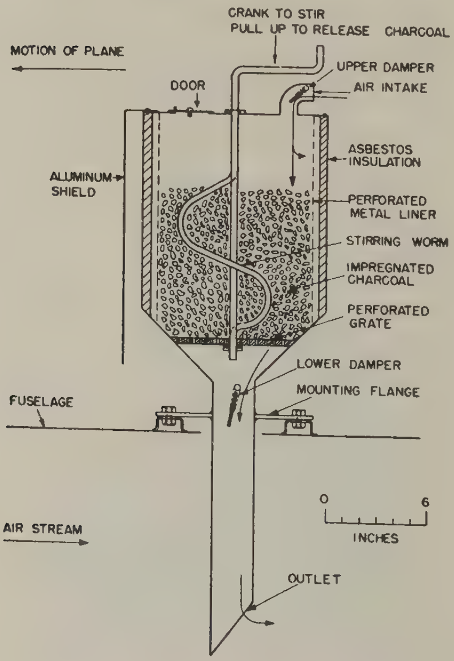

FIG. 3. Airplane charcoal igniter.

in which burning pieces of charcoal were balanced in a stream of air moving upwards through a glass tube. The total distance through which the charcoal fell was determined by measuring the total volume of air which had passed through the tube and dividing it by the cross sectional area of the tube. The results of these experiments, along with the experiments made in the same way on dry ice, are shown in Fig. 4. The air used was at atmospheric pressure and room temperature. The charcoal used in most experiments is of a size which would have a range of one to two thousand feet. It is designated by the manufacturer[1] as No. 3 charcoal and has particles about $\frac{1}{2} \times \frac{1}{4} \times \frac{1}{8}$ in. For seeding clouds thicker than 2,000 ft., it is probably desirable to use pieces that are somewhat larger so that they will fall through the depth of the cloud.

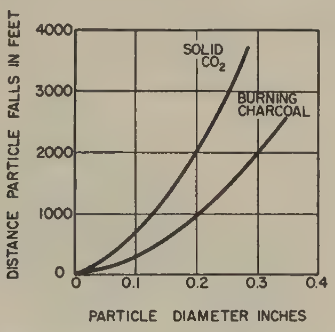

FIG. 4. Falling distance of burning charcoal and solid CO_2 particles.

In order to determine whether the charcoal particles would burn at high altitudes, tests were made in the laboratory under reduced pressures. At pressures corresponding to 50,000 ft., the charcoal appeared to burn as well as at sea level pressures. As a safety precaution in airplane operations, it is desirable to have means of extinguishing burning charcoal in the burner. It has been found that while carbon dioxide and carbon tetrachloride extinguishers are not at all effective, water is very satisfactory.

In order to be absolutely sure that none of the burning-charcoal particles reach the ground, it is desirable that seedings should be made from altitudes above the ground that are several times the measured trajectory of the charcoal particles used.

Experiments have been made to determine whether the burning of the falling charcoal particles would be seriously affected by the moisture in clouds. Pieces of burning charcoal held in a small wind tunnel with a spray of water giving a concentration of the order of 1 g./m.^{3} appeared to be unaffected by the water drops. It is concluded that the burning of the charcoal is not seriously affected by clouds if the charcoal is thoroughly ignited when it encounters the cloud.

---

[1] Flower City Charcoal Company, Rochester, New York.

Spray-Nozzle Type Smoke Generator

The spray-nozzle type of generator is one of the simplest and most efficient methods for producing large numbers of silver iodide nuclei. The spray-nozzle generator shown in Fig. 5 is made from a standard commercial air atomizing spray nozzle of the sort that is used in paint spraying and humidifying. In the conventional use of this type of nozzle, water or paint is atomized by the action of a jet of compressed air. In the use of the spray nozzle for silver iodide smoke generation, the nozzle is used to atomize an acetone solution of silver and sodium iodide with compressed hydrogen gas. The mixture of hydrogen gas and silver iodide solution is ignited as it leaves the spray nozzle. Because of the small size of the solution droplets, they are very rapidly vaporized in the flame. The silver iodide vapor in the flame rapidly condenses when it mixes with the cool air of the atmosphere to form a smoke of very small silver iodide particles.

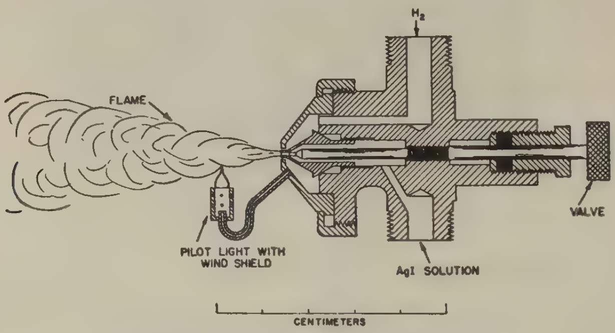

FIG. 5. Spray-nozzle type smoke generator.

By varying the concentration and the rate of flow of silver iodide solution to the spray nozzle, the size of the resulting particles can be varied over a wide range. In general, the greater the flow rate of silver iodide to the nozzle, the larger will be the resulting particles. The results of experiments carried out on the properties of smokes produced from a spray-nozzle generator have been published by the author (6). Fig. 6 shows the number of nuclei produced by the generator as a function of the rate of silver iodide consumption. Since this work, minor changes have been made in the spray-nozzle type generator which have somewhat improved its operation. The spray nozzle now being used is a "Sprayco," Model 125.[2] This type of nozzle has been found easy to clean and maintain, and it has the advantage that the central orifice where the solution is introduced can be cleaned merely by closing the valve. This type of nozzle is illustrated in Fig. 5. The annular orifice through which the gas flows is somewhat large as supplied by the manufacturer, and it has been found desirable to reduce the size of this hole by closing it with silver solder and then drilling it out with a smaller size drill. This greatly reduces the consumption of gas by the nozzle. Originally, the diameter of the hole is .059 in., and it is reduced to .052 in. (a No. 55 drill is used). When operated at a pressure of 20 lb./sq. in. this nozzle uses of the order of 1 cu. ft. of hydrogen/min. This means that a standard hydrogen tank containing 220 cu. ft. of gas lasts for about 4 hr. Heat released by the flame is of the order of 300 B.t.u./min. which would correspond to about 5 kw. of electrical heating.

---

[2] Manufactured by Spray Engineering Company, 114 Central Street, Sommerville, Massachusetts.

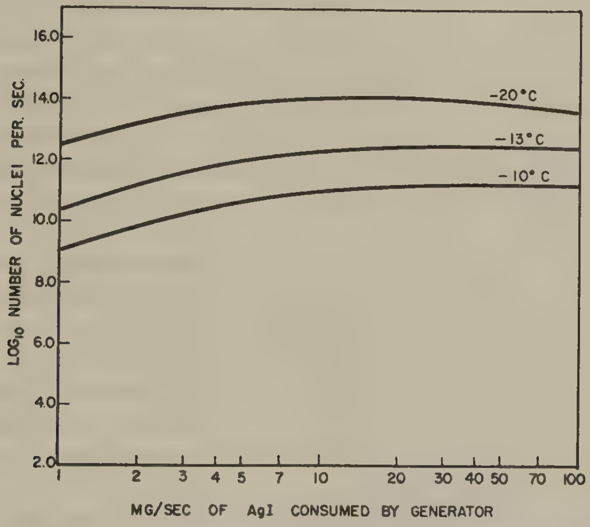

FIG. 6. Number of nuclei produced by spray-nozzle type generator.

If there is much wind where the generator is operated, measures must be taken to prevent the flame from being blown out. This can be done by using a flame holder made of a piece of pipe a few inches long placed an inch in front of the spray nozzle. After several hours of operation, the inside of the flame holder accumulates quite a thick layer of silver iodide and silver, and it must be cleaned. A more satisfactory method of maintaining the flame is to use a small pilot light. The end of the small tube supplying gas to the pilot light is pinched down to give a small rate of flow sufficient to maintain a small flame. The pilot light has been found very satisfactory. With it, the generator can be operated with a high rate of silver iodide consumption which gives a large particle size. At high rates of consumption, a flame holder has been found to clog very rapidly and to waste appreciable amounts of silver iodide.

There is a wide latitude in the concentrations of silver iodide solution which can be used in the spray-nozzle type of burner. A 10% solution seems to be quite satisfactory. This concentration is far below saturation so that the nozzle is not likely to clog from evaporation of the acetone.

The optimum setting for the spray-nozzle generator will doubtless depend on the temperature of the clouds to be seeded. In general, larger sized particles are desirable when the temperature of the cloud is close to the freezing point. A rough estimate of the particle size of the smoke being produced by the generator can be made from the appearance of the smoke. Smokes having a very small particle size are almost invisible. With bright sunlight against a dark background, smokes having a particle diameter of the order of 100 A can be seen to have a faint blue color. Smokes with larger sized particles are easily visible.

It is believed that the spray-nozzle type of generator is well adapted to the generation of silver iodide smokes from the ground. The apparatus is simple to operate and requires very little attention. For experiments requiring a mobile type of generator, a small two wheel trailer has been equipped to carry three 220-cu. ft. hydrogen tanks. The generator is mounted on the end of the trailer, and it is shielded from the wind by a housing made of stove pipe.

While the spray-nozzle type generator is being considered primarily for use in generating smokes on the ground, this type of generator may also be useful for airplane operation. Work is underway at the present time on installing one of these generators on an airplane.

The spray-nozzle type of generator which has been described produces about 10^{14} nuclei/sec. with a consumption of about 1 l. of 10% solution or 100 g. of silver iodide/hr. The cost of the hydrogen and silver iodide is about $3/hr. for one generator.

Combustible gases other than hydrogen can be used to operate the spray-nozzle type of generator. Some work has been done using commercial bottled gas. It has been found that such gas is satisfactory; however, it does not burn as readily as hydrogen and greater precautions must be taken to shield the flame from the wind.

Compressed air has been used instead of a combustible gas. With this arrangement, the acetone in the solution provides all of the fuel for the flame. In this case, it is difficult to maintain the flame, and only dilute solutions can be used because large concentrations of silver and sodium iodide make combustion difficult.

Turbo-Jet Smoke Generator

Some work has been done with the cooperation of the Thermal Power Systems Division of the General Engineering and Consulting Laboratory of the General Electric Company on the utilization of a turbo-jet burner as a silver iodide smoke generator. The turbo-jet burner is a very simple, lightweight, and efficient kerosene burner. The exhaust leaves the burner as a large, very hot flame. It was suggested by Mr. K. Maynard of the General Electric Research Laboratory that such a burner might be advantageously used as a basis for a large silver iodide smoke generator.

Through the cooperation of the Thermal Power Systems Division, a burner with an electric air blower was supplied. The burner used consumed about 10 gal. of kerosene/hr. and provided a flame about 4 in. in diameter and 2 ft. long. The unit was used as a silver iodide smoke generator by atomizing a 40% silver and sodium iodide acetone solution into its flame with an air atomizing nozzle operated with compressed air. This type of generator can be considered as an enlarged version of the spray-nozzle generator which has been described.

No satisfactory measurements of the nuclei production of this generator have been made because the size of the flame was such that it was not possible to use the existing smoke measuring wind tunnel. Because of the much larger flame and the much larger quantity of heat available, this generator can be expected to produce nuclei at a much higher rate than the smaller spray-nozzle generator. On the basis of a comparison of the ratio of the heat evolved by the two generators, the turbo-jet unit might provide 10^{15} to 10^{16} nuclei/sec. with a consumption of perhaps 5 lb. of silver iodide/hr.

This extrapolation of the performance of a small generator is somewhat risky. With a larger generator, there is the possibility that coagulation of the smoke particles may lower the output. Also, for a large flame, the rate of quenching of the hot gases will probably be somewhat different than that for a small flame. This would be expected to modify the performance of the smoke generator.

Should it appear desirable to make much larger silver iodide smoke generators, the turbo-jet burner appears to be a simple way to do it. Evaluation of the performance of such generators will have to be determined by further tests.

ACKNOWLEDGMENTS

This work was made possible through support extended the Research Laboratory of the General Electric Company jointly by the Signal Corps and the Navy Department (Office of Naval Research) under Signal Corps Contract No. W-36-039-sc-38141.

The author wishes to acknowledge the assistance and valuable suggestions of K. Maynard, R. E. A. Falconer, and D. C. Blanchard of the G. E. Research Laboratory and the personnel of Project CIRRUS. The author is also indebted to I. Benson, R. W. Abbot R. A. Doak, L. W. Crooks, and J. B. Gaffney of the Thermal Power Systems Division of the G. E. General Engineering and Consulting Laboratory who constructed the turbo-jet burner system used in the large silver iodide smoke generator.

SUMMARY

Generators are described which are capable of producing large numbers of silver iodide smoke particles for nucleating natural clouds. These

generators are of two kinds, the charcoal-burning type and the spray-nozzle type. The charcoal-burning generator produces silver iodide smokes by burning wood charcoal which has been impregnated with silver iodide. The spray-nozzle generator produces smokes by burning silver iodide solution atomized from a small spray nozzle with compressed hydrogen gas. The construction and operation of these smoke generators is described. In addition, a larger generator employing a turbo-jet burner is described. The preparation of the silver iodide solutions used in these smoke generators is outlined.

References

1. Schaefer, V. J., *Science* **104**, 457 (1946).
2. Schaefer, V. J., *Chem. Revs.* **44**, 291 (1949).
3. Bergeron, T., *Tellus* **1**, 1 (1949).
4. Vonnegut, B., *J. Applied Phys.* **18**, 593 (1947).
5. Trillat, J. J., and Laloeuf, A., *Compt. rend.* **228**, 81 (1949).
6. Vonnegut, B., *Chem. Revs.* **44**, 277 (1949).
7. Vonnegut, B., Supplement to First Quarterly Progress Report, Meteorological Research. General Electric Research Laboratory, Contract No. W-36-039-sc-32427, November, 1947.

GENERAL THEORY OF THE STRUCTURE, TRANSFORMATIONS AND MECHANICAL PROPERTIES OF MONOLAYERS

M. Joly

Service de Chimie-Physique, Institut Pasteur, Paris

Received June 28, 1949

The different methods of study of monolayers: the construction of isotherms, the measurements of surface potential and of surface viscosity, all lead to the detection of transformations in monolayers: ordinary changes of phase and homogeneous transformations.

Ordinary Changes of State

With isothermal curves $p(\sigma)$ (p is surface pressure, σ is molecular area), ordinary changes of state, such as liquefaction, vaporization and sublimation (1, 2) are characterized by flats in the curve. These correspond to zones of "demixtion" (entmischung), that is to say, to equilibrium between two nonmiscible phases. As we are dealing with a single constituent, this equilibrium is between two nonmiscible "forms" or "molecular states" of the same substance.

It may be helpful to recall the molecular mechanism of such a transformation of the first kind. Consider a compression of the monolayer starting from M (Fig. 1). When we reach A each molecule occupies the area σ_A. If we continue to reduce the surface, even by the smallest amount, the area occupied by each molecule is not $\sigma_A - d\sigma$: most of the molecules retain their molecular area while a certain number between

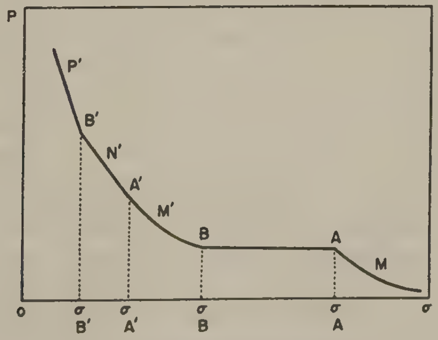

FIG. 1. Isothermal curve.

them jump suddenly to the area σ_B (which can be considerably smaller than σ_A) and cluster together in a new phase. The appearance of this phase reduces the degrees of freedom of the system by one, explaining the constancy of pressure during the process. As the representative point of the film moves from A to B, the number of molecules passing from area σ_A to area σ_B increases, and as soon as the point B is reached, all the molecules occupy the molecular area σ_B. We are again in the presence of a single phase and the degrees of freedom of the system revert to the initial value.

Mayer and Streeter (3) have emphasized the difficulty of distinguishing experimentally, in the case of ordinary bulk systems, between anomalous or diffuse first order transformations and λ transformations. In the same way, for surface systems very small variations of experimental conditions suffice for passing from one to the other of these different types of transformation. Thus, in the isotherms of the C_{18}, C_{19} and C_{20} alcohols studied by Harkins and Copeland (4), the transformation: liquid condensed-super liquid, displays these 3 different types in a narrow temperature range. That a transformation is of the first order, and not of higher order, can be shown by the surface potential examination, which can prove the existence of two phases. Thus, for pentadecylic acid Harkins, Young and Boyd (5) have shown that, despite the absence of a definite flat portion the transformation: liquid (liquid expanded)-expanded mesomorphous (intermediate liquid), is a diffuse first order transformation. The same conclusion was drawn by Schulman and Hughes (6) for the corresponding transformation of myristic acid and by Adam and Harding (7) for the C_{17} nitrile.

Homogeneous Transformations

We have shown, with Dervichian (8), that the thermodynamic classification of transformations introduced by Ehrenfest (9) extends without difficulty to transformations in monolayers providing a term for the surface energy is introduced into the thermodynamic expressions. By taking temperature and pressure as independent variables, the transformations correspond to successive derivatives with respect to the surface pressure of the Gibbs thermodynamic potential $G = E - TS + PV + p\sigma$, $\frac{\partial G}{\partial p} = \sigma$, $\frac{\partial^2 G}{\partial p^2} = \frac{\partial \sigma}{\partial p}$, . . . ($P$ is the bulk pressure, E and S the internal energy and total entropy of the system). An ordinary change of state by compression or expansion is a first order transformation, since there is a corresponding discontinuity in σ and, therefore, of the first derivative of G. When there is a sudden variation of compressibility $K = -\frac{1}{\sigma}\frac{\partial \sigma}{\partial p}$ without discontinuity of σ, it is the second derivative of G which is discontinuous, and not the first, and we are dealing with a second order transformation. These definitions do not presume any particular molecular mechanism of the transformations.

Points of transformation of high order in monolayers are extremely frequent as has been shown by Dervichian and Joly (8, 10, 11), as well as by Harkins and his collaborators (4, 5, 12).

Molecular Mechanism of the Transformations

It is often considered that homogeneous transformations correspond to a change of degree of symmetry of the lattice or of the molecules. This is precisely the point of view developed by Lifschitz (13), following Landau, for the case of monolayers. According to these authors (14,15, 16), a second order transformation is always associated with a change in the symmetry properties. Any change of symmetry will not work: the symmetry group of one of the phases must be a sub-group of the other. This necessary condition is, moreover, not sufficient; thus reducing the number of possibilities of transformations further. The types of symmetry able to exist in a film are very limited since, according to Lifschitz following Landau (14) and Peierls (17), there cannot be elements of translation, but only point groups with axes and planes of symmetry perpendicular to the plane of the film.

It can be conceded only with difficulty that transformation in the bulk of fluid phases correspond to changes of symmetry. The idea can even be contested for liquid-crystal or crystal-crystal transformations (18). Moreover, even if this concept were satisfactory for small molecules, it would be no longer valid for large molecules where different parts of the molecule cannot be considered to retain the same relative positions. Each molecule is a structure extending in three dimensions and it is a gross simplification to consider a monolayer as a two-dimensional structure.

According to Lifschitz's theory, the number of points of transformation of a film should be very limited while experiment shows a large number, sometimes of the order of 10. Furthermore, if the deformability of the molecules is neglected, and if we consider only possible changes of symmetry, we conclude with Lifschitz and Landau that transformations of higher order than the second cannot exist in monolayers, when experiment shows such higher transformations very frequently: for example with ethyl II-oxystearate on water at 20°C. for 120Å^2 and 150Å^2, with triricinoleine on H_2O at 20°C. for 100Å^2 and 140Å^2 or with tritaririne on $KMnO_4 + H_2SO_4$ at 21.6°C. for 156Å^2 (8) as well as during the passage from the mesomorphous to the expanded mesomorphous states (2, 8).

We are thus led to the conclusion that, in the higher order transformations, it is not only the state of order and of symmetry of the molecules that has changed, but also the form of the molecule itself.

In the study of the homogeneous transformations of ordinary bulk systems, it is often more or less implied that the whole transformation occurs in the neighborhood of a point (Curie point, for example), and that on either side of this point exist two different states of the system. In fact, this is not so. As Mayer and Streeter (3) have pointed out, a point of transformation of the second order corresponds to the end of a transformation, to the achievement of a complete transformation. Thus, for order-disorder transformations in alloys, the transition point appears when 100% disorder is attained. In the same way, for transformations corresponding to the appearence of a free rotation, the point of transformation occurs when complete rotation is attained. This significance of points of transformation, as the observed sign of the achievement of a transformation, comes out very clearly in the work of Bragg and Williams (19), Bethe (20), and Peierls (21).

In monolayers, the situation is just the same. All observed points of transformation correspond to the beginning or the end of homogeneous or heterogeneous transformations. This leads us to compare once more what happens on the portion of the isotherm $A'B'$ and the flat portion AB. We have previously seen the meaning of the flat AB. By analogy, we say that, when the film is compressed from A', all the molecules which occupy the area $\sigma_{A'}$ pass suddenly, but some after others, to the area $\sigma_{B'}$, and that, because of the miscibility of these two corresponding molecular forms, a new distinct macroscopic phase does not appear. The degrees of freedom of the system do not change and so the flat is absent. When B' is reached all the molecules occupy the area $\sigma_{B'}$. The homogeneous transformation is achieved and we observe the point of transformation B' of higher order.

Discontinuity of Molecular Forms

The preceding considerations lead us to make the following postulate (22, 23):

The molecules of a monolayer can exist only in a finite number of stable equilibrium states corresponding to a discontinuous series of energy states and, correlatively, can only occupy a series of discrete molecular areas, these areas being precisely those which correspond to points of transformation of the different orders.

These points of transformation appear, then, as the only points of the isotherms which correspond to a film formed of all identical molecules. All the points of an isotherm of a monolayer other than these single points correspond to a mixture of two neighboring molecular forms. This obviously does not apply to the gaseous state (at least for molecular areas above the critical molecular area) where all the molecules are most probably lying on the surface of the water, and sufficiently far apart from one another to be in a maximum state of disorder compatible with their anchorage on the surface of the water, so that the variations of the interaction energies with distance are sufficiently small not to involve deformation of molecules. The molecules are then all in the same state and the mean molecular area occupied by each of them can vary in a continuous way with pressure.

As each molecule of a film can only occupy a finite number of discrete molecular areas $\sigma_1, \sigma_2, \ldots, \sigma_i, \ldots$ corresponding to stable molecular states $1, 2, \ldots, i, i + 1, \ldots$ and to different molecular forms, the measured molecular area has only a statistical significance corresponding to a mixture of molecules in stable neighboring states. Thus, for each point on the isotherm we have $\sigma = (1 - x)\sigma_i + x\sigma_{i+1}$ with $x = \dfrac{\sigma - \sigma_i}{\sigma_{i+1} - \sigma_i}$, σ_i and σ_{i+1} being the molecular areas of the nearest neighboring points of transformation i and $i + 1$ on either side of σ; x is the proportion of molecules in the state $i + 1$ compared with the total number.

This statistical conception of the observed molecular area is not incompatible with the quasi hexagonal structure envisaged for fluid films (22). Indeed, it is generally considered that the mean position of the molecules of fluid films correspond at short range to a crystal structure, equivalent in two dimensions to the conception of the structure of liquid, the mean positions being locally nearly arranged on a central hexagonal lattice. This type of lattice is compatible with the fluid state, the iostropy of the film in its plane, and the close packing of the molecules. This means that molecules of fluid films have a symmetry of revolution, equivalent to free rotation of the molecules about a vertical to the surface of the water passing through their polar group. As the order is only defined at small distances and is only approximate, it can be realized that the unit cell of the plane quasi-lattice considered has not necessarily the same dimensions at every point on the film. As, moreover, the discrepancy between the molecular distances corresponding to two stable neighboring states is generally small compared with the mean observed value of the intermolecular distance, it is easy to admit that, on the molecular scale, two neighboring domains of the film are characterized statistically by different molecular areas.

Viscosity of Monolayers

In several previous publications (22, 24) the principal peculiarities of viscosity of monolayers of aliphatic compounds have been described and a large number of numerical values of the viscosity coefficient μ given. We shall see that the theory of structure developed above allows a quantitative treatment of surface viscosity.

Beforehand we must define the relationship between the monolayer and the underlying water. We usually say that the fixation of the molecules of the film on water is due to dipolar interactions and hydrogen bonds. The frequency of exchange of hydrogen bonds is very high and a polar group can interact simultaneously with all its neighbors. As a result, all the neighboring water molecules close to the polar groups of a molecule of the film behave as if they were effectively bound to this molecule. Moreover, since the potentials of dipolar interaction decrease very rapidly with distance, the molecules of water not adjacent to the polar groups are not "bound" to the molecules of the film.

For small molecular areas, a molecule of water can be bound to several molecules of the film. That is why, when there is no displacement of the molecules of the film with respect to each other, the number of molecules of water bound to each molecule of the film is independant of σ. When there is displacement of the molecules, it is no longer possible for a molecule of water to be bound simultaneously to two molecules of the film moving with respect to each other, because there is no slipping between a mobile monolayer and the water substrate, as shown by numerous experiments (25, 26, 27). Accordingly, when there is flow of the film, the number of molecules of water bound to each molecule of the film necessarily varies with the molecular area, provided this area is sufficiently small so that all the surface molecules of water can be bound to molecules of the film.

Free Energy of Activation of Viscous Flow

Eyring and his collaborators have developed a theory of viscosity considered as a particular case of activation reaction (28, 29, 30) and have applied it to monolayers (31). According to this theory, in a fluid each molecule is situated in a potential trough, each potential trough corresponding to a possible equilibrium position for the molecule. So, for the movement of a molecule to occur, it must acquire the energy of activation necessary to pass over the potential barrier which separates it from the neighboring equilibrium position.

With the notation used in the present work, Eyring and Moore's relation becomes $\mu = \frac{h}{\sigma} e^{\frac{\Delta F}{kT}}$ where ΔF is the free energy of activation per molecule, h is Planck's constant, k is Boltzmann's constant, and T the absolute temperature. Since a film is generally made up of a mixture of the two molecular forms i and $i + 1$, the energy of activation will be a mean value, and $\Delta F = (1 - x)\Delta F_i + x\Delta F_{i+1}$ (which brings us back to the idea that the probability of activation of a molecular type is proportional to the number of molecules of this type). In replacing x by its value $x = \frac{\sigma - \sigma_i}{\sigma_{i+1} - \sigma_i}$, we get $\Delta F = \frac{\sigma_{i+1} - \sigma}{\sigma_{i+1} - \sigma_i} \Delta F_i + \frac{\sigma - \sigma_i}{\sigma_{i+1} - \sigma_i} \Delta F_{i+1}$ which shows that the energy of activation is a linear function of σ in each interval

$\sigma_i\sigma_{i+1}$. As a result the curve $\Delta F(\sigma)$ is a kinked line, the angular points corresponding precisely to the successive points of transformation of the film. This is in good agreement with experiment.

We know that the measured surface viscosity is that of the system formed by the insoluble monolayer and the first layer of water molecules, and we can write that the energy of activation is equal to the sum of the activation energies relating to the film and to the water: $\Delta F = \Delta F_{(c)} + \Delta F_{(\mathrm{H_2O})}$. This additivity explains the variation of μ with σ. Indeed, as we shall see later, the work of displacement of the molecules of the film can be represented by a sum of terms which are proportional as a first approximation to σ^{-3} and $\sigma^{-\frac{3}{2}}$ while the work of displacement of water molecules adjacent to each molecule of the film increases linearly with σ. We realize, accordingly, that, for small values of σ, μ is a decreasing function of σ, while for high values it is an increasing function, which agrees with observations of surface viscosity measurements.

Direct Calculation of Activation Energy of Flow

While the aim of Eyring and Moore was to express ΔF from thermodynamic data, I have attempted (22) the direct calculation of energy of activation from structural data on films. The relation $\Delta F = (1 - x)\Delta F_i + x\Delta F_{i+1}$ shows that it is sufficient to calculate activation energy only at each one of the points of transformation. Further, this energy can be decomposed into two terms: the energy required to make a hole in the film into which an activated neighboring molecule may be moved, and the energy necessary to cause a molecule to pass from one equilibrium position to a free neighboring position.

As the forces of molecular interaction are negligible beyond three or four intermolecular distances, we only have to consider in the calculations very small regions around the molecule considered and we can treat the film as a small domain of a hexagonal network.

The energy necessary to make a hole in the film is the variation of energy when, for a domain of the film of definite surface, we pass from an initial state where all the possible positions for the molecules are occupied to a final state for which there is a free space of area σ_i. I have shown (22) that this energy is equal to W if W is the energy of interaction per molecule between a molecule in state i and its neighbors (total energy is $2W$, W relative to the molecule considered and W relative to the whole of the neighboring molecules). The energy required for a molecule to pass from an equilibrium position to a neighboring free space can be divided into 3 parts. First, the energy necessary for the translation of the molecule; second, the energy corresponding to the local deformation of the network during this translation; and third, the energy of the change of equliibrium stable form of the molecules during their displacement.

The energy of translation results from the fact that, during the displacement of a molecule from its initial position to the neighboring free place, the distance of this molecule from all the others varies. The energy of deformation of the network can be explained in the following way. If r_i is the lattice distance, and the mobile molecule is displaced without deformation of the hexagonal lattice, it should approach, in the course of its movement, a distance $r_i\sqrt{\frac{3}{2}}$ from two of its neighbors. Now for an extended domain of molecular areas the value of $r_i\sqrt{\frac{3}{2}}$ is less than the minimum possible intermolecular distance (4.44Å corresponding to the spacing of paraffin chains in the solid state); we must, therefore, displace its neighbors for the movement of a molecule to be possible. The existence of an activation energy of equilibrium change of state is a consequence of our hypothesis on the discontinuity of possible stable molecular states. Since, during the flow of a film in state i, the distance between certain molecules becomes lower than r_i (the calculation shows that the minimum molecular distance is 0.94 r_i), the corresponding molecules cannot remain in the state i. They are forced to jump suddenly into the state corresponding to the possible lattice distance immediately below the smallest distance attained.

It must be emphasized that, in all calculations, when energy of interaction between molecules of the film is mentioned without further precision we mean the energy of interaction between the "kinetic units" of the film, that is to say, between systems formed by the molecules of the insoluble film itself and the whole of the molecules of water which are "rigidly bound" to these molecules.

For the details of the calculation of these different terms, see the paper on the theory of viscosity of monolayers in the *Journal de Physique* (22). Let us indicate here only that the sum of the energy of translation and of the energy of deformation is found to be $w_j(r_i)$. This notation indicates the value per molecule of the energy of interaction between two molecules assumed to be in the state j but at a distance r_i, the state j being the one of the possible molecular states such that r_j is the greatest stable lattice distance immediately below the minimum attained by the intermolecular distance during the displacements of the molecules. The energy of change of state of equilibrium is equal to 6 $[W_i(r_i) - W_j(r_i)]$. Finally, the value of the free energy of activation of viscous flow for a film in the state i is, per molecule: $\Delta F_i = 7W_i(r_i) + w_j(r_i) - 6W_j(r_i)$.

Let us recall the relation which exists between w and W. Putting v for the energy of interaction per molecule between the nonpolar parts of two molecules, and v' the same quantity relating to the polar parts ($w = v + v'$). Also, V and V' are the corresponding terms for the energy of interaction per molecule between a molecule and the whole of its neighbors ($W = V + V'$). We have, in the case of a centered hexagonal network,

$V = 6.4v$ and $V' = 9v'$. These relations assume, as London has shown (32), that, as a first approximation, the forces of interaction between nonpolar groups are uniquely of the type dispersion forces, and that those which occur between polar groups oriented on the surface are uniquely of the dipolar orientation forces.

Let us summarize the calculation of w_i (22): the molecule of the film and the group of molecules of water rigidly bound to this molecule can be considered as an ensemble of $\Sigma_m n_m$ nonpolar groups m and of $\Sigma_{m'} n_{m'}$ polar groups m'. We shall admit the autonomy of different functional groups of organic molecules, that is to say, that each group behaves (as a first approximation) from the point of view of interaction with neighboring molecules as if it were alone in the molecule which contains it.

In the state i of the film, the potential of interaction between two molecules will be $w_i(r_i) = \Sigma_m n_m v_{im}(r_i) + \Sigma_{m'} n'_{m'} v'_{im'}(r_i)$, $v_{im}(r_i)$ and $v'_{im'}(r_i)$ being the "equivalent" potentials of interaction between two homologous groups (including water) m or m' (in the same position on a carbon chain for example) belonging to the neighboring molecules. This "equivalent" potential is equal to the sum of real interaction potential between each of the two considered groups and the whole of all the functional groups of the molecule to which they belong.

In the absence of thermal agitation, we have $v_{im}(r_i) = -B_m r_i^{-6}$ and $v'_{im'}(r_i) = -B'_{m'} r_i^{-3}$; but if two homologous groups can approach one another at a minimum distance ρ_m or $\rho_{m'}$ as a result of agitation of molecules about their mean position, or of their rotation about the normals to the surface, or from their deformation, we then have (22):

$$v_{im}(r_i) = \frac{-B_m[(\rho_m)^{-5} - (2r_i - \rho_m)^{-5}]}{10\,(r_i - \rho_m)}$$

$$\text{and } v'_{im'}(r_i) = \frac{-B'_{m'}[(\rho_{m'})^{-2} - (2r_i - \rho_{m'})^{-2}]}{4\,(r_i - \rho_{m'})}.$$

To render the calculation completely explicit, it only remains to determine the values of B_m and $B'_{m'}$. The principle of autonomy of functional groups allows, from calorimetric measurements in the bulk phase, the determination for each group of an increment for the heat of cohesion (33, 34). Let V_m or $V'_{m'}$ be the potential of interaction between a group and the whole of its homologs in a condensed volume phase. When we remove this group to infinity its potential varies from V_m or $V'_{m'}$ to zero while the sum of the energies of interaction of the surrounding homologs diminishes by the same amount. As a result, the energy of cohesion measured is equal to $2V_m$ or $2V'_{m'}$. To relate V_m or $V'_{m'}$ to B_m or $B'_{m'}$ attach a number to each molecule. The group m or m' of the molecule 0 is surrounded by the homologous groups of the molecules 1;2, . . . , l, . . . at distances $r_1, r_2, \ldots, r_l, \ldots$, and $V_m = -B_m \Sigma_l r_l^{-6}$ and

$V'_{m'} = -B'_{m'}\Sigma_l r_l^{-3}$. The value of r_l in the volume phases considered are known from X-ray data. The calculation for different functional groups has been developed previously (22); here are several values obtained in Å.g.s. units: $B_{-CH_2-} = 4.1 \times 10^5$, $B_{-CH_3} = 5.61 \times 10^5$, $B'_{H_2O} = 4.12 \times 10^3$, $B'_{-COOH} = 2.08 \times 10^4$, $B'_{-OH} = 1.68 \times 10^4$, $B'_{-COOCH_2-COOCH-COOCH_2-} = 3.21 \times 10^4$. Consiquently we can calculate ΔF_i completely if we know the form of the molecules in the state i.

Molecular Forms and Equivalent Pictures

In the fluid states of monolayers, the carbon skeletons do not remain planar. They are deformed each moment by rotation around C-C links and take up the configurations resulting from effects of thermal agitation, Van der Waals forces, steric hindrances due to neighboring molecules, and constancy of the angles of aliphatic linkages. The molecules in each possible equilibrium state have not a permanent form. Although they are not fixed in an immutable structure, their configuration is not arbitrary: there is a sort of mean outline representing the statistical mean of the possible configurations of each molecule. A precise idea of this mean form can be given by adopting a simple rigid model capable of turning only as a whole about the normals to the surface, but equivalent to the real mean configuration from the point of view of molecular interactions, since it has been chosen so that it leads to theoretical values of surface viscosity equal to those given by experiment. The calculation of these equivalent configurations has been made for a large number of fatty acids and triglycerides, and the description has been given in previous papers (22, 23).

This method of determining equivalent molecular structures is capable of very great precision. Indeed, the experimental values of the energy of activation are known with a very small relative error, since they are a linear function of log $\mu\sigma$; σ is known to less than about 1% and μ to about 2%. Further, the calculation of ΔF from the molecular pictures shows that a small modification of these involves considerable difference in corresponding values of the energy of activation.

In a very recent paper (35), Dervichian has shown that most of the steric properties indicated by the preceding schemes can be understood and explained by envisaging a helical curling of the carbon chains. This conception interprets certain peculiarities of X-ray diagrams of soaps, in particular, the considerable shortening of the long spacing by rise of temperature. From the point of view of molecular interactions and, therefore, activation energies of flow, it seems that Dervichian's hypothesis leads practically to the same values as those obtained by consideration of the preceding equivalent pictures. The great advantages of the model of Dervichian is that it will probably enable the *a priori* calculation of discrete possible molecular areas, while, with the model I have used, it is necessary to take the areas at different points of transformation as given experimental data to be used as starting elements in the calculations.

Mechanism of Passage from One Molecular Form to Another

Consider the system formed by a molecule of the film and all the surrounding molecules of water adjacent to its polar group. Let W_i be the energy of interaction between this system and its neighbors when all the molecules of the film are in the state i; let W_{i+1} be the value of this energy when all the molecules are in the state $i + 1$. Put $\Delta W_i = W_i - W_{i+1}$. When, in the course of a compression or expansion, the area occupied by each molecule jumps from σ_i to σ_{i+1} the energy of interaction changes suddenly by ΔW_i. Call $\Delta S_i = S_i - S_{i+1}$ the relative entropy variation for the same transformation. The work against the external

TABLE I

Variations of Entropy

Compound	i	$i+1$	ΔW_i	ΔA_i	ΔE_i	$\Delta E_i/kT/2$	m_i
Stearic acid on $N/100$ HCl at 20°C.	A	B	626	21	605	3	3
Palmitic acid on $N/100$ HCl at 17°C.	B′	C	444	18	426	2.1	2
Palmitic acid on $N/100$ HCl at 25°C.	C	D	847	22	826	4	4
	D	E	406	12	394	1.9	2
Myristic acid on $N/100$ HCl at 17°C.	A	B	466	31	435	2.1	2
	B	B′	635	27	608	3	3
	B′	C	397	21	376	1.9	2
Myristic acid on $N/100$ HCl at 22°C.	F	G	729	82	641	3.2	3
	G	H	229	27	202	1	1
	H	I	597	21	576	2.8	3
Oleic acid on $N/100$ HCl at 17°C.	F	H	1178	180	998	5	5
	H	I	602	48	554	2.8	3
Tricaproïn on H_2O at 20°C.	F	H	3494	690	2814	13.9	14
	J	J′	846	210	636	3.2	3
	J′	K	581	390	191	1	1
Tricaprylin on H_2O at 20°C.	F	H	4215	610	3605	18	18
	H	J	730	120	610	3	3
Tricaprin on H_2O at 19.5°C.	F	H	3863	630	3233	16.1	16
	H	I	673	60	613	3	3
Trilaurin on H_2O at 16.25°C.	F	I	2994	200	2794	14	14
Triolein on H_2O at 20°C.	F	H	1379	190	1189	5.9	6
	H	I	677	50	627	3.1	3
Triricinolein on H_2O at 20°C.	F	H	1508	330	1178	5.9	6
	H	J	1354	570	784	3.9	3

forces corresponding to the same variation of surface is $\Delta A_i = \int_{\sigma_i}^{\sigma_{i+1}} p(\sigma)d\sigma$, $p(\sigma)$ being the surface pressure for the mean molecular area.

According to the general relations of thermodynamics we have the equation $|\Delta A_i| = |\Delta W_i| - T|\Delta S_i|$. Almost always $|\Delta A_i|$ is small compared with $|\Delta W_i|$, which means that, during the passage from state i to state $i + 1$, the major part of the variation of potential energy of interaction is not transformed into external work and that there is a notable change óf entropy of the system. The entropy of a system is related to the number of possible configurations in a given energy state. Now here the configurations which must be considered are not only the different possible dispositions of the molecules with respect to one another. The number of these is practically independant of σ_i at constant temperature as a result of the quasi-hexagonal structure of the film. We must consider as different possible configurations of each molecule the totality of relative possible dispositions of all the functional groups of each molecule compatible with the same value of interaction energy.

The calculation of ΔW_i has been developed in the preceding paragraphs, and thus the values of $\Delta E_i = |\Delta W_i| - |\Delta A_i|$ can be calculated. Now, as can be seen from the examples in Table I, the values of ΔE_i are not distributed at random but grouped around integer multiples of $kT/2$. We can then write to a close approximation $\Delta E_i = m_i kT/2$.

Molecular Forms and Degrees of Freedom

We know that $kT/2$ is the mean kinetic energy of thermal agitation per degree of freedom, whence the following interpretation: the discontinuous passage from molecular state i to state $i + 1$ is accompanied by the liberation (or blocking) of one or serveral degrees of freedom in the molecule. Table II gives variations in the number of degrees of freedom for different transitions studied.

For small molecular areas, the steric hindrances and the strong Van der Waals forces inhibit rotation around the C—C links; when the molecular area increases, the constraints diminish and deformations of the chains become possible, partial or total rotations appear around the different C—C links as well as the possibility of tilting of the chain by rotation around the polar group. Each one of these rotations corresponds to the liberation of a degree of freedom. Beyond a certain molecular area, translations of the whole of the molecule become possible, liberating two new degrees of freedom. It is to be seen readily that these successive liberations of possibilities of movement accompany the steric and energetic discontinuity of the different stable molecular states. Indeed, a movement is or is not possible, and it can be understood why a certain well-defined free space is necessary for a rotation about a C—C link to appear, and that the molecules of the film can only occupy a discrete series of areas characteristic of their number of degrees of freedom.

We see also that, by increase of the available space and by elevation of temperature, the number of points of transformation can increase up to a maximum determined by the length of the chain. The longer a chain, the larger is the maximum number of possible elementary movements around the C—C linkages, and so also the limiting number of discrete theoretically possible molecular states. This explains the possibility of appearance of new states (superliquid of Harkins and Stenhagen, for example) in the case of substances with very long chains. It is to be noted that this limitation of the number of possible points of transformation due to the length of the chains slightly restricts the validity of the length of chain-temperature equivalence: however large the variation of tem-

TABLE II

Variations in the Number of Degrees of Freedom

Compound	$i =$	A	B	B′	C	D	E	F	G	H	I
Stearic acid on $N/100$ HCl at 20°C.	$m_i =$		3	4	3						
Palmitic acid on $N/100$ HCl at 17°C.	$m_i =$		2	4	2	2	1	2			
Palmitic acid on $N/100$ HCl at 25.3°C.	$m_i =$		2	3	2	4	2				
Myristic acid on $N/100$ HCl at 17°C.	$m_i =$		2	3	2	1	1	2	2	1	2
Myristic acid on $N/100$ HCl at 22°C.	$m_i =$								3	1	3

	$i =$	F	H	I
Oleic acid on $N/100$ HCl at 17°C.	$m_i =$		5	3
Tricaprin on H_2O at 19.5°C.	$m_i =$		16	3
Triolein on H_2O at 20°C.	$m_i =$		6	3

	$i =$	F	H	J	J′	K
Tricaproïn on H_2O at 20°C.	$m_i =$		14	1	3	1
Tricaprylin on H_2O at 20°C.	$m_i =$		18	3	1	

	$i =$	F	H	J	I
Triricinolein on H_2O at 20°C.	$m_i =$		6	4	1

	$i =$	F	I
Trilaurin on H_2O at 16.25°C.	$m_i =$		14

perature, the family of isotherms of a film of lauric acid will present fewer points of transformation than the family of isotherms of behenic acid, for example. Besides, the fact that certain points of transformation can only exist in a narrow range of temperature indicates that the independance of certain degrees of freedom, that is to say, the autonomy of certain rotations or of certain groups of rotations, is only possible in fairly narrow limits of the mean energy of thermal agitation.

Relationship between Points of Transformation of Different Orders

Let us consider what becomes of the different points of transformation with variation of temperature or chain length as well as of pH or number of double bonds or polar groups. From the point of view of changes of state, these different factors play comparable roles; Harkins and Copeland (4) and Stenhagen (36) have shown that the increase of length of the chain by one carbon atom was equivalent to a lowering in temperature of 5°C. We can thus take as unique variables the temperature T and the area per chain σ, allowing us to systematize a collection of apparently complex phenomena and to plot a family of curves independent of the chain length.

I have insisted recently (11) on the division of points of transformation into two large groups according to whether they are fixed or mobile; that is to say, according to whether the molecular area at which they occur remains constant or not when the temperature varies.

There has been some controversy about the constancy of area of the points considered here as fixed. Being given that a precision greater than $\pm 0.05\text{Å}^2$ in the measurement of molecular areas per chain is illusory and that an ordinary thermal expansion of the equilibrium molecular forms cannot be neglected for large temperature separations, we could consider as fixed every point of transformation for which the total amplitude of relative variation of the molecular area remains within $\pm 1.5\%$ of the mean value. This does not exclude the possibility of certain points of transformation from being eventually defined between much narrower limits. From this convention the point of transformation which for C_{18} alcohol moves from 20.25Å^2 to $20.8\ \text{Å}^2$ when the temperature varies from 8.65° to 34.85°C. can be considered as a fixed point of transformation and called, for example, the point 20.5Å^2, while the point of vaporization of myristic acid, which varies from 39Å^2 to 50Å^2 when the temperature passes from 6° to 22°C. will be the mobile type of point of transformation.

With Dervichian (8, 10, 37) we have especially emphasized the points of transformation which are produced from constant values of the areas, and shown that the position of these points was independent, not only of the temperature and of the length of the chain, but also of the order of the transformation. Thus, the transformation for trimyristin at 63Å^2 is first order at 19°C. and higher order at 22°C. (38). Similarly, the transformation at 20Å^2 for C_{18} alcohol is of the second kind below 8°C., of the first kind above, and no longer exists above 16°C. (4). This point, 20Å^2 in the case of C_{22} acid (36), is of the first kind between 4° and 10°C. and seems to disappear between 10° and 20°C. For 25° and 30°C. it reappears as a point of the first order, then, above 40°C., as a point of the second kind. These examples show that increase of temperature can lower as well as raise the order of the transformation which takes place for a given area. This appears very clearly for C_{18} alcohol, for example, where the point 20.5Å^2 is of the second kind below 8°C., of the first kind between 8° and 16°C., and again of the second kind above 16°C. This means that two stable neighboring molecular forms (here the forms 20Å^2 and 20.5Å^2) may or may not be miscible according to the temperature range they are in. Still another example is given by the change in the point 22Å^2 for behenic acid (36): from higher order (or uncertain existence) below 5°C. it passes to first order between 6° and 21°C., but the details of the equilibrium vary with temperature. In fact, between 6° and 10°C. it is the 20.5Å^2 which separates from the 22Å^2 form, while at 10°C. it is the form 21.5Å^2 which appears and is not miscible with the 22Å^2 form, the 20Å^2 being then miscible. On the other hand, at 21°C. the 22Å^2 form being again of higher order the 21.5Å^2 has disappeared. It should be mentioned that the form 21.5Å^2 does not exist with stearic acid on $N/1000$ HCl at room temperature, while certain series of viscosity measurements show its presence on $N/100$ HCl. The poor reproducibility of the measurements between 21.3Å^2 and 21.8Å^2 seems to indicate that we are at the point of disappearance of the form 21.5Å^2 which has not been found on stearic acid isotherms.

A change of order of the transformations can correspond to the appearance of new points of transformation. It is thus that the point 23.5Å^2, which is of the first order for stearic acid at 11°C., becomes third order at 35°C. because a new first order transition point appears at 24.5Å^2. The existence of a transformation at a given point is independent of the physical state of the film at this point. Thus, the transformation at 20.5Å^2 for fatty acids occurs in a fluid phase for relatively short chains while it occurs in a solid phase when the chain is very long (36).

I have shown previously (11) that the connection between mobile points of transformation can be followed and that, apart from the amplitude of their displacements, their properties are the same as those of fixed points.

When the temperature varies, it may happen that the number of points of transformation within a physical state do not vary but that their positions change. This happens with myristic acid in the liquid (liquid expanded) state between 17° and 22°C. At 17°C. the areas at the points of transformation are 30Å^2, 33.5Å^2, 37Å^2 and 45Å^2, while at 22°C.

they are 26Å², 32.5Å², 37Å² and 50Å². It often happens that, with rise of temperature, new points of transformation become apparent within a widened domain. This happens for palmitic acid in the expanded mesomorphous (liquid intermediate) state. While at 17°C. there are transformations for 24.5Å² and 26Å², at 22°C. transformations occur at 24.5Å², 25Å², 26Å² and 27.5Å²; the point 24.5Å² remains, the point 26Å² (first order) is displaced (in a continuous manner) to 27.5Å² and there have appeared two new points of higher order for 25Å² and 26Å². A temperature rise can equally well cause disappearance of points of transformation. Thus, for palmitic acid in the expanded mesomorphous state, when we go from 22° to 25.3°C. the first order point 27.5Å² moves to 31Å² and the higher order points 26Å² goes to 27.5Å², but the points 24.5Å and 25Å disappear.

When temperature variation makes a new physical state appear with first order change of phase, one first order point can split into two first order points. Thus, for palmitic acid at about 6°C. the liquid state appears. The point 33Å² of the first kind (vaporization of the expanded mesomorphous state at 5°C.) contracts to 32Å², which is the extremity of the flat part of the curve corresponding to liquefaction. At the same time, the triple point appears at 39Å². When the temperature continues to rise, the point 39Å² splits into two points of the first kind, extremities of the liquid state (36Å² and 40Å² at 12°C., for example), and still remains as a point of the second or third kind at 39Å². It may be shown similarly that the points 32.Å² and 33. 5Å² of liquid myristic acid, at 17° and 22°C. are "continuations" or "survivals" of the point 33Å², maximum area of the expanded mesomorphous state.

General Diagram of Monomolecular Films

The experimental data are now sufficient to allow the construction of curves relating the position σ of these points of transformation to the temperature. We know that the points of transformation represent the possible stable equilibrium states of the molecules of the film. The curves (T, σ) obtained represent the regions of existence of each molecular "form," these regions being lines and not surfaces (except for the gaseous state beyond the critical area). Zones limited by these lines are of two types, according to the nature of their boundaries but always correspond to a mixture of two distinct molecular forms. When the two boundaries of a zone are loci of points of the first kind, that is to say, domains of two non-miscible molecular forms, this zone is a zone of phase separation and the film is composed of two distinct macroscopic phases. In the other cases we are dealing with a homogeneous mixture of two miscible molecular forms constituting a single macroscopic phase.

The different zones of the diagram also have, as boundaries, segments of straight lines parallel to the σ axis. These correspond to the appearance (or the disappearance) for certain temperatures of new points of transformation; that is to say, of new molecular forms. We shall call them lines of transition. At each point of these lines the film can exist in two phases of different compositions made up of three molecular forms. It is to be expected that these lines of transition are for the film domains of instability with respect to temperature.

Fig. 2 gives the picture of the general diagram, valid for all phases of any surface film of long-chain molecules in the case where the critical temperature of crystallization is below the critical temperature of liquefaction. Fig. 3 gives the details of the diagram for condensed states. The analogy is apparent between these diagrams of transformation of monolayers and the diagrams of solubility, of mixing, or of equilibrium in bulk phases. This expresses the close relationship between these corresponding phenomena.

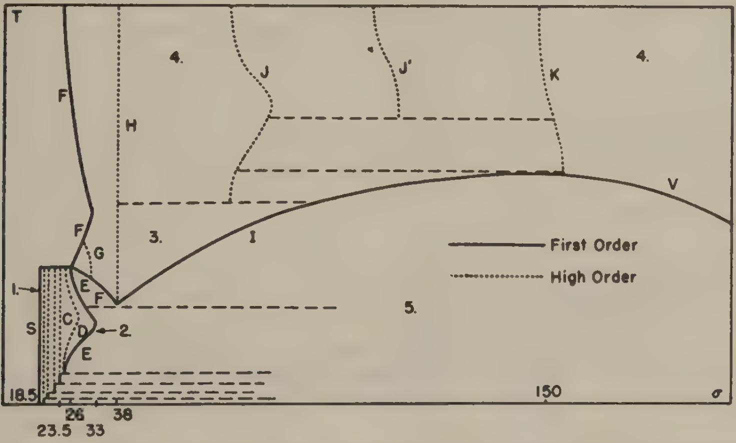

FIG. 2. General diagram of monomolecular films. 1. Solid state; 2. Mesomorphous state; 3. Liquid state; 4. Gaseous state; 5. Zone of phase separation.

On these diagrams, displacement parallel to the σ axis corresponds to plotting an isotherm and enables the areas at points of transformation to be determined. Inside each zone on the diagram the properties of the film (pressure, viscosity, etc.) vary continuously with the composition of the phase. Changes of slope or discontinuities of different orders appear only when passing the frontiers of the successive zones; that is to say, at the crossing of the domains of existence of each molecular form.

Displacement parallel to the T axis corresponds to a temperature variation at constant surface. If we are in a zone limited by the loci of fixed transformation points, there is no singularity at all during the temperature variation. If the properties of the film show variations, they are continuous and of small amplitude, since they correspond to variations with temperature of properties of stable molecular types in constant proportions. On the other hand, if we move inside a zone where the frontiers are loci of mobile points of transformation, the composition of the phase varies regularly with the temperature and, as a result, the variation of the properties of the film can be of large amplitude, and even change direction during the temperature change. By crossing zone frontiers, that is to say, the domains of pure forms, sudden changes in the properties will occur. We shall be dealing with homogeneous points of transformation with respect to temperature corresponding to the passage through a pure constituent and to the change in the nature of the other

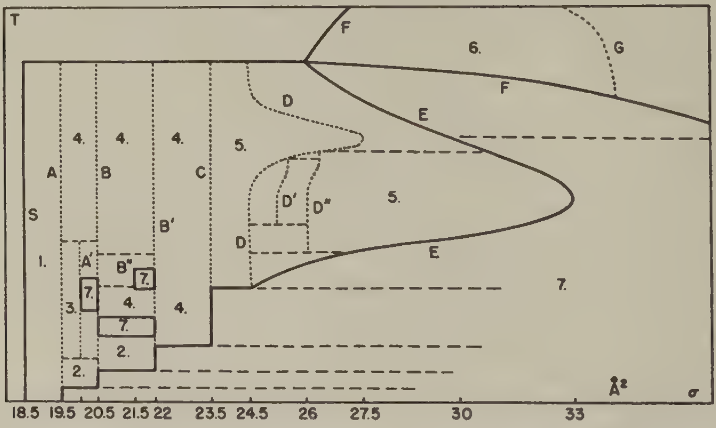

FIG. 3. General diagram of monomolecular films (condensed states). 1. Solid; 2. Solid expanded; 3. Condensed mesomorphous; 4. Mesomorphous; 5. Expanded mesomorphous; 6. Liquid; 7. Zones of phase separation.

constituent. One molecular form disappears progressively to the advantage of the other. When it has all gone a new form appears progressively, molecule by molecule. When there is a sudden change of composition on crossing the lines of transition all the molecules of one form suddenly change to molecules of another form. We are here dealing with a first order transformation with respect to temperature which can appear by a sudden variation of pressure at constant surface. This explains why, in the region of the appearance of a new equilibrium molecular form, the curves of a family of isotherms can cross one another, *e.g.*, isotherms of long-chain alcohols (4), or why the different kinds of measurements are reproducible with difficulty because of a kind of instability of the film due to an extreme sensitivity to variations of temperature, *e.g.*, palmitic acid at 22°C. in the expanded mesomorphous state.

Nomenclature of Molecular States

Consideration of the preceding diagram allows us to characterize the molecular states corresponding to different possible areas per chain independently of the nature of the film studied. I have proposed (11) the nomenclature of Table III. It should be emphasized once more that these discrete states characterize types of molecular forms and not physical states. Thus, between 19.5Å^2 and 22Å^2 per chain, the same molecular states can correspond according to the temperature or the length of the chain to fluid or solid films. We are dealing with films of the same structure (which justifies the use of the same nomenclature) of which the mechanical properties are different only because of the temperature difference or the length of the chains. The solid phase when the area per chain is above 19.5Å^2 could be called "solid expanded" to distinguish it from the true solid phase.

TABLE III

Molecular States in Monolayers

State	Area per chain	Order of the transformation	Peculiarities
S	18.5	1st order	Lower limit of crystalline state
A	19.5	2nd order	Upper limit of crystalline state
A′	20	1st or higher	Upper limit of condensed mesomorphous state
B	20.5	—	
B″	21.5	—	
B′	22	—	Upper limit of solid expanded state
C	23.5	—	Upper limit of mesomorphous state
D	24.5 to 27.5	Higher order	
D′,*D″*,···	$24.5<\sigma<33$	—	
E	24.5 to 33	1st order	Upper limit of expanded mesomorphous state
F	26 to 39	—	Lower limit of liquid state
G	$26<\sigma<37$	Higher order	Survival of the upper limit of E
H	37 to 41	—	Survival of the triple point
I	39 to $\sigma_{\text{crit.}}$	1st order	Upper limit of liquid state
J,*J′*,*J″*,···	$\sigma>39$	Higher order	
K	$150<\sigma<\sigma_{\text{crit.}}$	—	Upper limit of transformation above critical temperature
V	$\sigma>\sigma_{\text{crit.}}$	1st order	Lower limit of gaseous state below critical temperature

Extension to Bulk Systems

The variation with the length of the chain of the number of possible degrees of freedom and their successive liberation in the course of temperature rise is in perfect accord with what happens in bulk phases, in particular in the variation of the molecular specific heat of aliphatic compounds with temperature and the number of carbon atoms. In the solid state, just as in the liquid state, the molecular specific heat generally increases with the temperature and varies almost linearly with the chain length.

The theory of structure and mechanism of transformation which has just been developed can be extended to certain 3-dimensional systems, such as the soaps, for example. Each layer of smectic phases of soap can be compared with a monolayer. This point of view allows us to understand why equilibrium diagrams of these substances show such a large number of distinct phases. It also gives the explanation of all the peculiarities found in the soaps either by dilatometry or by thermal analysis.

As a matter of fact, these measurements are made at constant pressure. Now if we intersect the family of isotherms of a monolayer by a straight line p-const. and if we follow this straight line in the direction of increasing temperature, we cross successively the regions of existence of different molecular forms. Hence, if we study correlatively the change of any property whatever of the bulk phase of which the monolayer constitutes an elementary layer, we must expect to find for this property the discontinuities corresponding to crossing of the points of transformation of the film. This is effectively shown by experiment. The density-temperature curves of sodium stearate (39) show discontinuities at 70°, 100°, 125°–130° and 200°C. These points of transformation are also found by thermal analysis (method of differential cooling). The same techniques have been applied to the series of palmitates of lithium, potassium, rubidium, and cesium (40). In particular, the specific volume-temperature curves show very definite discontinuities, these curves being formed by three (Rb, Cs) or four (Li, K) segments of straight line joined by short flat portions. Vold has recently studied (41) the system water-sodium oleate. For very concentrated solutions, the points of transformation shown by thermal analysis are independent of the concentration, which proves that they are characteristic of the oleate. These points appear at 28°, 66°, 89° and 112°C. For anhydrous sodium oleate there are 6 points of transition: 40°C., change in crystalline form; 65°C., transition curd-subwaxy; 115°C., subwaxy-waxy; 180°C., waxy-superwaxy; 219°C., superwaxy-subneat; 246°C., subneat-isotropic liquid.

ACKNOWLEDGMENTS

For the presentation of this work, the numerous discussions I have had with Dr. D. G. Dervichian have been of the greatest help and I wish to express my gratitude to him. I wish to thank professors Bernal, Rideal and Bauer for their suggestions and encouragements. My thanks are due also to Dr. V. R. Gray for kindly translating this paper into English.

SUMMARY

The transformations of different orders in monolayers are discribed and an interpretation attempted, based on the following postulate: Molecules in a monolayer can only exist in a finite number of energy states corresponding to a discrete series of molecular "forms" and hence molecular areas, these last being precisely the areas of points of transformation. The transformations of the different orders correspond to the discontinuous passage from one molecular form to another, the order of the transformation depending on the miscibility or non-miscibility of the successive molecular forms. This structure theory is applied to the direct calculation of the energy of activation of flow. The comparison of the values obtained for different simple molecular models with these deduced from surface viscosity measurements by the relation of Eyring and Moore leads to a conception of the mean configuration of the molecules of the film in each of the possible stable molecular states. The discontinuous passage from one molecular form to another is shown to be accompanied by liberation or blocking of a certain number of degrees of freedom in the molecule. Connection is established between the different transformation points of the monolayers as the chain length and temperature are altered. From this, a unique nomenclature for the different possible molecular states is deduced, and an equilibrium phase diagram valid for all monomolecular films is proposed. These conceptions can be extended to bulk systems and can be used particularly to explain certain pecularities in phases of soaps.

REFERENCES

1. DERVICHIAN, D. G., *Ann. phys.* [XI] **8**, 361 (1937).
2. DERVICHIAN, D. G., *J. phys.* **10**, 333 (1939).
3. MAYER, J. E., AND S. F. STREETER, *J. Chem. Phys.* **7**, 1019 (1939).
4. HARKINS, W. D., AND COPELAND, L. E., *ibid.* **10**, 272 (1942).
5. HARKINS, W. D., YOUNG, J. F., AND BOYD, G. E., *ibid.* **8**, 954 (1940).
6. SCHULMAN, J. H., AND HUGHES, A. H., *Proc. Roy. Soc. London* **138A**, 30 (1932).
7. ADAM, N. K., AND HARDING, J. B., *Proc. Roy. Soc. London* **143A**, 104 (1933).
8. DERVICHIAN, D. G., AND JOLY, M., *J. phys. radium* **10**, 375 (1939).
9. EHRENFEST, P., *Proc. koninkl. Akad. wetensch. Amsterdam* **36**, 153 (1933).
10. DERVICHIAN, D. G., AND JOLY, M., *Compt. rend.* **206**, 326 (1938).
11. JOLY, M., *Advances in Surface Chem.* 37, (1948).
12. COPELAND, L. E., HARKINS, W. D., AND BOYD, G. E., *J. Chem. Phys.* **10**, 357 (1942).
13. LIFSCHITZ, E., *Acta Physicochim. U.R.S.S.* **19**, 248 (1944).
14. LANDAU, L., *Physik. Z. Sowjetunion* **11**, 26, 545 (1937).
15. LANDAU, L., AND LIFSCHITZ, E., Statistical Physics, Chap. XI, Oxford, 1939.
16. LIFSCHITZ, E., *J. phys. radium* **6**, 61, 251 (1942).
17. PEIERLS, R., *Helv. Phys. Acta* **7** (Suppl. 2), 81 (1934).
18. EISENSCHITZ, R., private communication.
19. BRAGG, W. L., AND WILLIAMS, E. J., *Proc. Roy. Soc. London* **145A**, 699 (1934); **151**, 540 (1935).
20. BETHE, H., *ibid.* **150A**, 552 (1935).

21. Peierls R., *ibid.* **154A**, 207 (1946).
22. Joly, M., *J. phys. radium* **7**, 83, 112 (1946).
23. Joly, M., *J. chim. phys.* **44**, 213 (1947).
24. Joly, M., *ibid.* **44**, 206 (1947).
25. Joly, M., *J. phys. radium* **9**, 345 (1938).
26. Mérigoux, R., *Compt. rend,* **202**, 2049 (1936); **203**, 848 (1936).
27. Schulman, J. H., and Teorell, T., *Trans. Faraday Soc.* **34**, 1337 (1938).
28. Ewell, R. H., and Eyring, H., *J. Chem. Phys.* **5**, 726 (1937).
29. Tobolsky, A., Powell, R. E., and Eyring, H., *Frontiers in Chem.*, **1**, 125 (1943).
30. Powell, R. E., and Eyring, H., *Advances in Colloid Sci.* **1**, 183 (1942).
31. Moore, W. J., and Eyring, H., *J. Chem. Phys.* **6**, 391 (1938).
32. London, F., *Trans. Faraday Soc.* **33**, 8 (1937).
33. Dunkel, M., *Z. physik. Chem.* **138A**, 42 (1928).
34. Dunkel, M., and Wolff, R. L., Müller-Pouillet, IV, 3, 579.
35. Dervichian, D. G., *Advances in Surface Chem.* **47** (1948).
36. Stenhagen, E., *Nature* **156**, 239 (1945).
37. Dervichian, D. G., and Joly, M., *Compt. rend.* **208**, 1488 (1939).
38. Dervichian, D. G., *J. Chem. Phys.* **7**, 931 (1939).
39. Gallay, W., and Puddington, I. E., *Can. J. Research* **21B**, 202 (1943).
40. Vold, M. S., and Vold, R. D., *J. Phys. Chem.* **49**, 32, 315 (1945).
41. Vold, M. S., *J. Phys. Colloid Chem.* **51**, 797 (1947).

IONIC EXCHANGE AND STATISTICAL THERMODYNAMICS
I. EQUILIBRIA IN SIMPLE EXCHANGE SYSTEMS

Lannes E. Davis

From the Division of Soils, University of California, Davis, California

Received June 27, 1949; revised October 31, 1949

Introduction

Classical Thermodynamics and Ionic Exchange Equilibria

The theoretical treatment of ionic exchange equilibria can be approached successfully from several directions. Kelley (11) has recently reviewed the various concepts in the literature. The prevailing tendencies have involved the treatment of ionic exchange as a chemical reaction (7,12,14,15) or as an ionic adsorption process (3,10). In recent years the author (2,3) has been interested in somewhat varied thermodynamic and statistical aspects of the problem. During the past year Krishnamoorthy, Overstreet, and the author (13) have become interested in the development of a straightforward attack involving a combination of classical thermodynamics and statistical mechanics. The results of these theoretical studies, as well as considerable experimental support in work done by Krishnamoorthy and Overstreet, have been prepared for publication.

The phenomena of ionic exchange are usually displayed by relatively complicated systems. In spite of this fact the conditions for equilibria can be derived in a simple and fairly rigorous manner. In the following discussion an attempt has been made to avoid thermodynamically undefined concepts of individual ionic species.

We may set up the following operational model: The system consists of two phases separated by an interface. Phase I contains a solution of simple electrolytes with at least two cationic species and a cation exchanger. Phase II contains only a solution of the electrolytes. The interface is permeable to the solvent and the various ions but not to the particles of the exchanger. When a steady state has been attained the system represents a Donnan equilibrium.

The exact thermodynamic treatment of Donnan equilibria was developed by Donnan and Guggenheim (1,4). At equilibrium the chemical potential of any diffusible electrolyte species has the same value for all phases.

We shall employ the activity concept of Lewis. It will be convenient to consider symmetrical electrolytes and assume that the activities can be determined in Phase II (the phase which contains no exchanger). We may then write the expression for any electrolyte present in the system,

$$a^{\mathrm{I}} = c_+{}^{\mathrm{I}} c_-{}^{\mathrm{I}} \gamma_\pm{}^2 = a^{\mathrm{II}}. \qquad [1]$$

The physical dimensions of the measurable concentration terms, c_+ and c_-, may be chosen in any convenient manner; the significance of $\gamma_\pm{}^2$ must be consistent with that of c_+ and c_-.

We may select any pair of electrolytes with different cations but a common anion. The cation concentrations in Phase I are c_A and c_B, while the values of $\gamma_\pm{}^2$ and a for the electrolytes are correspondingly indexed. We then derive from Eq. 1 the expression,

$$(c_A{}^{\mathrm{I}}/c_B{}^{\mathrm{I}})[\gamma_\pm{}^2(A)/\gamma_\pm{}^2(B)] = a_A{}^{\mathrm{II}}/a_B{}^{\mathrm{II}}. \qquad [2]$$

Solution may now be reversibly transferred from Phase I to Phase II until Phase I consists almost entirely of the exchanger. The operational model will approach a hypothetical model in which the amount of electrolyte in Phase I is infinitesimal. We may write $c_A = c_A' + c_A''$ where c_A' is the ionic concentration somewhat arbitrarily assigned to the exchanger, while c_A'' is the virtually negligible quantity assigned to the "intermicellar liquid." Then, we have

$$c_A/c_B = (c_A' + c_A'')/(c_B' + c_B'') \sim c_A'/c_B'. \qquad [3]$$

An equation having the form of a mass action equation can be derived from [2] and [3],

$$c_A' a_B{}^{\mathrm{II}}/c'_B a_A{}^{\mathrm{II}} \sim \gamma_\pm{}^2(B)/\gamma_\pm{}^2(A) = k. \qquad [4]$$

Although the system is still a system in Donnan equilibrium, to which Eq. 2 applies exactly, Eq. 4 represents not the Donnan equilibrium but the ionic exchange equilibrium.

In general we may say that k is not necessarily a constant, *i.e.*, it may vary when the concentrations are varied. "Successful" ionic exchange equations of the mass action type employ formulations of c_A' and c_B' for which k is experimentally determined to be a constant. Such equations are useful, for example, in deriving the appropriate exchange isotherms to be employed in the study of ionic exchange during flow of solution through a column of exchanger. From a broader viewpoint, the critical study of the assumptions and hypotheses utilized in the derivation of such equations may involve a useful contribution to the theory of ionic exchange.

Discussion

1. *An Approach from the Viewpoint of Statistical Mechanics. The Perfectly Regular Localized Monolayer of Exchangeable Ions*

The surface of an exchanger may be regarded as a system of identical discrete sites. Each site consists of one unit of electrical charge. The exchangeable ions constitute a more or less diffuse layer. This layer is a monolayer in the important sense that the total number of ionic unit charges is not greater than the number of oppositely charged sites. We may now state a useful hypothesis: The monolayer of ions may be regarded as equivalent to a localized monolayer, *i.e.*, to a simple model in which each ionic unit charge is assigned to one site. Finally, there are no empty sites, *i.e.*, the total number of ionic unit charges is never less than the number of oppositely charged sites. In this respect the surface of an ionic exchanger differs from ordinary adsorbents of gases or liquids which have been treated by Freundlich, Langmuir, and others.

In general, the ionic monolayer is not an ideal monolayer since the ions undoubtedly display mutual repulsive interaction. We shall now use an hypothesis which is a modified form of the postulate established by Brønsted (16) that ions of the same sign do not display specific interaction. For any given surface, with fixed sites, the energy of mutual ionic interaction is invariant with respect to the distribution of ions of different species among the sites provided that the ions all have the same valence. A monolayer of this type may be called a perfectly regular localized monolayer. The case of ions of different valences will be discussed in a later section. We shall also assume that the energy of the bond between any ion and its site is not affected by neighboring ions.

2. Application of the Method of Fowler and Guggenheim. A Preliminary Statement

Fowler and Guggenheim (6) have presented a very thorough treatment of localized monolayers by the methods of statistical mechanics derived by Fowler (5). Guggenheim (8) has given us an extension of this treatment to cases in which various molecules of different valences occupy varied numbers of sites. These writers have applied their theory primarily to the adsorption of gases on surfaces. For an ideal localized monolayer they derive the equation which was first presented by Langmuir and which is known as the "Langmuir adsorption isotherm."

The treatment to be described has been briefly outlined in a preliminary paper (13). The method of Fowler and Guggenheim forms the essential basis for the derivation but in addition to changes in terminology three important modifications are adopted.

1. Fowler and Guggenheim derive an equation in terms of the partial potential μ. We do not wish to discuss the significance of the concepts of the free energy, activity, etc., of ionic species. We attempt to avoid the consideration of thermodynamically undefined concepts by a derivation which by-passes the transition from statistical terminology to thermodynamic terminology.

2. Ionic exchange systems have no empty sites. This fact requires a minor alteration in the derivation.

3. We have called our monolayer a perfectly regular monolayer. A regular monolayer has the following characteristics:

a) Any configuration of the monolayer can be described when we specify the number and geometric arrangement of sites and how each site is occupied.

b) We may neglect interactions between pairs of molecules that are not nearest neighbors, so that the total interaction energy of the ions can be expressed as the sum of contributions from each pair of nearest neighbors.

c) The internal degrees of freedom of each ion are independent of its neighbors. In this we paraphrase Fowler and Guggenheim.

A perfectly regular monolayer may be defined as follows: *a* and *c* remain as defined for a regular monolayer. *b* is restated: When all the ions have the same valence, interactions between all pairs of neighboring ions are identical. Thus, the total interaction energy of the ions is independent of the configuration, *i.e.*, of the distribution of ions of different species. In other words the energy of mixing is zero. We can accordingly neglect the interaction energy and treat the system as if it were an ideal localized monolayer. We shall consider unsymmetrical exchanges in a later section.

Not all ionic exchange systems can be treated as if they contained ideal monolayers. In a later paper we shall discuss monolayers which cannot be treated as ideal. We may state here that many of the common simple exchangers behave as if they possessed ideal monolayers when the latter consist entirely of the common basic cations in the case of cation exchangers and of the common acidic anions in the case of anion exchangers. On the other hand, hydrogen ions, hydroxyl ions, and probably some complex ions may be expected to produce irregular systems.

3. Derivation of the Equations for Uni-Univalent Exchanges

It will be convenient to restrict our attention at first to uni-univalent exchanges. Each ion occupies only one site and the distribution is always at random.

We may denote by $y = y(T)$ the partition function for the internal degrees of freedom of an adsorbed ion referred to an appropriate energy zero. (T is the absolute temperature.) The number of sites on the surface is N_S and the number which are occupied by ions of species A, B, etc., are denoted by the terms N_A, N_B, etc., with N_I used as a general term, while N_J represents any unspecified particular term. Let $\pi = \pi(N_A, N_B \cdots)$ denote the contribution to the complete partition function which is represented by the mutual interaction energy of all the pairs of ions. In view of the invariance of this quantity, as described in the preceding section, it is not necessary to be more specific in regard to the partition for individual pairs. Then, for an interchange of an A ion for a B ion, $(\partial\pi/\partial N_A)dN_A = -(\partial\pi/\partial N_B)dN_B$, since the total mutual interaction energy is not altered by an interchange in a perfectly regular monolayer. Therefore, since $dN_A = -dN_B$, we have $\partial\pi/\partial N_A = \partial\pi/\partial N_B$.

The complete partition function for the monolayer is

$$f = g(N_A, N_B, \cdots)(y_A{}^{N_A}y_B{}^{N_B}\cdots)\pi, \tag{5}$$

where $g(N_A, N_B, \cdots)$ is the number of distinguishable ways of distributing the exchangeable ions among the sites,

$$g(N_A, N_B, \cdots) = \frac{N_S!}{N_A!N_B!\cdots}. \tag{6}$$

We may now substitute [6] in [5], take the logarithm of f and apply Stirling's approximation formula for factorials,

$$\ln n! = n \ln n - n.$$

We then get, since $N_S = \Sigma_{\mathrm{I}}N_{\mathrm{I}}$,

$$\ln f = N_S \ln N_S - \Sigma_{\mathrm{I}}N_{\mathrm{I}} \ln N_{\mathrm{I}} + \Sigma_{\mathrm{I}}N_{\mathrm{I}} \ln y_{\mathrm{I}} + \ln \pi. \tag{7}$$

The appropriate partial function for the energy partition with respect to any particular ionic species J can then be found by taking the partial derivative of $\ln f$ with respect to N_J. This is analogous to the usual procedure in statistical thermodynamics for the derivation of the chemical potential. However, we are not concerned with the undefinable chemical potential of ionic species. Our requirements will be satisfied by specification of the resultant distribution of the ionic species in the monolayer, when the latter is in equilibrium with Phase II.

We thus get

$$-\partial \ln f/\partial N_J = (1 + \ln N_J) - \ln y_J - \partial \ln \pi/\partial N_J. \tag{8}$$

For the distribution of any two ionic species A and B on the surface, in equilibrium with Phase II, we have

$$(\partial \ln f/\partial N_A - \partial \ln f/\partial N_B) = \ln (N_B/N_A) + \ln (y_A/y_B) \tag{9}$$

since the terms in π are eliminated.

It will be desirable to translate our terminology into one more commonly used in chemical mass action equations. Let $[J]$ be the number of mols of the ionic species J on the surface, while (J) is the activity in Phase II of the corresponding electrolyte species. Then $N_J = N°[J]$, where $N°$ is Avogadro's number, while $N_B/N_A = [B]/[A]$, etc. A comparison of Eq. 9 with Eq. 4 indicates that the terms c_A' and c_B' can be replaced by $[A]$ and $[B]$, respectively, so that we have

$$[A](B)/[B](A) = k, \tag{10}$$

where k will now be a constant if the model here is valid.

4. Exchanges Involving Polyvalent Ions

When the ions in an exchange system are not all univalent, we have to consider two special problems: (*a*) Whenever one or more of the ionic species is polyvalent, there is some loss of freedom in the distribution of the ions with respect to the sites. For example, if one site is occupied by one valence of a divalent ion, the site occupied by the other valence must always be a neighboring site. The latter is then not available for occupancy by another ion. (*b*) Unless the ions all have the same valence the monolayer cannot be truly a perfectly regular monolayer as this term is defined in Section 3.

A brief formal treatment of the first problem will be found in an accompanying paper by Davis and Rible. This analysis is based upon a procedure developed by Guggenheim (8) for the theoretical consideration of mixed liquids. For continuity, the results are very briefly summarized below:

Let N_{I} = number of ions of any type I.
r_{I} = number of sites occupied by one ion of type I (r_{I} = valence of ion).
z = number of sites which are nearest neighbors of any given site in a regular array.
q_{I} = a function of z and r_{I} which determines the frequency with which a valence element of an ion of type I will occupy a site adjacent to another occupied site.

The frequency $P(nJ)$ of occupancy of a set of r sites by n ions of type J is

$$P(nJ) = (Kr_JN_J/\Sigma_{\mathrm{I}}r_{\mathrm{I}}N_{\mathrm{I}})(K'q_JN_J/\Sigma_{\mathrm{I}}q_{\mathrm{I}}N_{\mathrm{I}})^{(r-r_J)/r_J}, \tag{11}$$

where K and K' are coefficients defined in the paper by Davis and Rible. The terms q_{I}, r_{I}, and z are related by the equation,

$$(z/2)(r_{\mathrm{I}} - q_{\mathrm{I}}) = r_{\mathrm{I}} - 1. \tag{12}$$

We may also note that

$$N_S = \Sigma_{\mathrm{I}}r_{\mathrm{I}}N_{\mathrm{I}},$$

where all the sites are occupied by ionic valences.

The number of possible arrangements, $g(N_{\mathrm{I}})$, of the ions will be greatly restricted because of the modified character of the distribution. Instead of Eq. 6, we have (in the logarithmic form)

$$\ln g(N_{\mathrm{I}}) = (z/2) \ln (\Sigma_{\mathrm{I}} q_{\mathrm{I}} N_{\mathrm{I}})! - \Sigma_{\mathrm{I}} \ln N_{\mathrm{I}}! - (z/2 - 1) \ln (\Sigma_{\mathrm{I}} r_{\mathrm{I}} N_{\mathrm{I}})! \quad [13]$$

When Eq. 13 is reduced by the use of Stirling's formula and the derivative with respect to N_J is taken, we have

$$\partial \ln g(N_{\mathrm{I}})/\partial N_J = (zq_J/2) \ln \Sigma_{\mathrm{I}} q_{\mathrm{I}} N_{\mathrm{I}} - \ln N_J - (z/2 - 1) r_J \ln \Sigma_{\mathrm{I}} r_{\mathrm{I}} N_{\mathrm{I}}. \quad [14]$$

When the ions do not all have the same valence the monolayer is not a perfectly regular monolayer. The energy of mixing will not be zero. Guggenheim (9) has treated cases of molecular mixing in which the energy is not zero. However, we shall attempt a somewhat crude analysis which may be applicable to ionic monolayers. In an ionic monolayer of ions of the same sign but varied charge, we may assume the interaction is entirely electrostatic; this greatly simplifies the problem.

Let us consider a surface covered with univalent ions. We now let one divalent ion replace a neighboring pair of univalent ions. The total interaction energy is independent of which pair of neighboring univalent ions is replaced, but it will be diminished by the amount of the mutual interaction energy of the pair. When a second divalent ion replaces two other neighboring univalent ions the interaction energy will be further reduced by the amount of the mutual interaction energy of the pair. If we may assume that the divalent ion interacts with other divalent ions and with univalent ions as if it were a fixed pair of univalent ions, the interaction energy will be independent of the location of this second divalent ion.

Let $\phi(B)$ represent the total interaction energy of a monolayer exclusively consisting of univalent B ions, while θ_B is the interaction energy of a pair of univalent B ions. Then the total interaction energy will be $\phi(B) - \theta_B N_A$ when N_A divalent ions have replaced $2N_A$ univalent ions. Likewise, if $\pi(B)$ represents the partition coefficient for mutual interaction energy of a surface composed solely of B ions, while π_B represents the individual partition coefficients for pairs of B ions, we may consider that π of Eq. 5 becomes $\pi(B)/\pi_B{}^{N_A}$ and $\partial \ln \pi/\partial N_B - \partial \ln \pi/\partial N_A = \ln \pi_B$.

For a pair of such ions we then get

$$\partial \ln f/\partial N_B - \partial \ln f/\partial N_A = \partial \ln g(N_A, N_B, \cdots)/\partial N_B - \partial \ln g(N_A, N_B, \cdots)/\partial N_A + \ln (y_B/y_A) + \ln \pi_B. \quad [15]$$

Only the quantities in $g(N_A, N_B, \cdots)$ are variables so that the mixed monolayer behaves for our purposes as if it were an ideal assembly. (π_B is taken into the equilibrium constant, k, in the mass action equation. Likewise, y_B/y_A is taken into k.) The analysis outlined above can be applied to any mixed monolayer of ions which interact as if the monolayer were ideal (*i.e.*, for our purposes).

We may now return to Eq. 14 which determines the ionic distribution in the monolayer and therefore, in part, the ionic distribution between Phases I and II. The form of the mass action equation may now be stated in general terms.

Consider any pair of ionic species A and B, with valencies r_A and r_B, respectively, which are present in a monolayer of various ionic spaces I, with valencies r_{I}. Then we may derive two simultaneous equations for A and B. We may eliminate the terms in $r_{\text{I}}N_{\text{I}}$ by cross multiplication and subtraction as indicated:

$$\begin{aligned}&[(r_B z q_A)/2] \ln (\Sigma_{\text{I}} q_{\text{I}} N_{\text{I}}) - r_B \ln N_A - (z/2 - 1) r_A r_B \ln \Sigma_{\text{I}} r_{\text{I}} N_{\text{I}} \\ &\quad - \{[(r_A z q_B)/2] \ln (\Sigma_{\text{I}} q_{\text{I}} N_{\text{I}}) - r_A \ln N_B - (z/2 - 1) r_A r_B \ln \Sigma_{\text{I}} r_{\text{I}} N_{\text{I}}\} \\ &\qquad = (z/2)(r_B q_A - r_A q_B) \ln (\Sigma_{\text{I}} q_{\text{I}} N_{\text{I}}) + r_A \ln N_B - r_B \ln N_A. \quad [16]\end{aligned}$$

Since $(z/2)(r_{\text{I}} - q_{\text{I}}) = r_{\text{I}} - 1$, we can see that

$$(z/2)(r_B q_A - r_A q_B) = r_B - r_A.$$

Let (J) be the mean ionic activity of the electrolyte species J in Phase II. Then the appropriate mass action equation for any pair of ionic species A and B is,

$$\frac{(A)^{r_B}[B]^{r_A}(\Sigma q_{\text{I}}[\text{I}])^{(r_B - r_A)}}{(B)^{r_A}[A]^{r_B}} = k, \qquad [17]$$

where k will now be a constant if the model here is valid.

The parameter z may not be known in many cases. The three most probable cases are:

1. A multi-linear array of widely spaced rows of sites: $z = 2$, $q_{\text{I}} = 1$.
2. An open-packed surface array of sites: $z = 4$, $q_{\text{I}} = (r_{\text{I}} + 1)/2$.
3. A closely packed surface array of sites: $z = 6$, $q_{\text{I}} = (2r_{\text{I}} + 1)/3$.

In the case of a symmetrical exchange ($r_A = r_B$) Eq. 17 becomes Eq. 10. All equations of the mass action type found in the literature have this form for symmetrical exchanges. Equation 17 becomes identical with the well known equation of Vanselow (15) when z is assumed to have the value 2 and $r_A \neq r_B$.

The approach to invariance of the values of k which may be experimentally estimated can be expected to be determined by the appropriate choice of z. Since z may not actually be known, there is a decidedly empirical element in the fitting of experimental results to the theory. The values of $q_{\text{I}} = f(r_{\text{I}}, z)$ are coefficients of [I] in a summation so that the effect of a choice of z may not be very critical in determining the invariance of k. Accordingly, although Vanselow's equation may be based on less rigorous theoretical assumptions than may be desired, it nevertheless is probably a good approximation in favorable cases. Vanselow's equation has been used extensively in recent years, particularly for uni-divalent exchanges, with satisfactory results.

Summary

1. The conditions for ionic exchange equilibria are derived by an application of classical thermodynamics. Only thermodynamically defined terms are used.

2. The appropriate ionic concentration terms are derived by a modification of a statistical theory of localized monolayers due to Fowler and Guggenheim.

3. The theory is first applied to a uni-univalent exchange. The resultant equation is of the simple mass action type.

4. Unsymmetrical exchanges are treated by combining a method first presented by Guggenheim with an analysis of the problem of mutual ionic interaction in a monolayer of mixed valence types. Equilibrium exchange equations of a mass action type are developed.

5. Vanselow's well known equation is an approximate form of the equations derived in this paper.

References

1. Davis, L. E., *Soil Sci.* **54**, 199 (1942).
2. Davis, L. E., *Soil Sci.* **59**, 379 (1945).
3. Davis, L. E., *J. Phys. Chem.* **49**, 473 (1945).
4. Donnan, F. G., and Guggenheim, E. A., *Z. physik. Chem.* (**A**), **162**, 346 (1932).
5. Fowler, R. H., Statistical Mechanics. Cambridge Press, 1929.
6. Fowler, R. H., and Guggenheim, E. A., Statistical Thermodynamics. Macmillan, 1939.
7. Gapon, E. N., *J. Gen. Chem.* (*U. S. S. R.*) **3**, 144 (1933).
8. Guggenheim, E. A., *Proc. Roy. Soc.* (*London*) **183A**, 203 (1944).
9. Guggenheim, E. A., *Proc. Roy. Soc.* (*London*) **183A**, 213 (1944).
10. Jenny, H., *J. Phys. Chem.* **40**, 501 (1936).
11. Kelley, W. P., Cation Exchange in Soils. Reinhold, 1948.
12. Kerr, H. W., *Soil Sci.* **26**, 384 (1928).
13. Krishnamoorthy, C., Davis, L. E., and Overstreet, R., *Science* **108**, 439 (1948).
14. Magistad, O. C., Fireman, M., and Mabry, B., *Soil Sci.* **57**, 371 (1944).
15. Vanselow, A. P., *Soil Sci.* **33**, 95 (1932).
16. Brønsted, J. N., *J. Am. Chem. Soc.* **44**, 877 (1922); **45**, 2898 (1923). La Mer and Cook, *ibid.* **51**, 2622 (1929).

MONOLAYERS CONTAINING POLYVALENT IONS

Lannes E. Davis and John M. Rible

From the Division of Soils, University of California, Davis, California

Received October 31, 1949

Theory

The authors have been guided by the theory of Guggenheim (1) which deals with mixed liquids. A somewhat different method of approach to the distribution of ions upon a fixed two-dimensional array of sites apparently justifies the discussion below. For the general background of this treatment, the reader is referred to the accompanying paper by Davis and to the reference (1) to the paper by Guggenheim.

Let N_I = number of ions of any type I.
r_I = number of sites occupied by an ion of type I (r_I = valence of ion).
z = number of sites which are nearest neighbors of any given site in a regular array.
q_I = a function (to be derived below) of z and r_I which determines the frequency with which a valence element of an ion of type I will occupy a site adjacent to another occupied site.

The frequency of the independent occupancy of a given site by a valence element of a J ion, with valence r_J, is

$$P'(J) = r_J N_J / \Sigma_\mathrm{I} r_\mathrm{I} N_\mathrm{I}. \qquad [1]$$

A polyvalent ion will occupy a set of r_J adjacent sites. For simplicity of description, we may fix our attention upon linear sets of adjacent sites in regular arrays. (When $r_J > 2$, we may suppose that an ion frequently will occupy a space element which covers a ring of sites. However, this case is somewhat difficult to deal with. Furthermore, for those ions which occupy only linear sets there will be no unpredictable competition for sites. It is necessary to choose one consistent model, which probably will be adequate, in view of the principle of detailed balancing.)

The frequency with which a J ion occupies a set of r_J sites, which includes a given site, will be

$$P(J) = K_r P(J) = K_r r_J N_J / \Sigma_\mathrm{I} r_\mathrm{I} N_\mathrm{I}, \qquad [2]$$

where K_r is a constant determined by the valence r and the array characteristics.

Consider a set of sites which is occupied by a J ion. Let a valence element of another J ion occupy a given site which is adjacent to the occupied set. Then, the frequency of occupancy of this given site may be expressed formally by the equation

$$P_J'(J) = q_J N_J / \Sigma_{\mathrm{I}} q_{\mathrm{I}} N_{\mathrm{I}}, \tag{3}$$

where q_J is defined at present only as a function of r_J and z.

Likewise, for the occupancy of a set of r_J sites by a neighboring ion, we have

$$P_J(J) = K_q q_J N_J / \Sigma_{\mathrm{I}} q_{\mathrm{I}} N_{\mathrm{I}}, \tag{4}$$

where K_q is determined by r_J, z, and also by the fact that the neighboring site is occupied.

Consider the case in which a set of r sites is occupied by n ions of type J with valence $r_J = r/n$. One ion may be considered to occupy r_J sites of the set independently, *i.e.*, in accordance with Eq. 2. A second J ion will occupy an adjacent subset of r_J sites in accordance with Eq. 4. A third J ion is faced by the same situation as that which confronted the second ion, so that Eq. 4 applies again. The over-all frequency of occupancy of the r sites is, therefore,

$$\begin{aligned} P(nJ) &= P(J) \cdot P_J(J)^{n-1} = P(J) P_J(J)^{(r-r_J)/r_J} \\ &= (K_r r_J N_J / \Sigma_{\mathrm{I}} r_{\mathrm{I}} N_{\mathrm{I}})(K_q q_J N_J / \Sigma_{\mathrm{I}} q_{\mathrm{I}} N_{\mathrm{I}})^{(r-r_J)/r_J}. \end{aligned} \tag{5}$$

The value of q_J may be determined from the following considerations: In a regular array, a series of intersecting lines will connect a chosen site with each of its nearest neighbors. Let an occupied linear set include the chosen site. Then the number of modes in which an occupied linear set may include the chosen site and lie along one of the lines is equal to r_J. The number of lines is $z/2$. The total number of modes in which an occupied linear set may include the chosen site is $r_J z/2$.

Let the chosen site be adjacent to a site occupied by a valence element of a J ion which lies in a set along one of the lines. Then the number of modes available to another J ion which utilizes the chosen site is not restricted along the $(z/2) - 1$ intersecting unoccupied lines but is restricted to one mode along the already occupied line.

The frequency of occurrence of occupiable modes adjacent to an occupied site will then be proportional to

$$m = m(r_J, z) = \frac{[(z/2) - 1]r_J + 1}{z r_J/2} = \frac{(z-2)r_J + 2}{z r_J}. \tag{6}$$

It should be clear that the frequency of occupancy of a site adjacent to a set of occupied sites will be proportional to the frequency of the occurrence of occupiable modes, *i.e.*, m, and to r_J. The frequency of occupancy of any set of sites which includes this adjacent site will also be proportional to m, so that from Eqs. 4 and 6 we can see that

$$q_J = m_J r_J = (z r_J - 2 r_J + 2)/z. \qquad [7]$$

This equation is identical with that derived by Guggenheim (his Eq. 2.1). It does not seem necessary to reproduce the remainder of the argument here which will be closely analogous to the treatment given by Guggenheim (Secs. 4–8). The term p_{I} in Eq. 8.2 of this reference may be neglected since it is a constant which does not occur in the summations $\Sigma_{\mathrm{I}} q_{\mathrm{I}} N_{\mathrm{I}}$ and, therefore, does not affect the form of the exchange equation.

REFERENCE

1. GUGGENHEIM, E. A., *Proc. Roy. Soc.* (*London*) **183A**, 203 (1944).

MATHEMATICAL ANALYSIS OF THE FORMATION OF PERIODIC PRECIPITATIONS

Carl Wagner*

From the Ordnance Research and Development Division Suboffice
(Rocket), Fort Bliss, Texas

Received November 1, 1949

INTRODUCTION

The formation of periodic precipitations was detected by Liesegang (5). Placing a drop of a concentrated silver nitrate solution upon a glass plate covered with a gelatin layer containing potassium dichromate, he observed that the resulting precipitation of silver chromate did not spread continuously or quasi continuously, but that separate precipitation zones evolved in the form of concentric circles. Similar phenomena were observed with many other reactions.

Numerous authors have dealt with the theory of these phenomena. It is obvious that the differential equation of diffusion is involved in all theories. As early as 1899, Ostwald (9) pointed out that the possibility of supersaturation and the existence of a metastable concentration limit for the formation of nuclei play an important part. Among others are Notboom (7) and Fricke (2) who have shown by means of quantitative chemical analyses that actually supersaturation occurs in the space between two precipitation zones. In spite of contrary opinions of some authors, Wilhelm Ostwald's "supersaturation theory" is now adopted by the majority of investigators. This idea likewise underlies the following considerations.

In addition to other theoretical investigations, which have been surveyed by Freundlich (1) and Van Hook (12), the present paper deals with the reasons for the necessity of periodic phenomena and contains a straightforward mathematical analysis of diffusion processes. Thus an approximate calculation of the distance of consecutive precipitation zones results.

MATHEMATICAL ANALYSIS IN THE CASE OF A CONTINUOUS PRECIPITATION ZONE

First we analyze mathematically the conditions in the case of formation of a continuous precipitation zone and subsequently we show the inconsistency of some of the underlying assumptions and the necessity for the occurrence of periodic precipitation zones.

---

* Present address: Department of Metallurgy, Massachusetts Institute of Technology Cambridge, Massachusetts.

Let us assume that two solutions, one containing ions of type A with initial concentration a_0 and another one containing ions of type B with initial concentration b_0 (in terms of equivalents/ml.), are placed above each other in a test tube at the time $t = 0$. The ions A and B are supposed to be the components of a virtually insoluble salt with the formula $A_{\nu_A}B_{\nu_B}$. Convection may be avoided by the presence of gelatin. This arrangement involves only one-dimensional diffusion and thus the subsequent calculations are somewhat simpler than for the conditions originally applied by Liesegang. We inquire into the concentrations a and b of the ions A and B as functions of the distance x from the boundary of the original solutions and time t. The distance in the direction of the solution containing ions of type B shall be assigned the positive sign. According to the above assumption that the precipitated compound is almost insoluble, the whole space falls into two regions in which either ions A or ions B are prevalent and accordingly the concentration of the other component is negligible. Consequently, the distance X of the boundary between these two regions is determined by the condition

$$a \cong b \cong 0 \qquad \text{at} \qquad x = X. \tag{1}$$

Formation of precipitation can take place only at $x = X$ where ions A and B, diffusing in opposite directions, encounter each other. Moreover, we conclude that at $x = X$ the diffusion rates must be equivalent, with opposite signs. To avoid lengthy expressions, we assume that the diffusion coefficients of the ions A and B are equal to each other and thus may be designated by the common symbol D. Hence

$$-D\frac{\partial a}{\partial x} = +D\frac{\partial b}{\partial x} \qquad \text{at} \qquad x = X. \tag{2}$$

In the region $x < X$, where ions A are prevalent, we can practically disregard the consumption of ions A by the precipitation reaction and therefore apply the second law of Fick to the ions A in the usual form

$$\frac{\partial a}{\partial t} = D\frac{\partial^2 a}{\partial x^2} \qquad \text{if} \qquad x < X. \tag{3}$$

Likewise,

$$\frac{\partial b}{\partial t} = D\frac{\partial^2 b}{\partial x^2} \qquad \text{if} \qquad x > X. \tag{4}$$

The initial conditions, as referred to above, are

$$a = a_0 \qquad \text{at} \qquad x < 0 \qquad \text{and} \qquad t = 0, \tag{5}$$

$$b = b_0 \qquad \text{at} \qquad x > 0 \qquad \text{and} \qquad t = 0. \tag{6}$$

The distance X, defined by Eq. 1, is to be expressed by a combination of other values and this combination must have the dimension of length. Thus we set

$$X = \gamma \cdot 2(Dt)^{\frac{1}{2}}, \tag{7}$$

where γ is a dimensionless constant which depends on the ratio of the initial concentrations and is determined below by Eq. 10.

Solutions of differential Eqs. 3 and 4, satisfying the initial conditions in Eqs. 5 and 6 and the additional condition in Eq. 2, are

$$a = \tfrac{1}{2}(a_0 - b_0) - \tfrac{1}{2}(a_0 + b_0) \operatorname{erf} [x/2(Dt)^{\frac{1}{2}}] \quad \text{if} \quad x < X, \tag{8}$$

$$b = -\tfrac{1}{2}(a_0 - b_0) + \tfrac{1}{2}(a_0 + b_0) \operatorname{erf} [x/2(Dt)^{\frac{1}{2}}] \quad \text{if} \quad x > X. \tag{9}$$

Setting $a = 0$ in Eq. 8 or $b = 0$ in Eq. 9 for $x = X$ according to Eq. 1, we obtain in view of Eq. 7

$$\frac{1 - \operatorname{erf}(\gamma)}{1 + \operatorname{erf}(\gamma)} = \frac{b_0}{a_0}. \tag{10}$$

From this equation the value of γ is to be calculated. To facilitate evaluation, a graph is shown in Fig. 1, which immediately yields the value of γ, the ratio a_0/b_0 being given.

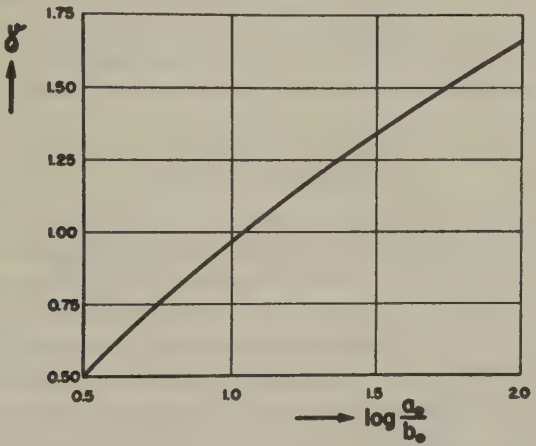

FIG. 1. Parameter γ as a function of the concentration ratio a_0/b_0.

If $b_0 \ll a_0$, the argument of the error function is large, so that the approximations

$$1 - \operatorname{erf}(\gamma) \cong \pi^{-\frac{1}{2}}\gamma^{-1} \exp(-\gamma^2) \quad \text{if} \quad \gamma > 1.5 \tag{11}$$

$$1 + \operatorname{erf}(\gamma) \cong 2 \quad \text{if} \quad \gamma > 1.5 \tag{12}$$

can be used. Upon introduction into Eq. 10,

$$\tfrac{1}{2}\pi^{-\frac{1}{2}}\gamma^{-1} \exp(-\gamma^2) \cong b_0/a_0 \quad \text{if} \quad \gamma > 1.5 \quad \text{or} \quad b_0/a_0 < 0.02. \tag{13}$$

Graphs of the concentrations a and b as functions of the distance x are shown in Fig. 2. Here $a_0 > b_0$ is assumed, so that ions of type A diffuse into the space $x > 0$, initially occupied by ions of type B. The same assumption is made in all further considerations.

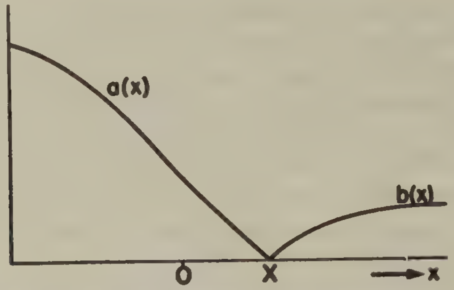

FIG. 2. Concentrations a and b as functions of the distance x from the boundary of the original solutions according to Eqs. 8 and 9.

After a given time the precipitation zone extends from $x = 0$ to $x = X$ and the characteristic distance X varies as the square root of time according to Eq. 7. Although in its derivation only a continuously advancing precipitation zone is assumed, Eq. 7 also applies approximately to periodic precipitations, as first shown by Morse and Pierce (8) and later corroborated by many other authors. Obviously the periodic interruptions can be considered as small perturbations of the general diffusion processes.

INVESTIGATION OF THE STABILITY OF A CONTINUOUS PRECIPITATION ZONE

If the concentration of a solution is only slightly greater than the saturation concentration, the formation rate of nuclei is very small, but rises considerably with increasing supersaturation. For many purposes we can approximately introduce the assumption that the formation of nuclei takes place only if the supersaturation exceeds a certain "metastable limit," although in principal the formation rate of nuclei is a continuous function of the concentration if it is greater than the saturation concentration. In the case of a salt consisting of ions A and B, we have to introduce the value of the "supersaturation product" K_N which has the same general form as the solubility product but a greater numerical value.

According to the preceding considerations, the precipitation zone will continuously advance in the direction of the x-axis. This requirement can be met without the formation of new nuclei only if the crystals evolve in the form of long needles parallel to the x-axis and grow with a rate corresponding to the increase of X according to Eq. 7. The growth of crystals in form of such long needles is, however, very unlikely in view of other observations. Actually the rate of growth of a crystal in various directions has the same order of magnitude unless there is an extreme concentration gradient in the solution, or one direction is greatly preferred for crystallographic reasons. This equalization of growth rates in various directions is due to the fact that the growth of a crystal involves formation of "two-dimensional nuclei" if a new lattice plane evolves, and therefore a small degree of supersaturation is necessary.

Auxiliary calculations show that in the case of approximately spherical crystals, the surface of the crystals advances with a velocity considerably less than the propagation velocity of the precipitation zone calculated in Eq. 7. In the immediate vicinity of a crystal, however, we have virtually saturation concentration unless the transition of ions or molecules from the solution into the crystal is hindered by special circumstances. Therefore, formation of new nuclei involving considerable supersaturation is possible only at a certain distance from the crystal previously formed.

To summarize, the end of a precipitation zone is due to the discrepancy between the linear growth rate of a crystal and the diffusion rate, and to the necessity of considerable supersaturation for a noticeable formation rate of new nuclei.

QUALITATIVE DESCRIPTION OF THE EVENTS IN THE CASE OF PERIODIC PRECIPITATION ZONES

We assume an initial state similar to that calculated in Eqs. 8 and 9. The concentrations as functions of x near $x = X$ are qualitatively shown in Fig. 3*a*. This initial state, involving a quasi-continuous precipitation zone can be obtained by introducing a sufficient number of nuclei capable of growing into the space $x < X$ at $t < 0$. As shown above, we have $a = b = 0$ at the end of the precipitation zone at $x = X$, and, according to Eq. 2, the diffusion rate of ions A in the positive direction of the x-axis equals that of ions B in the negative direction. If nuclei are missing in the region $x > X$, the precipitation can no longer advance for reasons indicated above. Since the curve $a(x)$, in accordance with Eq. 8, is concave upward, the concentration $a(x)$ increases in the course of time; conversely, the curve $b(x)$ is concave downward, and accordingly the concentration $b(x)$ decreases. Thus more ions A than ions B arrive at $x = X$, and, consequently, ions A enter the region $x > X$ as shown in Fig. 3*b*. According to the continuing precipitation and consumption of ions A at $x = X$, there is a discontinuity of the slope of the curve $a(x)$ at $x = X$.

In the region $x > X$ a new precipitation zone is formed only if the supersaturation product is reached. The position of the beginning of the new precipitation zone can be obtained by calculating the position of the spatial maximum of the product of the concentrations as a function of time and then determining the position $X + \xi_N$ at which the maximum of the concentration product equals the supersaturation product. Immediately after the formation of new nuclei, ions B are prevalent and thus the concentration of ions A decreases practically to zero as indicated in Fig. 3*c*. Later on the diffusion rate of ions A arriving at $X + \xi_N$ increases and conversely that of ions B decreases until the diffusion rates of ions A and B are equivalent. Thus conditions similar to the initial conditions are reached as indicated in Fig. 3*d*. In this manner a large number of distinctly separate precipitation zones can be formed. In contrast to Fig. 3*a*, Fig. 3*d* shows a small concentration of ions A in the region beyond the new precipitation zone at $x > X + \xi_N$, but this difference may be disregarded.

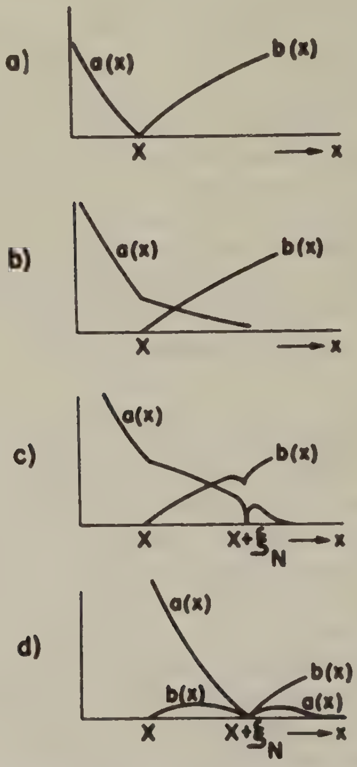

FIG. 3. Concentrations a and b as functions of the distance $\xi = x - X$ at different times after the formation of a quasi-continuous precipitation zone.

CALCULATION OF THE DISTANCE BETWEEN ADJACENT PRECIPITATION ZONES

We then calculate the concentration distribution under the assumptions of the foregoing Section in order to obtain approximately the distance between consecutive precipitation zones. As mentioned above, we assume a quasi continuous precipitation zone in the region $x < X$ at the time $t = T$ and concentration distributions according to Eqs. 8 and 9. It is convenient to introduce new variables of distance and time

$$\xi = x - X, \tag{14}$$

$$\vartheta = t - T. \tag{15}$$

In accordance with Eqs. 8 and 9, we have the conditions

$$a = b = 0 \qquad \text{at} \qquad \xi = 0 \qquad \text{and} \qquad \vartheta = 0, \tag{16}$$

$$\partial a/\partial \xi = -\,\partial b/\partial \xi \qquad \text{at} \qquad \xi = 0 \qquad \text{and} \qquad \vartheta = 0. \tag{17}$$

We then inquire into the concentrations $a(\xi, \vartheta)$ and $b(\xi, \vartheta)$ at $\vartheta > 0$ when the precipitation zone ceases to advance. The initial distribution

$$b(\xi, \vartheta = 0) \equiv f(\xi) \tag{18}$$

is given by Eq. 9. At $\xi = 0$, the concentration b is kept practically equal to zero for $\vartheta > 0$ because there is an excess of ions A in the presence of the virtually insoluble precipitation. The well-known solution of the differential equation of diffusion involving these boundary conditions is

$$b(\xi, \vartheta) = \frac{1}{2(\pi D\vartheta)^{\frac12}} \int_0^\infty f(\alpha)\left\{\exp\left[-\frac{(\alpha - \xi)^2}{4D\vartheta}\right] - \exp\left[-\frac{(\alpha + \xi)^2}{4D\vartheta}\right]\right\} d\alpha \qquad \text{for} \qquad \xi > 0, \tag{19}$$

where α is an auxiliary variable.

For $f(\xi) = b(\xi, \vartheta = 0)$ we use the series expansion

$$f(\xi) = \xi(\partial b/\partial \xi)_{x=X,\, t=T} + \tfrac12 \xi^2(\partial^2 b/\partial \xi^2)_{x=X,\, t=T} + \cdots, \tag{20}$$

and accordingly

$$f(\alpha) = \alpha(\partial b/\partial x)_{x=X,\, t=T} + \tfrac12 \alpha^2(\partial^2 b/\partial x^2)_{x=X,\, t=T} + \cdots. \tag{21}$$

Upon differentiation of Eq. 19 with respect to ξ, introduction of Eq. 21, and evaluation of integrals with $\alpha/2(D\vartheta)^{\frac12}$ as variable of integration, it follows that

$$\left(\frac{\partial b}{\partial \xi}\right)_{\xi=0,\,\vartheta} = \frac{1}{2\pi^{\frac12}D^{\frac32}\vartheta^{\frac32}} \int_0^\infty f(\alpha)\cdot\alpha\cdot\exp\left(-\frac{\alpha^2}{4D\vartheta}\right)\cdot d\alpha$$
$$= \left(\frac{\partial b}{\partial x}\right)_{x=X,\, t=T} + 2(D\vartheta/\pi)^{\frac12}\left(\frac{\partial^2 b}{\partial x^2}\right)_{x=X,\, t=T} + \cdots. \tag{22}$$

A first approximation of $b(\xi, \vartheta)$ is obtained if we disregard the dependency of expression [22] on time. Consequently we set, using Eqs. 9 and 7,

$$b(\xi, \vartheta) \cong \xi \left(\frac{\partial b}{\partial x} \right)_{x=X,\, t=T} = \xi \frac{a_0 + b_0}{2(\pi D T)^{\frac{1}{2}}} \exp \left(- \frac{X^2}{4DT} \right)$$
$$= (\xi/X)(a_0 + b_0)(\gamma/\pi^{\frac{1}{2}}) \exp (-\gamma^2). \quad [23]$$

We then consider the function $a(\xi, \vartheta)$. The initial distribution $a(\xi, \vartheta = 0)$ at $\xi < 0$ is given by Eq. 8. In contrast to the foregoing investigation of the function $b(\xi, \vartheta)$, the concentration at $\xi = 0$ and $\vartheta > 0$ is not given. However, we have another condition in that there is a sink at $\xi = 0$ the intensity of which is given by the rate of ions B diffusing from the region $\xi > 0$ to $\xi = 0$. Thus

$$\lim_{\epsilon=0} \left\{ - D \left[\left(\frac{\partial a}{\partial \xi} \right)_{\xi=-\epsilon} - \left(\frac{\partial a}{\partial \xi} \right)_{\xi=+\epsilon} \right] = D \left(\frac{\partial b}{\partial \xi} \right)_{\xi=+\epsilon} \right\}. \quad [24]$$

The unknown solution $a(\xi, \vartheta)$ can be built up by superposition of the functions $a_1(\xi, \vartheta)$ and $a_2(\xi, \vartheta)$ each of which must satisfy the general differential Eq. 3. In addition, we have the following boundary conditions

$$a_1(\xi, \vartheta = 0) = a(\xi, \vartheta = 0), \quad [25]$$

$$a_1(\xi = 0, \vartheta > 0) = 0, \quad [26]$$

$$a_2(\xi, \vartheta = 0) = 0, \quad [27]$$

$$\lim_{\epsilon=0} \{ - D[(\partial a_1/\partial \xi)_{\xi=-\epsilon} + (\partial a_2/\partial \xi)_{\xi=-\epsilon}$$
$$- (\partial a_1/\partial \xi)_{\xi=+\epsilon} - (\partial a_2/\partial \xi)_{\xi=+\epsilon}] = D(\partial b/\partial \xi)_{\xi=+\epsilon} \}. \quad [28]$$

The solution $a_1(\xi, \vartheta)$ is similar to the solution $b(\xi, \vartheta)$, but it must be borne in mind that here the initial concentration is given at $\xi < 0$ instead of $\xi > 0$ so that the sign of terms involving uneven derivatives needs to be changed. Thus we obtain in analogy to Eq. 22

$$\lim_{\epsilon=0} \left[- \left(\frac{\partial a_1}{\partial \xi} \right)_{\xi=-\epsilon} \right]$$
$$= - \left(\frac{\partial a}{\partial x} \right)_{x=X,\, t=T} + 2 \left(\frac{D\vartheta}{\pi} \right)^{\frac{1}{2}} \left(\frac{\partial^2 a}{\partial x^2} \right)_{x=X,\, t=T} - \cdots. \quad [29]$$

In the region $\xi > 0$, the function a_1 vanishes because of the initial condition $a(\xi > 0, \vartheta = 0) = 0$ and the boundary condition [26]. Thus

$$\lim_{\epsilon=0} [(\partial a_1/\partial \xi)_{\xi=+\epsilon}] = 0 \qquad \text{for} \qquad \vartheta > 0. \quad [30]$$

Upon introduction of Eqs. 22, 29, and 30 into Eq. 28 and rearrangement, it follows that

$$\lim_{\epsilon\to 0}\left[\left(\frac{\partial a_2}{\partial \xi}\right)_{\xi=-\epsilon}-\left(\frac{\partial a_2}{\partial \xi}\right)_{\xi=+\epsilon}\right]$$
$$=-\left(\frac{\partial a}{\partial x}\right)_{x=X,\,t=T}+2\left(\frac{D\vartheta}{\pi}\right)^{\frac{1}{2}}\left(\frac{\partial^2 a}{\partial x^2}\right)_{x=X,\,t=T}$$
$$-\left(\frac{\partial b}{\partial x}\right)_{x=X,\,t=T}-2\left(\frac{D\vartheta}{\pi}\right)^{\frac{1}{2}}\left(\frac{\partial^2 b}{\partial x^2}\right)_{x=X,\,t=T}. \quad [31]$$

Introduction of Eqs. 8 and 9 yields

$$\lim_{\epsilon\to 0}\left[\left(\frac{\partial a_2}{\partial \xi}\right)_{\xi=-\epsilon}-\left(\frac{\partial a_2}{\partial \xi}\right)_{\xi=+\epsilon}\right]=\frac{(a_0+b_0)X\vartheta^{\frac{1}{2}}}{\pi D T^{\frac{3}{2}}}\exp\left(-\frac{X^2}{4DT}\right). \quad [32]$$

The condition [32] is equivalent to a source at $\xi = 0$ with an intensity proportional to $\vartheta^{\frac{1}{2}}$. Upon integration of the product of the known solution for an instantaneous source and an intensity factor proportional to $\vartheta^{\frac{1}{2}}$ according to Eq. 32 with respect to time, it follows that

$$a_2(\xi, \vartheta)=\frac{(a_0+b_0)X\vartheta}{2\pi^{\frac{1}{2}}D^{\frac{1}{2}}T^{\frac{3}{2}}}\exp\left(-\frac{X^2}{4DT}\right)$$
$$\cdot\left\{\left(\frac{1}{2}+\frac{\xi^2}{4D\vartheta}\right)\left[1-\operatorname{erf}\left(\frac{|\xi|}{2(D\vartheta)^{\frac{1}{2}}}\right)\right]\right.$$
$$\left.-\frac{|\xi|}{2(\pi D\vartheta)^{\frac{1}{2}}}\exp\left(-\frac{\xi^2}{4D\vartheta}\right)\right\}. \quad [33]$$

This solution can be easily checked by introduction into Eqs. 3, 27, and 32 which must be satisfied.

Since $a_1(\xi, \vartheta)$ vanishes at $\xi > 0$, $a_2(\xi, \vartheta)$ represents the complete function $a(\xi, \vartheta)$ for $\xi > 0$. Substituting $X = 2\gamma(DT)^{\frac{1}{2}}$ in [33], we have

$$a(\xi, \vartheta)=(a_0+b_0)\frac{\gamma\exp(-\gamma^2)}{\pi^{\frac{1}{2}}}\frac{\vartheta}{T}\left\{\left(\tfrac{1}{2}+\frac{\xi^2}{4D\vartheta}\right)\left[1-\operatorname{erf}\left(\frac{\xi}{2(D\vartheta)^{\frac{1}{2}}}\right)\right]\right.$$
$$\left.-\frac{\xi}{2(\pi D\vartheta)^{\frac{1}{2}}}\exp\left(-\frac{\xi^2}{4D\vartheta}\right)\right\} \quad \text{if} \quad \xi > 0. \quad [34]$$

Assuming that the solid compound consists of ν_A ions A and ν_B ions B, we have to calculate the "concentration product" $a^{\nu_A}b^{\nu_B}$, which must equal the supersaturation product K_N at the beginning of the new precipitation zone. First we calculate the coordinate ξ_m at which the concentration product as a function of ξ has a maximum value, which is to be obtained from the condition

$$\frac{\partial}{\partial \xi}(a^{\nu_A}b^{\nu_B})=\frac{1}{\xi}a^{\nu_A}b^{\nu_B}\left(\nu_A\frac{\partial \ln a}{\partial \ln \xi}+\nu_B\frac{\partial \ln b}{\partial \ln \xi}\right)=0. \quad [35]$$

Upon rearrangement and introduction of Eqs. 23 and 34 and the auxiliary value

$$y = \xi_m/2(D\vartheta)^{\frac{1}{2}}, \qquad [36]$$

we obtain

$$-\frac{\partial \ln a/\partial\xi}{\partial \ln b/\partial\xi} = \frac{2\{y\pi^{-\frac{1}{2}}\exp(-y^2) - y^2[1-\operatorname{erf}(y)]\}}{(\frac{1}{2}+y^2)[1-\operatorname{erf}(y)] - y\pi^{-\frac{1}{2}}\exp(-y^2)} = \frac{\nu_A}{\nu_B}. \qquad [37]$$

This equation determines the auxiliary value y, depending only on the ratio ν_A/ν_B. Numerical values for various values of ν_A and ν_B are compiled in Table I.

TABLE I

Numerical Values of Constants

ν_A	ν_B	y	G	H
1	1	0.37	0.20	0.6
1	2	0.65	0.090	0.9
2	1	0.20	0.31	0.3
1	3	0.89	0.042	1.0
3	1	0.14	0.36	0.2
2	3	0.52	0.13	0.5
3	2	0.26	0.27	0.3

Combining Eqs. 23 and 34 for $\xi = \xi_m$, eliminating ϑ and T with the help of Eqs. 36 and 7, we have

$$\begin{aligned} a^{\nu_A}b^{\nu_B} = {} & G^{\nu_A}\gamma^{(3\nu_A+\nu_B)}y^{-2\nu_A}\pi^{-\frac{1}{2}(\nu_A+\nu_B)} \\ & \cdot[\exp(-\gamma^2)]^{(\nu_A+\nu_B)}(a_0+b_0)^{(\nu_A+\nu_B)}(\xi_m/X)^{(2\nu_A+\nu_B)} \\ & \text{at} \quad \xi = \xi_m, \qquad [38] \end{aligned}$$

where G is a further auxiliary value according to the definition

$$G = (\tfrac{1}{2}+y^2)[1-\operatorname{erf}(y)] - y\pi^{-1}\exp(-y^2). \qquad [39]$$

The formation of new nuclei and thus the beginning of a new precipitation zone is to be expected when the spatial maximum value of the concentration product calculated in Eq. 39 equals the supersaturation product K_N. Equating expression [38] to K_N, setting $\xi_m = \xi_N$ as distance of the formation of a new precipitation zone, and solving for ξ_N/X, we obtain

$$\frac{\xi_N}{X} = \left\{\frac{y^{2\nu_A}\pi^{\frac{1}{2}(\nu_A+\nu_B)}[\exp(\gamma^2)]^{(\nu_A+\nu_B)}K_N}{G^{\nu_A}\gamma^{(3\nu_A+\nu_B)}(a_0+b_0)^{(\nu_A+\nu_B)}}\right\}^{1/(2\nu_A+\nu_B)} \qquad [40]$$

Upon introduction of the approximation

$$\exp(\gamma^2) = \tfrac{1}{2}\pi^{-1}\gamma^{-1}(a_0/b_0) \qquad \text{if} \qquad a_0 \gg b_0 \qquad [41]$$

according to Eq. 13 and introduction of the auxiliary value H, depending only on the values ν_A and ν_B,

$$H = (y^{2\nu_A}/2^{(\nu_A+\nu_B)}G^{\nu_A})^{1/(2\nu_A+\nu_B)}, \qquad [42]$$

Eq. 40 becomes

$$\frac{\xi_N}{X} = \frac{H}{\gamma^2}\left\{\frac{K_N}{[b_0(1+b_0/a_0)]^{(\nu_A+\nu_B)}}\right\}^{1/(2\nu_A+\nu_B)}$$

$$\cong \frac{H}{\gamma^2}\left[\frac{K_N}{b_0{}^{(\nu_A+\nu_B)}}\right]^{1/(2\nu_A+\nu_B)} \qquad \text{if} \qquad a_0 \gg b_0. \qquad [43]$$

DISCUSSION

The distance ξ_N calculated in Eqs. 40 and 43 represents the distance between the beginning of a new precipitation zone and the end of the first quasi continuous precipitation zone. However, the distance ξ_N also represents approximately the distance between two consecutive precipitation zones in a long series of periodic precipitations, because the conditions at the end of a long quasi continuous precipitation zone as calculated in Eqs. 1 to 10 are not expected to differ widely from the conditions which occur when the growth of the new precipitation zone at $x = X + \xi_N$ ceases. Thus Eq. 43 can be generalized by the introduction of a correction factor of the order of unity. Practically, however, this equation cannot be used to precalculate the characteristic quotient ξ_N/X, for values of supersaturation products are not adequately known, especially under the rather complex conditions of most experiments. However, we can draw four general conclusions from Eqs. 40 and 43.

1. The distance ξ_N between consecutive precipitation zones is proportional to the distance X from the boundary of the original solutions. This relation has been found empirically by several investigators, *e.g.*, Jablczynski (3), Schleussner (10), and Lakhani and Mathur (4). In part, these relations look different, but they can easily be transformed into the relation ξ_N/X = constant with the aid of Eq. 7. A general theoretical interpretation on the basis of the supersaturation theory has been given by Neumann and Costeanu (6).
2. The ratio ξ_N/X is inversely proportional to the $[(\nu_A + \nu_B)/(2\nu_A + \nu_B)]^{\text{th}}$ power of the initial concentration a_0 or b_0 if the concentration ratio a_0/b_0 is kept constant. Qualitatively it is known that the distance between two consecutive precipitation zones is greater, the more dilute the solutions.
3. If the concentration a_0 is much greater than b_0, the value of γ does not vary considerably. Therefore the characteristic ratio ξ_N/X depends only slightly on the concentration a_0, if the concentration b_0 is kept constant. The ratio ξ_N/X is, however, approximately inversely proportional to the $[(\nu_A + \nu_B)/(2\nu_A + \nu_B)]^{\text{th}}$ power of the concentration b_0.

4. When different precipitation reactions with equal values of ν_A and ν_B and equal initial concentrations are compared with each other, the characteristic ratio ξ_N/X is expected to be less, the lower the solubility of the salt formed by the reaction between the ions A and B.

The relations [2], [3], and [4] are in accordance with many experiments reported in the literature. Most of the experiments were performed under rather complex conditions. Therefore quantitative confirmations of the above relations can hardly be expected. Many investigators dealt with the reaction between silver nitrate and potassium dichromate, but this particular system involves considerable complications, for in the potassium dichromate solution there is the equilibrium $2HCrO_4^- = Cr_2O_7^{--} + 2H_2O$ and, in addition, hydrogen ions are formed by the reaction $2Ag^+ + HCrO_4^- = Ag_2CrO_4 + H^+$, affecting equilibrium and supersaturation conditions.

Another point not considered thus far is the variation of the supersaturation product K_N with the composition of the solution, for the supersaturation depends on the interface energy, as shown *e.g.*, by Volmer (13), and the interface energy in turn depends on the concentrations of the various constituents of the solution according to the well-known equation of Gibbs, interrelating adsorption and interface energy.

Furthermore, the assumption of unhindered growth of crystals after the formation of nuclei does not hold in all systems, according to Van Hook (12).

Consequently, numerous deviations from the above relations are to be expected. The objective of this paper is not to present a theory fitting all systems but to show how the occurrence of periodic precipitation zones can be interpreted quantitatively under certain ideal assumptions.

SUMMARY

It is shown how the formation of periodic precipitation zones (Liesegang rings) and the diffusion phenomena involved can be interpreted quantitatively under certain ideal assumptions. A formula for the distance of consecutive precipitation zones based upon solutions of the diffusion equation with interruptions produced by periodic supersaturation is given.

REFERENCES

1. FREUNDLICH, H., Kapillarchemie, 4th Ed., p. 701. Leipzig, 1932.
2. FRICKE, R., AND SWALAK, O., *Z. physik. Chem.* **124**, 359 (1926). FRICKE, R., LUEKE, J., AND MEYRING, K., *Z. Elektrochem.* **39**, 629 (1933).
3. JABLCZYNSKI, K., *Bull. soc. chim.* (4) **33**, 1592 (1923).
4. LAKHANI, M. P., AND MATHUR, R. N., *Kolloid-Z.* **67**, 59 (1934).
5. LIESEGANG, R. E., *Naturw. Wochschr.* **11**, 353 (1896); Chemische Reaktionen in Gallerten, Duesseldorf, 1898.

6. Neumann, K., and Costeanu, V., *Kolloid-Z.* **84**, 130 (1938).
7. Notboom, K., *Kolloid-Z.* **32**, 247 (1923).
8. Morse, H. W., and Pierce, G. W., *Z. physik. Chem.* **45**, 589 (1903).
9. Ostwald, W., *Z. physik. Chem.* **22**, 365 (1897).
10. Schleussner, C. A., *Kolloid-Z.* **34**, 338 (1924).
11. Van Hook, A., Liesegang Rings. In: Colloid Chemistry. Collected and edited by Alexander, J., Vol. 5, p. 513. New York, 1944.
12. Van Hook, A., *J. Phys. Chem.* **42**, 1191, 1201 (1938); *Kolloid-Z.* **87**, 125 (1939).
13. Volmer, M., Kinetik der Phasenbildung. Dresden and Leipzig, 1939; Edwards Bros. Ann Arbor, Mich., 1945.

ASSOCIATION PHENOMENA II. THEORIES OF CHAIN MOLECULES AND THEIR APPLICATION TO HYDROGEN BONDING IN GASEOUS HYDROGEN FLUORIDE: *A CORRECTION*

The equation following Eq. 16 in the original paper (1) should be

$$-\Delta\nu = \sum_j jn_j - \frac{\sum_j jn_j}{P_N}.$$

This changes Eq. 17 to

$$\Delta\nu = \frac{1}{P_N} - 1.$$

Consequently Table IV has been recalculated.

TABLE IV

K_p and ΔH Calculated by the Theories of Blatz and Tobolsky and of this Paper from the Data of Simons and Hildebrand

Temp.	V.P.	Average M.W.	P_N	K_p, this paper	K_p, B & T	ΔH, this paper	ΔH, B & T	No. of determ. of M.W.
°*K*	*Atm.*							
234	.0739	87.4	4.37	18.043	219.586	—	—	6
252	.1895	81.6	4.08	7.932	88.222	5348	5934	3
263	.3079	74.3	3.715	4.861	47.713	5529	6435	2
273	.4789	67.6	3.38	3.129	27.019	5700	6817	5
278.3	.5737	69.3	3.465	2.957	25.364	5281	6303	1
281.6	.6461	64.3	3.215	2.399	19.332	5548	6682	1
285.0	.7579	69.5	3.475	1.381	12.388	6675	7468	1
289.0	.8697	47.7	2.385	.283	1.486	6811	12201	1
	Average (all values)					5842±515	7406±1388	
	Average (excluding last two values)					5481±133	6434±253	

The conclusions are not changed but the values of ΔH are brought closer in line with those calculated from the hexamer–monomer equilibrium theory for the association of hydrogen fluoride (2).

References

1. Ginell, R., *J. Colloid Sci.* **3**, 1 (1948).
2. Long, R. W., Hildebrand, J. H., and Morrell, W. E., *J. Am. Chem. Soc.* **65**, 182 (1943).

Robert Ginell

Chemistry Department,
Brooklyn College,
Brooklyn, N. Y.
Received November 23, 1949

THE ELECTROPHORETIC MOBILITY IN RELATION TO SUSPENDABILITY AND DETERGENCY

In recent papers several investigators have attempted to correlate their observations on the suspendability of powders and detergency with postulated changes in the zeta potential of the soils and substrates. Goette (1) attributes the removal of soils from fibers to the action of the detergent in simultaneously raising the zeta potential of both soil and fiber. The fact that cationic surface-active agents are not good detergents is explained by the assumption that these materials are not adsorbed in washing operations by cellulosic and other fibers and consequently do not change their zeta potential.

Measurements of the electrophoretic mobility of cellulose in solutions of cationic surface-active agents, using a microelectrophoretic cell of the Abramson design (2), had been carried out in these laboratories, and the results are reported in Table I.

TABLE I

System	Electrophoretic mobility *μ/sec./volt/cm.*
0.5% Cellulose in distilled water	−1.3
0.5% Cellulose in 0.001% Hyamine 1622 [a]	+0.30
0.5% Cellulose in 0.01% Hyamine 1622	+1.8
0.5% Cellulose in 0.1% Hyamine 1622	+2.8
0.5% Cellulose in 1.0% Hyamine 1622	+3.0
0.5% Cellulose in 3.0% Hyamine 1622	+3.2

[a] Hyamine 1622 (Phemerol), Rohm and Haas Co., is 100% diisobutyl phenoxy ethyl dimethyl benzyl ammonium chloride, monohydrate.

In order to study further the action of the cationic agents, experiments were made on the mobility of carbon blacks suspended in Hyamine solutions, and the results are reported in Table II.

Since very dilute solutions of the cationic agents are sufficient to cause a significant increase in the mobility of both a polar fiber and a nonpolar soil, it is unlikely that preferential adsorption of the cationic agent by either one in actual washing operations would lead to only one having a positive charge.

Further light on the behavior of the cationic agents may be obtained by considering their ability to suspend powders, such as carbon and manganese dioxide, in aqueous media. Suspension isotherms of manganese dioxide in Hyamine solutions were obtained by Vold and Greiner (4), and their results indicated a sharp rise in suspendability at low concentrations of Hyamine followed by a maximum at 0.4%, and then a sharp drop at higher concentrations, so that a 1.0% solution of Hyamine was no better a suspending medium than pure water. Since manganese dioxide may be expected to be negatively charged in pure water, the suspension isotherm and electrophoretic mobilities were obtained for Malacco carbon, a positive carbon (3), in Hyamine solutions. The results are given in Table III.

TABLE II

Electrophoretic Mobility of Carbon Blacks in Hyamine 1622 Solutions

0.2% Excelsior carbon, a negative carbon (3)	Mobility *μ/sec./volt/cm.*	0.2% Malacco carbon, a positive carbon (3)	Mobility *μ/sec./volt/cm.*
In distilled water	−1.8	In distilled water	+2.1
In 0.01% Hyamine 1622	+3.8	In 0.01% Hyamine 1622	+6.2
In 0.10% Hyamine 1622	+6.8	In 0.10% Hyamine 1622	+8.5
In 0.25% Hyamine 1622	+7.3	In 0.50% Hyamine 1622	+9.5
In 0.75% Hyamine 1622	+7.0	In 1.5% Hyamine 1622	+8.8
In 1.5% Hyamine 1622	+7.6	In 3.0% Hyamine 1622	+9.2
In 3.0% Hyamine 1622	+7.9		

TABLE III

Suspendability and Electrophoretic Mobilities of Malacco Carbon in Hyamine 1622

System 0.2% Malacco carbon	Suspendability *g./l.*[a]	Mobility *μ/sec./volt/cm.*
In water	0.1	+2.1
In 0.01% Hyamine	1.7	+6.2
In 0.10% Hyamine	1.9	+8.5
In 0.50% Hyamine	1.9	+9.5
In 1.0% Hyamine	1.8	—
In 1.5% Hyamine	0.2	+8.8
In 3.0% Hyamine	0.0	+9.2

[a] Suspension isotherms were obtained as in Ref. (3).

It is apparent from the above data that the suspension isotherm for the positive carbon is similar to that for the negative powder, manganese dioxide, and hence cannot be attributed to neutralization of charge, nor can it be attributed to any sharp drop in the zeta potential as suggested by Vold and Greiner (4), and by Vold and Konecny (3).

An alternative explanation for the inability of the cationic materials to suspend powders and their inefficiency as detergents at concentrations between 1.0 and 3.0% may be related to the tendency of these materials to be sorbed on surfaces as charged aggregates and micelles, above the critical concentration, rather than as simple ions (5). The sorption of these aggregates evidently results in a hydrophobic exterior regardless of the substrate to which they are attached (6). Since the charges on these aggregates will be distributed rather than concentrated at a single point (7), interaction of the hydrophobic surfaces on one particle with those on another may occur and result in the formation of bridges and the consequent reprecipitation of the soil. This behavior would account for the negative cleansing effects observed by Goette (1) upon placing a piece of soiled fabric together with an unsoiled piece in a solution of cationic surface active material.

That the cationic agents aggregate extensively is shown by their ability to solubilize dyes much more extensively than anionic and non-ionic surface active materials (8), and that these aggregates are charged is shown by the increase in transport number of the cation with concentration and other conductivity effects (9).

The foregoing data strongly suggest that it is not the change in zeta potential, per se, which gives rise to suspendability or detergency, but whether or not the detergent can be adsorbed on dirt and fabric, in ionized or non-ionized form, and the resulting nature of the exposed surfaces—whether hydrophobic or hydrophilic. To illustrate further this point, suspension isotherms and electrophoretic mobilities were obtained with Excelsior carbon in solutions of Renex, Atlas Powder Co., a non-ionic surface-active agent. From the results shown in Table IV, it is apparent that the suspendability increased with practically no change in the zeta potential.

TABLE IV

Suspendability and Electrophoretic Mobility of Excelsior Carbon in Renex Solutions

System 0.2% Excelsior	Suspendability *g./l.*	Mobility *μ/sec./volt/cm.*
In water	0.0	−1.8
In 0.01% Renex	0.2	−2.0
In 0.10% Renex	1.4	−2.0
In 1.0% Renex	1.9	−1.9
In 3.0% Renex	1.8	−1.9
In 5.0% Renex	1.8	−1.9

Finally, sodium oleate has been reported to suspend Excelsior carbon and manganese dioxide with no evidence of a maximum in suspendability, but with Malacco carbon a sharp maximum was observed (3,4). Just as in the preceding example (Table III), no correlation was found when the electrophoretic mobilities were determined between the latter and the suspendability. The positive Malacco carbon may cause a head-on adsorption of the negatively charged soap aggregates, thus producing hydrophobic surfaces which are capable of aggregating and resulting in precipitation of the carbon.

References

1. Goette, E. K., *J. Colloid Sci.* **4**, 459 (1949).
2. Abramson, H. A., Moyer, L. S., and Gorin, M. H., Electrophoresis of Proteins, Reinhold, New York, 1942.
3. Vold, R. D., and Konecny, C. C., *J. Phys. & Colloid Chem.* **53**, 1262 (1949).
4. Greiner, L., and Vold, R. D., *J. Phys. & Colloid Chem.* **53**, 67 (1949).
5. Corrin, M. L., Lind, E. L., Roginsky, A., and Harkins, W. D., *J. Colloid Sci.* **4**, 485 (1949).
6. Neville, H. A., and Jeanson, C. A., *J. Phys. Chem.* **37**, 1001 (1937); see also Goette, E. K., *Die Chemie* **57**, 67 (1944).
7. McBain, J. W., and Betz, M. D., *J. Am. Chem. Soc.* **57**, 1909 (1934).
8. McBain, J. W., and Huff, H. M., *J. Colloid Sci.* **4**, 383 (1949).
9. Hartley, G. S., Collie, B., and Samis, C. S., *Trans. Faraday Soc.* **32**, 795 (1936).

Todd M. Doscher

Department of Chemistry,
University of Southern California,
Los Angeles 7, California

Received January 6, 1950

SOLUBILIZATION IN AQUEOUS SOLUTIONS OF BOVINE SERUM ALBUMIN

It has been found that an aqueous solution of bovine serum albumin will solubilize so-called fat-soluble dyes. The phenomenon appears to be reversible as indicated by dialysis experiments as well as experiments involving the effect of temperature. The solubilization can be observed in a few minutes after the solid dye and protein solution are mixed. Several days are required, nevertheless, to obtain equilibrium values.

The results are given in Fig. 1 for the effect of the native protein on dimethylaminoazobenzene. All solutions were maintained at pH 6.8 with 0.07 M phosphate buffer. The values of the optical density at the absorption maximum ($\lambda = 4200$ A) are plotted against the concentration of albumin in Fig. 2. The linear relation indicates that the ratio of solubilized (or adsorbed) dye to protein is constant.

To obtain a numerical value for this ratio, the absorption of a series of alcohol–water solutions of the dye was determined. The best match was obtained for a 1:1 alcohol–water solution. This solvent gave a value (1) for $E/C = 0.1080$ mg./l. at $\lambda = 4200$ A for dimethylaminoazobenzene. The molar ratio of dye to protein was very close to 1:6.

The linear relation between the solubilization of dye and concentration of albumin may be seen by considering the protein molecules as a separate phase. Since the dye is limited to the surface of the serum albumin molecule, a surface activity function, n^*, may be set up which in the ideal case is equal to n, the number of molecules of dye per unit area of protein surface. The two-dimensional activity coefficient of the dye molecule

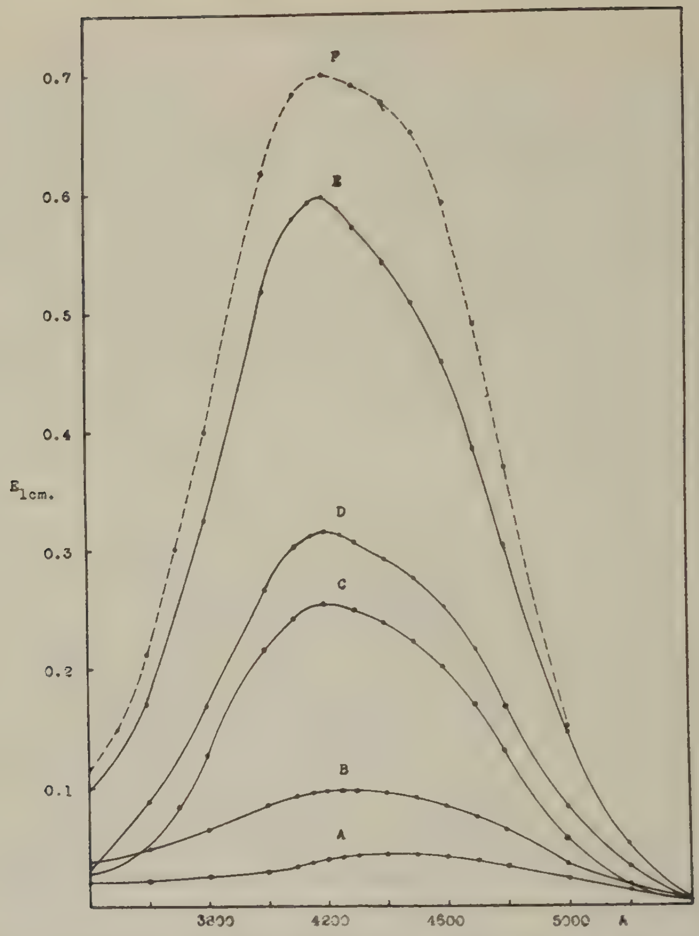

FIG. 1. The optical density for bovine serum albumin solution which has been in contact with dimethylaminoazobenzene. pH 6.8, 0.07 *M* phosphate buffer, temperature 27 ± 0.1°C.

	Per Cent Albumin Concentration
A	0.0
B	0.1
C	0.4
D	0.5
E	1.0
F	Dimethylaminoazobenzene 6.5 mg./l. in 1:1 alcohol–water solution.

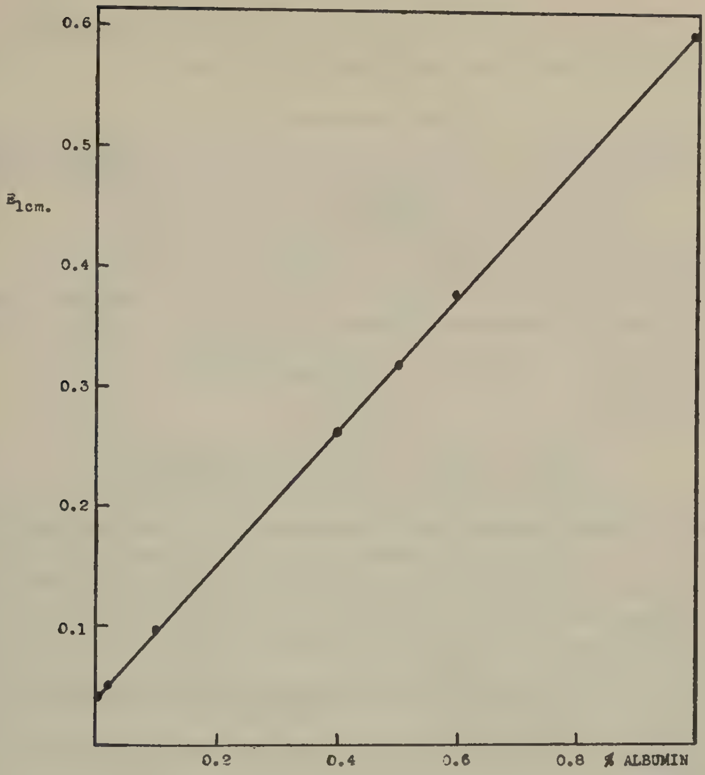

FIG. 2. The optical density at λ = 4200 A for bovine serum albumin solution which has been in contact with dimethylaminoazobenzene. pH 6.8, 0.07 M phosphate buffer, temperature 27 ± 0.1°C.

may be defined by (2)

$$f = n^*/n.$$

The chemical potential of the adsorbed dye is

$$u_2 = u_2^0 + kT \ln n^*,$$

and that for the dye in solution is

$$u_2' = u_2^{0\prime} + kT \ln a_2.$$

At equilibrium

$$u_2 = u_2' \qquad \text{and}$$

$$n^* = Ca_2 \text{ where } C \text{ is a constant.}$$

Since the solution is saturated with respect to the dye and the concentration of buffer is kept at the same value in all experiments, a_2 remains constant. The surface of the albumin molecule is so sparsely populated with dye molecules that the two-dimensional activity coefficient can be set equal to unity with the result that n is constant.

ACKNOWLEDGMENT

The suggestions of Prof. A. W. Thomas in this work is gratefully acknowledged.

REFERENCES

1. KOLTHOFF AND STRICKS, *J. Phys. & Colloid Chem.* **52**, 915 (1948).
2. WARD AND TORDAI, *Trans. Faraday Soc.* **42**, 413 (1946).

BENJAMIN CARROLL

Newark Colleges of Rutgers University, Newark, N. J.
and
Department of Chemistry, Columbia University, New York, N. Y.

Received January 13, 1950

BOOKS RECEIVED FOR REVIEW

Abriss der Chemischen Technologie der Textilfasern, H. E. Fierz-David and E. Merian, Verlag Birkhäuser, Basel, 1948, 295 pp.

An Introduction to Biochemistry, Roger J. Williams. D. Van Nostrand and Co., Inc., 2nd edition, 1948, 736 pp., $5.75.

Advances in Catalysis, Vol. I, Frankenburg, Komarewsky and Rideal, editors, Academic Press Inc., 1948, 321 pp., $7.80.

Proceedings of the Congress on Rheology, Holland, 1948, Interscience Publ. Inc., $11.00.

Vierteljahresband Chemisches Zentralblatt IV Quartal, 1945, Akademie-Verlag, Berlin, 1948, 1876 pp.

The Science of Plastics, H. Mark and E. S. Proskauer, Interscience Publ. Inc., 1948, 632 pp., $9.00.

Elastomers and Plastomers, Vol. II, R. Houwink, Elsevier Publ. Co., 1948, 515 pp., $9.00.

High-Polymer Physics, A Symposium, Howard A. Robinson, editor, Remsen Press Division, Chem. Publ. Co., Brooklyn, 1948, 572 pp.

The Colloid Chemistry of the Silicate Minerals, C. E. Marshall, Academic Press Inc.

Chemistry of Specific, Selective and Sensitive Reactions, Fritz Feigl, Academic Press Inc.

Acetylene Chemistry (translated from German), J. W. Reppe, Charles A. Meyer & Co., New York, 209 pp., $10.00.

Torchbearers of Chemistry, H. M. Smith, Academic Press Inc., 1949, 270 pp., $8.00.

Advances in Carbohydrate Chemistry, Pigman and Wolfrom, editors, Academic Press Inc., 1949, Vol. IV, 378 pp., $7.80.

Die Thermodynamik des Wärme- und Stoffaustauches in der Verfahrenstechnik, W. Matz, Verlag Dr. Dietrich Steinkopff, Frankfurt, Main, 1949, 355 pp.

Colloid Science II. Reversible Systems, H. R. Krüyt, editor, Elsevier Publ. Co., Inc., New York, 1949, 753 pp., $11.50.

Strength of Plastics and Glass, R. N. Haward, Interscience Publ. Inc., New York, 1949, 245 pp., $5.50.

IONIC EXCHANGE AND STATISTICAL THERMODYNAMICS. II. EQUILIBRIA IN IRREGULAR SYSTEMS

Lannes E. Davis

Division of Soils, University of California, Davis, California

Received December 9, 1949

Introduction

1. Simple (Regular) and Irregular Systems

A simple model for ionic exchange has been described in an earlier paper (1). A localized monolayer of ions is assumed to be distributed on a regular array of charged sites. The monolayer behaves as if it were ideal although the ions actually interact. A statistical method was applied to this model. Exchange isotherm equations of a mass action form were derived.

A simple (or regular) ion exchange system may be defined as one which is found to behave experimentally in conformity with the statistically treated model. The criterion is the invariance of the equilibrium "constant," k. Apparently, many systems which comply with the following specifications are simple systems:

(*a*) The exchanger is a single substance, not a mixture of different exchangers.

(*b*) The ions consist of ordinary basic cations or acidic anions. When hydrogen ions (or hydroxyl) ions are present (*i.e.*, in appreciable concentrations) along with two or more basic (or acidic) ionic species, the system may behave regularly for an equation which expresses exchange between any two of the ordinary basic (or acidic) ions.

One may conceive of at least three types of irregular systems:

(*a*) Both the simple model and the statistical method are inappropriate. This case falls outside the discussion and will not be considered further.

(*b*) The simple model is inadequate in some respects. The array may be very irregular. For example, isolated individual sites may not be able to adsorb polyvalent ions. A special case of irregularity is a mixture of regular arrays. This model corresponds to a mixture of very different real exchangers and it will be discussed later.

(*c*) The model is appropriate. In this case the statistical method may be assumed to be applicable in principle. However, certain assumptions made in the application of the method may not be relevant. A particular possibility is considered in the following sections.

2. Variance of the Internal Partition Functions for Completely Dissociated Ions

The complete partition function f, for the monolayer, is composed of a distribution term $g(N_A, N_B, \ldots)$, a group of internal partition functions for each of the I ionic species, and an interaction term π, so that we have

$$f = g(N_A, N_B, \ldots)(y_A{}^{N_A} y_B{}^{N_B} \ldots)\pi. \qquad [1]$$

The equilibrium "constant" k for an exchange involving A ions, of valence r_A, and B ions, of valence r_B, is represented by the ratio $y_B{}^{r_A}/y_A{}^{r_B}$. Thus, k will be invariant, in reality, only when this ratio is invariant. It is not necessary (although sufficient) that y_A or y_B should be constants.

The terms y_I are exponential functions of the energy of adsorption. They are of the type $y_I(e^{\epsilon_I/kT})$, where ϵ_I represents this energy. It will be convenient to discuss the forces which presumably are involved: (*a*) Short range forces, *i.e.*, ion-dipole, van der Waals, and covalent bond forces. (*b*) Long range forces, *i.e.*, electrostatic (Coulomb) forces.

It is probable that many exchangers form strong salts with complete dissociation of ordinary basic or acidic ions. Then the van der Waals and covalent bond forces will be negligible. It has frequently been assumed that ion-dipole forces for any given ionic species are invariant in electrolyte solutions. The validity of this assumption is probably debatable, but is not a proper subject for consideration here. We may, perhaps, assume that the variability for any two ionic species may be approximately proportional within the limited domain of the ion swarm adjacent to a charged surface.

The average value of the long range electrostatic forces might presumably vary inversely with the so-called "thickness of the double layer" which is assumed to decrease as the electrolyte concentration increases. Although we cannot be certain about this concept, we may assume with safety that any variation is identical for the appropriate powers in the ratio $y_B{}^{r_A}/y_A{}^{r_B}$, where A and B are completely dissociated ionic species.

3. Variance of the Internal Partition Functions for Incompletely Dissociated Ions

We may safely assume that any ionic species which exhibits appreciable short range interaction with the adsorbing surface will display marked variability of y_I. The variability will not be closely similar to that for a completely dissociated species. Then $y_B^{r_A}/y_A^{r_B}$ will not be invariant if either A or B represents this type of ion.

Let us consider specifically a cation exchanger and an exchange involving H and K ions. We shall discuss the exchange in the sense that the K exchanger is treated with the acid so that the "reaction" may be written

$$KX + \mathrm{H}^+ \rightleftarrows \mathrm{H}X + K^+, \qquad [2]$$

where X represents the exchanger. The intensity of interaction of both of these ions will vary with the ionic strength μ of the electrolyte. It will be convenient, however, to consider the effect of variation of the activity $a_{\mathrm{H}A}$ of the acid species HA which supplies the H ions. We shall use the logarithmic form for the variance of k,

$$\partial \ln k/\partial a_{\mathrm{H}A} = (\partial \ln k/\partial N_{\mathrm{H}})(dN_{\mathrm{H}}/da_{\mathrm{H}A}). \qquad [3]$$

We are thus committed to derive an expression for $\partial \ln k/\partial N_{\mathrm{H}}$.

In general, although $\partial \ln y_I/\partial \mu \neq 0$, we should expect that for ordinary basic or acid ions $\partial \ln y_I/\partial N_I = 0$. Thus in the derivation of the fundamental differential equation for a pair of ordinary ions the latter derivative does not appear. However, N_{H} is a function of $a_{\mathrm{H}A}$ and we can be sure that $(\partial \ln y_{\mathrm{H}}/\partial a_{\mathrm{H}A}) \neq 0$. Therefore, we should expect that $\partial \ln y_{\mathrm{H}}/\partial N_{\mathrm{H}} \neq 0$. The equation for an exchange of the type indicated in Eq. 2 will then be

$$(\partial \ln f/\partial N_{\mathrm{H}} - \partial \ln f/\partial N_K) = \ln(N_K/N_{\mathrm{H}}) + \ln(y_{\mathrm{H}}/y_K) + N_{\mathrm{H}}(\partial \ln y_{\mathrm{H}}/\partial N_{\mathrm{H}}). \qquad [4]$$

The expression $(\partial \ln f/\partial N_{\mathrm{H}} - \partial \ln f/\partial N_K)$ is the statistical analog of $-[\bar{F}_{\mathrm{H}A} - \bar{F}_{KA}]/RT = [\bar{F}_{KA} - \bar{F}_{\mathrm{H}A}]/RT = \ln(a_{KA}/a_{\mathrm{H}A})$. Also, we should note that k is an experimentally derived value. If we use the mass action equation acceptable for uni-univalent exchanges, we will have the expression

$$\ln k = \ln(a_{KA}/a_{\mathrm{H}A}) + \ln(N_{\mathrm{H}}/N_K). \qquad [5]$$

We, therefore, see from Eq. 4 that

$$\ln k = \ln(y_{\mathrm{H}}/y_K) + N_{\mathrm{H}}(\partial \ln y_{\mathrm{H}}/\partial N_{\mathrm{H}}) + j \qquad [6]$$

where j is a constant.

We now take the derivative

$$\partial \ln k/\partial N_{\mathrm{H}} = 2(\partial \ln y_{\mathrm{H}}/\partial N_{\mathrm{H}}) + N_{\mathrm{H}}(\partial^2 \ln y_{\mathrm{H}}/\partial N_{\mathrm{H}}^2). \qquad [7]$$

It is reasonable to assume that the first derivative on the right is positive in sign. As the value of N_{H} increases, y_{H} will increase toward a maximum which represents the lowest energy levels of the H ion adsorbed on the exchanger. The second derivative presumably will be a decreasing function so that it will be negative in sign. The coefficient of the second derivative is a large number, being an ionic (not a molal) quantity. It is conceivable that the entire term frequently will be an appreciable negative number, somewhat greater in magnitude than the first term. Then, ln k will vary inversely with N_H and with a_{HCl}. Experimental evidence indicates that this conclusion is valid in several cases, while in other cases ln k varies directly with N_H.

Discussion

1. Strong Acidic and Basic Ion-Exchangers

Weak acid cation-exchangers and weak base anion-exchangers will be expected to behave "irregularly." The properties of strong acid cation-exchangers and strong base anion-exchangers are interesting because they also are "irregular." Overstreet and Krishnamoorthy (7) added varied amounts of acid to a fixed quantity of cation exchanger saturated with a basic ion. This procedure corresponds to the conditions set forth in the preceding discussion, where the "reaction" is expressed formally by Eq. 2. The mass action equation is thus

$$\frac{[\mathrm{H}X]\,(K^+)}{[KX]\,(\mathrm{H}^+)} = k. \qquad [8]$$

The value of k decreased as the amount of acid added increased for bentonite and Amberlite IR 100. Recent work by Heyman and O'Donnell (2) involves the reverse process. In one set of experiments, they added varied amounts of NaCl and LiCl to a fixed quantity of H-Amberlite IR 100. The reaction equation is the reverse of Eq. 2, while the mass action equation is the reciprocal of Eq. 8, so that their term K' represents the reciprocal of the k derived by Overstreet and Krishnamoorthy. K' decreased as the amount of salt increased. In another experiment, Heyman and O'Donnell added varied amounts of H-Amberlite IR 100 to a fixed amount of LiCl. The value of K' increased as the amount of H-exchanger increased. These results are qualitatively consistent with the theory described in Sec. 3, with reference to the variation of k with N_H.

H-Amberlite IR 100 is apparently a strong acid. The active sulfonic acid groups readily dissociate H ions. The form of the titration curves obtained by Heyman and O'Donnell are consistent with this viewpoint. Furthermore, these authors (3) found that the electrical conductivity of a plug of H-Amberlite IR 100 is comparable to that for the salts of this resin when the data are correlated with the relative mobilities of H ion and alkali metal ions in dilute aqueous solutions of ordinary electrolytes. Kunin and Barry (4) have found evidence that H ion is preferentially replaced by basic ions on the strong acid-exchanger Amberlite IR 105. Similarly Kunin and McGarvey (5) present data which indicate that the strong base-exchanger Amberlite IRA-400 preferentially adsorbs several common anions in comparison with hydroxyl ion. The exchange data do not indicate a constant value of k for exchanges involving hydroxyl ion. Application of the information found in the paper by Kunin and McGarvey to Eq. 7 indicates that this anion exchanger is analogous to the cation exchangers bentonite and Amberlite IR 100 for replacement of OH ions by formate ions, but for replacements by the other anions it displays the reverse behavior. The OH-formate exchange provides a nearly invariant value of k.

Although H-Amberlite IR 105 and OH-Amberlite IRA 400 are undoubtedly strong electrolytes, it does not follow that the H ions and OH ions, respectively, are completely dissociated. We now know that certain strong acids, *e.g.*, HNO_3, are not completely dissociated, whereas solutions of the corresponding salts are generally free from molecular species. The rather appreciable "exchange acidity" found by Kunin and Barry with H Amberlite IR 105 and the corresponding "exchange basicity" of OH-Amberlite IRA 400, as shown by Kunin and McGarvey, when these resins are mixed with neutral salts perhaps implies that these exchangers may not be completely dissociated. One may be inclined to suggest that the "exchange acidity and basicity" are only evidences of ionic exchange involving H or OH ions as the conventional terms imply. Actually, exchange as an observable phenomenon does not occur until a phase separation is achieved. "Exchange acidity and basicity" involve microredistributions within the ion swarms which are loosely analogous to exchange. Such redistributions would probably occur even with completely dissociated systems. The evidence for complete or incomplete dissociation is accordingly not conclusive.

The "irregular" nature of many exchanges involving H (or OH) ions may or may not be primarily due to the conditions suggested in Sec. 3. Equation 7 may be interpreted as an expression pertinent to a hypothetical model which would be expected to exhibit irregular behavior corresponding to experimental results obtained from many acid or base exchangers.

2. Ionic Exchange Equilibria in Mixed Exchangers

We shall now consider an electrolyte solution in exchange equilibrium with a suspension of two exchangers. We may designate the two exchangers and the corresponding terms by single and double primes, while the terms which are not primed represent the complete mixed exchanger. Thus, $N_J = N_J' + N_J''$ represents the number of J ions adsorbed on the mixed exchanger.

The complete partition function for the assembly which contains the two different types of monolayers is then

$$f = f'f'' = g'g''(y_A^{N_A} y_B^{N_B} \ . \ . \ .)'(y_A^{N_A} y_B^{N_B} \ . \ . \ .)'' \qquad [9]$$

omitting ionic interaction terms to simplify the equations.

We may then write,

$$\ln f = \ln f' + \ln f'' \qquad [10]$$

and

$$\begin{aligned}\partial \ln f/\partial N_J &= \partial \ln f'/\partial N_J + \partial \ln f''/\partial N_J \\ &= (\partial \ln f'/\partial N_J')dN_J'/dN_J + (\partial \ln f''/\partial N_J'')dN_J''/dN_J. \qquad [11]\end{aligned}$$

We now note that

$$-\partial \ln f/\partial N_J = (1 + \ln N_J) - \ln y_J. \qquad [12]$$

(We omit the interaction terms since the resultant will vanish in the exchange equation.)

For the exchange of two ionic species, A and B, on the two exchangers we may write

$$\begin{aligned}&\partial \ln f/\partial N_A - \partial \ln f/\partial N_B = (\partial \ln f'/\partial N_A')dN_A'/dN_A + (\partial \ln f''/\partial N_A'') \\ &\quad \times dN_A''/dN_A - (\partial \ln f'/\partial N_B')dN_B'/dN_B - (\partial \ln f''/\partial N_B'') \\ &\quad \times dN_B''/dN_B = [(1 + \ln N_B') - \ln y_B']dN_B'/dN_B \\ &\quad + [(1 + \ln N_B'') - \ln y_B'']dN_B''/dN_B - [(1 + \ln N_A') \\ &\qquad - \ln y_A']dN_A'/dN_A - [(1 + \ln N_A'') - \ln y_A'']dN_A''/dN_A. \qquad [13]\end{aligned}$$

It can now be shown that k for the complete exchange will not be invariant in general, although the terms k' and k'' for the individual exchanges may be invariant. In terms of the mass action equation, we can write

$$\begin{aligned}\ln k' - \ln k'' &= [\ln(N_B'/N_A') + \ln(a_A/a_B)] - [\ln(N_B''/N_A'') \\ &\quad + \ln(a_A/a_B)] = \ln(N_B'/N_A') - \ln(N_B''/N_A''). \qquad [14]\end{aligned}$$

Since k' is proportional to y_A'/y_B', *etc.*, we can also write

$$\ln k' - \ln k'' = \ln(y_A'/y_B') - \ln(y_A''/y_B''). \qquad [15]$$

There are three cases to be considered:

(*a*) The trivial case in which the two so-called different exchangers are actually or nearly identical. Then $\ln y_A' = \ln y_A''$, $\ln N_A' = \ln N_A''$, *etc.* and $\ln k' - \ln k'' = 0$. Thus k will be invariant in this case.

(*b*) The special case in which the exchangers are different but have the same exchange constants; *i.e.*, $k' = k''$. Then, we have $\ln(y_A'/y_B') = \ln(y_A''/y_B'')$ and $\ln(N_B'/N_A') = \ln(N_B''/N_A'')$.

Since $dN_B'/dN_B + dN_B''/dN_B = dN_B/dN_B = 1$, Eq. 11 can be simplified in both cases (*a*) and (*b*). In this connection, we may now write the mass action equation,

$$k = \frac{[B](A)}{[A](B)} = \frac{\{[B'] + [B'']\}(A)}{\{[A'] + [A'']\}(B)}. \qquad [16]$$

If $[B'] = [B'']$ and $[A'] = [A'']$, which is case (*a*), k will be invariant. Likewise, whenever $[B']/[A'] = [B'']/[A'']$, which is case (*b*), k will be invariant.

(*c*) The exchangers are different and $k' \neq k$. Then none of the conditions in cases (*a*) or (*b*) can be met. Equation 11 will not have a simple form. Inspection of Eq. 16 shows that k will not regularly be invariant with respect to changes in the variables, *i.e.*, concentrations of A and B or amounts of the two exchangers.

It is well-known that many exchangers behave in a "regular" manner, especially for symmetrical exchanges of ordinary basic or acidic ions. It is possible that exchangers which behave in an "irregular" manner are actually mixed systems with markedly irregular mosaics of sites. The weak base anion-exchange resin Amberlite Ir 4 B described by Kunin and Myers (6) may be of this character.

SUMMARY

1. Two types of irregular models for ionic-exchange systems are described.

2. Whenever the internal partition function for any ionic species is markedly affected by strong bond forces, we may expect "irregular" behavior for any exchange involving this species.

3. A mixture of two "regular" systems, with different invariant values of the equilibrium exchange constant k, will display a variable value of k for the mixed system.

REFERENCES

1. DAVIS, L. E., *J. Colloid Sci.*, in press.
2. HEYMAN, E., AND O'DONNELL, I. J., *J. Colloid Sci.* 4, 395 (1949).
3. HEYMAN, E., AND O'DONNELL, I. J., *J. Colloid Sci.* 4, 405 (1949).
4. KUNIN, R., AND BARRY, R. E., *Ind. Eng. Chem.* 41, 1269 (1949).
5. KUNIN, R., AND MCGARVEY, F. X., *Ind. Eng. Chem.* 41, 1265 (1949).
6. KUNIN, R., AND MYERS, R. J., *J. Am. Chem. Soc.* 69, 2874 (1947).
7. OVERSTREET, R., AND KRISHNAMOORTHY, C., *Soil Sci.* 69, 87 (1950). See also: *Science* 111, 231 (1950); *Soil Sci.* 68, 307 (1949); 69, 41 (1950).

THE EFFECT OF SALTS ON THE VISCOSITY OF SOLUTIONS OF POLYACRYLIC ACID [1]

Hershel Markovitz[2] **and George E. Kimball**

Department of Chemistry, Columbia University, New York, New York

Received November 3, 1949

INTRODUCTION

The properties of solutions of large charged molecules have been of interest for a long time. Until rather recently this interest had been centered mainly on proteins. Since little is known about the details of the structure of proteins, an investigation of synthetic polyelectrolytes was begun. This work was initiated by Staudinger and his school who prepared and studied polyacrylic acid solutions.[3] Thus far, not even a satisfactory qualitative explanation for the behavior of these solutions has been given. In this work, the effect of salts on the viscosity of polyacrylic acid solutions was explored in greater detail to see if a clue to a reasonable explanation might be found.

REVIEW OF LITERATURE

Most of the work on polyacrylic acid has been done by Staudinger and his school (1–8). They studied its solubility in various solvents (1), some chemical reactions (1), and the effect of various conditions on the polymerization of acrylic acid (2). They investigated the viscosity of solutions of polyacrylic acids as a function of molecular weight, concentration of polymer, and degree of neutralization (3). They showed that solutions of the lower molecular weight PAA are Newtonian liquids. However the behavior of the solution is peculiar in comparison to that of other polymer solutions. With ordinary polymer solutions, for example, it had been found that η_{sp}/c is an increasing linear function of the concentration of polymer.

---

[1] Submitted by Hershel Markovitz in partial fulfillment of the requirements for the degree of Doctor of Philosophy at Columbia University. One of us (H. M.) wishes to thank the Charles A. Coffin Foundation for a fellowship awarded to him.

[2] Present address: Mellon Institute of Industrial Research, Pittsburgh, Pennsylvania.

[3] The term "polyacrylic acid" will be used in two senses in this paper: (*1*) for the unneutralized polyacrylic acid and (*2*) for polyacrylic acid of varying degrees of neutralization. In most cases the more general meaning will be intended. It is hoped that the sense will be clear from the context. The term is frequently abbreviated to PAA.

$$\eta_{sp} = (\eta - \eta_0)/\eta_0,$$

η = viscosity of solution,

η_0 = viscosity of solvent,

c = concentration of polymer.

In the case of PAA solutions, on the other hand, this linear dependence no longer exists. In fact, η_{sp}/c becomes larger and larger as the concentration of polymer gets smaller.

Electrolytes greatly affect the viscosity of solutions of PAA. The addition of sodium hydroxide increases the viscosity considerably until an equivalent amount is added. Further addition of NaOH causes a sharp drop in the viscosity. Sodium chloride, added to a solution of PAA, causes the viscosity to decrease. The sodium salt of PAA shows an η_{sp}/c behavior similar to the acid. However a solution with a large excess of sodium hydroxide, like most polymer solutions, gives values of η_{sp}/c which are linear in the concentration of polymer.

Solutions of higher molecular weight PAA are non-Newtonian liquids and the sodium salt of PAA shows an even stronger dependence of the viscosity on shearing stress. However with an excess of NaOH, the non-Newtonian behavior diminishes greatly or disappears.

Staudinger and Trommsdorf (4) made a more careful study of the relationship between molecular weight and the viscosity of solutions of PAA in 2 *N* NaOH.

Kern (5–8) studied the titration curve of PAA and the conductance and osmotic pressure of PAA and its salts. He found that the pH, specific conductance, and osmotic pressure of a solution or its salt at a given grundmolarity[4] are independent of the molecular weight. In the osmotic pressure measurements, the sodium salt acts as if it were 20% dissociated, and in the conductance measurements, it acts as if it were 50–60% dissociated. Other univalent salts of PAA give the same osmotic pressure. Kern (6) attributed the behavior of the viscosity of PAA at low concentrations to electrical effects and at higher concentrations to ordinary polymer effects.

A. G. Evans and E. Tyrrall (9) determined the heat of polymerization of acrylic acid.

Some work has been done on other polyelectrolytes. A. Katchalsky and P. Spitnik (10) have reported on the potentiometric titration of polymethacrylic acid. A. H. Aten, Jr. (11) published a note on the effect of added salt on the viscosity of solutions of sodium polymethacrylate.

---

[4] In this paper concentrations are expressed in terms of "grundmolarity" (sometimes abbreviated "gdmol."). This is the weight of polymer per liter of solution divided by the molecular weight of the monomer.

Fuoss and co-workers have made studies on the picrates of 4-vinylpyridine–styrene copolymers (12), poly-4-vinyl-*N*-*n*-butylpyridonium bromide (13, 14, 15), and on the polyelectrolytes formed by the addition of methyl bromide to the polyester from methyldiethanolamine and succinic anhydride (16) with results similar to those on polyacrylic acid. S. Johanson (17) has reported a few data on a copolymer of vinyl acetate and crotonic acid. D. T. F. Pals and J. J. Hermans (18) have studied the effect of sodium chloride on the viscosity of sodium pectinate.

Experimental Materials and Apparatus

1. Preparation of Acrylic Acid

A 65% aqueous solution of crude acrylic acid was obtained from Rohm and Haas Company. This was purified according to a method suggested by H. T. Neher of the Rohm and Haas Company (19). The acrylic acid was extracted from the crude solution with ethylene dichloride. Beta-naphthol and the extract were put into a Claisen flask whose side arm had been packed with single-turn copper helices and the solution distilled under atmospheric pressure until most of the ethylene chloride had been boiled off. The residue was distilled under vacuum at 61 mm. Hg. The fraction that came over between 74–75° was collected.

2. Polyacrylic Acid

The acrylic acid was polymerized by the "reduction–activation" technique used by Evans and Tyrrall (9). Nine-hundred fifty ml. of water, 50 ml. acrylic acid, 6.7 ml. 3 N H_2SO_4, and 20 ml. 0.1 M $FeSO_4$ were mixed in a large round-bottomed flask, and the solution was deoxidized by bubbling N_2 through it for 45 min. Then 20 ml. of 0.1 M H_2O_2 solution was added while stirring. The acrylic acid polymerized in a few minutes at room temperature. The polyacrylic acid was precipitated by the addition of sulfuric acid and redissolved with just enough sodium hydroxide. This solution was dialyzed against distilled water until no test for sulfate was given by the dialyzate. The solution was then acidified until the polymer began to precipitate again. This solution was then dialyzed until again no sulfate was present in the dialyzate. No sulfate was present in the resulting polymer solution on testing with barium chloride.

The concentration of polymer in the solution was determined by titration with sodium hydroxide using either a pH meter or phenolphthalein indicator according to the method of Staudinger (3).

The molecular weight of this polyacrylic acid was not determined exactly. However by comparison with the viscosity data of Staudinger (3) the molecular weight was estimated to be about 35,000 (degree of polymerization, 500).

3. *Measurement of Viscosity*

The viscosities were determined with Bingham (20) viscometers. The time of flow was measured by means of an electric stopwatch graduated in 0.01 sec. The pressure was read on a manometer whose scale was mounted over a mirror to avoid parallax. The scale was calibrated with a cathetometer. Each pressure reading was corrected (*a*) with the calibration curve for the scale, (*b*) for temperature, (*c*) for difference in height of manometer and viscometer, and (*d*) for varying height of liquid as the liquid flowed through the viscometer. The pressure was supplied by tank nitrogen and was kept constant by a "bubbler" type of regulator to within ±0.04 cm. of water. The viscometers were calibrated with water at various applied pressures. The time and pressure were each measured to 0.1%. All viscosity measurements were taken at two applied pressures in the range 40–100 cm. of water. At a given pressure, the viscosities checked to 0.2%. All measurements were made at 30.00 ± 0.02°C. with the temperature held constant to within 0.002°.

4. *Non-Newtonian Behavior*

If the solutions of PAA obeyed Newton's law of viscous flow (i.e., if the velocity gradient were exactly proportional to the shearing stress), the viscosity calculated from

$$\eta = A(P \pm h\rho)t - B\rho/t$$

should be independent of the driving pressure. Here A and B are constants of the viscometer, t is the time of flow, P is the driving pressure in centimeters of H_2O at 25°C., ρ is the specific gravity of the solution, and h is the difference in height of the bulbs of the viscometer. In the double sign, the positive sign was used for flow from right to left and the negative sign for the opposite direction.

As Staudinger (3) has previously observed, some solutions of PAA are non-Newtonian liquids. With the molecular weight used in these experiments, the departure from Newtonian behavior amounted to as much as a 2.3% difference in viscosity for a difference in applied pressures of 15 cm. of H_2O in the worst case. Except for a few cases to be mentioned later, there was less than a 0.5% difference in viscosities for a difference in applied pressure of 25 cm. of H_2O. This departure from Newtonian behavior is the largest source of uncertainty in these experiments. Since this effect is much smaller than those studied here and since the proper method for correcting for it is uncertain, no correction has been made. The viscosities obtained from both pressures were averaged together.

EXPERIMENTAL RESULTS

In most of the experiments, the concentration and degree of neutralization of the PAA were maintained constant, and the molarity of the added salt was varied. In such a series of runs, it was found that the viscosity could be expressed by the equation

$$\eta = \eta_\infty + \frac{a}{M + b} \qquad [1]$$

where

η = viscosity of the solution,
M = molarity of salt added, and
a, b, η_∞ are constants during the series.

Results were fitted to this equation by choosing trial values of b, and plotting η against $1/(M + b)$. The value of b was varied until the plot became a straight line. The slope and intercept of the straight line then gave the values of a and η_∞. Typical plots are shown in Fig. 2.

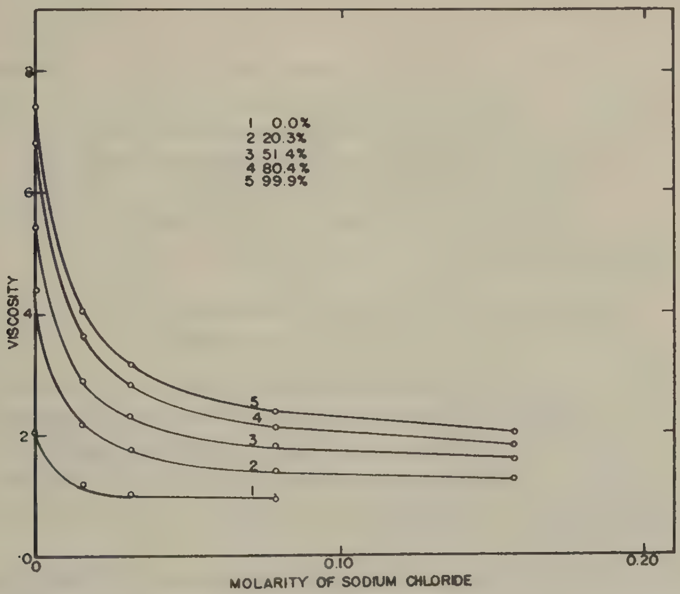

FIG. 1. Variation of viscosity of 0.0336 gdmol. PAA with molarity (M) of added sodium chloride for varying degrees of neutralization.

Equation 1 was obtained after several attempts at getting an empirical expression to represent the data. The only other expression which seemed to have promise was

$$\eta = G + HM^{-0.5} \qquad [2]$$

which fits the data at higher concentrations of salt but fails at low concentrations. Equation 1 was used throughout this paper even though there were a few points at high salt concentrations which did not fall on this

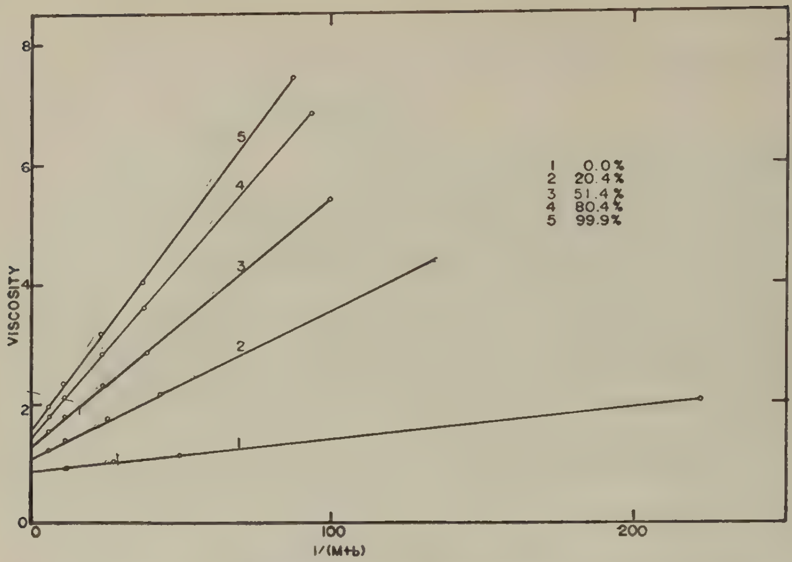

FIG. 2. Viscosity of 0.0336 gdmol. PAA as a function of sodium chloride concentration for various degrees of neutralization.

type of curve. (See Fig. 6.) The use of [2] rather than [1] would not affect the general results.

1. Effect of Adding Sodium Chloride to Solutions of Varying Degrees of Neutralization

Data were obtained for the variation of viscosity with added sodium chloride as a function of degree of neutralization at a concentration of 0.0336 grundmolar PAA. These viscosities are plotted against concentration of salt in Fig. 1. The curves are obtained from Eq. 1 with parameters as listed in Table I. The data are plotted as straight lines against $1/(M + b)$ in Fig. 2.

Figure 3 is a plot of these constants as a function of the fraction neutralized. From this figure it appears that a and η_∞ might be linearly re-

TABLE I

The Constants of Eq. 1 as a Function of Fraction Neutralized in a Solution of 0.0336 Grundmolar PAA

Fraction neutralized	0	0.203	0.514	0.804	0.999
η_∞	0.87	1.09	1.30	1.46	1.61
b	0.0047	0.0076	0.0102	0.0107	0.0114
a	0.0055	0.0248	0.0412	0.0568	0.0660

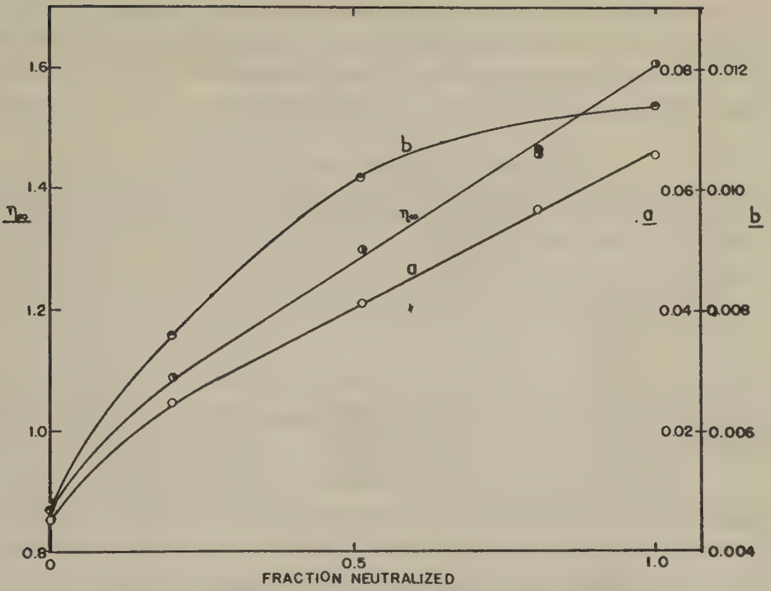

FIG. 3. Variation of parameters of Eq. 1 with degree of neutralization for 0.0336 gdmol. PAA.

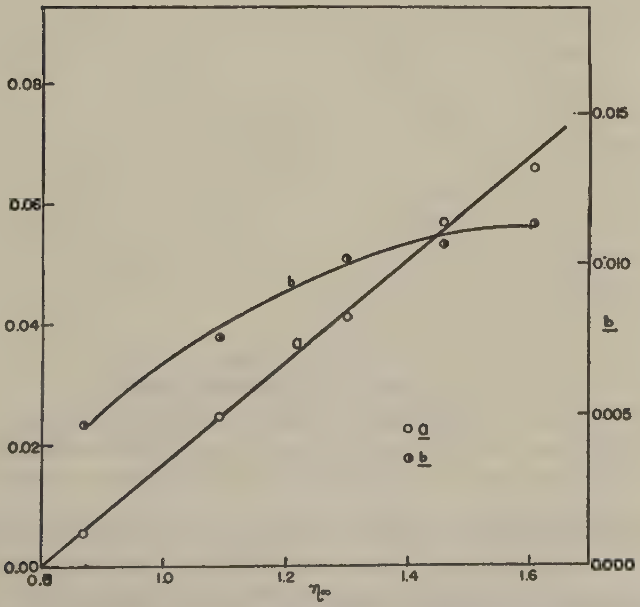

FIG. 4. Variation of the parameters *a* and *b* with the parameter η_∞ for varying degrees of neutralization in 0.0336 gdmol. PAA.

lated, so Fig. 4 shows a and b as a function of η_∞. Indeed it seems that $a = k_1(\eta_\infty - \eta_0)$ where $\eta_0 = 0.800$ is the viscosity of water at 30° and k_1 is a constant independent of the degree of neutralization. The parameter b shows no simple behavior in a plot of this type.

2. Effect of Concentration of Polymer

The viscosity of 0.514 neutralized PAA was studied at various concentrations of polymer as a function of concentration of sodium chloride.

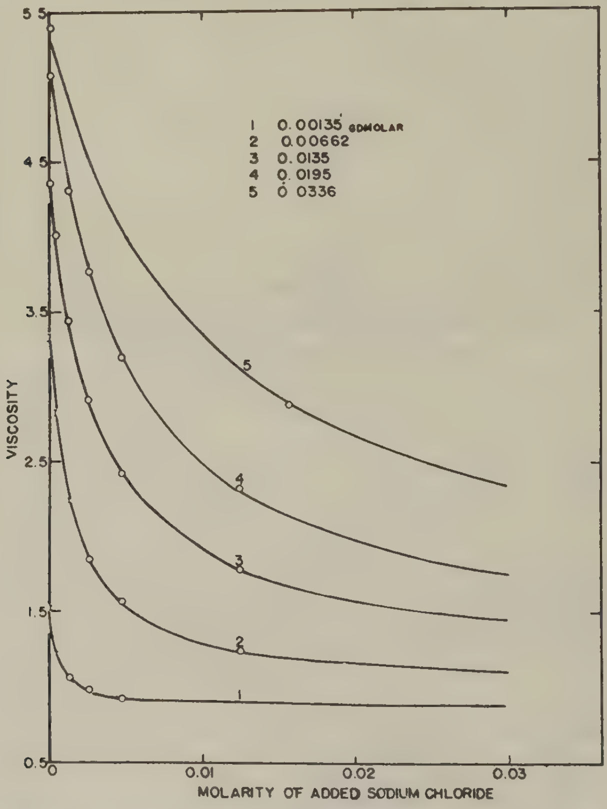

FIG. 5. Variation of viscosity with added salt concentration for various concentrations of 51.4% neutralized PAA. The extent of non-Newtonian behavior is indicated by the mark (1) where the ends are the extreme values of the viscosity observed.

These data are plotted in Fig. 5. Here again the curves are drawn from Eq. 1 with the parameters listed in Table II. Two measurements were taken at concentrations of salt much greater than plotted in Fig. 5. These did not fall on the curve. They are indicated in Fig. 6 which is a straight line plot based on Eq. 1.

TABLE II

The Parameters of Eq. 1 as a Function of Concentration for 0.514 Neutralized PAA Solutions

Grundmolarity of PAA	η_∞	a	b
0.00135	0.88	0.000296	0.00045
0.00662	1.02	0.0033	0.00145
0.0135	1.15	0.0099	0.0031
0.0198	1.22	0.0189	0.0049
0.0336	1.30	0.0412	0.0102

At the lowest two concentrations, the difficulty with non-Newtonian behavior appeared in the case of no added salt and the two lowest salt concentrations. Fuoss (21) obtained a similar result in his experiments with poly-4-vinyl-*N*-*n*-butylpyridonium bromide.

Various attempts were made to find a functional relationship between the parameters and the concentration of polymer. These parameters are plotted as functions of the concentration in Fig. 7. a seems to be proportional to the concentration to the $\frac{3}{2}$ power as can be seen in Fig. 8

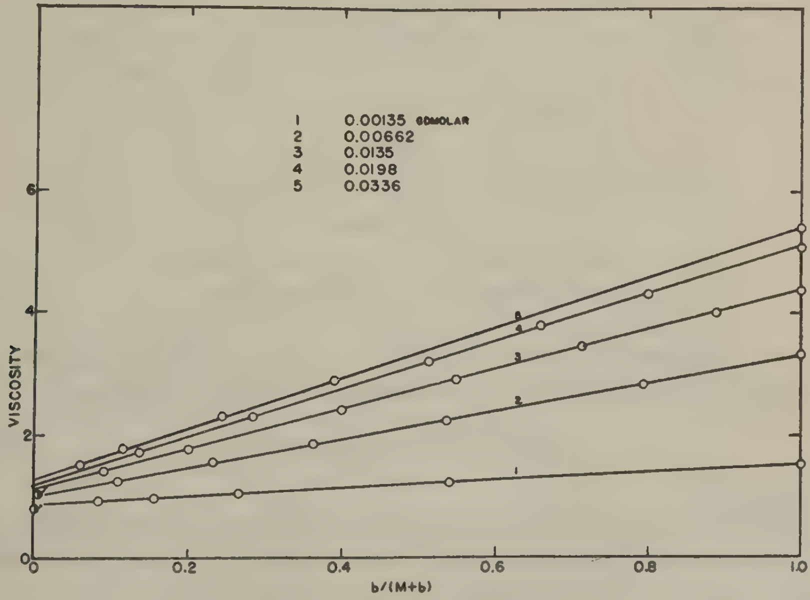

FIG. 6. Variation of viscosity of 51.4% neutralized PAA with molarity, M, of added sodium chloride for various grundmolarities, c, of PAA. The two points indicated by ◑ are those at large M which are not fitted by Eq. 1.

where a/c is plotted against $c^{\frac{1}{2}}$.

$$a = 6.33c^{\frac{1}{2}}. \qquad [3]$$

c is the concentration of polymer expressed as grundmolarity.

It was found that

$$\frac{c\eta_0}{\eta_\infty - \eta_0} = 0.0046 + 0.235c^{\frac{1}{2}} \qquad [4]$$

as shown in Fig. 9.

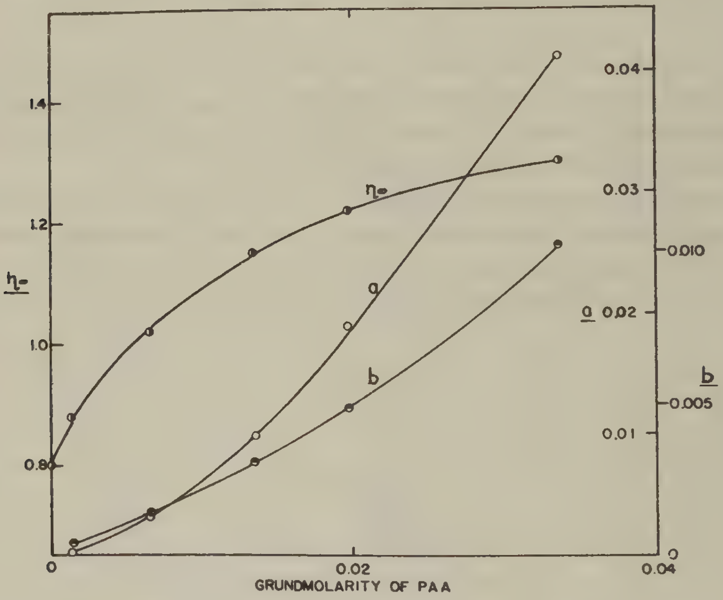

FIG. 7. Variation of parameters of Eq. 1 with concentration of PAA (51.4% neutralized).

The parameter b seemed to be least tractable; no simple relationship was found. The best empirical equation which could be found was

$$b = 0.00023 + 0.16c + 4.07c^2. \qquad [5]$$

See Fig. 10.

Putting the concentration dependencies into Eq. 1 we get the following expression for the viscosity of the 0.514 neutralized PAA as a function of concentration of polymer c and sodium chloride M

$$\eta_{sp}/c = \frac{1}{0.00046 + 0.235c^{\frac{1}{2}}} + \frac{7.91c^{\frac{1}{2}}}{M + 0.00023 + 0.16c + 4.07c^2}. \qquad [6]$$

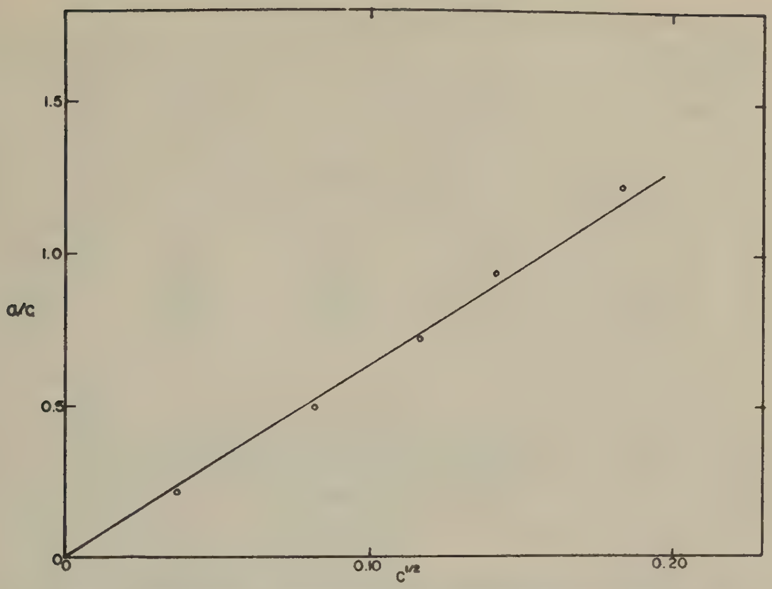

FIG. 8. Variation of the parameter a/c with concentration of 51.4% neutralized polyacrylic acid; c is grundmolarity of PAA.

Figure 11 shows η_{sp}/c as a function of concentration of polymer for various salt concentrations as calculated from the above expression [6]. The dots represent points calculated for $M = 0$, 0.001, 0.003, and 0.01 from the parameters obtained at concentrations of PAA where measure-

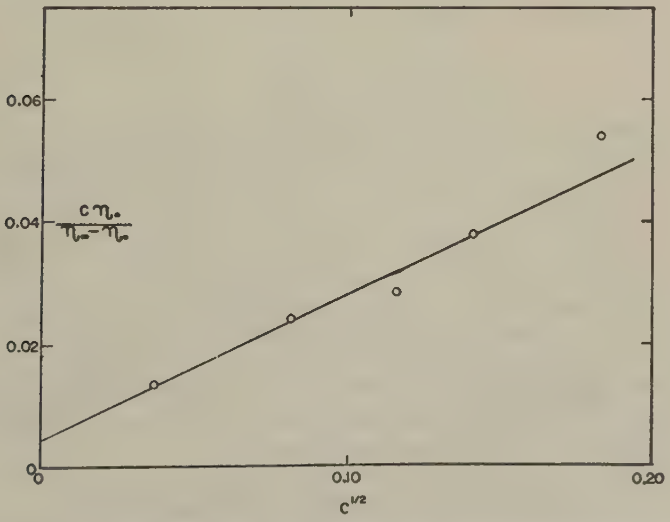

FIG. 9. Variation of $c\eta_0/(\eta_\infty - \eta_0)$ with $c^{\frac{1}{2}}$ for 51.4% neutralized PAA.

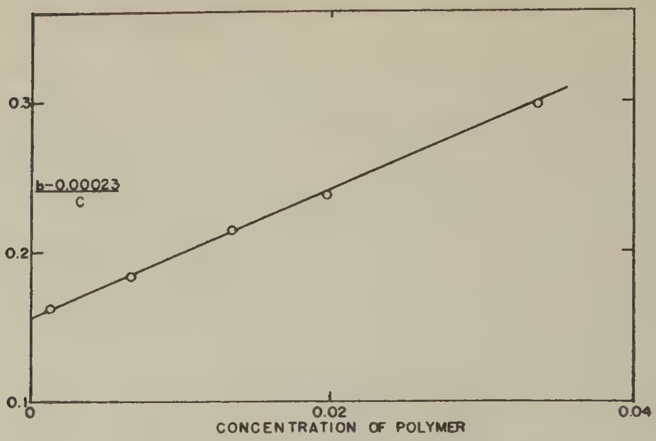

FIG. 10. Variation of $(b - 0.00023)/c$ with grundmolarity of 51.4% neutralized PAA.

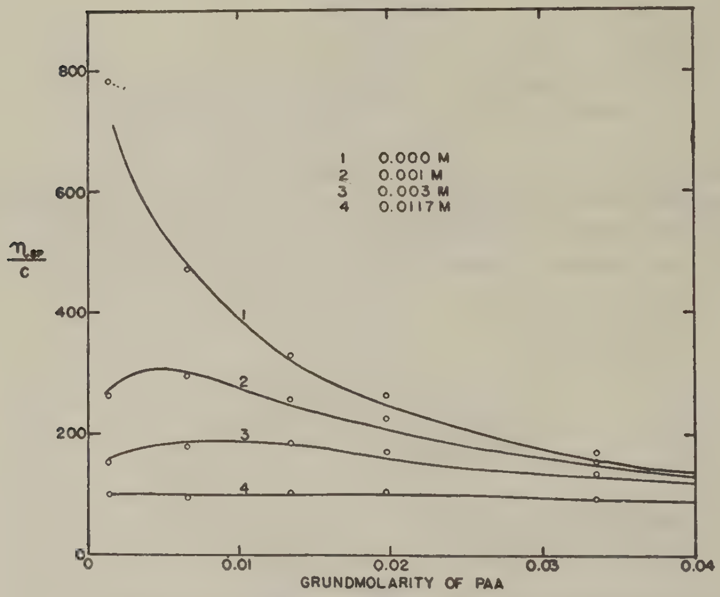

FIG. 11. Variation of η_{sp}/c with grundmolarity of 51.4% neutralized PAA for various molarities, M, of added sodium chloride.

ments were made. Fuoss and Strauss (14) obtained similar curves for poly-4-vinyl-*N*-*n*-butylpyridonium bromide. Pals and Hermans (18) show similar curves for sodium pectinate.

3. Effect of Salts Other Than Sodium Chloride

A. Salts with univalent cations. The viscosity of a polyacrylic acid solution with added salt is independent of the charge on the anion and

TABLE III

Viscosities of Solutions PAA to Which Salts Other Than NaCl Have Been Added. $\eta_{calc.}$ Is Calculated from Eq. 1 Using the Constants Found in the NaCl Experiments but Substituting for M the Molarity of Univalent Cation

Salt added	Grundmolarity of polymer c	Fraction neutralized	Conc. of univalent cation M	$\eta_{calc.}$	$\eta_{exp.}$
Na_2SO_4	0.0135	0.514	0.0141	1.73	1.71
KCl	0.0135	0.514	0.0252	1.43	1.47
Na_2SO_4	0.0336	0.203	0.00705	2.78	2.74
Na_2SO_4	0.0336	0.203	0.0141	2.23	2.19
KCl	0.0336	0.203	0.0132	2.28	2.32

depends only on the charge of the cation. In Table III data of Na_2SO_4 and KCl experiments are compared with the data from NaCl experiments.

It is to be noted that ionic strength is not the controlling factor but rather the concentration of the cation. This is further borne out by the experiments on barium chloride.

B. Barium chloride. Figures 12 and 13 show the viscosity data taken with $BaCl_2$ added to PAA. The parameters of Eq. 1 used to represent these data are given in Table IV.

It is to be noted that at least in this case, η_∞ cannot have any physical significance, but is only a parameter used to represent the data, since it has values much lower than the viscosity of the solvent.

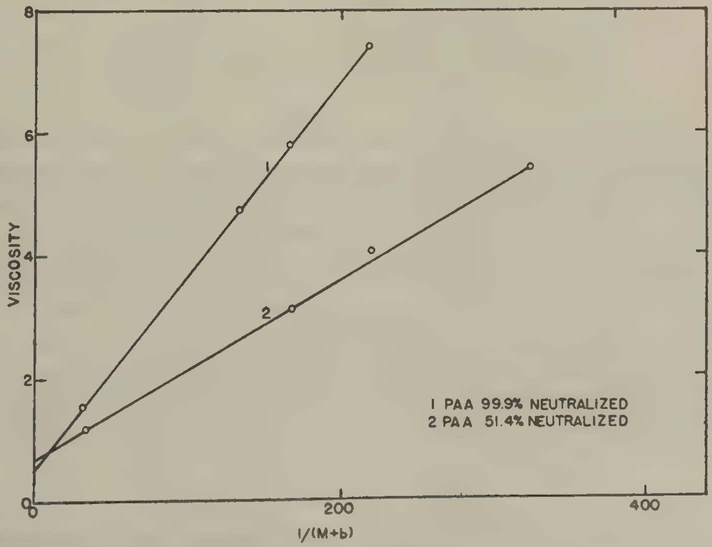

FIG. 12. Viscosity of 0.0336 gdmol. PAA solutions as function of molarity, M, of added barium chloride.

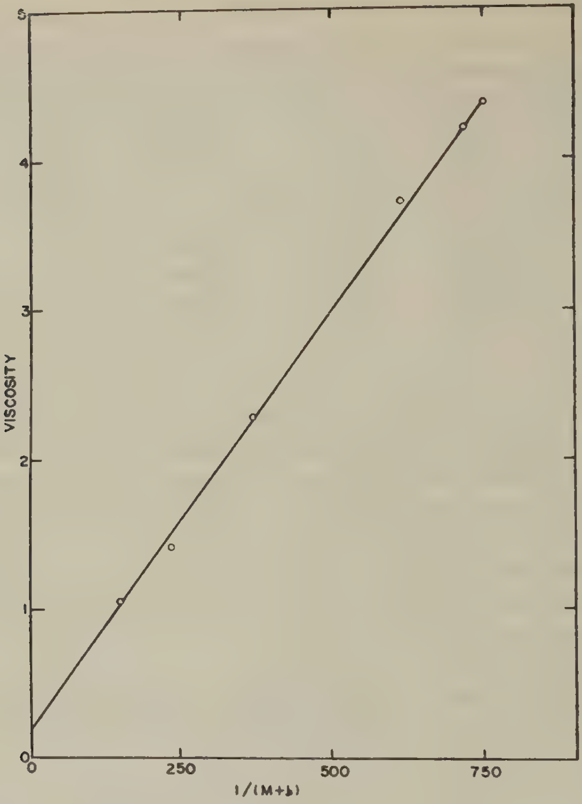

FIG. 13. Viscosity of 0.0135 gdmol. PAA (51.4% neutralized) as function of molarity, M, of added barium chloride.

A comparison between the effectiveness of sodium chloride and barium chloride can be seen if we plot the concentration of NaCl against the "equivalent" concentration of $BaCl_2$. By equivalent concentration we mean a concentration of $BaCl_2$ which depresses the viscosity of a PAA solution by the same amount as a given concentration of NaCl. In Fig. 14

TABLE IV

Parameters of Eq. 1 for Experiments with Barium Chloride

Conc. of polymer fraction neutralized	0.0336 0.999	0.0336 0.514	0.0135 0.514
η_∞	0.55	0.70	0.20
a	0.0324	0.0148	0.00456
b	0.0046	0.0031	0.00134

is shown such a plot. Figure 15 is a plot of the ratio of equivalent concentrations of sodium chloride and barium chloride as a function of the concentration of sodium chloride. If ionic strength were the determining factor, this line would be horizontal through the ordinate at 3. This is not the case.

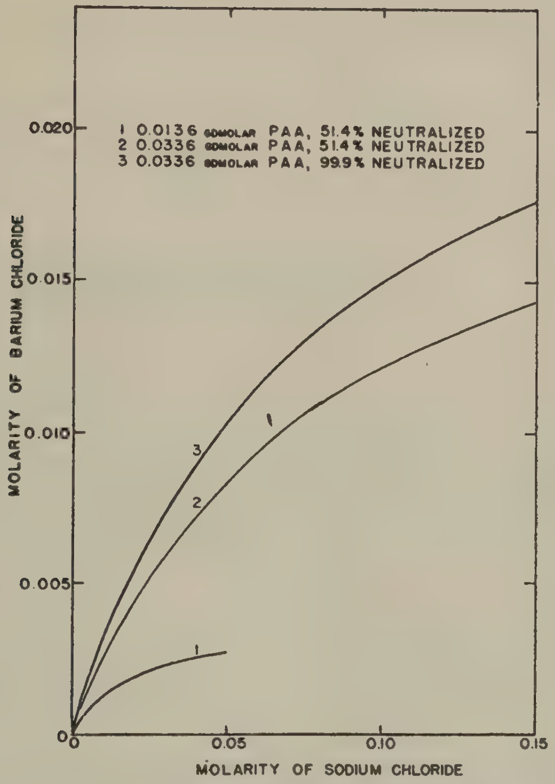

FIG. 14. Equivalent concentrations of sodium chloride and barium chloride.

It is to be noted that with $BaCl_2$ values of the viscosity can be obtained which are less than the η_∞ of the corresponding NaCl data.

C. Magnesium sulfate. One run was made with a magnesium sulfate concentration of 0.00329 M, polyacrylic acid, 0.999 neutralized, and 0.0336 gdmol. The viscosity was measured to be 4.64. The value calculted from the parameters obtained with barium chloride at the same grundmolarity and degree of neutralization was 4.70.

RELATED WORK PREVIOUSLY DONE

Since some work has been done in the past on the viscosity of polyelectrolytes and proteins as a function of concentration of added salt, it is interesting to see whether they obey the relationship [1] found above. Staudinger (3) reported one set of data on the viscosity of completely neutralized PAA (degree of polymerization 800, 0.02 gdmol.) as a function of the concentration of added sodium chloride. This is plotted according to [1] in Fig. 16.

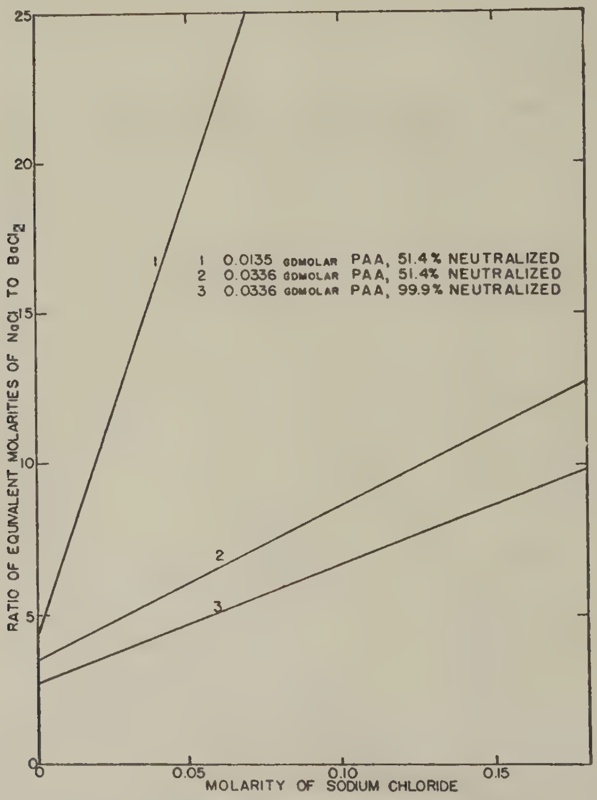

Fig. 15. Ratio of equivalent molarities of sodium chloride to barium chloride as function of molarity of sodium chloride.

Aten (11) gives a few data on 83% neutralized polymethacrylic acid, 0.00395 gdmol. These data are plotted in Fig. 17.

Jacques Loeb (22) investigated the effect of the addition of salt on the viscosity of gelatin solutions. Figure 18 is an example of a plot of his data according to Eq. 1.

Discussion

1. Comparison of Theories

The outstanding difference between polyacrylic acid and most other polymers is its charge. Therefore we turn to the electrical nature of the

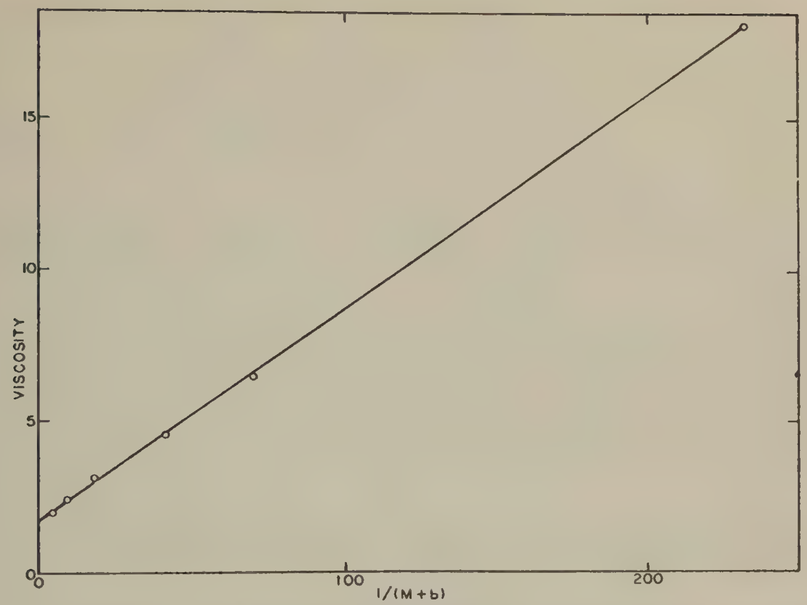

FIG. 16. Viscosity of 0.02 gdmol. PAA (DP = 800, 100% neutralized) as function of molarity, *M*, of added sodium chloride. [From data of Staudinger (3) table 250.]

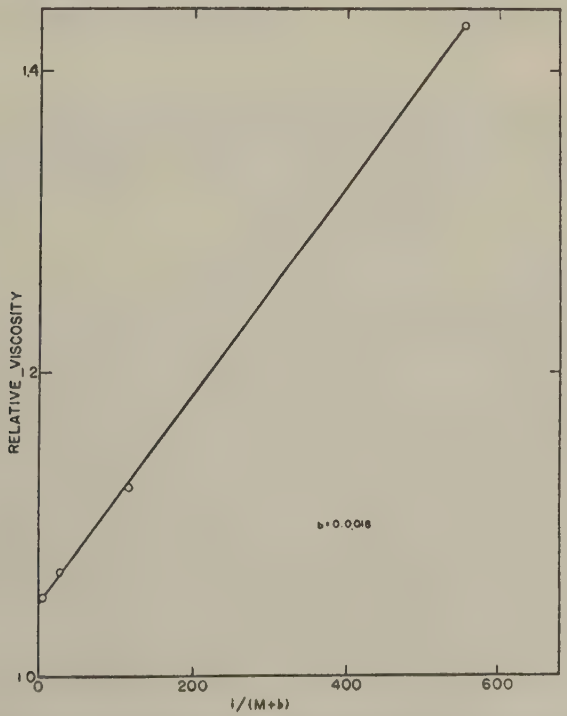

FIG. 17. Viscosity of 0.0040 gdmol. polymethacrylic acid (83% neutralized) as function of molarity, *M*, of added sodium chloride (Aten, 12).

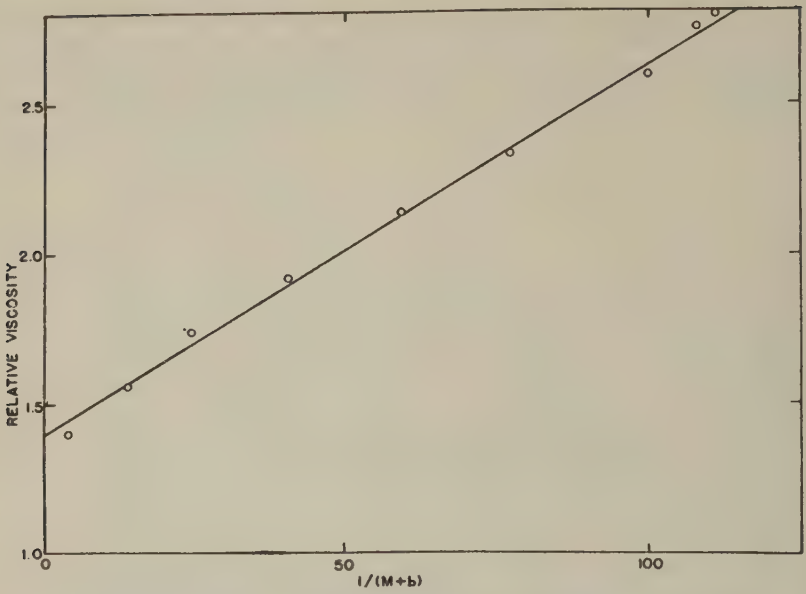

FIG. 18. Variation of viscosity of a gelatin solution (pH = 3.0) with molarity, *M*, of added sodium chloride (Loeb, 23, p. 104).

polymer for an explanation of its abnormal behavior. Various approaches can be made:

A. The viscometric behavior can be ascribed mainly to the presence of electrical charges on the polymer and to its ion-atmosphere in solution, without regard to secondary effects such as changes of size, shape, or state of aggregation (Electrical Theory).

B. The configuration of the individual polyions may vary because of the changes in the electrical environment and thus cause changes in the viscosity (Folding-chain Theory) (10, 11, 13).

C. The effects may be due to the changes in the degree of association of the polyions. This was the explanation suggested by Staudinger (Swarm Theory).

D. Some combination of the above approaches may be necessary.

In the electrical theory the effect on the viscosity is due to the distortion of the ionic atmosphere by the shear gradient. This causes an increase in the rate of dissipation of energy and hence in the viscosity of the solution. Smoluchowski (23, 24) proposed an expression for the viscosity of a solution of charged spheres.

$$(\eta - \eta_0)/\phi = 2.5\{1 + [(D\zeta)^2/4\pi^2\sigma\eta_0R^2]\}. \qquad [7]$$

Here

σ = specific conductance of the solution,
ζ = difference in potential in the double layer,
R = radius of the sphere,
D = dielectric constant,
ϕ = volume fraction of solute in solution.

On the basis of this one can explain qualitatively the behavior of solutions of PAA. Whenever the potential increases, the viscosity goes up. More will be said later.

According to the folding-chain theory, the charges on the polyion repel one another. As a result of changes in the electrical environment the amount of this repulsion will vary. Under conditions such that the repulsion is strong, the molecule will be stretched out. When these forces are reduced, the polymer will more nearly approach the random coil. The more spread out and the more asymmetric the molecule is, the higher will be the viscosity.

From hydrodynamical considerations it has been shown (25, 26) that for solutions of particles that could be represented as spheroids or cylinders

$$\eta = \eta_0[1 + \phi f(\psi)] \tag{8}$$

where ϕ is the volume fraction of solute, ψ is the axial ratio, and $f(\psi)$ is a monotonically increasing function of ψ. If we further make the substitution

$$\phi = H\phi_0$$

where ϕ_0 is the volume fraction due to the solute itself and H is the factor necessary to multiply by ϕ_0 to get the effective volume fraction (hydration), we obtain

$$\eta_{sp} = (\eta - \eta_0)/\eta_0 = H\phi_0 f(\psi) \tag{9}$$

and

$$\eta_{sp}/\phi_0 = Hf(\psi). \tag{10}$$

On the basis of this equation, an increase in the observed value of η_{sp}/c can be caused by increases in H or in ψ.

A similar sort of dependence on the shape of the molecule can be obtained from the "pearl necklace" models of Huggins (27) and Debye (28).

The swarm theory, as explained by Staudinger, states that both the acid and the polyion are stretched-out chains. In the case of the salt, a negative polyion is surrounded mostly by small positive ions. These in turn have polyions as part of their ion atmosphere. In this way aggregates may be built up. In most of the following discussion of the swarm theory we will use Staudinger's explanations.

Let us see how these three theories explain some of the behavior of solutions of polyacrylic acid.

TABLE V

Summary of Theories

Observation	Electrical theory	Folding-chain theory	Swarm theory
1. Viscosity of PAA solutions increases as sodium hydroxide is added.	As the acid gets neutralized, the molecule gets charged. Its potential goes up. The viscosity of the solution increases.	The polymer is getting charged. The various parts repel each other more. The molecule spreads and stretches out. It becomes more asymmetrical. The viscosity increases.	As the molecule gets charged, the ion atmospheres develop. As explained before, swarms form. The viscosity increases.
2. η_{sp}/c for unneutralized PAA increases to a very high value with increasing *dilution* of the polymer.	At low concentrations, the PAA is more ionized than at higher ones. Therefore the charge and potential of the polymer molecule go up with dilution. η_{sp}/c increases.	Since there is a higher degree of ionization at lower concentrations, the the chain is more highly charged. The molecule is more stretched out in more dilute solutions. η_{sp}/c increases.	Since the chain is more charged at low concentrations, larger swarms form. η_{sp}/c increases as the solution is diluted.
3. η_{sp}/c for completely neutralized PAA gets large at small concentrations of polymer.	The polyion has lots of charge constrained to be in a small volume. The sodium ions are therefore rather tightly held. As the solution is diluted, more sodium ions get away from the neighborhood of the polymer. The potential increases, the specific conductance goes down. η_{sp}/c goes up with dilution.	Since more sodium ions can get away, the effective charge on the polymer goes up. The polymer stretches out. η_{sp}/c increases.	Staudinger says: At low concentrations where acid and salt are both ionized, one expects similar behavior. This explanation is hard to understand, since in the case of the acid, the chains were getting charged during the dilution. However, in the case of the completely neutralized PAA, dilution increases the effective charge. Swarms form. η_{sp}/c goes up. This is in spite of the fact that dilution decreases both the concentration of cement (i.e. small ions) and also polymer chains.

TABLE V—*Continued.*

Observation	Electrical theory	Folding-chain theory	Swarm theory
4. The viscosity decreases when salt is added to solutions of PAA.	When salt is added, there is a great increase in the number of small positive ions which surround the large polyion. The potential goes down. Conductivity goes up. The viscosity decreases.	Since there are more positive ions around the negative charges on the polymer molecule, the effective charge is smaller. As a result, there is less repulsion between parts of the polymer molecule. It coils up. Viscosity goes down.	Added salt decreases the effective charge on the polymer. Also small negative ions can take the place of the large polyions in the ion atmosphere. The swarms are smaller. The viscosity goes down.
5. At large concentrations of sodium chloride, the viscosity varies with the degree of neutralization of the PAA.	This is very surprising. The conductivity should be high enough to bring the viscosity to the same level for all degrees of neutralization even if there are still small differences of potential.	The negative charges on the polyions are not completely "neutralized" by the small positive ions. Therefore the polymer molecule is not completely coiled up even with a large concentration of sodium chloride. The amount of the stretching out will depend on the degree of neutralization.	This is hard to understand. The sodium chloride should have completely destroyed the electrostatic interaction between the chains. Therefore one expects to get the same viscosity for all fractions neutralized—namely the viscosity due to the individual chains.

It is seen that any of the theories can explain qualitatively almost all of the observed phenomena in a reasonable fashion. The one point with which there seems to be any difficulty is the fact that at large concentrations of sodium chloride, the viscosity of the PAA solutions seems to depend on the degree of neutralization. This is a result that could be expected on the basis of the folding-chain theory but not on the basis of either of the others. Therefore it seems reasonable to conclude that the polymer does change its configuration.

Before discussing the various approaches further let us look at the order of magnitude of the changes in η_{sp}/c which must be explained. Staudinger reported some data on his sample of polyacrylic acid P50 (degree of polymerization about 350). This material has a low η_{sp}/c value of 4.3 for the unneutralized acid (0.2 grundmolar). The highest measured η_{sp}/c value was 378 for the completely neutralized PAA at a concentration of 0.0005 grundmolar. Therefore increases of the order of a hundred fold in η_{sp}/c must be explained.

Swarm theory. Staudinger's straight-chain, stretched-out molecule is a very long, thin particle with a very high axial ratio. If swarms form, it is not likely that the resulting "particles" will be more asymmetric. Even if the original molecule is a random coil, swarms would not increase the axial ratio to such an extent as to affect the viscosity greatly. This is borne out by the work of Doty, Wagner, and Singer (29) who found evidence for association of polyvinyl chloride from osmotic pressure, light scattering, and ultracentrifuge measurements. However the viscosity was not affected by the association.

There is a possibility that the polymer would associate end to end as does tobacco mosaic virus (30, 31) but there does not seem to be any special reason why it should do this. Staudinger's picture of swarming, at least, leads to a more random type of association.

It seems then that the changes in viscosity on the basis of this theory will have to be explained in terms of variations in the effective volume fraction of the particles. This might be caused by increased hydration or trapping of some solvent in the swarm, but it is hard to imagine the hundred fold increase which would be necessary because of the proportionality between effective volume fraction and η_{sp}/c.

From the same mechanism which leads to "attraction" between chains and therefore to swarms, one might expect to get "attraction" between parts of the same polyion. In fact a more highly charged polymer molecule would be more tightly coiled. At large salt concentrations, then, the viscosity would be the same or lower for a higher degree of neutralization. The opposite effect is observed.

The whole idea of two bodies of the same charge being held together by small ions is weakened further by the theoretical work of Verwey and Overbeek (32) who show that the interaction of two double layers always gives rise to a repulsion between the surfaces bearing them. It is only a large Van der Waals force which can cause two such surfaces to come together as they do, for example, in the case of soap micelles. With PAA, however, the Van der Waals forces would probably not vary greatly with increased charge, but the repulsion would increase.

Folding-chain theory. To get some idea of what to expect from this apprach, we will use some expressions from Debye's (28) first viscosity theory. Using a pearl-necklace model, he gets the expression

$$\eta - \eta_0 = \tfrac{1}{6} n f \sum \langle r^2 \rangle \qquad [11]$$

where n is the number of polymer molecules/cc., f is the frictional force per unit velocity for the particles in the polymer chain, and r is the distance of the particle in the chain from the center of gravity. Debye works out this equation for a solution of randomly coiled chains and finds its viscosity η_{ran}:

$$\eta_{\mathrm{ran}} - \eta = \tfrac{1}{36} nf \frac{1 + \rho}{1 - \rho} N^2 l^2 \qquad [12]$$

where ρ is the cosine of the angle between two consecutive links in the chain, N is the number of particles in the chain, and l is the length of a link. If the chains are completely stretched out the viscosity η_{st} is given by

$$\eta_{\mathrm{st}} - \eta = nfN^3l^2(1 + \rho)/144 \qquad [13]$$

and

$$\frac{(\eta_{\mathrm{sp}}/c)_{\mathrm{st}}}{(\eta_{\mathrm{sp}}/c)_{\mathrm{ran}}} = N(1 - \rho)/4. \qquad [14]$$

If the angle between links in the chain is the tetrahedral angle and $N =$ 700, the above ratio is about 120. This should correspond to the case of Staudinger's P50 mentioned above. There the ratio of the highest to lowest η_{sp}/c values measured was 90. However, the experimental values obtained are not necessarily the extreme values of η_{sp}/c possible. On the other hand the theoretical assumptions are too extreme. It is hardly likely that the sodium salt of PAA is completely stretched out or that unneutralized PAA is a random coil. Therefore it seems as if the folding-chain theory may not be able to explain the results by itself.

Electrical theory. It is expected that there should be an important contribution to the viscosity from this source. Even in the case of small carboxylic acids the viscosity of the salt is considerably greater than that of the undissociated acid (3). To estimate the amount of this contribution to the viscosity is a more difficult matter. The equation of Smoluchowski and Krasny-Ergen was based on the model of a rigid sphere with a charge distributed on its surface. This is not a very good approximation to the PAA molecule. Furthermore, even if one were satisfied with this simplification, it is difficult to evaluate the quantities entering into the equation. An attempt was made to evaluate the potential by means of a Debye-Hückel type of computation. However, it turned out the potential was too high to allow the approximations used in setting up the equations. Qualitatively it can be seen that the electrical effect will be most important when the potential is high and the conductivity is low. This condition will obtain when the concentrations of polymer and of added salt are small.

Summary. The behavior of PAA solutions can be accounted for by the electrical and folding-chain theories. The former is probably more important at low concentrations of polymer and salt, and the latter at higher concentrations.

2. Concentration Experiments

In the experiments where the concentration of polymer varied, the main feature seems to be that at a given M (concentration of salt), η_{sp}/c goes through a maximum as c (the concentration of polymer) increases if M is not too large. At low c, M is much greater than c. This case is similar to point *4* in the table and a low η_{sp}/c is expected. As the relative amount of salt decreases, η_{sp}/c increases. When the concentration of polymer is higher, the situation is similar to point *2* in the table and η_{sp}/c decreases with increasing concentration of polymer.

3. Experiment With Other Salts

That the viscosity of PAA solutions depends only on the charge and concentration of the positive ions and not on the ionic strength, can be understood in terms of the high potential on the polyacrylate ion. In regions of high negative potential, there will be very few small negative ions. Almost all of the small ions near the polyion will be positive ones. It will be these which will determine the electrical environment around the polyion and therefore the properties of PAA solutions.

4. The Recent Theory of Hermans and Overbeek

Recently Hermans and Overbeek (33) have proposed a theory of the electroviscous effect. Essentially it is an attempt to work out the folding-chain theory in mathematical terms. However their treatment is not applicable here. It ignores the "electrical" effect and uses the Debye-Hückel approximation. As a result of the latter the significant variable at a given degree of charging is the ionic strength. It has been shown in our case, however, that the important variable is not the ionic strength but rather the charge and concentration of the cation.

SUMMARY

1. The viscosity of polyacrylic acid solutions has been studied as a function of concentration of added sodium chloride and degree of neutralization at a given concentration of polymer.
2. The viscosity of PAA solutions has been measured as a function of concentration of sodium chloride and concentration of polymer at a given degree of neutralization.
3. The effect of salts other than sodium chloride was found to depend on the charge and concentration of the cation rather than on ionic strength. A doubly charged cation is much more effective than a univalent positive ion.
4. An empirical expression [1] was found to express the viscosity as a function of salt concentration which was valid at least for low salt concentrations.

5. Empirical expressions were found for the variation of the parameter in the relationship mentioned in Item 4 with concentration of polymer.

6. A comparison of the various theories explaining the behavior of PAA solutions was made.

REFERENCES

1. STAUDINGER, H., AND URECH, E., *Helv. Chim. Acta* **12**, 1107 (1929).
2. STAUDINGER, H., AND KOHLSCHUETTER, H. W., *Ber.* **64**, 2091 (1931).
3. STAUDINGER, H., Die hochmolekularen organischen Verbindungen, Second Part, Section D. Julius Springer, Berlin, 1932.
4. STAUDINGER, H., AND TROMMSDORF, E., *Ann.* **502**, 201 (1933).
5. KERN, W., *Z. physik. Chem.* **A181**, 249 (1938).
6. KERN, W., *Z. physik. Chem.* **A181**, 283 (1938).
7. KERN, W., *Z. physik. Chem.* **A184**, 197 (1939).
8. KERN, W., *Z. physik. Chem.* **A184**, 302 (1939).
9. EVANS, A. G., AND TYRRALL, E., *J. Polymer Sci.* **2**, 387 (1947).
10. KATCHALSKY, A., AND SPITNIK, P., *J. Polymer Sci.* **2**, 432 (1947).
11. ATEN, A. H., JR., *J. Chem. Phys.* **16**, 636 (1948).
12. FUOSS, R. M., AND CATHERS, G. I., *J. Polymer Sci.* **2**, 12 (1947).
13. FUOSS, R. M., AND STRAUSS, U. P., *J. Polymer Sci.* **3**, 246 (1948).
14. FUOSS, R. M., AND STRAUSS, U. P., *J. Polymer Sci.* **3**, 602 (1948).
15. FUOSS, R. M., *J. Polymer Sci.* **3**, 603 (1948).
16. FUOSS, R. M., AND EDELSON, D., *J. Am. Chem. Soc.* **70**, 2832 (1948).
17. JOHANSON, S., *Svensk Kem. Tid.* **60**, 122 (1948).
18. PALS, D. T. F., AND HERMANS, J. J., *J. Polymer Sci.* **3**, 898 (1948).
19. Private communication.
20. BINGHAM, E. C., Fluidity and Plasticity, McGraw-Hill, New York, 1922.
21. FUOSS, R. M., private communication.
22. LOEB, JACQUES, Proteins and the Theory of Colloidal Behavior, pp. 88 ff. McGraw-Hill, New York, 1922.
23. SMOLUCHOWSKI, M. v., *Kolloid Z.* **18**, 190 (1916).
24. KRASNY-ERGEN, W., *Kolloid Z.* **74**, 172 (1936).
25. PHILIPPOFF, W. Viskosität der Kolloide, pp. 11 ff. Theodor Steinkopff, Dresden and Leipzig, 1942.
26. BURGERS, J. M., *Second Report on Viscosity and Plasticity, Verhandel. Koninkl. Nederland. Akad. Wetenschap., Afdeel. Natuurk. Sect. I*, **16** (4), pp. 134 ff. Each of the books in Refs. 25 and 26 lists many references.
27. HUGGINS, M. L., *J. Phys. Chem.* **42**, 911 (1938); *ibid.* **43**, 439 (1939); *J. Applied Phys.* **10**, 700 (1939).
28. DEBYE, P., *J. Chem. Phys.* **14**, 636 (1946).
29. DOTY, P., WAGNER, H., AND SINGER, S., *J. Phys. & Colloid Chem.* **51**, 32 (1947).
30. SCHACHMAN, H. K., *J. Am. Chem. Soc.* **69**, 1841 (1947).
31. LAUFFER, M. A., *J. Biol. Chem.* **126**, 443 (1938).
32. VERWEY, E. J. W., AND OVERBEEK, J. TH. G., Theory of Stability of Lyophobic Colloids, Elsevier Publishing Co., New York, 1948.
33. HERMANS, J. J., AND OVERBEEK, J. TH. G., *Bull. soc. chim. Belg.* **57**, 154 (1948).

THE ADSORPTION OF HYDROGEN ON NICKEL CATALYSTS. II. SORPTION ISOBARS FROM 20°K. TO ROOM TEMPERATURE

O. Beeck, J. W. Givens and A. W. Ritchie

Shell Development Company, Emeryville, California

Received November 9, 1949

INTRODUCTION

The first paper of this series (1) gives an account of studies of the adsorption of hydrogen on evaporated nickel films in which the effect of sintering the films before adsorption takes place was investigated. In this work it was found that the ratio of slowly sorbed hydrogen to rapidly adsorbed hydrogen increases with the sintering temperature of the film and it was shown that the slow "activated adsorption" of hydrogen on nickel, which has been previously observed by other investigators, was actually slow sorption of hydrogen into the interior of the metal structure rather than adsorption. This work further showed that sites occupied by hydrogen that is slowly sorbed into the interior of the metal structure are not accessible to chemisorption of carbon monoxide or van der Waals' adsorption of krypton, nor are they accessible to ethylene. It was concluded that the very fast chemisorption of hydrogen at liquid nitrogen temperature is a true measure of the surface available for chemisorption of carbon monoxide, for van der Waals' adsorption of krypton, and for surface reactions such as the hydrogenation of ethylene.

It is the purpose of this paper to present the results of measurement of sorption isobars from 20°K. to room temperature This work was undertaken to elucidate further the nature of adsorption by metal films and to obtain further confirmation of the results obtained in the first paper. It will be seen that the conclusions from the low temperature results are in good agreement with those from the earlier work. As a result a clear picture of the sorption process on evaporated metal films has been obtained.

EXPERIMENTAL

The evaporated metal films were made by the technique previously described (2). The films used in these experiments were evaporated in a high vacuum (10^{-5} mm.) and were deposited on the surface of a cylindrical adsorption vessel kept at 0°C. by an ice-bath. The films were subsequently sintered at either 23°C. or 200°C. All adsorption measurements were carried out in a Collins helium cryostat (3). This apparatus is admirably suited for carrying out a wide variety of measurements over the temperature range from 1.5°K. to room temperature. In this work the adsorption vessel containing the deposited film was inserted into a brass cylinder on which was wound a heating coil of manganin wire and to which was soldered the copper–constantan thermocouple used for measuring the temperature. This thermocouple, designated Copper–Constantan Thermocouple No. 1, consists of five parallel No. 30 glass covered especially selected constantan wires soldered to one No. 24 thermocouple grade copper wire. This thermocouple was calibrated against a helium gas thermometer and against the boiling point of helium at one atmosphere. All thermocouple potentials were measured by means of a Wenner potentiometer. In carrying out the adsorption measurements, the temperature of the vessel was regulated manually by balancing the heat input to the brass cylinder against the cooling rate produced by the cryostat engines. In this way the adsorption vessel could be brought to any predetermined temperature and held there with a variation of only 0.1°K.

RESULTS

In Fig. 1 are shown adsorption isobars at 0.1 mm. hydrogen pressure for hydrogen on evaporated nickel films. The solid curves represent the isobars for increasing and decreasing temperature. With increasing temperature (the part between 20 and 80°K. will be discussed later), sorption increases rapidly between 80 and 170°K. While initial sorption at each point, after raising the temperature, was fairly rapid, it was followed by a very slow sorption, and true equilibrium values were not obtained in the time of about 30 min. allowed for equilibration. It is possible, therefore, that the maximum at about 170°K. would have shifted to lower temperatures if long enough waiting periods had been used. In the descending branch of the isobar, true equilibrium was obtained very rapidly and, as indicated by the squares, this isobar could be traced exactly when again increasing the temperature, without any intermediate outgassing of the system. When the system was pumped to high vacuum for 15 min. at 80°K. the subsequently measured isobar starting at 20°K. with increasing temperature exactly retraced the isobar obtained initially on the branch of decreasing temperatures, assuming identity of the two curves at the temperature of pumping. After the system was pumped to high vacuum for 15 min. at 175°K., the isobar for increasing temperature showed a pronounced minimum and maximum, the amount taken up at the 80°K. minimum agreeing well with the amount which was taken up in the first isobar when 175°K. had been reached on the branch of descending temperatures, again assuming identity of the two curves at the temperature of pumping. After pumping the system to high vacuum for 15 min. at 296°K., the subsequently measured isobar for increasing temperature (starting again at 20°K.) showed at its minimum value an uptake practically identical with the uptake found at 296°K. on the ascending branch of the very first isobar. As in the two previous cases, identity of the two curves at 296°K. is assumed. These facts are of interest because they show that the amount of hydrogen which can be removed from the system by pumping to high vacuum for 15 min. at 175°K. and 296°K. is being resorbed almost completely in the lower temperature region between 20 and 80°K. More important, however, is the fact that the rise of the initial isobar with decreasing temperature down to about 80°K. must also be partly due to absorption. Further proof of this will be given in the next paragraph.

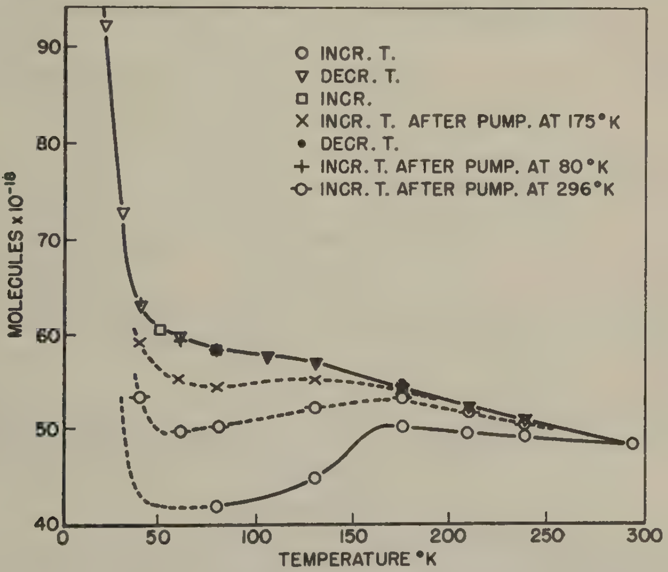

Fig. 1. Sorption isobar of hydrogen at 0.1 mm. on evaporated nickel film sintered at 23°C. (To obtain the ordinate in molecules × 10^{-18}/100 mg., divide by 9.07.)

Figure 2 shows the ascending and descending branch of a hydrogen isobar at 0.1 mm. pressure on a nickel film previously sintered at 200°C. If the 80°K. point of the ascending isobar in this figure is compared with the 80°K. point of the ascending isobar in Fig. 1 (after converting the ordinate in Fig. 1 to molecules × 10^{-18}/100 mg. of nickel film as indicated below the figure), it is noted that the initial hydrogen adsorption at 80°K. is nine times larger per weight unit for the film sintered at 23° than for the film sintered at 200°C. At the same time it is seen that the difference of hydrogen sorption between the descending and ascending branch of the isobar at 80°K. is the same for both types of films and, thus, evidently a weight effect. Furthermore, the ratio of total sorption at 80°K to that at room temperature on the decreasing branch of the two isobars is the same for both types of films, indicating that the relative decrease of total sorption with temperature is independent of surface. Figure 2 shows clearly that the major portion of the hydrogen sorption at room temperature of a film sintered at 200°C. is absorption into the interior of the structure. It is interesting to note that the total van der Waals' adsorption as given by the differences of sorption between 20° and 80°K. is practically the same for the ascending and the descending part of the isobar. Furthermore, the numerical value of the van der Waals' adsorption for the film sintered at 200°C. is seen to be approximately 4 times lower than the van der Waals' adsorption observed on a film sintered at 23°C. as shown by Figs. 1 and 2. The reason that the ratio of the van der Waals' adsorption in the two types of film is not equal to the ratio of the surfaces as measured by the adsorption at 80°K. in the ascending part of the isobars of the two types of film will become clear after the following discussion of Fig. 3, which represents an isobar on the same type of film in the region between 20 and 120°K. All points of this isobar with increasing or decreasing temperature are numbered in the sequence in which they were measured. It is seen that, starting with point No. 1 at 20°K. and proceeding to 50°K., the isobar can be traced back to point No. 3 at 20°K., which coincides with point No. 1. Ascending again with the temperature, point No. 4 falls on the same curve and, after obtaining point No. 5, the isobar can be traced back and forth to point No. 9. Since the isobar flattens out completely at 80°K. with the value of 7.2 × 10^{18} molecules/100 mg. it can

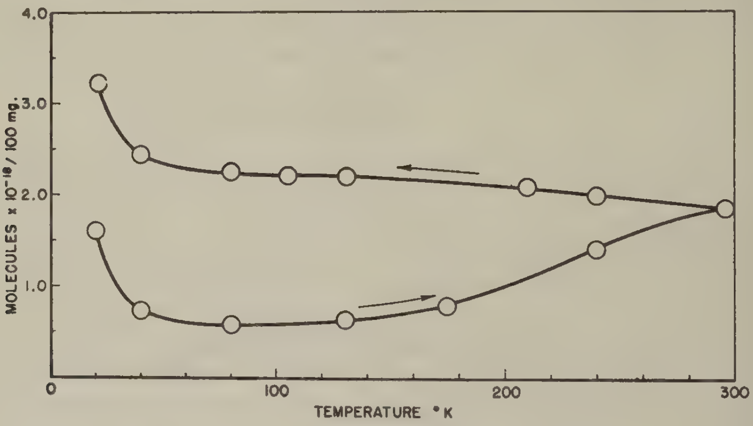

FIG. 2. Sorption isobar of hydrogen at 0.1 mm. on evaporated nickel film sintered at 200°C.

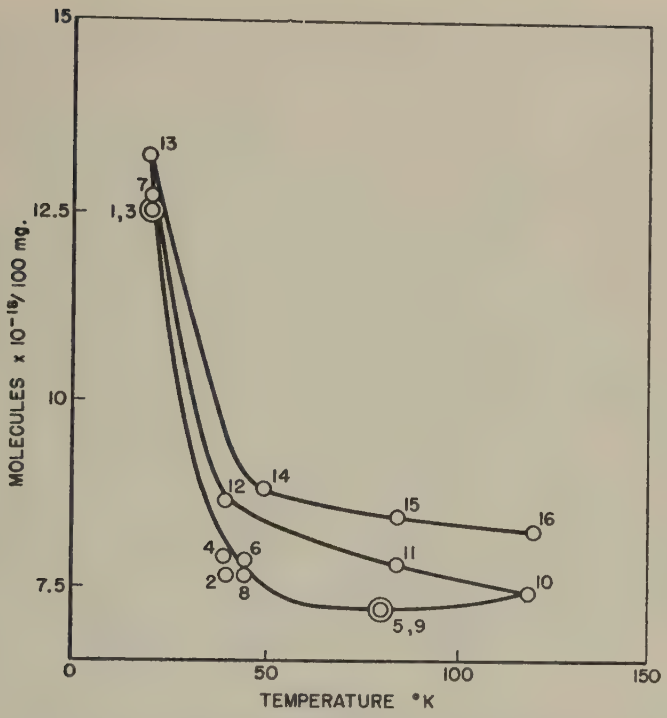

FIG. 3. Sorption isobar between 20°K. and 120°K. of hydrogen at 0.1 mm. on evaporated nickel film sintered at 23°C.

be concluded that the total adsorption of hydrogen at 20°K. consists of 7.2 × 10^{18} molecules/100 mg. of nickel of chemisorption and of 6.0 × 10^{18} molecules/100 mg. van der Waals' adsorption.

DISCUSSION

Measurements made in these laboratories (3*a*) have shown the heat of adsorption of hydrogen at liquid air temperature to be 30,000 cal./mole for the sparsely covered surface decreasing to 18,000 cal./mole for the completely covered surface. These values are in complete agreement with those obtained at room temperature. Since the isobar in Fig. 3, starting at 20°K. can be retraced back and forth to 80°K., it is evident that the chemisorption observed at 80°K. must already have occurred at 20°K. By tracing the isobar further to point No. 10, it is seen that a small amount of sorption into the interior of the structure has taken place. After initiation of this process, which is activated by the energy supplied by raising the temperature from 80°K. to 120°K., it is interesting to note that this process will continue, even at an increasing rate, upon lowering the temperature again to point No. 11. Upon tracing the isobar down to

20°K., it is found that the total sorption value of point No. 13 is higher (within the limits of experimental error) by an amount corresponding to the absorption that has taken place during this time. Upon retracing the isobar back through points 14, 15, and 16, more gas is absorbed and the process could presumably have been continued until the total *ab*sorption would have been identical with that of the descending branch in Fig. 1, the absolute value at 80°K. being higher by the difference in *ad*sorption of the two films. These measurements show clearly that after the absorption process has once been started by raising the temperature from 80° to 120°K., it will continue even at lower temperatures. It should be pointed out that several repetitions of this experiment have shown that absorption was sometimes initiated at temperatures as low as 70° to 80°K., if sufficient time were allowed. The increase observed with lower temperatures seems to be due to the higher surface concentration of molecules in the van der Waals' adsorption layer. Once the formation of the "hydride phase" was initiated at lower temperatures, the growth of this new phase, even at temperatures below the initiation temperature, is probably due to the assistance of nuclei of the new phase that have opened up the passage into the interior. It is concluded that this process is an exothermic type of absorption or solution, possibly the formation of a hydride. In comparing Figs. 2 and 3 it is seen that the van der Waals' adsorption at 20°K. of an unsintered film as measured by the difference of the ordinates of points 1 and 5 in Fig. 3 is five times as large as that of the sintered film in Fig. 2 (difference between adsorption at 20°K. and 80°K.), while the chemisorption is thirteen times larger for the unsintered than the sintered film. This discrepancy may possibly be explained by the increased capillary condensation in the sintered film. Additional studies at very low temperatures are necessary to clarify this point.

It is of interest to note that in the measurement of the hydrogen absorption on the ascending isobar of Fig. 1, a sudden desorption of hydrogen took place, after raising the temperature, followed by a slow sorption that exceeded the initial desorption. This phenomenon is identical to that reported by Taylor and Chou-Shou Liang (4) and earlier by Frankenburger and Messner (4*a*) and suggests that their experiments may deserve reexamination in the light of the findings on nickel, inasmuch as it is possible that Taylor and Chou-Shou Liang may have interpreted an activated absorption process as activated adsorption in the absence of further proof.

From the nature of the isobars, it is clear that the absorption process must be exothermic and that, like adsorption, it is reversible at higher temperature. The heat of *ab*sorption must be considerably lower than the heat of *ad*sorption, inasmuch as the absorption process, which is definitely of the activated type with a measurable temperature-dependent rate, is more readily reversible at high temperatures than the adsorption process. An interesting side light on the nature of the absorption process was obtained through the measurement of sorption isobars on palladium. The adsorption on palladium at liquid nitrogen temperature was shown (through rates of hydrogenation measurements and by CO adsorption) to be comparable to the adsorption on the other metal films investigated, although the initial fast hydrogen adsorption is always followed by a slow sorption that seems to continue indefinitely. When the temperature is raised, the uptake of hydrogen increases in the neighborhood of −100°C. to an amount which is approximately equal to the absorption of one hydrogen atom per atom of palladium. This absorption decreases again rapidly when increasing the temperture to room temperature and more slowly when increasing the temperature further to 100°C., at which point the sorption again is low (about four times larger than that obtained at −196°C.). The 1:1 ratio of hydrogen atoms to palladium leaves no doubt that hydride formation is involved, and reports in the literature (5) have indeed shown that low temperature solution of hydrogen in palladium leads first to a hydride of cubic structure and that raising of the temperature causes this hydride to lose hydrogen with the formation of a hexagonal hydride with a palladium-hydrogen ratio of 3:1. These reports show also that upon raising the temperature still higher the hydride decomposes again. In the case of nickel, the number of hydrogen atoms in solution is too small to be detected by diffraction methods.

Summary

1. Sorption isobars for hydrogen at 0.1 mm. on evaporated nickel films have been obtained from 20°K. to room temperature by aid of a Collins helium cryostat.

2. Slow activated sorption, which is interpreted as sorption of the hydrogen into the metal structure, has been observed in confirmation of the results previously reported.

3. Slow sorption or "hydride phase" formation is exothermic and after initiation by raising the temperature to about 120°K. will continue at much lower temperatures. This effect is probably due to the assistance of nuclei of the new phase that have opened up passage into the interior.

References

1. Beeck, O., Ritchie, A. W., and Wheeler, A., *J. Colloid Sci.* **3**, 505 (1948).
2. Beeck, O., Smith, A. E., and Wheeler, A., *Proc. Roy. Soc.* (*London*) **A177**, 62 (1940).
3. Collins, S. C., *Rev. Sci. Instruments* **18**, 157 (1947).
3a. Beeck, O., *Rev. Modern Phys.* **17**, 61 (1945).
4. Taylor, H. S., and Chou–Shou Liang, *J. Am. Chem. Soc.* **69**, 1306 (1947).
4a. Messner, G., and Frankenburger, W., *Z. physik. Chem.* Bodenstein Festband 593 (1931).
5. Michel, A., *et al.*, *Bull. soc. chim.* [5] **12**, 336 (1945); Owen, E. A., and Jones, J. I., *Proc. Phys. Soc.* (*London*) **49**, 603 (1937). Michel, A., and Gallissot, M., *Compt. rend.* **208**, 434 (1939).

BIOELECTRIC PHENOMENA IN THE MYXOMYCETE PLASMODIUM AND THEIR RELATION TO PROTOPLASMIC FLOW [1]

Noburô Kamiya and Shigemi Abe

From the Department of Biology, Faculty of Science,
Osaka University, Nakanoshima, Osaka

Received November 23, 1949

INTRODUCTION

The possible relation between changes in the electromotive force that may be generated in a plasmodium and the flow of the endoplasm has been an important problem. Watanabe, Kodati and Kinoshita (1937) found that the potential difference between the front and caudal part of the slime mold, *Didymium nigripes*, rises and falls as the protoplasm flows back and forth. Important phases of the problem, however, still remain to be dealt with.

To deal with this problem, one must first measure exactly the variations in the potential difference between the anterior and the posterior part of the flow and, secondly, represent the type of changes in the protoplasmic flow with an adequate scale. The insertion of microelectrodes into the protoplasm in order to measure the potential difference in a plasmodium is not always satisfactory. In addition to damaging a portion of the protoplasm, the measurement is made difficult because of the high resistance of the microelectrodes. Even after the protoplasm has recovered from the injury, a new protoplasmic membrane invariably forms at the place where the electrodes came in contact with the protoplasm; in such an event, all that is measured is the potential across a membrane.

In the present experiment, using *Physarum polycephalum*, we tried the following technique which enabled us to determine the electromotive force of the slime mold directly with a potentiometer without having to use a vacuum tube amplifier.

---

[1] The present work was supported by a grant from the Ministry of Education of the Japanese Government. A part of the experiment was carried out at the Tokugawa Biological Institute (4 Chome, Mejiro, Tokyo) and also at the Botanical Institute of the University of Tokyo.

I. The Electromotive Force of the Slime Mold

(a) *Method of Measurement*

A pair of L-form glass tubes (*A*, *B*) opening in the form of a bowl at one end were filled with agar and placed opposite to each other at a distance of 1–2 cm. (Fig. 1). A small amount of mold *a* and *b* was put on the surface of the agar at the bowl-form openings of the two glass tubes. These two masses of protoplasm were made to connect with each other through a strand of protoplasm suspended in moist air. Before long, these two masses spread over the surface of the agar while the connecting strand fused with them; the whole thus formed one plasmodium. Upon observing the connecting strand under the microscope after fusion had occurred, we noticed a lively back and forth movement of the protoplasm. This completed preparatory steps to be taken with respect to the plasmodium. Our purpose was now to measure the potential difference between the two protoplasmic masses joined by a hanging strand. The total resistance between the two electrodes was usually 0.3–1.0 megohm including that of the connecting strand measuring 70–150 μ in diameter and that of the protoplasmic membrane of *a* and *b* kept in contact with the agar.

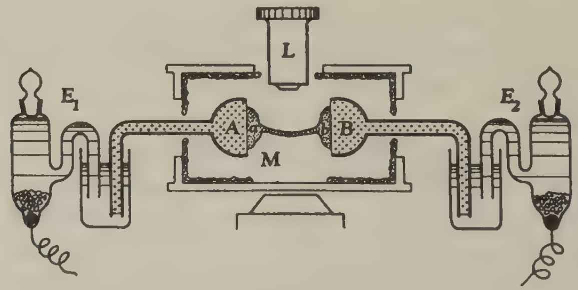

Fig. 1. Slime mold protoplasm between non-polarizable electrodes. *a*, *b*: Masses of protoplasm connected with a strand of the protoplasm suspended in moist air. These masses spread on the surfaces of agar at the bowl-like openings of L-form glass tubes *A* and *B*. *M*: Moist chamber. *L*: Microscopic lens. E_1, E_2: Calomel electrodes.

Since the stock culture was cultivated with tap water and oatmeal on filter paper (cf. Camp, 1936), we used 2 per cent tap water agar for the electrodes *A* and *B* without adding any particular electrolytes. As shown in Fig. 1, *A* and *B* are connected with the calomel electrodes E_1 and E_2 through the pools of a saturated KCl solution. The two calomel electrodes are led to the potentiometer through the current reverser. The galvanometer used had a sensitivity of 1.7×10^{-10} ampere, with an undamped period of 7.7 sec.

The experiment consisted in controlling the position of the sliding contact of the potentiometer without interruption so that no current passed through the galvanometer, and in reading the balancing potentials every 15 sec. with the help of the automatic sound signal.

(b) *The Graphical Representation of the Cyclic Change in the Electromotive Force*

If we plot a series of values of the balancing potential as the ordinate against time as the abscissa, undulating curves are obtained which faithfully show the manner in which the electric potential of the protoplasmic blob *b* varies against that of *a*. Figure 2 is one example of the curves thus obtained. Small circles representing the measured values come most satisfactorily in a smooth undulating line. The error of the measurement is estimated to be not more than 0.1 mv., since the uninterrupted compensation of the electromotive force by means of a potentiometer can be performed keeping the deflection of the galvanometer within 1 mm. from the zero point on the lamp scale.

Such a graph representing the difference in the electric potential in one and the same protoplasmic system may be termed an "electroplasmogram" (EPG) in contrast to the word "dynamoplasmogram" (DPG) which represents the power of protoplasm to flow[2] (Kamiya, 1942, 1943), or the power to do mechanical work.

The period [3] of the EPG is kept nearly constant in regard to one and the same individual insofar as its environment is kept constant, while the amplitude[4] may change markedly on its own accord. In Fig. 2 the mean period amounts to 3 min. 51 sec. and its average amplitude to 6.6 mv.

In Fig. 2 the wave train is found as a whole on the plus side of the base line before it gradually comes down. Let us visualize a smooth line cutting the undulating curves equally into its upper and lower portions. Such a curve can be drawn with a certain degree of accuracy by the same procedure applied to the analysis of the DPG (Kamiya, *loc. cit.*). This is represented in Fig. 2 by a dash-dot line, XY, the ordinate of which is the measure of the electric polarity of the organism. As the line thus drawn in the DPG was called the "polarity-line," the line XY in Fig. 2 is also the

---

[2] By the "power of flow" is meant the motive force responsible for the protoplasmic flow as referred to by Kamiya in his previous papers. In order to prevent confusion of the word "motive force" with the "electromotive force," we should like to avoid Kamiya's former terminology and simply call it the "power to flow."

[3] We should like to refer to the difference between the time coordinates for successive maxima or minima as the period. Even though exactly the same wave form is not repeated, this interval is nearly constant as long as the cyclic oscillation of the wave is vigorous.

[4] Whereas in physics the word "amplitude" means the maximum departure of the value of the wave from the average value, we want to use this term, for the sake of convenience, as indicating the ordinate difference between the maximum of a wave and the point with the same time coordinate on a line connecting its immediately preceding and following minima.

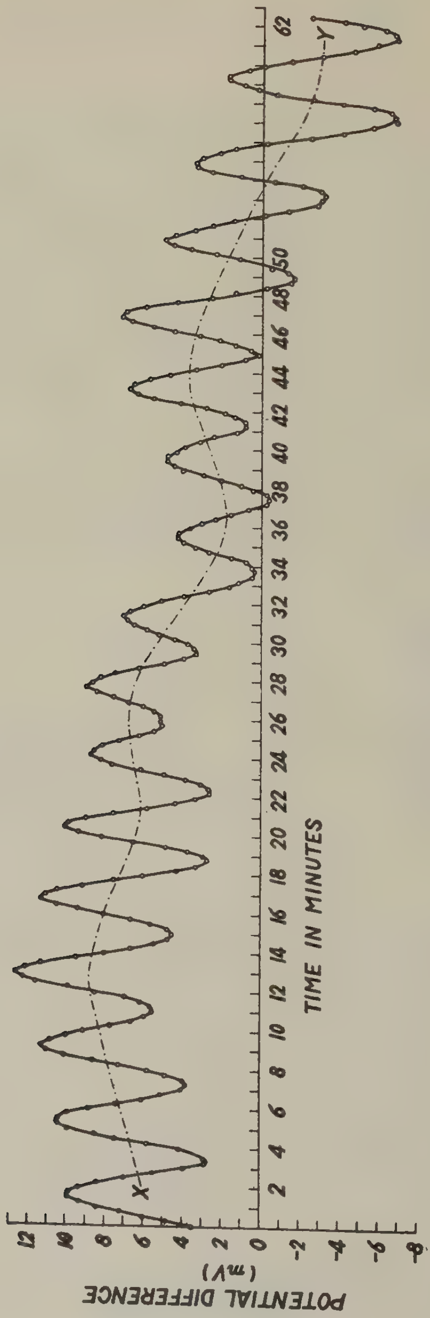

Fig. 2. Cyclic changes with time.

polarity-line with respect to the electric potential. If polarity can be represented as a constant, similar to many oscillatory phenomena in physics, the polarity-line will run parallel to the base line; whereas in the case of the EPG, it is not parallel, but changes spontaneously according to the protoplasm's own scheme, sometimes intersecting the base line, as is also the case in Fig. 2, which shows that the electric polarity of the protoplasm not only changes but also reverses its direction. In Fig. 2, the polarity-line appears as if it had another cycle of a longer period.

(c) *Stoppage of the Protoplasmic Flow and Its Bearing to the Potential Changes*

If we record the time of the reversal of flow while measuring the potential, we realize that the period of the potential variation coincides with that of the back and forth flow of protoplasm, as Watanabe *et al.* have already pointed out.

As a preliminary experiment to determine the causal relation between these periodic potential variations and the protoplasmic flow, we first tried to subject the central part of the connecting strand to local coagulation. Such a coagulation may be brought about by dehydration through use of a concentrated sucrose solution. In this case the back and forth flow of the endoplasm along the connecting tube is stopped because of its blockage. We would like to emphasize that even when the connecting tube was subjected to such a condition locally, the potential difference between the two masses of protoplasm *a* and *b* continued to change as if the streaming were unhindered. Rhythmic changes in potential can be seen even when a part of the connecting strand is entirely eliminated and replaced by a wet cotton thread. Such facts demonstrate that the rhythmic potential variation can proceed quite independently of the protoplasmic streaming and that consequently it cannot be regarded as the so-called streaming potential resulting from the streaming as has been discussed elsewhere (Seifriz, 1937, 1943).

Our next object is to find how the bioelectrical potential changes in relation to the protoplasmic flow. In order to express the streaming exactly, it is not sufficient simply to observe the flow under the microscope and to record the time of reversal as Watanabe *et al.* did. In attacking this problem, we tried to combine dynamoplasmometry and the above mentioned potentiometry using the double-chamber method (Kamiya, *loc. cit.*).

II. Simultaneous Measurement of the Potential Difference and the "Power to Flow"

(a) *Method*

For the purpose of analyzing the streaming phenomena of the protoplasm, it is more adequate to measure its balance-pressure, or the counter pressure just sufficient to stop the flow, than to measure its rate. Our measurements, therefore, were made using a null method both in case of the potential difference and the protoplasmic flow. The setup is shown diagrammatically in Fig. 3. The method of measurement of the power to flow resembles Kamiya's former method and the arrangement for the measurement of the potential is the same as that described in Section I. The structure of the double-chamber and the method of mounting the material are slightly different from either of the two methods just mentioned.

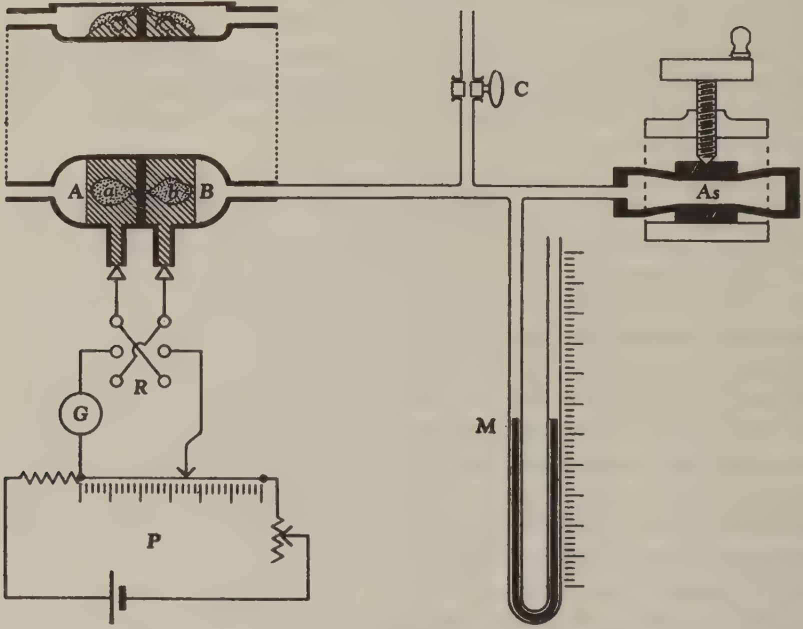

FIG. 3. A diagrammatic illustration of the arrangement for the simultaneous measurement of both the electromotive force and the power to flow. *a*, *b*: protoplasmic masses spreading on the surfaces of agar placed in the compartments *A* and *B* of the double-chamber, the side view of which is shown above. The agar parts in the two compartments which are shaded from upper left to lower right are led to the potentiometer *P* through calomel electrodes (not shown in the figure) and current reverser *R*. *G*: Galvanometer. The right half of the diagram is a setup for controlling and measuring the difference in air pressure between the compartments *A* and *B*. *M*: Manometer. *As*: Rubber aspirator. *C*: Stopcock.

The double-chamber shown in Fig. 3 is made entirely of glass. The partition between the compartments *A* and *B* is 2 mm. in thickness, and on the upper center edge there is a tiny channel measuring 0.5 mm. both in depth and width. The strand connecting the protoplasm *a* and *b* passes through this channel. The possible slight gap between this strand and the channel is filled with vaseline [*cf.* Kamiya (1950)]. The protoplasmic masses *a* and *b* are spread out on the surface of the agar in the compartments *A* and *B*. These pieces of agar are insulated from each other except through the connecting strand of protoplasm and are led to the potentiometer through the calomel electrodes and a current reverser.

The experiment was conducted by two observers. One watched the protoplasmic flow within the connecting tube, adjusting the counter-pressure so that the flow was kept at a standstill. The values of this counter-pressure, or so-called balance-pressure, were recorded from the manometer every 15 sec. upon the sounding of a time signal. The values of the compensation potential were read every 15 sec. simultaneously with the first observer. Such a simultaneous measurement can be achieved satisfactorily with a little skill on the part of the two observers. Before conducting the experiment, we ascertained that, without material, the difference in pressure alone between the two compartments does not cause any perceptible changes in electric potential between them.

(*b*) *Comparison Between the Electroplasmogram* (*EPG*) *and Dynamoplasmogram* (*DPG*)

By plotting on a graph two series of values obtained in the manner mentioned above, we can express simultaneously the changes in the potential difference in the protoplasm and those in the power to flow in the two waves. In the following figures, the potential difference is, corresponding with Fig. 2, designated as plus when the potential of *b* is higher than that of *a*, and as minus in the reverse situation. The balance-pressure is designated with a plus sign when the pressure in compartment *B* is higher than that in *A*, or when the protoplasm has a tendency to flow from *a* to *b*, and with a minus sign for the opposite state.

Figure 4 is one of the examples obtained. The smoothness of the curve is an indication of the precision with which the balancing operation was performed both with respect to the electromotive force and the power of the protoplasm to flow. The upper curve in Fig. 4 is entirely of the same nature as that of Fig. 2. The average periods of the waves of the two curves coincide exactly at 2 min. 35 sec., while the amplitudes fluctuate moderately, averaging 6.4 mv. in the EPG, and 55 mm. hydrostatic head in the DPG. XY and $X'Y'$ represent the polarity-lines of the two waves.

While Fig. 4 is an example of a case when relatively similar waves repeat themselves for a period of time, both EPG and DPG generally change their amplitudes spontaneously to a lesser or greater extent. In Fig. 5 we see conspicuous variations in the amplitudes, but the periods are exactly coincident with each other averaging 3 min. 36 sec. Such pronounced variations in the amplitude as seen in Fig. 5 often appear by turns with a definite interval. The reinforced amplitude period and the

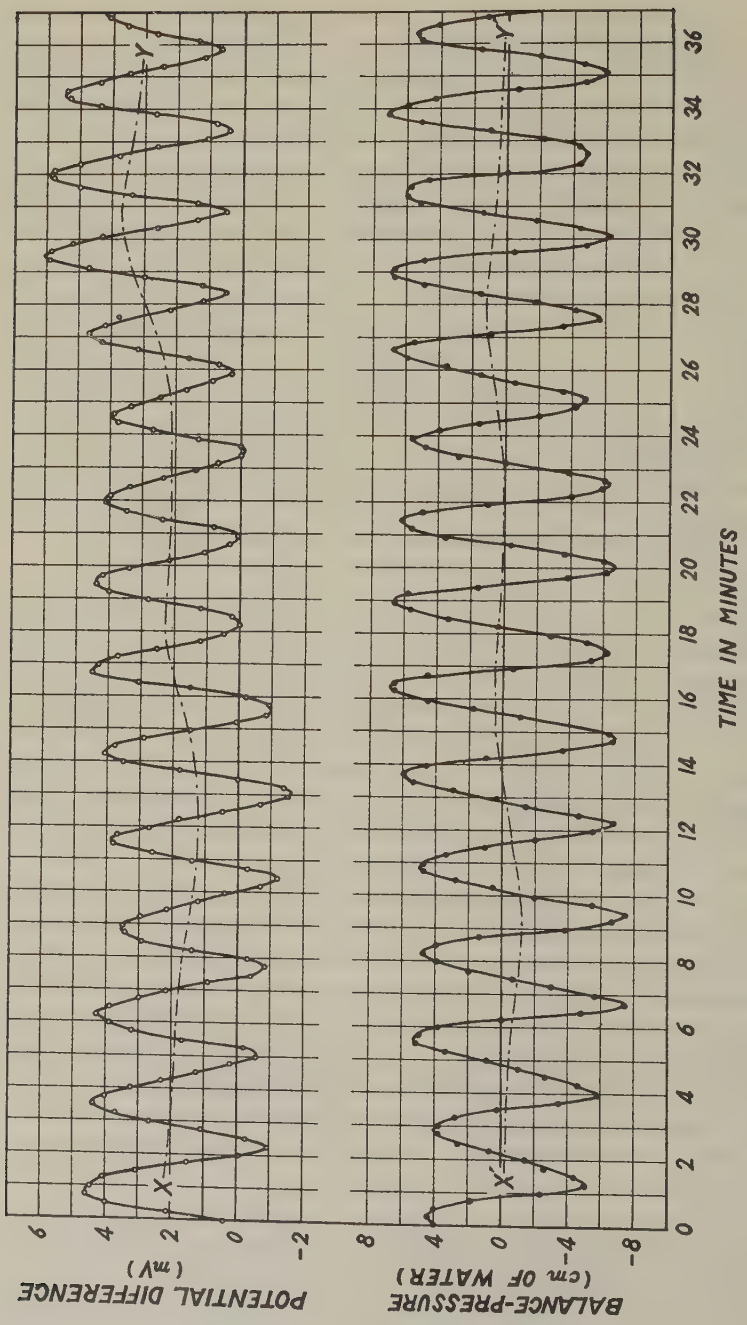

FIG. 4. Cyclic changes with time.

diminished amplitude period thus alternate, forming a beat wave pattern. Such a phenomenon seen in DPG has been explained as a resultant of the interference of two component waves having slightly different periods generated in one and the same protoplasmic system. The undulating curve formed by joining the black circles in Fig. 6 is an example of a DPG of this kind. In Fig. 6 the two waves have been drawn superposed upon each other so as to facilitate the comparison of DPG with EPG as expressed by the open circles.

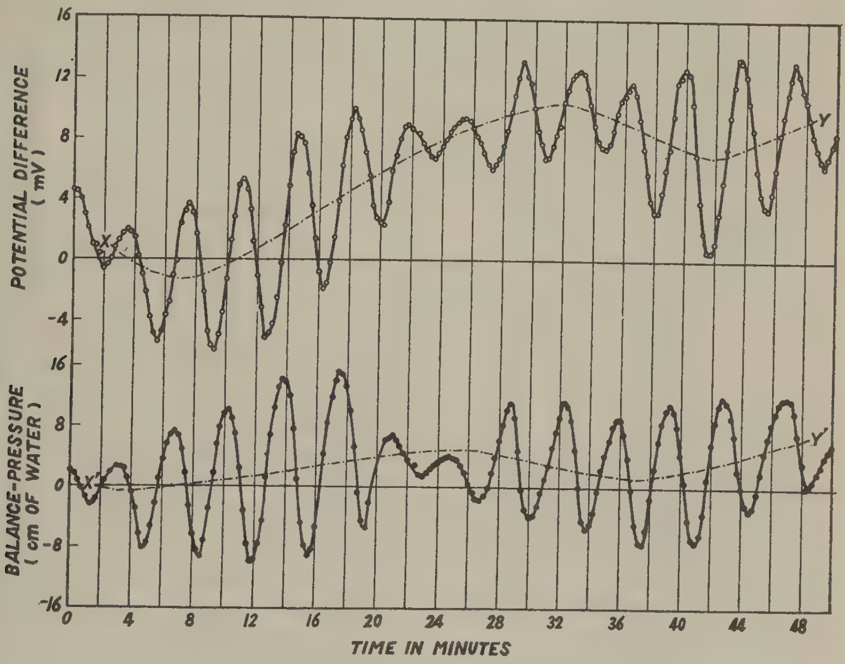

Fig. 5. Cyclic changes with time.

All these figures, which were selected from more than 20 experiments conducted on different samples, show well the relation between the potential difference in the plasmodium and the power of the protoplasm to flow. In these graphs, we have demonstrated most clearly that the period of EPG and DPG is the same. Let us now compare the two kinds of wave from the standpoints of amplitude, wave form, phase relation, and polarity.

In general, the amplitude of EPG changes correspondingly when the amplitude of DPG changes and also the wave form of EPG changes correspondingly when the wave form of DPG changes. This fact is evident in Figs. 5 and 6 which show a striking correlation between the amplitude and the wave form.

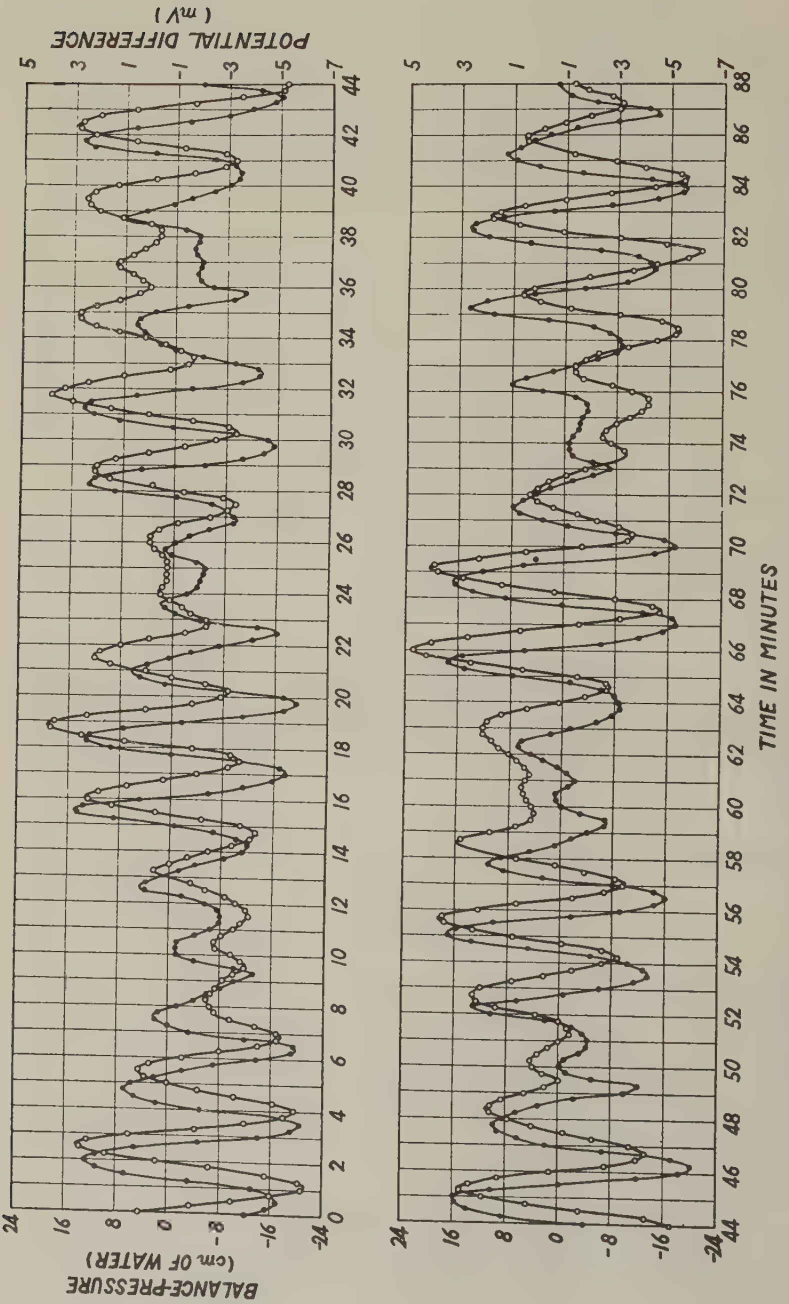

FIG. 6. Superposed representation of the beat-like waves of EPG and DPG. Successive values of the potential difference are shown by open circles while those of the balance pressure are shown by black circles.

By virtue of the perfect coincidence of the periods in EPG and DPG and the high correlation of the wave form and the amplitude, we are in a position to know easily to what wave in the EPG a wave in the DPG corresponds. Comparing the relative phases of two corresponding waves in the EPG and DPG, we find the remarkable fact that the phase of the changes in the power of the protoplasm to flow always preceded the phase of the changes in the electromotive force. No exception has been found to this in all of the experiments so far conducted. This finding utterly contradicts the observations made by Watanabe *et al.* who claimed that the phase of the wave representing the potential variation in a slime mold (*Didymium nigripes*) slightly precedes that of the protoplasmic streaming.

TABLE I

Phase Differences Between EPG and DPG of Different Specimens at Different Temperatures

Exp. no.	Temperature	Period[a] T	Phase difference[b] D	Relative phase difference	
				D/T	$(D/T) \times 100$
	°C	min.	min.		per cent
1	18	5.4 (24)	−2.1	−1/2.6	−39
2	18	3.3 (14)	−0.9	−1/3.7	−27
3	18.5	3.0 (46)	−1.0	−1/3.0	−33
4	19	4.9 (66)	−1.4	−1/3.5	−29
5	19	3.5 (30)	−0.9	−1/3.9	−26
6	20	3.6 (48)	−0.7	−1/5.1	−19
7	21	2.0 (32)	−0.5	−1/4.0	−25
8	21	3.2 (23)	−0.6	−1/5.3	−19
9	22	2.6 (66)	−0.6	−1/4.3	−23
10	23	2.0 (32)	−0.5	−1/4.0	−25
11	23	3.0 (67)	−0.5	−1/6.0	−17
12	23	3.0 (75)	−0.5	−1/6.0	−17
13	24.5	3.5 (16)	−0.5	−1/7.0	−14

[a] Numbers in parenthesis show the number of waves taken for calculating the mean period.

[b] Minus signs of the phase difference mean lag of the phase of the EPG behind that of the DPG.

The precedence of the phase of the DPG to that of the EPG, however, is not always the same, varying considerably according to the temperature and possibly also according to the individual. In Table I are shown the mean values of the phase differences obtained from the results of some experiments carried out at different room temperatures with different specimens.

Figures 4, 5 and 6 are taken from Expts. 9, 6, and 12 respectively. From the above table, we find that the time lag of the phase of the potential difference behind that of the balance-pressure at room temperatures (18–25°C.) is usually 30–90 sec., that is, 2/5–1/7 or 40–15% of the period at the stated temperatures, and furthermore, that the time lag diminishes rapidly with the rise in temperature.

Next we note that there is an intimate correlation between EPG and DPG with respect to their polarities. The changes in polarity are expressed by polarity-lines. In Fig. 4, the same tendency in the rise and fall of the polarity-line of DPG ($X'Y'$) is seen in the polarity-line of EPG (XY). It is remarkable that with respect to the polarity changes there is also a time lag in EPG against DPG. In Fig. 4, the time lag of the polarity of EPG against that of DPG amounts to 3 min., approximately. In that figure the polarity lines XY and $X'Y'$ themselves appear like a wave with a long period. We cannot however, from these data alone, determine whether they merely appear like waves or whether a relatively weak wave with such a long period actually exists as a physical entity comparable to an ordinary cyclic wave.

The fact that the phase lag of a polarity-line is greater than that of the periodic wave is evident also from Fig. 5. Though the polarity-line of EPG in Fig. 5 is far more accentuated than that of DPG, it is sufficiently clear that a common general trend exists in the rise and fall of the polarity-lines XY and $X'Y'$.

Discussion

The power of the protoplasm to flow in the connecting tube, which is shown as the balance-pressure, can be interpreted as the resultant of the summation of the workings of many infinitesimal parts in the protoplasmic masses *a* and *b*; the electromotive force of the plasmodium compensated by the potentiometer can likewise be interpreted as the resultant of the summation of the action of infinitesimal parts in the same protoplasmic masses. The manner of their summation may, however, not be the same for the electromotive force and the power to flow. This is a point to be borne in mind when comparing the two curves of EPG and DPG. But it can be inferred from the close correlation found between the two curves obtained by the above methods that this objection does not appear a serious one with respect to our present purpose.

In the foregoing sections we have dealt with the aspects of the changes in the electric potential which show a close parallel to the protoplasmic flow. The fact that no differences can be observed in the EPG pattern, no matter whether the protoplasmic flow proceeds freely or whether it is stopped by blocking a part of the connecting tube, has led to the conclusion that the potential difference we are measuring is not brought about as a direct result of the flow. In other words, it is not a streaming potential. This conclusion has been further confirmed through the double-chamber method. For we have made clear that not only when the flow has been stopped, but also when on the contrary pressure has been added in such a manner as to accelerate its speed far more than in its natural condition, the potential difference between *a* and *b* is not affected in any discernible manner.

On the other hand, however, the fact that the phase of the potential wave lags always behind that of the balance-pressure wave indicates that the electric potential cannot be the direct cause generating the power to flow. As a further proof of this, it may be added that the difference of an electric potential (0.01–4.0 v.) applied artificially between the compartments *A* and *B* for a short period of time does not exert any noticeable effect upon the wave pattern of DPG and its polarity-line. Therefore any attempt to ascribe the flow in the slime mold to the localized potential difference, or to regard the flow as a phenomenon of electroendosmosis, must be discarded in the light of the above findings.

The foregoing facts have clearly indicated that even though a high correlation is seen between the potential difference and the protoplasmic flow, it does not mean a simple relation of cause and effect exists between them. Why is it then that the protoplasm manifests such a close correlation between its electromotive force and the power to flow under normal conditions? This is an important problem directly connected with the nature and origin of the bioelectric potential and also with the mechanism of the protoplasmic flow itself. Though in the present paper our purpose has been only to demonstrate the parallelism between the bioelectric phenomena and the protoplasmic flow in the material left under normal conditions, it is our hope that a series of experiments we are conducting at present may throw some light on this problem. The results of these experiments show that when the plasmodium is treated with various chemicals such as substances inhibiting respiration, the electric potential and the power to flow mostly manifest a different mode of reaction. In such cases the parallelism thus no longer exists between EPG and DPG as to the wave pattern, amplitude, and polarity.

We should like to add that besides the slow cyclic changes in the electromotive force described above, there can be discerned in the plasmodium other rapid, transient changes. These transient changes in the bioelectric potential are sometimes repeated spontaneously at irregular intervals and intensity. This is shown by the sudden swing in the galvanometer used as zero-pointer, the deflecting beam on the lamp scale being soon restored to a position that is approximately the same as formerly.

We found that similar transient changes in the electric potential can be very easily induced artificially by giving a slight tap on a part of the double-chamber from the outside, or, in case of a setup like the one shown in Fig. 1, also by giving a light mechanical shock to one of the electrodes. And we ascertained that the protoplasm on that electrode which had received the mechanical stimulus always became negative in relation to the one that had not received it. Within certain limits, this negative variation is the more intense the stronger the mechanical shock, so that the all-or-none law does not seem to exist between the stimulus and the electric response. Yet, as hinted by the above simple experiments, this is none other than the "action potential" of the plasmodium. A detailed report as to its nature will be presented elsewhere (Tasaki and Kamiya, 1950). We can say that the cyclic changes in the electric potential having periods of several minutes we have dealt with in this report are to be considered as entirely different from those transient changes with respect to the mechanism of their generation.

SUMMARY

1. Potential differences between the two loci of the slime mold (*Physarum polycephalum*) connected with a single strand of protoplasm were determined successively and the mode of their variation in relation to time was represented graphically.

2. The electromotive force of the slime mold changes according to a rhythmic pattern, the period of which is the same as that of the cyclic back and forth steaming, and the amplitude of which increases and decreases spontaneously under constant conditions, usually within 10 mv.

3. The rhythmic change in the potential occurs whether the flow along the connecting strand is allowed to take place freely, or if it is made to stop by means of local blocking of the strand, or by application of a balancing pressure.

4. Satisfactory results have been obtained in an attempt to represent graphically the simultaneous variation in potential (electroplasmogram or EPG) and the power to flow (dynamoplasmogram or DPG) from one and the same plasmodium with the aid of a double-chamber method.

5. In addition to the periods of these two curves being the same, a close relationship between them under normal conditions is seen with respect to amplitude, wave form, and polarity.

6. The phases of the two waves do not coincide with each other, that of the EPG always lagging behind that of the DPG usually by 30–100 sec., or 2/5–1/7 of their period.

7. The local differences in the bioelectric potential in a plasmodium cannot be regarded as the direct result of the protoplasmic flow or as the streaming potential. Nor is it to be considered as the direct cause responsible for the flow; in other words, the protoplasmic flow is not explained as a phenomenon of electroendosmosis.

8. Besides the slow cyclic variation mentioned above, there is a quick, transient potential variation which is elicited not only spontaneously at times, but also artificially through use of weak mechanical shocks.

REFERENCES

CAMP, W. G., *Bull. Torrey Botan. Club* **63**, 205 (1936).

KAMIYA, N., Physical aspects of protoplasmic streaming. In The Structure of Protoplasm (edited by W. SEIFRIZ), pp. 199–244. Ames, Iowa, 1942.

KAMIYA, N., *Kagaku* [*Science* (*Japan*)] **13**, 351, 390, 438 (1943) (in Japanese).

KAMIYA, N., The protoplasmic flow in the myxomycete plasmodium as revealed by volumetric analysis. *Protoplasma*, in press (1950).

SEIFRIZ, W., *Science* **86**, 397 (1937).

SEIFRIZ, W., *Botan. Rev.* **9**, 49 (1943).

TASAKI, I., AND KAMIYA, N., Electrical response of a slime mold to mechanical and electrical stimuli. *Protoplasma*, in press (1950).

WATANABE, A., KODATI, M. UND KINOSHITA, S., *Botan. Mag.* (*Tokyo*) **51**, 337 (1937) (in Japanese with German résumé).

THE USE OF WHITE LIGHT IN DETERMINING PARTICLE RADIUS BY THE POLARIZATION RATIO OF THE SCATTERED LIGHT

Milton Kerker

From the Chemistry Department, Clarkson College of Technology, Potsdam, New York

Received October 26, 1949

The polarization ratio, ρ, of the light scattered by a spherical particle illuminated with parallel, unpolarized, monochromatic light is given by Rayleigh's law when $\alpha = \frac{2\pi r}{\lambda} < 0.05$. r is the particle radius and λ is the wavelength of the light.
Thus

$$\rho = \frac{b}{a} = \cos^2 \gamma, \qquad [1]$$

where a and b are the intensities of the vertical and horizontal components of the scattered light and γ is the angle between the direction of propagation of the scattered light and the reversed direction of propagation of the incident light.

ρ increases for larger values of α until $\alpha > 2.5$ when it is no longer monotonic. La Mer (1, 2, 3) and others (4) have used the value of ρ in this intermediate size range to characterize the particle radius.

The measurement of ρ is generally difficult for dilute systems of small colloidal particles because of the low intensity of the scattered light. The difficulty of measurement can be decreased considerably if white light instead of monochromatic light is used. Although existing tables of polarization ratio as a function of radius are applicable only to monochromatic light, it is possible to calculate the dependence of ρ on radius for white light.

The intensity of light scattered at wavelength λ is

$$\begin{aligned} a &= k\lambda^2 i_1 S(\lambda) P(\lambda) \\ b &= k\lambda^2 i_2 S(\lambda) P(\lambda), \end{aligned} \qquad [2]$$

where i_1 and i_2 are functions which have been tabulated for various values of index of refraction, angle of observation and α (5); $S(\lambda)$ is the relative sensitivity of the eye or photosurface; $P(\lambda)$ is the relative intensity of the light source. For a given particle radius, the values of a and b will vary as a function of wavelength. The intensity scattered by white light is obtained by intergrating over all wavelengths, and the polarization ratio is given by

$$\rho_w = \frac{\int_\lambda b d\lambda}{\int_\lambda a d\lambda}. \qquad [3]$$

The polarization ratio calculated as a function of radius for index of refraction 1.44 and $\gamma = 90°$ and $\gamma = 110°$ is shown in Table I and plotted in Fig. 1. The average of the photopic and scotopic sensitivity of the eye (6) and the spectral output of a tungsten filament lamp at 2700°C. were used for $S(\lambda)$ amd $P(\lambda)$.

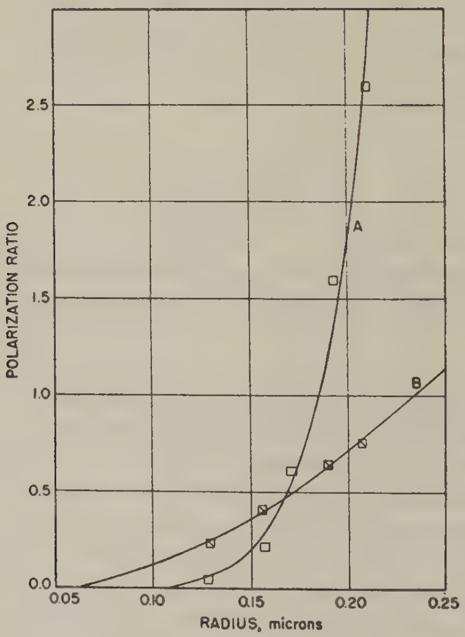

FIG. 1. Polarization ratio *vs.* particle radius.
A. $\gamma = 90°$. □ Calculated for $\lambda = 0.545\mu$.
B. $\gamma = 110°$. ⧅ Calculated for $\lambda = 0.540\mu$.

The curves are smooth monotonic functions of particle radius. Furthermore, they resemble the curves for monochromatic light so that it is possible by choosing an appropriate wavelength to treat the data as if the light used were monochromatic. The square points in Fig. 1 were cal-

TABLE I

Polarization Ratio as a Function of Particle Radius for White Light

Radius	Polarization ratio, $\gamma = 90°$	Calculated radius, $\lambda = 0.545\mu$ $\gamma = 90°$	Polarization ratio, $\gamma = 110°$	Calculated radius, $\lambda = 0.540\mu$ $\gamma = 110°$
μ		μ		μ
0.06	0.002	0.078	0.13	—
0.08	0.003	0.091	0.13	0.06
0.10	0.012	0.108	0.16	0.095
0.12	0.050	0.134	0.23	0.125
0.14	0.150	0.148	0.35	0.146
0.16	0.33	0.164	0.44	0.159
0.18	0.74	0.176	0.58	0.180
0.20	1.49	0.185	0.69	0.194
0.22	2.59	0.206	0.91	0.219

culated for monochromatic light using $\lambda = 0.545\mu$ at $\gamma = 90°$ and $\lambda = 0.540\mu$ at $\gamma = 110°$. The results obtained with these wavelengths agree with those for white light to within 0.01μ of radius.

REFERENCES

1. SINCLAIR, D., AND LA MER, V. K., *Chem. Revs.* **44**, 245 (1949).
2. KERKER, M., AND LA MER, V. K., "Particle Size Distribution in Sulfur Hydrosols by Polarimetric Analysis of the Scattered Light." To be published.
3. LA MER, V. K., INN, C. Y., AND WILSON, I., "The Methods of Forming, Detecting and Measuring the Size and Concentration of Liquid Aerosols in the Size Range of 0.01 to 0.25 Microns Diameter." To be published.
4. WHITE AND HILL, *J. Colloid Sci.* **3**, 251 (1948).
5. LOWAN, A. N., Tables of Scattering Functions for Spherical Particles. Applied Mathematics Series, 4. Department of Commerce, National Bureau of Standards.
6. HECHT, S., AND WILLIAMS, R. E., *J. Gen. Physiol.* **5**, 1 (1922).

MICELLES AND X-RAYS

W. Philippoff[1,2]

Chemistry Department, Stanford University, Stanford University, California

Received June 20, 1949; revised December 27, 1949

Introduction

The particles of colloidal solutions can be small crystals as in the case of inorganic sols, aggregates of small molecules as in the case of association colloids such as detergents and dyes, or single molecules as in the case of high polymers. The aggregates of the association colloids, which can dissociate reversibly with change of the concentration, are called micelles.

This paper is concerned with the results of the application of x-ray diffraction analysis to the investigation of the structure of the micelles of soaps or detergents. All the results available in the literature have been summarized and supplemented with new, as yet not completely published results of the author. From these results the basic phenomena are summarized and the known quantitative mathematical relations indicated. Then by a generalizing treatment of all the evidence a tentative picture is evolved which would have to be tested by further experiments.

Experimental

Following a few scattered observations (1, 2), the subject of the investigation of the micellar structure by means of x-rays has received an intensive treatment, beginning in 1936, by Hess and his associates (3–12). It was taken up in the United States in 1943 in connection with rubber research, chiefly by the Stanford group under McBain (13–15), the Chicago group under Harkins (16–18), and the Shell Development Company of Emeryville (19).

The following points or theses can be extracted from the mass of experimental evidence available and seem important to use in developing a picture of the phenomenon.

Conditions for an X-Ray Pattern

The x-ray diffraction pattern of concentrated solutions of detergents is confined to the *colloidal state* or the existence of micelles. Alcoholic solu-

---

[1] Lever Brothers Postdoctorate Research fellow.

[2] Present address: School of Mines, University of Minnesota, Minneapolis, Minnesota.

tions of detergents, for example, which are ordinary solutions even at concentrations of 60% solute, do not give any patterns (8, 10), whereas much more dilute colloidal solutions in water give sharp patterns. As the example of Aerosol OT[3] shows (20, 25), one can get patterns in nonpolar solvents in some cases.

Detergent properties are *not* correlated with the formation of x-ray diffracting planes which appear only at higher concentrations. Indeed there are some detergents that do not give any patterns at all (15).

X-ray diffracting planes appear independently of the sign of the electric charge of the micelle: ordinary anionic soaps, cationic detergents and even nonionic ones all show the x-ray patterns with much the same experimental relations. This encourages one to generalize and use ionic, nonionic or even nonaqueous solutions of detergents for the elucidation of the micellar structure. This procedure may be questionable, but the results appearing subsequently show that it works.

Kinds of Patterns

The x-ray investigation of a concentrated solution of a detergent gives generally 3 diffraction rings besides the "water halo." An outer one, called the "short spacing," corresponds to 4.5 A calculated by the Bragg equation. This spacing is common to many detergents and, since it shows very little variation with different influences, will not be discussed at length. The second is a spacing nearly equal to the double length of a soap molecule. It was called the "M-Band" by Harkins and Mattoon (21) and is apparently independent of the concentration of the detergent. The innermost "I-Band" shows a remarkable dependence on many factors and will be dealt with principally. This band is generally related to a spacing definitely larger than the double length of the soap molecule.

Concentration Dependence of the "I-Band"

The first experimental variable investigated (5) was that of the concentration (in wt. %) on the "I-Band" for isotropic micellar solutions. As an example of this effect, data on potassium laurate and sodium oleate, measured by several independent investigators, are shown in Fig. 1. In both cases the relation is essentially the same: a linear decrease of the long spacing with increasing concentration, with all the values being greater than the calculated or measured length of the double molecule of the anhydrous soap. The question arises as to whether this linear relationship is valid beyond the concentration range investigated, where the solubility determines the maximum possible concentration. Investigations of substances having a very great solubility, or even complete miscibility with the solvent can give an answer.[4] In Fig. 2 the concentration dependence of the long-spacing for nonionic water-miscible detergents is shown, together with the aqueous and nonaqueous systems with Aerosol OT. These investigations show that the linear relation between the long-spacing and the concentration is valid in practically the whole range of concentrations when there are no phase changes. At very high concentrations the spacings of the solutions sometimes merge exactly into the values of the solid.

---

[3] Sodium salt of di-(2-ethylhexyl) ester of sulfosuccinic acid. American Cyanamid Co.

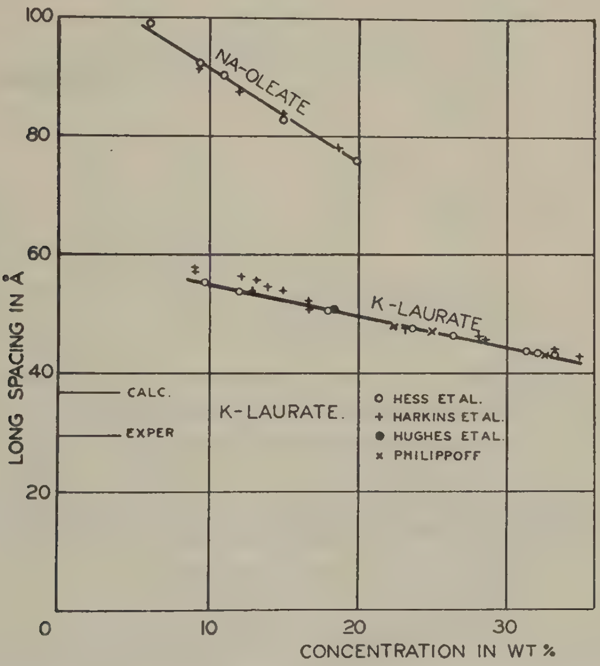

FIG. 1. Dependence of the long-spacing of aqueous solutions of potassium laurate and sodium oleate on concentration. Calculated and experimental values for the length of two potassium laurate molecules included (15).

This linear law seems to be generally valid for the *micellar state*. For some nonionic detergents (14) other relations have been obtained, but only in the liquid–crystalline state.

From the investigation of the dependence of the "I-Band" on concentration, it can be definitely concluded that the diffractions appear at a concentration much higher than the "first critical concentration of

---

[4] Of course, only such experiments can be considered valid that are performed in a concentration range in which no phase changes occur. Detergents form liquid crystals very easily at higher concentrations. In dubious cases the investigation of the binary phase-diagram, using the fusion or transition points, has proved valuable.

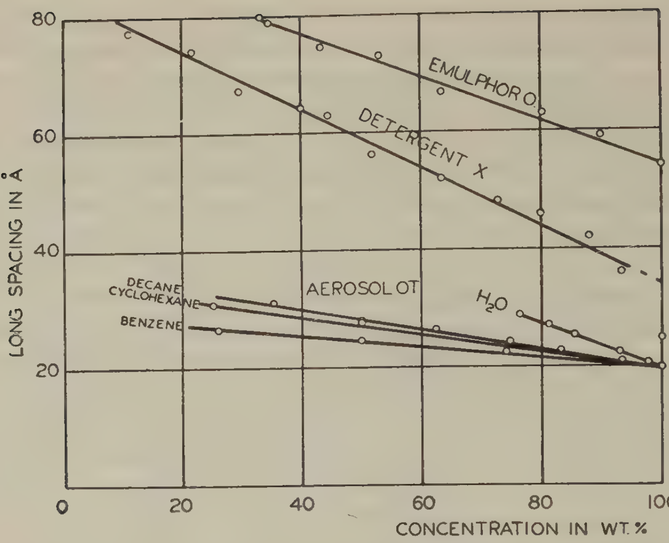

FIG. 2. Dependence of the long-spacing of aqueous solutions of Detergent X and Emulphor O aqueous and nonaqueous solutions of Aerosol OT on concentration.

micelle formation CMC," the usual limit being 10–20% detergent. The lowest concentration ever measured is 6% sodium oleate. One has therefore to refer to a second or "x-ray CMC" as we did in 1939 (4). The "M-Band" however appears at much lower concentrations, sometimes even comparable to CMC: the lowest concentration measured is 1.28% potassium palmitate (18). The lowest measurable concentration depends in all cases on the solute and solvent investigated.

X-Ray Investigation of Solubilization

It is a well-known phenomenon that solutions of detergents have the property of dissolving water-insoluble substances, such as liquid hydrocarbons and even dyes, to form clear isotropic solutions. This has been called "Solubilization" by McBain (22). In nonaqueous solutions of detergents, water can be solubilized to an appreciable extent; this has been called "Blending" by McBain and Palit (23). When one compares the x-ray results on a solubilized (ternary) system with those of the binary system it is observed (6) that the intensity of the pattern and its sharpness increase, the long-spacing itself is changed by a usually positive amount Δd, whereas the short-spacing is unchanged. This increase in long-spacing, for both the I- and M-bands, with solubilization follows a linear empirical law (6):

$$\Delta d = k \text{ (gram "oil"/gram detergent).} \qquad [1]$$

This relation has been extensively investigated in this country in connection with the emulsion-polymerization of synthetic rubber. In Fig. 3 the solubilization curve for heptane in a 25% aqueous solution of potassium laurate is shown (17). In Fig. 4 is shown the counterpart, the solubilization of water in nonaqueous solutions of Aerosol OT (20). In this case the enormous amount of solubilized substance, together with an increase of long-spacing of about 90 A, is to be noted. The values are nearly 10 times those for aqueous systems.

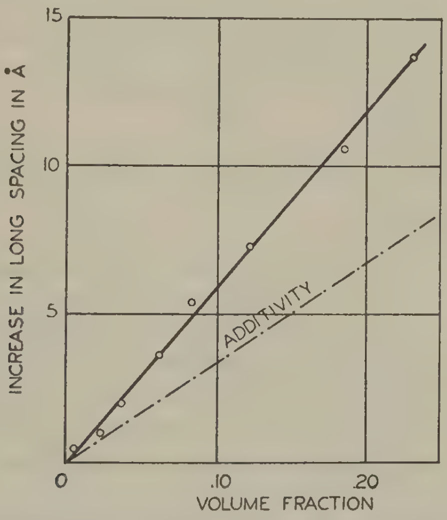

FIG. 3. Solubilization curve of heptane in aqueous 25% potassium laurate [Mattoon(17)].

The effect of increase in long-spacing is confined to the solubilization of nonpolar "oils" in aqueous solutions of detergents, and water in hydrocarbon ones. *m*-Cresol gives *negative* values of Δd (9), but the linear law is fulfilled as is shown in Fig. 5. This has been recently more fully investigated for the solubilization of alcohols in solutions of sodium dodecylsulfate by Harkins and Mittelmann (24). It is interesting to note that dimethylphthalate, insoluble both in water and hydrocarbons, is solubilized in aqueous solutions of detergents with a negative Δd (15).

Added electrolytes influence the long-spacing of anionic and cationic detergents only very slightly, causing a decrease or small increase (6, 10, 15, 17).

It is well-known that sometimes a small amount of solubilized substance is needed to induce an x-ray diffracting structure. Examples are aqueous solutions of laurylsulfonic acid (26), and the nonionic Triton X-100[5] (14). In the case of nonaqueous solutions of hexanolamineoleate

[5] A condensation product of diisobutylphenol and ethylene oxide. Rohm & Haas Co.

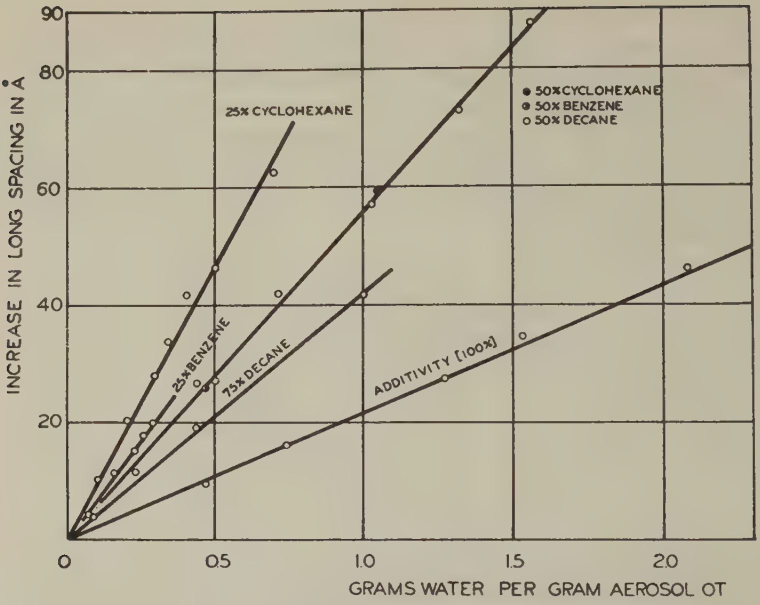

FIG. 4. Solubilization curves for water in nonaqueous solutions of Aerosol OT. Percentages refer to g. Aerosol OT/100 g. (Aerosol OT + solvent) (20).

(15) and especially Aerosol OT in decane (or dodecane) (20, 25), the building up of the structure by adding 0.25–0.30 g.H_2O/g. Aerosol OT could be shown.

Related to the solubilization curve is the phenomenon investigated by the Shell Dev. Co. (19). One would expect from the greater x-ray scattering of liquids containing heavy atoms, such as bromine and iodine,

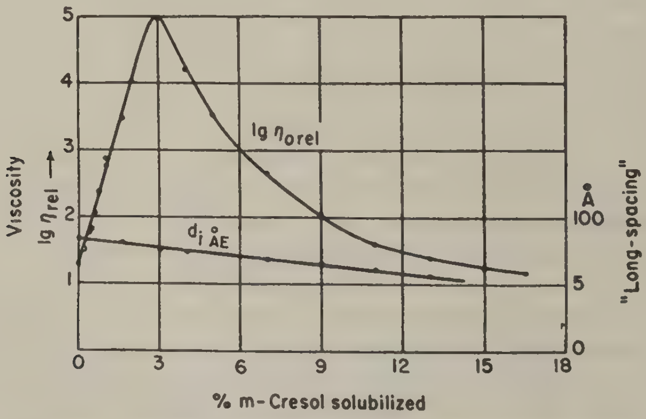

FIG. 5. Solubilization curve and viscosity for *m*-cresol in aqueous solutions (13, 85 w%) of sodium oleate (9).

that solubilization of these compounds would give exceptionally intense patterns; but this is not the case. For instance when bromoform is solubilized in aqueous solutions of potassium laurate the lines first fade out and then reappear at higher amounts solubilized. Hydrocarbons, however, as previously mentioned, enhance both the intensity and the sharpness of the pattern.

Influence of Temperature

There is *no* great effect of temperature on the long-spacing. Sodium oleate solutions and 25% potassium laurate failed to show any temperature effects on the long-spacing (27). Whether there is an effect on the intensity and sharpness of the x-ray pattern, remains to be ascertained. This matter deserves further investigation.

Mechanical Properties and X-Ray Diffraction Patterns

The first experiments performed (6, 10) showed that the mechanical properties of soap solutions, especially the viscosity, have apparently *no* relation to the x-ray pattern. Investigations of the effect of solubilized *m*-cresol on the long-spacing and on the viscosity of aqueous sodium oleate solutions (9) showed an increase in viscosity of 10,000-fold at the maximum (Fig. 5), whereas the long-spacing showed a gradual linear decrease. Some nonionic detergents such as Emulphor O[6] give a transparent gel at about 50% concentration, the long-spacing only showing the usual increase with decreasing concentration (14); see similar phenomena with solutions of sodium dodecyl sulfate (24). It has already been said that additions of electrolytes scarcely affect the I-Band, the viscosity been strongly affected (10).

Our work has demonstrated that if soap solutions show a non-Newtonian flow (or structural viscosity), one also has an orientation effect in the streaming system, investigated by x-rays. The long-spacing alone shows orientation, the diffracting planes being oriented parallel to the axis of the capillary (3, 11, 28). These solutions also show flow-birefringence (29, 28, 9).

X-Ray Patterns of Mixtures

Not only do the pure soaps or detergents show an x-ray diffraction pattern, but so also do natural or artificial mixtures (30). In the solid or in solution, only one spacing for the mixture is measurable. This spacing shows a linear dependence on the molar concentration of the mixture, as has been found by Harkins (16) and by Hess and Kiessig (12) for C_6-, C_{12}-, C_{14}-, and C_{18}-soaps. This is analogous to the Vegard-rule for the spacing of binary metal alloys which form solid solutions, such as copper–gold. The same phenomenon occurs for the fatty acids and even paraffins. The existence of only one spacing has been proved for a ternary system $C_6 + C_{12} + C_{18}$ (12). However with the salts of the long-chain dibasic acids (12) spacings of both the constituents showed up.

---

[6] A condensation product of oleyl alcohol and ethylene oxide. General Dyestuffs Co.

Intensity and Sharpness of the Patterns

The intensity of the short-spacing at different concentrations was investigated by Stauff in 1939 (5), that of the long-spacings in first approximation by Mattoon in 1948 (18). These last measurements are shown in Fig. 6. Both the "M-Band" and "I-Band" were measured over a wide range of concentrations.

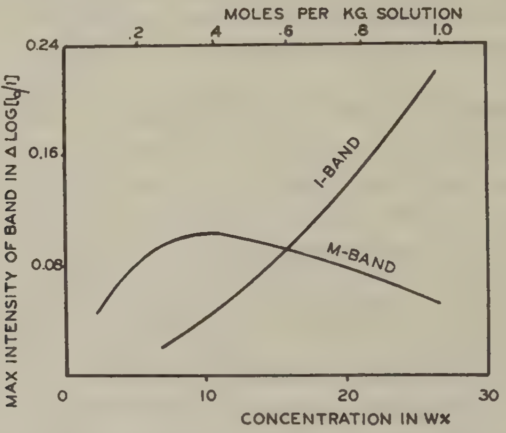

FIG. 6. Dependence of the intensity of the "M" and "I"-Bands on concentration for aqueous solutions of potassium myristate [Mattoon (18)].

The sharpness of the short-spacing was found to be comparable with that of liquid palmitic acid (5). That of the long-spacing could not as yet be referred to any number of diffracting planes, approximations of 3–7 planes being given in literature.[7]

Formation of Liquid Crystals

Besides micelle formation, soap or more generally detergent systems form so-called "liquid crystals" readily with the solvent alone, or with solubilized substances. The liquid crystals are to be distinguished experimentally from a micellar solution by giving much sharper x-ray patterns, usually with higher orders present. They also show orientation in the capillary generally used to contain the sample in these experiments, the diffraction planes being parallel to the axis of the capillary. In some systems even point-diffractions have been observed (26). Liquid systems can change their long-spacing with concentration, and in one system there can be several different structures of liquid crystals (26). They show a very brilliant birefringence under the polarizing microscope, generally in spots of uniform orientation. Liquid crystals have usually a high and anomalous viscosity or a yield value.

---

[7] W. Philippoff and J. T. Davies [*Nature* **165** (1950)] determined experimentally that generally about 4 diffracting planes could account for the sharpness of the diffraction patterns of micellar solutions.

From all these phenomena, the following quantitative mathematical relationships can be obtained and must be explained by a satisfactory theory.

A. The essentially linear decrease of the long-spacing with increasing concentration.

B. The linearity of the curve for the long-spacing vs. amount solubilized (solubilization curve).

C. The validity of the "Vegard rule" for the long-spacing of mixtures.

Discussion

A. Models for the Micelle

For the simplest form of theory, one has to make assumptions as to the arrangement of the molecules of the detergent in the micelle and as to the mechanism of solubilization. The assumption made by us in 1937 (3, 7) and 1939 (6) is the laminar x-ray micelle in which the soap molecules are arranged in planes like a brush. The possibility of such an arrangement could be conclusively proved by the work of Langmuir (31) on monolayers, Harkins (32) on surface phenomena, and Perrin (33) on soap films in 1915–17. The concept of "neutral micelles" as double layers of soap molecules has been used by McBain in his lecture demonstrations since 1923, a model having been published in 1929 (34).

This first assumption explains many of the observed effects, even if one does not assume any definite lateral size of the micelle or any definite number of diffracting planes in the kinetic unit. The "short-spacing" is then the lateral distance between the parallel chains. From this separation, the area per chain can be calculated. Depending on the specific assumptions made, values between 19.5 (4) and 28 sq. A (16) have been given in the literature, 25 sq. A being a fair approximation. This "side spacing" occurs also in the diffraction patterns of liquid hydrocarbons and melted fatty acids (7). A comprehensive treatment of the problem, taking into account the interaction of the carbon atoms of neighboring chains with each other and the theory of x-ray diffractions of liquids, was given by Warren (35) and Zachariasen (36). The values calculated are slightly larger than those determined from measurements on compressed (solid) monolayers : 20.5 sq. A.

The long-spacing would then be measured in the direction of the length of the molecules. We see here that the minimum value for this is the length of the double molecule. The preliminary assumption of Hess and Gundermann (3) of the identity of the long-spacing (I-Band) with the double length of the molecule has not been substantiated, the measured long-spacing being *longer* than the double length of the molecule either calculated or measured in the solid. This led us in 1939 (4) to assume a *water layer* between the double layers of molecules. Part of the water layer could be accounted for by the hydration of the micelle. Solubilization was explained by the formation of a layer of "oil" between the hydrophobic ends of the soap molecules (6), the long-spacing measuring the combination of the soap molecules, the water layer, and the "oil" layer.

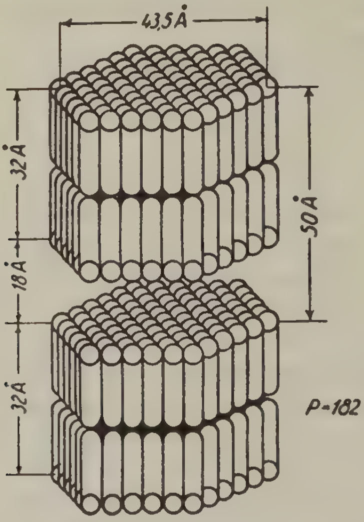

FIG. 7. Tentative model of a micelle of potassium laurate (9) (1941).

The next step is to decide how large the diffracting unit is, how many planes are included in a micelle, and how large it is laterally. The first assumption of Hess and Gundermann (3) that the micelle is a small crystal is disproved by the notable dependence of the long-spacing on concentration. Stauff (7) assumed "Grossmizellen" including the whole diffracting unit. His specific assumptions of 5–7 diffracting planes (~ 250 A) and a plate shaped particle of 2000–3000 A laterally (~ 2500 A) give with the above mentioned area of 25 sq. A/molecule and a molecular weight of 250/chain a micelle of a molecular weight of 300 million, which would have to be checked by other methods.

The author in 1941 (9) assumed the micelle to consist of only *one* double-layer of molecules, the definite lateral extension being fixed by the micelle size measured at or near the CMC (about 50–100 molecules/micelle) Fig. 7. The long-spacing would then be caused by the "spatial lattice" or arrangement of these small micelles in the solution. From data published before 1941, Dervichian developed independently the same picture (37). It is important that according to this model the micelles are practically spherical, but not isotropic, the hydrophilic surfaces being oriented to each other. The conclusions made for the laminar micelle of indefinite lateral size are all valid for this model. Harkins in 1948 (38) advocated the same idea, assigning the "M-Band" to diffractions arising from the single double-layer. It thus seems that the short-spacing and the "M-Band" are "inner effects," arising from the order in a single micelle; the "I-Band" is an "outer effect" determined by the interaction of the micelles, using the terminology of the x-ray diffractions of gases and liquids.

A strong support for the laminar micelle (of any size) is the measurement of diffractions of the solutions of salts of dibasic acids (hexadecandicarbonic acid) (12), which give very similar patterns to the usual soap solutions, including the "water layer" increment, but do *not* show any solubilization of hydrocarbons as the hydrophobic inner surface is not present.

Several investigators, beginning with Reychler (39), McBain (40) (ionic micelle), and Hartley (41, 42), have advocated a spherical micelle the outer surface of which is formed by the hydrophilic "heads," the inside of the hydrocarbon "tails" of the soap molecules. To explain the x-ray diffractions, an "outer effect" is then postulated. Corrin (43) applied the theory of the x-ray diffractions of gases or liquids to this model and pointed out that a laminar micelle was not essential to cause diffractions in soap solutions when one assumed an appropriate distribution curve for the micelles. The discussion of this model as to the occurrence of the short-spacing and "M-Band" has as yet not been published.

Without going into the explicit theory of the x-ray diffractions, we can develop several quantitative relations that allow us to understand some of the effects described.

B. Binary Soap-Water Systems

Considering a laminar micelle with no definite lateral size, one can calculate geometrically how the long-spacing should depend on concentration. Three cases can be distinguished.

1. The water goes only between the lamellar diffracting planes of the solid, *i.e.*, one-dimensional swelling.
2. The water swells a structure of rods, one dimension of the structure being approximately constant, *i.e.*, two-dimensional swelling.
3. The micelles of constant size are distributed in equipartition in space, the structure swelling up in all directions, *i.e.*, three-dimensional swelling.

If one tries to apply geometry to this problem, it is clear that only the *volume* is important, not the mole ratio or weight percentage. One must therefore recalculate all the experimental data on the basis of the volume fraction c_v = volume of soap/volume of solution. For many detergents, however, the density is very near unity, so that the weight per cent give approximately $100 \times c_v$.

In the first case, one calculates the spacing of the binary system d from the spacing d_0 of the solid and the volume fraction c_v as follows:

$$d = d_0/c_v. \tag{2}$$

It is convenient, as we shall see further on, to use the amount in grams of added solvent per gram solid. The increase in long-spacing Δd is then:

$$\Delta d = d_0\ (\rho_{\text{solid}}/\rho_{\text{solvent}}) \times \text{g.}_{\text{solvent}}/\text{g.}_{\text{solid.}} \tag{2a}$$

This gives a linear relation between Δd and the solvent added (in g./g.) which is easily tested on experimental data. The slope of the straight line is exactly determined. Only when the slope has the theoretical value ($d_0\ \rho_{\text{solid}}/\rho_{\text{solvent}}$) does the log d − log g./g. plot give a straight line with the slope − 1, as has been used by Marsden (14) for the interpretation of his numerous results. Equation [2] is valid when the volumes of both components are additive, but the plot of d against $1/c$ as is sometimes used gives a straight line also when additivity is *not* present.

In the second case (two-dimensional swelling), we calculate the long-spacing to be:

$$d = d_0/\sqrt{c_v}. \tag{3}$$

In the third case (three-dimensional swelling):

$$d = d_0/\sqrt[3]{c_v}. \tag{4}$$

Plotted on log-log paper, these equations give straight lines with the slopes − 1, − ½ and − ⅓, passing through d_o at 100% solid. One can, therefore, obtain a graphical indication as to which mechanism is present. The d_o value determined in this way does not have to coincide with the measured one for the solid, as many substances are supposed to have the molecules inclined to the diffracting planes under an angle β mainly to account for the discrepancy of the calculated length of the molecule and the measured one of the solid. Other substances as the polyoxyethylene derivatives (*i.e.* Emulphor O) form hydrates at high concentrations of the detergent. One is sometimes inclined, for the sake of simplicity, to assume that the molecules are perpendicular to the diffracting planes and use the calculated theoretical value for d_o. The short-spacings of micellar solutions change to diffuse bands from the sharp ones of the solid state, indicating a less ideal structure with the possibility of a rotation of the molecules about their long axis (3).

The experimental check of these equations shows that in the *micellar* systems they are definitely *not* followed over a large range of concentrations. The empirical linear relation between Δd and $(1 - c_v)$ (volume fraction of the solvent) is valid in so great a concentration range, see Fig. 2, that there is no doubt that it is a definite relationship. In the mostly liquid crystalline systems of nonionics investigated by Marsden (14) all three equations can be experimentally verified (53); the general case for liquid crystals seems to be the lamellar swelling system case 1; whereas, in some ethylene oxide derivatives the square- and cube-root equations are valid. This is also the case for tobacco mosaic virus solutions and gels as investigated by Bernal and Fankuchen (44). This is a swelling system of rods following Eq. [3], for case 2. In this case the sequence of the diffractions is not the usual one of 1 : 2 : 3, but 1 : $\sqrt{3}$: 2 : $\sqrt{7}$, as calculated for the hexagonal lattice (26).

Making the specific assumption that the structure of the micellar solution can be approximated as a close packing of spheres (equipartition), Harkins (18) and Hartley (42) calculated the *size* of the micelles. According to Harkins the number N_m of soap molecules/micelle is:

$$N_m = N \cdot \rho \cdot c_{\text{mol}} \cdot (d/10)^3/\sqrt{2} \cong 0.426 \cdot c_{\text{mol}} \cdot (d/10)^3 \quad [4a]$$

Here N is the Avogadro number, c_{mol} the molar concentration in moles/l., d the long-spacing in A. Hartley calculates in exactly the same way the radius of the assumed spherical micelle. The micelle sizes calculated according to Eq. [4*a*] are of the same order of magnitude as generally assumed, but unfortunately have not yet been checked by other methods on the same system. This calculation (as well as the other equations derived) is no proof for any specific shape of the micelle. Especially Eq. [4*a*] is derived for the "outer effect of a point lattice" without any assumptions as to the shape of the micelle. This has been stated by Harkins (18), so that the proof of the calculation as supporting a spherical micelle (42) does not appear warranted. This calculation is valid for equipartition, interrelating the "I-Band" with the size of the micelle. This is made more complicated by the independence of the "I-Band" and the viscosity of the solutions.

Equation [2] gives the maximum possible swelling of a binary system. Liquid crystals, with their optically observable structure, comply with these geometrical concepts. It seems probable that liquid crystals are greatly enlarged micelles, each "spot" seen in the polarizing microscope being a region of uniform orientation.

All the experimentally investigated *micellar systems*, especially at small concentrations, give values for the increase in long-spacing appreciably *smaller* than calculated from Eq. [2]. One must therefore assume that some solvent is distributed, not between the diffracting planes, but say between the micelles of finite lateral size. On the other hand there is no exact equipartition in space, as then Eq. [4] would have to be valid in the whole isotropic concentration range, which is not the case. The empirical results approach Eq. [4] at the highest concentrations, taking the value of d_o as *measured* in the solid. This would mean that some attractive forces between the micelles cause the structure to depart from the ideal equipartition at high concentrations.

The concentration dependence of the lateral spacing of the micelles has, it would seem, no special importance. It follows from Eq. [4*a*] that the lateral spacing is a hyperbolic function of the concentration.

This is about all that the still meager theory of the dependence of the long-spacing on concentration for binary systems can definitely give. Similar calculations have been made for quaternary systems of soap–"oil"–alcohol–water by Schulman and Riley (45) assuming different models for the micelle.

C. Ternary Soap–Oil–Water Systems

The first experiments of Kiessig and the author in 1939 (6) led to the concept of the solubilized "oil" going into the lamellar micelle. Logically the increase in long-spacing is then calculated according to Eq. [2*a*], no molecular data being needed. In this case d_o is the value as *measured* in the solid (anhydrous) detergent, the "solvent" being the solubilized "oil." Kiessig (4, 6) and Harkins (17) made a similar calculation, giving entirely identical results, using an *assumed* area per molecule, the molecular weight of the solid and the Avogadro number to calculate the expected increase in long-spacing, τ. Kiessig found that the values so calculated for the system sodium oleate–benzene–water corresponded to the experimental ones and so developed the model. But this seems *not* to be the general rule for all systems (17), as we shall presently see.

The validity of this linear relationship between Δd and the amount solubilized (in g./g. see Eq. [1]) leads to the assumption of a *lamellar* swelling of the diffracting planes, any two- or three-dimensional swelling being incompatible with this *linear* relation.

It is important to note that Eq. [2*a*] not only describes the concentration dependence of the increase in long-spacing for a binary system (liquid crystals), but also accounts for the increase in long-spacing of a ternary solubilized system.

However, it has been experimentally demonstrated that Eq. [2*a*] is *not* entirely adequate to account for the experimental data. The increase in long-spacing is linear as in Eq. [2*a*], but the slope is much greater (up to 3 or 4 times as much), as has been remarked by Harkins (17). This is seen from the two solubilization curves in Figs. 3 and 4. The slope is not only dependent on the concentration of the solid in the solvent, but also on the chemical composition of the solubilized material. For the sake of comparison one can calculate values of d_o according to Eq. [2*a*] and compare these values with the measured d_o values for the anhydrous detergent. This has been done in Table I for all 49 systems investigated up to now. The calculated d_o amounts to the value $\Delta d/\tau$ introduced by Harkins (17). From Table I it follows as a general rule that d_o as calculated from Eq. [2*a*] is smaller at higher concentrations, the limit for isotropic systems seeming to be d_o of the solid, corresponding to additivity. Also, the values depend very much on the chemical structure of the solubilized substance, benzene giving the lowest values (practically additivity). This explains why we found additivity in the sodium oleate–benzene experiments with Kiessig (6). Paraffinic hydrocarbons show increasing values of d_o with increasing chain length, alkylbenzenes occupying an intermediate position. The values of d_o of different investigators check as well as

TABLE I

Solubilization Data for the "I-Band"

$$d_0 = \Delta d' \times [\rho_{oil}/\rho_{solid}] \times [g._{solid}/g._{oil}]$$

Detergent	Conc.	Oil	d_0A	Author
	wt.-%			
Potassium laurate	15	Benzene	39	Mattoon
$d_0 = 29.4$ A	18	Benzene	29	Kiessig
	20	Benzene	40	Mattoon
	22.1	Benzene	34	Hughes
	24.8	Benzene	31	Philippoff
	22.1	Pentane	56	Hughes
	22.1	Hexane	58	Hughes
	22.1	Heptane	64	Hughes
	25.0	Heptane	59	Mattoon
	25.0	Triptane	60	Mattoon
	22.1	Octane	66	Hughes
	22.1	Decane	72	Hughes
	22.1	Dodecane	76	Hughes
	20	Cyclohexane	59	Mattoon
	22.1	Toluene	40	Hughes
	22.1	*o*-Xylene	41	Hughes
	15.0	Ethylbenzene	59	Mattoon
	22.1	Ethylbenzene	50	Hughes
	26.5	Ethylbenzene	34	Philippoff
	20.0	Mesitylene	48	Mattoon
	22.1	Mesitylene	47	Hughes
	22.1	Butylbenzene	54	Hughes
	25.0	Bromoform	39	Philippoff
	32.6	Methyleneiodide	−14	Philippoff
	50	Cumene	27	Hoffman
	50	Bromobenzene	27	Hoffman

TABLE I—*Continued*

Detergent	Conc.	Oil	d_0A	Author
	wt.-%			
Sodium oleate	9.1	Benzene	40	Kiessig
$d_0 = 44.5$ A	15.0	Benzene	36	Kiessig
	13.8	*m*-Cresol	−27	Philippoff
Laurylpyridiniumchloride	42	Benzene	8	Kiessig
Cetylpyridiniumchloride	20	Benzene	22	Hoffman
$d_0 = 28.8$ A	20	Methylenechloride	9	Hoffman
	20	Ethylenebromide	57	Hoffman
	20	Cumene	60	Hoffman
	25	Methylphthalate	−22	Hoffman
Sodium dodecylsulfate	24.8	Benzene	38	Mittelmann
$d_0 \sim 37$ A	20.0	Methanol	−9	Mittelmann
	20.0	Ethanol	−5	Mittelmann
Aerosol OT/H_2O	25	Cyclohexane	84	Philippoff
$d_0 = 19.9$ A	26	Benzene	61	Philippoff
	50	Cyclohexane	51	Philippoff
	50	Benzene	51	Philippoff
	50	Decane	51	Philippoff
	75	Decane	40	Philippoff
	100	———	20	Philippoff
Zinc-Aerosol[a] $d_0 \sim 20$ A	25	Toluene	75	Philippoff
	50	Toluene	43	Philippoff
	25	Xylene	75	Philippoff
	50	Xylene	40	Philippoff

[a] Zinc salt of di (2-ethylhexyl) ester of sulfosuccinic acid. American Cyanamid Co.

can be expected, taking into account the experimental difficulties of work with minute quantities of mixtures including volatile solvents.

The above applies to the usually investigated "I-Band." For the "M-Band," which is referred to the thickness of the micelle, it is logical to apply the same concepts, and an additivity for all concentrations and solubilized substances is to be expected, the solvent not affecting the results. Measurements of Mattoon (18) and Mittelmann (24) show that in some cases (see Table II) this is indeed the case for solubilized hydrocarbons. The experiments are extremely difficult to evaluate due to the diffuse bands. In other cases (potassium myristate) (18), a large dependence of d_0 on concentration was found, but it is possible that experimental errors are present. Butanol gave a negative value of d_0 (24). The results are still not conclusive and require further investigation.

A correlation of the calculated d_0 values with any other properties of the solubilized compounds has until now not been possible. If, however, one takes the maximum amount solubilized in ml. hydrocarbon/ml. soap as abscissa, all the measured d_0 values fall onto one, approximately straight, line as is shown in Fig. 8, curve 1. The solubilization values of Harkins and co-workers (46), measured in 15% potassium laurate, have been taken along with the d_0 values (Table I) from the work of the Shell Dev. Co. (19), measured at 22.1%. For three substances, benzene, ethylbenzene, and heptane, the solubilization data obtained at the same concentration could be used (curve 2), as these substances had been investigated at different concentrations of potassium laurate. No essential difference results from this correction. The linear relation seems to hold for all concentrations of potassium laurate and all solubilized substances. By this means we have correlated the maximum amount solubilized with the over-proportional increase of the long-spacing, the full meaning of which has yet to be ascertained.

TABLE II

Solubilization Data for the "M-Band"

Detergent	Conc.	Oil	d_0A	Author
	wt.-%			
Potassium laurate	7.00	Ethylbenzene	27.6	Mattoon
$d_0 = 29.4$ A	8.84	Ethylbenzene	27.0	Mattoon
	10.09	Ethylbenzene	27.6	Mattoon
	12.05	Ethylbenzene	27.4	Mattoon
	13.60	Ethylbenzene	27.0	Mattoon
		Mean:	27.3	
Potassium myristate $d_0 = 36.3$ A	7.16	Ethylbenzene	33.4	Mattoon
Sodium dodecylsulfate $d_0 \sim 37$ A	8.65	Ethylbenzene	27.0	Mittelmann
	8.65	Heptane	42	Mittelmann
	15.7	Butanol	−6	Mittelmann

This lack of additivity in solubilized systems is apparently a general rule for the micellar state. Normal soaps, cationic detergents [Hoffman (15)], nonionics [Marsden (14)], and even nonaqueous systems of Aerosol OT in hydrocarbons (20) show it. It is certainly difficult to understand why this occurs. Possibly not all micelles participate in solubilization, the "x-ray micelles" taking all or most of the solubilized "oil," the amount in them being calculated on the basis of additivity of the volumes by Eq. [2a]. The variability of the increase of the long-spacing with concentration of the detergent being caused by the varying amount of "x-ray micelles" present. It is more difficult to account for the influence of different substances. Solubilization without an x-ray pattern (at small concentrations of the detergent) and some Aerosol OT experiments mentioned above seem to exclude this possibility.

Likewise it has been proposed to explain the increase of intensity of the x-ray pattern on solubilization by assuming more or larger (better oriented) "x-ray micelles" being formed under the influence of the solubilized substance.

If one assumes micelles of a limited lateral size, one arrives at different conclusions. Already the investigation of the long-spacing with concentration showed that a definite layer of *solvent* must be assumed to exist between the double layers of molecules. When one calculates the increase in long-spacing in solubilized systems according to Eq. [2*a*], one assumes that this layer of solvent between the micelles is completely independent

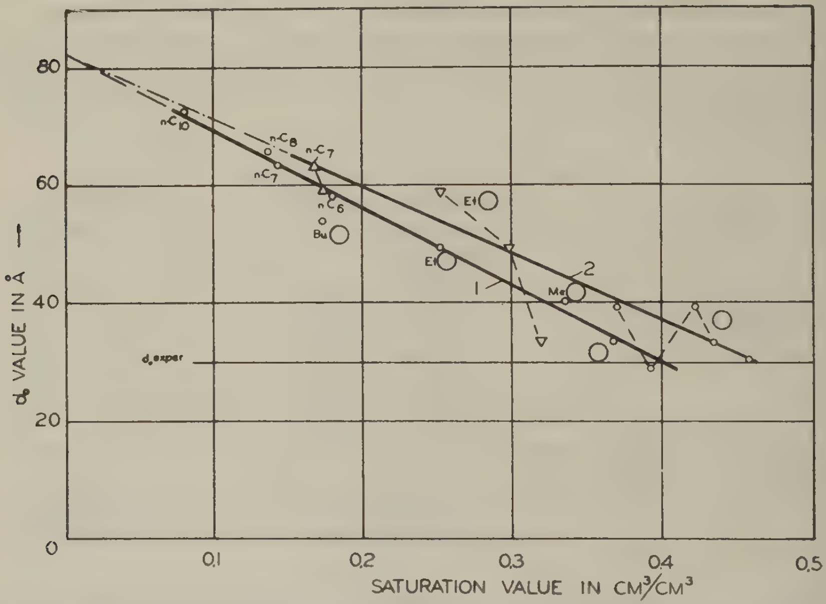

FIG. 8. Dependence of the d_0 value for aqueous solutions of potassium laurate on the maximum amount solubilized.

of the solubilized material, both concentration and solubilization increases being independent and superimposable, as found by the Shell Dev. Co. investigators (19). But the lack of agreement between the experimental and calculated values forces us to abandon this assumption. We assume then that both increases are interrelated, the solubilized material causing a simultaneous increase in intermicellar solvent. But of course it is amazing that the relationship in this case should remain linear to such a great extent. Equation [2*a*] gives the minimum amount of swelling, without changing the solvent layer. In the few cases where the long-spacing decreases with the amount solubilized (9, 10, 15, 24) there is still however a finite layer of solvent between the micelles. We cannot as yet imagine a mechanism that would cause such a "secondary swelling" of the structure by solubilization, but it seems the only hypothesis which explains the experimental findings. Of course negative d_o-values have no physical significance, merely showing that the decrease in long-spacing with concentration is of the same order of magnitude as in the case of an increase.

For the decrease in long-spacing of solutions of dodecyl sodium sulfate and normal alcohols, Harkins and Mittelmann (24) proposed a mechanism of "interpenetration" of the layers of the soap molecules by the alcohol molecules. As these are generally shorter, the soap molecules "curl back" to eliminate holes in the structure and so give a decrease in the long-spacing.

The phenomenon of the "fading out" of the x-ray diffractions on solubilization of heavy atoms has an intimate relation with the assumption of a laminar structure for the micelle, as has been remarked by previous investigators (15, 19). The x-ray diffraction of a system of layers is dependent on the distribution of electron density in successive planes. Both the surplus of electron density at the ionic "head" of the molecule and the deficiency at the methyl group at the "end" contribute to the intensity. If hydrocarbons with a low electron density are solubilized this deficiency against the water solvent is increased, as is also the diffracted intensity. When substances of high electron density are solubilized they change at first the deficiency at the "end" to zero; then their contribution of a surplus in electron density cancels the one of the ionic "head" and the diffractions disappear. When still more is solubilized the diffractions reappear "with a phase-shift of 180°," according to Hughes, Sawyer, and Vinograd (19), because the electron density surplus in the solubilized layer supersedes all other influences. No other explanation for this phenomenon involving spherical micelles has been proposed and it seems quite probable. In any case, the d_o values for fading-out systems are not too different from the usual ones. Similar phenomena are known for the higher orders of the diffractions of paraffin derivatives as theoretically calculated by Shearer (47). Related phenomena have been described by Harkins and co-workers (17) for halogenated hydrocarbons and $Pb(C_2H_5)_4$. The new band described can possibly be the *second* order of the "I-Band" that does not fade out as the first order does.

D. Further Phenomena

After discussing at length the main effects, we will consider some as yet less fully-investigated phenomena in their relations to the micellar structure.

The temperature effect has been investigated in a very incomplete way, but it is sure to give more information concerning the forces involved in micelle formation. A possible decrease in intensity with increase in temperature as found by Hoffman (27) has to be checked on more material. In the case of sodium oleate solutions no effect was found even with about 30 A of water between the layers.

The independence of the viscosity from the x-ray pattern is a point not sufficiently emphasized lately. It would invalidate any direct relations between the micelle size and the x-ray pattern (I-Band). The experimentally ascertained effects could only be explained by an unordered aggregation of the diffracting units which influences their kinetic motion, but does not contribute to the structural order (6, 9).

The orientation of the x-ray patterns by flow is very difficult to understand. The quantitative investigation by Snellman (29) has shown that the theory of orientation of anisometric particles by flow, which requires a 45° orientation at zero velocity, is *not* fulfilled.

The validity of the Vegard-rule for mixtures as applied to micellar systems cannot be explained at the moment in another way than proposed by Hess and Kiessig (12); they assumed a flexibility of the hydrocarbon chains so that they fold back and show the mean spacing of the constituents. This assumption has also been used by Harkins and Mittelmann (24) with reference to the "interpenetration phenomenon."

The quantitative measurement of the *intensity* as a function of the concentration of the short-spacing and "I-Band" does not give anything new; it merely states that the amount of diffracting matter increases with concentration. The peculiar result for the "M-Band" (see Fig. 6) requires checking.

The size of the x-ray diffracting unit deserves a more detailed treatment. Is it a "Hess-micelle" (15) or "Grossmizelle" (7) or is it an "outer effect" of small micelles? This controversy that began in 1941 (48) cannot of course be decided by x-ray data alone and additional evidence from other independent methods is required. The main difficulty is that the high concentration of the detergent required to give x-ray diffractions makes the application of thermodynamic data and reasoning somewhat difficult. To exclude the possibility of some particles escaping detection, the particle size determination should be made at the *same concentration* as the x-ray experiments. To demonstrate the experimental side of the problem, the example of the best investigated "classical" system potassium laurate in water is shown in Fig. 9. The data on freezing point lowering, electrical conductivity and solubilization of the dye Orange OT[8] are taken from the unique collection of data of McBain's school at Stanford (49, 50, 51). To this may be added the data on the density, viscosity, surface tension, diffusion, and solubilization of liquid hydrocarbons, measured by different investigators. The x-ray diffractions appear about 9–10% and *no break in*

---

[8] *1-*o*-Tolylazo-2-naphtol.

any curve is noticeable. Should the formation of new micelles be the cause of the x-ray patterns, they are not indicated by any other method. This is a strong argument against such a possibility. The approximate size of a "Grossmizelle" has been given above. All the colloidal properties appear at the "first CMC."

Such complete evidence is only available for very few systems and its further elaboration using other methods such as light-scattering (52), ultracentrifuge, and diffusion or others *in the same range of concentrations as the x-ray experiments* would certainly give a decision. Harkins and Mittelmann (24) gave a recent survey of micelle size determinations.

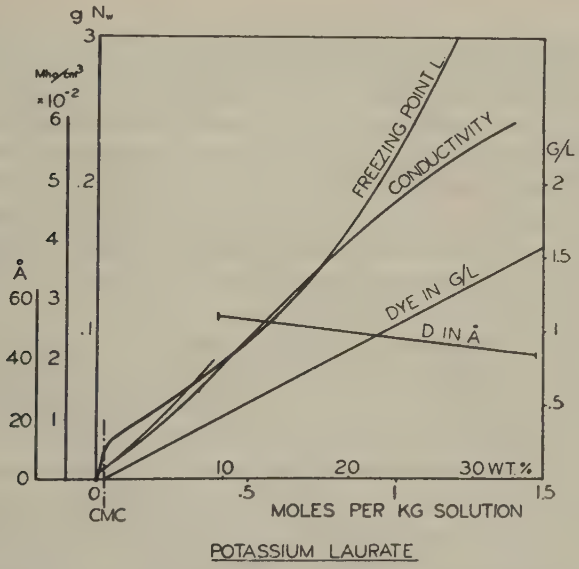

FIG. 9. Dependence of several properties of solutions of potassium laurate in water after McBain and co-workers (49–51) (short curve g. N_w for 25° C.).

Another important point for the comprehension of the phenomenon of solubilization is : Does the micelle present in the solution previous to solubilization change in size only on an additive basis, or is there an over-proportional increase in size? This would of course complicate the conditions considerably. *Decisive* experiments on this point are still wanting.

The quantitative investigation of the solubilization shows that a definite structure, in micellar solutions as well as in liquid crystals, can persist at extraordinary long distances. In the case of Aerosol OT–water systems, Eq. [2*a*] was fulfilled up to a ratio of water/Aerosol OT of 5 : 1 (53). In approximately 16% solutions, definite sharp spacings (liquid crystals) of 110 A could be measured accurately. Even at this distance the structure persists, determined by molecules only 10 A long in the direction of the diffracting distances. In ternary systems, repeating distances of over 150 A occur, but each layer is thinner than the one mentioned. This gives the possibility of measuring the surface forces involved in a very direct manner. We are here in a completely new field where the possibilities are not known.

ACKNOWLEDGMENTS

The author is especially grateful to Prof. J. W. McBain for taking such an interest in this work, to Dr. A. Brown for the amiable help in wording the manuscript and helpful criticism, and to the Lever Bros. Co. which made this reaserch possible by a generous Fellowship.

CONCLUSIONS

From all the accumulated experimental evidence we see how the application of x-ray diffraction analysis has demonstrated a micellar structure in otherwise isotropic solutions. The concept of solubilization in layers in these micelles has been mainly founded on x-ray evidence. It seems that the model of small micelles with molecules oriented in a double layer is the most adequate as yet advanced to account for the experimental facts, the "I-Band" being caused by their relative positions in space. Simple geometric formulas have been derived to account for the variation of the long-spacing with concentration.

After the chief experimental relations have been established, the next step should be to ascertain, preferably by several methods in the same range of concentration as the x-ray experiments, how large the x-ray diffracting units are, then to extend the conclusions from the x-ray experiments to more dilute solutions in the practical range. A more detailed investigation of solubilization, perhaps also in liquid crystals, is sure to give positive information concerning the forces involved in micelle formation and solubilization. A complete theory of the micellar state, taking into account all of the experimental evidence concerning the forces involved in micelle formation, has yet to be developed.

REFERENCES

1. FRIEDEL, G., *Ann. phys.* (9) **18**, 273 (1922).
2. KRISHNAMURTI, P., *Indian J. Phys.* **3**, 307 (1929).
3. HESS, K., and GUNDERMANN, J., *Ber.* **70**, 1800 (1937).
4. HESS, K., PHILIPPOFF, W., AND KIESSIG, H., *Kolloid-Z.* **88**, 40 (1939).
5. STAUFF, J., *Kolloid-Z.* **89**, 224 (1939).
6. KIESSIG, H., AND PHILIPPOFF, W., *Naturwissenschaften* **27**, 593 (1939).
7. STAUFF, J., *Kolloid-Z.* **96**, 244 (1941).
8. KIESSIG, H., *Kolloid-Z.* **96**, 252 (1941).
9. PHILIPPOFF, W., *Kolloid-Z.* **96**, 255 (1941).
10. HESS, K., KIESSIG, H., AND PHILIPPOFF, W., *Fette u. Seifen* **48**, 377 (1941).
11. KIESSIG, H., *Kolloid-Z.* **98**, 213 (1942).
12. HESS, K., AND KIESSIG, H., *Ber.* **81**, 327 (1948).

13. Ross, S., and McBain, J. W., *J. Am. Chem. Soc.* **68**, 296 (1946).
14. Marsden, S. S., and McBain, J. W., *J. Phys. Coll. Chem.* **52**, 110 (1948).
15. McBain, J. W., and Hoffman, O. A., *J. Phys. Coll. Chem.* **53**, 39 (1949).
16. Harkins, W. D., Mattoon, R. W., and Corrin, M. L., *J. Am. Chem. Soc.* **68**, 220 (1946).
17. Harkins, W. D., Mattoon, R. W., and Corrin, M. L., *J. Colloid Sci.* **1**, 105 (1946).
18. Mattoon, R. W., Stearns, R. S., and Harkins, W. D., *J. Chem. Phys.* **16**, 644 (1948).
19. Hughes, E. W., Sawyer, W. M., and Vinograd, J. R., *J. Chem. Phys.* **13**, 131 (1945).
20. Philippoff, W., and McBain, J. W., paper presented at the ACS meeting, March 1949, in San Francisco, Calif.
21. Mattoon, R. W., Stearns, R. S., and Harkins, W. D., *J. Chem. Phys.* **15**, 209 (1947).
22. McBain, J. W., and Merrill, R. C., *Ind. Eng. Chem.* **34**, 915 (1942).
23. Palit, S. R., and McBain, J. W., *J. Soc. Chem. Ind.* **66**, 3 (1947).
24. Harkins, W. D., and Mittelmann, R., *J. Colloid Sci.* **4**, 367 (1949).
25. Mattoon, R. W., and Mathews, M. B., *J. Chem. Phys.* **17**, 496 (1949).
26. Marsden, S. S., and McBain, J. W., *J. Am. Chem. Soc.* **70**, 1973 (1948).
27. Hoffman, O. A., *Rev. Sci. Instruments* **19**, 277 (1948); and Kiessig, H., unpublished data; see also Ref. 12.
28. Hess, K., Kiessig, H., and Philippoff, W., *Naturwissenschaften* **26**, 184 (1938).
29. Snellman, O., *Arkiv Kemi, Mineral. Geol.* **19B**, 1 (1944).
30. Hattiangdi, G. S., *Bur. Standards J. Research* **42**, 331 (1949).
31. Langmuir, I., *Met. Chem. Eng.* **15**, 468 (1916); *idem, J. Am. Chem. Soc.* **39**, 1848 (1917).
32. Harkins, W. D., Brown, F. E., and Davies, E. C. H., *J. Am. Chem. Soc.* **39**, 354 (1917); Harkins, W. D., Davies, E. C. H., and Clark, G. L., *J. Am. Chem. Soc.* **39**, 541 (1917).
33. Perrin, J., *Ann. phys.* (8) **10**, 160 (1915); *idem, Kolloid-Z.* **51**, 2 (1930).
34. McBain, J. W., *J. Chem. Education* **6**, 2121 (1929).
35. Warren, B. E., *Phys. Rev.* **44**, 969 (1933).
36. Zachariasen, W. H., *J. Chem. Phys.* **3**, 158 (1935).
37. Dervichian, D. G., *J. chim. phys.* **38**, 59 (1941).
38. Harkins, W. D., *J. Chem. Phys.* **16**, 156 (1948).
39. Reychler, A., *Kolloid-Z.* **13**, 252 (1913); *idem, Bull. soc. chim. Belg.* **27**, 113 (1913).
40. McBain, J. W., and Salmon, C. S., *J. Chem. Soc.* **42**, 426 (1920); *idem, Proc. Roy. Soc. (London)* **A 97**, 44 (1920).
41. Hartley, G. S., Aqueous Solutions of Paraffin Chain Salts. Paris, 1937.
42. Hartley, G. S., *Nature* **163**, 767 (1949).
43. Corrin, M. L., *J. Chem. Phys.* **16**, 844 (1948).
44. Bernal, J. D., and Fankuchen, I., *J. Gen. Physiol.* **25**, 111 (1941).
45. Schulman, J. H., and Riley, D. P., *J. Colloid Sci.* **3**, 383 (1948).
46. Stearns, R. S., Oppenheimer, H., Simon, E., and Harkins, W. D., *J. Chem. Phys.* **15**, 496 (1947).
47. Shearer, G., *Proc. Roy Soc. (London)* **A 108**, 655 (1925).
48. Discussion in *Kolloid-Z.* **96**, 258–60 (1941).
49. McBain, J. W., Laing, M. E., and Titley, E. F., *J. Chem. Soc.* **115**, 1279 (1919).
50. McBain, J. W., and Bolduan, O. E. A., *J. Phys. & Coll. Chem.* **47**, 94 (1943).
51. McBain, J. W., and Green, Sister A. A., *J. Am. Chem. Soc.* **68**, 1731 (1946).
52. Debye, P., *J. Colloid Sci.* **3**, 407 (1948); *idem., J. Phys. & Coll. Chem.* **53**, 1 (1949).
53. McBain, J. W., and Philippoff, W., *Nature* **164**, 885 (1949).

BOOK REVIEWS

Electron Microscopy, Technique and Applications. By Ralph W. G. Wyckoff. Interscience Publishers, Inc., New York, 1949. 248 pp. Price $5.00.

This book will be welcomed by everyone interested in the growing use of the electron microscope in so many fields of modern science. The small volume contains a vast amount of technical knowledge the author has accumulated with this new tool of research.

After an introduction dealing with the principle, development, and characteristics of modern electron microscopes, followed by a brief outline of the procedure for adjustment of the instrument, the reader will find a detailed discussion of different methods for preparation of samples for electron microscopy. Everyone who has had experience with an electron microscope knows that preparation of a sample remains the most difficult step. It is appropriate that the author has devoted almost 80 pages to this important question including an interesting chapter on metal shadowing and surface replicas. The following chapters present problems concerning microphotography of particle suspensions, viruses, and macromolecules. The last part sums up the information about the structure of macromolecular solids.

The magnificent collection of electron microphotographs (almost 200, with a special index), most of them prepared in the author's own laboratory, is the impressive feature of the book. The author's acquaintance with the literature has found expression in long lists of references attached to each chapter.

It is difficult to criticize this book. Some readers may feel disappointed by a certain discrepancy between the title and the character of the book rather than by its contents. Many of them may disagree with the author's statement that (p. 4) "electron microscopy is far too young to be a subject of an exhaustive monograph." They may feel that now when the electron microscope wins so much recognition the publication of such a monograph is more necessary than ever. According to the quoted statement, the author has omitted the entire theory of electron waves, and has reduced the discussion of the theoretical principles to a few sentences. While concentrating heavily on biological specimens, he stressed only very slightly applications of the microscope to colloidal and metallurgical investigations.

V. A. Gordieyeff, New York, N. Y.

Chemistry of Specific, Selective, and Sensitive Reactions. By Fritz Feigl. Translated by Ralph E. Oesper. Academic Press, New York, N. Y. xiv + 740 pp. Price: $13.50.

Feigl's popularity derives from the fact that he is the founder of the spot test analysis and the author of well-known books on this field. However, his international reputation is not based on these achievements alone. His research activities, concerned directly and indirectly with the problems of analytical application of chemical reactions, are equally important and fundamental. These include his studies on the relationship between atomic groupings in organic compounds and specificity, on complexes, on induced precipitations, masking of reactions and other anomalies, the use of catalysis in trace analysis, etc.

Feigl's new book "Chemistry of Specific, Selective, and Sensitive Reactions" is a fascinating monograph of the scientific bases of analytical problems. As the author states in the preface, his aim has been to summarize the present knowledge of the scientific background of specificity, selectivity, and sensitivity of analytical procedures by collecting and classifying the relevant experimental material, considering at the same time the close relationship between the problems and results of analytical chemistry and other fields of chemistry. This novel and difficult task has been undertaken by Feigl in a manner deserving of the highest admiration. His book is not a mere enumeration of facts but through his complete mastery of the subject the author has been able to coördinate apparently unconnected results.

Thanks to the excellent translation of the German manuscript by Dr. Oesper, the author's personal style and approach have been preserved so that the reading of the book is a real pleasure. The material considered by Feigl is by no means derived exlcusively from analytical papers; many other sources have been taken into account. It is shown that many findings widely dispersed throughout the literature and partly sunk into oblivion can gain new importance from more than one point of view in the light of the problems of specificity, selectivity, and sensitivity. Feigl further points out that analytical papers often contain reports which are of greater importance for other specialized fields of chemistry than for purely analytical problems. These few indications make it obvious that an immense amount of factual material has to be incorporated. Feigl classified and discussed it in twelve chapters. No review can do justice to the amazingly varied contents. No abstract can be made of the 693 pages of the text, every one of which contains an overwhelming mass of facts. However, it may be said that every chapter of the book stimulates and suggests a number of new experiments not only for the analytical chemist but for any chemist.

The readers of this journal will be particularly interested in Chapter 10 (surface effects, etc.) which is a 179-page monograph referring to all those phenomena of colloid chemistry which are directly or indirectly connected with analytical chemistry. The author's thoroughness may be illustrated by a footnote on p. 601 to the effect that Tswett's chromatographic analysis had a precursor in the work of L. Reed (1892), a fact which remained unknown even to authors of special texts on chromotography. Feigl also refers to the fact that the Schönbein-Goppelsröder technique of capillary analysis which gave him the impetus to his first spot test experiment contains the elements of adsorption analysis, especially paper chromatography. Considerable interest attaches to the author's treatment of chemical adsorption. Stressing the requirement that no new phase must be formed during the process of adsorption, Feigl arrives at a clear picture and an appropriate definition of color lakes with metals and of adsorption compounds. Up to now color lakes were generally considered as inner complex salts in accord with an assumption of Werner (1908) the reddish violet aluminum alizarin lake being given as a typical example. Feigl points out that an entire generation of chemists appears to have overlooked a paper by Möhlau (1913) in which he describes the preparation of the inner complex Al-alizarinate and its properties which differ considerably from those of the Al-alizarin lake. According to Feigl the great majority of color lakes are not inner complexes at all but products of chemical bonding of dyestuff molecules to sol or gel particles of oxide hydrates without the formation of a new phase. The bonds may be both primary and secondary in nature or due to secondary valences only. This view is experimentally supported by as yet unpublished work with H. Zocher (p. 676). Similarly, the tannin precipitates investigated so thoroughly by Schöller and applied in analytical procedures are considered products of surface reactions of phenolic groups of the dissolved or colloidally suspended tannin with acid or basic metallic oxides in the form of hydrosols, and not, as believed hitherto, products of flocculation of oppositely charged colloid particles. A number of facts which concern the colloid chemist are also included in Chapter 11 (genetic formation of materials and topochemical reactions). The examples of induced precipitations, collector effects, and protecting layer effects quoted there and in Chapter 5 (enhancement of reactivity of compounds and reaction systems) are important beyond their application to analytical problems. The same applies to the material contained in Chapters 8 and 9 regarding group effects in solute–solvent systems. Chapter 6 is a treasure trove for suggestions on the study of organic reagents, which are critically surveyed in an excellent 200-page review of this up-to-date field.

This book must have involved an enormous amount of work; 1500 literature-references are quoted. Although most chapters include references to papers by Feigl, many of them fundamental, his part in the development of the field is not stressed sufficiently. In great modesty he always points out the merits of other authors. His amazing knowledge of the literature, including the most difficultly available sources, gives him ample opportunity to discuss critically all relevant material. It can be accepted as a certainty that Feigl will attempt to add to the material treated in the text. Undoubtedly he will want to include the facts and views advanced in his lecture on the role of organic reagents in the chemistry of specific selective and sensitive reactions presented before the Amercan Chemical Society in the summer of 1949 [Anal. Chem. **21**, 1298 (1949)] and not yet contained in Chapter 6 of his book which had been published somewhat earlier. Additions will also become necessary as research and publications in the field are influenced by aspects and critical observations found in the text. It is hoped that he will then refer to the papers of Warburg and Sakuma [Biochem. Z. **142**, 68 (1923)] and Bjerrum [J. Biol. Chem. **114**, 357 (1936)] on the oxidation of thioacids catalyzed by Cu^{++} which would have been included in Chapter 5. Furthermore, some footnotes rightly belong into the main text and the subject index is inadequate as it fails to give a true picture of the impressive contents.

Feigl's book is a poineer work and therefore one of the truly great contributions in the field of chemistry. It is the first presentation of the scientific basis of the systematic search for analytically applicable reactions and reagents. And beyond this, by the collection and classification of the store of knowledge directly or indirectly connected with the specificity, selectivity, and sensitivity of analytical procedures, he has laid the foundation for an experimental chemistry of value for all branches of chemistry and for chemical education.

C. NEUBERG, New York, N. Y.

Elastomers and Plastomers, Their Chemistry, Physics and Technology. Volume II. Manufacture, Properties and Applications. Edited by R. HOUWINK. Elsevier Publishing Co., Inc., New York and Amsterdam, 1949. 515 pp. Price $7.00.

The second volume of Houwink's Elastomers and Plastomers series contains the following Chapters:

"Phenol-Formaldehydė Plastomers" by R. Houwink consists of an introduction which is followed by a discussion of the raw materials, the maunfacture of the resins, and their hardening. Section 5 written by C. P. A. Kappelmeier deals with *Phenol-Formaldehyde Resins for Varnishes, Paints and Lacquers* followed among others by paragraphs on molding components and laminated materials. The properties of the various phenol-formaldehyde plastomers are presented in different paragraphs. A. von Royen's "Synthetic Resin Ion-Exchangers" gives a concise discussion of the subject. In G. Widmer and K. Frey's "Urea and Melamine Resins" the discussion of the raw materials is followed by a chapter on the condensations reaction. The last and most extensive paragraphs of this chapter deal with the properties and production of carbamide and aminotriazine resins. "Polymers from Ethylene Derivatives" by H. T. Neher gives the preparation of a number of monomers, a brief discussion of polymerization, and a discussion of the properties and uses of these polymers.

"The Cellulose Derivatives" by V. E. Yarsley, H. Kitchen, and W. J. Grant is introduced by a paragraph on the structure of cellulose followed by a discussion of various derivatives and the processes of solvation and plasticization. The manufacture, properties, analysis, and applications are extensively treated. The chapter on "Protein Plastics" consists of two parts: I. *Protein Plastics other than Fibers* by A. D. Whitehead and S. H. Pinner, and II. *Fibers from Proteins* by C. Diamond. The first part contains a short chemistry of proteins followed by the discussion of some proteins and paragraphs on the theories of hardening of proteins with formaldehyde, modifying agents, manufacture, and uses. The second part mentions some theories on fiber structure, and after technological remarks briefly describes a number of fibers. After-treatment, physical properties, and general properties are briefly discussed. "Synthetic Polymides" by L. F. Salisbury follows the usual pattern, too briefly, perhaps, in discussing chemical reactions, commercial processes, properties, and applications. In "Silicone Polymers" by J. R. Elliott a short chemistry of silicones is followed by a discussion of properties and applications of silicone oils, rubber, resins, and water-repellent films. "Alkyd Resins" by J. R. Patterson discusses raw materials, the process of resinification, applications, and manufacturing. J. C. Clare's "Natural Resins and Their Derivatives" is introduced by a "classification; production" and followed by an extensive discussion of natural resins, rosin, and lac and shellac. T. R. Dawson's "Derivatives of Natural Rubber" discusses all too briefly: sulfur derivatives, rubber isomers, oxidation and hydrogenation derivatives, halogenated rubber, rubber hydrochloride, acrylonitrile and maleic anhydride, addition products, and miscellaneous derivatives. The chapter on "Synthetic Rubbers" by W. J. S. Naunton discusses the types of rubber-like materials followed by the chemistry and production of monomers, the technology of polymerization, and the properties of synthetic rubbers. A brief but thorough treatment of processing and of applications follows. The last chapter by R. N. Traxler deals with "Asphalts," giving sources, chemical composition, rheological and colloidal properties, and applications.

It is probably an intrinsic difficulty in a work of this nature to achieve the proper balance for the different topics, particularly since by necessity the physical size of the volume has to be limited. This reviewer does not know of any fundamental principle which could have guided Dr. Houwink's editorial policy, but he would have liked to be able to detect even an arbitrary principle. It seems as if the authors have been given no directives beyond some rather liberal limits of number of pages. Consequently, each chapter makes pleasant reading, but read in sequence as the reviewer has been obliged to do, the volume is disturbingly unharmonious. To illustrate with a random example: "Derivatives of Natural Rubber" (23 pp.) which includes Section 2 "Sulfur Derivatives (Vulcanizad Rubber)" (1½ pp.) is believed excessively scant as compared with "Natural Resins and Their Derivatives" (38 pp.).

This drawback, however, will affect only a few readers and is greatly compensated by the thorough treatment (within the space limitations) of most subjects. Its usefulness will be apparent as a first source of reference particularly since the chapters are followed by an extensive list of references.

George Goldfinger, Buffalo, New York

Introduction of

HENRY EYRING

Hugh S. Taylor

I met Henry Eyring for the first time in Berkeley, California, in September 1930 through Professor G. N. Lewis who, convinced of Eyring's future as a scientist, was unable to foresee opportunities for him on the West Coast. My second encounter was at the meeting of the American Chemical Society in Indianapolis the following spring. I was struck by Eyring's *calculations* that both flourine atoms and molecules should react slowly with hydrogen. All the textbooks said differently, but just about the same time von Wartenburg in Germany was showing experimentally that Eyring's calculations were right and the textbooks wrong. I invited Eyring to Princeton within a quarter of an hour after his Indianapolis lecture. He stayed with us for 15 most fruitful years in the development of rate theory in chemistry and in physical processes.

Eyring had examined the interaction of atomic and molecular hydrogen with Polanyi in Berlin in 1929–30 and had extended these theoretical calculations to the interaction of the halogens with hydrogen in 1930–1 in the University of California. On coming to Princeton he immediately extended the methods of calculation to the problem of the activation energy required for the chemisorption of hydrogen on a charcoal surface. Out of this came the important relation that the activation energy of adsorption is a function of the lattice distances of the atoms in the solid surface. From all of these kinetic studies there emerged a clear picture of the activated complex as the intermediate between reactant and product, the potential energy of which complex determined activation energy. One immediate consequence was an understanding of the significance of zero-point energy in the rates of the newly found isotope reactions.

The next major advance was Eyring's formulation of the activated complex as a system, similar in every respect to a polyatomic molecule, save that one degree of freedom was in process of becoming a translational decomposition. To the complex, as well as to reactants and products, statistical methods were applicable and hence was developed the absolute rate theory of chemical reactions. The velocity of a process could be represented by the equation $v = (kT/h)e^{-\Delta F^*/RT}$. They were happy days in

---

[1] Presented at the Annual Meeting of the Society of Rheology, New York, N. Y., November 4–5, 1949.

Princeton as Eyring and his students worked out the details of this development.

There was in principle no basis for restricting these advances to chemical reactions and by 1936 the application of absolute rate theory to physical processes was in full swing. Viscosity of liquids was the first physical rate process to be considered. The activated state was a state of high energy as two molecules passed by one another from an initial to a final equilibrium state during which change their relative positions one to another had been interchanged. Free volume was necessary to permit such flow and Eyring found in the Cailletet-Mathias Law of Rectilinear Diameters the concept of holes or free volume in liquid measured by the volume of the molecules in the saturated vapor. The activation energy of viscous flow was the energy required to make a hole of size sufficient to permit the motion of the molecules past one another. Associated liquids had to break hydrogen bonds as well as have free volume in order to flow. Large molecules had to move in segments rather than as a unit. Newtonian and non-Newtonian flow were formulated in terms of absolute rate theory. Perhaps one of the most interesting cases of viscosity thereby interpreted was that of liquid sulfur anomalous in that a limpid liquid changes on *heating* to a viscous fluid. The motion of S_8 rings accounts for the former, of S_n chains for the latter, and the frontier from simple molecules to high-polymeric substances is crossed in one system.

The writer can remember the first seminar on viscous flow and recalls how the principles formulated brought understanding to him of isolated empirical facts in the earlier studies of diffusion. Viscosity in mixtures and diffusion phenomena were then clarified by Eyring and his colleagues, the role of activity in nonideal systems exhibited, and the concepts applied to conductance, transport of ions, overvoltage and other electrochemical rate processes. Laidler worked up the kinetics of heterogeneous processes, adsorption, and reaction, while Glasstone prepared the manuscript for the "Theory of Rate Processes" which was shortly to emerge under Eyring's constant and critical direction.

The war years broke up the natural sequence of developments in this area; in the archives of the war effort are recorded the yield from those years. Of Eyring one must record that his approach to every problem is fresh, original, and very frequently unorthodox. He tends to discover the facts of science for himself rather than to read what others have found. For Eyring a scientific fact becomes a fact when he has discovered it and discovered why it is a fact. He does not live by scientific bread alone. His intense activity in science is complemented by a dedication to the Mormon faith which he is anxious to interpret to any who will listen. How often our conversations in science drifted off into expositions of the Mormon and the Roman Catholic points of view. The writer can at any rate record his own vigorous defense of Mormonism at a Jesuit college in Baltimore on the occasion of an American Chemical Society's meeting. That his own expositions may not have been entirely vain is indicated by a remark of Eyring's in the war years that the position taken by Pope Pius XII concerning the war most nearly coincided with his (Eyring's) own.

Salt Lake City was his Mecca, certainly the Mecca of Mrs. Eyring in the interest of her three growing sons. Throughout the 15 years at Princeton there was a strong polarization westwards. Pittsburgh to which he was early invited was said to have this advantage over Princeton, that it was 400 miles nearer to Utah. Finally, he made the break in 1946. Is it not significant that the Bingham medallist of 1949, in his new environment, seeing, as he has remarked, during the morning shave, through the bathroom window, the lovely city ringed around with its snow-capped mountains, should turn to the problems of viscosity and fluidity whereby in geologic times the mountains were thrust up to form the valley which greeted the Mormon pioneers.

HUGH S. TAYLOR

ACCEPTANCE OF THE BINGHAM MEDAL[1]

Henry Eyring

University of Utah, Salt Lake City, Utah

I greatly appreciate the honor accompanying the award of the Bingham Medal. Professor Bingham, more than anyone else I know, was dedicated to the study of the flow properties of matter. His book is known to all students in this field, and among my very pleasant memories are the visits I had with him. My own contributions to rheology were usually in association with very able collaborators so that I think of myself, this evening, as the spokesman for this rather large group.

Our active interest in the subject dates back to 1936. The activated-complex theory of reaction rates had been formulated in a generalized form the year before. Thus, in 1936, as now, one believed that using quantum mechanics and statistical mechanics all rate processes were calculable. Dr. Raymond Ewell, who was then a graduate student at Princeton, insisted on a literal demonstration for viscosity. His own preoccupation with the preliminary Ph.D. examinations kept him out of the initial effort, but with the examinations out of the way we went to work in earnest. Since that time we have always been struggling to understand some aspect of the question of how matter relaxes under stress. Chemical reaction rate theory is tailor-made for the study of relaxation. Thus, the formal theory applied to experimental data helps in arriving at the mechanism.

Two guiding principles are especially useful in estimating the probability of a mechanism. (*1*) Of all possible mechanisms that which is most economical of energy will be most important when energy is scarce, *i.e.*, at low temperatures and under lower stresses. This helps us to understand the absence of turbulence and the fact that ordinary Poiseuille flow proceeds by the movement of molecules rather than by aggregates of molecules. (*2*) In a condensed system the provision of maneuver space for the molecule to move into is indispensable. This principle explains the Batchinski result that the fluidity of liquids increases linearly with the molal volume. Also the idea that this maneuver space must be provided against any external as well as internal pressure explains the effect of pressure on viscosity.

The relaxation theory leads to the notion that substances flow, even though very slowly, under the smallest stresses. The old idea that flow begins only when a critical stress is reached parallels the outworn concept that chemical decomposition begins only above a certain temperature.

---

[1] Presented at the Annual Meeting of the Society of Rheology, New York, N. Y., November 4–5, 1949.

Plasticizers and chemicals which modify structure are to be understood also in terms of rate processes.

As we look to the future we see much profit to be gained by mechanical engineers and physicists willing to study the statistical-mechanical methods of equilibrium and rate theory, while chemists need to apply more of the methods of hydrodynamics and elasticity.

In any case we confidently expect great developments in the understanding of the flow properties of matter in the immediate future.

Finally I again wish to express my appreciation for the Bingham medal and for the kind wishes of my friends.

RHEOLOGICAL PROPERTIES OF PHENOLIC RESINS. EFFECT OF REACTION WITH HEXAMETHYLENETETRAMINE ON PROPERTIES OF A PHENOL-FORMALDEHYDE NOVOLAK [1, 2]

A. J. Guzzetti and G. J. Dienes [3]

Development Laboratories, Bakelite Division, Union Carbide and Carbon Corporation, Bound Brook, New Jersey

Turner Alfrey, Jr.

Polymer Research Institute, Polytechnic Institute of Brooklyn, Brooklyn, New York

Received February 17, 1950

INTRODUCTION

The purpose of the work described herein was the study of the rheological properties of phenolic resins of intermediate degrees of cross-linking.

There are several varieties of phenolic resins. The one used in this work was of the novolak or two-stage type made from unsubstituted phenol and formaldehyde.[4] Novolaks are prepared in acid solution with an aldehyde to phenol mole ratio usually in the range 0.7–0.9. They are not heat reactive and require the addition of a cross-linking agent, such as hexamethylenetetramine (hexa)[5] to convert them to heat-hardenable resins.[6]

The commonly accepted structure of phenol-formaldehyde novolaks is that of relatively short chains of various lengths, which consist of phenolic nuclei joined by methylene bridges in the positions *ortho* and *para* to the hydroxyl groups (6,7,8,9,13,14). A typical molecule may be represented as:

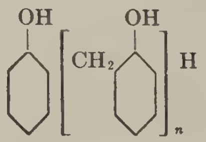

---

[1] Presented at the Annual Meeting of the Society of Rheology, New York, N. Y., November 4–5, 1949.

[2] From Master's thesis by A. J. Guzzetti at Polytechnic Institute of Brooklyn.

[3] Present address: North American Aviation Corporation, Los Angeles, California.

[4] Phenolic resins may also be prepared from alkyl-substituted phenols (cresols, *etc.*) containing open *ortho* and *para* positions and from other aldehydes, as furfural.

[5] The commonly employed abbreviation "hexa" is used throughout this paper to denote hexamethylenetetramine.

[6] The heat-hardenable resols, or one-step resins, are prepared in alkaline solution, with an aldehyde to phenol mole ratio in excess of 1.0.

Unreacted phenol may also be present. The trifunctionality of phenol indicates a possibility of branched chains (4,10).

At room temperature, most novolak resins are weak brittle solids. At elevated temperatures, they are Newtonian liquids characterized by high activation energies of viscous flow (3).

While novolaks are pyrolyzed at high temperatures (9) (250–450°C.), they are chemically stable over the temperature range used in this work. Conversion to highly cross-linked structures requires the addition of some substance which reacts with and joins the chains. Hexa is the most satisfactory and most commonly empolyed hardener. The mechanism of reaction between hexa and novolaks is not known. Very little is known of the structure of the gelled and highly cross-linked resins but it is generally believed that they consist of phenolic nuclei joined in a three-dimensional network by methylene bridges. Evidences of the presence of other types of linkages have been reported.

A profound change in physical properties occurs when a novolak resin reacts with hexa. Ultimate strength and toughness are greatly increased and the highly cross-linked products are typical viscoelastic materials of a high order of rigidity (5,12). There are almost no data in the literature on the rheological properties of resins of degrees of cross-linking intermediate between those of the novolaks and the highly cross-linked "cured" resins of commerce. It is difficult to measure the rheological properties of these intermediate resins because of their reactivity at the elevated temperatures at which their properties are of interest. In order to avoid this difficulty and gain some insight into the sequence of structures occurring during actual curing with full amounts of hexa, a series of samples were prepared from a single novolak resin by more or less complete reaction with intermediate amounts of hexa, and the rheological properties of the resultant resins were studied at elevated temperatures.

EXPERIMENTAL

The novolak resin used in this work (hereinafter referred to as resin A) was prepared by refluxing for 3 hr., at atmospheric pressure 2000 g. (21.26 mols) phenol crystals, U.S.P.; 1382 g. (16.65 mols CH_2O) 36.15% formaldehyde solution, U.S.P.; and 52.11 ml. 1.004 *N* HCl solution. The hydrochloric acid was then neutralized with an exactly equivalent amount of 1 *N* NaOH solution, and the water and other volatile matter distilled off at atmospheric pressure until a resin temperature of 155°C. was reached. The resultant resin had intrinsic viscosities at 25°C. in acetone and methanol of 0.046 and 0.043, respectively. Its free- (unreacted) phenol content was 7.0% by weight.

The hexa employed in preparing cross-linked samples was C.P. grade and assayed 99.0% hexa by Kjeldahl determination.

Preliminary trials indicated that a mechanical mixture of resin A and hexa (prepared by grinding in a mortar) containing as little as 0.25% hexa yielded, after reaction, a relatively small amount of gelled particles in a mass of soluble resin. Molecular dispersions of hexa in resin A were therefore prepared by dissolving both in a low-boiling mutual solvent and removing the solvent at room temperature to prevent uncontrolled reaction. Methanol was found to be suitable. The methanol solutions were spread on glass plates and allowed to air-dry until the residues could be scraped off in the form of flakes (several days were required). The flakes were futher air-dried until they could be powdered in a mortar. Residual methanol and absorbed water were driven off during subsequent reaction at elevated temperature.

The resin A–hexa mixtures were caused to react by heat alone under controlled conditions. In order that the resultant resins be sufficiently reacted to prevent appreciable change in properties during subsequent rheological testing, it was necessary to determine the time–temperature treatment required to attain substantially complete reaction. In the region below the gel point, this was done by noting the change in specific viscosity with reaction time; the criterion of complete reaction was taken as the absence of further viscosity increase with increased reaction time. Samples were heated in open test tubes placed in a constant-temperature bath. Specific viscosities of 2 g./100 ml. solutions in methanol were determined with Ostwald pipets at 25.00 ± .05°C. The results obtained with 1.00 and 1.10% hexa are shown in Fig. 1. It is seen that substantially the same limiting viscosity was obtained with the 1.00% hexa-resin A mixture at reaction temperatures of 150, 170, and 190°C., although the rates, of course, were temperature dependent. The curve for the 1.10% hexa mixture indicates that a higher viscosity was attained with higher hexa content and a longer time was required to reach the limiting value. The two lines at the bottom of the graph indicate the absence of appreciable change in resin A without hexa when heated 2 hr. at 170°C. in either an open or a sealed tube. Based upon these results and the fact that 1.10% was the highest hexa concentration employed which did not cause gelation, 2.0-2.5 hr. reaction at 170°C. was chosen for the preparation of ungelled resin samples for rheological testing.

Gelation was found to occur with a hexa content between 1.1 and 1.2%. Samples containing 1.10% or less hexa remained completely and readily soluble in methanol and acetone after 4 hr. reaction at 170°C. Those containing 1.20% or more hexa gelled when heated only 1 hr. at 170°C., and the products swelled but gave no visible evidence of dissolving in these solvents even after prolonged contact.

Two methods were available for following the course of reaction in resin A–hexa mixtures which gelled. The first of these, chemical determination of residual nitrogen, indicated that complete elimination of nitrogen, if indeed ever attained, required a very long time at elevated temperatures. Samples of a 1.50% hexa–resin A mixture heated at 170°C. lost nitrogen at a diminishing rate as heating time was increased, and still contained appreciable amounts after 16 hr. at this temperature. The second method, comparison of creep curves obtained under like conditions in the parallel plate plastometer, was therefore employed to estimate the heating time at 170°C. required to effect sufficient reaction to prevent appreciable further change during measurement of rheological properties. This was not entirely satisfactory because of the lack of information as to whether differences in creep behavior resulting from longer heating were due to further reaction, loss of volatile matter (as phenol) which may have acted as plasticizer, or both. The odor of phenol was detectible in all samples at temperatures well below that employed for reaction.

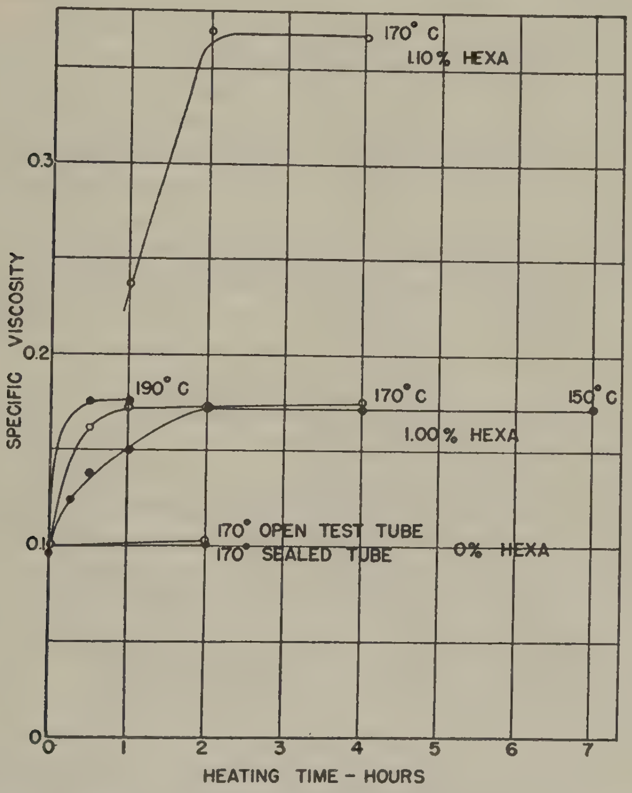

FIG. 1. Specific viscosity vs. reaction time for 2-g./100 ml. methanol solutions of resin A and resin A-hexa reaction products.

Preliminary tests with samples of the 1.20% hexa–resin A mixture heated 2, 4, and 8 hr. at 170°C. indicated a sharp reduction in creep in going from 2 to 4 hr. reaction time, but negligible further reduction as a result of heating 8 hr. The final sample, employed for determination of rheological properties, was allowed to react 8 hr. A portion of this final sample was heated an additional 2 hr. at 170°C. in a sealed tube and its creep compared with that of the material heated 8 hr. There was no appreciable difference.

In spite of this evidence of substantially complete reaction, it was found that exposure to the atmosphere in the plastometer at much lower temperatures (100–130°C.) resulted in small but consistent reductions in creep. When preheat time was increased from 0.5 hr. to 2 hr. (which doubled the total time of exposure to plastometer air), total creep at the end of 4000 sec. was reduced by about 10–20% depending on the temperature. This effect was small compared with that caused by changing temperature, and negligible compared with differences among the samples, but it indicated that it was probably useless to extend the reaction time further in an attempt to produce samples which would be entirely stable under test conditions. For this reason, hexa–resin A mixtures containing more than 1.2% hexa were simply allowed to react at 170°C. for somewhat longer than 8 hr., and their behavior was checked to be sure that their loss in plasticity on exposure to test conditions was no greater than that of the sample made with 1.2% hexa.

It may be noted that exposure of resin A and the resin–hexa mixtures to the atmosphere during reaction at 170°C. resulted in the formation of a small amount of a dark brown, insoluble oxidation product. In the case of the fusible resins, this material consisted of a surface skin which was easily removed. But the gelled resins, which took the form of foam, were darkened throughout so that it was necessary to heat all mixtures containing more than 1.1% hexa in a reducing atmosphere.

The resin samples prepared for rheological testing were as follows:

TABLE I

Designation	Composition unreached mixture		Reaction time at 170°C.
	Resin A	Hexa	
	per cent	*per cent*	*hr.*
B	100.	0	2
C	99.5	0.50	2
D	99.0	1.00	2
E	98.9	1.10	2.5
F	98.8	1.20	8
G	98.7	1.30	10
H	98.6	1.40	12

The reacted samples were cooled, ground in a mortar, and stored in airtight containers or in a desiccator. For all comparisons, resin B was used as the unreacted reference material. This sample was identical with resin A except that it received a heat treatment similar to that of the reacted samples.

The rheological properties were determined by means of the parallel-plate plastometer. This instrument and its application to various high polymers have been described in previous papers (1,2,3). Techniques of sample preparation peculiar to the materials under investigation were somewhat different from those reported previously. All test specimens were prepared by compressing the ground resins at room temperature into 0.50-in. diameter pellets at about 10,000 p.s.i. in a steel mold. It was found that this method was satisfactory for the gelled as well as ungelled resins as they apparently contained sufficient fusible matter for the individual particles to fuse together and yield a fairly clear specimen at the end of the test.

Test specimens of ungelled resins B–E were preheated thoroughly and allowed to flow for 900–1500 sec. Specimens of gelled resins were all preheated 30 min. and creep was observed for 4000 sec. at loads of 5, 10, and 20 kg.

RESULTS AND DISCUSSION

1. Rheological Properties and the Effect of Temperature

Tests on the ungelled resins A–E indicated no measurable load dependence or elastic effects. For example, tests on resin E at 85°C. and various loads gave the following results:

Load, *kg.*	5	10	30	60
Viscosity, *poise* $\times 10^{-7}$	3.60	3.75	3.28	3.49

This is in agreement with previous observations that novolak resins are Newtonian liquids (3). Linear $1/h^4$-t curves were obtained passing substantially through the origin and the viscosities were calculated by the equation:

$$\eta = \frac{8.21 \times 10^6 W}{MV^2} \text{ poise,} \qquad [1]$$

where W = load in kg., M = slope of $1/h^4$–t graph in cm.$^{-4}$-sec.$^{-1}$, and V = volume in cm^3.

The log viscosity versus $1/T$ graphs are shown in Fig. 2. The straight lines indicate adherence to the Arrhenius equation:

$$\eta = Ae^{Ea/RT}.$$

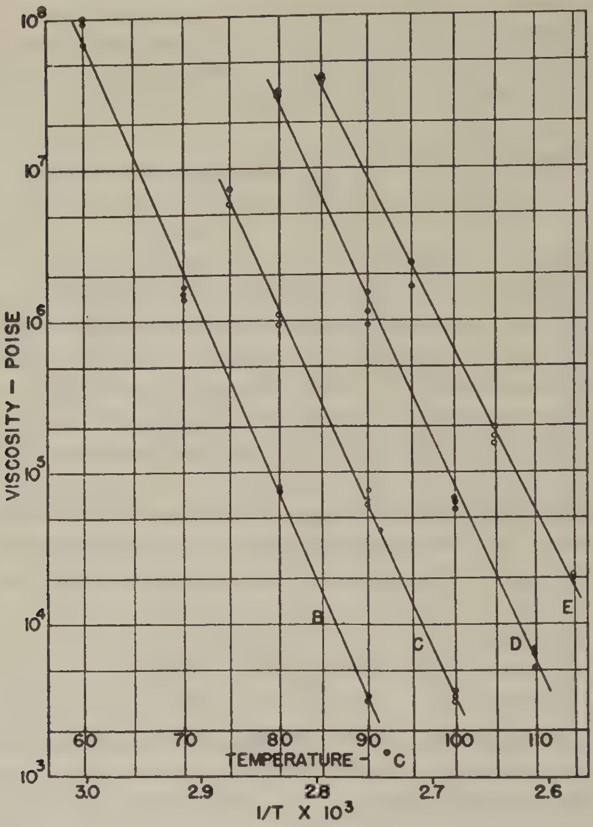

FIG. 2. Log viscosity vs. $1/T$ for ungelled resins B–E.

The slope of each line was calculated by the method of least squares (11) and the corresponding activation energies and 95% confidence limits were computed with the following results:

TABLE II

Resin	Initial hexa *per cent*	$Ea \pm d$ (.05, Ea) *cal.*
B	0	79,940±900
C	0.50	76,770±910
D	1.00	77,190±900
E	1.10	68,980±900

These data and those of Fig. 2 indicate a regular increase in viscosity and small decrease in activation energy with increased percentage hexa below the gel point.

The behavior of the gelled resins (F–H) was in sharp contrast to that of the ungelled ones. True flow was not observed even with resin F, a large amount of recovery occurred on removal of load, and considerable load dependence was observed. The method of treating the data obtained from parallel-plate plastometer tests was of necessity somewhat different from that employed for the ungelled resins because the creep curves were no longer straight lines. From the plate separation (h) vs. time (t) readings, a creep curve was computed according to the formula:

$$F\left(\frac{1}{h^4} - \frac{1}{h_0^4}\right) = g\ (t), \qquad [2]$$

where: $F = \dfrac{V^2 \times 10^{-6}}{8.21\ W}$,

h_0 = initial sample height

$g\ (t)$ = creep function (*i.e.*, normalized deformation).

As has been shown previously (2), the curve described by Eq. 2 is independent of applied load and specimen size (within well-defined limits) for any linear viscoelastic material.

The standard 4000-sec. creep time was extended to 10,000 sec. in one experiment with resin F in an attempt to determine whether true flow

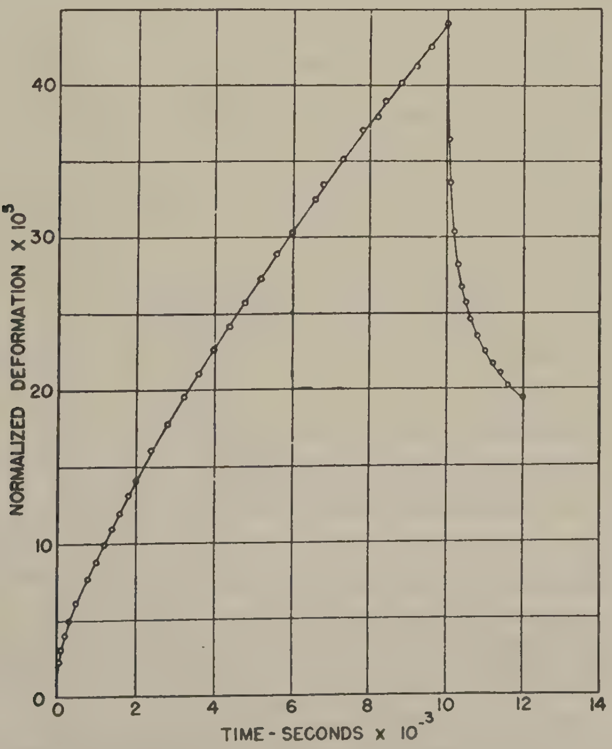

Fig. 3. Creep of resin F (1.2% hexa) at 110°C. and 10-kg. load, and recovery at 0.1 kg.

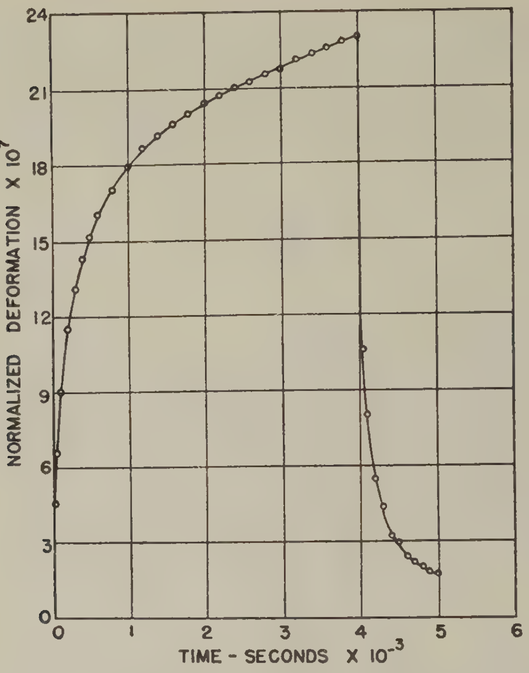

FIG. 4. Creep of resin H (1.4% hexa) at 110°C. and 20-kg. load, and recovery at 0.1 kg.

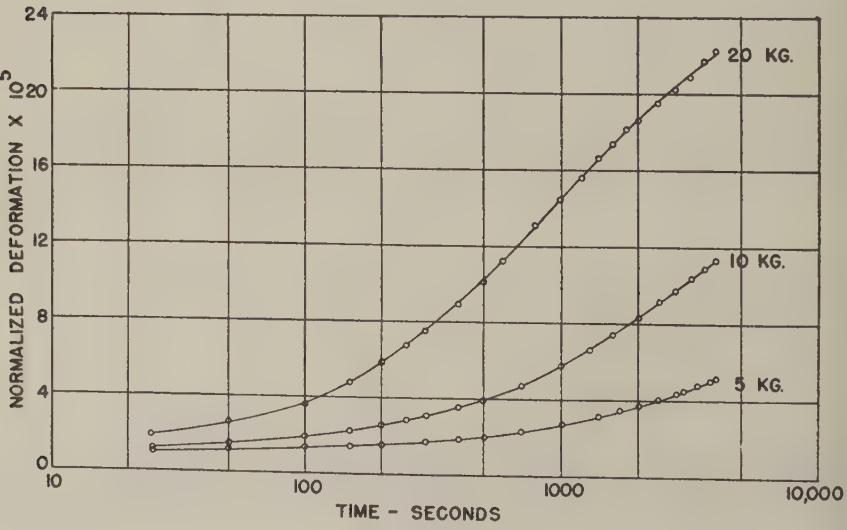

FIG. 5. Effect of load on creep of resin G (1.3% hexa) at 130°C.

occurred. The normalized deformation–time curve (Fig. 3) did not become linear within the limits of the test. This may have indicated that true flow did not occur, but it is also possible that the contribution of true flow was too small to be distinguishable from elastic deformation or that exposure to air at the test temperature resulted in a continual increase in principal viscosity. However, the large recovery observed in the first 2000 sec. after removal of load indicated the predominance, at least, of elastic effects. Recovery was measured in only a few cases because of the poor precision of such measurements in the plastometer (2). An example of recovery with resin H is given in Fig. 4.

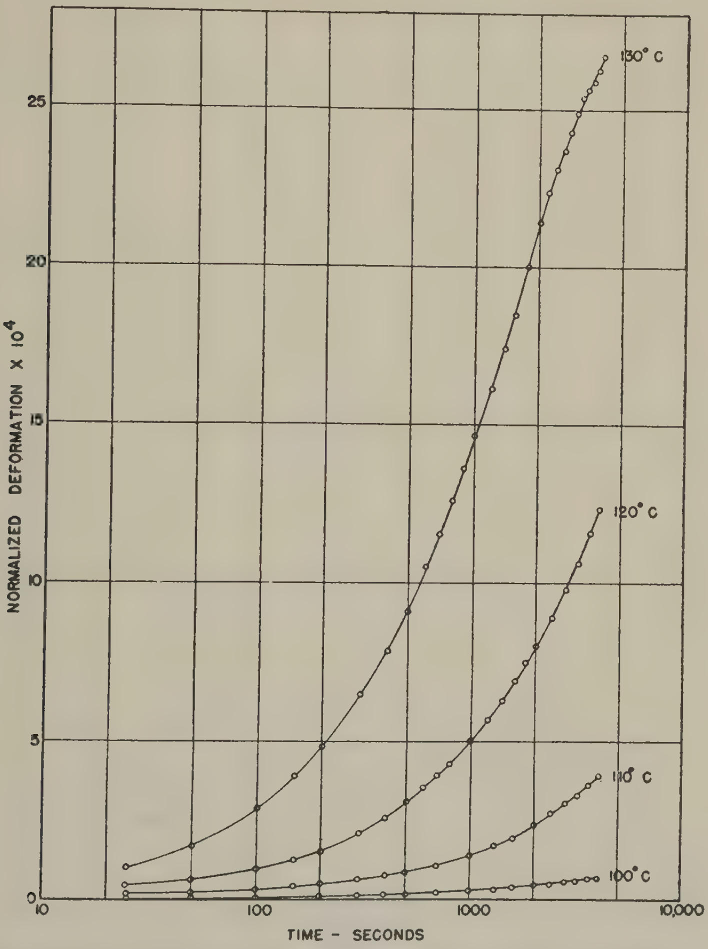

FIG. 6. Effect of temperature on creep of resin F (1.2% hexa) at 20-kg. load.

Increasing the load on the specimens resulted in considerable increase in normalized deformation. An example of this is shown in Fig. 5 in which the normalized deformations of resin G at the three loads and at 130°C. are plotted against log time. Similar results were obtained at other temperatures and with resins F and H.

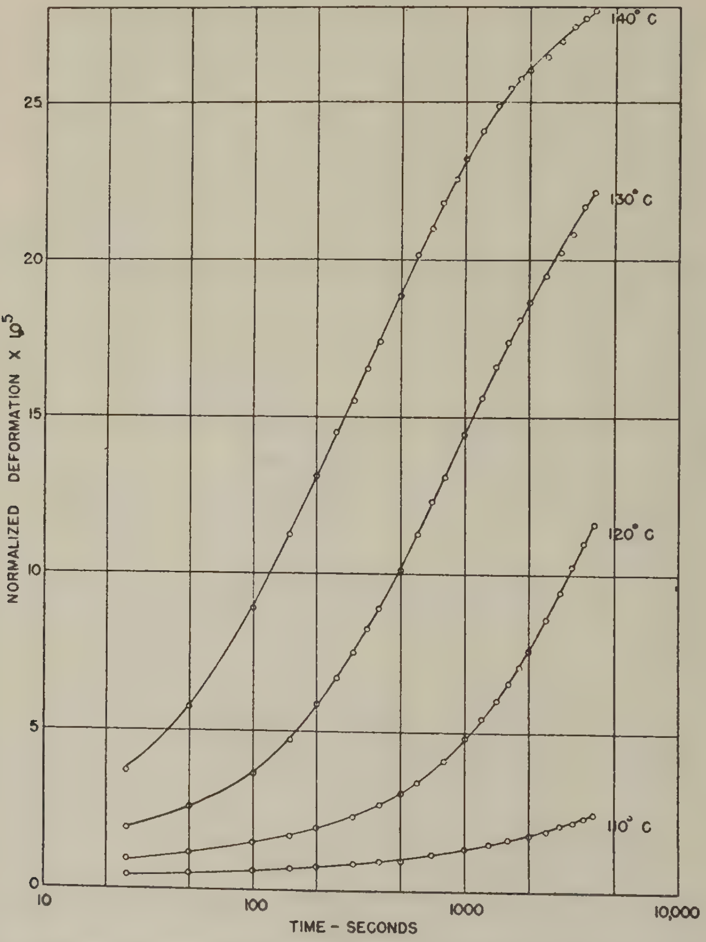

Fig. 7. Effect of temperature on creep of resin G (1.3% hexa) at 20-kg. load.

The effects of temperature on normalized creep of the three gelled resins are shown by Figs. 6–8 which represent the data obtained at 20-kg. load. It is seen that a higher temperature resulted in a closer approach to equilibrium deformation in the fixed time of test (4000 sec.). It was found that the log time required to attain a given normalized deformation with any one resin under the same load varied approximately linearly with $1/T$.

This permitted calculation of the over-all activation energy of all the molecular processes which were responsible for the deformation properties of each resin. The slopes of the log time versus $1/T$ lines were calculated by the method of least squares for each resin at each load and for two or three different values of deformation, and all slopes for a given resin were

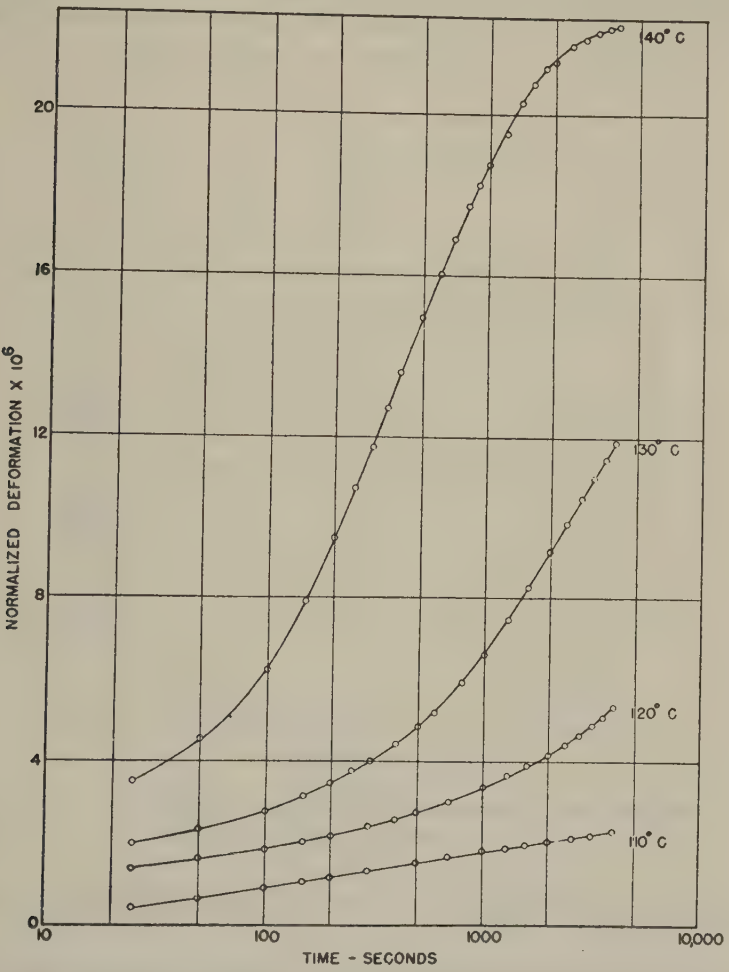

FIG. 8. Effect of temperature on creep of resin H (1.4% hexa) at 20-kg. load.

veraged. The activation energies were 55,700 ± 6500, 50,600 ± 6500, nd 59,500 ± 6500 cal. for resins F, G, and H, respectively. It is seen that alues for the three resins did not differ significantly from each other and at the average of 55,300 cal was appreciably lower than the activation ergies of viscous flow of the ungelled resins (69,000–80,000 cal).

It was found that the creep curves could be fitted fairly well by empirical five-parameter mechanical models whose constants were calculated by a modification of the method of successive residuals (2). However, the physical significance of these models was limited by the fact that deformation was not continued to equilibrium and because of nonlinearity with respect to applied load. It was possible to extrapolate some, but not all, of the parameters to zero load to obtain a single set of constants for each resin at each temperature. In general, the viscous and elastic constants decreased with increasing temperature and increased about tenfold for each 0.1% increase in hexa.

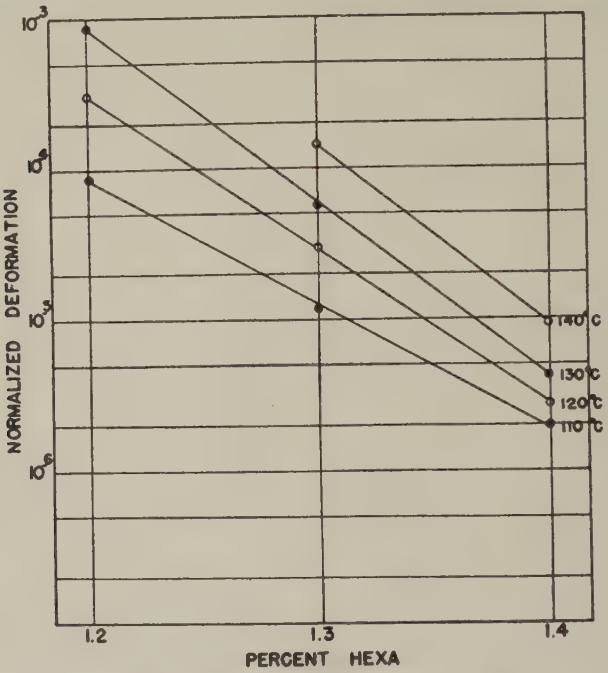

Fig. 9. Log normalized deformation at 1000 sec. and 10-kg. load vs. per cent hexa for gelled resins.

2. *Flow Properties as a Function of Initial Hexa Content*

The effect of variations in the proportion of hexa with which resin A had reacted on the properties of the resultant resins cannot be simply represented in terms of viscous and elastic constants over the whole range from 0–1.4% hexa. In the region below the gel point only viscosities were observed and the differences in activation energies of viscous flow were not great. A fair approximation of the behavior over a rather wide temperature range could therefore be obtained by comparison at a single temperature. It was found that log viscosity increased approximately linearly with the percentage hexa up to slightly below the gel point and then rose at a rapidly increasing rate as the gel point was approached (see left hand part of Fig. 11).

In the region above the gel point no such satisfactory comparison was possible, but comparisons were made on a basis of total creep at a given time, temperature, and load. An example of the behavior is given in Fig. 9 in which log normalized deformation at 1000 sec. and 10-kg. load is plotted against percentage hexa. The linearity of these graphs is probably fortuitous, but the data demonstrate the roughly tenfold decrease in total creep with each 0.1% increase in hexa.

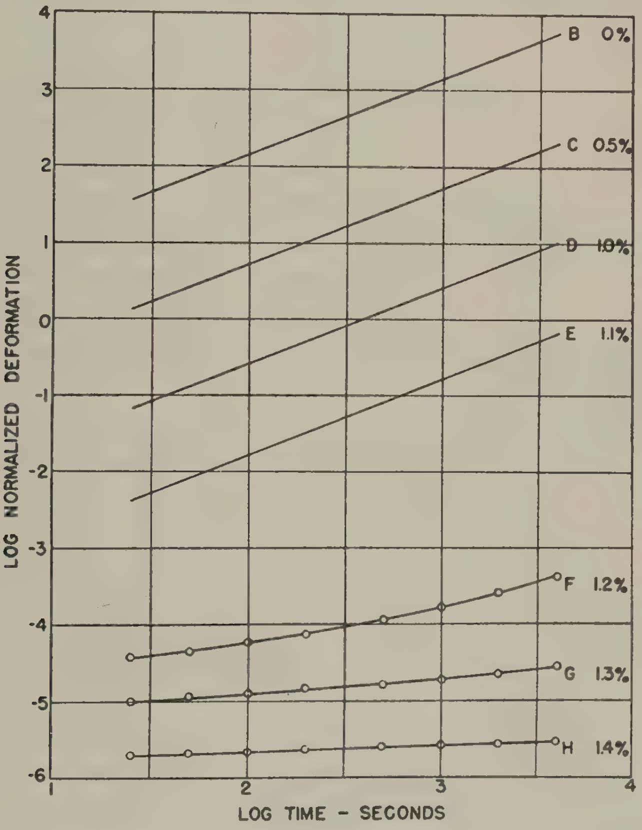

FIG. 10. Effect of per cent hexa on creep curves at 120°C. and 5-kg. load.

Some idea of the over-all variation in properties with hexa concentration may be obtained by plotting the normalized creep curves for all resins at a fixed temperature on the same graph. Figure 10 shows the log normalized deformation-log time curves for resins B–H inclusive at 120°C. and 5-kg. load. Those for resins B–E were calculated from the viscosities extrapolated from Fig. 2 and are, of course, independent of load.

Another method, though arbitrary, of tracing the change in properties over the entire range is on the basis of apparent viscosity (inverse normalized deformation rate) at some particular temperature and time after application of load. Figure 11 shows the change in log apparent viscosity (η_a) at 120°C. and 1000 sec. with percentage hexa. The values for the ungelled resins are the true viscosities obtained from Fig. 2 by extrapolation. Those for the gelled resins were obtained by extrapolating to zero load the values of η_a obtained graphically from the creep curves. In spite of the arbitrary nature of this comparison, it emphasizes the sharp break

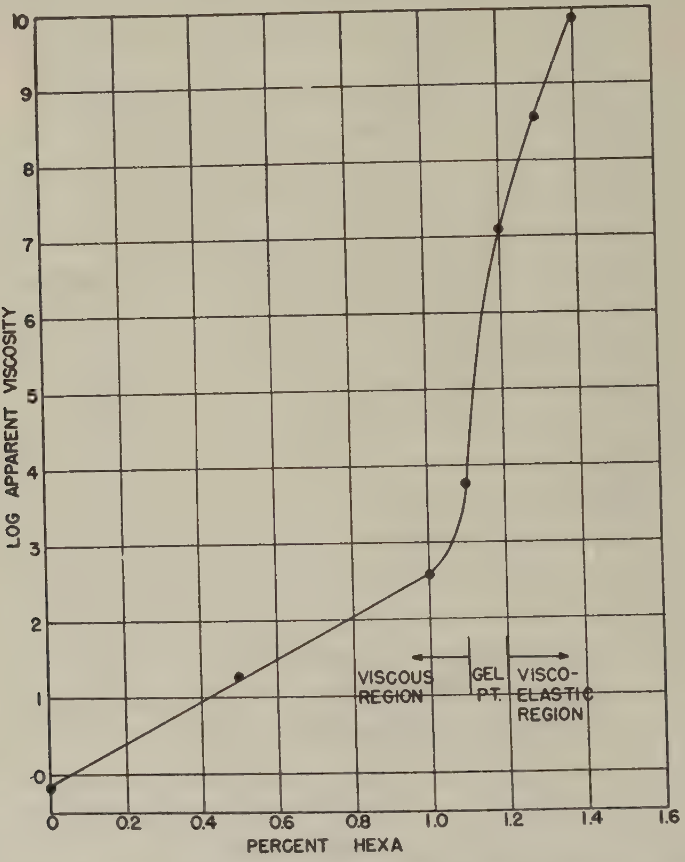

FIG. 11. Log apparent viscosity at 120°C. and 1000 sec. vs. per cent hexa.

in properties in the neighborhood of the gel point and the continued rapid change in properties with increasing amounts of hexa in the region immediately beyond.

ACKNOWLEDGMENTS

The authors wish to express their appreciation to Mr. F. D. Dexter and Dr. E. A. Barr (both of the Development Laboratories, Bakelite Division) for helpful discussions during the course of the work and review of the manuscript, and to the Bakelite Corporation for permission to use the parallel plate plastometer and auxiliary equipment.

REFERENCES

1. Dienes, G. J., and Klemm, H. F., *J. Applied Phys.* **17**, 458 (1946).
2. Dienes, G. J., *J. Colloid Sci.* **2**, 131 (1947).
3. Dienes, G. J., *J. Colloid Sci.* **4**, 254 (1949).
4. Flory, P. J., *Chem. Revs.* **39**, 137 (1946).
5. Gailus, W. J., and Telfair, D., *Modern Plastics* **22**, 149 (May, 1945).
6. Koebner, M., *Chem.-Ztg.* **54**, 619 (1930); *C. A.* **24**, 6039 (1930).
7. Koebner, M., *Brit. Plastics* **2**, 197, (1930); *C. A.* **26**, 609 (1932).
8. Lilley, H. S., *J. Oil & Colour Chemists Assoc.* **26**, 88 (1943).
9. Megson, N. J. L., *Trans. Faraday Soc.* **32**, 336 (1936).
10. Nickerson, H., *Brit. Plastics* **19**, 345 (1947).
11. Snedecor, G. W., Statistical Methods. Iowa State College Press, Ames, Iowa, 1948.
12. Telfair, D., Carswell, T. S., and Nason, H. K., *Modern Plastics* **21**, 137 (Feb., 1944).
13. U. S. Patent No. 2,464,207.
14. Vansheidt, A., Itenberg, A., and Andreeva, T., *Ber.* **69**, 1900 (1936).

PLASTIC FLOW PROPERTIES OF CASEIN[1, 2]

Leif Hougen[3] **and N. J. Hipp**

Eastern Regional Research Laboratory, Philadelphia, Pa.

Received February 17, 1950

INTRODUCTION

The flow properties of casein during extrusion and molding are important to the manufacturer of casein plastic. Variations in flow due to differences in the quality of caseins or other factors produce undesirable variations in the product. Several papers have dealt with flow characteristics of casein plastics. Cooper and Hand (1) have described a test for quality control of rennet casein in which a Scott Plastomoter was used. Haller (2) demonstrated a relationship of flow to pressure and water content at room temperature. He found that there was a sudden increase of flow when the water content was increased to 20–21%, which he considered to be caused by a change in the structure of the casein gel. The effect of different pH, and ash and lactose contents on plastic flow was studied by Gallay and Tapp (3), who extruded casein with a laboratory extruder at pressures from 20,000 to 77,000 p.s.i.

It appeared desirable to extend the study on the flow properties of casein to include pressures and temperatures nearer to those generally employed in the manufacture of casein plastics and to compare the flow properties of acid casein with those of rennet casein and modified caseins.

MATERIALS AND TESTING PROCEDURE

For testing the effect of composition of casein on flow properties the following samples of casein were used:

(*1*). *High-grade commercial acid casein containing 0.67% ash.*[4]

(*2*). *Commercial rennet casein containing 8.5% ash.*

(*3*). *Rennet casein prepared from acid casein by the following method:* 500 g. of acid casein was dissolved with sodium hydroxide in 17 l. of water. Water solutions containing 32 g. of calcium hydroxide

---

[1] Presented at the Annual Meeting of the Society of Rheology, New York, N. Y., November 4–5, 1949.

[2] A contribution from the Eastern Regional Research Laboratory, one of the laboratories of the Bureau of Agricultural and Industrial Chemistry, Agricultural Research Administration, U. S. Dept. of Agriculture.

[3] Norwegian Government Fellow, 1947–48.

[4] All ash values are on a moisture-free basis.

and 53 g. of dihydrogen calcium phosphate were added simultaneously with rapid stirring in order to obtain a colloidal dispersion of insoluble calcium phosphate in the casein solution. The resulting solution contained about the same amount of casein, calcium, and phosphorus as skim milk. The final pH of the solution was adjusted to 6.7 with dilute hydrochloric acid. To this solution was added 0.35 g. of Hansen's rennet. After coagulation, the mixture was heated to 40°C. and the casein was filtered, washed, and dried at 50°C. The ash content of this casein was 13.5%.

(*4*). *Para casein prepared from acid casein by the following method:* 600 g. acid casein was dissolved in sodium hydroxide and diluted to 15 l. with water. Calcium chloride (95 g.) was added, and the pH was adjusted to 6.7. The solution was clotted by the addition of 0.5 g. Hansen's rennet. After clotting, the casein was filtered, washed, dissolved in sodium hydroxide, and diluted to 15 l. The casein was precipitated by adding dilute hydrochloric acid to pH 4.6, washed free of chloride ions, and dried at 50°C. The ash content was 1.3%.

(*5*). *Carbamido casein* prepared and described by Hipp *et al.* (4): by treating casein with potassium cyanate.

(*6*). *Reprecipitated commercial acid casein.*

To determine whether dissolving and reprecipitating affect the flow properties of casein, a sample was prepared by dissolving acid casein in dilute sodium hydroxide and precipitating with hydrochloric acid. After the casein was filtered and washed, it was dried at 50°C.

The Rossi-Peakes flow tester (5), a constant-force, vertical-orifice type machine was used to determine plastic flow. The Rossi-Peakes apparatus was chosen for this work because (*1*) the measurements of plastic flow are obtained under dynamic conditions, (*2*) temperature and pressure are easily adjusted to obtain measurable plastic flow with reasonable variations in water content, (*3*) the measurement is made within an enclosed chamber which prevents the loss of moisture, and consequently the plastic flow value is obtained on material with a constant moisture content, (*4*) the actual flow measurement requires only 2 min., which minimizes the changes in physical properties that occur in different degree when casein is heated in the dry state or in the presence of moisture, and (*5*) the results are precise and highly reproducible. The Rossi-Peakes machine is substantially free of the kneading or shearing action present in commercial extruders for casein plastics.

The test specimen, a cylinder ⅜-in. in diameter and ⅜-in. in height, was made at room temperature on a hand-operated tablet machine. It was found that a variation in the density of the test specimen between the weights of 0.70–0.75 g. for a roughly constant volume did not measurably affect the plastic flow. The plastic material under the influence of heat and pressure was forced into an orifice ⅛-in. in diameter and 2 in. long. The distance of flow into the orifice was measured by a follower rod and was recorded on a time graph with a mechanical ratio of 3:1. By this device the plastic flow can be precisely measured to ± 0.01 in.

For normal operation of the flow tester at 100°C. or higher, steam at the required pressure was circulated in passages around the orifice and the material chamber. By the use of two pressure-regulating valves, the temperature within a series was maintained within ± 0.2°C. For temperatures below 100°C., hot water from a thermostatically controlled, electrically heated water bath was circulated by means of a centrifugal pump.

EXPERIMENTAL

In testing the plastic flow of casein, it is difficult to keep the water content of the test specimens constant because samples lose water by evaporation during their preparation. Samples were prepared as follows: to the ground casein, water was added in amounts that gave the approximate water content desired. The moistened casein was sifted through a 40-mesh sieve and placed in a closed container. A portion of the moistened casein was made into pellets by use of a tablet press and then placed back in the container with the moistened ground casein and allowed to equilibrate in the refrigerator for 6–7 days. The exact water content of the pellets was determined at the same time as the flow test by drying them at 105°C. for 3 hr. or more, or until they reached constant weight. In all cases, the water content of the test specimen was in equilibrium with the powdered casein.

The caseins tested for plastic flow at various water contents are listed in Tables I and II; the measurements are the average of three closely checking values. The tests were performed at temperatures from 50 to 140°C. and pressures of 500–3000 p.s.i. For each water content, the plastic flow can be expressed as a function of either pressure or temperature. Figures 1 and 2 are graphs for commercial acid casein with a 19.10% water content. The plastic flow in this instance is defined as the distance the material is forced into the orifice during a period of 2 min. It is not possible to compare the flow properties of two caseins by means of these curves alone, since the water content of each sample differs because of experimental difficulties, and the relation between the water content and flow is unknown. The American Society for Testing Materials term "flow temperature" has been adopted. They define the flow temperature (6) as the temperature at which the material flows 1 in. when subjected to a pressure of 1500 p.s.i. over a period of 2 min. For our work, however, it was necessary to modify this definition in order to cover a reasonable range of the three parameters—temperature, pressure, and water content. The tem-

TABLE I

Plastic Flow Measurements of Commercial Type Caseins

Water content	Temperature	Pressure of (p.s.i.)					
		500	1000	1500	2000	2500	3000
		(*1*) Commercial acid casein					
per cent	*°C.*	*in.*	*in.*	*in.*	*in.*	*in.*	*in.*
8.70	110	—	—	—	—	—	0.10
	120	—	—	—	—	—	0.21
	130	—	—	0.17	—	—	0.50
	140	—	—	0.28	0.42	0.60	0.88
	150	—	—	0.38	0.75	1.09	1.43
13.00	100	—	—	0.18	0.25	0.34	0.43
	110	—	0.21	0.37	0.55	0.70	0.90
	120	—	0.36	0.62	0.90	1.31	—
	130	0.10	0.40	1.05	—	—	—
	140	0.16	1.40	—	—	—	—
15.20	80	—	—	0.15	—	—	0.39
	90	—	0.17	0.27	0.36	—	0.55
	100	—	0.24	0.42	0.52	0.74	0.86
	110	0.10	0.32	0.55	0.70	1.02	1.58
	120	0.22	0.68	1.40	—	—	—
19.10	70	—	—	0.25	0.40	0.51	0.61
	80	—	0.25	0.40	0.55	0.70	0.95
	90	0.15	0.42	0.64	0.92	1.19	1.52
	100	0.20	0.59	1.03	1.55	—	—
	110	0.32	0.90	—	—	—	—
27.50	50	—	0.30	0.50	0.83	1.10	1.35
	60	0.20	0.57	0.93	1.30	—	—
	70	0.48	1.05	—	—	—	—
	80	0.95	—	—	—	—	—
		(*2*) Commercial rennet casein					
10.60	110	—	—	0.18	—	0.27	0.33
	120	—	—	0.21	0.26	0.36	0.44
	130	—	—	0.27	0.40	0.55	0.70
	140	—	—	0.44	0.70	0.86	1.19
	147.5	—	—	—	0.92	1.16	1.50
13.25	102	—	—	0.22	0.30	0.40	0.46
	106	0.12	0.22	0.35	0.42	0.50	0.62
	110	0.14	0.25	0.35	0.50	0.61	0.70
	120	0.14	—	0.50	0.68	0.92	—
	130	0.17	—	0.67	1.22	—	—

TABLE I—*Continued.*

Water content	Temperature	Pressure of (p.s.i.)					
		500	1000	1500	2000	2500	3000
(*2*) Commercial rennet casein							
per cent	*°C.*	*in.*	*in.*	*in.*	*in.*	*in.*	*in.*
15.00	100	—	0.40	0.65	0.85	1.03	1.20
	105	—	0.47	0.73	1.00	1.30	—
	110	—	0.56	0.90	1.20	—	—
	115	0.22	0.68	1.05	—	—	—
	120	0.28	0.76	1.39	—	—	—
19.40	70	—	—	0.33	0.45	0.56	0.70
	80	0.15	0.40	0.58	0.82	1.20	—
	90	0.20	0.50	0.82	1.30	—	—
	100	0.40	0.95	—	—	—	—
23.25	60	—	0.32	0.42	0.55	0.70	0.87
	70	—	0.50	0.68	0.92	1.32	—
	80	—	0.72	1.43	—	—	—
	90	0.37	1.00	—	—	—	—
27.90	40	—	0.15	0.28	0.40	0.50	0.60
	50	—	0.28	0.43	0.70	0.87	1.08
	60	0.20	0.40	0.90	1.10	—	—
	70	0.35	1.10	—	—	—	—
(*3*) Laboratory-prepared rennet casein							
14.30	100	—	0.19	0.30	0.38	0.48	0.61
	110	0.15	0.32	0.65	0.91	1.05	1.15
	120	0.15	0.45	0.92	1.23	—	—
18.70	70	—	—	0.30	0.38	0.49	—
	80	—	—	0.33	0.63	0.78	1.00
	84	—	0.46	0.97	1.12	—	1.46
22.90	60	—	—	0.43	0.64	0.78	1.00
	70	0.20	0.53	0.80	1.20	—	—
	80	0.40	0.95	—	—	—	—

perature where the casein flows 0.75 in. under the same conditions was used as the "flow temperature."

To determine flow temperatures for the caseins at the various water contents in Tables I and II, the flow at the pressure of 1500 p.s.i. is plotted against temperature. The data for acid casein are presented in Fig. 3.

TABLE II

Plastic Flow Measurements of Modified Casein

Water Content	Temperature	Pressure of (p.s.i.)	
		1500	2000
(4) Para casein			
per cent	*°C.*	*in.*	*in.*
13.50	115	0.75	1.00
16.70	71	0.25	0.32
	78	0.38	0.60
	84	0.62	0.90
	88	0.95	1.11
20.80	61	0.30	0.40
	71	0.70	0.90
	84	1.04	1.28
(5) Carbamido casein			
14.00	110	0.45	
	116	0.76	
	123.5	0.92	
17.50	85	0.67	
	101	1.16	
	111	1.40	
21.50	50	0.19	
	67	0.70	
	73	0.90	
27.50	50	0.70	
	56.5	0.93	
	67	1.30	
(6) Reprecipitated acid casein			
14.00	115	0.40	0.57
	121	0.60	0.90
	132	0.90	1.40
16.30	100	0.44	0.65
	105	0.62	0.81
	113	0.98	1.16
23.20	61	0.30	0.50
	71	0.65	1.00
	78	0.96	—

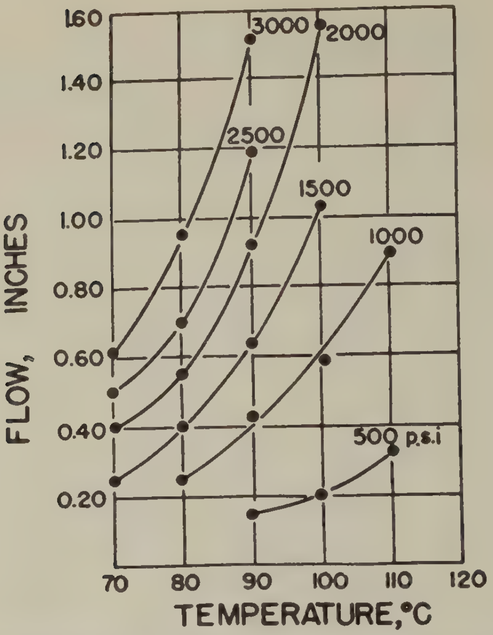

FIG. 1. Effect of temperature on plastic flow of commercial acid casein with 19.10% water content at various pressures.

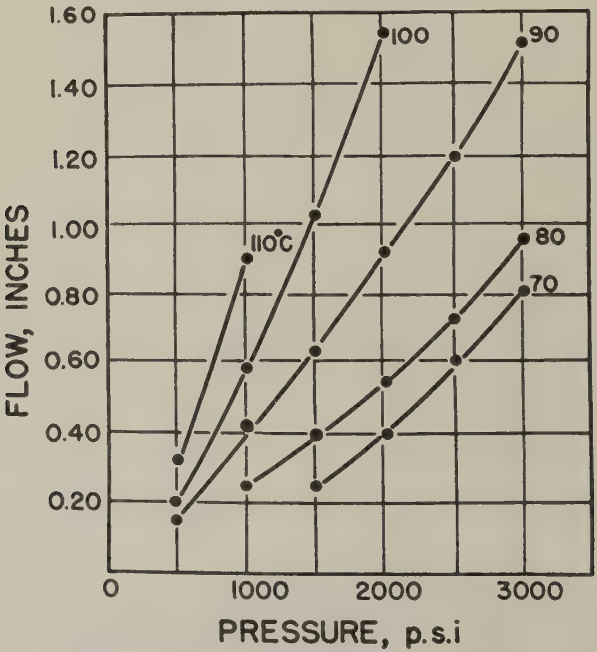

FIG. 2. Effect of pressure on plastic flow of commercial acid casein with 19.10% water content at various temperatures.

Figure 4 shows the effect of water content on the flow temperature for all the caseins studied. The tridimensional graph in Fig. 5 shows the temperature, pressure, and water-content relationship required to obtain a flow of 0.75 in. for commercial rennet casein. The values on the temperature axis are the temperatures required to give a flow of 0.75 in. at the indicated pressures and water content, and are not to be confused with "flow temperature," which refers to a fixed pressure of 1500 p.s.i. The data for Fig. 5 are obtained from families of curves (shown for example in Fig. 1, which gives the data for a single water content) by reading the temperature required to obtain a flow of 0.75 in. at each pressure. Similarly, the data for each water content are obtained from the isobars. A few of the values in Fig. 5 were obtained from extrapolated curves.

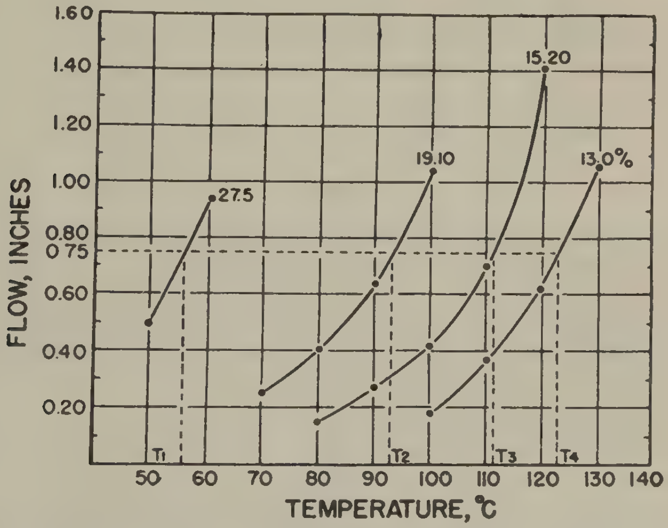

FIG. 3. Effect of temperature on plastic flow of commercial acid caseins with various water contents at 1500 p. s. i. T_1, T_2, etc., are the "flow temperatures."

DISCUSSION OF RESULTS

The data in Fig. 4 show that there are no great differences between the flow temperature-water content plots for the caseins studied, and therefore one may conclude that, for industrial use, difficulties arising from uneven flow may be overcome by altering the water content or the extrusion temperature. None of the data shows the sudden rise in plastic flow at 20–21% water content recorded by Haller (2). The apparent deviation from a smooth curve at 13.25 and 15.00% water content for rennet casein shown in Fig. 5 may be due to a chemical change of the protein induced by temperatures above 110°C. The rate at which the flow temperature in-

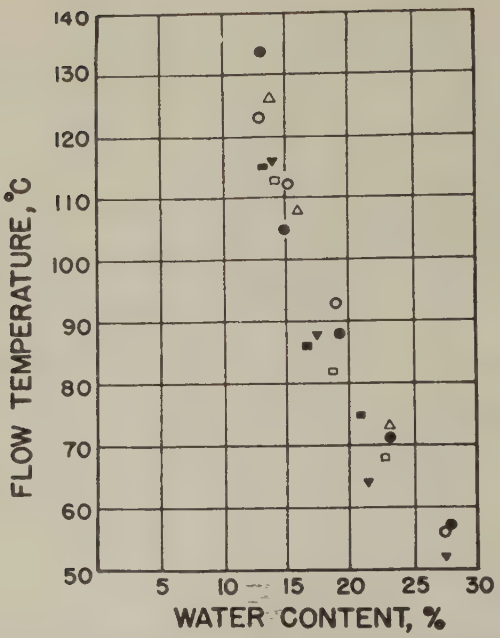

FIG. 4. Flow temperature for caseins of different water contents. ○ Commercial acid casein; ● commercial rennet casein; □ laboratory-prepared rennet casein; ■ para casein; △ reprecipitated acid casein; ▼ carbamido casein.

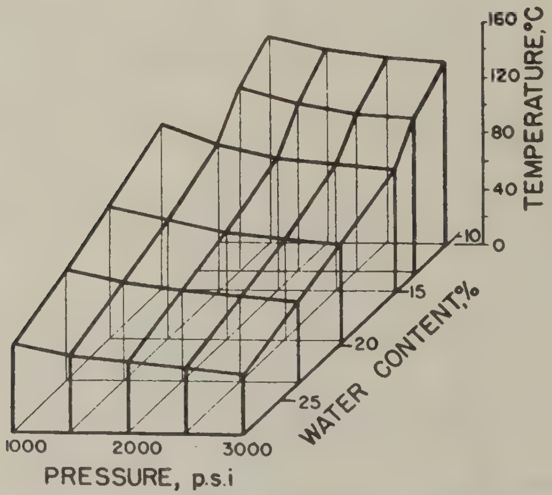

FIG. 5. Temperature, pressure, and water content required to give a plastic flow of 0.75 in. for commercial rennet casein.

creases at water contents lower than 15% is much greater than the rate of change at water contents above 15% (Fig. 4). Figures 1 and 2 show that the rate of increase in the plastic flow at a given water content increases with temperature and with pressure. The combined effect of temperature and pressure in relation to water content to produce a given plastic flow is shown in Fig. 5.

Our results on flow properties of casein are consistent with those of Gallay and Tapp (3), but greatly extend their measurements with respect to temperature and water content. By extending the temperature from that of the room to a range of 50–140°C., the flow data may be applied directly to commercial practice.

Although rennet casein is favored in the manufacture of casein plastics, the results on flow properties do not reveal significant differences between rennet and high-grade acid caseins. Any superiority of rennet casein due to desirable flow properties can be obtained with acid casein by minor changes in the water content or temperature of extrusion.

Summary

Plastic flow measurements of commercial and laboratory-prepared caseins were made with the Rossi-Peakes flow tester. Flow properties of casein samples containing different amounts of moisture were determined at temperatures from 50° to 140°C and pressures from 500 to 3000 p.s.i. Only minor differences were found in the "flow temperature." The transition in flow properties, corresponding to a water content of about 21%, as described by Haller, could not be demonstrated. A tridimensional graph for rennet casein is presented which illustrates the temperature, pressure, and water-content requirements necessary to obtain a given plastic flow.

References

1. Cooper, C. A., and Hand, P. G. T., *Brit. Plastics* **10**, 572–77 (1939).
2. Haller, W., *Kolloid-Z.* **57**, 197–203 (1931).
3. Gallay, W., and Tapp, J. S., *Can. J. Research* **16B**, 345–60 (1938).
4. Hipp, N. J., Groves, M. L., Swain, A. P., and Jackson, R. W., *Modern Plastics* **26**, 205 (Sept., 1948).
5. Rossi, L. M., and Peakes, G. L., assignors to Bakelite Corp., U. S. Patent 2,066,016, Dec. 29, 1936.
6. "Tentative method of test for measuring flow temperature of thermoplastic materials," A. S. T. M. Designation D569–44T.

EXTRUSION BEHAVIOR OF VISCOELASTIC MATERIALS[1]

F. D. Dexter and G. J. Dienes[2]

From the Development Laboratories, Bakelite Division, Union Carbide and Carbon Corporation, Bound Brook, New Jersey

Received February 17, 1950

Abstract

The relation between viscoelastic properties and extrusion characteristics is discussed. It is shown that materials characterized by nonlinear deformation–time properties necessarily exhibit a nonlinear relation between volume rate of discharge and pressure in extrusion. Specifically, the presence of delayed elastic elements leads to a relation which shows that, for linear viscoelastic materials, the volume rate of discharge increases more than proportionately with increasing pressure. The important factor to be recognized is time the material spends in the die. This time, on a volume average basis, is determined by the material, pressure, and die geometry. For a given viscoelastic material the time spent in the die may be altered by changing the pressure or the die geometry. Increasing pressure, for example, decreases the average time spent in the tube and thereby lowers the apparent or effective viscosity. A simple quantitative theory is presented based on a conventional viscoelastic model. Even in simple cases, however, such a mathematical representation appears to be unduly complex. More tractable equations are derived assuming a power function for the deformation–time curve. It is of interest to note that, in this case, a power function describes also the corresponding volume rate of discharge–pressure curve. The influence of die geometry is also shown. The present analysis is limited to linear viscoelastic materials, *i.e.*, to substances whose deformation at any given time is proportional to the applied stress. Some preliminary experiments are described which can be used to compare deformation–time and extrusion behavior. The experimental results are in quite good agreement with the proposed theory.

I. Introduction

The use of extrusion-type measurements for the characterization of flow properties of high polymeric materials is proving to be of increasing value. Work by Spencer and Dillon (1,2), Greenblatt and Fensom (3) and Nason (4) are noteworthy examples of this type of data and their analysis. The common denominator for most of the results is the nonlinear relation between the volume rate of discharge and applied pressure (or rate of shear and shearing stress). It is the purpose of this paper to consider theoretically the relation between such nonlinear response to stress and the complex time-dependent deformation properties of many materials of high viscosity.

---

[1] Presented at the Annual Meeting of the Society of Rheology, New York, N. Y., November 4–5, 1949.

[2] Present address: North American Aviation, Inc., Downey, California.

In extrusion type tests material is forced through a small tube (or die) by application of a known pressure and the volume rate of discharge measured. Since the area of the sample cavity is usually large compared to that of the die, the only significant deformation occurs while the material is in the die. Therefore, it lasts for a fixed and relatively short interval of time for any given element of material. If the material possesses nonlinear time-dependent deformation properties this factor assumes considerable importance in determining the relation between the volume rate of discharge and the pressure. A particular class of such materials whose properties have become more or less well-defined in recent years,[3] are called linear viscoelastic materials. These are characterized by nonlinear deformation-time properties with the deformation at any particular time directly proportional to the applied stress.

The present discussion will be limited to the extrusion properties of such substances. Incompressibility and perfect adherence of the material to the wall of the tube are further limiting assumptions.

II. QUALITATIVE DISCUSSION

Under the action of a constant stress, purely viscous (or Newtonian) materials are characterized by a linear relation between the deformation and time. Viscoelastic materials, on the other hand, show a nonlinear response which subsequently approaches linearity as the purely viscous component becomes predominant. Such a deformation–time curve is shown in Fig. 1(*a*).

The portion *A–B* of the curve represents deformation due to delayed elastic and viscous components acting simultaneously. Usually part of *A–B* is considered to be purely elastic indicating that a certain amount of deformation occurs instantaneously. The magnitude of a truly elastic component is difficult to measure since, for viscoelastic materials, the "instantaneous" deformation depends on the time scale of the experiment. Further clarification of this point will have to come from vibrational experiments. In any case, the "purely" elastic deformation obtained from a static test is unboubtedly an integration of many rapid delayed elastic elements (7).

The purely viscous portion of the curve is given by *B–C* and is linear with time. For many viscoelastic materials the deformation at any time is proportional to the applied stress; that is, from the mechanical model standpoint, they are made up of Hookean springs and Newtonian dashpots. The present paper considers only such linear viscoelastic substances.

In order to obtain the type of deformation–time curve previously described, the testing process must be such that the strains are cumulative. That is, after application of the load (zero time), any given element of the material will continually be strained until the test is terminated by release of the load. Under these conditions elastic components of the deformation reach a limiting value after a certain length of time and the purely viscous component may be measured.

---

[3] For a thorough discussion and review see Ref. (5). For specific application of viscoelastic theory to the behavior of high polymers at elevated temperatures see Ref. (6).

In extrusion-type instruments the material is forced through a small tube or die by application of pressure. Any given element of material undergoes relatively little deformation in shear until it enters the die. Immediately upon entry into the die this element starts to deform and continues to do so until it emerges. Thus, any element is strained for a finite period of time which is equal to the length of time it is in the die. This finite period of time does not necessarily bear any relation to the total testing time. Under such conditions the strains are noncumulative and the time under stress becomes an important factor.

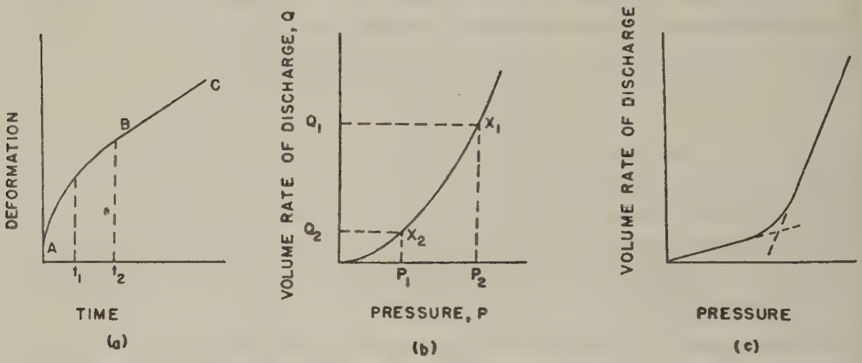

FIG. 1. Typical deformation–time and volume rate of discharge–pressure curves for viscoelastic materials.

Consider, for instance, a viscoelastic material being extruded through a given die by some moderate pressure P_1. Under these conditions the time any given element is under stress is relatively long and might be represented as t_2 in Fig. 1(*a*). The rate of strain is then given by the slope of the deformation–time curve at time t_2. An effective viscosity may be defined which is proportional to the reciprocal of the slope. A volume rate of discharge Q_1 corresponds to this effective viscosity giving a point X_1 in Fig. 1(*b*). Increasing the pressure to P_2 decreases the time any given element is under stress and might be represented as t_1 in Fig. 1(*a*). The rate of strain is then given by the slope of the curve at time t_1. The effective viscosity is, in this case, evidently less than at t_2 (corresponding to P_1). Thus, the new volume rate of discharge, Q_2, is larger than Q_1 by a greater amount than the ratio between the two pressures (P_2/P_1) would predict. The resulting point is plotted as X_2 in Fig. 1(*b*). A series of similar tests at various pressures would result in a curve of the type shown in Fig. 1(*b*) passing through X_1 and X_2; this is a familiar type volume rate of discharge–pressure relation for many thermoplastic materials. Note that zero pressure in Fig. 1(*b*) corresponds to infinite time in Fig. 1 and both are a measure of the purely viscous element. This fact has been verified experimentally by the work of Spencer and Dillon (2) and Dienes and Dexter (8).

This behavior is to be compared to that of a Newtonian or purely viscous material for which the deformation–time curve is linear from zero time. In this case, the time under shear stress in extrusion does not change the effective viscosity which under all conditions of pressure is equal to the absolute viscosity. The volume rate of discharge for a purely viscous material is linear with applied pressure.

While all linear viscoelastic materials give the characteristic Q vs. P curve shown in Fig. 1(*b*) the converse is not necessarily true. Other materials, such as thixotropic substances or those exhibiting nonlinear stress response, may also show this same general flow–pressure relation. Extrusion data are not valid criteria for determining the existence of delayed elastic elements. Thus the analysis presented here is valid only for materials known to be linearly viscoelastic, *i.e.*, materials whose deformation at any time is proportional to applied stress. It is to be emphasized, however, that the presence of "elastic" properties necessarily results in nonlinear volume rate of discharge–pressure relations.

III. Mathematical Formulation

In formulating the mathematics for the extrusion of viscoelastic materials, it is necessary, at this point in the development, to recognize certain conditions. The material is assumed to exhibit laminar flow, to adhere to the tube wall, and to be incompressible. However, the usual simplifying assumption of shear rate being a function only of shearing stress is not valid (9). From the previous discussion it is evident that the rate of shear is also a function of the time under stress, because of the nonlinear time-dependent properties of the material. The following simple theory deals only with volume average properties since a detailed picture of the velocity front has not yet been worked out.

The simplest relation for the extrusion process is that representing the behavior of a purely viscous or Newtonian material. This is the well-known Poiseuille's law:

$$Q = \frac{\pi R^4 P}{8L\eta}, \qquad [1]$$

where

Q = volume rate of discharge,
R = radius of tube (capillary),
P = pressure,
L = length of tube, and
η = Newtonian viscosity.

The fact that this equation holds for high-viscosity materials has been demonstrated by Dienes (10). His data showed that a material (novolac resin) exhibiting a linear deformation–time curve will also show a linear volume rate of discharge pressure curve. This is a necessary condition as can be seen from the deformation time relation

$$D = \frac{1}{\eta} t, \tag{2}$$

where

D = normalized deformation and
t = time under stress.

It is evident that the value of the viscosity coefficient will be independent of the time under stress. Thus, in extrusion, the viscosity will remain a constant when the time under stress is changed by changing the pressure or the size of the die.

The concept of time under stress becomes important when the extrusion process for a material having complex time-dependent deformation properties is considered. The normalized deformation–time relation for a typical linear viscoelastic material, characterized by one retarded element and a viscous element, is (5)

$$D = \frac{1}{\eta_0} t + \frac{1}{G_1} (1 - e^{-t/\tau_1}), \tag{3}$$

where

η_0 = principal or Newtonian viscosity,
G_1 = delayed elastic modulus,
τ_1 = retardation time = η_1/G_1, and
η_1 = delayed viscosity.

A material of the type described by Eq. 3 is deforming, at any particular time, at a rate equivalent to a viscosity value which can be termed the "effective viscosity." Thus, the effective viscosity, η_e, is defined for the purposes of this analysis, as

$$\frac{1}{\eta_e} = \frac{dD}{dt} \tag{4}$$

or from Eq. 3

$$\frac{1}{\eta_e} = \frac{dD}{dt} = \frac{1}{\eta_0} + \frac{1}{\eta_1} e^{-t/\tau_1}. \tag{5}$$

If the effective viscosity at a given volume rate of discharge in extrusion is defined on the basis of Poiseuille's law as

$$\frac{1}{\eta_e} = \frac{8LQ}{\pi R^4 P}, \tag{6}$$

then the volume rate of discharge for a substance obeying Eq. 3 is given by

$$Q = \frac{\pi R^4 P}{8L\eta_e} = \frac{\pi R^4 P}{8L}\left(\frac{1}{\eta_0} + \frac{1}{\eta_1} e^{-t/\tau_1}\right). \qquad [7]$$

The time, t, in Eq. 7 is now the average time (on a volume basis) spent in the die and bears no relation to the testing time used to obtain the value of the volume rate of discharge. It is evident from previous discussion that constant values of pressure and die geometry correspond to a fixed value of the time under stress and result in a constant volume rate of discharge. This point has been verified experimentally (1,4). The time spent in the tube can be most easily altered by changing the pressure. At very long values of time under stress ($t \gg \tau_1$) which corresponds to low pressures, essentially the purely viscous element is being measured (1,2,8) and Eq. 7 becomes

$$Q = \frac{\pi R^4 P}{8L\eta_0}, \qquad [8]$$

and for very short values of time ($t \ll \tau_1$), corresponding to high pressure,

$$Q = \frac{\pi R^4 P}{8L}\left(\frac{1}{\eta_0} + \frac{1}{\eta_1}\right). \qquad [9]$$

The resultant volume rate of discharge–pressure curve would have the general shape shown in Fig. 1(*c*), being represented by two straight lines of different slope connected by a curved transition region. For a material characterized by more complex viscoelastic behavior (more elements) than that represented by Eq. 3 the curvature would extend over a much greater range of pressures. It is interesting to note that a material having an apparent yield value (Bingham body) can be easily produced by viscoelasticity. Such a material would have a very high value of η_0 relative to η_1.

Unfortunately the time spent in the die (time under stress) is a function of both pressure and die geometry. An average time spent in the die can be obtained by dividing the volume of the die by the volume rate of discharge. Theoretically, therefore, a Q vs. P plot can be constructed on the basis of Eq. 7 by a point by point calculation. However, the reverse process of determining the constants from the Q vs. P curve is extremely difficult even from this equation because of the presence of combined linear and exponential functions of Q. The calculations become prohibitive when more than one retarded element is involved.

This situation can be more easily handled if the general deformation–time equation is expressed differently. Over a short range of time, the deformation properties of many viscoelastic materials can be represented by a power function,

$$D = At^n. \qquad [10]$$

Where A and n are constants. The effective viscosity in this case is

$$dD/dt = \frac{1}{\eta_e} = nAt^{n-1}. \qquad [11]$$

From Eq. 6

$$\frac{1}{\eta_e} = \frac{8QL}{\pi R^4 P} = nAt^{n-1}. \qquad [12]$$

If this is placed in terms of shearing stress and rate of shear at the wall,

$$\frac{1}{\eta_e} = \frac{4Q}{\pi R^3 \tau} = nAt^{n-1}, \qquad [13]$$

where $\tau = \dfrac{PR}{2L}$. The time, t, which is the time under stress, can again be approximated by a simple volume averaging process. This previously mentioned value is the volume of the tube, V_t, divided by the volume rate of discharge, Q,

$$t = V_t/Q = \frac{\pi R^2 L}{Q} \qquad [14]$$

or

$$t = \frac{\pi R^3}{Q} \frac{L}{R}.$$

Equation [13] then becomes

$$\frac{1}{\tau} \frac{4Q}{\pi R^3} = nA \left(\frac{\pi R^3}{Q} \frac{L}{R} \right)^{n-1}, \qquad [15]$$

and

$$\tau = \frac{4}{nA} \left(\frac{Q}{\pi R^3} \right)^n \left(\frac{L}{R} \right)^{1-n} \qquad [16]$$

On the basis of Eq. 16 a plot of τ vs. $Q/\pi R^3$ would be different for different values of L/R. However, since n is expected to be a number less than unity, the variation would be rather small and large differences in L/R would be required to separate the effect from the experimental error. Because of this it has not been possible to test the relation with respect to changes in L/R, through any of the published data.

It is of interest to note that the linear log-log relation with respect to time leads to a linear log-log relation between shearing stress and rate of shear for any given L/R. Such relations have been proposed many times in the literature to describe variations in viscosity with shearing stress (or rate of shear). Many of these "non-Newtonian" behaviors may find their origin in the viscoelastic nature of the material.

It is recognized that in extrusion the effective viscosity could be defined as the slope of the volume rate of discharge–pressure curve. Such a procedure leads to a slightly different equation of the same general form.

The choice between the two must be based on experimental data, and to date insufficient data have been collected to test any of the proposed equations conclusively. However, the general aspects of the role of viscoelasticity in extrusion are believed to be sound. That is, nonlinear deformation–time properties must lead to nonlinear volume rate of discharge–pressure data. This is true even though stresswise the response may be linear, *i.e.*, deformation proportional to stress at any given time. The reverse is of course not necessarily true since nonlinear volume rate of discharge–pressure data may arise from thixotropy, slippage at the wall, *etc.*

IV. Preliminary Experiments

There are several experimental difficulties involved in testing the theoretical relations derived on the basis of the somewhat idealized picture presented here. First, it is necessary to carry out the experiments using a material which will not slip on the wall of the die and which is known to be linearly viscoelastic. Second, in comparing extrusion and deformation–time data, the time scale of the experiment should be of the same order of magnitude. This requires the measurements of the static deformation–time properties (for example, by the parallel-plate plastometer) at low values of time. The measurements are usually not very accurate in this region.

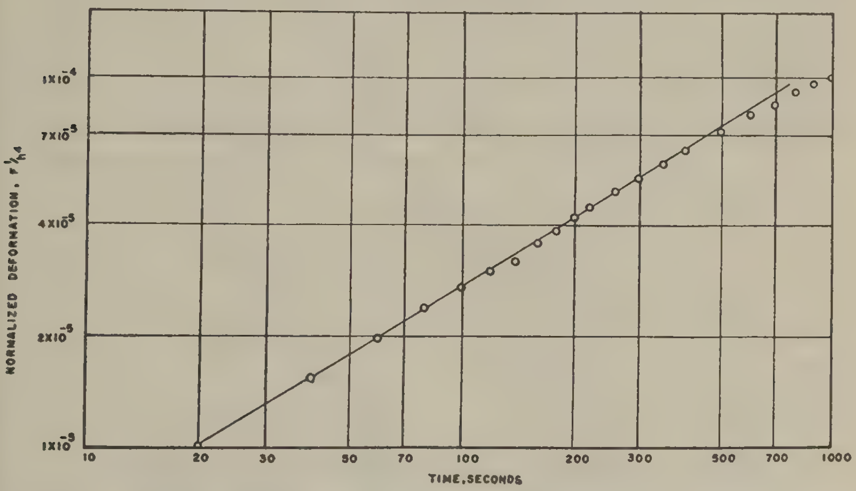

Fig. 2. Normalized deformation–time curve for a VYNS grade vinyl chloride-acetate resin compound at 160°C. Parallel-plate plastometer data.

Only a few preliminary experiments can be described at this time which were obtained using a material that meets fairly well the requirements outlined above. Stabilized VYNS grade vinyl chloride-acetate resin containing no lubricant appeared to be sufficiently adherent at 160°C. to serve for these experiments. This compound is known to be linearly visoelastic (6), at least at relatively low stresses. Its high-temperature deformation–time properties can be measured by the parallel-plate plastometer as described by Dienes (6).

The early portion of the deformation–time curve of this VYNS resin compound was measured at 160°C. using the parallel-plate plastometer.

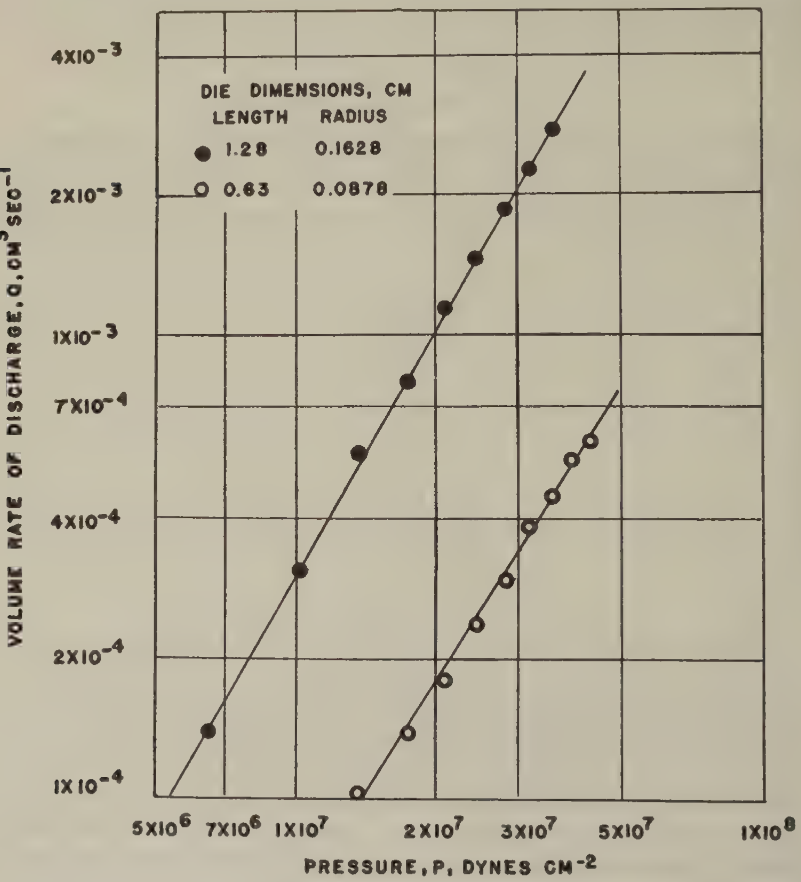

FIG. 3. Volume rate of discharge–pressure curves for a VYNS grade vinyl chloride-acetate resin compound at 160°C. Die dimensions as shown.

The complete normalized $1/h^4$ vs. time curve is not described by Eq. 11. However the early portion of the curve, which is of most interest in connection with the extrusion data, is satisfactorily fitted by a linear log-log relation as shown in Fig. 2 (average of two tests). From this curve the constants A and n are easily determined.

Volume rate of discharge–pressure data were obtained on the same compound at 160°C. using a simple extrusion plastometer. Two dies of different dimensions were used in this work (dimensions shown on Fig. 3). The data are presented in the form of log-log volume rate of discharge-pressure plots as shown in Fig. 3 (average of two tests).

These data can be used to check the validity of Eq. 16. According to this relation the volume rate of discharge, Q, and pressure, P, should be linearly related on a log-log basis. This conclusion is experimentally proven by the lines of Fig. 3. Furthermore, if Eqs. 11 and 16 apply to this material, the constants A and n obtained from the parallel-plate plastometer (Eq. 11) and the extrusion data (Eq. 16) should be the same. From the plots of Fig. 3, A and n obtained in the extrusion experiments are easily calculated.

Comparison of A and n from the two types of experiments gave the results listed in Table I. The agreement is quite satisfactory, particularly for the n values. The larger discrepancy in A can easily be caused by relatively small errors in the early portion of the deformation–time curve. The good agreement between the n values emphasizes the essential connection between deformation–time and extrusion behavior.

TABLE I

Comparison of A and n from Deformation–Time and Extrusion Data.
VYNS resin compound at 160°C.

	cm.	$A \times 10^6$	n
Extrusion data			
Die A:	$L = 1.28$	2.8	0.586
	$R = 0.1623$		
Die B:	$L = 0.63$	2.4	0.598
	$R = 0.0878$		
Deformation–time data (parallel plate)		1.6	0.614

Equation [16] predicts that at any given value of $Q/\pi R^3$ the shearing stress will be a function of the die geometry, specifically of the ratio L/R. The L/R ratios for the two dies used in these experiments do not differ sufficiently to permit one to draw any conclusions concerning this point—the τ vs. $Q/\pi R^3$ curves coincide within experimental error. Large differences in L/R will be required to investigate this effect thoroughly.

It is felt that, while these experiments are preliminary, they lend considerable support to the theoretical analysis presented.

While this paper was being prepared for publication, an article by Wilson and Smith (11) appeared in which somewhat similar ideas were advanced. These authors point out the importance of "residence time" but their treatment is based on thixotropic rather than viscoelastic behavior and treats a different experimental condition. Thus, while there are some mathematical similarities in the two treatments, the appropriate physical interpretations for the two cases are quite different.

ACKNOWLEDGMENT

The helpful suggestions and criticisms of our associates, particularly V. E. Meharg, R. F. Clash, Jr., and W. A. Zinzow, are gratefully acknowledged.

REFERENCES

1. Spencer, R. S., and Dillon, R. E., *J. Colloid Sci.* **4**, 241 (1949).
2. Spencer, R. S., and Dillon, R. E., *J. Colloid Sci.* **3**, 163 (1948).
3. Greenblatt, J. H., and Fensom, P. H., *Ind. Eng. Chem.* **3**, 1037 (1947).
4. Nason, H. K., *J. Applied Phys.* **16**, 338 (1945).
5. Alfrey, T., Mechanical Behavior of High Polymers, pp. 93–228. Interscience Publishers, N. Y., 1948.
6. Dienes, G. J., *J. Colloid Sci.* **2**, 131 (1947).
7. Brenschede, W., *Kolloid-Z.* **104**, 1–13 (1943).
8. Dienes, G. J., and Dexter, F. D., *J. Colloid Sci.* **3**, 181 (1948).
9. Burgers, J. M., First Report on Viscosity and Plasticity. Amsterdam Academy of Sciences, 1939.
10. Dienes, G. J., *J. Colloid Sci.* **4**, 257 (1949).
11. Wilson, H. W., and Smith, G. H., *Ind. Eng. Chem.* **41**, 770 (1949).

FITTING MATHEMATICAL THEORIES OF PLASTICITY TO EXPERIMENTAL RESULTS [1, 2]

F. D. Stockton and D. C. Drucker

Brown University, Providence, Rhode Island

Received February 17, 1950

INTRODUCTION

At present the analytical development of mathematical theories of plasticity for work hardening metals has far outstripped application and comparison with experimental information. However, despite the considerable generality of existing theory it is not known whether all data can be correlated even when, as is assumed throughout the rest of this paper, time and temperature effects are negligible. Also, much must be learned about the applicability of simple forms of the theories when the path of loading is not too complicated (1,2).

It is the purpose of this paper to show what experiment may demand of theory using the classical data of Taylor and Quinney (3) for illustration. The analysis will demonstrate that the more varied the data the stress–strain law must fit, the more elaborate the mathematical relation must become. Two fundamental questions are also considered: Are the strain increments linear in the stress increments? Is the plastic work per unit volume independent of the path of loading provided unloading is not taking place? The linearity assumption is implicit in all explicit stress–strain relations now in use, and the more drastic work assumption appears in many. Obviously, a large number of experiments must be run and studied before final answers can be obtained. All conclusions presented here are therefore tentative.

STRESS–STRAIN RELATIONS

The incremental stress–strain law which will be used is based upon the reasonable assumption, in the absence of time and temperature effects, of the existence of a loading function, f, a criterion of further plastic deformation (2). A simple example is the Mises' function, J_2, which represents the

---

[1] The conclusions presented here were obtained in the course of research conducted under Contract N7onr-358 sponsored jointly by the Office of Naval Research and the Bureau of Ships.

[2] Presented at the Annual Meeting of the Society of Rheology, New York, N. Y., November 4–5, 1949.

elastic shear strain energy. The octahedral shearing stress, a constant times $\sqrt{J_2}$, is essentially the same loading function.

The increments of plastic strain, in tensor notation, for a general f are

$$d\epsilon^p{}_{ij} = G \frac{\partial f}{\partial \sigma_{ij}} \left(\frac{\partial f}{\partial \sigma_{kn}} d\sigma_{kn} \right). \qquad [1]$$

The elastic strain increments, $d\epsilon^e{}_{ij}$, must be added to the plastic to obtain the total strain increments

$$d\epsilon_{ij} = d\epsilon^e{}_{ij} + d\epsilon^p{}_{ij}.$$

Both functions f and G may depend on instantaneous values of stress, strain, and on their history. If the basic assumption of linearity between the increments of stress and strain is correct, Eq. 1 is the most general stress–strain law possible for a work hardening material.

Taking f as J_2 gives the simplest form:

$$d\epsilon^p{}_{ij} = G s_{ij}\, dJ_2, \qquad [2]$$

where $s_{ij} = \dfrac{\partial J_2}{\partial \sigma_{ij}}$ is the stress deviation $\sigma_{ij} - \frac{1}{3}\sigma_{kk}\delta_{ij}$.

Taking f as $f(J_2,J_3)$ adds a little complexity (4):

$$d\epsilon^p{}_{ij} = G \left(\frac{\partial f}{\partial J_2} s_{ij} + \frac{\partial f}{\partial J_3} t_{ij} \right) df, \qquad [3]$$

where t_{ij} is the deviation of the square of the stress deviation, $s_{ik}s_{kj} - \frac{2}{3}J_2\delta_{ij}$.

Taking $f = \frac{1}{2}(s_{ij} - m\epsilon^p{}_{ij})\,(s_{ij} - m\epsilon^p{}_{ij})$ or equally well $f = J_2 - m s_{ij}\epsilon^p{}_{ij}$ or $J_2 - m\sigma_{ij}\epsilon^p{}_{ij}$, as the sum of the normal strains $\epsilon^p{}_{kk}$ is 0 (plastic incompressibility), introduces strain explicitly and gives

$$d\epsilon^p{}_{ij} = G(s_{ij} - m\epsilon^p{}_{ij})[(s_{kn} - m\epsilon^p{}_{kn})d\sigma_{kn}]. \qquad [4]$$

Any number of more complicated incremental forms may be written down by other choices of f, but only [2], [3], and [4] will be employed in the following discussion.

Experiments of Taylor and Quinney (3)

Taylor and Quinney tested tubes under independently applied axial pull and twist producing various combinations of tensile and shearing stresses on the cross section. As shown in Fig. 2, the tubes were first pulled far into the plastic range to a tensile stress, P_0, then partially unloaded to mP_0 and twisted under constant axial force. Torque was applied by adding weights, p, to pans attached through threads and pulleys to a torque drum. Extension, δL (l is used by Taylor and Quinney), angle of twist, χ, and change in internal volume were measured. Assuming no change in the

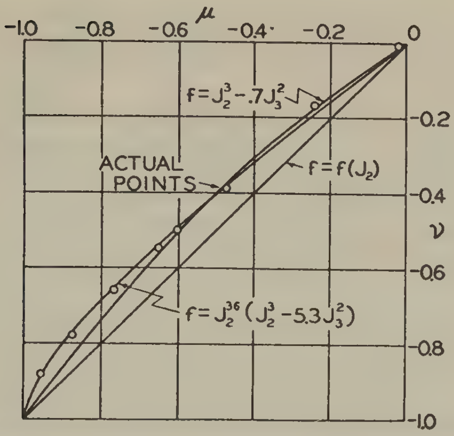

FIG. 1. Predicted μ vs. ν curves for copper compared to experimental points (3).

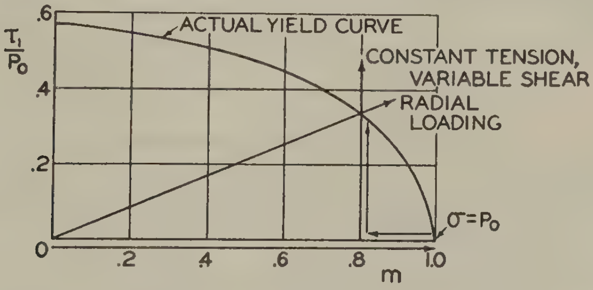

FIG. 2. Yield curve for copper, and loading paths.

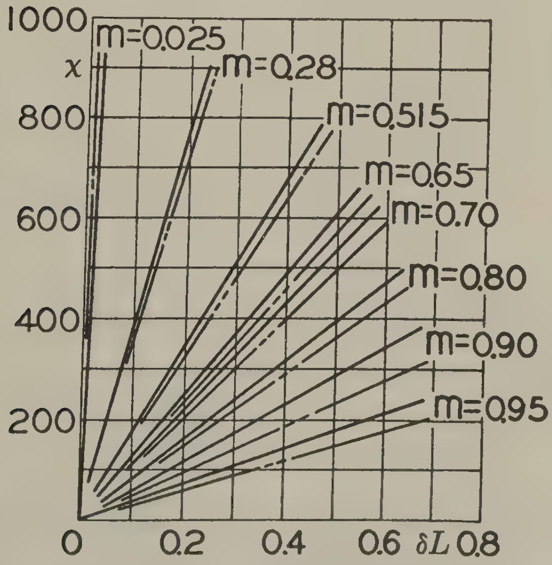

FIG. 3. Total angle of twist, χ, vs. increase in extension of copper tubes, δL. ———— Experimental (3); ———— – – ———— Predicted using $f = J_2^{36}(J_2^3 - 5.3\, J_3^2)$.

volume of the metal, a hypothesis checked experimentally during application of the tensile stress, P_0, the circumferential and the radial strains could be computed.

A number of curves were plotted from the data, but the following information, sufficient for a reasonably complete analysis, is given for copper, of nearly electrolytic purity, only:

1. Tensile stress, σ, vs. strain, ϵ, diagram.
2. Shear stress, τ, vs. shear strain, γ, diagram $\left(\text{modified to } 2\tau \text{ vs. } \frac{\gamma}{2}\right)$ (Taylor and Quinney use the symbols S and s).
3. Yield curve or loading function in the form $\frac{\tau_1}{P_0}$ vs. m, where τ_1 is the shear stress required for further plastic deformation after reduction of the axial tension to $\sigma = mP_0$ and subsequent application of shear.
4. μ vs. ν curve, where μ and ν are approximations to Lode's variables
$$\mu = 2\,\frac{\sigma_2 - \sigma_3}{\sigma_1 - \sigma_3} - 1; \qquad \nu = 2\,\frac{d\epsilon_2 - d\epsilon_3}{d\epsilon_1 - d\epsilon_3} - 1$$
in which σ_1, σ_2, and σ_3 are principal stresses and $d\epsilon_1$, $d\epsilon_2$, and $d\epsilon_3$ are principal values of the strain increments.
5. Torque vs. extension diagram in the form of load in torque pans, p, vs. axial extension, δL.
6. Angle of twist, χ, vs. extension, δL, diagram.

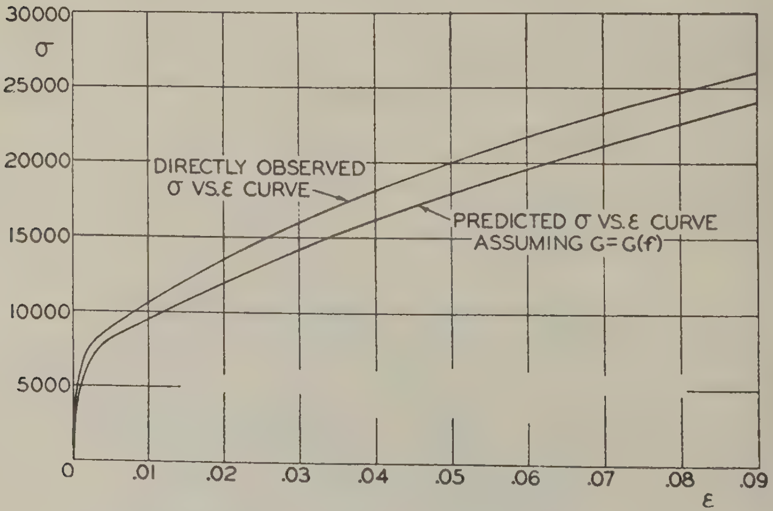

FIG. 4. Actual and predicted stress–strain curves for copper (3). σ in pounds per square inch.

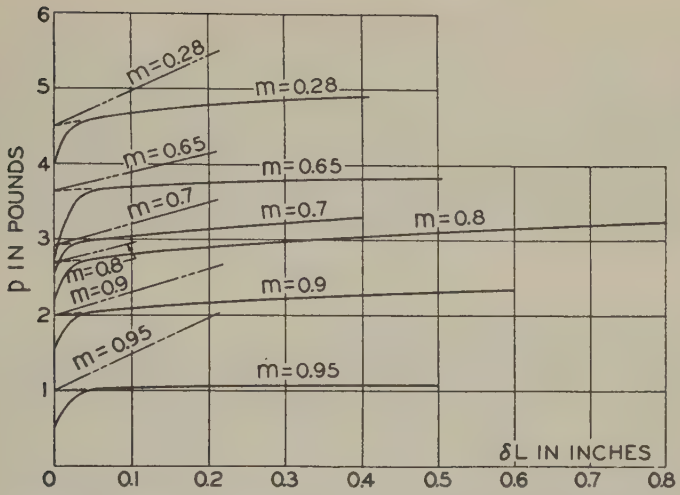

FIG. 5. p vs. δL curves for copper tubes. ——— experimental (3); — — - - — predicted using $f = J_2^{36}(J_2^3 - 5.3\ J_3^2)$, and $c_1 = 1.35$.

Among the significant results are:

(*a*) χ vs. δL (Fig. 3) and p vs. δL (Fig. 5) are practically straight lines in the region of interest: ν remains constant as τ increases (a little) beyond the yield value.

(*b*) μ vs. ν deviates appreciably from the straight line $\mu = \nu$ (Fig. 1).

(*c*) The yield curve is close to the prediction of the J_2 theory (Fig. 2).

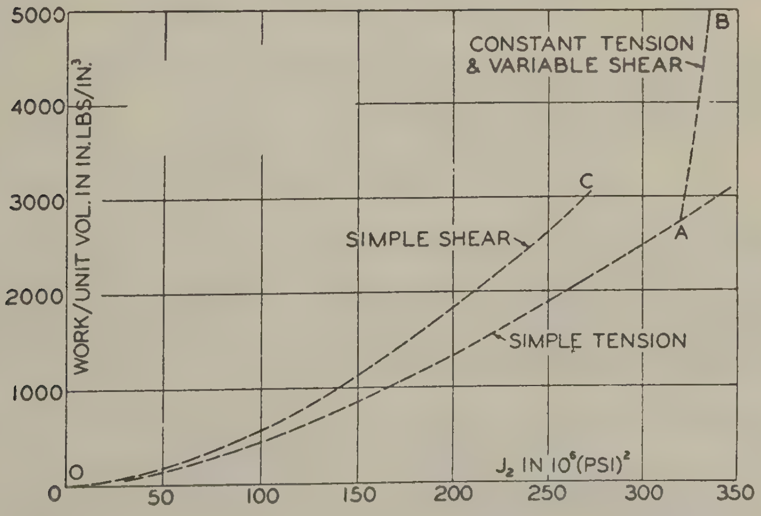

FIG. 6. Work/unit vol. vs. J_2 curves for various loading paths for copper tube.

Possible Forms of f and G

The fact (*c*) that the yield curve is near J_2 = constant despite the large tensile prestrain indicates the possibility of isotropic work (stress) hardening (2) (*i.e.*, the loading function depending upon the invariants of stress alone). Deviation (*b*) of ν from μ then requires the inclusion of J_3 since $f = f(J_2 \text{ only})$ would yield $\nu = \mu$. Constancy (*a*) of ν in addition might seem almost conclusive evidence for a loading function of the type

$$f = f(J_2,J_3)$$

homogeneous in the stress components.

A simple form, $f = J_2^3 - cJ_3^2$ with $c = 0.7$, provides sufficient deviation of ν from μ without much departure from the J_2 yield curve, but the bulge in the μ vs. ν curve is too near the origin (Fig. 1). A much better fit is obtained with $f = J_2^{36}(J_2^3 - 5.3J_3^2)$ which also checks very closely with the yield data (Fig. 2). Thus, as has been demonstrated, it is easy to take into account accurately the yield curve and the μ vs. ν curve with a J_2,J_3 incremental theory. However, the very best agreement in these two respects is no guarantee of a more general validity of such a form; the remaining data must also be fitted. No trouble is encountered with curves of χ vs. δL (Fig. 3), which are essentially plots of $d\epsilon_{xy}$ vs. $d\epsilon_x$ and so depend upon the form of f alone and not at all upon G. Although not perfect, the agreement between prediction and experiment is reasonably good.

If G, in Eq. 3, is taken to be a function of f, a highly desirable simplification which apparently is satisfactory for other tests on tubes (5,6), then

$$d\epsilon^p{}_{ij} = G(f)\left(\frac{\partial f}{\partial J_2}\, s_{ij} + \frac{\partial f}{\partial J_3}\, t_{ij}\right) df. \qquad [5]$$

With this form of the stress–strain relation, axial tension, σ_x, alone produces plastic axial strain increments

$$d\epsilon_x{}^p = G(f)\left(\frac{\partial f}{\partial J_2}\frac{2}{3}\,\sigma_x + \frac{\partial f}{\partial J_3}\frac{2}{9}\,\sigma_x{}^2\right) df, \qquad [6]$$

where G, $\frac{\partial f}{\partial J_2}$, and $\frac{\partial f}{\partial J_3}$ all reduce to functions of σ_x, and df becomes $d\sigma_x$ times a function of σ_x. The tensile stress–strain diagram thus completely determines G. Also, with this same form of the stress–strain relation, shear stress τ_{xy} alone produces plastic shear strain

$$d\gamma^p{}_{xy} = 2d\epsilon_{xy}{}^p = 2G(f)\,\frac{\partial f}{\partial J_2}\,\tau_{xy}\,df \qquad [7]$$

as $t_{xy} = 0$. Therefore, G is determined even more easily from a shear stress–strain diagram.

However, assuming $G = G(f)$ does not make it so. The functions $G(f)$ obtained from the two simples tress–strain curves mentioned may not turn out the same. A method of comparison is to compute G from one curve and plot the other curve on the basis of the theory. Although in most cases the agreement will be very good, Fig. 4 shows that for Taylor and Quinney's tests it is poor. A more general form is required, say $G = G(J_2,J_3)$. The simplest choice which produces a good correlation between prediction and actual data is

$$G = g(f)\left(1 - c_1\frac{J_3^{\,2}}{J_2^{\,3}}\right), \qquad [8]$$

where g depends upon f alone and c_1 is only slightly dependent on the particular form of f chosen. For $f = J_2^{36}(J_2^3 - 5.3J_3^2)$, $c_1 = 1.35$, which appears to be an average figure. Many more complicated forms of G will, of course, work equally well, and have greater flexibility.

The predicted initial slope, $\dfrac{dp}{d(\delta L)}$, of the p vs. δL curve may now be found, without explicitly determining $g(f)$, from the slope of the tensile stress–strain curve at $\sigma = P_0$, $\left(\dfrac{d\sigma}{d\epsilon}\right)_{P_0}$, and the values of the stresses at yield, $\sigma = mP_0$, $\tau = \tau_1$. This is apparent from the expression for the increment of the plastic extension

$$d\epsilon^p = G\frac{\partial f}{\partial\sigma}df = g(f)\left(1 - c_1\frac{J_3^{\,2}}{J_2^{\,3}}\right)\frac{\partial f}{\partial\sigma}\left(\frac{\partial f}{\partial\sigma}d\sigma + \frac{\partial f}{\partial\tau}d\tau\right), \qquad [9]$$

where $\dfrac{\partial f}{\partial\sigma}$ and $\dfrac{\partial f}{\partial\tau}$ are known functions of σ and τ alone. For simple tension alone

$$d\epsilon_\sigma{}^p = g(f)\left(1 - c_1\frac{J_{3_\sigma}^{\,2}}{J_{2_\sigma}^{\,3}}\right)\left(\frac{\partial f}{\partial\sigma}\right)_\sigma^2 d\sigma, \qquad [10]$$

while for the shear stress increment $d\tau$ at constant tension, $\sigma = mP_0$, the normal strain increment is

$$d\epsilon_m{}^p = g(f)\left(1 - c_1\frac{J_{3_m}^{\,2}}{J_{2_m}^{\,3}}\right)\left(\frac{\partial f}{\partial\sigma}\right)_m\left(\frac{\partial f}{\partial\tau}\right)_m d\tau, \qquad [11]$$

where the subscript m is to be interpreted as requiring the value of the quantity at $\sigma = mP_0$ and $\tau = \tau_1$. Therefore, using conversion factors to change $d\epsilon$ to δL, $d\tau$ to dp, *etc.*, and, remembering that f is the same for $\sigma = mP_0$, $\tau = \tau_1$, $\dfrac{dp}{d(\delta L)}\bigg/\left(\dfrac{\partial\sigma}{\partial\epsilon}\right)_{P_0}$ is a function of mP_0 and τ_1, independent of g. For most of the data, f changes very little as the increase in τ is small, so that the computed p vs. L curves are practically straight lines. However, although the experimental lines also are straight when f does not change appreciably, the predicted slopes of the p vs. δL curves are found to be far too great or, equivalently, the inverse slopes, $\frac{d\epsilon}{d\tau}$, are too small (Fig. 5). In no case was the predicted slope of p vs. δL less than two times the value Taylor and Quinney reported; and the average is almost ten times too great. There is no important difference in this respect betwen the elementary or J_2 form of f and the more general J_2,J_3 forms.

As has been stated previously, the more complicated the data to be taken into account, the more elaborate the theory needed. Therefore, in itself the lack of agreement at this stage of theory and data is not too discouraging. Within the framework of a J_2,J_3 theory there must exist a function $g_2(J_2,J_3)$ which is unity for simple tension and also for simple shear and which will predict the p vs. δL curves correctly;

$$G = g(f)\, g_1\,(J_2,J_3)\left(1 - c_1 \frac{J_3^2}{J_2^3}\right). \qquad [12]$$

The previous agreement with experiment will not be altered.

Now that the available data can be fitted completely, the question of the generality of the stress–strain relation developed still remains. Suppose one more different kind of test were run. Would the prediction of the theory agree with the data obtained? In particular, how about radial loading paths, *i.e.*, combined stress tests in which all the components of stress are increased in ratio: $\sigma_{ij} = k\sigma^0_{ij}$. It has been shown (7) that for radial loading paths μ vs. ν, yield curves, and stress–strain diagrams all fit very well under a J_2, J_3 theory. However, in the present analysis nonradial loading tests were matched by a J_2,J_3 form and the predictions for radial loading turn out to be quite unreasonable. This positive statement can be made despite the absence of test data because plots of octahedral shearing stress (proportional to $\sqrt{J_2}$) vs. octahedral shearing strain ($\propto \int \sqrt{d\epsilon_{ij}d\epsilon_{ij}}$) have been used often for radial loading. Curves are always obtained whose stress ordinates do not differ from each other by more than 20% for metals reasonably isotropic to start with, and usually are within better than 15%. As

$$\sqrt{d\epsilon^p{}_{ij}d\epsilon^p{}_{ij}} = G\sqrt{\frac{\partial f}{\partial \sigma_{ij}}\frac{\partial f}{\partial \sigma_{ij}}}\,df$$

$$= g(f)\, g_1(J_2,J_3)\left(1 - c_1\frac{J_3^2}{J_2^3}\right)\sqrt{\frac{\partial f}{\partial \sigma_{ij}}\frac{\partial f}{\partial \sigma_{ij}}}\,df \qquad [13]$$

the factor which must average about 10 inserted by g_1 to match p vs. δL appears in the slope $\frac{d\gamma_0}{d\tau_0}$ for radial loading. It is extremely unlikely that had these experiments been made, this enormous difference in slope on a τ_0 vs.

γ_0 plot between tensile and combined tension and shear stress curves would have been found. The presumption must be that the form [12] is not correct, although it is useful if predictions are required for the same types of test as those matched.

What has been established so far is that a J_2,J_3 theory provides answers for a considerable number of tests but does not really fit the data of Taylor and Quinney for copper. This does not necessarily mean that similar data for some other metal may not be correlated well by a simple theory but the presumption is rather strong. However, the result is not a complete surprise because no metal actually hardens isotropically as assumed in a stress theory of plasticity, *i.e.*, f a function of stress alone.

Possibly the correct way to look at the J_2, J_3 expression is that it represents the general form

$$d\epsilon^p{}_{ij} = G \frac{\partial f}{\partial \sigma_{ij}} \left(\frac{\partial f}{\partial \sigma_{kn}} d\sigma_{kn} \right)$$

with f and G functions of stress, strain, and history. At the particular stage of deformation being considered, f and G are functions of stress and J_2 may be translated as $\frac{1}{3}\sigma^2 + \tau^2$ and J_3 as $\frac{\sigma}{3}\left(\frac{2}{9}\sigma^2 + \tau^2\right)$ rather than as true invariants.

Another, more unfortunate possibility also exists whose importance transcends the immediate problem of correlation. The same factor averaging almost 10 appears in both radial loading and in the Taylor-Quinney loading path (Fig. 2) because of the assumption of linearity between the differentials of stress and strain. No matter how complicated a "linear" theory is chosen, if G is a function of stress alone and the yield or loading surfaces for radial loading are close to those established by initial tension, the factor 10 must carry through. Only if different loading surfaces are produced by different paths will the factors be independent to any extent.

A brief investigation of the properties of such a stress–strain relation as Eq. 4 where f depends upon strain explicitly will serve as illustration.

Simple tension in the x-direction to P_0 produces $\epsilon_x{}^p = \epsilon_0$, $\epsilon_y{}^p = \epsilon_z{}^p = -\frac{\epsilon_0}{2}$. At this stage of plastic deformation consider stresses σ_x and $\tau_{xy} = \tau_{xy}$ to be acting and producing further plastic strains. Substitution in [4] gives

$$\begin{aligned}
d\epsilon_x &= G(\tfrac{2}{3}\sigma_x - m\epsilon)[(\tfrac{2}{3}\sigma_x - m\epsilon)d\sigma_x + 2\tau_{xy}\,d\tau_{xy}],\\
d\epsilon_y &= d\epsilon_z = -G\left(\frac{1}{3}\sigma_x - m\frac{\epsilon}{2}\right)[(\tfrac{2}{3}\sigma_x - m\epsilon)d\sigma_x + 2\tau_{xy}\,d\tau_{xy}], \qquad [14]\\
d\gamma_{xy} &= 2d\epsilon_{xy} = 2G\tau_{xy}[(\tfrac{2}{3}\sigma_x - m\epsilon)d\sigma_x + 2\tau_{xy}\,d\tau_{xy}],\\
d\gamma_{yz} &= d\gamma_{zx} = 0,
\end{aligned}$$

while for radial loading to σ_x and τ_{xy} which causes strains $\epsilon_x = \epsilon'$ and $\gamma_{xy} = \gamma'$ quite different factors appear.

$$\begin{aligned} d\epsilon_x' &= G(\tfrac{2}{3}\sigma_x - m\epsilon')\left[(\tfrac{2}{3}\sigma_x - m\epsilon')d\sigma_x + 2\left(\tau_{xy} - m\frac{\gamma'}{2}\right)d\tau_{xy}\right], \\ d\gamma_{xy} &= 2G\left(\tau_{xy} - m\frac{\gamma'}{3}\right)\left[(\tfrac{2}{3}\sigma_x - m\epsilon')d\sigma_x + 2\left(\tau_{xy} - m\frac{\gamma'}{2}\right)d\tau_{xy}\right]. \end{aligned} \tag{15}$$

However, despite the different factors appearing, and although G may be taken as a function of both stress and strain, it is doubtful in this relatively simple theory that reasonable forms can be obtained which will give the proper correlation for p vs. δL and also radial loading. A considerably more complicated f would certainly be required.

Still another possibility which cannot be ignored is that the large thickness of the tubes (outside diameter 0.248 in. with wall thickness 0.036 in.) make the experimental data somewhat unreliable. However, the conclusion appears to be either that G and f are strongly path- and strain-dependent, or that linearity is not a good assumption.

PLASTIC WORK

As previously mentioned, the total plastic work per unit volume, W^p, has often been assumed to depend on the loading function only. This corresponds to the simple choice of f as a homogeneous function of stress only and $G = G(f)$, so that

$$d\epsilon^p{}_{ij} = G(f)\,\frac{\partial f}{\partial \sigma_{ij}}\,df$$

and

$$dW^p = \sigma_{ij}d\epsilon^p{}_{ij} = G(f)nf\,df, \tag{16}$$

where n is the degree of f in the stress components. This result means that the value of W^p must be independent of the path of loading. It does not depend upon the manner in which the final value of f is reached, provided, of course, that plastic deformation is occurring and not elastic unloading. Although Fig. 4 shows that this hypothesis is certainly not entirely true, it has given correlation within close limits for radial paths (5,6,7).

More complicated paths of loading provide a more severe test. Figure 6 is a work vs. J_2 diagram, on the assumption that J_2 is approximately the actual loading function, for (*a*) simple shear, (*b*) simple tension, and (*c*) Taylor-Quinney's loading path. It is seen that at point A the change in slope of the W vs. J_2 curve is enormous; and, as mentioned before, the difference between the shear and tension curves is large. These are certainly rather conclusive indications that the work is really strongly path-dependent and is not a function of the final state of stress alone.

Thus, G cannot depend upon f but must be path-dependent even in quite simple cases.

ALTERNATIVE MATHEMATICAL THEORIES OF PLASTICITY

Having established that considerable complexity is required within the framework of "linear" incremental theory, it is logical to inquire about other existing theories. It might be thought possible that despite its mathematical and physical incompatibility with the existence of a loading function, deformation theory might work out better than incremental theory for Taylor and Quinney's tests. Deformation theory postulates a unique relation between stress and strain. In its currently used J_2 form, $\epsilon_{ij} = F(J_2)s_{ij}$, ignoring the major inconsistency, it would predict a unique curve of work vs. J_2. Also, in shifting from $\sigma = P_0$ to $\sigma = mP_0$, $\tau = \tau_1$ the plastic increment in the extension due to $d\tau$ is

$$d\epsilon^p = \frac{\partial F}{\partial \tau}\frac{2}{3}\, mP_0\, d\tau,$$

which has the same form as incremental theory and cannot be made to agree with experiment.

Another type of theory has been advanced by Batdorf and Budiansky (8) in which the shear stress on each possible slip plane is considered the basic quantity. Their theory is not a "linear" one and so might be expected to agree with the data. However, such a theory would not give a loading surface at all close to J_2 and so also could not agree with the data.

Thus, present alternatives would not do as well as "linear" incremental theory.

SUMMARY AND CONCLUSIONS

It has been shown that stress–strain relations become more and more complicated the more data they have to fit. Although useful relations were found for only part of the data of Taylor and Quinney on copper tubes, many tests can be fitted by simple incremental theories.

The difficulty in matching all the data offered is tentatively attributed to one or more of the following:

1. Excessive thickness of the tube walls rendered the analysis given invalid.
2. The loading function f and the function G depend strongly on the strain and strain–history as well as on the stress.
3. The assumption of the linearity of the strain increments in the stress increments is not valid for the data examined.

REFERENCES

1. Prager, W., *J. Applied Phys.* **20**, 235–41 (1949).
2. Drucker, D. C., *J. Colloid Sci.* **4**, 299–311 (1949).
3. Taylor, G. I., and Quinney, H., *Trans. Roy. Soc.* (*London*) **A230**, 232–362 (1932).
4. Hodge, P., and Prager, W., *J. Math. Phys.* **27**, 1–10 (1948).
5. Schmidt, R., *Ing. Arch.* **3** 215–35 (1935).
6. Davis, E. A., *J. Applied Mechanics, Trans. ASME* **65**, A-187ff (1943).
7. Drucker, D. C., *J. Applied Mechanics, Trans. ASME* **71**, A349, (1949).
8. Batdorf, S. B., and Budiansky, B., Nat. Advisory Comm. Aeronaut., Repts., Tech. Mem., Notes p. 1871 (April 1949).

DILUTE-SOLUTION VISCOSITY OF POLYMETHYL METHACRYLATE AND A METHYL METHACRYLATE-STYRENE COPOLYMER [1]

Turner Alfrey, Jr., A. I. Goldberg and John A. Price [2]

From the Institute of Polymer Research, Polytechnic Institute of Brooklyn,
Brooklyn, New York

Received February 17, 1950

INTRODUCTION

The behavior of high polymer molecules in dilute solution has been correlated with the nature of the polymer and the composition of the solvent (1–6). In the case of noncrystalline, nonpolar polymers, Gee (4) has shown that Hildebrand's (7) concept of cohesive energy density (CED) yields a useful indication of solvent power. The best solvents for such polymers are those whose cohesive energy densities most closely match that of the polymer. In the case of polar polymers, a greater degree of specificity can be expected in the poylmer–solvent interaction. Spurlin (3) has suggested the desirability of classifying polar substances on the basis of their "acidic" or "basic" character (in the generalized Lewis sense), as well as on the basis of their cohesive energy densities. Specific solvation can be expected between an "acidic" polar solvent of the proper cohesive energy density and a "basic" polymer, and vice versa.

A number of different experimental methods have been used to estimate the solvent power of various solvents for a given polymer. The Flory-Huggins relationship involves the use of the constant μ, which has a direct thermodynamic significance. It may be evaluated from the reduced osmotic pressure–concentration curve or from the swelling of cross-linked polymers (4,8,9). The dilution–ratio method, in which the solvent is characterized by the amount of nonsolvent needed to bring a solution to initial turbidity, is useful but is complicated by the possibility that the solvent power may pass through an optimum on addition of the diluent. Another general approach utilizes the viscosity behavior of dilute solutions. In general, flexible polymer molecules are extended in good solvents, thus exhibiting high intrinsic viscosities, and are more tightly coiled in poor solvents. In addition, the *slope* of a specific viscosity curve, divided by the square of the intrinsic viscosity, yields a constant k' which also serves as a measure of solubility. This empirical constant has higher values in poor solvents and lower values in good solvents (2,3). Thus the viscosity method enables us to obtain two criteria of solvent power with a relatively simple experimental technique.

---

[1] Presented at the Annual Meeting of the Society of Rheology, New York, N. Y. November 4–5, 1949.

[2] Taken in part from a thesis submitted by John A. Price in partial fulfillment of the requirements for the degree of Master of Science in Chemistry, Polytechnic Institute of Brooklyn, June 1949.

In this investigation, the intrinsic viscosity of polymethyl methacrylate was determined in a variety of solvents. Similar studies were made on a copolymer of methyl methacrylate–styrene and on polystyrene, to observe the corresponding effects of these solvents on the three polymers.

EXPERIMENTAL

A commercial sample of methyl methacrylate was redistilled through a 2-ft. column packed with glass helices, and the fraction distilling between 46.5–47.0°C. at 100 mm. pressure was used; refractive index at 20°C. was 1.4142. The commercial styrene monomer was similarly distilled and the fraction boiling at 46.0–46.5°C. at 20 mm. was utilized; $n_D^{20} = 1.5462$.

Methyl methacrylate was polymerized in bulk with 0.2% recrystallized benzoyl peroxide at 70°C. for about 1 hr. to a 12% conversion. The polymer was precipitated with methanol and purified by redissolving in acetone and reprecipitating twice, the final time in water. The polymer was dried to a constant weight in a vacuum oven for 10 hr. at 50°C. and was ground to a fine white powder, 25 g. yield.

The copolymerization was carried out in the same manner, using equimolar quantities of the co-monomers. The polymerization was carried to an 8% conversion in 200 min. at 70°C. and the polymer was isolated, purified, and dried as above: 23 g. yield. Chemical analysis gave: 74.73% C, 7.71% H.

The carbon analysis corresponds to a ratio of 55.4 mole-% methyl methacrylate and 44.6 mole-% styrene. This ratio would give a hydrogen analysis of 7.86%, which is in fair agreement with the average found value of 7.71%.

Styrene itself was not polymerized for this work, but a sample of fractionated polystyrene from The Dow Chemical Company was used.

A modification of the conventional Ostwald viscometer was used in most of the viscosity determinations. This type of vicosmeter has the same design as the Ostwald type but has a large reservoir bulb of about 30 ml. capacity. It was therefore possible to make a series of dilutions within the viscometer itself without the necessity of cleaning and drying the viscometer between concentrations. A set of three viscometers, varying appreciably in their kinematic viscosity, was used in order to keep the flow times of the solvents used at approximately 100 sec. Cyclohexanone was the only solvent used which was too viscous for these viscometers and in this case, a faster flowing Fenske modified-Ostwald viscometer (10) was used.

The three viscometers were put into the thermostat and clamped to the side wall. The flow times of each solvent were determined in the appropriate viscometer for volumes of 5, 10, 15, 20, and 25 ml. for calibration purposes. The temperature of the thermostat was maintained at 25.00 ± 0.02°C. The flow times at each volume were repeated until triplicate runs checked within 0.3 sec.

Five milliliters of the 1.0% polymer solution was added to the clean, dry viscometer and its flow time determined in triplicate. Then an additional 5 ml. of solvent was introduced and the resulting 0.50% polymer solution was made homogeneous by blowing air gently through a calcium chloride drying tube attached to an inverted U-tube connected to the viscometer. A few seconds of agitation was all that was necessary to make the solution uniform in composition. The flow time of this solution was determined and then the process was repeated for 15 ml. (0.33%), 20 ml. (0.25%), and 25 ml. (0.20%). The final solution was then drawn out through the U-tube by suction. The viscometer was rinsed out with acetone or benzene and then dried by drawing air through it for a few minutes (11). The viscometer was not removed from the thermostat during the whole process. In this way any error in alignment would be cancelled out.

The Huggins-Kraemer viscosity relationship

$$\eta_{sp}/C = \{\eta\} + k'\{\eta\}^2C, \tag{1}$$

was assumed to hold in the various systems studied and was utilized to determine the values of $[\eta]$ and k'. These values were calculated from the experimental points using the method of least squares.

RESULTS

The intrinsic viscosities and k' values of the three polymers in the various solvents investigated are listed in Table I, along with the (estimated) cohesive energy densities for the various solvents and nonsolvents. The solvents are listed in order of decreasing intrinsic viscosity for polymethyl methacrylate. The degree of precision obtained is illustrated in Fig. 1, which shows typical η_{ps}/C vs. C curves.

Similar data for polymethyl methacrylate in the mixed solvents, chloroform–toluene and chloroform–ethyl methyl ketone are shown in Table II.

The variation of the intrinsic viscosity of polymethyl methacrylate in solvent–nonsolvent mixtures was also observed. Ethyl methyl ketone was selected as the solvent and methanol was the nonsolvent. The limiting solubility composition was determined by titrating 25 ml. of a 0.50%

TABLE I

Intrinsic Viscosity and k′ Values for Three Polymers in Various Solvents

CED polymer		Methyl methacrylate		Copolymer		Styrene	
Solvent	CED	$[\eta]$	k'	$[\eta]$	k'	$[\eta]$	k'
	cal./cc.						
Chloroform	86	1.75	0.36	1.13	0.37	2.55	0.39
Dioxane	92	1.37	0.29	0.91	0.31	2.11	0.36
Benzene	83	1.34	0.29	0.99	0.29	2.54	0.35
Nitroethane	120	1.15	0.35	0.57	0.47	I	—
Toluene	76	0.97	0.38	0.88	0.31	2.40	0.35
Ethyl methyl ketone	83	0.92	0.44	0.64	0.37	1.20	0.50
Cyclohexanone	89	0.91	0.52	0.77	0.47	2.20	0.32
Ethyl acetate	78	0.79	0.56	0.62	0.41	1.11	0.60
Acetone	93	0.75	0.64	0.38	0.80	I	—
Isopropyl acetate	70	0.50	1.10	0.49	0.57	0.90	0.75
Carbon tetrachloride	75	0.44	0.80	0.9	0.4	2.25	0.39
m-Xylene	64	0.40	1.38	0.73	0.45	2.25	0.30
Hexane	52	I	—	I	—	I	—
Methanol	210	I	—	I	—	I	—

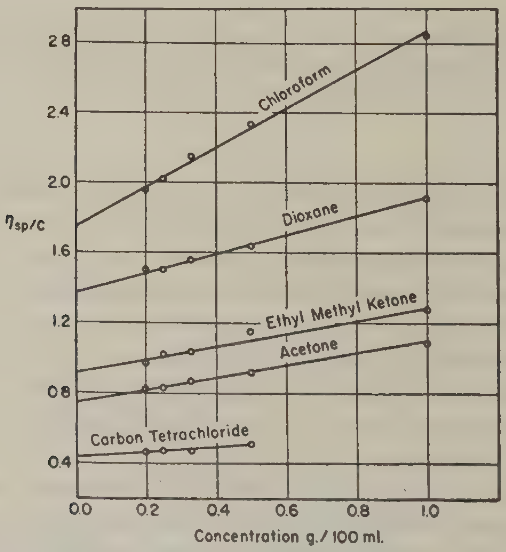

FIG. 1. Viscosity of polymethyl methacrylate in pure solvents.

TABLE II

Intrinsic Viscosity and k′ Values of Polymethyl Methacrylate in Mixed Solvents

Mixed solvent Chloroform *per cent*	 Toluene *per cent*	[η]	k′
80	20	1.675	0.328
60	40	1.544	0.336
50	50	1.464	0.320
40	60	1.405	0.346
20	80	1.231	0.352
	Ethyl methyl ketone *per cent*		
75	25	1.592	0.330
50	50	1.350	0.343
25	75	1.085	0.401

solution of polymethyl methacrylate in ethyl methyl ketone to the cloud point with methanol. This titration required 28.5 ml. of methanol, hence the solvent–nonsolvent mixture contained 53.4% methanol at the precipitation point. Values of the intrinsic viscosity and k′ for three different compositions are listed in Table III.

Discussion

The intrinsic viscosity of polymethyl methacrylate in twelve solvents varied from 0.4 in *m*-xylene and carbon tetrachloride to 1.75 in chloroform. This fourfold variation indicates that the methacrylate molecule is quite flexible in solution.

In Fig. 2, the intrinsic viscosities of polymethyl methacrylate in the twelve solvents are plotted against the cohesive energy density (CED) of the solvents. It can be seen from this figure that there is no obvious correlation between intrinsic viscosity and CED of the solvent. Evidently there are additional factors which influence the intrinsic viscosity of polymethyl methacrylate.

However, these results can be qualitatively rationalized if one adopts the point of view of Spurlin, and considers the generalized "acidic" or "basic" properties of the various solvents, as well as their cohesive energy densities. Chloroform and nitroethane are both known to complex with

TABLE III

Intrinsic Viscosity and k′ Data for Polymethyl Methacrylate in Solvent–Nonsolvent Mixtures

Solvent Ethyl methyl ketone	Nonsolvent Methanol	[η]	k′
per cent	*per cent*		
85	15	0.853	0.487
70	30	0.697	0.608
55	45	0.451	1.200

ketones and esters; the oxygen of the carboxyl group has nonbonded electrons which it can "donate" to an electron-accepting, or "acidic," molecule such as chloroform or nitroethane. These two solvents, as a result, exhibit much greater solvent power for polymethyl methacrylate than would be predicted on the basis of their cohesive energy densities alone. (As a matter of fact, nitroethane has such a large cohesive energy density that one would not expect it to dissovle polymethyl methacrylate at all if no specific solvation effect were operating.) On the other hand, the ketonic solvents are all relatively poor solvents for polymethyl methacrylate, even when their cohesive energy densities are favorable. Thus we are led to the following generalization which we must carefully qualify as being qualitative and tentative: Polymethyl methacrylate has a cohesive energy density of approximately 80–90 cal./cc. Furthermore, it can act as an electron donor (Lewis base). The solvent power of a "neutral" solvent depends upon the matching of the cohesive energy densities of solvent and polymer. (Cf. the regular decrease in solvent power in the benzene–toluene–xylene series.) "Acidic" solvents, such as chloroform and nitroethane, exhibit greater solvent power than would be predicted on the basis of cohesive energy density alone. "Basic" solvents, such as ketones, exhibit poorer solvent power than would be predicted on the basis of cohesive energy density alone.

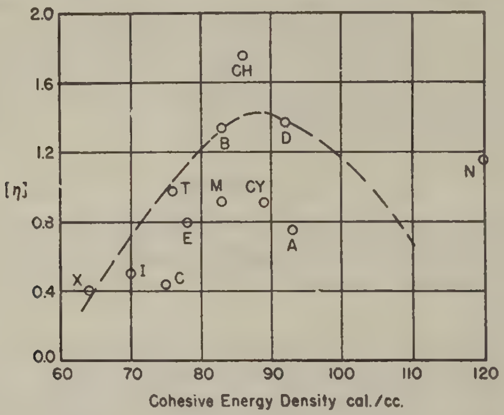

FIG. 2. Variation of intrinsic viscosity with the cohesive energy density of the solvent in the case of polymethyl methacrylate. A acetone, B benzene, C carbon tetrachloride, CH chloroform, D dioxane, E ethyl acetate, I isopropyl acetate, M ethyl methyl ketone, N nitroethane, T toluene, X *m*-xylene.

The intrinsic viscosities of the polymer in chloroform–toluene mixtures were somewhat higher (Fig. 3) than would be anticipated if a linear relationship with varying compositions of the two solvents existed. This is probably due to the fact that the solvating, hydrogen-bonding property of the chloroform still persists somewhat upon dilution, as the toluene behaves essentially as an inert solvent. In the case of the mixed solvent, chloroform–ethyl methyl ketone (Fig. 4), the ethyl methyl ketone also may form associated complexes with the chloroform, minimizing the association with the carbonyl groups in the polymer. The solvating property of the chloroform therefore becomes "neutralized" by the ethyl methyl ketone, and the intrinsic viscosity shows a straight-line relationship with varying compositions of the two solvents.

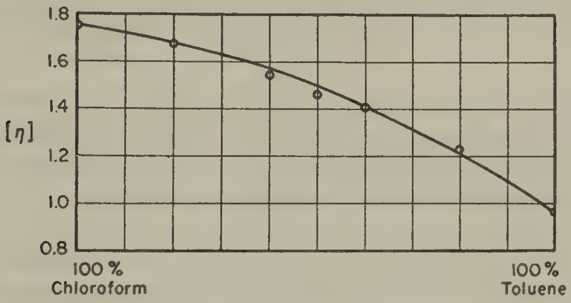

FIG. 3. Intrinsic viscosity of polymethyl methacrylate in mixtures of chloroform and toluene.

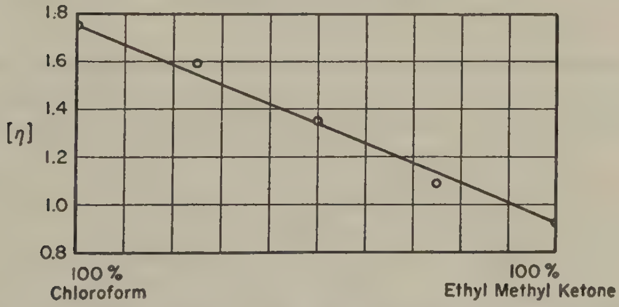

FIG. 4. Intrinsic viscosity of polymethyl methacrylate in mixtures of chloroform and ethyl methyl ketone.

The intrinsic viscosity of polymethyl methacrylate was determined in the solvent–nonsolvent system, ethyl methyl ketone–methanol (Fig. 5). The intrinsic viscosity was found to decrease as the volume per cent of the nonsolvent (methanol) was increased. This decrease in intrinsic viscosity did not show a linear relationship with solvent composition, but decreased more sharply with larger proportions of methanol, until it had approached a limiting value of about 0.3 which was obtained by extrapolating the curve to the limiting solubility composition.

In the viscosity relationship expressed above (1), the constant k' (12) is referred to as a solvent–solute interaction term. The value of k' depends

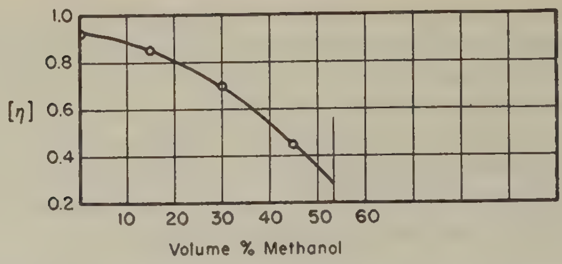

FIG. 5. Variation of intrinsic viscosity with composition of mixed solvent: polymethyl methacrylate in ethyl methyl ketone-methanol.

on the number and permanence of polymer-polymer contacts in solution, and its value decreases with increasing solvent action. In Fig. 6, the values of k' are plotted against the intrinsic viscosities for polymethyl methacrylate. (These include some data unreported above.)

It is interesting to note that the plotted points fall, within experimental error, along a hyperbola (13). From the data it appears that the limiting value of $[\eta]$ is about 0.3 and (by coincidence) the limiting value of k' is also 0.3. The limiting value of $[\eta] = 0.3$ is the same as that independently determined from Fig. 5 based on limiting solubility measurements. The limiting k' value in good solvents is of the same magnitude as indicated by previous workers.

It can be seen from Table I that the general interaction with solvent of the styrene–methyl methacrylate copolymer is intermediate between that of polystyrene and that of polymethyl methacrylate. For example,

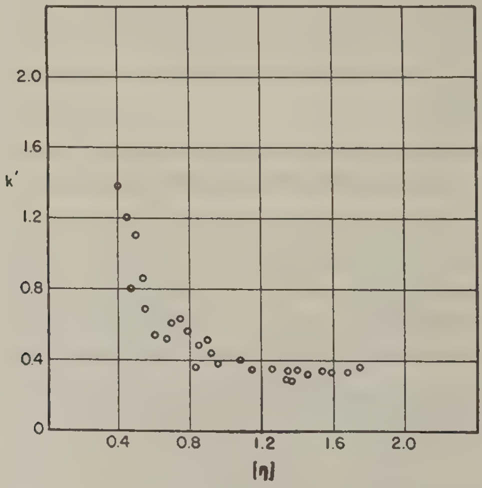

FIG. 6. Variation of k' with intrinsic viscosity in solutions of polymethyl methacrylate.

benzene, toluene, and xylene are all good solvents for polystyrene; they differ markedly in their solvent power for polymethyl methacrylate; for the copolymer, a similar trend in solvent power is observed, but is much less pronounced than in the case of polymethyl methacrylate. Similar consistencies were found in the case of other solvent series.

The designation of solvents as "acidic" or "basic" appears to be necessary in interpreting the variations observed with polystyrene as well as with the more polar polymethyl methacrylate. In addition, a steric or symmetry factor is quite possibly operative, making the entire picture fairly complex. Further experimental work is planned to aid in clarifying these various influences.

SUMMARY

Specific viscosity data were obtained for polymethyl methacrylate, polystyrene, and a methyl methacrylate–styrene copolymer, in a variety of solvents. The "solvent power" of a given solvent for the methyl methacrylate group in the polymer and the copolymer depends not only upon the cohesive energy density of the solvent but also upon the electron-donating or electron-accepting properties of the solvent. In the case of polymethyl methacrylate, a definite inverse correlation between intrinsic viscosity and k' value was observed.

REFERENCES

1. ALFREY, BARTOVICS, AND MARK, *J. Am. Chem. Soc.* **64**, 1557 (1944).
2. ALFREY, T., *J. Colloid Sci.* **2**, 99 (1947).
3. SPURLIN, H. H., *J. Polymer Sci.* **3**, 714 (1948).
4. GEE, G., *Trans. Faraday Soc.* **40**, 463 (1944).
5. CRAGG, L. H., AND ROGERS, T. M., *Can. J. Research* **26B**, 230 (1945).
6. ALFREY, JUSTICE, AND NELSON, *Trans. Faraday Soc.* **42B**, 50 (1946).
7. HILDEBRAND, J. H., Solubility of Nonelectrolytes. Reinhold, New York, 1936.
8. DOTY, P., *J. chim. phys.* **44**, 107 (1947).
9. BOYER, R. F., *J. Chem. Phys.* **13**, 363 (1945).
10. CANNON, M. R., AND FENSKE, M. R., *Ind. Eng. Chem., Anal. Ed.* **10**, 297 (1938).
11. WAGNER, R. H., AND RUSSELL, J., *Anal. Chem.* **20**, 151 (1948).
11a. See also: DAVIS, W. E., AND ELLIOTT, J. H., *J. Colloid Sci.* **4**, 313 (1949).
12. HUGGINS, N. L., *J. Am. Chem. Soc.* **64**, 2716 (1942).
13. See also: EIRICH AND RISEMAN, *J. Polymer Sci.* **4**, 417 (1949).

MEASUREMENTS OF PROPERTIES OF CORN STARCH GELS [1]

Welker G. Bechtel [2]

Corn Industries Research Foundation [3]

Received February 17, 1950

INTRODUCTION

There is extensive literature on the fundamental theory of gel formation and structure, on pectin, gelatin, and other gels. However, starch gels have not been as extensively studied, and the findings are based largely on experiments with native, or unmodified starches (1–5).

Gel properties of starches, both native and chemically modified, are of great importance commercially. Starch is frequently used in puddings, and as a thickening agent in pie fillings, salad dressings, gum candies, and other food products. It is also employed industrially as a gelling agent: for example, in the pastes for dry cells. For many other purposes it is desirable that the gelling tendency be minimized so that when the cooked starch is cooled, or is allowed to age, it will remain fluid. Certain native starches such as tapioca, potato, and waxy maize, have less tendency to form firm gels than do the ordinary cereal starches such as corn and wheat. However there are processes for modifying starches chemically so that the gelling tendency may be either increased or diminished.

The objectives of this study were (*a*) to compare the application of different gel testing methods and instruments to starch gels and to correlate the results, (*b*) to determine some of the properties of gels of both native and modified corn starch, and (*c*) to compare the gel properties of a series of commercial grades of acid-modified corn starches.

EXPERIMENTAL METHODS

Instruments

For measurement of the modulus of rigidity, the rigidometer of Brimhall and Hixon (6) was used. Empirical gelometers employed were the Saxl (7), Bloom (8), and Delaware (9), all of the plunger type. Also an embedded-disk instrument was devised for these experiments. The commercial gelometers were used as recommended in the descriptions referred to above. With the Delaware jelly tester, only the breaking strength of gels can be obtained. While the Bloom gelometer is designed to measure the elasticity of gelatin gels, it was found that it broke the surface of every starch gel tested. Thus it gave a measure of the breaking strength of starch gels. It was used with the plunger of 1-in. diameter and the adapter to restrict the flow of shot. The Saxl and embedded-disk instruments give readings both of load vs. deformation and of yield point.

---

[1] Presented at the Annual Meeting of the Society of Rheology, New York, N. Y., November 4–5, 1949.

[2] Present address: American Institute of Baking, Chicago, Illinois.

[3] Research Fellow.

The embedded-disk gelometer is a modification of the method of Saare and Martens (10), which has been used in other forms for the study of starch gels by Kerr (11) and Hamer (4). The apparatus devised for these experiments is shown schematically in Fig. 1. Jars used for the gels were wide-mouthed, of 150-ml. capacity, 59 mm. inside diameter, and 85 mm. in over-all height. Disks were of copper, 19 mm. in diameter and 1.5 mm. thick, attached centrally to a stiff wire with a hook at the end. As soon as the hot starch paste was poured into the jar, the disk was embedded in it at a depth of 3.0 cm., and a slotted metal cover was placed over the top. By moving the wire to the end of the slot the disk was centered in the jar.

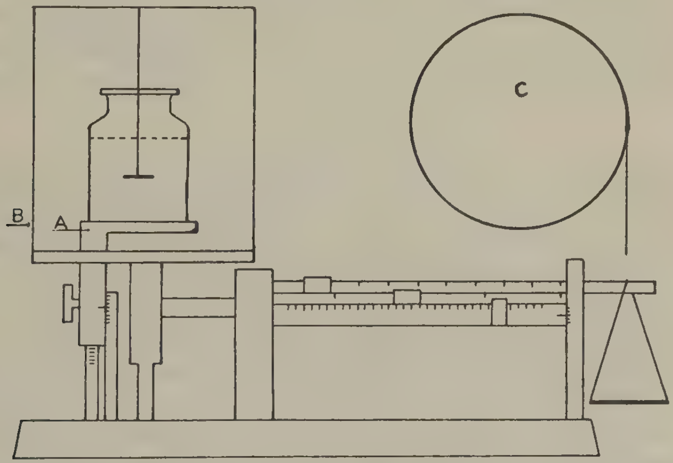

FIG. 1. Schematic drawing of embedded-disk gelometer. A is a platform adjustable in height. B is a frame attached to the pan of a triple beam laboratory balance. C represents a means of applying a continuously increasing load to the disk.

To make a test, the jar containing a gel was placed on platform *A*, which is vertically adjustable by a rack and pinion. The wire from the embedded disk was hooked to the frame *B* which was attached to the pan of a triple-beam laboratory balance. A balance with sensitivity of 0.1 g. is adequate. Platform *A* was then lowered 1 mm. and the load was applied to the beam until the pan was balanced. This step was repeated until the disk broke the gel. Thus readings of load vs. deformation to the yield point were obtained. Two means were used to apply the load. In early experiments, the riders on the beams of the balance were suitably adjusted. In subsequent ones, a chain was wound around a drum C which was supported above an auxiliary pan at the end of the beam. To apply the load, the chain was unreeled from the drum onto the pan by turning the drum. This added to the convenience of the apparatus and eliminated the vibration of the gel which occurred when the riders were moved.

Starches

Typical starches of regular commercial grades including unmodified and acid-modified corn starches of alkali fluidity from 10 to 70 were used. The usual grade designation for these modified starches is in terms of fluidity, the grades being numbered at intervals of 10 from 10 to 90. With increasing numbers a higher degree of modification is indicated. The basis for this method of grading has been described by Bechtel and Fischer (12).

Preparation of Gels

The properties of starch gels depend on the natural variety of the starch and its treatment during manufacture, and on all the conditions to which the starch is subjected during the cooking process. These conditions which are the same as those which affect starch consistency, have been discussed by Kesler and Bechtel (13). When starch is cooked it undergoes a complex series of changes including swelling, followed by collapse of the granules, solution of some of the constituents, and later, more or less complete granule disintegration. The rate of change depends on agitation, temperature and time of cooking, pH, and the presence of materials other than starch. Starches were all cooked under standardized conditions in the Corn Industries viscometer (13). Unless otherwise stated they were cooked to 91°C. in distilled water. The hot paste was poured into molds and immediately covered with petroleum oil to prevent evaporation and skin formation. Gels were stored in a water bath at 25°C. for 24 hr. before testing.

RESULTS AND DISCUSSION

Precision of Tests

The precision of replicate tests was found to be as follows: rigidometer ± 4.5%; Delaware tester ± 4.5%; Saxl gelometer ± 4%; Bloom gelometer ± 4%; embedded-disk gelometer ± 3%. All are within the range considered satisfactory for industrial evaluation of starch gel.

Elasticity

It was demonstrated by Hixon and Brimhall (3,6) that gels of unmodified corn starch follow Hooke's law and are elastic to the yield point, at

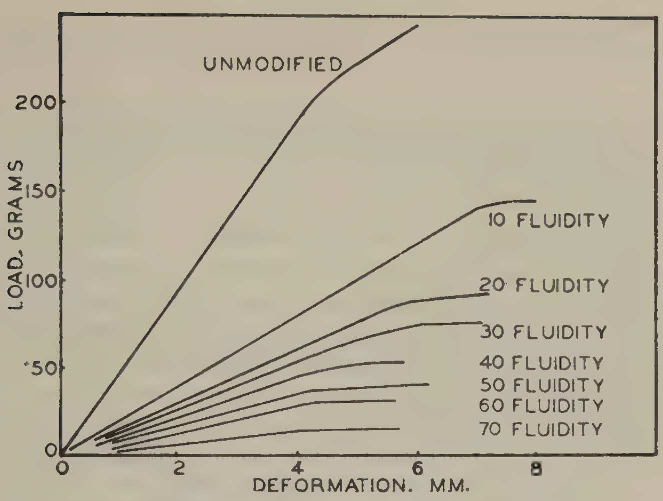

FIG. 2. Load vs. deformation characteristics of corn starch gels.

which a sharp break occurs. In the present study it was found (Fig. 2) that under the experimental conditions used for their preparation, gels of all of the modified starches tested were also elastic.

Correlation of Results with Different Instruments

Load vs. Deformation. Tests of load vs. deformation below the yield point were made with the rigidometer, Saxl gelometer, and embedded-disk instrument. With the rigidometer the modulus of rigidity was found in absolute units using the formula of Hatschek and Jane (14),

$$E = \frac{N}{4\pi h}\left(\frac{1}{R_0^2} - \frac{1}{R_1^2}\right)\frac{\delta}{\omega}.$$

E is the modulus of rigidity in dynes/cm.^{2}, N is the torsional moment of the wire, h is the height of the gel on the inner cylinder, R_0 and R_1 are the radii of the inner and outer cylinders respectively, δ is the angular twist given the wire, and ω is the corresponding deflection of the inner cylinder. By including all of the instrument constants in a constant k the formula reduces to

$$E = \frac{k}{h} \times \frac{\delta}{\omega}.$$

The empirical gel testers which were used either compressed the gel with a plunger or stretched it as stress was applied to the embedded disk. For elastic gels results should be proportional to Young's modulus Y, which is related to the modulus of rigidity by the formula $Y = 2E(1+\sigma)$ where σ is Poisson's ratio. It seems reasonable to expect Poisson's ratio to be essentially constant for gels of various starches. Tests with plunger and embedded-disk gelometers should then be proportional to the modulus of rigidity.

From the data in Table I for Saxl and embedded-disk tests, regression lines on the rigidometer data were found by least squares. These are:

Saxl gelometer vs. rigidometer $E = 71.4S$
Embedded-disk gelometer vs. rigidometer $E = 20.9P$,

where S and P represent the load required to deform the gel 1 mm. with the Saxl and embedded-disk gelometers, respectively. Moduli of rigidity were calculated from the above equations. These are given in the last two columns of the table for comparison with rigidometer results in column 4. Coefficients of linear correlation found are:

Saxl gelometer vs. rigidometer $r = 0.915$,
Embedded-disk gelometer vs. rigidometer $r = 0.988$.

Since the value $r = 1$ indicates that all points fall on the regression line while $r = 0$ indicates complete lack of linear correlation, it is apparent that results of embedded-disk tests were in close agreement with those of the rigidometer. Agreement between the Saxl gelometer and the rigidometer was good but not as close.

TABLE I

Measurement of the Elasticity of Corn Starch Gels

Gel no.	Load/mm. deformation		Modulus of rigidity		
	Saxl	Embedded disk	Rigidometer	Saxl	Embedded disk
	g.	*g.*	*dynes/cm.*^{2}	*dynes/cm.*^{2}	*dynes/cm.*^{2}
1	2.63	7.5	136	188	156
2	2.20	7.7	148	157	160
3	3.97	11.3	251	283	236
4	4.90	12.0	253	350	249
5	3.93	18.5	335	281	385
6	5.43	16.7	346	388	348
7	6.93	22.9	505	495	478
8	5.80	25.2	512	414	525
9	8.63	27.0	582	616	563

Some of the variation between the instruments, especially in the gels of low rigidity, is accounted for by the greater sensitivity of the embedded-disk gelometer. A second cause of variation is that with any plunger-type gelometer the plunger should be in complete contact with the gel surface at the start of the test. However, gels prepared from more concentrated pastes of corn starches of low fluidity are plastic when poured into molds. Even if the jars are tapped gently or are swirled the surface is rarely, if ever, level. On cooling, such gels usually form a more or less wrinkled surface which makes complete plunger contact impossible.

Wall and Bottom Effects. A third cause of variation is the effect of the wall of the vessel which contains the gel. Sheppard and Sweet (15) found that results of plunger tests were affected by the bottom of the jar unless the gel exceeded a minimum depth, and by the side wall unless the ratio of jar diameter to that of the plunger exceeded a minimum value. It was found experimentally that for starch gels the bottom effect could be avoided by using gels at least 4 cm. deep. In these experiments all gels were made 5 cm. deep.

Distortion due to the side wall cannot be avoided as readily. It would be inconvenient to use a jar of sufficient diameter to minimize the effect. It would also be impractical to use a plunger of smaller diameter, as this would decrease the load required to produce a given deformation, thus reducing the sensitivity of the test. No effect due to wall or bottom was found with the embedded-disk gelometer.

Yield Point and Breaking Strength. Yield points of starch gels differ little from the points of rupture. Since yield points could not be measured with the Delaware or Bloom gelometers, breaking-strength values are given in the experimental results.

It has often been assumed that values of rigidity and yield point are interdependent and that it is unnecessary to make both tests. While the values frequently increase or decrease together, this is not always the case. Saxl demonstrated this for gelatin (7), Meschter and Lataillade for pectin (16), and the experiment below illustrates a similar result for starch gels. Here the use of calcium bicarbonate solution instead of distilled water for preparing the gels caused a marked increase in breaking strength with little change in rigidity. In these gels unmodified corn starch was used at a 6% concentration.

Added agent	Rigidity	Deformation at break	Breaking strength
	dynes/cm.²	*mm.*	*dynes/cm.²*
None (control)	450	4.5	22.6
Calcium ion, 60 p.p.m. (as bicarbonate)	462	6.0	33.0

It follows that both load vs. deformation and breaking strength (or yield point) measurements should be made except, perhaps, in routine testing when it is known what a single property is important for a specific application of the gel.

Comparative tests of breaking strength were made with the Saxl, Delaware, Bloom, and embedded-disk gelometers. Values are given in Table II as pressures in grams per square centimeter. One should not expect them to agree numerically, since they are affected by the rate of addition of load and the sharpness of the edge of the plunger as well as the depth of the disk. However the results were found to be nearly proportional, with coefficients of linear correlation as follows:

Bloom vs. embedded-disk gelometer $r = 0.911$,
Saxl vs. embedded-disk gelometer $r = 0.946$,
Delaware vs. embedded-disk gelometer $r = 0.943$.

Thus the instruments are in reasonably good agreement.

In industrial testing, the total load rather than the pressure is usually taken as the breaking strength. If this is done the numerical value of the test may be made greater by increasing the area of the plunger or disk. This gives greater separation of results with different gels and increases the sensitivity of the test. In addition, with the embedded disk the depth of the disk can be increased. Hamer (4) found that the load at the break point varied exponentially with the depth of the disk.

TABLE II

Measurement of the Breaking Strength of Corn Starch Gels

Gel no.	Breaking strength			
	Saxl	Embedded disk	Delaware	Bloom
	g./cm.^{2}	*g./cm.*^{2}	*g./cm.*^{2}	*g./cm.*^{2}
1	14.8	23.6	19.9	10.5
2	13.7	26.5	23.0	8.9
3	19.0	32.3	32.1	14.0
4	18.6	39.0	37.6	12.3
5	24.7	50.2	46.3	15.6
6	25.8	53.3	49.5	16.3
7	36.4	61.1	69.9	21.9
8	39.8	71.5	78.9	23.6
9	50.8	118.0	92.3	—

The embedded-disk gelometer is sufficiently sensitive to distinguish clearly between gels of the commercial grades of acid-modified corn starch, and between those of the same starch which differ by 0.5% in concentration. This is illustrated in Table III. The other gelometers gave results in which there was more or less overlapping of the extreme values.

Change in Gel Properties with Time

The greatest increase in rigidity and breaking strength of corn starch gels occurs during the first few hours and thereafter it becomes progressively slower. However, the rate of change is not the same for all starches when measured at the same concentration.

TABLE III

Total Load at Break Point of Gels Measured with the Embedded-Disk Gelometer

Starch fluidity	Starch concentration	Load at break point of gel	
		Average	Range
	%	g.	g.
10	6.0	75	71–80
10	6.5	111	105–15
10	7.0	142	135–47
Unmodified	9.0	550	525–75
10	9.0	335	321–40
20	9.0	203	196–206
30	9.0	173	162–80
40	9.0	114	105–22
50	9.0	92	85–96
60	9.0	67	59–76
70	9.0	38	35–40

In Table IV, data are given for the rigidity and breaking strength of a series of corn starch gels after 4 and 24 hr. aging. Measurements made with the embedded-disk gelometer show that with increasing starch modification there is a greater percentage increase in both rigidity and breaking strength during this time interval.

Effect of Temperature of Cooking

The effect of temperature of cooking unmodified corn starch on the rigidity of its gels was studied by Brimhall and Hixon (6). In the present study, the effect of cooking temperature on both rigidity and breaking strength of gels of unmodified and acid-modified corn starches of intermediate and high fluidity was determined.

TABLE IV

Change in Gel Properties with Time

(Starch concentration: 6%)

Starch fluidity	Rigidity			Breaking strength		
	4 hr.	24 hr.	Increase	4 hr.	24 hr.	Increase
	dynes/cm.^{2}	dynes/cm.^{2}	%	g./cm.^{2}	g./cm.^{2}	%
Unmodified	437	518	19	40.0	48.7	22
5[a]	229	335	48	24.9	34.8	39
10	123	233	90	15.2	26.4	74
20	—	—	—	8.5	16.4	93

[a] This was a specially prepared laboratory sample.

The results in Table V show that the effect of cooking temperature on the properties of gels of modified starches cannot be inferred from its effect on gels of unmodified corn starch. The breaking strength of gels of unmodified corn starch increased with temperature to 94°C., then decreased, while for 30-fluidity starch it remained nearly constant through the range 92–96°. For 60-fluidity starch it increased as the cooking temperature was raised from 88° to 96°. Changes in rigidity given in the table show the same general trends.

This illustrates the importance of close control of starch cooking temperature. It shows also that comparative laboratory tests may be misleading if they are intended for control of starches which are to be used commercially for gels unless the cooking temperature used in the laboratory approximates that used by the consumer.

TABLE V

Effect of Cooking Temperature on Gel Properties

Temperature (°C.)		88	92	94	96	88	92	94	96
Starch fluidity	Starch concentration	Rigidity, *dynes/cm.*^{2}				Breaking strength, *g./cm.*^{2}			
	%								
Unmodified	7.0	476	793	835	602	31.4	80.8	100.0	90.5
30	9.0	685	—	665	687	54.8	73.3	79.0	78.0
60	9.0	314	359	380	450	20.8	25.4	36.0	54.5
60	12.0	—	1120	1300	1640	—	81.4	97.5	138.0

Commercial Grades of Acid-modified Corn Starch

Woodruff and MacMasters (1) found that there was no relationship between the consistency of hot pastes of unmodified corn starch and the properties of its gels. It is also known that when corn starch is oxidized, rigidity and breaking strength of the gels decrease more than does hot-paste consistency. However when corn starch is modified with acid there is a smaller decrease in rigidity and breaking strength than in hot-paste consistency (17).

Gel properties of commercial acid-modified corn starches were studied to obtain quantitative data for their evaluation. Gels were compared at 9% concentration, the lowest at which 70-fluidity starch formed a firm gel under the conditions of preparation. Since the properties of these gels are affected by pH, all gels were of approximately pH 6. In Table VI the values of rigidity and breaking strength were found with the embedded-disk gelometer. Ratios of consistency, rigidity, and breaking strength of each starch to the corresponding property of unmodified corn starch are given. Consistency measured in the Corn Industries viscometer

TABLE VI

Consistency of Pastes; Rigidity and Breaking Strength of Corn Starch Gels
(Nine per cent concentration. Consistency after 30 min. at 91°C.)

Starch fluidity	Consistency	Rigidity	Breaking strength	Ratios to unmodified corn starch		
				Consistency	Rigidity	Breaking strength
	poises	*dynes/cm.*^{2}	*g./cm.*^{2}			
Unmodified	34.0	1850	194	1.000	1.000	1.000
10	15.1	1140	118	0.444	0.615	0.610
20	8.5	810	71.5	.250	.438	.368
30	6.0	738	61.1	.175	.398	.314
40	3.6	510	40.3	.105	.276	.207
50	3.0	422	32.6	.088	.238	.166
60	1.1	318	23.6	.031	.172	.121
70	0.2	156	13.4	.006	.085	.069

after cooking the starches 30 min. decreased with degree of starch modification to a much greater extent than did the gel properties.

SUMMARY

1. By means of an embedded-disk gelometer the properties of starch gels can be determined with adequate precision to distinguish between consecutive commercial grades of acid-modified corn starches, and between gels of the same starch which differ by 0.5% in starch concentration.

2. Gels of acid-modified as well as unmodified corn starch are elastic to the yield point.

3. The percentage increase in rigidity and breaking strength of gels during aging from 4 to 24 hr. depends on the modification of the starch. The increase is greater for starches of higher modification.

4. The effect of temperature of cooking starches on the properties of their gels varies with the degree of modification of the starch.

5. With increasing modification of the starch, the consistency of the hot pastes of acid-modified corn starches decreases to a greater extent than do the rigidity and breaking strength of their gels.

ACKNOWLEDGMENT

This research is part of a program undertaken by the Corn Industries Research Foundation and is published with its permission.

REFERENCES

1. WOODRUFF, S., AND MACMASTERS, M. M., Illinois Agr. Exptl. Sta., Bull. 445 (1938).
2. HARRIS, R. H., AND JESPERSON, E., *Food Research* **11**, 216–28 (1946).
3. HIXON, R. M., AND BRIMHALL, B., *Ind. Eng. Chem., Anal. Ed.* **13**, 193–4 (1941).
4. HAMER, W. J., *J. Research Natl. Bur. Standards* **39**, 29–37 (1947).

5. Whittenberger, R. T., and Nutting, G. C., *Ind. Eng. Chem.* **40**, 1407–13 (1948).
6. Brimhall, B., and Hixon, R. M., *Ind. Eng. Chem., Anal. Ed.* **11**, 358–61 (1939).
7. Saxl, E. J., *Ind. Eng. Chem., Anal. Ed.* **10**, 82–6 (1938).
8. DeBeaukelaer, F. L., *et al., Ind. Eng. Chem., Anal. Ed.* **2**, 348–51 (1930).
9. Baker, G. L., *Fruit Products J.* 17, 329–30 (1938).
10. Saare, O., and Martens, P., *Z. Spiritusind.* **26**, 436 (1903).
11. Kerr, R. W., Chemistry and Industry of Starch, p. 97. Academic Press, New York, 1944.
12. Bechtel, W. G., and Fischer, E. K., *J. Colloid Sci.* **4**, 265–82 (1949).
13. Kesler, C. C., and Bechtel, W. G., *Anal. Chem.* **19**, 16–21 (1947).
14. Hatschek, E., and Jane, R. S., *Kolloid-Z.* **39**, 300–13 (1926).
15. Sheppard, S. E., and Sweet, S. S., *Ind. Eng. Chem.* **15**, 571–6 (1923).
16. Meschter, E. E., and Lataillade, L. J., *Food Technol.* **3**, 28–33 (1949).
17. Ref. 11, p. 235; p. 402.

RHEOLOGICAL PROPERTIES OF COMMERCIAL PAINTS[1]

Earl K. Fischer[2]

Received February 17, 1950

INTRODUCTION

The flow properties of protective coatings are of primary importance in establishing the working qualities with respect to initial application and to subsequent leveling. Consistency is controlled empirically by choice of vehicle components, pigment volume, and reagents added to induce either flocculation or deflocculation of the suspended pigment particles. Various control methods and instruments are used to measure the flow properties during manufacture, among them being several types of "flow cups" (efflux viscometers), the Mobilometer, and rotational instruments usually equipped with paddle-type rotors (12). Although useful for manufacturing control purposes, these methods provide empirical data which are significant only in terms of the instrument and the test method. Despite a considerable literature on the subject, there are few measurements of typical paints and other finishes which are reported in standard physical units.

This paper presents (*1*) viscometric data on a variety of commercial paints, (*2*) a comparison of results obtained by certain other testing methods, and (*3*) a brief evaluation of the rheological properties of paints as related to brush and spray-gun application. The measurements were made with a cylindrical rotational viscometer described previously (9,10) which is well suited for the consistency range of these materials. The paint samples were typical consumer products and included high-gloss enamels, semi-matte wall finishes, flat paints and primers, exterior house and trim paints, and emulsion paints.

The rheological properties of paints are of interest in connection with the early investigations of Bingham on plastic flow, and the terminology adopted has been applied to other systems. *Consistency* is a qualitative, descriptive term representing a subjective merging of the various attributes of non-Newtonian flow. The *yield value* (f) as used by Bingham and subsequent investigators, is the minimum stress which must be applied to initiate laminar flow. *Plastic viscosity* (U) is the resistance-to-flow when the material has been subjected to a stress in excess of the yield value. For paints, the term *false body* is often used, and its meaning is variable; it frequently refers to a material exhibiting thixotropic properties in which the time for restoration of high consistency is very short.

---

[1] Presented at the Annual Meeting of the Society of Rheology, New York, N. Y., November 4–5, 1949.

[2] Present address of author: National Bureau of Standards, Washington 25, D. C.

The early investigations of Bingham and Green (3,13) demonstrated the essential fact that paints exhibited plastic-flow properties and established, for the first time, magnitudes for plastic viscosity (expressed as its reciprocal, mobility), and yield value. This work was considerably extended a few years later by the coöperative effort of several laboratories (4). Measurements on a selected variety of paint samples by different investigators showed fairly good reproducibility, and variations in the values were attributed partly to actual differences in the samples as a consequence of mixing, aging, evaporation, etc. The yield value for the paint samples was less than 500 dynes/cm.^{2}, except for a flat white which had a yield value in excess of 1300 dynes/cm.^{2}. The plastic viscosities for all except one sample were included between 0.9 and 5 poises. Perhaps the most important conclusion drawn from the data was the linearity of the curve of efflux volume vs. shearing stress. It became evident at this time to many discerning investigators that to attempt a single numerical definition of consistency, based on some combination or ratio of the two flow factors, was a futile endeavor. Subsequent investigations will be noted later.

The rotational cylindrical viscometer is advantageous for these measurements and the rationale for its use has been established (8,9,14,15). Industrial laboratories, however, utilize instruments which yield only limited information, probably because of convenience in measuring technique (2,12,24).

EXPERIMENTAL PROCEDURES

Measurements were made by means of the modified Stromer viscometer described previously (9,10). The clearance between cup and bob was 1.81 mm.; bob height, 3.53 cm. Calculations were made from the working equations $U = K_v \times (W - W_f)/\text{r.p.m.}$ and $f = K_f \times W_f$ where U is the plastic viscosity in poises, W is the weight (g.) at a given r.p.m. ,W_f is the intercept on the weight (stress) axis of the experimental curve of r.p.m. vs. weight, and f is the yield value in dynes/cm.^{2}. The constants had the following numerical values: $K_v = 1.93$; $K_f = 1.85$. At viscosities below 0.8 poise, a special correction factor, related to the end effect, was used (9). For determination of the rate of shear S (in sec.$^{-1}$) at a given r.p.m., $S = K_s \times \text{r.p.m.}$; $K_s = 0.95$.

The procedure was to introduce the paint into the cup, wait for temperature equilibrium, and take a series of readings by varying the weights systematically and without interruption from low loads to a maximum providing close to 400 r.p.m., and then to reduce the weights in sequence. Data so obtained are shown in Figs. 1 and 2. The reproducibility of the technique was excellent, and the curves of Fig. 1 show repeat runs using different samples of the same paint. All measurements were made at 30° ± 0.1°C.

Paint samples, obtained from local retail stores, were representative consumer products representing 15 different manufacturers. Although such a selection of samples does not take into account factors as age condition of storage, formula variations, *etc.*, it does indicate the range of flow properties encountered by the average consumer of "ready-mix" products. All samples were taken from new containers freshly opened, and were stirred adequately to ensure that all the settled solid components had been resuspended.

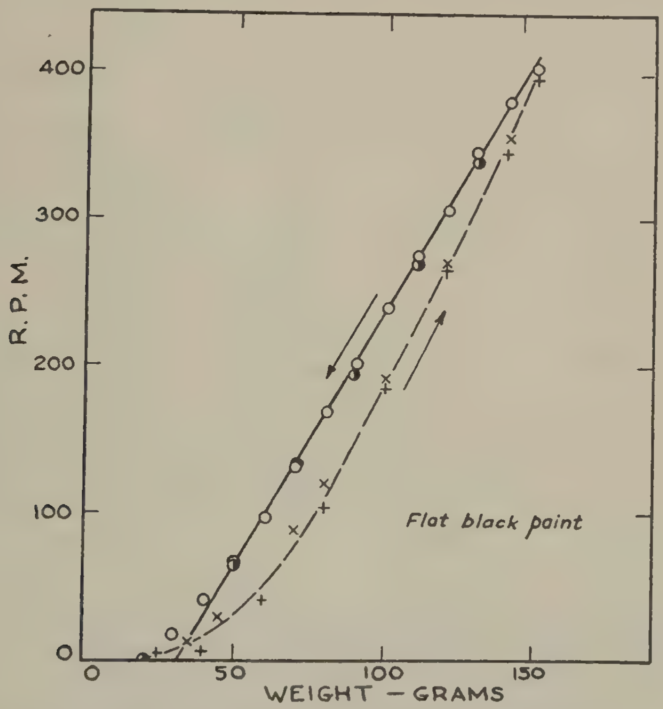

Fig. 1. Experimental curve of a thixotropic flat black paint.

Results and Discussion

Data obtained are collected in Table I, and curves typical of a thixotropic paint and one showing no loop in the flow curve are given in Figs. 1 and 2. It will be noted that the plastic viscosities of all samples were less than 4 poises, but it is not possible to characterize definitely a class of finishes in terms of the viscosity. In general, high-gloss enamels, house and trim paints, and semi-gloss finishes have plastic viscosities in the range of 1.5–3.9 poises; primers, flat (or matte-finish), and emulsion wall paints are generally lower, approximately 0.4–2.5 poises. However, the yield values as measured, and the variation in thixotropic properties as estimated from the loop in the flow curve (14), show differences between the different types. The enamels are characterized by low yield values (all less than 30 dynes/cm.^{2}), and some are clearly Newtonian in flow properties. It is possible that some of the low values are uncertain and can be considered as zero. No thixotropic breakdown was observed in many specimens, although a few cases were noted where it was slight. Flat, semi-matte, and outside white paints were found with the highest yield values. Most of the samples were under 100 dynes/cm.^{2}, and three were in the range of 100–200 dynes/cm.^{2}. These products also exhibited varying degrees of thixotropy.

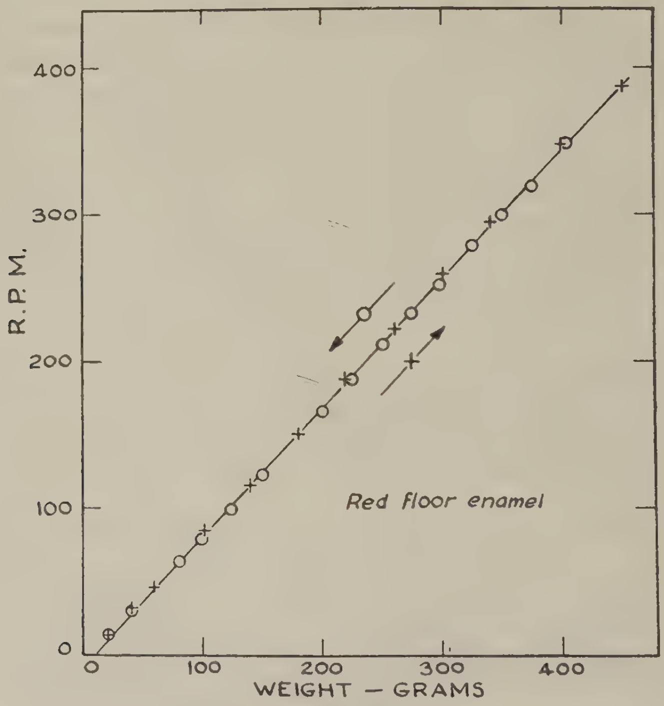

FIG. 2. Experimental curve of a high-gloss deck or floor enamel showing coincidence of points obtained at increasing and decreasing rates of shear.

Several varnishes, unpigmented, were measured and the viscosities were in the range of 0.9–2.9 poises.

TABLE I

Rheological Data on Different Types of Paints

Mfr.	Color	*U*	*f*	Thixotropy rating
Enamels (gloss deck or floor)				
		poises	*dynes/cm.*^{2}	
A	Grey	2.2	15	Nil
I	Grey	1.8	10	Nil
F	Green	1.9	19	Nil
F	Maroon	1.9	0	Nil
F	Red	1.8	8	Nil
F	Yellow	2.5	20	Very slight
Enamels (gloss; varied purpose)				
E	Black	0.81	0	Very slight
L	Black	1.4	0	Nil
O	Black	1.6	20	Nil
D	Black	2.3	15	Nil
B	Grey	1.5	15	Nil
I	Grey	1.8	6	Nil
M	Red	2.6	0	Nil
J	Red	2.6	18	Nil
F	White	2.7	0	Nil
G	White	2.0	15	Nil
H	White	3.9	28	Very slight
Semi-matte (interior wall or trim)				
A	Ivory	1.6	100	Slight
F	Oyster	1.7	74	Slight
F	Cream	2.6	70	Slight
F	White	2.3	65	Slight
K	Olive	2.7	110	Marked
N	White	3.5	120	Marked
Exterior				
A	White	3.4	170	Marked
N	White	3.8	110	Marked
A	Brown	1.1	20	Slight
G	Green	3.5	25	Slight
Primers (metal)				
G	Grey	1.2	20	Slight
D	Black	1.3	70	Marked
A	Brown	0.30	10	Marked

TABLE I—*Continued*

Flat				
A	Black	0.50	60	Marked
N	White	2.5	50	Marked
P	White	0.59	40	Marked
Emulsion (water-reduced)				
A	Pink	0.75	40	Slight
A	Blue	1.1	75	Slight
N	White	0.60	25	Slight
B	White	0.40	50	Slight

DISCUSSION

Rheological information on paints can serve several purposes. Data on the finished product serves to standardize a given line, and it provides an indication of what the artisan rates subjectively as "workability," "brushability," "sprayability," etc. The special requirements for different methods of application can also be estimated. Williamson and co-workers (25) measured a series of paints and correlated the rheological data with ratings of experienced painters. They estimated that brushing produces a rate of shear ranging from 100 to 200 sec.$^{-1}$. The plastic viscosities of paints with acceptable brushing properties were between 2 and 5 poises. Droste (7) considers paint to have good brushing properties when the plastic viscosity is in the range of 3.5–4.0 poises and the yield value lies between 400 and 1400 dynes/cm.^{2}. The viscosity limits noted are in accord with the data on commercial paints, but the yield values are considerably higher. Nitrocellulose lacquers are said to have good brushing properties if the viscosity is 0.16–0.18 poises (6). Aldrich (1) states that hot plastic paints, applied at temperatures in the range of 275–300 F., should have a viscosity of less than 1.5 poises; higher viscosities produce an uneven spray. Viscosities of gel lacquers have been noted by Malm and Smith (20) These compositions are applied by dipping, and each coat may be as thick as 0.015 in., as contrasted with the usual dip lacquer finish which is approximately one-tenth this thickness. The usual range for application is 20–40 poises.

It is evident that rheological data on the bulk composition before application is useful chiefly for estimating properties incident to initial application. A very low viscosity results in easy brushing properties, while viscosities in the neighborhood of 3–4 poises cause a "drag" on the brush. The viscosity of lacquers for spray-gun application is usually adjusted to fall within the approximate range of 0.2–1.2 poises by appropriate solvent additions. The dilution serves two main purposes: to allow efficient atomizing in the spray gun and to leave sufficient solvent in the applied film for adequate flowout.

The appearance of a film of paint or other coating is determined only partly by the flow properties of the bulk composition at the time of application. The rate at which the consistency changes immediately after application influences to a large extent the final smoothness of the film and its freedom from surface imperfections (5,16). Irregularities in the surface of many types of decorative and protective coatings are so common as to be considered almost unavoidable. Although these defects do not appreciably impair the service of a coating, the appearance is usually considered marred, and elaborate buffing and polishing means are sometimes employed to achieve uniformly smooth surfaces. Familiar examples are the following: sag marks and "curtains" result from any method of application where the film has been applied in a layer too thick to prevent excessive flow before the composition sets; brush marks are parallel ridges and valleys where the matted hairs of a paint brush leave an imprint; surface ripples, usually termed "orange-peel" by analogy with the skin of an orange, result from spray-gun application of lacquers and enamels.

The requirements for complete leveling of an applied finish have been stated by several investigators (5,11,16,17,21,25). The general conditions are the following: surface forces tend to produce flow of the applied film, smoothing the surface irregularities incidental to application by brushing or spraying; thixotropic build-up of the pigment structure within the film tends to reduce the rate of leveling; solvent evaporation increases the plastic viscosity and yield value, thus slowing down flowout of the film.

Waring (23) presented an interesting analysis of the leveling of paint films as a rheological process, deriving the following expression, $h = d^2f/8\gamma$, where h is the height of the brush mark and d the width, f is the yield value, and γ is the surface tension. Assuming that typical brush marks have a width of 0.1 cm., that the surface tension is 35 dynes/cm., and that the surface appears level when h is less than 0.0001 cm., Waring concluded that a yield value of less than 3 dynes/cm.^{2} will result in perfect leveling. This value appears unreasonably low. It means that a yield value lower than that measurable with certainty would result in brush marking. It may be inferred that the analysis presumes extremely low viscosity and film thickness. A further defect is failure to consider the effects of thixotropy. McMillen (21) developed a more complicated expression in which thixotropic build-up is considered. The actual conditions during paint application cannot be fully included in measurements made on the bulk composition, however, because the change in rheological properties with solvent evaporation is neglected.

The effect of viscosity and film thickness on flowout may be readily demonstrated by brushing or spraying oils of different viscosities onto a nonporous surface and observing the time for leveling. An oil with a viscosity of less than 0.5 poise levels in less than a minute at film thicknesses from 0.5 to 5 mil. An oil of 2 poises requires about 5 min. to flow to a smooth film if the film thickness is about 0.5 mil, but at higher film thickness leveling proceeds more rapidly and with thick films is complete in less than 30 sec. When the viscosity reaches 10 poises, thin films do not flow out in less than several hours, and thick films require about 10 min. These simple experiments suggest that flowout should occur in a film in a relatively short time, perhaps 2 min., to level completely. If any thixotropic build-up occurs, it should not be complete in the flowout time. Brush marks and "orange-peel" are inevitable if yield value of any appreciable magnitude is observed in the paint film. The actual change in flow properties is rapid, of course, when volatile solvents are present. Within 5 min. after application, the plastic viscosity of a typical enamel increases to 10 poises or more and the yield value builds up proportionately.

During application by brush, the paint is subjected to a moderate amount of shearing, and the thixotropic structure often present is broken down momentarily. After the brush has left the layer of paint on the surface, several competing processes start: the paint layer begins to flow and the dispersed pigment particles begin to rebuild the original thixotropic structure. If rebuilding takes place quickly, leveling and flowout cease, and brush marks are formed. On the other hand, if the development of structure is protracted, flowout continues and the applied paint film forms sag marks, particularly on vertical surfaces. The balance between these properties establishes the performance of the paint (see Table II). Saunders (22) obtained fair correlation of leveling and rheological data, and states that paints which are considerably reduced in consistency on agitation and which show a slow rate of thixotropic recovery exhibit the best leveling. On the other hand, when the thixotripoc recovery is rapid, poor leveling results.

TABLE II

Change in Flow Properties of a Brushed Black Enamel on Solvent Evaporation

Time	Plastic viscosity (U)	Yield value (f)	Type flow
min.	*poises*	*dynes/cm.²*	
0	1.9	0	Newtonian
2.5	14.	24	Plastic
5.0	30.	520	Plastic-thixotropic
7.5	167.	6200	Plastic-thixotropic

An over-all picture of the formation of an "orange-peel" surface pattern from spray application may be theorized as follows. The clearest case is that obtained from a spray gun in which the atomization of the liquid is imperfect and particles of abnormal size are projected toward the panel, resulting in a very uneven application. With spray equipment in good condition, however, the likelihood of imperfect atomizing of the liquid is much smaller. Nevertheless, the liquid particles from the gun coalesce to some extent after leaving the spray nozzle, particularly at the center of the spray cone, and to some extent also by deposition of successive droplets adjacent to each other, forming relatively large irregularly-shaped lakes of the composition. In addition, at the time of deposition, the surface is subjected to an air blast of extremely high velocity and turbulence which set up ripples on the layer of viscous material deposited.

The solvent loss and high air-velocity during spraying are of considerable importance in analyzing flowout since they account for the important rheological changes which occur during atomization. The ratio of air to fluid delivery for commercial spray guns is very great, from 5 to 15 cu. ft./min. being required for adequate atomization. Bogin found that 47–74% of the solvents initially present were lost during spraying, at distances between gun and object from 8–18 in. (5). There is, first, the effect of cooling: the composition as applied is at a lower temperature than the bulk material as a consequence of solvent evaporation, and the plastic viscosity of the film is accordingly higher. The solvent loss also results in a rapid increase in plastic viscosity. The change for a typical material is from 0.5–3 poises for normal spraying distance. Even higher values have been observed at greater spraying distances, and one black baking enamel increased to more than 30 poises. The yield value of the applied composition increases with solvent loss. Finally, the turbulent spray fan or cone impinging on the film as applied sets up ripples and waves.

After deposition of the coating, the surface is left momentarily with irregularities, and the related processes of continued evaporation of solvent, leveling under the surface forces at the interface, and the gradual increase of viscosity begin. If the composition immediately after deposition exhibits a yield value (or a rapid thixotropic build-up), the structure is set by the low mobility of the composition. If the flow properties are those of a Newtonian or pseudoplastic type, then at the low shearing stresses operating under the conditions of leveling, the initial viscosity and the solvent volatility at the time determine entirely whether or not the surface will level to perfect smoothness. In thin layers (less than 25μ) the time for oils to flow to a smooth layer becomes excessively long if the viscosity exceeds 2–3 poises, although thick films level quickly—within a fraction of a minute. The flowout time for films of greater thickness is much more rapid.

For most commercial types of finishes, however, the evaporation of solvent proceeds with resultant increase of plastic viscosity. If the viscosity for 1 min. after spraying is less than 1 poise, the flowout will be complete, even for very thin films. This result is accomplished in practice by considerable dilution of the composition with solvents. Most compositions, however, are applied with a higher total-solid content, and as a consequence, the viscosity of the deposited film is considerably greater, requiring correspondingly greater flowout time.

A cause of "orange-peel" frequently listed is that of moisture in the composition or a high humidity during spraying. Hochwalt and Marling (18) consider removal of water, present in the lacquer solvent, as a vital condition. In the author's experience, however, the presence of water is of small effect with many typical compositions, provided the pigment combination is not flocculated. When water-sensitive pigments are present, then "orange-peel," reduced gloss, and numerous other defects become prominent.

Summary

1. Rheological properties of a variety of commercial paints as measured by a rotational viscometer may be classified approximately as follows: (*a*) all samples had a plastic viscosity less than 4 poises; (*b*) high-gloss enamels exhibited very low or zero-yield values, and thixotropy was absent or of low magnitude; (*c*) exterior house paints, flat or matte paints, and water-reduced emulsion paints exhibited the highest yield values (maximum less than 200 dynes/cm.^{2}) and the most evident thixotropic properties.

2. Data on the bulk composition is chiefly of value in establishing uniformity during manufacturing and in setting the working properties during application; leveling of the applied finish requires information on the rate of change of the rheological properties during flowout and setting of the applied film.

3. In general terms, flowout of the applied film is facilitated by low viscosity, maximum film thickness, and by deflocculation of the pigmenting components of the paint, as indicated by low or zero-yield value. At present only approximate estimates can be assigned to these factors.

4. The rotational cylindrical viscometer as adapted from the Stormer viscometer is well suited for the range of viscosities represented by commercial paints, and its use has a decided advantage over many empirical testing procedures in that the data are given in dimensionally consistent units and an analysis of the non-Newtonian flow characteristics is possible.

References

1. Aldrich, H. L., *Paint, Oil, Chem. Rev.* **110**, No. 2, pp. 8, 30, 31, 34 (Jan. 23, 1947).
2. *Am. Soc. Testing Materials, Standards*, D 562-44.
3. Bingham, E. C., and Green, H., *Am. Soc. Testing Materials, Proc.*, **II**, **19**, 640–75 (1919).
4. Booge, J. E., Bingham. E. C., and Bruce, H. D., *ibid.*, **II**, **22**, 420–63 (1922); cf. also, Bingham, E. C., Fluidity and Plasticity, p. 220 ff.

5. Bogin, C., *Paint, Oil, Chem. Rev.* **103**, No. 15, p. 7, and No. 16, p. 16 (July 17 and 31, 1941); Mattiello, J. J., Ed., Protective and Decorative Coatings, Vol. 1, pp. 641–736. John Wiley & Sons, 1941; Bogin, C., and Wampner, H. L., *Ind. Eng. Chem.* **29**, 1012–8 (1937).
6. Coughlin, J. J., and Wint, R. F., *Official Digest, Federation Paint & Varnish Production Clubs*, No. 263, 694–6 (1946).
7. Droste, W. H., *Farben-Ztg.* **37**, 619–20; 655–7; 694–5 (1932); *Chem. Fabrik* **7**, 249–50 (1934).
8. Fischer, E. K., and Jerome, C. W., *Ind. Eng. Chem.* **35**, 336–43 (1943).
9. Fischer, E. K., and Lindsley, C. H., *Textile Research J.* **13**, 325–37 (1948); *J. Applied Phys.* **18**, 988–96 (1947).
10. Fischer, E. K., and Lindsley, C. H., *J. Colloid Sci.* **3**, 111–28 (1948); Bechtel W. G., and Fischer, E. K., *ibid.* **4**, 265–82 (1949).
11. Gamble, D. L., *Ind. Eng. Chem.* **28**, 1204–10 (1936); Symposium on Consistency, pp. 15–22. Am. Soc. Testing Materials, Philadelphia, Pa., 1938.
12. Gardner, H. A., and Sward, G. G., Physical and Chemical Examination of Paints, Varnishes, Lacquers and Colors, 10th Ed., pp. 299–331. Henry A. Gardner Laboratory, Bethesda, Md., 1946.
13. Green, H., *Ind. Eng. Chem.* **15**, 122–6 (1923); Green, H., and Haslam, G. S., *ibid.* **17**, 726–9 (1925).
14. Green, H., and Weltmann, R. W., *Ind. Eng. Chem., Anal. Ed.* **15**, 201–6 (1943); *J. Applied Phys.* **15**, 414–20 (1944).
15. Green, H., *J. Colloid Sci.* **3**, 93–8 (1947); *ibid.* **4**, 129–33 (1948).
16. Harvey, E. N., Jr., and Fischer, E. K., Paper presented at the Society of Rheology meeting, New York City, Oct. 29, 1943; cf. *Rheol. Bull.* **14**, No. 3, p. 11 (1943).
17. Haslam, G. S., and Grady, L. D., Jr., *Ind. Eng. Chem., Anal. Ed.* **2**, 66–9 (1930).
18. Hochwalt, C. A., and Marling, P. E., *Ind. Eng. Chem.* **27**, 190–2 (1935).
19. Kewish, R. W., and Wilcock, D. F., *ibid.* **31**, 76–83 (1939).
20. Malm, C. J., and Smith, H. L., *Ind. Eng. Chem.* **38**, 937–41 (1946).
21. McMillen, E. L., *J. Rheol.* **3**, 163–78 (1932); *Ind. Eng. Chem.* **23**, 676–9 (1931).
22. Saunders, B., *J. Oil and Colour Chemists' Assoc.* **31**, 95–106 (1948). This subject has also been discussed by Jarrett, M. E. D., *ibid.* **31**, 357–78 (1948).
23. Waring, R. K., *J. Rheol.* **2**, 307–14 (1931).
24. Wicker, C. R., and Geddes, J. A., *ASTM Bull.* No. 120, 11–18 (1943).
25. Williamson, R. V., Patterson, G. D., and Hunt, J. K., *Ind. Eng. Chem.* **21**, 1111–15 (1929).

VISCOELASTIC AND PHOTOELASTIC PROPERTIES OF POLYSTYRENE ABOVE ITS SOFTENING TEMPERATURE[1]

Lawrence E. Nielsen and Rolf Buchdahl

From the Plastics Research Laboratory, Monsanto Chemical Company,
Springfield, Massachusetts

Received February 17, 1950

Introduction

Considerable quantities of data are available on polystyrene at temperatures high enough so the material is essentially liquid in nature (1–6). Likewise, much is known about the mechanical properties of polystyrene at much lower temperatures where it is a rigid material (13–15). However, very few data are available at intermediate temperatures where the polymer is quite rubbery in behavoir (16). In this softened state the material can readily be deformed so that orientation effects may be studied. In this paper data will be presented on creep, recovery, stress relaxation, and birefringence of polystyrene in the rubbery state.

Experimental Details

Most of the work was carried out on polystyrene films cast from ethyl methyl ketone according to a previously described procedure (7). Several days of drying at temperatures as high as 105°C. were required to remove most of the solvent from the films, which were approximately 0.015 in. thick. Most of the films were made from an unfractionated mass polymer whose intrinsic viscosity was 1.1 in toluene. Other experiments were carried out on fractions of polystyrene of weight-average molecular weights of 160,000 and 660,000 as determined by light scattering measurements. Creep experiments were also made on this latter fraction plasticized with 10% bibenzyl by weight.

The creep experiments were carried out in a circulating oven having windows by applying a tensile weight to a film 3 or 4 in. long and 1 in. wide. The elongation was determined as a function of time by measuring the distance between two ink lines with a cathetometer. At the same time the optical anisotropy (birefringence) was measured by a conventional method. The light source was either a tungsten or sodium vapor lamp. The light beam, made parallel by a lens, was polarized by a Polaroid disk.

---

[1] Presented at the Annual Meeting of the Society of Rheology, New York, N. Y., November 4–5, 1949.

After the light passed through the film, the birefringence was measured with a Babinet compensator. The birefringence in angstrom units/mil of thickness was determined from the compensator reading and the thickness at any elongation assuming a Poisson's ratio of 0.5.

In such a creep test the stress is not constant but continually increases as the elongation increases since the cross-sectional area decreases. In the following graphs, the birefringence and stress have been corrected to take into account the actual thickness and cross-sectional area at each elongation. In most of the recovery experiments after creep, not all of the tensile load was removed as this was not easily done without opening the oven and changing the temperature. Actually, in many cases it is advantageous to keep a small tensile load so that the ratio of birefringence to stress can be calculated during recovery. This ratio becomes indeterminate if all the load is removed.

Stress-relaxation experiments, with simultaneous measurements of birefringence, were carried out in which the stress was determined by means of a modified balance to the arm of which was attached the stretched polystyrene film. By changing the weights on the balance, the stress could be adjusted to keep the elongation constant. The birefringence was measured in the same manner as in the creep experiments.

Results

Figure 1 shows how the creep differs for three different initial stresses. Part of a recovery curve is also shown for the intermediate stress. This is not a true recovery curve as a stress of about 3 p.s.i. was still applied to

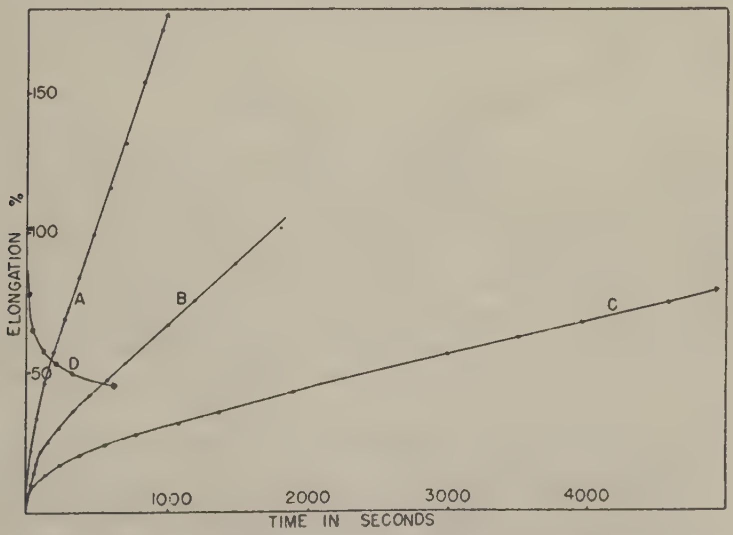

Fig. 1. Creep as a function of stress at 110°C. Original stress in pounds per square inch (p.s.i.): *A* = 24.4, *B* = 14.1, *C* = 10.5, *D* is part of a recovery curve.

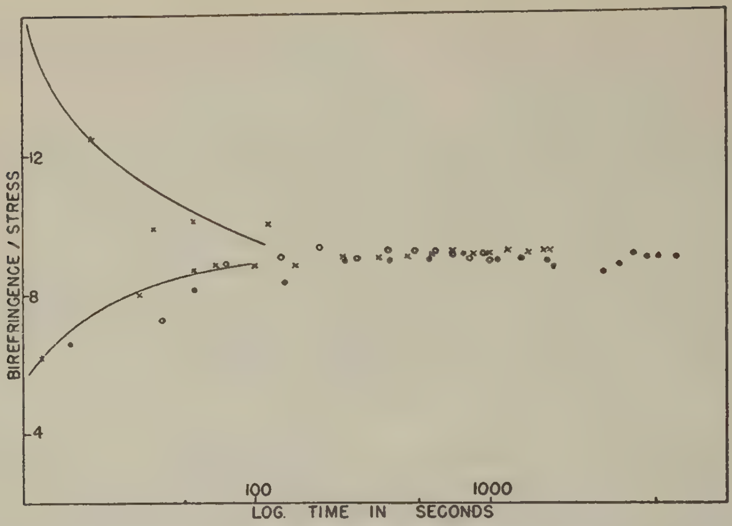

FIG. 2. Effect of stress on birefringence to stress ratio, B/σ, at 110°C. B/σ given in angstrom units/mil/p.s.i. Original stress in p.s.i.: ● 10.5, × 14.1, ○ 24.4. One recovery curve shown.

the specimen. Figure 2 shows the corresponding ratios of birefringence to stress.

In Figs. 3 and 4 curves are given for creep, recovery, and ratio of birefringence to stress at 100, 105, 110, and 120°C. Two values of stress are given for 110°C. Figures 5 and 6 illustrate the effect of cycling in

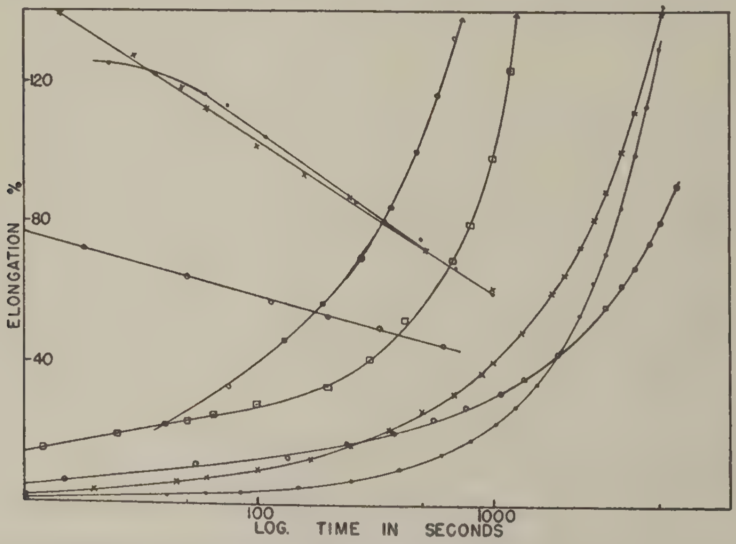

FIG. 3. Effect of temperature on creep and recovery. ● 100°C., × 105°C., ○ 110°C., □ 120°C.

which a creep test is carried out, the stress is removed so that partial recovery takes place, and then another creep test is made. The data shown in Figs. 1–6 were determined on films made from the unfractionated polymer.

The effect of molecular weight on creep, recovery, and the birefringence to stress ratio at 110°C. is shown in Figs. 7 and 8. In these experiments a creep test was carried out with an initial stress of about 14.5 p.s.i.; later the stress was increased to approximately 40 p.s.i. and the creep test continued without any recovery taking place. The weight-average molecular weights of the films as determined by light-scattering measurements were 160,000 and 660,000. Their intrinsic viscosities in toulene were 0.59 and 1.56, respectively. In Fig. 8 the data for both the high and low stresses are given, but curves have been drawn only for the low stress.

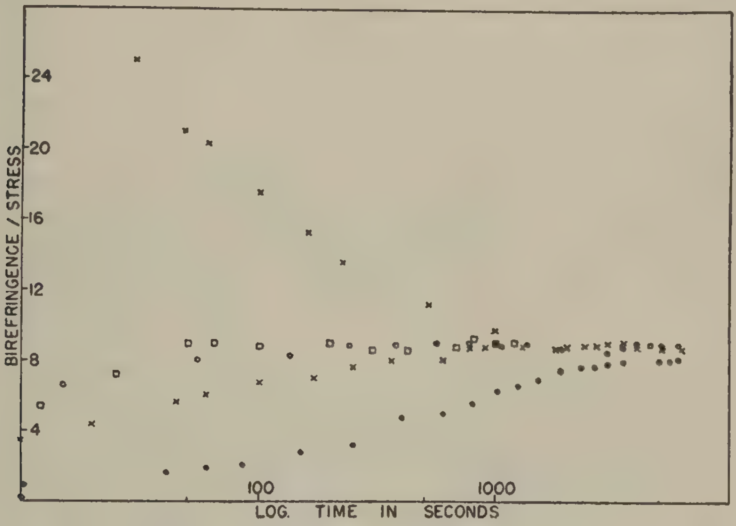

Fig. 4. Effect of temperature on birefringence to stress ratio. (Symbols same as for Fig. 3.)

The effect of plasticizer on creep and on the birefringence to stress ratio is illustrated by the data in Fig. 9. Two creep cycles are shown. The polystyrene was plasticized with 10% by weight of bibenzyl. The softening action of the plasticizer allowed the creep test to be easily carried out at 90°C.

In looking over the creep and birefringence data, two facts should be pointed out. Since polystyrene is more polarizable perpendicular to the molecular chain than parallel to it, the birefringence should have a negative sign, but it has been omitted here for the sake of simplicity. The value of the birefringence to stress ratio for recovery is not as accurate as the value for creep. In recovery experiments, both the birefringence and stress are small, so the value of their ratio may be in error by as much as 25%.

Data for a typical stress-relaxation experiment at 110°C. are plotted in Fig. 10. The material was the same polystyrene as used in most of the creep experiments. The stress and birefringence to stress ratio were measured on a specimen elongated 95%. With the somewhat crude stress-relaxation

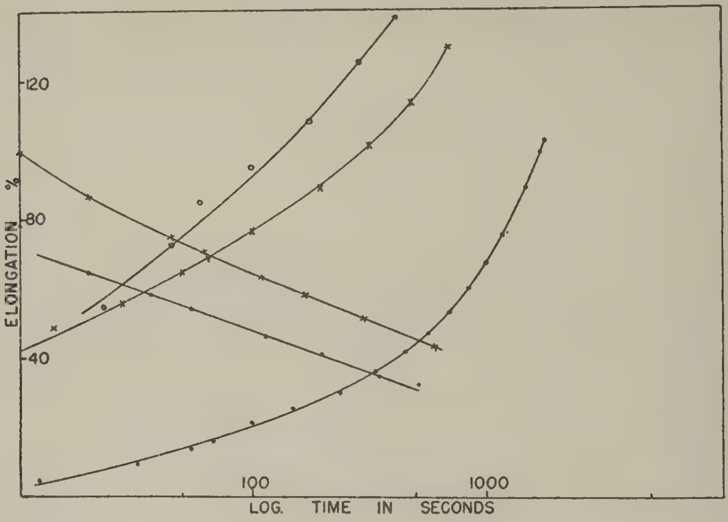

FIG. 5. Effect of cycling on creep at 110°C. ● First cycle, × second cycle, ○ third cycle.

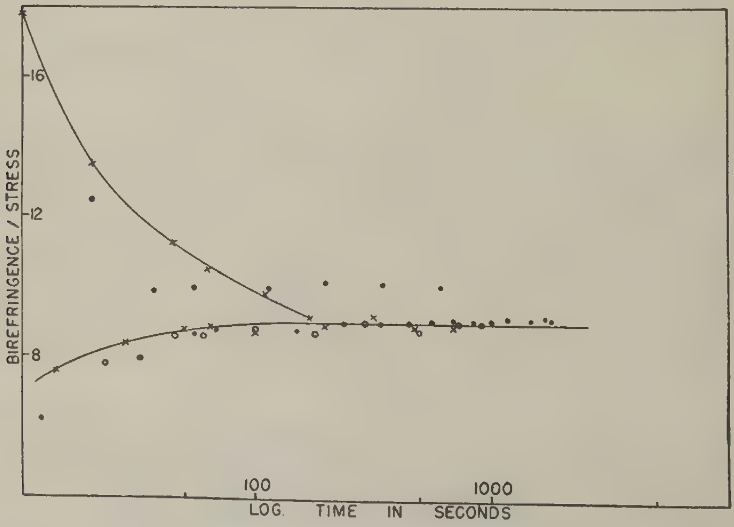

FIG. 6. Effect of cycling on B/σ at 110°C. (Symbols same as for Fig. 5.)

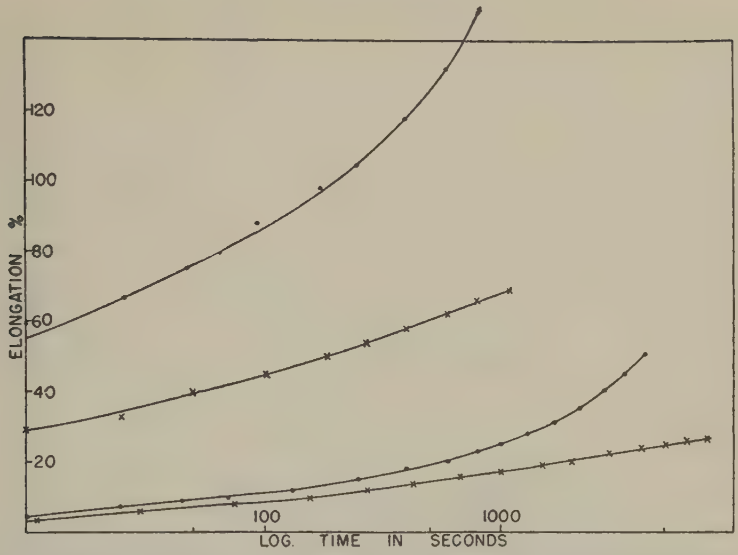

FIG. 7. Effect of molecular weight on creep at 110°C. Weight-average molecular weights: ● 160,000; × 660,000. Lower curves with initial stress of 14.5 p.s.i.; upper curves at 40 p.s.i.

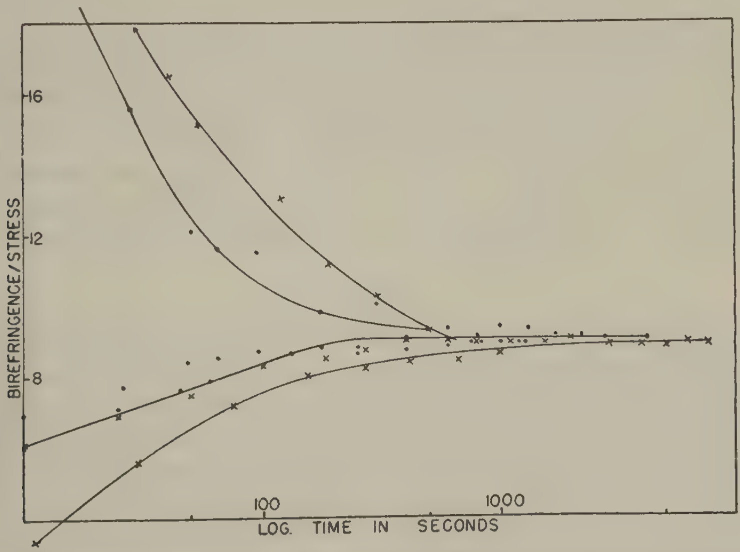

FIG. 8. Effect of molecular weight on B/σ at 110°C. (Symbols same as for Fig. 7.)

apparatus used in these experiments, the B/σ ratio had reached its limiting value in most cases by the time measurements could be taken.

Figure 11 illustrates the manner in which the birefringence–time curve changes if more than one stress-relaxation experiment is carried out on the

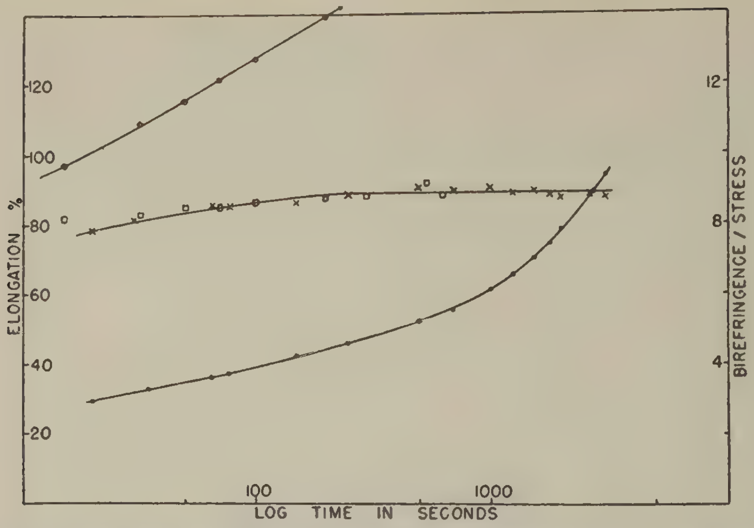

FIG. 9. Creep and B/σ at 90°C. of polystyrene plasticized with 10% bibenzyl. ● Second cycle of creep, ○ third cycle of creep, × second cycle B/σ, □ third cycle B/σ.

same sample of film. (The breaks in some of these curves are due to a slight increase in temperature when the oven heater is turned on.)

From time-to-time experiments were made to find out how much of the elongation taking place in a specimen during a creep or stress-relaxation experiment was recoverable. For instance a stress-relaxation experiment

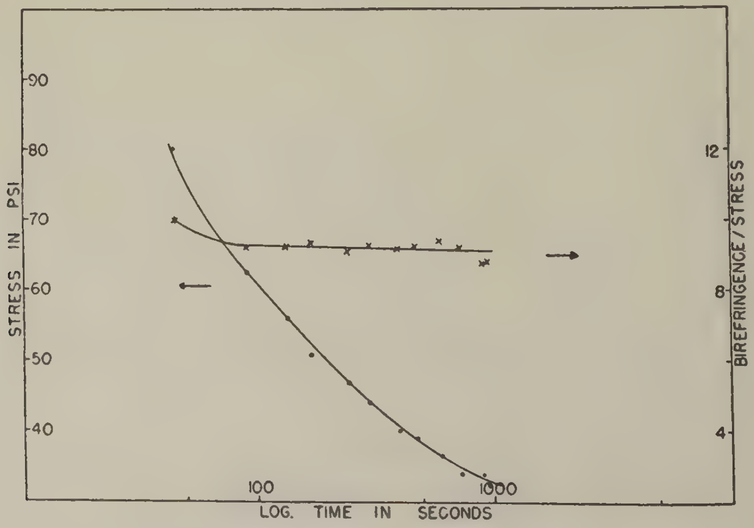

FIG. 10. Stress relaxation and B/σ at 110°C. Elongation = 95%.

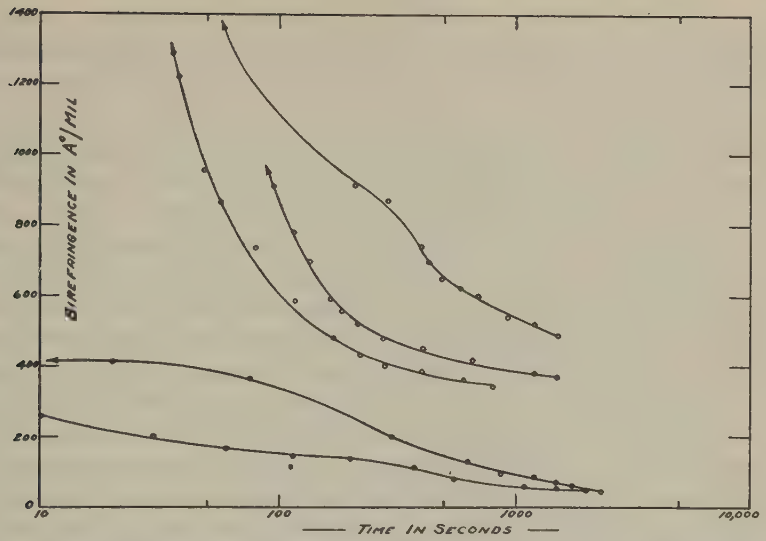

FIG. 11. Effect of cycling on birefringence relaxation and recovery at 103°C. First cycle on right; third cycle on left. Two lowest curves are the recovery curves.

was made at 112°C. for 1500 sec. with the film elongated 85%; on removing the stress it was found that 95% of the initial elongation was recoverable even though the stress had decreased from a value greater than 51 p.s.i. to 23 p.s.i. during the course of the experiment. In a creep test at 110°C. (shown in Fig. 1), the specimen was elongated 90% at the end of 6200 sec. A recovery test lasting several thousand more seconds brought the specimen back to a final elongation of only 11%. Probably the recovery would have been even more complete except for the fact that the weight of the specimen itself gives rise to a force tending to stretch the film.

DISCUSSION

The data presented here clearly show that the ratio of birefringence to stress, B/σ, is a constant, except at short times, for polystyrene at temperatures above its softening temperature. Furthermore, this constant B/σ is practically independent of stress, elongation, temperature, and molecular weight of the polystyrene even though other properties such as creep and stress relaxation are very dependent on such variables. During a creep test the short-time value of B/σ is less than the limiting value, but during a recovery experiment the initial value of B/σ is larger than the limiting long-time value.

The compliance calculated from creep is not independent of the applied stress. However, the creep tests were not true creep tests because the stress was not constant but continuously increased with elongation. On making corrections for this, it is still found that the compliance is somewhat dependent on the stress. The greater the stress the greater is the compliance; that is, increasing the stress seems to make the material softer.

Temperature has a marked effect on the rate of creep. Changing the temperature from 100°C. to 120°C. increases the compliance by many times as can be seen from inspection of Fig. 3. Temperature also changes the shape of the B/σ versus time curves. The lower the temperature the greater is the time required for B/σ to reach its limiting value, but the limiting value seems to be practically independent of temperature.

Cycling, *i.e.*, repeating a creep or a stress-relaxation run on the same sample, has the effect of increasing the creep or compliance and the initial rate at which the stress and birefringence relax out. The longer the time between cycles the less pronounced is the observed effect. From Fig. 11 it is seen that the birefringence at first dies down more rapidly on the second than on the first cycle, but then at longer times the birefringence dies down more slowly on the second cycle. The very striking differences in the rate at which the initial birefringence died down on successive cycles was easily observed with the Babinet Compensator, but unfortunately the changes were so rapid it was practically impossible to record them.

The lower the molecular weight the greater is the creep or compliance. However, this difference in the shape of the creep curves does not change the limiting value of B/σ. Likewise, the addition of plasticizers does not noticeably change this constant.

The data presented here can be readily interpreted by postulating a semipermanent network structure for polystyrene.[2] This network is probably formed by the intertwining of the molecules and not due to chemical cross-linking or crystallites. To explain the observed phenomena, especially at the longer times, it is only necessary to assume that a small percentage of the total number of molecular segments is actually involved in the network at any time. Without the hypothesis of such a network it is difficult to visualize nearly complete recovery after the stress may have decayed several hundred per cent in a stress-relaxation experiment. Also the fact that the ratio of birefringence to stress becomes constant in a creep experiment, yet the elongation is recoverable, becomes reasonable on the basis of a network structure.

We visualize something like the following occurring in a creep or stress-relaxation experiment. In a creep test, when the load is first applied a large percentage of the molecules help carry the stress by becoming partially oriented or by deformation of their bond angles. However, in a

---

[2] Such a network structure has been previously proposed by one of the authors: BUCHDAHL, R., *J. Colloid Sci.* **3**, 87 (1948). Similar network structures have been suggested for raw rubber. For example, see LONG, SINGER, AND DAVEY, *Ind. Eng. Chem.* **26**, 543 (1934), and TRELOAR, *Trans. Faraday Soc.* **36**, 538 (1940).

short time the stress on many of these molecules or molecular segments is relieved by relatively small amounts of rotation, or movement, or by breaking of weak entanglements. As this relaxation process occurs, more and more stress is put on the molecules in the network which have very strong entanglements. As a result most of the molecular segments are, after a period of time, in a relaxed state while the small number of molecules in the network becomes more and more oriented or elongated. Thus there is something analogous to Ostwald's two-phase theory of rubber elasticity, in which one phase is composed of the network and the other phase being the liquid-like material filling the loose structure of the network. Actually, of course, the two phases are the same except for the restriction of certain types of motion in the network; the relative amount of material in each phase continually changes with time. On removing the stress nearly complete recovery would be expected because of the spring-like action of the deformed network. The last part of this recovery would take a long time as the relatively small number of molecular segments in the network would give rise to only very small restoring forces; these must drag the network through the viscous medium composed of the greater portion of the material. Now on repeating the creep test a second time, the creep would be greater at short times than before since some of the entanglements broken during the first creep test would not have had time to re-form. Similar ideas can be used to explain stress relaxation.

The birefringence measurements substantiate the above theory. For a molecule in which there are no deformed bond angles or other energy effects, the birefringence is an entropy effect, *i.e.*, it is a measure of the orientation in the molecule (8). In such a case, the birefringence is a linear function of the stress (9,10). At the beginning of a creep test some time is required for the molecules to adjust themselves, and some processes such as bond-angle deformations will occur in some of the more restrained molecules. Initially some of the stress is carried by mechanisms other than the restoring force created by the Brownian motion of elongated molecules. Thus, the short time values of the ratio of the birefringence to stress should be less than the long time limiting value of this ratio. The constancy of the B/σ ratio at long times implies either viscous flow or a retarded elastic process. The nearly complete recovery of a deformation indicates that nonrecoverable viscous flow can play only a small part at these temperatures. Thus one is forced to assume a retarded elastic process. The fact that this ratio remains constant even though the birefringence in a stress-relaxation experiment can decrease by several hundred per cent is good evidence that a network structure exists in polystyrene. The fact that the B/σ ratio remains constant implies that only relatively few molecular segments become more oriented as the elongation increases, while at the same time an equivalent number of molecular segments must become deoriented and assume a relaxed state, since the same value of B/σ is obtained whether the elongation is 2% or 200%. If the B/σ ratio had continued to increase with elongation, it would have been necessary to assume a different mechanism in which more and more molecular segments became oriented as the elongation increased.

Other experimental evidence which supports a network theory has been published by Buchdahl (5). The striking decrease in the apparent viscosity of polystyrene with large deformations in a rotational viscometer of the Stormer type can be attributed to the destruction of the network structure. Holding the material at a temperature above its softening point without stresses will gradually allow the network to rebuild itself because the continuous segmental motion of the molecules will cause the chains to again become entangled. However, it will take a relatively long time to re-form as strong a network as originally existed since the mid portions of the chains must become looped over one another as well as just the ends of the chains.

If the assumption is made that the stress and birefringence are purely entropy effects, then it is possible to put the network theory on a more quantitative basis and to predict what percentage of the molecular segments is in the network phase. One may simply borrow the equations already developed in the theory of rubber elasticity (11). An equation useful for our purpose is:

$$\sigma = \frac{RTd}{Mc}\left(1 - 2\frac{Mc}{M}\right)(\alpha - 1/\alpha^2).$$

σ is the force per unit area based on the cross-sectional area before stretching, R is the gas constant, T is the absolute temperature, d is the density of the material, α is the ratio of the stretched to the unstretched length, M is the number-average molecular weight of the material, and Mc is the molecular weight between crosslinks, here between entanglement points. In using this equation one must keep in mind the restrictions imposed by the assumptions and approximations used in deriving it. It seems, in general, that this equation predicts for a given value of Mc a stress considerably less than that found experimentally (11). However, on substituting data on both creep and stress relaxation into this equation, reasonable values are found for Mc. This is illustrated by Table I.

The number-average molecular weight of the polystyrene used for the experiments given in Table I was approximately 180,000. The stresses listed are on the basis of the original cross-sectional area. The calculated values of Mc indicate there are about 4 to 20 points of chain entanglements for each of the polystyrene molecules on an average. The lower value applies to tests carried out for long times where much of the network structure has been destroyed.

It is of interest to compare the results obtained here on polystyrene with those of a similar nature recently published on plasticized polyvinyl chloride where the cross-links were shown as being due to crystallites (9). The shapes of the stress relaxation–time curves and the birefringence to stress ratio versus time curves are very similar to those presented here. In the case of polystyrene there is no evidence of crystallinity on the basis of X-ray diffraction data (12). The facts, that the creep in polyvinyl chloride never stops, and that the second cycle of a creep test gives a greater compliance than the first cycle, are good evidence for a semipermanent network structure, but by themselves are not necessarily indicative of crystallinity. Such phenomena reveal much about the nature of the network, but other data are required to clarify the nature of the cross-links in the structure such as the X-ray diffraction patterns given in the polyvinyl chloride studies mentioned above.

TABLE I

Calculation of Mc from Creep and Stress-Relaxation Experiments on Polystyrene at 110°C.

Type of expt.	Time	Stress	Elongation	Mc
	sec.	*dynes/cm.²*	%	
Stress relaxation	90	2.21×10^6	95	19,000
Stress relaxation	950	1.15×10^6	95	31,000
Creep	55	7.3×10^5	9.2	10,000
Creep	565	7.3×10^5	24	20,000
Creep	6040	7.3×10^5	90	40,000

ACKNOWLEDGMENTS

The interest shown in this work by Dr. N. N. T. Samaras, Mr. H. W. Mohrman, and others of the Plastics Research Laboratory of the Monsanto Chemical Company has been greatly appreciated.

SUMMARY

Creep, recovery, and stress-relaxation experiments with simultaneous measurements of birefringence have been carried out on polystyrene films above their softening temperature.

The ratio of birefringence to stress is a constant independent of the stress, elongation, temperature, and molecular weight of the polystyrene.

The data indicate that polystyrene has a semipermanent network structure. The network is most likely caused by the strong intertwining of the polymer molecules.

REFERENCES

1. Wiley, F. E., *Ind. Eng. Chem.* **33**, 1377 (1941).
2. Foote, N. M., *Ibid.* **36**, 244 (1944).
3. Nason, H. K., *J. Applied Phys.* **16**, 338 (1945).

4. Fox, T. G., Jr., and Flory, P. J., *J. Am. Chem. Soc.* **70**, 2384 (1948).
5. Buchdahl, R., *J. Colloid Sci.* **3**, 87 (1948).
6. Spencer, R. S., and Dillon, R. E., *J. Colloid Sci.* **3**, 163 (1948), and **4**, 241 (1949).
7. Merz, E., Nielsen, L., and Buchdahl, R., *J. Polymer Sci.* **4**, 605 (1949).
8. Stein, R. S., and Tobolsky, A. V., *Textile Research J.* **18**, 201, 302 (1948); *ibid.* **19**, 8 (1949).
9. Alfrey, T., Wiederhorn, N., Stein, R., and Tobolsky, A., *J. Colloid Sci.* **4**, 211 (1949); *idem, Ind. Eng. Chem.* **41**, 701 (1949).
10. Treloar, L. R. G., *Trans. Faraday Soc.* **43**, 277 (1947).
11. Flory, P. J., *Chem. Revs.* **35**, 50 (1944); *idem, J. Polymer Sci.* **4**, 225 (1949).
12. Katz, J., *Trans. Faraday Soc.* **32**, 77 (1936); *idem, Rubber Chem. and Technol.* **9**, 357 (1936). Also, unpublished data, Monsanto Chemical Company.
13. Sauer, J., Marin, J., and Hsiao, C., *J. Applied Phys.* **20**, 507 (1949).
14. Maxwell, B., and Rahm, L., *Ind. Eng. Chem.* **41**, 1988 (1949).
15. Merz, E., Nielsen, L., and Buchdahl, R., in press.
16. Nielsen, L. E., and Buchdahl, R., *J. Chem. Phys.* **17**, 839 (1949).

INSTRUMENTS FOR THE DETERMINATION OF RHEOLOGICAL PARAMETERS OF LIQUID BODIES [1]

R. N. Weltmann [2]

Received February 17, 1950

The laboratory investigator who needs to determine the flow characteristics of a variety of substances such as asphalt, printing ink, and blood finds in his study of the literature of instrumentation references to many devices. He is soon confronted with the question whether he should use as simple an instrument as the Ford cup or as complicated an equipment as a rotational viscometer with an automatic recorder and a pressurizing chamber. This investigator will soon realize that not any one device will suffice to obtain the required information for the wide range of consistencies found in different materials. In addition, he will recognize that the term *consistency* not only relates to the internal friction of a material as expressed by the coefficient of viscosity for Newtonian liquids but includes also such factors as the yield value, the thixotropic breakdown, pseudoplasticity, and dilatancy.

Even the more experienced worker in the field of rheology might be surprised to learn that viscosities of apparently Newtonian materials can vary in magnitude from 1 to 10^{12} and possibly more. Yield values of plastic materials also cover a very wide range, but no data are presently available to permit making a more specific statement. The breakdown curves of thixotropic materials have only been investigated over a restricted range of rates of shear due to a lack of suitable measuring devices. The study of dilatancy is still in an embryonic state, since few instruments are strong enough to allow measurements at even conventional rates of shear, because of the rapid increase in dilatant consistency. Pseudoplastic materials, on the other hand, have been studied extensively. These materials seem to compound the widest scale of consistencies and thus a variety of instruments and methods for evaluating the flow properties of these materials has been proposed. But still there is need for instruments which will provide information on both ends of the consistency scale.

When an attempt is made to classify the available devices for rheological instrumentation (16), it becomes apparent that they can be divided into three classes. To the first class belong all the instruments which express in some arbitrary terms the consistency of the material when this material is subjected to any given set of flow conditions. Values obtained from instruments of this group are frequently calibrated in terms of a standard material of known consistency. Such measurements, although meaningful only for Newtonian materials, can be used to compare different factory batches of the same non-Newtonian formulation. When more than one set of flow conditions can be produced by the same instrument, it is possible to evaluate the plastic viscosity of true plastic materials, but only if the data obtained from the various flow conditions yield a large straight portion when properly plotted.

---

[1] Presented at the Annual Meeting of the Society of Rheology, New York, N. Y., November 4–5, 1949.

[2] Consultant in rheology to the Research Laboratories, Interchemical Corporation, New York, N. Y., and a member of the staff of NACA, Lewis Flight Propulsion Research Laboratory, Cleveland, Ohio.

Devices like the Gardner bubble tubes (5), extrusion type viscometers, Stokes' type viscometers (19), and others fall into this classification. The same is true for rotational viscometers employing a rotor and stator of such a design that a mathematical interpretation of the model of flow has not been achieved.

The extrusion type viscometers include the commonly used Ford cup, the Saybold viscometer, which is most frequently employed in the oil industry, and others. The best known Stokes' type viscometer is the Hoeppler (10) of which many varieties are used in industry, particularly in the textile field. A typical rotational viscometer of this group employs a paddle as rotor. Any experimenter can add many more constructional arrangements to the already existing substantial variety of devices. In each special case consideration will have to be given to the required consistency range. Physical properties, for example, transparency, opaqueness, degree of evaporation, test temperature requirements, and others, are decisive factors for the design.

The second group of devices differs from the first one in so far as it is possible to represent the flow conditions mathematically. Whenever the picture of the model of flow is available, the instrument can be applied to the rigid investigation of Newtonian materials. On the other hand, these devices are not applicable to the study of non-Newtonian materials since the rate of shear to which the material is subjected varies to such an extent that the non-Newtonian parameters cannot be properly correlated. Some devices of the first group might be transferred into the second group by a change in design, such as to produce flow conditions which are susceptible to calculations. The most prominent instruments of the second group are the parallel-plate and capillary-tube viscometers, which are widely used in industry.

In 1874, Stefan (18) proposed a model of flow for a parallel-plate viscometer, in which the material under test is located between two approaching and separating plates. The instrument can only be used for obtaining viscosities of Newtonian and of true plastic materials where the rate of shear–shearing force relationship is linear at least over an extended range. Furthermore, the rates of shear which can be applied to the test material are extremely low.

The parallel-plate viscometer has lately found much use in the investigation of materials with high solid content. Dienes and Klemm (4) measured viscosities of high polymers ranging from 10^4 to 10^9 poises on a specially designed parallel-plate viscometer. Williams' (27) viscometer is reported to measure rubber viscosities in the order of 10^6 poises. Resin solutions up to 10^8 poises were measured on H. Green's (6) Tackmeter. All three parallel-plate viscometers measured the high consistency material at such low rates of shear that the materials seemed to behave like Newtonian liquids. Hence, the viscosities referred to are apparently the intrinsic viscosities of those materials.

In the year 1842, Poiseuille (14) established the model of flow in capillary tubes. From his equation it becomes apparent that the rate of shear at the center of the capillary is zero, hence also the shearing force, and that both increase towards the walls of the capillary. This means that the rate of shear of the material when sheared in a capillary varies considerably over the cross section even in the smallest capillaries. Such a variation does not matter when dealing with Newtonian liquids where the viscosity is proportional to the rate of shear, but it interferes when measuring a true plastic material which is characterized by its yield value (1). The yield value is the shearing force per unit area which will just cause flow. Since the shearing force is zero at the center of any capillary, the required yield-value-force can never be reached in the center layer but only at layers closer to the wall. Therefore, a true plastic will never start flowing in the last minute center layer of the capillary. This will result in a nonlinear flow curve which resembles flow curves characteristic of pseudoplastic materials.

The instruments of the third group are so designed that they not only permit making consistency measurements under controllable flow conditions but they also make possible the establishment of an accurate relationship between the shearing force and the rate of shear. This means that the material under test must be subjected to essentially only one rate of shear at any one instant.

In these instruments the substance to be measured is always placed between two members, one of which moves relative to the other one at various known speeds. Furthermore, provisions must be made to establish the forces which are associated with such relative motion. It is, of course, immaterial whether the magnitude of motion is changed and the forces are determined, or whether the forces are changed and the motion is measured.

The rotational viscometer of proper design (3) and the band viscometer are the most prominent representatives of this group. The investigator who is ignorant of the type of material he is dealing with should always use these viscometers to determine whether non-Newtonian parameters (25) need consideration. This is especially important in the study of thixotropic materials (8), where, in addition, the viscometer has to be capable of subjecting the test sample to increasing and decreasing rates of shear (9).

At first glance the band viscometer, as suggested by Wachholz and Asbeck (23), seems to be the ideal instrument, since it is designed in accordance with Newton's model of flow. In Newton's model of flow the material is located between two parallel plates which move with respect to each other. The force causing this relative motion is proportional to the rate of shear between the plates. The proportionality constant is the Newtonian viscosity. This equation has been extended by Bingham (1)to true plastic materials by subtracting the yield value force from the shearing force. This model of flow is ideal since the rate of shear and velocity gradient in the material are constant over the complete separation of the plates. In Wachholz and Asbeck's band viscometer an endless band moves for a portion of its length in the center between two parallel stationary plates with the test material between the plates and the band. Such a structure represents in essence the relative motion of two plane-parallel plates. Therefore, it seems to lend itself to a rather simple mathematical interpretation. However, its disadvantages are many. Most of the difficulties are caused by end effects. To minimize the end effect, the tape has to have a small width and depth compared with those of the container, and the tape should be wide in relation to its thickness. The tape has to enter and leave the trough containing the test material, hence end effects are introduced also at those locations. To make them negligibly small compared to the shearing effect, the tape passing through the trough has to be made rather long. This, however, makes it mechanically difficult to maintain the tape parallel to the stationary plates and well-centered over its entire length, especially at high shearing stresses and for heavy consistency materials. In the Wachholz and Asbeck instrument the order of magnitude of the rates of shear reaches about 1000 sec.$^{-1}$ for viscosities of only a couple of poises and decreases linearly with an increase in viscosity of the material to be tested. Band viscometers, however, show interesting possibilities for the measurement of non-Newtonian materials. It is entirely conceivable that an improved band viscometer can be designed which is well suited to measurements of higher consistency materials permitting at the same time high rates of shear application. For instance, a highly flexible endless ribbon might be used which is maintained straight and parallel to a stationary plate by an appropriate backing support.

For high-speed applications, the rotational viscometer is the only one presently available. However, this viscometer also introduces several problems. The rate of shear and velocity gradient vary over the distance between rotor and stator. In a properly designed rotational viscometer this variation in rate of shear over the clearance can be reduced by using a very small clearance and by selecting suitable diameters for the stator and rotor. With increasing diameters the difference in rate of shear from one to the other surface of the two members becomes smaller for a constant distance between them. Hence, it would seem that large diameters should be used. That, however, has three severe disadvantages. To obtain the same rate of shear with increasing diameter, a higher torque is required. This might become mechanically difficult, especially for high consistency materials. With larger diameters the inertia of the stationary member is increased which can introduce difficult oscillatory conditions when a spring deflection system is being imployed (26). Finally, the centering of large members is much more critical and becomes mechanically almost impossible for very large diameters. Thus, a compromise diameter has to be chosen.

For Newtonian materials the nonconstant rate of shear across the clearance does not matter. But already for true plastics this varying rate is noticed by the fact that the rate of shear–shearing stress curve is nonlinear at low rates of shear, and becomes linear only when the rate of shear at the outer member corresponds to a shearing force which is just higher than the yield–value force. This is in accordance with calculations made by Reiner and Riwlin (15) for the flow of true plastic materials in a rotational viscometer. Their mathematical interpretation of the model of flow makes the rotational viscometer most useful for measuring non-Newtonian materials. By employing their concept of flow, shearing stresses and rates of shear can be calculated and an average rate of shear can be postulated; this will differ only slightly from the rates of shear at any point between the rotor and the stator. The end effects can be extrapolated experimentally (11,24) and thus can be included in the calculated solutions for the consistency. Some investigators (13) have used specially designed rotors and stators to eliminate them altogether.

Because the rotational viscometer is susceptible to a mathematical interpretation, the development of such viscometers has lately received considerable impetus. The literature of recent years is full of descriptive material of rotational type viscometers having special design features to meet the conditions for specific studies. However, only a few instruments have been described which will measure materials at the extreme ends of the consistency scale at high enough rates of shear.

The Mooney-Ewart (13) rotational type viscometer although built for relatively low consistency materials—down to the order of 0.01 poise,—can only employ rates of shear up to a maximum of about 100/sec. This is too low for most practical applications.

The rotational viscometer built at the Interchemical Corporation for a still lower consistency range and employing relatively high rates of shear, up to about 4000/sec. has been briefly described by H. Green (8). With this instrument, materials of non-Newtonian consistencies down to a plastic viscosity of 0.005 poise and a yield value of 5 dynes/cm.^{2} can be measured. This is accomplished by using a very lightweight stator assembly with a needle shaft. To lighten the weight further, a multiple pointer rather than a dial is carried on the shaft. Flow curves of industrial finishes, paper coatings, gravure inks, and biological samples have been obtained. Without the availability of such an instrument a casual observer could have misinterpreted those materials to be Newtonian liquids, but a flow curve study showed some of them to be thixotropic plastics and others to be pseudoplastics. Such knowledge will frequently explain their peculiar behavior upon application and will make it possible to suggest changes which will overcome difficulties experienced in practice.

For the determination of flow properties of high consistency materials, Traxler *et al.* (20,21) built a rotational viscometer. This instrument is designed to measure asphalts ranging in viscosity from 10^3 to 10^9 poises. The maximum rate of shear which can be applied is only about 10 sec.$^{-1}$ when testing the lower viscosity materials and becomes accordingly less when measuring the more viscous substances. To obtain a useful portion of the flow curve, as for instance the linear part when dealing with true plastics, high rates of shear are required. This introduces considerable mechanical difficulties when measuring high-consistency materials, since considerable shearing forces have to be generated. Also, when dealing with materials of high solid content, adhesion between the movable members and the test material often becomes a problem. Means must be found to prevent slippage of the material at the interfaces with the movable members. For this reason grooved members have been suggested in the literature (7,20), but have only been used for asphalts and lower viscosity materials. The problem of slippage will probably differ for each material to be tested, depending on its physical nature.

Even with substances of high-solid-pigment content like printing inks, paper coatings, and others but of only medium consistency having plastic viscosities in the order of a couple of hundred poises and yield values in the order of a couple of thousand dynes per square centimeter, no investigations have been made to extend the flow curve into the region of the rate of shear of the operating conditions. Although three rotational viscometers of the MacMichael type (12), designed for materials of just that consistency range have recently been described (2,7,17), none of them enables the operator to test these materials at the extreme high speeds of modern industrial machinery in the application field.

For rapid measuring procedures and high rate of shear applications, it is desirable that automatic indicating means be provided. This is especially important for thixotropic materials where very rapid indication is required, since the flow conditions change continuously with time. The stator, if made to deflect against a torsional restoring force, requires time to complete its path and to reach its equilibrium position. It has been shown (26) that the time of deflection depends on the instrumental constants, the inertia of the stator system, the amount of deflection, the type of torsional restoring force, the applied angular velocity, and the consistency of the test material which supplies the damping to the oscillatory system. To get away from the deficiencies of such a mechanical arrangement and to obtain a more rapid measurement, a few of the viscometers employ a strain gage as a force indicator which is coupled to a high-speed reading or recording device.

It would be of still greater advantage if means could be found to substitute the measurements of force and mechanical action by some electric analog such as dielectric constant or magnetic permeability. Research along these lines has been conducted by Voet (22) in correlating the dielectric behavior of substances with consistency measurements. This might eventually lead to a novel, rapid, and high-speed measurement of flow behavior.

For the rheologist who concerns himself with instrumentation problems, there is still a considerable territory of no-man's-land. It is an unavoidable trend that modern electronic practices which heretofore have found little use in rheological instrumentation will have to be employed to an ever-incresing degree, especially if testing at high rates of shear is to be accomplished.

Summary

Instruments for rheological measurements of liquid bodies can be classified into three groups. Devices of the first and second group provide accurate information on Newtonian viscosities. For non-Newtonian materials, instruments of both groups can be employed only when taking data for purposes of comparison. With instruments of the second group, in distinction to those of the first group, a model of flow can be associated. That means that Newtonian and plastic viscosities can be calculated directly without referring to a standard material which is required when using instruments of the first group.

The third group includes instruments with which controllable flow conditions can be established in such a manner that a specific rate of shear can be correlated to a shearing stress. This requires that the material is subjected to essentially one rate of shear at any one instant. Only the third group of instruments can be used for the determination of all parameters of non-Newtonian materials.

The merits and disadvantages of most frequently employed instruments of all three classes are briefly discussed. The range of presently available devices of the third group is not wide enough to permit investigation of very low and very high consistency materials. In many instances, conditions as they exist in the practical use of industrial materials cannot be simulated. Suggestions are made with regard to the design of improved measuring equipment.

REFERENCES

1. BINGHAM, E. C., Fluidity and Plasticity. McGraw-Hill, New York, N. Y., 1922.
2. BUCHDAHL, R., *et al.*, *Rev. Sci. Instruments* **18**, 168 (1947).
3. COUETTE, M., *Ann. chim. et phys.* **21**, (1890); *idem, J. phys.* **9**, 566 (1890).
4. DIENES, G. J., AND KLEMM, H. F., *J. Applied Phys.* **17**, 458 (1946).
5. GARDNER, H. A., AND PARKS, H. C., Paint Mfrs. Assoc. of U. S., *Circ. No. 265*, pp. 414–28, 1926.
6. GREEN, H., *Ind. Eng. Chem., Anal. Ed.* **13**, 632 (1941).
7. GREEN, H., *Ind. Eng. Chem., Anal. Ed.* **14**, 576 (1942).
8. GREEN, H., Industrial Rheology and Reological Structures, p. 197. John Wiley and Sons, New York, N. Y., 1949.
9. GREEN, H., AND WELTMANN, R. N., Colloid Chemistry, Chap. 6, p. 328. Edited by J. ALEXANDER, Reinhold Publishing Co., 1946.
10. HOEPPLER, F., *Chem. Ztg.* **57**, 62–3 (1933).
11. LINDSLEY, C. H., AND FISCHER, E. K., *J. Applied Phys.* **18**, 988 (1947).
12. MACMICHAEL, R. F., *J. Ind. Eng. Chem.* **7**, 961 (1915).
13. MOONEY, M., AND EWART, R., *J. Applied Phys.* **5**, 350 (1934).
14. POISEUILLE, J. L. M., *Compt. rend.* **15**, 1167 (1842).
15. REINER, M., AND RIWLIN, R., *Kolloid Z.* **43**, 1, (1927).
16. SCOTT BLAIR, G. W., A Survey of General and Applied Rheology, p. 89. Pitman Publishing Co., 1944.
17. SMITH, J. W., AND APPLEGATE, P. D., *Paper Trade J.* **126**, 23, 60–66 (1948).
18. STEFAN, M. J., *Sitzber. Akad. Wiss. Wien, Math.-naturw. Klasse Abt. II*, **69**, 713 (1874).
19. STOKES, G., *Trans. Cambridge Phil. Soc. II*, 8–9 (1851).
20. TRAXLER, R. N., ROMBERG, J. W., AND SCHWEYER, H. E., *Ind. Eng. Chem., Anal. Ed.* **14**, 340 (1942).
21. TRAXLER, R. N., *et al.*, *Ind. Eng. Chem.* **36**, 823 (1944).
22. VOET, A., *J. Phys. & Colloid Chem.* **51**, 5 (1947).
23. WACHHOLZ, F., AND ASBECK, W. K., *Kolloid-Z.* **93**, 280–97 (1940).
24. WELTMANN, R. N., *Interchem. Rev.* **2**, 43 (1943).
25. WELTMANN, R. N., *Ind. Eng. Chem., Anal. Ed.* **15**, 424 (1943).
26. WELTMANN, R. N., *J. Applied Phys.* **18**, 933 (1947).
27. WILLIAMS, I., *Ind. Eng. Chem.* **16**, 362 (1924).

FLOW BEHAVIOR OF CONCENTRATED GR-S RUBBER SOLUTIONS[1, 2]

A. B. Bestul and H. V. Belcher

National Bureau of Standards, Washington 25, D. C.

Received February 17, 1950

INTRODUCTION

The application of the McKee-White worker-consistometer (1), which was originally developed for investigating the flow of lubricating greases, to flow measurements on solutions of 5–30 wt.–% X–418 GR-S rubber in *o*-dichlorobenzene has recently been reported to the Office of Rubber Reserve, Reconstruction Finance Corporation by White and Belcher (2). These measurements covered nominal rates of shear from about 200 to 6000 sec.$^{-1}$ with shear stresses from about 5000 to 100,000 dynes/cm.^{2} These shearing stresses and rates of shear are higher than those attainable for substances as viscous as these solutions (apparent viscosities 1–1000 poises) in more conventional viscometers. Since it is important, in studying the flow behavior of any material, to observe the shearing stress–rate of shear relation over as wide a range as possible, it seemed desirable to combine results for a given material in the worker-consistometer with results for the same material in more conventional viscometers. The present paper deals with results obtained on GR-S solutions of concentrations from 3.5 to 10 wt.–% in the worker-consistometer and of concentrations from 0.1 to 10 wt.–% in several Bingham viscometers.

EXPERIMENTAL METHODS

Solutions

Solutions of 0.1, 0.5, 1.5, 3, 5, 7.5, and 10 wt.–% X–418 GR-S, prepared by placing weighed quantities of rubber (milled 25 passes in a tight mill) and *o*-dichlorobenzene in cylindrical bottles and rolling them slowly at room temperature until solution was complete, were furnished by Mr. F. W. Quinn of the National Bureau of Standards Rubber Section. It was necessary to filter the 0.1% solution through a fine sintered-glass filter in order to obtain reproducible flow times for this solution in the capillary of smallest diameter.

---

[1] The investigations reported herein are part of a research program sponsored by the Office of Rubber Reserve, Reconstruction Finance Corporation.

[2] Presented at the Annual Meeting of the Society of Rheology, New York, N. Y., November 4–5, 1949.

Worker-Consistometer

A complete description of the worker-consistometer and its operation is given by McKee and White [see Ref. (1)]. It consists essentially of a capillary shearing element clamped between flanges on the ends of two coaxial steel cylinders, each of which is equipped with a close-fitting piston. The experimental material is situated between the pistons and can be forced through the capillary by means of them. When the material is forced out of one cylinder, through the capillary, it is collected in the opposed cylinder and is immediately in position to be forced back through the capillary in the opposite direction. Any number of measurements may thus be made with one filling of the instrument. The shearing element used to obtain the data reported in this paper is a capillary of $\frac{1}{4}$-in. length and 0.0158 in. diameter.

Measurements were made in the worker-consistometer at 37.8±0.6°C. (100±1°F.) on 3, 5, 7.5, and 10% solutions. Each solution was observed under about eight different loads giving flow times from about 4 to 600 sec./in. travel. These loads were all in the range from 0.5 to 80 lb. Each flow rate reported is the average of three observations. Kinetic energy corrections were necessary for the faster rates of flow of the 3% and the 5% solutions. These were calculated using the equation

$$P'' = \frac{m\rho Q^2}{\pi^2 R^4}, \qquad [1]$$

where
P'' = pressure drop in capillary due to kinetic energy effect (dynes/cm.^{2}),
m = dimenensionless constant estimated from unreported measurements as 0.8,
ρ = density (g./cm.^{3})
Q = volume rate of flow through capillary (cm.^{3}/sec.), and
R = radius of capillary (cm.).

The largest correction, for the fastest rate of flow for the 3% solution, amounted to about 35% of the total applied load.

Bingham Viscometers

Three Bingham capillary viscometers were used. These were calibrated at 37.6°C. (99.7°F.) according to the general techniques outlined by Swindells (3). All subsequent measurements with these viscometers were made within 0.05°C. of the above temperature. The radii of these capillaries, obtained from the calibrations, are

Viscometer designation	Radius of capillary *cm.*
GE 20	0.0109
GE 36	0.0187
GE 70	0.0363

Within the accuracy of the calibrations, no kinetic energy corrections were required. The capillary radii were calculated using a value of 12 cm. for the capillary length and a nominal value of 5 cm.^{3} for the volume between fiducial marks in all cases.

Measurements were made in each viscometer on all solutions for which flow times of 1–30 min. could be obtained with pressure heads of 4–150 cm. Hg. These measurements covered the range from 0.1 to 10% rubber.

RESULTS

The results are all plotted in Fig. 1. The open and half-shaded circles are logarithmic plots of nominal rate of shear at the capillary wall (D_w) versus shearing stress at the wall (s_w). These are obtained from the observed quantities by using the relations

$$D_w = \frac{4Q}{\pi R^3};\ s_w = \frac{PR}{2L}, \tag{2}$$

where
$$\begin{cases} Q = \text{volume rate of flow through capillary, cm.}^3\text{/sec.,} \\ P = \text{pressure drop across capillary, dynes/cm.}^2\text{,} \\ R = \text{capillary radius, cm., and} \\ L = \text{capillary length, cm.} \end{cases}$$

The numerical conversion factors giving these values from the observed quantities are as follows:

Instrument	Shearing stress at wall, s_w, dynes/cm.^{2}	Nominal rate of shear at wall, D_w, sec.$^{-1}$
GE 20	$6.05 \times P$ (*cm.* Hg, *C.*)	$9.82 \times 10^5 \times Q$ (*cm.*^{3}/*sec.*)
GE 36	$10.4 \times P$ (*cm.* Hg, *C.*)	$1.94 \times 10^5 \times Q$ (*cm.*^{3}/*sec.*)
GE 70	$20.2 \times P$ (*cm.* Hg, *C.*)	$2.66 \times 10^4 \times Q$ (*cm.*^{3}/*sec.*)
Worker-consistometer	$5400 \times P'$ (lb. load)	$1.58 \times 10^6 \times Q$ (*cm.*^{3}/*sec.*)

Q is obtained by dividing the volume between fiducial marks (3.3 cm.^{3} in the worker-consistometer) by the observed time of flow. The pressures in cm. Hg at 0°C. are obtained by correction of observations on a mercury monometer at room temperature. For converting lb. load on the worker-consistometer to dimensions of pressure the areas of the cylinders are calculated from a diameter of 0.506 in.

The plots in Fig. 1 show that the flow of the GR-S solutions is non-Newtonian, since they are not straight lines of unit slope as result for Newtonian flow, although they do approach this condition at the lowest concentrations and lowest rates of shear. These plots also show reasonably good agreement among the different instruments since all the points for a given solution fall on a single line. This is expected since, although in non-Newtonian flow D_w is not the actual rate of shear at the capillary wall—as it is in Newtonian flow— it retains the role of a correlating function.

The actual rate of shear at the capillary wall ($\dot{\gamma}_w$) can be obtained from D_w, as has been pointed out by many authors (4), without assuming the particular form of the functional relationship between rate of shear and shearing stress, but only assuming that some functional relation does apply. The solution of the (general) differential equation, followed by integration of the flow over the cross section of the capillary, and the conversion of Q and P into D_w and s_w, and of dD_w/ds_w into $d \log D_w/d \log s_w$, gives the relation

$$\dot{\gamma}_w = (D_w/4)\,(3 + d \log D_w/d \log s_w). \qquad [3]$$

According to Eq. [3], if the tangential slope of a log D_w vs. log s_w curve, such as those plotted in Fig. 1, exceeds unity, as is the case for the solutions throughout Fig. 1, $\dot{\gamma}_w$ is greater than D_w, and the deviation of the slope from unity determines the extent of this inequality, *i.e.*, is a measure of the magnitude of the deviation of the flow from Newtonian.

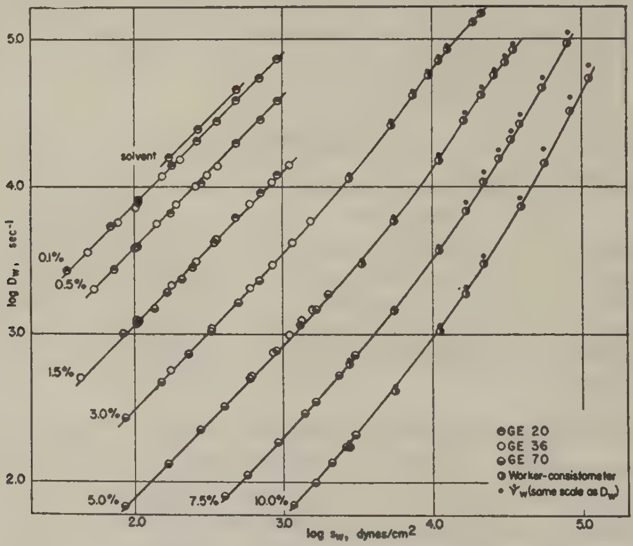

FIG. 1. Composite flow curves.

By using Eq. [3], with the slopes of the D_w plots in Fig. 1, as determined graphically from an expanded plot, it is possible to evaluate $\dot{\gamma}_w$. The results of such evaluation are plotted as the small, completely shaded circles in Fig. 1. For values of concentration $<7.5\%$ rubber and log $s_w < 3.4$, the deviations of the slopes from unity are so small that on the scale of Fig. 1 $\dot{\gamma}_w$ in this region can be considered identical with D_w, and no separate $\dot{\gamma}_w$ plots are given.

DISCUSSION

The Expression $\dot{\gamma} = \mathrm{as} + \mathrm{bs}^2$ *as a Flow Law of Limited Applicability*

In order to interpret the flow behavior in terms of the properties of the system it is desirable to describe the flow curves analytically. No expression has been found which can serve as a general analytical representation of non-Newtonian flow. However, the relation

$$\dot{\gamma} = as + bs^2, \tag{4}$$

where a and b are constants, which has been suggested by many authors, has been found to represent most of the present data. Consideration of the present, and other, flow curves for GR-S solutions shows that this relation cannot have general validity. Since its second derivative is a constant, the expression cannot represent inflections such as are indicated in the upper parts of the curves for the 3% and the 5% solutions in Fig. 1 and are often present in flow curves for polymer solutions at high rates of shear. It can, however, represent the parts of those curves which are below the inflections. A second limitation is that the expression cannot represent data for which the slopes of the log D_w vs. log s_w plots are greater than two, since a polynomial cannot represent a logarithmic plot having a slope exceeding the greatest exponent in the polynomial. Such slopes are not shown by any of the present data but they are shown by the data of White and Belcher (1) at concentrations somewhat above 10% rubber, and often appear in logarithmic flow curves for polymer solutions of relatively high concentration. However, since there is no inherent reason why this expression cannot represent all of the data reported here except that in the upper parts of the flow curves for the 3% and the 5% solutions, and since the constants in the expression can be evaluated conveniently and interpreted in physical terms, as discussed below, its application to the present data has seemed of interest.

In the form

$$(1/a)\dot{\gamma} = s[1 + (b/a)s] \tag{5}$$

the expression can easily be compared with the Newtonian equation

$$\eta\dot{\gamma} = s. \tag{6}$$

The viscosity at zero shearing stress is given by $1/a$; b/a is some kind of a measure of the deviation of the flow from Newtonian. The variation of these quantities with concentration should be of interest. When $1/a$ is converted into terms of reduced viscosity,

$$\eta_{\text{red}} = \frac{\eta_{\text{sp}}}{c} = \frac{(\text{viscosity of solution/viscosity of solvent}) - 1}{\text{concentration in g./100 ml.}} \tag{8}$$

it is found to be related to concentration by Martin's (5) equation

$$\eta_{sp}/c = [\eta] \exp\{k' [\eta] c\}, \qquad [9]$$

which transforms to

$$\log (\eta_{sp}/c) = \log [\eta] + k' c[\eta]/2.303, \qquad [10]$$

in all of which $[\eta]$ is the intrinsic viscosity, or reduced viscosity extrapolated to zero concentration, and k' is a constant for any polymer homologous series in a given solvent.

The ratio b/a has been tentatively identified by Ferry (6) as the reciprocal of a static modulus of internal rigidity by the following argument. A polymeric solution in steady flow is in a state of steady internal strain, γ_i, which may be defined formally as

$$\gamma_i = s/G_i, \qquad [11]$$

where s is the same shearing stress which is sumultaneously producing external flow, and G_i is a static modulus of internal rigidity. Ferry assumes that the ratio of the viscosity at a given shearing stress $(s/\dot{\gamma})$ to the viscosity at zero shearing stress $(1/a)$ is a function of the internal strain, *i.e.*,

$$as/\dot{\gamma} = f(\gamma_i). \qquad [12]$$

Now Eq. [4] transforms to

$$\dot{\gamma}/as = 1 + (b/a)s, \qquad [13]$$

or,

$$as/\dot{\gamma} = 1/[1 + (b/a)s], \qquad [14]$$

which suggests that

$$as/\dot{\gamma} = f(\gamma_i) = 1/(1 + \gamma_i) = 1/(1 + s/G_i) = 1/[1 + s/(a/b)], \qquad [15]$$

or

$$a/b = G_i. \qquad [16]$$

Leaderman (7) has found in several instances that values of a/b agree in order of magnitude with the values of the modulus (G_k) calculated from the kinetic theory of high elasticity, specifically,

$$G_k = \frac{cRT\rho}{M}, \qquad [17]$$

where
c = concentration in g./100 ml.,
R = gas constant,
T = absolute temperature,
ρ = density, and
M = molecular weight.

This modulus is directly proportional to the concentration, and suggests a similar concentration dependence for a/b. This may be the case at moderate values of the concentration. However, it is not possible at high dilution, since it is obvious from inspection of Eq. [5] that in order for this equation to reduce to the Newtonian equation in the case of the pure solvent ($c = 0$), as it must, a/b must approach infinity as the concentration approaches zero. This situation is in no sense self-contradictory since it is not expected that the kinetic theory of high elasticity should apply to solutions of high dilution.

If Eq. [4] is solved for velocity, the flow through a capillary integrated over its cross section, and the result expressed in terms of D_w and s_w, there results

$$D_w = a\, s_w + (4/5)\, b\, s_w^2, \qquad [18]$$

or

$$(D_w/s_w) = a + (4/5)\, b\, s_w. \qquad [19]$$

Accordingly, when Eq. [4] is valid, a plot of D_w/s_w vs. s_w will be a straight line of intercept a and slope $(4/5)b$.

The data shown in the logarithmic plots in Fig. 1 have subsequently been plotted in terms of D_w/s_w vs. s_w. Since the plots for different concentrations exhibit large differences in the magnitude of D_w/s_w, it is impossible to condense them all into a reasonable number of figures, and no attempt is made to show them all in this paper. As an example, Fig. 2 is such a plot for the 7.5% solution. The inset in this figure is an expansion of the lower end of the main plot. Some of the plots show considerably more scattering of the points than does Fig. 2, but, in general, straight lines do represent the plots reasonably well below the inflections in the

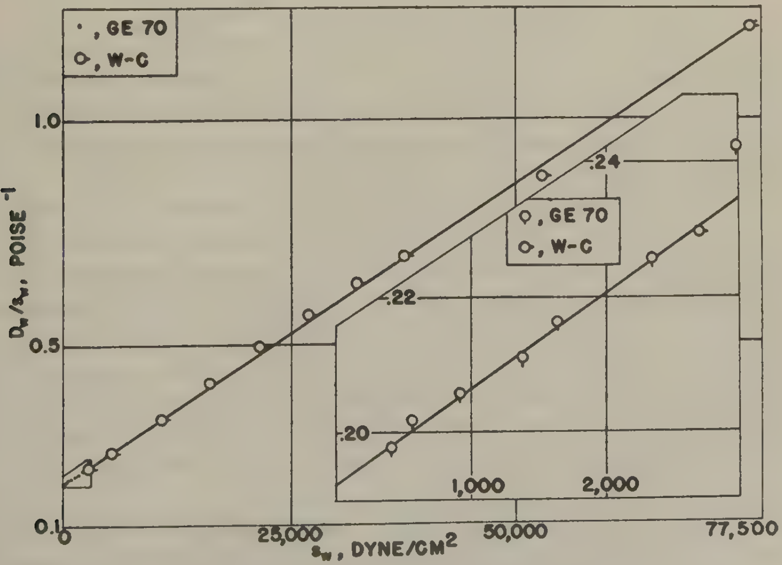

Fig. 2. Apparent fluidity of 7.5% GR-S solution.

logarithmic plots. The relatively greater scattering in these plots, as compared with the logarithmic plots, indicates their greater sensitivity to uncertaintities in the data. The plots for the 3% and the 5% solutions show systematic deviations from linearity in the regions above the inflections in Fig. 1.

TABLE I

Constants for Quadratic Flow Relations

GR-S	*a*		*b* × 10^6	
	Best value	Range	Best value	Range
%	*poise*$^{-1}$	*poise*$^{-1}$	*cm.*^{2} *dyne*$^{-1}$ *poise*$^{-1}$	*cm.*^{2} *dyne*$^{-1}$ *poise*$^{-1}$
0.0	92.0	91.0–93.0	0	
0.1	75.9	73.4–77.6	3260	1450–7050
0.5	37.6	36.4–38.6	4820	2760–7140
1.5	11.4	11.1–11.8	2290	1740–2810
3	3.27	3.13–3.30	378	375–390
5	.795	0.793–0.845	71.8	69.2–89.3
7.5	.192	0.192–0.197	16.6	16.6–18.9
10	.0545	0.0520–0.0570	5.19	5.17–5.22

The intercepts and slopes of these straight lines give values for the constants *a* and *b*. Table I gives these values of *a* and *b* for the different concentrations. Both best values and range of experimental uncertainty are given in the table.

Viscosity at Zero Shearing Stress: 1/*a*

The values of *a* were converted to reduced viscosity, η_{red} and Fig. 3 is a plot of log η_{red} vs. concentration. These fall quite well on a straight line, as required by Martin's equation. Concentration in g./100 ml. is obtained by assuming that the density of the solutions can be obtained by proportional addition of the densities of the components (GR-S = 0.935 g./cm.,^{3} *o*-dichlorobenzene = 1.30 g./cm.^{3}). The viscosity of the solvent is taken as 0.0107 poise, which is believed to be a better value than (1/92.0) = 0.0109, from Table I. Where the limits of experimental uncertainty are outside the circles in the figure, they are indicated by vertical lines attached to the circles. The intercept in Fig. 3 yields $[\eta] = 1.9$ (100 ml./g.), and the slope gives $k' = 0.18$. The value $[\eta] = 1.9$ is in fair agreement with data obtained at low rates of shear at the University of Akron Government Laboratories; these data indicate that the intrinsic viscosity of a rubber similar to X-418 GR-S should be about 2 in a good solvent, such as *o*-dichlorobenzene.

The value of 0.18 for k' is lower than the values of 0.3–0.4 usually found for solutions of linear polymers in good solvents (8), or than the values of 0.3–1.3 obtained for solutions of crepe rubber in various solvents from the data of Gee (9) and of Kemp and Peters (10). The knowledge of the significance of k' is in such a nebulous state that an adequate discussion of the apparent lowness of the experimental value for the present system is beyond the scope of this paper.

Coefficient of s^2 Term: Internal Modulus

Figure 4 is a plot of a/b vs. weight per cent rubber. The range of experimental uncertainty is shown for each point by the vertical lines attached to the circles in the figure. The larger uncertainties at lower concentrations are due to the fact that here the absolute slopes of the D_w/s_w vs. s_w plots become smaller in comparison to the scattering. At the lower concentrations, a/b increases quite rapidly as the concentration decreases.

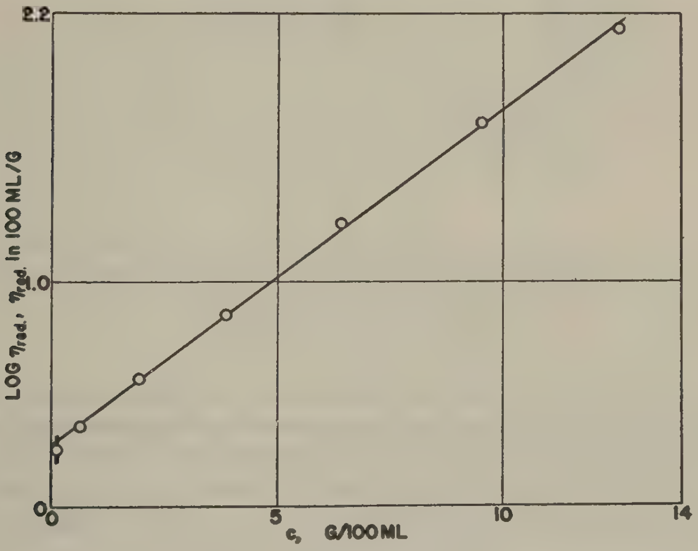

FIG. 3. Reduced viscosity.

This is in accord with the requirement that a/b approach infinity as the concentration approaches zero. In the neighborhood of 3% GR-S, a/b increases with concentration, and the plot is not inconsistent with a direct proportionality between a/b and concentration. At higher concentrations, the values of a/b level off. This change in behavior probably indicates that the interpretation of a/b as G_i becomes less valid at the higher concentrations. It has been mentioned previously that there is evidence to indicate that the quadratic flow equation will fail at concentrations somewhat above 10 wt.–%. This failure may well be preceded by a nonconforming behavior of the constants at still lower concentrations extending down into the range examined here.

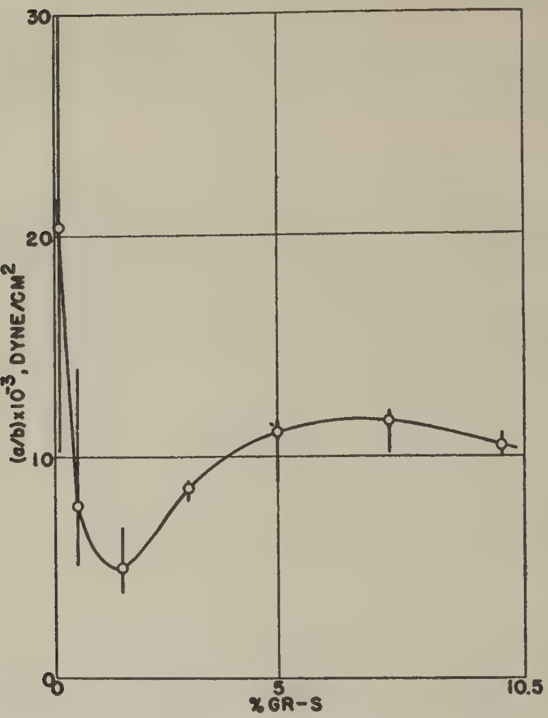

FIG. 4. Internal modulus.

The following numerical example applies the kinetic theory equation to the 3% solution, which is in the range where a/b is proportional to concentration. For $c = 4$ g./100 ml., $M = 125{,}000$, $T = 300$°K., and $\rho = 1$, there results $G_k = 16 \times 10^3$ dynes/cm.^{2} This is in rough agreement with the approximate experimental value $a/b = 8.6 \times 10^3$ dynes/cm.^{2}

Nonapplicability of Suggested Flow Equation $\dot{\gamma} = \mathrm{as} + \mathrm{cs}^3$

Several theoretical considerations have indicated that the relation

$$\dot{\gamma} = as + cs^3 \text{ (}a\text{ and }c\text{ being constants)} \qquad [20]$$

should be a more valid flow equation than the quadratic relation. Reiner (11) argues that $\dot{\gamma}$ should change sign when the sign of s is changed. This allows only odd terms and suggests the deleted power series of which the above expression constitutes the first two terms. Eisenschitz (12) has deduced, on the basis of Hencky's hydrodynamic considerations (13), that the relation between viscosity and internal strain should be of the form

$$as/\dot{\gamma} = 1/(1 + \gamma_i^2), \qquad [21]$$

which also leads to the above expression. The applicability of this expression requires that plots of D_w/s_w vs. s_w^2 be straight lines. Such plots have been made for the present data and are found to be curved in all cases. Accordingly, the expression is not applicable to the flow observed here. Apparently the concepts on which the expression is based are not valid for the present system, and require revision.

ACKNOWLEDGMENTS

The authors wish to thank Messrs. S. A. McKee and H. S. White for helpful advice concerning the operation of the worker-consistometer, and Dr. H. Leaderman for valuable discussions regarding the interpretation of the data.

SUMMARY

1. Flow curves have been obtained at 37.8°C. (100°F.) for 0.1, 0.5, 1.5, 3, 5, 7.5, and 10 wt.–% solutions of milled X-418 GR-S in *o*-dichlorobenzene. Results from the NBS worker-consistometer and from Bingham capillary viscometers were combined to cover the range from 60 to 100,000 sec.$^{-1}$ rate of shear and 30–100,000 dynes /cm.^{2} shearing stress.

2. Except for the higher regions for the 3% and the 5% solutions, these flow curves can be represented by the quadratic equation

$$\dot{\gamma} = as + bs.^2$$

3. The reciprocal of the coefficient *a* gives the viscosity at zero shearing stress; a plot of log reduced viscosity (obtained from $1/a$) vs. concentration in g./100 ml. is a straight line as predicted by Martin's equation

$$\eta_{sp}/c = [\eta] \exp\{k' [\eta] c\}.$$

This plot gives an intrinsic viscosity $[\eta]$ of 1.9 (100 ml./g.) in good agreement with the value obtained elsewhere from measurements at lower rates of shear. The constant k' has a value of 0.18 which is relatively low.

4. The ratio a/b has been interpreted by Ferry as a static modulus of internal rigidity. At low concentrations it increases with decreasing concentration, and in the neighborhood of 3 wt.–% it shows a nearly direct proportionality with concentration, and is in fair agreement with the modulus

$$G_k = c\,R\,T\,\rho/M,$$

calculated from the kinetic theory of elasticity.

5. The equation, $\dot{\gamma} = as + cs^3$ (a and c being constants), which has been suggested by several theoretical considerations, does not fit the present flow data.

REFERENCES

1. Cf. McKee, S. A., and White, H. S., *ASTM Bull.* No. 153, 90 (1948).
2. White, H. S., and Belcher, H. V., "Apparent Viscosity of 5 to 30 Percent GR-S Rubber Solutions," technical report to Reconstruction Finance Corporation, Office of Rubber Reserve, from National Bureau of Standards, August 10, 1948.

3. Swindells, J. F., *J. Colloid Sci.* **2**, 177 (1947).
4. Cf., *e.g.*, Philippoff, W., Viskosität der Kolloide, p. 42. Steinkopff, Dresden and Leipzig, 1942.
5. Cf. Huggins, M. L., *J. Am. Chem. Soc.* **64**, 2716 (1942).
6. Ferry, J. D., *J. Am. Chem. Soc.* **64**, 1330 (1942).
7. Leaderman, H., report to be submitted to the Office of Naval Research.
8. Bawn, C. E. H., The Chemistry of High Polymers, p. 167. Interscience Publishers, New York, 1948.
9. Gee, G., *Trans. Faraday Soc.* **36**, 1171 (1942).
10. Kemp, A. R., and Peters, H., *J. Phys. Chem.* **43**, 1063 (1939).
11. Reiner, M., Ten Lectures on Theoretical Rheology, pp. 139, 140. Rubin Mass, Jerusalem, 1943.
12. Eisenschitz, R., *Kolloid Z.* **64**, 184 (1933).
13. Hencky, H., *Ann. Physik* [5], **2**, 617 (1929).

THE EFFECT OF ULTRASONIC IRRADIATION ON THE FORMATION OF COLLOIDAL SULFUR AND ICE

C. F. Turner and Andrew Van Hook

Department of Chemistry, College of the Holy Cross, Worcester, Massachusetts

Received July 11, 1949

The following experiments were performed in connection with our experiments on the promotion of nucleation in sugar solutions by ultrasonic irradiation (1).

EXPERIMENTAL

Sulfur

The effects reported by La Mer and Yates (2) and Weissler (3) for sulfur sol formation were completely confirmed by irradiation of 50-ml. samples at room temperature in 8 in. test tubes at 340 kc. and 300 w. input. In addition, if unboiled water is boiled immediately after irradiation, the otherwise prolonged induction period assumes the usual value of about 12 min. for solutions 0.006 M in HCl and 0.003 M in $Na_2S_2O_3$. Addition of traces of a wide variety of salts (Ni^{++}, Fe^{++}, Fe^{+++}, Cu^+, Mn^{++}, Na^+, NH_4^+, NO_3^-, Cl^-, SO_4^{--}, H_2O_2, *etc.*) was observed to have no marked effect on the normal induction period (4) except for cupric and nitrite ions. The following table summarizes the effect of added nitrite ion. These observations indicate a strong inhibiting action of nitrite ion, a likely contaminant upon irradiation at high frequency (3,5).

TABLE I

Induction Period Upon Addition of KNO_2 to Solutions 0.006 M in HCl and 0.003 M in $Na_2S_2O_3$, at Approximately 27°C.

$KNO_2/Na_2S_2O_3$ moles/moles	Time min.
0	12
10^{-5}	12
10^{-4}	18
10^{-3}	37
10^{-2}	50
10^{-1}	3 hr.

The possibility that foreign nuclei, rather than homogeneous nucleation (6), might be the normal base upon which the majority of sol particles form seems improbable since prior boiling (2) of the water used, proper sterilization of all solutions and glassware and exclusion of air, centrifuging, partial freezing, and ultrafiltration—all have no effect upon the normal (not irradiated) induction time. Although no one of these treatments assures absolutely mote-free water, it seems likely that the collected precautions would reveal any activity in this way (7).

We have observed (1) that low-frequency high-power sonic waves are very effective in causing the crystallization of various sugar solutions under conditions when low power or high frequency (high and low power) ultrasonic irradiation are ineffective. Upon irradiating freshly mixed sulfur sols at 8 or 16 kc. and 300 w., coagulation is immediate, and frequently visible outside the Tyndallscope. Previous irradiation of the water, or separate solutions, at 8 kc., does not alter the normal induction period, so that, presumably, the effect is the usual nucleating one due to low-frequency sonic waves. Even the most strongly inhibited solutions listed in the table coagulate immediately at 8 kc.

Water

The same difference was observed in the case of ice formation from supercooled water. The particular distilled water used could be supercooled rather readily from 5 to 10°, even when surrounding the nickel bar of the magnetostriction generator. This limit of supercooling was extended to about 15° after irradiating the water at the high frequency (8) previously specified. The low frequency had no effect. However, if the irradiation is performed while the water is in the supercooled state (even if only 1 or 2°), ice formation is immediate at the low frequency whereas the high frequency has no particular effect.

Previous treatment of the water or addition of traces of the various substances mentioned above has no significant effect upon the freezing pattern described, even though the extention of supercooling possible after irradiation at high frequency (8) is strongly suggestive of the formation of an inhibitor (3), or dispersion of foreign nuclei (2). The prompt formation of ice crystals when irradiated at low frequency, even when only slightly supercooled, suggests a strongly accelerated, homogenizing mechanism.

Conclusion

Low-frequency sonic waves, of sufficient power, enhance the nucleation of several systems which are unaffected or even inhibited by high-frequency ultrasonic irradiation.

References

1. Van Hook, A., and Turner, C., to be published.
2. La Mer, V. K., and Yates, J. W., *Science* **106**, 508 (1947).
3. Weissler, A. J., *J. Colloid Sci.* **3**, 67 (1948).
4. Zaiser, E. M., and La Mer, V. K., *J. Colloid Sci.* **3**, 575 (1948).
5. Nomoto, O., and Okui, S., *J. Phys. Soc. Japan* **3**, 47 (1948); *C. A.* **43**, 4084.
6. Dorsey, N. E., *Trans. Am. Phil. Soc.* **38**, 247 (1948).
7. Van Hook, A., and Brumo, A. J., Faraday Soc., Symposium on Crystal Growth, April 1949.
8. Smith-Johannsen, R., *Science* **108**, 652 (1948).

STABILIZATION OF CARBON-BLACK DISPERSIONS IN HYDROCARBONS

M. van der Waarden

From the Koninklijke/Shell Laboratory, Amsterdam, Holland

Received February 2, 1950

Introduction

The factors determining the stability of dispersions in liquids with a very low dielectric constant (ϵ) are still imperfectly understood. It may be assumed that dispersed particles of the same nature are attracted towards each other in such a system by van der Waals-London forces, and in some cases by permanent or induced dipoles, or both. This attraction may be prevented or reduced by adsorption of suitable molecules (stabilizers) on the surface of the dispersed particles. The present article is meant as a contribution towards explaining the way in which the particles are stabilized by these adsorbed molecules. The investigation here described deals with the special case of carbon-black dispersions in a hydrocarbon medium stabilized by hydrocarbons.

The medium has a very low ϵ (2–3), while the substances intended to stabilize the dispersions are not ionogenic. Even though electrical charges at the surface of stabilized particles might play a part in such a medium, which is not certain, they may no doubt be neglected in this investigation.

Experimental

Carbon black is rubbed in a mortar with 20 parts of a white vaseline. As a result of mechanical forces a very fine dispersion is formed, which is stable because the particles cannot move freely after dispersion owing to the rigidity of vaseline at room temperature. Upon heating, this property disappears and the carbon black particles at once conglomerate to form coarse flakes. If one volume of the fine dispersion in vaseline is lightly rubbed with excess hydrocarbon oil (50 vol.), the vaseline dissolves, the carbon-black particles are released and flocculate unless the oil contains sufficient material to stabilize the dispersion. Though flocculation during dilution may occur at moments when the adsorption of stabilizing components has not yet reached equilibrium, the results are reproducible. The results obtained with various dilution oils are therefore comparable.

The 0.1% dispersions obtained are compared for degree of flocculation by reference to 6 microphotographs of dispersions with varying degree of flocculation made in transmitted light,[1] magn. 380 ×. The degree of flocculation is expressed by the figures 0–6, 0 indicating a dispersion in which no particles are visible by direct microscopic observation and 6 the presence of very large floccules. Differences of 0.5 point are clearly perceptible. In independent duplicate determinations the differences are smaller than 0.5 point. The degree of flocculation is estimated accurate to 0.25 point, though differences of 0.25 point are doubtful. In many cases the degree of flocculation was determined after 1 day's storage at 20°C. or 1 hr. at 100°C. taking a fresh sample for each microscopic examination.

Carbon black consists of primary particles, probably somewhat elliptical, with a diameter of 10–300 mμ, part of which are tightly bound together (1,2,3), and a density of *ca.* 1.8 (4). They consist very probably of parallel layers of condensed six-carbon rings (3,5), with oxygen and some hydrogen bound to the more or less rough surface. They readily form aggregates and floccules. Our product, after removal of 9.2% by wt. of water, contained (in per cent by weight): 91.5% of C; 0.7% of H; 0.1% of S; 6.0% of O (direct determination); 0.2% of ash; no N. About 50% of the oxygen can easily be removed, and may therefore be considered to be adsorbed; the remainder is still present after prolonged heating in a nitrogen current at 200°C. and must herefore be considered as chemically bound oxygen. According to Verwey and de Boer (6) and Villars (7) this oxygen is found at the surface of the carbon black, chiefly in ether bond and further perhaps as hydroxyl, keto, or carboxyl oxygen (8).

The active surface area, determined according to Brunauer, Emmett, and Teller (9), with nitrogen at − 195°C., is 325 sq. m./g. After heating at 1000°C. in vacuum to remove all oxygen, the surface area is practically unchanged (320 sq. m./g). From the maximum adsorption of the dye Sudan III dissolved in an aromatic-free mineral oil, the active surface area is calculated to be 75 sq. m./g, assuming that the flat dye molecules are adsorbed in a horizontal position, occupying a surface area of 2.0 sq. mμ.

The carbon black was used in an untreated condition, after removing water and volatile products (vacuum, 125°C.) with and without extraction with benzene, and after heating at 1000°C. in vacuum and in a hydrogen current (removal of nitrogen or alternatively nitrogen and sulfur).

Hydrocarbons used were:

1. *Individual hydrocarbons.*
2. *Synthetic (mixtures of) alkylated aromatics.* The aromatics (individual aromatics and benzene or naphthalene derivatives from a mineral oil fraction with b.p. *ca.* 180–250°C.) are alkylated with α-olefin fractions with $AlCl_3$ as the catalyst.[2]

---

[1] According to unpublished work of van der Minne and Hermanie of this laboratory.

[2] Prepared by Mr. C. M. van Battum of this laboratory.

3. *Mineral oil fractions:*
   - *a.* distillates, obtained by separating mineral oil into fractions with specified boiling ranges;
   - *b.* residual oil, obtained as distillation residue of an asphaltene-free mineral oil;
   - *c.* raffinates, obtained by partial extraction of aromatic and colored components from distillates by means of a selective solvent;
   - *d.* white oils, obtained by freeing raffinates completely from aromatic and colored constituents by treatment with oleum;
   - *e.* extracts (consisting of aromatic and colored constituents) obtained in solvent refining of distillates.

In various cases these products were freed from acids and resins by distillation over caustic solution and percolation through silica gel. The average molecular weight was determined ebullioscopically; the percentage of carbon in the aromatic structure was calculated according to the ring analysis of Vlugter, Waterman, and van Westen (10); this method has been further elaborated in this laboratory and will be shortly reported on elsewhere.

RESULTS

1. In aromatic-*free* hydrocarbons (mixtures) with av. mol. wt. (M), M = 72–500, the carbon-black dispersions showed pronounced flocculation; the degree of flocculation (F) decreases somewhat (to a minimum of 3.5) with increasing M of the hydrocarbons. The floccules in low molecular hydrocarbons (to M = about 200) have a very compact structure; those in high molecular hydrocarbons (M = 300–500) have a loose structure. The carbon black had been freed from water and other volatile components

TABLE I

Degree of Flocculation F of 0.1% Carbon-Black Dispersions in Hydrocarbon Mixtures Containing Polynuclear Nonsubstituted Aromatics

Solvent	Aromatic admixed			F of dispersion
	Name	% by wt.	M[a]	
White oil	—	—	—	4.5
White oil	Naphthalene	10	128	4.5
White oil	Retene[b]	10	234	4
α-Methylnaphthalene	—	—	—	3.5
α-Methylnaphthalene	Anthracene	2	178	3.25
α-Methylnaphthalene	Phenanthrene	10	178	3.5
α-Methylnaphthalene	Fluorene	10	178	3.5
α-Methylnaphthalene	α-α′-Dinaphthyl	6	254	2

[a] Molecular weight.

[b] 7-Isopropyl-1-methylphenanthrene.

TABLE II

Degree of Flocculation F of 0.1% Carbon-Black Dispersions in Alkylated Aromatics (Alkylate)

No.	Alkylate	Average number of side chains	Average number of C per side chain	Total number of C in side chains	F of carbon black dispersions in													
					100% Alkylate		20% Wt. alkylate in white oil		10% Wt. alkylate in w. o.		5% Wt. alkylate in w. o.		1% Wt. alkylate in w. o.		0.2 % Wt. alkylate in w. o.		0% Alkylate in w. o.	
					Direct	After 1 hr. at 100°C.	Direct	After 1 hr. at 100°C.	Direct	After 1 hr. at 100°C.	Direct	After 1 hr. at 100°C.	Direct	After 1 hr. at 100°C.	Direct	After 1 hr. at 100°C.	Direct	After 1 hr. at 100°C.
1	Alkylated benzene	1	16(pure)	16	2.5	3	—	—	—	—	—	—	—	—	—	—	4.5	4.5
2	Alkylated toluene	1	16	16	1	2	1	1.5	1.25	1.5	1.5	3	2	2.5	—	—	4.5	4.5
3	Alkylated xylene	1	16	16	1.5	2.5	2	3	—	—	2.5	4	3	4	—	—	4.5	4.5
4	Alkylated xylene	1.25	16	20	1	2.25	—	—	—	—	—	—	—	—	—	—	4.5	4.5
5	Alkylated xylene	2	16	32	0	1	1.25	1.5	1.5	1.75	—	—	2	2.5	2.5	4	4.5	4.5
6	Alkylated benzene-derivatives mixture[a]	1	16	16	1	1.25	2	1.75	—	—	—	—	—	—	—	—	4.5	4.5
7	Alkylated naphthalene	1	8(pure)	8	1.25	2	—	—	—	—	—	—	—	—	—	—	4.5	4.5
8	Alkylated naphthalene	1	8	8	1.25	1.5	3.5	4.75	—	—	—	—	—	—	—	—	4.5	4.5
9	Alkylated naphthalene	1	16(pure)	16	0	0	1.5	3	2.5	3.75	2.75	3.75	—	—	—	—	4.5	4.5
10	Alkylated naphthalene	3	13	39	0	1	1	1.5	1.25	2.25	2	2.5	—	—	—	—	4.5	4.5
11	Alkylated naphthalene	2.5	14	35	0	1	1	1.5	1.25	2	2.25	2.5	—	—	—	—	4.5	4.5
12	Alkylated naphthalene	2	16	32	0	1	1	2	1.5	2.25	2.25	2.75	—	—	—	—	4.5	4.5
13	Alkylated naphthalene	2	17	34	0	1	1.25	2	1.75	2	2	2.5	—	—	—	—	4.5	4.5
14	Alkylated naphthalene-derivatives mixture[a]	2 and more	10	>20	1	1	2	2	—	—	—	—	—	—	—	—	4.5	4.5
15	Alkylated naphthalene-derivatives mixture[a]	1	16	16	1	2	2.75	3.25	—	—	—	—	—	—	—	—	4.5	4.5

[a] From a mineral oil fraction with boiling range from *ca.* 180–250°C.

at 125°C. in vacuum. Also in low molecular *aromatics* this carbon black forms floccules which are compact in benzene, toluene, and xylene, and looser in α-methyl naphthalene. The aromatics which are solid at room temperature were used as solutions in white oil (M = 300, aromatic-free), or if their solubility was insufficient, in α-methyl naphthalene. The degree of flocculation of carbon black dispersions in these solutions is given in Table I.

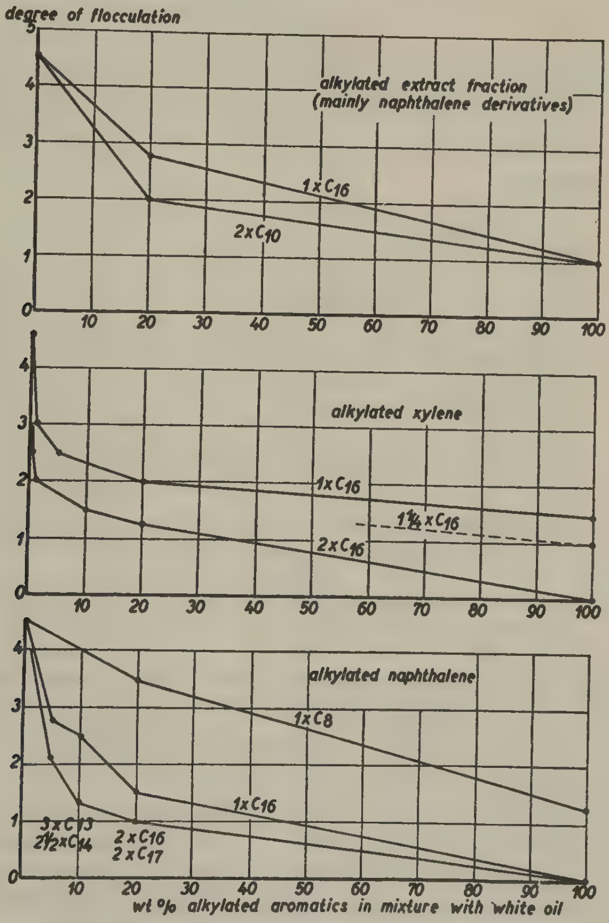

FIG. 1. Influence of alkylated aromatics on the degree of flocculation of 0.1% carbon-black dispersions in white oil.

With the exception of α-α′-dinaphthyl, these aromatics therefore have also a negligible stabilizing effect; the floccules have a loose structure.

2. The results of similar experiments with alkylated aromatics (benzene, toluene, xylene, naphthalene, aromatic extracts mainly with 1 or 2 condensed nuclei) are collected in Table II.

Contrary to the aforementioned experiments, all these cases show a distinct or even pronounced stabilization. In most cases flocculation increases somewhat upon heating for 1 hr. at 100°C. The stabilizing power of aromatics with 2 or more C_{10} alkyl chains or higher is distinctly better than that of aromatics with 1 chain; this is demonstrated in Fig. 1 in which various alkylates of one and the same aromatic are compared.

A comparison of various aromatics having about the same alkyl chains shows that there is no difference in activity between toluene and naphthalene with two C_{16} chains. For aromatics with one C_{16} side chain, the order for high aromatic concentration, is in various cases different from that for low concentrations (Fig. 2). Mention should be made of the great activity of the toluene derivative at low concentration and the low activity of the benzene derivative.

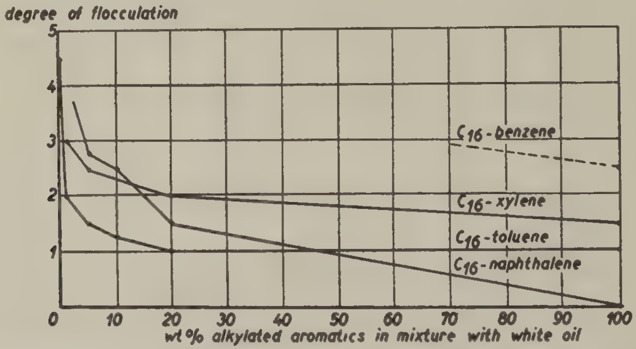

FIG. 2. Influence of aromatics alkylated once with C_{16} on the degree of flocculation of 0.1% carbon-black dispersion in white oil.

3. The results of experiments with carbon-black dispersions in various mineral oil fractions are shown in Table III. The carbon black was in these cases untreated. The fractions are primarily arranged according to aromatic content,[3] and in each group of about the same aromatic content according to molecular weight. Not all the fractions are from the same base material, so that at the same av. mol. wt. and aromatic content, differences in composition may occur owing to the presence of various contaminants such as resinous products. These products may have a stabilizing effect themselves or influence stabilization by other substances, as was shown by van der Minne (11).

The degree of flocculation in these experiments shows hardly if any change on storage or heating at 100°C. These results, too, indicate that stabilization is only effected in the presence of a sufficient amount of high molecular aromatics; since these aromatics have mainly 1, 2, or 3 nuclei, it means that part of them have long side chains.

---

[3] Percentage of carbon in aromatic structure.

Using a centrifuge method, Krein, Lipshtein, and Alexandrov (12) found in 7 mineral oils that residual oils have a stronger stabilizing activity towards carbon-black dispersions than have distillates, the latter, again, being stronger than raffinates. These results are in agreement with ours.

4. The influence of the condition of the carbon-black surface on stabilization by hydrocarbons was studied by comparable experiments with: I. untreated carbon black; II. carbon black from which the volatile components (chiefly water) had been removed; previous extraction with benzene had no influence; III. carbon black from which the chemically bound oxygen had also been removed; additional removal of sulfur had no effect.

TABLE III

Degree of Flocculation F of 0.1% Carbon-Black Dispersions in Mineral-Oil Fractions

Min.-oil fraction	Average mol. wt.	C_A[a]	F		
			Direct	After 1 day at 20°C.	After 1 hr. at 100°C.
		%			
White oil 1	320	0	4.5	4.5	4.5
White oil 2	400	0	3.5	3.5	3.5
White oil 3	500–600	0	4	—	—
Raffinate 1	500	5	0	0	1
Distillate 1	94	10	5	—	—
Distillate 2	170	9	4.75	5	5
Distillate 3 (acid-free)	392	8	3.25	3.5	3.5
Residual oil 1 (acid-free)	712	8	1	1	1
Distillate 4	236	14	4.25	5	5
Raffinate 2	375	12	2	2.5	2.5
Distillate 5 (acid-free)	283	22	3.75	4	4
Distillate 6 (acid-free)	278	25	3.75	3.75	3.75
Distillate 7 (acid-free)	310	28	3	2.75	3
Distillate 8 (acid-free)	356	25	1.75	1.75	1.75
Distillate 9 (acid-free)	513	26	0	0	1
Extract 1	130	53	4.5	4.5	4.5
Extract 2 (resin and acid-free)	240	47	1.75	1.75	—
Extract 3 (resin and acid-free)	300	49	0	0	—

[a] Percentage of carbon in aromatic structure.

The results given in Table IV show that the susceptibility of the carbon black to be stabilized by aromatics can be considerably increased by removal of adsorbed volatile products (chiefly water) from the carbon black. If, however, also the chemically bound oxygen is removed this increase is neutralized again. A comparison of the results obtained with dispersions II and III shows therefore that the chemically bound oxygen of carbon black plays an important part in stabilization.

TABLE IV

Degree of Flocculation F of 0.1% Dispersions of Carbon Black, Subjected to Various Pretreatments, in a Number of Mineral-Oil Fractions

Min.-oil fractions	Average mol. wt.	C_A	F (direct determination)		
		%	I[a]	II	III
White oil 1	320	0	4.5	4	4
Raffinate 3 (resin-free)	500	5	1	1	2
Residual oil 1	712	8	1	1	1
Distillate 5 (acid-free)	283	22	3.75	1.5	3.75
Distillate 6 (acid-free)	278	25	3.75	2.5	3.5
Distillate 7 (acid-free)	310	28	3	1.75	2.5
Distillate 8 (acid-free)	356	25	1.75	1.25	2
Distillate 9 (acid-free)	513	26	0	0	0
Extract 4 (acid-free, but containing resin)	247	47	3	1.5	2.5
Extract 5 (as in Extract 4)	310	49	1	0	0

[a] I untreated carbon black;
II volatile components removed;
III volatile components and chemically-bound oxygen removed.

DISCUSSION

On the strength of these results we assume that stabilization of carbon black by hydrocarbons in a hydrocarbon medium takes place as follows:

The surface area of the carbon-black particles is probably densely set with polar carbon–oxygen bonds; there may also be polar groups owing to the presence of ash-forming constituents. These dipoles attract polar or highly polarizable molecules. Aromatic hydrocarbons show a far greater interaction with polar molecules than aliphatic molecules do, which may be ascribed to the pronounced polarizability of aromatics in the plane of the rings (Kerr effect) or to the presence of a number of partial dipoles in the rings (13) and a small dipole moment of alkylated aromatics. Aromatics will thus be more strongly adsorbed on a polar surface. It is possible that oxygen removal from carbon black causes the formation of residual chemical valencies, which may function as centers of attraction.

Adsorbed aromatics without aliphatic side chains or with short side chains (the chains being assumed to be rather mobile in the medium) have no stabilizing effect, because the carbon-black particles with these adsorbed aromatics may enter each other's sphere of attraction. This possibility decreases as the side chains are longer, as a result of which the stabilizing power of the alkyl aromatics may increase to approach constancy. A higher amount of aliphatic chains in the aromatic nucleus improves the protection against flocculation for each adsorbed molecule. The stabilizing effect of a long aliphatic chain of a molecule adsorbed on a dispersed particle in a hydrocarbon medium was also found by Rehbinder (14) for dispersions in benzene stabilized by carboxylic acids, and by Verwey and de Boer (15) for highly concentrated suspensions stabilized with oleic acid.

Acknowledgment

The author is indebted to Mr. J. M. Hörchner for the careful way in which he carried out the experiments.

Summary

1. The degree to which hydrocarbons prevent flocculation of finely-divided carbon black in hydrocarbon medium was determined.

2. Only aromatic hydrocarbons with aliphatic chains of sufficient length were found to stabilize the dispersion. Their activity increases with the length of the aliphatic chain (investigated to C_{16}) and with the number of chains per molecule (investigated to 2).

3. It is supposed that adsorbed molecules can only have a stabilizing effect, if they are able to prevent the carbon-black particles from approaching each other to such a short distance as to enter each other's sphere of attraction.

References

1. Voet, A., *J. Phys. & Colloid Chem.* **51**, 1037 (1947).
2. Venuto, L. J., *Paint, Oil Chem. Rev.* **102**, No. 7, 32 (1940).
3. Watson, J. H. L., *J. Applied Phys.* **20**, 747 (1949). Ladd, W. A., and Wiegand, W. B., *Rubber Age* **57**, 299 (1945).
4. Dawson, T. R., and Hartshorne, N. H., *Trans. Inst. Rubber Ind.* **5**, 48 (1929).
5. Akamatu, H., and Nagamatsu, K., *J. Colloid Sci.* **2**, 593 (1947).
6. Verwey, E. J. W., and de Boer, J. H., *Rec. trav. chim.* **55**, 675 (1936).
7. Villars, D. S., *J. Am. Chem. Soc.* **70**, 3655 (1948).
8. Kruyt, H. R., and de Kadt, G. S., *Kolloidchem. Beihefte* **32**, 249 (1932).
9. Brunauer, S., Emmett, P. H., and Teller, E., *J. Am. Chem. Soc.* **60**, 309 (1938).
10. Vlugter, J. C., Waterman, H. I., and van Westen, H. A., *J. Inst. Petroleum Tech.* **21**, 661, 701 (1935).
11. Van der Minne, J. L., *Rec. trav. chim.* **65**, 549 (1946).
12. Krein, S. E., Lipshtein, R. A., and Alexandrov, A. N., *Neftyanoe Khoz.* **26**, 43 (1948); *C. A.* **42**, 8453i (1948).
13. Van Arkel, A. E., *Trans. Faraday Soc.* **42B**, 81 (1946).
14. Rehbinder, P., *Z. physik. Chem.* **A146**, 63 (1930).
15. Verwey, E. J. W., and de Boer, J. H., *Rec. trav. chim.* **57**, 383 (1938).

INTRINSIC VISCOSITY OF COTTONSEED GLOBULIN SOLUTIONS

Jett C. Arthur, Jr., and Barbara H. Saik

Southern Regional Research Laboratory, New Orleans, Louisiana[1]

Received December 30, 1949; revised February 13, 1950

ABSTRACT

Intrinsic viscosity of macromolecular solutions has become a very useful tool in evaluating high polymeric substances for various industrial applications. The shape characteristics of cottonseed globulin molecules in solution as determined by viscosity data are important in adapting the globulin for use in making synthetic fibers or adhesives and in evaluating chemical and physical modification of the globulin.

These characteristics of cottonseed globulin (18.06% nitrogen), extracted from solvent-extracted cottonseed meal by means of 0.5 *M* sodium chloride solution, precipitated by dialysis, and lyophilized, are reported. The intrinsic viscosity of the globulin in urea solutions was calculated to be 0.093, equivalent to a viscosity increment of 12.3 and an axial ratio (Simha equation) of 9.4 assuming elongated macromolecules or of 16.3 assuming flattened-disc-type macromolecules. These values are comparable with reported axial ratios of other vegetable protein macromolecules.

INTRODUCTION

Intrinsic viscosity has been recognized as an important characteristic of high polymeric substances since the concept was introduced by Kraemer and van Natta (1). As reasonably satisfactory theories, which quantitatively relate the intrinsic viscosity of macromolecular solutions to molecular size, shape, and thermodynamic properties, have been proposed, viscometry has become a very useful tool in evaluating colloidal and biological substances (2). Intrinsic viscosity may be defined as:

$$\underset{\lim C\to 0}{(\eta_{sp}/C)} = \underset{\lim C\to 0}{(\eta/\eta_0 - 1)/C},$$

where η is the viscosity of the solution, η_0 is the viscosity of the solvent, C is the concentration of polymer in grams per 100 ml. of solution, and η_{sp} is the specific viscosity (3). If η_{sp}/C is plotted versus C, a curve is obtained which approaches linearity at low concentrations. The limiting value of this curve at zero concentration is the intrinsic viscosity of the high polymer.

Fontaine (4) recently reviewed the characterization of cottonseed proteins as to type, amino acid content, solubility phenomena, and color, and the methods of preparation for industrial uses. A knowledge of some of the physical chemical properties of the cottonseed globulins, such as shape characteristics of the globulin molecules in solution, would also be important to the development of their protein technology in adapting them for making synthetic fibers and adhesives. The purpose of this report is to present data on the viscosity of dilute cottonseed globulin solutions and to propose some interpretations of these data.

---

[1] One of the laboratories of the Bureau of Agricultural and Industrial Chemistry, Agricultural Research Administration, United States Department of Agriculture.

EXPERIMENTAL

The cottonseed globulin was peptized from solvent-extracted (commercial hexane) and unheated cottonseed meal by suspending the meal in a 0.5 *M* sodium chloride solution at 25°C. in a 1:10 weight ratio and stirring for 3 hr. The extract solution was clarified by supercentrifuging and then was poured into cellophane sacks and dialyzed against running distilled water at 4°C. (5). The globulin which precipitated from the salt-free solution, was washed several times with water, and finally dried by means of lyophilization (6). The globulin analyzed on a moisture-free basis: 18.06% N, 1.57% ash, 0.50% P, and 0.009% Cl. The low chloride content indicates the efficiency of the dialysis. If the phosphorus content of phytic acid-protein component is calculated as P_2O_5, about 75% of the ash content is explained.

The cottonseed globulin used is the fraction defined by D. Breese Jones and F. A. Csonka in their poineer work with this vegetable protein (5).

The viscosities were measured in Cannon-Fenske (7) or modified Ostwald-type viscometers, American Society of Testing Materials (ASTM) designation D-445. The viscometers were calibrated with distilled water, and only those were selected which had a kinetic energy correction less than 0.2%. All of the viscosities were determined at 25 ± 0.02°C.

The globulin concentration of the solutions was measured by dialyzing portions of the solutions to remove the non-protein constituents and then by determining the nitrogen content of these aliquots by means of the macro-Kjeldahl method.

The globulin solutions were prepared by dissolving the protein in the solvents. After thoroughly mixing, the solutions were then clarified and equilibrated for about 3 hr. after which very little change in the absolute viscosities of the globulin solutions was observed.

The use of urea solution as the solvent was based on two reasons: (*a*) to obtain minimum association of the protein molecules in solution and (*b*) to obtain as nearly as possible a maximum unfolding or denaturation of the protein molecules in solution for purposes of uniformity (8). Several concentrations of urea were used to demonstrate the effect on the intrinsic viscosity of the protein.

Experimental techniques and interpretations used in this paper are similar to those used by other investigators, such as Neurath and Saum (9), who investigated the viscosity increment of serum albumin in water and in urea solutions of varying concentrations by means of the Ostwald viscometer. The Simha equation, initially developed for Couette-type flow, was also applied by these authors to the interpretation of viscosity data obtained by means of capillary-flow instruments.

RESULTS

The relations between the viscosity of cottonseed globulin in urea solutions are shown in Table I and Fig. 1. The effect of the concentration

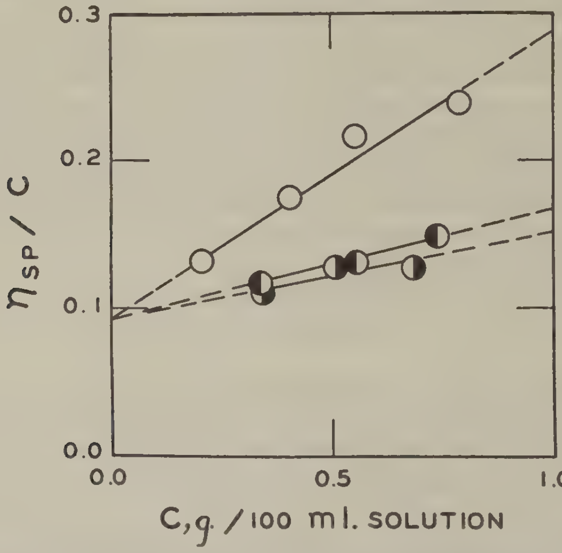

FIG. 1. Relation between η_{sp}/C and C of cottonseed globulin in urea solutions. ○, 5.25 *M* urea; ◐, 3.15 *M* urea; ◑, 1.58 urea.

TABLE I

Viscosity Characteristics of Cottonseed Globulins in Urea Solutions at 25°C.[a,b]

Solvent (urea) *M*	η_r	η_{sp}/C	$[\eta]$	k
5.25	1.095	0.19	0.093	0.195
3.15	1.065	0.13	0.093	0.075
1.58	1.060	0.12	0.093	0.060

[a] $\eta_r = \eta/\eta_0$ = relative viscosity of 0.5% globulin solutions in urea at pH 8.7; $[\eta]$ = intrinsic viscosity; k = slope of η_{sp}/C vs. C curve.

[b] $[\eta]$ of casein in 5.25 *M* urea at pH 8.7 was found to be 0.275.

of the urea solution on the viscosity was to increase the slope of the η_{sp}/C vs. C curve as the urea concentration increased. The intercepts of the curves at zero concentration of globulin are about the same for all urea solutions used and are believed to be a function of the axial ratio of the dispersed particles.

The viscosity increment of the globulin solutions was calculated using the relationship

$$\frac{[\eta]}{\gamma} = \frac{V}{100},$$

where $[\eta]$ is the intrinsic viscosity, V is the partial specific volume of the globulin [for proteins usually 0.75 ± 0.03, see Ref. (8)], and γ is the viscosity increment. Neglecting solvation effects, the viscosity increment of the globulin was calculated to be 12.3. The axial ratio of the globulin was evaluated by means of the Simha equation (10) and the calculated viscosity increment. Comparisons of this value and the ratios for other vegetable proteins reported in the literature are made in Table II.

TABLE II

Comparisons of the Axial Ratio (a/b) of Cottonseed Globulin Macromolecules with Other Vegetable Proteins

Protein	a/b for elongated molecules	b/a for flattened molecules	Reference
Cottonseed globulin	9.4	16.3	
Gliadin[a]	10.5	21	(11)
Edestin[b]	8	—	(12)
Zein[b]	7	—	(13)
Secalin[a]	10	—	(14)

[a] Calculated from diffusion constants.

[b] Calculated from dielectric properties of protein solutions.

SUMMARY

The intrinsic viscosity of the globulin in urea solutions was calculated to be 0.093, equivalent to a viscosity increment of 12.3 and an axial ratio (Simha equation) of 9.4 assuming elongated macromolecules, or of 16.3 assuming flattened-disc-type macromolecules. These values are comparable with reported axial ratios of other vegetable protein macromolecules.

REFERENCES

1. KRAEMER, E. O., AND VAN NATTA, F. J., *J. Phys. Chem.* **36**, 3175–86 (1932).
2. GREEN, D. E., Currents in Biochemical Research, pp. 241–60. Interscience Publishers, Inc., New York, 1946.
3. CRAGG, L. H., *J. Colloid Sci.* **1**, 261–9 (1946).

4. Bailey, A. E., Cottonseed and Cottonseed Products, pp. 409–65. Interscience Publishers, Inc., New York, 1948.
5. Jones, D. B., and Csonka, F. A., *J. Biol. Chem.* **64**, 673–83 (1925).
6. Pomes, A. F., and Irving, G. W., Jr., *Science* **101**, 22 (1945).
7. Cannon, M. R., and Fenske, M. R., *Ind. Eng. Chem., Anal. Ed.* **10**, 297–301 (1938).
8. Cohn, E. J., and Edsall, J. T., Proteins, Amino Acids, and Peptides, pp. 506–42. Reinhold Publishing Corp., New York, 1943.
9. Neurath, H., and Saum, A. M., *J. Biol. Chem.* **128**, 347–62 (1939).
10. Simha, R., *J. Phys. Chem.* **44**, 25 (1940).
11. Polson, A., *Kolloid Z.* **88**, 51 (1939).
12. Oncley, J. L., *J. Am. Chem. Soc.* **60**, 1115–23 (1938).
13. Elliott, M. A., and Williams, J. W., *J. Am. Chem. Soc.* **61**, 718–23 (1939).
14. Andrews, A. C., *J. Am. Chem. Soc.* **62**, 942–8 (1940).

VISCOSITY, SEDIMENTATION, AND DIFFUSION OF LONG-CHAIN MOLECULES IN SOLUTION AS DETERMINED BY EXPERIMENTS ON LARGE-SCALE MODELS

Hans Kuhn

Institute of Physical Chemistry, University of Basel, Switzerland

Received March 30, 1950

INTRODUCTION

It has been suggested by Werner Kuhn (1) that long-chain molecules, such as cellulose acetate or polystyrene, when in a suitable solvent, assume the shape of a very loose coil (Fig. 1).

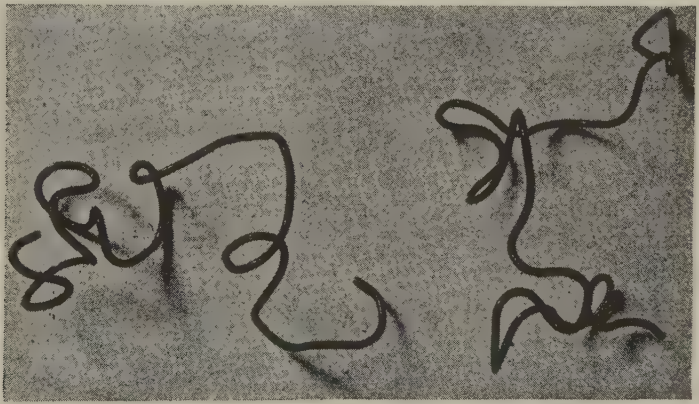

FIG. 1. Macroscopic models of a randomly coiled molecule with N_m (number of preferential statistical elements) equal to 25. These models represent geometric approximations of two probable constellations of a cellulose acetate molecule of a degree of polymerization $Z = 540$.

Many properties of the solutions of these molecules, such as the viscosity, diffusion, and sedimentation velocity, are connected with the motion of the coil or parts of the coil relative to its surrounding solvent. For a quantitative study of these properties, several approximations have been proposed to describe the hydrodynamical behavior of the coil.

W. Kuhn (1) originally had assumed that the liquid inside the coil was completely immobilized when the molecule is performing a translational motion or when the coil is brought into a liquid where there is a velocity gradient. On the basis of this assumption he found that the intrinsic viscosity η_{sp}/c of a homologous series of polymers ought to be proportional to the square root of the degree of polymerization, Z.

M. L. Huggins (2) on the other hand, by assuming that there was free draining of the solvent through the coil under these same conditions, found that the intrinsic viscosity η_{sp}/c should be proportional to the degree of polymerization, Z. This is as would be expected from Staudinger's empirical rule.

Later on it had been found by W. Kuhn and H. Kuhn (3) that the two approximations of completely hampered flow and free draining through the coil are two limiting cases and that real molecules behave somewhere between these limits. There is nearly free draining through a molecule of a moderate degree of polymerization, while an increasing amount of solvent is immobilized inside the coil if the degree of polymerization Z is increased. The intrinsic viscosity η_{sp}/c of a homologous series of unbranched long-chain molecules was thus expected to be proportional to the degree of polymerization in the region of moderate values of Z, and proportional to $\sqrt{Z}$ in the region of large values of Z. The correctness of this prediction and the validity of the derived equations for the sedimentation velocity, diffusion, and flow birefringence in the case of homologous series of polymers was shown to be in agreement with experimental data.[1,2]

In order that the intrinsic viscosity and similar quantities may be determined more accurately than was done in the 1943 paper just mentioned (here mainly the case of free draining was treated), one must assess the degree of immobilization as a function of the parameters which describe the shape of the coil.

A theoretical treatment which would specify the amount of immobilization inside a randomly coiled molecule with any degree of accuracy seems to be very difficult to evolve. The calculations of J. J. Hermans (6), H. C. Brinkman (7), P. Debye and A. M. Bueche (8, 9), and J. G. Kirkwood and J. Riseman (10) have been carried out with a number of assumptions to simplify the hydrodynamical problem involved.

A further attempt to measure the extent of immobilization of solvent inside a coil was made a few years ago when experiments on large-scale models were carried out by using a theorem of hydrodynamical similarity (11,12).[3] As these papers are not readily available, it seems appropriate to give here a short description of the translational and rotational

---

[1] See Ref. (3), especially pp. 1397 *et seq.*, 1420, 1443 *et seq.*

[2] The partial immobilization of solvent inside the coil is neglected by P. Debye (4) and H. A. Kramers (5).

[3] For an application of the results to calculations of diffusion, sedimentation, and viscosity constants in the case of solutions of branched-chain molecules, *see* KUHN, W., AND KUHN, H., *Helv. Chim. Acta* **30**, 1233 (1947).

experiments that were carried out with such models, and to repeat the conclusions to be drawn from these results concerning the sedimentation, diffusion, and viscosity of long-chain molecules in solution.

It has to be pointed out that the experiments on models are based on the hypothesis that hydrodynamics can still be used to describe the behavior of chain molecules in solution. Such a description is permissible as long as the free passages through the coil (*i.e.*, the channels through which the solvent moves in a translational or rotational motion of the particle) are large compared to the molecules of the solvent, and as long as the thickness of the molecular chain is approximately equal to or larger than the diameter of the solvent molecules. These two conditions are fulfilled in most actual cases. They are not fulfilled when the degree of polymerization is very low; in such cases there occur marked deviations of the experimental data from the results given by the hydrodynamical picture. This has been demonstrated by J. J. Hermans (13), W. Kuhn (14), and others.

1. External Dimensions of a Randomly Coiled Molecule

Construction of Large-Scale Models

The hydrodynamic properties are dependent primarily on the total volume of the coil and it will therefore be useful to know some average values of its outside dimensions such as, *e.g.*, the average diameter.

a) *End-to-end Distance h.*—Eyring (15) was the first to calculate the average of the square of the distance h (Fig. 2*b*) between the two ends of a randomly coiled molecule but for a rather special case. He assumed that the chain was composed of links of length l, bound together with a given valence angle $180° - \beta$ (Fig. 2*c*), but such that there was otherwise completely free rotation about the chain bonds. The average of the square of the distance h between the end points of the chain is then given by the expression

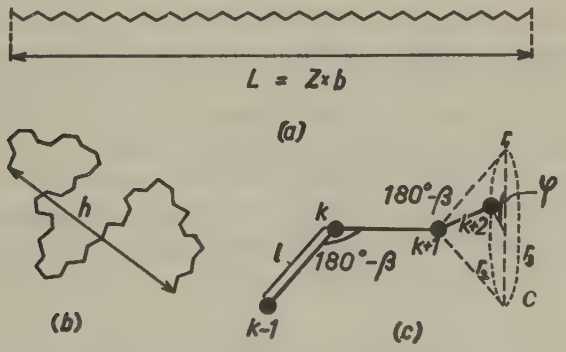

FIG. 2.

$$\overline{h^2} = L\left(l\,\frac{\cos\beta/2}{\sin^2\beta/2}\right) \quad (\text{for } Z \gg 1). \qquad [1]$$

Here L is the so-called hydrodynamic length, *i.e.*, the fully extended length of the chain (Fig. 2*a*), as can be obtained without distortion of valence angles or atomic distances. Obviously then

$$L = Z \cdot b, \qquad [2]$$

where b is the hydrodynamic length of the monomer residue, *i.e.*, its length in the direction of the extended zigzag chain. (In the simple case considered here $b = l \cos \beta/2$.)

In actual molecules there never is completely free rotation about valence bonds. On the contrary, rotation is very strongly restricted due to the steric and energetic influences of the chain substituents. Therefore, not every point on the circle C (Fig. 2*c*) is an equally probable position for atom number $k + 2$. (In the case of hydrocarbons, the regions r_1, r_2, and r_3 on this circle—corresponding to a staggered arrangement of the substituents of C-atoms number k and $k + 1$—are preferred.) In this case of restricted bond rotation, the average of the square of the distance h is found to be equal to (12,16,17,18)

$$\overline{h^2} = L\left[l \frac{\cos \beta/2}{\sin^2 \beta/2}\left(1 + \frac{2\,\overline{\cos \varphi}}{1 - \overline{\cos \varphi}}\right)\right] \quad (\text{for } Z \gg 1), \qquad [3]$$

where

$$\overline{\cos \varphi} = \int_0^{2\pi} W(\varphi) \cos \varphi d\varphi. \qquad [3a]$$

φ is the angle of rotation (angle between the two planes containing the centers of atoms number $k - 1$, k, $k + 1$, and k, $k + 1$, $k + 2$, respectively; see Fig. 2*c*), and $W(\varphi)$ represents the probability that the angle of rotation about a chain bond lies between φ and $\varphi + d\varphi$. Equation [3, 3*a*] is valid for arbitrary but even functions $W(\varphi)$.

There is not much known about the steric and energetic influence of the neighboring parts of the chain in actual molecules, so that $W(\varphi)$ must remain undefined in practical cases. Let us in these cases put (3)

$$\overline{h^2} = LA_m, \qquad [4]$$

where A_m is a constant which corresponds to the terms in brackets in Eq. [3] and which has a characteristic value in the case of each homologous series of polymers.

In the case of cellulose acetate, $A_m = 110 \times 10^{-8}$ cm. (3,12), a value found from sedimentation velocity and viscosity (see sections 2 and 4 following). X-ray data show that the hydrodynamic length of the monomer unit, b, is equal to 5.15×10^{-8} cm.; hence, according to Eq. [2], the hydrodynamic length of a cellulose acetate molecule of a degree of polymerization $Z = 1000$ is equal to 5.15×10^{-5} cm., and the average of the end-to-end distance $\sqrt{\overline{h^2}}$, according to Eq. [4], is equal to

$$\sqrt{5.15 \times 10^{-5} \times 110 \times 10^{-8}} = 7 \times 10^{-6} \text{ cm.},$$

i.e., equal to one-seventh of the hydrodynamic length.

b) External Dimensions of the Coil (19,20).—The external dimensions of the coil are quite obviously connected with the end-to-end distance h. It has been shown that the average diameter $\bar{X}$ of the coil, *i.e.*, the average of the maximum extension X of the coil in an arbitrary direction (Fig. 3)

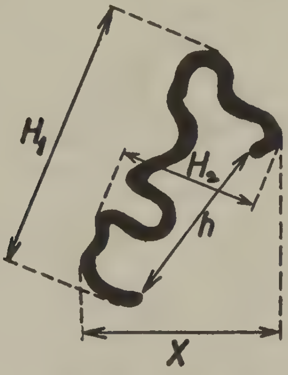

FIG. 3.

is equal to

$$\bar{X} = 0.92\sqrt{\overline{h^2}} = 0.92\sqrt{LA_m}. \qquad [5]$$

The coil can thus be described in very rough approximation as a sphere of diameter $\bar{X}$ and volume

$$V = \frac{4\pi}{3}\left(\frac{\bar{X}}{2}\right)^3 = 0.41(LA_m)^{\frac{3}{2}}. \qquad [6]$$

For a better approximation, the maximum coil diameter H_1 and the cross-sectional diameter H_2 (Fig. 3) should be known. H_1 is obviously larger than or equal to h; the average of this parameter is found to be equal to

$$\overline{H}_1 \cong 1.4\sqrt{\overline{h^2}} = 1.4\sqrt{LA_m}. \qquad [7]$$

The average cross-sectional dimension, *i.e.*, the average diameter of the coil perpendicular to H_1, is equal to

$$\overline{H}_2 \cong 0.5\overline{H}_1 \cong 0.7\sqrt{LA_m}. \qquad [8]$$

c) Preferential Statistical Element.—The constant A_m in Eq. [4] is a parameter which is independent of the degree of polymerization. It has an interesting significance (3). Let us consider a chain molecule which may assume its unlikely stretched form (Fig. 4*a*) or any coiled shape (Fig. 4*b*). Let us now compare it with a model, consisting of a number

$$N_m = L/A_m \qquad [9]$$

of segments of length A_m (so-called preferential statistical elements), which are connected together in a chain (Fig. 4), and let us assume that

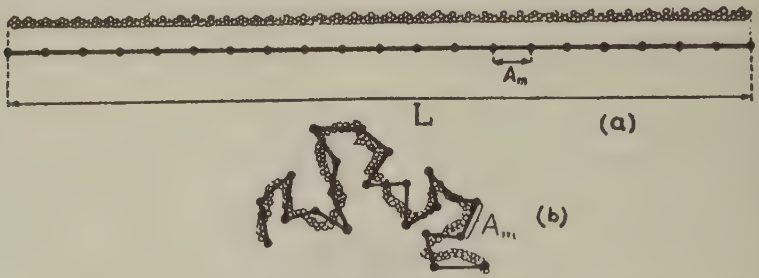

FIG. 4. Chain molecule and corresponding model consisting of N_m preferential statistical elements of length A_m. *a*) In its unlikely stretched shape. *b*) In a coiled shape.

each segment can be oriented in an arbitrary direction; *i.e.*, the orientation of a given statistical element will be independent of the orientation of neighboring elements. This model, consisting of a number N_m of preferential statistical elements of length A_m, has the same total chain length L as the corresponding molecule. Furthermore, the square average of the end-to-end distance h of this model and of the corresponding molecule are the same, and corresponding shapes of the model and of the molecule (see Fig. 4) have the same relative probability.

d) *Construction of Large-scale Models* (12).—With this picture as a basis, large-scale models can be constructed which ought to be good geometric approximations of chain molecules. Such a model can be formed from a piece of wire of circular cross section, which has the same hydrodynamic length L and the same average thickness d_h (hydrodynamic thickness) as the corresponding molecular chain but multiplied with a certain scale factor. The wire is divided into N_m equal sections of length A_m (times scale factor), and is bent between each of these sections through an arbitrary angle. In order to do this bending process in a really random manner, we take a sphere marked with a dot, and roll it first quite arbitrarily on a level surface and then suddenly arrest it. We then bend the wire so that the new direction of the axis of the wire is given by the direction of that diameter of the sphere which passes through the mark.

In Fig. 1 are shown models obtained in this way, corresponding to two probable constellations of a molecule with $N_m = 25$ preferential elements. They correspond to a cellulose acetate molecule of a degree of polymerization $Z = 540$ when in acetone solution.

The models shown in Fig. 1 and those which have been used for the experiments described below have been constructed in a somewhat improved manner which differs slightly from that described above.

As before, the model of a molecule characterized by the parameters L, A_m, and d_h was made from a piece of wire of the same hydrodynamic length L and the same thickness d_h as the molecule (multiplied by a certain scale factor). The wire is now however divided into $N_\sigma = 0.76 \times N_m$ (instead of N_m) equal sections of length $A_\sigma = (1/0.76) \times A_m$ (instead of A_m). Each section is bent in the form of segment of a circle which can be less than or equal to a semicircle. The directions of the wire at the beginning and end of each segment are chosen by the use of a marked sphere in the arbitrary manner described above.

It can be shown (12) that the models thus obtained consisting of N_σ so-called statistical circle-segments of length A_σ have the same root mean square end-to-end distance as the corresponding models consisting of N_m preferential statistical elements of length A_m. The models consisting of circle-segments are, however, easier to construct than the models consisting of preferential elements, and are also somewhat better approximations to the corresponding molecules. [For details, see Ref. (12).]

2. Translational Resistance of Long-Chain Molecules, Diffusion, and Sedimentation Constant

a) *Frictional Force as Determined by Experiments on Models*

Let a chain molecule carry out a translational motion through a viscous liquid. The frictional force F_{coil} thus produced is proportional to the velocity u, to the viscosity η_0 of the solvent, and to any selected linear dimension of the coil, such as, *e.g.*, its hydrodynamic length L. We can thus set up (3) the equation

$$F_{\text{coil}} = \lambda_{\text{trans}} \eta_0 L u, \qquad [10]$$

where λ_{trans} is a numerical factor, depending on the shape of the molecule and thus on the degree of immobilization of solvent inside the coil.

Its value can be estimated in the two limiting cases mentioned in the introduction. In the case of free draining, λ_{trans} is independent of the length L, and, according to W. Kuhn (21), approximately equals $3\pi/2$. In the case of complete immobilization, the resistance F_{coil} is approximately equal to the resistance of a sphere of diameter $\bar{X}$, *i.e.*, according to Stokes' law, equal to

$$F_{\text{coil}} = 6\pi\eta_0\bar{X}u \text{ (estimated for large values of } N_m\text{).} \qquad [11]$$

From Eqs. [10], [11], and [5], it follows that $\lambda_{\text{trans}} = \dfrac{8.7}{\sqrt{N_m}}$.

In the general case of partial immobilization of the solvent inside the coil, λ_{trans} will be dependent on the parameters that characterize the shape of the coil, *i.e.*, the number N_m of preferential elements and the ratio A_m/d_h, A_m being the length of a statistical element and d_h the thickness of the chain.

The dependence of λ_{trans} on these parameters has been determined experimentally with large-scale models (11,12). For given values of N_m and A_m/d_h, a number of models were made as described in the last section. The frictional factor λ_{trans} of these models was determined by measuring the sedimentation velocity of the models in a viscous liquid. From the dimensions and the weight of the models and the viscosity of the solvent, λ_{trans} was calculated on the basis of Eq. [10].[4] The sedimentation velocity was found to be somewhat dependent on the orientation of the coil axis with respect to the direction of motion, and differences of 10–20% between the sedimentation velocities of different models with the same values of N_m and A_m/d_h have been found. By averaging the values of the frictional factors thus obtained, we first found a value of λ_{trans} for one set of values of the parameters N_m and A_m/d_h. Experiments on a number of models with various values of N_m and A_m/d_h showed that λ_{trans} is approximately given by the following equation:

$$\lambda_{\text{trans}} = (0.16 \log_{10}(A_m/d_h) + 0.02 + 0.1\sqrt{N_m})^{-1}. \qquad [12]$$

Therefore, according to [10],

$$F_{\text{coil}} = \frac{\eta_0 L u}{0.16 \log_{10}(A_m/d_h) + 0.02 + 0.1\sqrt{N_m}}. \qquad [13]$$

(Translational resistance of random coil)

For large values of N_m (complete immobilization), we find from [12] that $\lambda_{\text{trans}} = \frac{10}{\sqrt{N_m}}$; this is close to the value $\frac{8.7}{\sqrt{N_m}}$ which (see above) has been estimated for this case.

It is of interest to compare [13] with recently published expressions by Debye and Bueche (8) and by Kirkwood and Riseman (10), namely

$$F_{\text{coil}} = \eta_0 L u \left[\frac{9.94}{\sqrt{N_m}} \frac{1 - \frac{1}{\sigma}\tanh\sigma}{1 + \frac{3}{2\sigma^2}\left(1 - \frac{1}{\sigma}\tanh\sigma\right)} \right] \qquad [14]$$

(Debye and Bueche)

and

$$F_{\text{coil}} = \frac{\eta_0 L u}{(b\eta_0/\zeta) + 0.195\sqrt{N_m}}. \qquad [15]$$

(Kirkwood and Riseman)

η_0, L, u, b, and N_m have been defined above, and σ and ζ are adjustable constants.

The term σ in Debye and Bueche's expression (the so-called shielding ratio) measures the amount of immobilization of solvent inside the coil; $\sigma = 0$ corresponds to the case of free draining, and $\sigma = \infty$ to the case of complete immobilization.

---

[4] From the laws of hydrodynamics it can be deduced that Eq. [10] is valid only on condition that Reynolds's number $\rho_0 u\bar{X}/(5\eta_0)$ is small compared with unity ($\bar{X}$ is the average diameter of the model and ρ_0 the density of the liquid). This was used to find the appropriate experimental conditions.

The term ζ in Kirkwood and Riseman's equation is a friction factor of the monomer and is supposed to be constant in a homologous series of polymers. Thus, according to Eq. [15], $1/F_{\text{coil}}$ is a linear function of $\sqrt{N_m}$, exactly as is seen from [13].

The adjustable constants σ and ζ disappear in the case of large values of the degree of polymerization (complete immobilization), and it follows from Debye and Bueche's expression that $F_{\text{coil}} = (9.94/\sqrt{N_m})\eta_0 Lu$, and from Kirkwood and Riseman's equation that $F_{\text{coil}} = (5.1/\sqrt{N_m})\eta_0 Lu$, while Eq. [13] gives $F_{\text{coil}} = (10/\sqrt{N_m})\eta_0 Lu$. Thus, in this case, Debye and Bueche's expression is very nearly equal to our expression, while Kirkwood and Riseman's result differs from ours by a factor of 0.51.

b) *Sedimentation and Diffusion Constant of a Random Coil*

From Eq. [13] and taking [2] and [9] into consideration, we can easily obtain the following expressions for the sedimentation constant s_0 and the diffusion constant D:

$$s_0 = a_1 + b_1\sqrt{Z}, \qquad [16]$$

$$D = (a_2 + b_2\sqrt{Z})Z^{-1}, \qquad [17]$$

where

$$a_1 = \frac{M_g}{N_A b}\frac{1 - v_{\text{part}}\rho_0}{\eta_0}\left(0.02 + 0.16 \log_{10}\frac{A_m}{d_h}\right), \qquad [16a]$$

$$b_1 = \frac{M_g}{N_A b}\frac{1 - v_{\text{part}}\rho_0}{\eta_0}0.1\sqrt{\frac{b}{A_m}}, \qquad [16b]$$

$$a_2 = \frac{kT}{\eta_0 b}\left(0.02 + 0.16 \log_{10}\frac{A_m}{d_h}\right), \qquad [17a]$$

$$b_2 = \frac{kT}{\eta_0 b}0.1\sqrt{\frac{b}{A_m}}, \qquad [17b]$$

and are independent of the degree of polymerization Z. N_A is Avogadro's number per mole, M_g the molecular weight of the monomer, v_{part} the partial specific volume of the solute, ρ_0 the density of the solvent, k Boltzmann's constant, T the absolute temperature, and b, as mentioned in Sec. 1, the hydrodynamic length of the monomer.

The dependence of s_0 and D on Z, as given by Eqs. [16] and [17], has been observed in actual experiments on nitrocellulose, methylcellulose, and cellulose acetate.[5] By introducing the values of the constants a_1, b_1, or a_2, b_2 found from such experiments into [16a] [16b] [17a] [17b], the parameters A_m and d_h can be determined, because all other parameters in these equations are known from the experimental conditions.

In Fig. 5 the sedimentation constant, s_0, is plotted against the square root of the degree of polymerization, Z, for the particular case of cellulose acetate in acetone. The experimental points taken from measurements by Kraemer and Nichols (22) are nearly on a straight line, as is to be expected from Eq. [16]. Measuring the y-intercept and the slope of that straight line, and using the values $M_g = 240$, $b = 5.15 \times 10^{-8}$ cm., and $v_{\text{part}} = 0.68$, it follows from [16*a*] and [16*b*] that $A_m = 110 \times 10^{-8}$ cm., and $d_h = 11 \times 10^{-8}$ cm. The latter value can be compared with the average diameter d_t of the molecular chain as determined from structural molecular data. Here one finds that; $d_t \cong 7 \times 10^{-8}$ cm. *The approximate agreement of the hydrodynamic thickness d_h and of the true thickness d_t of the coil is remarkable, and it justifies our assumption that hydrodynamics is applicable and can be used to describe the behavior of these molecules.*

---

[5] Measurements by Mosimann, Kraemer, and Nichols and by Polson [*see* Ref. (12)].

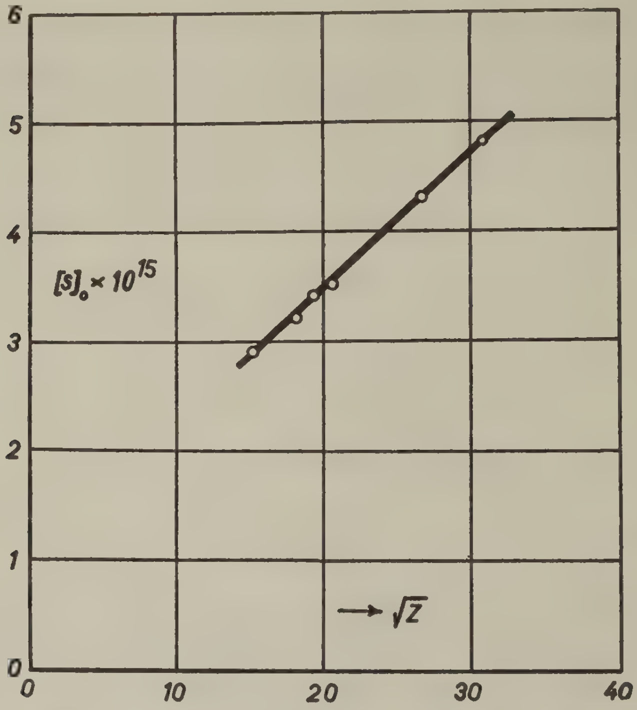

FIG. 5. Ordinate: intrinsic sedimentation constant $[s]_0$ [*i.e.*, sedimentation constant s_0 times the factor $\eta_0 v_{\text{part}}/(1 - v_{\text{part}}\rho_0)$]. Abscissa: $\sqrt{Z}$ (Z is the degree of polymerization). The points marked by circles correspond to measurements by Kraemer and Nichols. They are on the straight line expected from Eq. [16].

This fact requires particular emphasis because the application of hydrodynamics to the macromolecular region has been doubted by several authors. Thus Sadron (23) is of the opinion that the degree of draining of the coil should be smaller than that obtained by the use of hydrodynamics. On the other hand from the work of Kirkwood and Riseman (10) and Newman, Riseman, and Eirich (24) an increased degree of draining has to be inferred in that they use for their friction factor ζ values which are about ten times smaller than those expected on the basis of hydrodynamics. It has however been pointed out[6] that the experimental results of these authors can be interpreted just as satisfactorily by using larger values of ζ which are in agreement with hydrodynamics.

3. Rotational Resistance of Long-Chain Molecules

The frictional resistance of a random coil in the process of rotation around its center of gravity has also been studied by experiments on large-scale models (11,12). It has been found from such experiments that the frictional moment M_{coil}, which occurs when rotating a coil with an angular velocity $\varphi^{\cdot}$ around the axis, which is perpendicular to the largest coil diameter H_1 and intersects H_1 in its center (see Fig. 6*a*), is, on the average, given by the expression

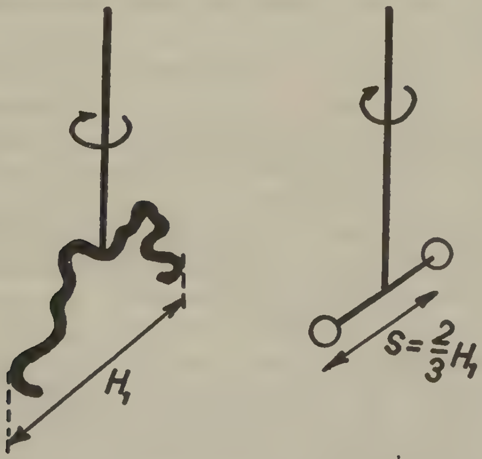

FIG. 6. Coil and corresponding dumbbell, which produce the same frictional couple by rotating around the axis shown.

$$M_{\text{coil}} = \frac{3.2}{-1.3 + 3.2\log_{10}(A_m/d_h) + \sqrt{N_m}}\,\eta_0 L^2 A_m \varphi^{\cdot}. \qquad [18]$$

The over-all average friction moment which occurs by rotating about an axis, which is oriented arbitrarily relative to H_1, is approximately equal to

$$m_{\text{coil}} = (3/4)M_{\text{coil}}. \qquad [18a]$$

---

[6] Discussion remark by H. Kuhn. [*See* Ref. (24), p. 388.]

As was to be expected from our introductory remarks, one finds in the two limiting cases of large and small values of N_m that this equation reduces to expressions similar to those derived theoretically in each of the two cases of complete immobilization and free draining. For instance, where the values of N_m are large it can be shown that the rotational resistance m_{coil} defined above is about the same as that of an equally large compact sphere, *i.e.*, a sphere of diameter $\bar{X}$ as given in Eq. [5]. According to Kirchhoff's law we find this resistance to be equal to $\pi\bar{X}^3\eta_0\varphi\cdot$. Substituting from [5] this gives $\pi(0.92\sqrt{LA_m})^3\eta_0\varphi\cdot = 2.5\eta_0L^{3/2}A_m^{3/2}\varphi\cdot$. In satisfactory agreement with this we find from Eq. [18*a*] by putting $N_m \gg 1$ the result $m_{\text{coil}} = \frac{3}{4}\eta_0L^2A_m\varphi\cdot/(0.31\sqrt{N_m}) = 2.4\eta_0L^{3/2}A_m^{3/2}\varphi\cdot$.

The resistance M_{coil} in this case of complete immobilization is expected to be about the same as that of an elongated ellipsoid of revolution with long axis $\bar{H}_1$ and short axis $\bar{H}_2$, when rotating about an axis perpendicular to $\bar{H}_1$. This resistance turns out (25)to be equal to $3.4\eta_0L^{3/2}A_m^{3/2}\varphi\cdot$; from Eq. [18] we find in good agreement with this result that $M_{\text{coil}} = 3.2\eta_0L^{3/2}A_m^{3/2}\varphi\cdot$.

Kirkwood and Riseman (10) recently have calculated the average rotational resistance m_{coil} of a chain molecule. Their equation in the case of the complete immobilization under discussion yields the result $m_{\text{coil}} = 1.2\eta_0L^{3/2}A_m^{3/2}\varphi\cdot$, which is considerably smaller than the above result $2.4\eta_0L^{3/2}A_m^{3/2}\varphi\cdot$ found from experiments on models.

4. INTRINSIC VISCOSITY OF SOLUTIONS OF CHAIN MOLECULES

The hydrodynamic behavior of long-chain molecules in a solution with velocity gradient has been treated in a series of papers by W. Kuhn and H. Kuhn (3,25,26). It has been shown that in a liquid with a velocity gradient, the motion of a coil relative to the surrounding solvent results from a competition between the hydrodynamical forces which tend to orient the axes of the coils and the thermal agitation which tends to achieve a homogeneous angular distribution of these axes. This motion of the coil relative to the solvent, which determines the viscosity of the solution, is determined to a large extent by the rotational diffusion constant and thus by the rotational resistance [18] of the coil.[7] A coil and any other particle which offers the same rotational resistance as the coil will thus produce approximately the same contribution to the viscosity. In a theoretical treatment of the intrinsic viscosity of solutions of chain molecules we can thus, for instance, replace the coils by dumbbells of the same dimensions as the coils.[8] (See Fig. 6.)

[7] This fact first mentioned in Ref. (3) has been recognized recently also by Kirkwood and Riseman (10). These authors find the following relation between Kraemer's intrinsic viscosity $[\eta]$ and over-all average rotational diffusion constant $d_{\text{rot}} = kT/(m_{\text{coil}}/\varphi\cdot)$,

$$[\eta] = (kTN_A)/(2 \times 10^2 M_g Z \eta_0 d_{\text{rot}}).$$

According to the results presented here and in earlier papers by W. Kuhn and H. Kuhn, the relation exists

$$[\eta] = (kTN_A)/(4.5 \times 10^2 M_g Z \eta_0 d_{\text{rot}}),$$

which differs from Kirkwood and Riseman's expression by a factor of 2.25.

[8] In Ref. (25) we have treated the intrinsic viscosity not only on the basis of a simple dumbbell, but also by using more satisfactory two- and three-dimensional models.

Let the distance S between the centers of the two spheres of the dumbbell be equal to

$$S = \frac{2}{3}\overline{H_1}, \qquad [19]$$

where $\overline{H_1}$ as mentioned before is the average of the largest diameter of the corresponding coil. The radius r of each of these spheres then has to be chosen in such a way, that the dumbbell, when rotating about the axis shown in Fig. 6*b*, offers the same resistance as the coil when rotating about the axis of Fig. 6*a*. The resistance couple acting on the dumbbell is easily found to be equal to

$$M_{\text{dumbbell}} = 2 \times 6\pi\eta_0 r \left(\frac{S}{2}\right)^2 \dot{\varphi}, \qquad [20]$$

while the corresponding resistance of the coil is given by Eq. [18]. By equating [18] and [20] and taking [7] and [19] into account, we obtain the following expression for the radius r:

$$r = \frac{0.39}{-1.3 + 3.2\log_{10}(A_m/d_h) + \sqrt{N_m}} \times L. \qquad [21]$$

The specific viscosity $\eta_{sp} = \dfrac{\eta - \eta_0}{\eta_0}$ of a dilute solution of dumbbells, according to W. Kuhn and H. Kuhn (27), equals[9]

$$\eta_{sp} = (\pi/2)GS^2r, \qquad [22]$$

where G is the number of particles/cc. The viscosity of a solution of chain molecules is found by introducing [19] and [21] in [22]. If in the resulting equation we substitute for the number G in terms of the concentration c of chain molecules in base moles/l., the molecular weight M_g of the monomer and the degree of polymerization Z, we obtain[10]

It was shown that such models lead to practically the same results as the simple dumbbell, which is as the above statement would lead us to expect.

[9] Equation [22] has been obtained under consideration of the influence of thermal rotatory motion of the particle. This influence of Brownian motion had been considered later by Kirkwood and Riseman (10) in a very different yet equivalent manner. (Compare with Brinkman, H. C., Hermans, J. J., Polder, D., and co-workers, Proceedings of the International Rheological Congress, Holland, 1948.)

[10] The Staudinger viscosity index $(\eta_{sp}/c)_{\lim c=0}$ in which the concentration is expressed in base moles per liter is related to Kraemer's definition of intrinsic viscosity $[\eta] = (\eta_{sp}/c'_{\text{g./100 ml.}})_{\lim c'=0}$ and to the intrinsic viscosity J where concentration is expressed in g./ml. by the following formula:

$$J = 100[\eta] = \frac{10^3}{M_g}\left(\frac{\eta_{sp}}{c}\right)_{\lim c=0}.$$

(25,28):

$$\left(\frac{\eta_{sp}}{c}\right)_{\lim\, c=0} = \frac{0.53}{-1.3 + 3.2 \log_{10}(A_m/d_h) + \sqrt{bZ/A_m}} \frac{A_m b^2 N_A}{10^3} \times Z \quad [23]$$

In Fig. 7, η_{sp}/c is plotted against the degree of polymerization Z in the case of cellulose acetate in acetone. Curve 1 shown in this figure represents η_{sp}/c as calculated from Eq. [23] for the case $A_m = 110 \times 10^{-8}$ cm., $d_h = 11 \times 10^{-8}$ cm., $b = 5.15 \times 10^{-8}$ cm., *i.e.*, for values of A_m and d_h obtained from the sedimentation measurements mentioned in Sec. 2*b*, and for the value of b as found from x-ray data. The points marked by circles represent measurements by Sookne and Harris (29) of the intrinsic viscosity of cellulose acetate in acetone. The measurements are in good agreement with the theory.

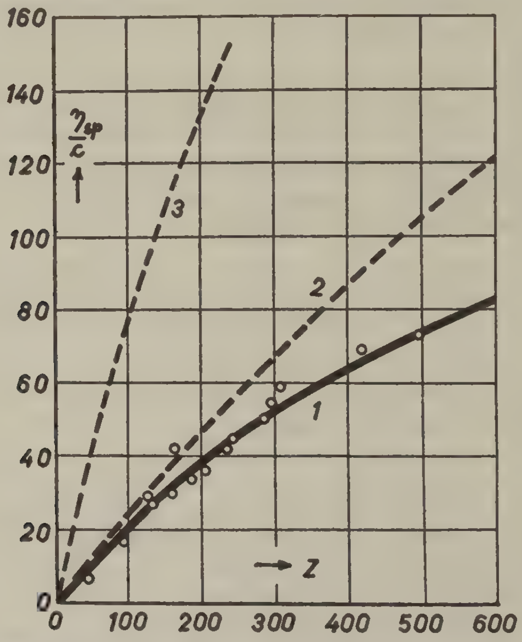

FIG. 7. Intrinsic viscosity $(\eta_{sp}/c)_{\lim\, c=0}$ of cellulose acetate in acetone plotted against the degree of polymerization Z. *Curve 1:* Theoretical curve according to Eq. [23] for $A_m = 110 \times 10^{-8}$ cm., $d_h = 11 \times 10^{-8}$ cm., and $b = 5.15 \times 10^{-8}$ cm. The values of A_m (length of the preferential statistical element) and d_h (hydrodynamical thickness of the chain) are those found from the sedimentation velocity of cellulose acetate, the value of b [see Eq. (2)] is found from x-ray data. *Curve 2 and Curve 3:* Theoretical curves resulting from the theories of Debye and Bueche and of Kirkwood and Riseman, also obtained by using the observed data of the sedimentation constant. *Points marked by circles:* Measurements by Sookne and Harris.

The dotted lines 2 and 3 result from the theories of Debye and Bueche (8) and Kirkwood and Riseman (10), respectively. Here also η_{sp}/c was calculated from the experimental values of the sedimentation constant as given by Kraemer and Nichols (22).

Debye and Bueche's expression for η_{sp}/c is as follows:

$$\left(\frac{\eta_{sp}}{c}\right)_{\lim c=0} = 1.52\,\frac{N_A b^{3/2} A_m{}^{3/2} Z^{1/2}}{10^3} \times \frac{1 + \dfrac{3}{\sigma^2} - \dfrac{3}{\sigma}\coth\sigma}{1 + \dfrac{10}{\sigma^2}\left(1 + \dfrac{3}{\sigma^2} - \dfrac{3}{\sigma}\coth\sigma\right)}. \qquad [24]$$

(Debye and Bueche)

The two parameters A_m and σ can be determined from the observed values of the sedimentation constant by using Debye and Bueche's equation [14]. In the case of high degrees of polymerization we obtain $A_m = 110 \times 10^{-8}$ cm.[11] From the sedimentation constants observed for $Z = 100$, 300, and 900, we find on the basis of Eq. [14] that $\sigma = 2.6$, 3.7, and 5.4, respectively. By introducing these values in [24], curve 2 in Fig. 7 is obtained.

Kirkwood and Riseman's equation for the intrinsic viscosity is as follows:

$$\left(\frac{\eta_{sp}}{c}\right)_{\lim c=0} = \frac{\zeta/\eta_0}{36}\,F\left(\frac{Z^{1/2}\zeta/\eta_0}{(A_m b \times 6\pi^3)^{1/2}}\right) \times \frac{A_m b N_A}{10^3} \times Z$$

$$F(X) = \frac{6}{\pi^2}\sum_{k=1}^{\infty}\frac{1}{k^2}\,\frac{1}{1 + X/(k)^{1/2}}. \qquad [25]$$

(Kirkwood and Riseman)

On the basis of Kirkwood and Riseman's Eq. [15] for the translational resistance, we easily find from Kraemer and Nichols measurements that $A_m = 405 \times 10^{-8}$cm.[12] $\zeta/\eta_0 = 29 \times 10^{-8}$cm. By introducing these values in [25] we obtain curve 3 in Fig. 7.

It is of interest to compare the expressions which follow from [23], [24], and [25], respectively, in the case of complete immobilization. Our Eq. [23] transforms in that case to the equation $(\eta_{sp}/c) = (0.53/10^3)N_A b^{3/2} A_m{}^{3/2} Z^{1/2}$. Debye and Bueche's expression gives $(\eta_{sp}/c) = (1.52/10^3)N_A b^{3/2} A_m{}^{3/2} Z^{1/2}$, and Kirkwood and Riseman's equation leads to the expression $(\eta_{sp}/c) = (0.60/10^3)N_A b^{3/2} A_m{}^{3/2} Z^{1/2}$. It is seen that Debye and Bueche's expression differs from ours by a factor of 3 while Kirkwood and Riseman's expression is nearly identical with ours in this case.

It has been found (30) from light-scattering data that the root mean square end-to-end distance $\sqrt{\overline{h^2}}$ of a polystyrene molecule of molecular weight $M = 1.1 \times 10^6$ and intrinsic viscosity $J = 195$ cc./g. is equal to 1120 Å. To find the value of $\sqrt{\overline{h^2}}$ which follows from viscosity we

[11] The same value of A_m has been found on the basis of our Eq. [13]. This has to be expected from the fact mentioned in Sec. 2 that Eq. [13] and Debye and Bueche's Eq. [14] are very nearly identical in the case of high degrees of polymerization.

[12] This value is about four times as large as the value of A_m which results from ours as well as from Debye and Bueche's equation. This has to be expected from the remarks made in section 2, where it has been shown that in the case of high degrees of polymerization Kirkwood and Riseman's Eq. [15] transforms to an equation, which differs from our corresponding equation by a factor of 0.5.

rewrite [23] using [2] and [4].

$$\left(\frac{\eta_{sp}}{c}\right)_{\lim c=0} = \frac{M_g}{10^3} J$$

$$= \frac{(\sqrt{\overline{h^2}})^3 N_A}{Z 10^3} \frac{0.53}{1 + (\sqrt{\overline{h^2}}/Zb)(-1.3 + 3.2 \log_{10}(\overline{h^2}/Zbd_h)}. \quad [26]$$

The value of $\sqrt{\overline{h^2}}$ can be determined from this equation by remembering that $M_g = 104$, $Z = M/M_g = 1.06 \times 10^4$, $N_A = 6.02 \times 10^{23}$, and by introducing a reasonable value for the parameter d_h. In this case of a very high degree of polymerization in which the solvent inside the coils is almost completely immobilized, it is clear that the value of $\sqrt{\overline{h^2}}$ cannot critically depend on an exact value of d_h, as a consideration of the above formula immediately shows. We may therefore put d_h equal to the average thickness d_t of the polystyrene chain as obtained from x-ray data, that is $d_h = d_t = 8$ Å. It follows then that $\sqrt{\overline{h^2}} = 880$ Å, a value about 25% smaller than the value found from light-scattering data. This discrepancy is not astonishing in view of the uncertainties involved in the experimental techniques.[13,14]

If we summarize the results thus obtained we can conclude that experiments on large-scale models are a conceivable approach to determine the hydrodynamical properties of randomly coiled molecules, which in turn will then determine the viscosity, sedimentation, and diffusion constants in dilute solutions.

ACKNOWLEDGMENTS

The author is grateful to Professor Werner Kuhn for many helpful discussions. He also wishes to thank Mr. Alexander Silberberg for help in the preparation of the manuscript.

SUMMARY

It is a consequence of a hydrodynamical similarity theorem that the forces acting on geometrically similar bodies under corresponding condi-

---

[13] A critical analysis of the uncertainties involved in light-scattering dissymmetry measurements is given by BLAKER, R. H., BADGER, R. M., and GILMANN, T. S., *J. Phys. Chem.* **53**, 794 (1949).

[14] Similar results are found on the basis of Debye and Bueche's (8) and Kirkwood and Riseman's (10) equations when reasonable values are assumed for their monomer friction factors f/η_0 and ζ/η_0. It does not seem likely that the frictional resistance of the monomer is either less than that of a sphere of radius 0.4 Å or larger than that of a sphere of radius 4 Å. These limits according to Stokes' law would correspond to outside values of 7.5 Å and 75 Å in the case of monomer friction factors. On this basis Debye and Bueche's treatment yields values of the root mean square distance $\sqrt{\overline{h^2}}$ which are between 640 Å and 740 Å while Kirkwood and Riseman's treatment gives the range 840 Å and 930 Å.

tions of flow are simple functions of the magnification parameter. This principle has been used to find the frictional resistance opposing translational or rotational motions of a randomly coiled molecule through a solvent by means of experiments on corresponding large-scale models. The geometrically similar models of the random coils whose translational and rotational resistance in a viscous liquid was measured were made by bending wire in a statistical manner.

Expressions for the sedimentation constant s_0, the diffusion constant D, and the intrinsic viscosity η_{sp}/c have been obtained from the results of these experiments on large-scale models, *viz.*, $s_0 = a_1 + b_1\sqrt{Z}$; $D = (a_2 + b_2\sqrt{Z})Z^{-1}$; $\eta_{sp}/c = Z(a_3 + b_3\sqrt{Z})^{-1}$. Z is the degree of polymerization and a_1, b_1, a_2, b_2, a_3, and b_3, are constants independent of Z but dependent on the length A_m of the preferential statistical chain element and the average thickness d_h of the polymer chain. These expressions are found to be in agreement with the experimental data. They have been compared with equations by Debye and Bueche and by Kirkwood and Riseman.

References

1. Kuhn, W., *Kolloid-Z.* **68**, 2 (1934).
2. Huggins, M. L., *J. Phys. Chem.* **43**, 439 (1939).
3. Kuhn, W., and Kuhn, H., *Helv. Chim. Acta* **26**, 1394 (1943).
4. Debye, P., *J. Chem. Phys.* **14**, 636 (1946).
5. Kramers, H. A., *J. Chem. Phys.* **14**, 415 (1946).
6. Hermans, J. J., *Rec. trav. chim.* **63**, 219 (1944).
7. Brinkman, H. C., *Applied Sci. Research A* **1**, 27 (1947); *Proc. Netherl. Acad. Sci. Amsterdam* **50**, 618 (1947).
8. Debye, P., and Bueche, A. M., *J. Chem. Phys.* **16**, 573 (1948).
9. Debye, P., *Phys. Rev.* **71**, 486 (1947).
10. Kirkwood, J. G., and Riseman, J., *J. Chem. Phys.* **16**, 565 (1948); *ibid.* **17**, 442 (1949).
11. Kuhn, H., *Schweiz. Chem.-Ztg.* **28**, 373 (1945) (preliminary report).
12. Kuhn, H., Habilitationsschrift, Basel, 1946. Proceedings of the International Congress on Rheology, Holland, 1948.
13. Hermans, J. J., Discussion at the International Rheological Congress, Holland, 1948.
14. Kuhn, W., *Exposé au Colloque des grosses molécules*, Paris, 1948.
15. Eyring, H., *Phys. Rev.* **39**, 746 (1932).
16. Benoit, H., Report of a lecture at the High-Polymer Conference, Strasbourg, November, 1946.
17. Kuhn, H., *J. Chem. Phys.* **15**, 843 (1947).
18. Taylor, W. J., *J. Chem. Phys.* **15**, 412 (1947); *ibid.* **16**, 257 (1948).
19. Daniels, H. E., *Proc. Cambridge Phil. Soc.* **37**, 244 (1941).
20. Kuhn, H., *Experientia*, 28 (1945); *Helv. Chim. Acta* **31**, 1677 (1948).
21. Kuhn, W., *Z. physik. Chem.* (*A*) **161**, 1 (1932).
22. Kraemer, E. O., and Nichols, J. B., in Th. Svedberg and Pedersen, K. O., Die Ultrazentrifuge, p. 392. Dresden and Leipzig, 1940.
23. Sadron, C., *J. Polymer Sci.* **3**, 812 (1948).

24. Newman, S., Riseman, J., and Eirich, F. R., Proceedings of International Colloquium on Macromolecules, Holland, 1949, D. B. Centen's Uitgevers-Maatschappij N. V. Amsterdam 1950.
25. Kuhn, H., and Kuhn, W., *J. Polymer. Sci.*, in press.
26. Kuhn, W., and Kuhn, H., *Helv. Chim. Acta* **28**, 1533 (1945); *ibid.* **29**, 71, 609, 830 (1946); *J. Colloid Sci.* **3**, 11 (1948).
27. Kuhn, W., and Kuhn, H., *Helv. Chim. Acta* **38**, 97 (1945).
28. Kuhn, W., and Kuhn, H., *Helv. Chim. Acta* **30**, 1233 (1947); Kuhn, H., Proceedings of the International Rheological Congress, Holland, 1948. *See also* Kuhn, W., and Kuhn, H., *J. Chem. Phys.* **16**, 838 (1948).
29. Sookne, A. M., and Harris, M., *Ind. Eng. Chem.* **37**, 475 (1945).
30. Kunst, E. D., Proceedings of the International Colloquium on Macromolecules, Holland, 1949, D. B. Centen's Uitgevers-Maatschappij N. V. Amsterdam 1950.

SLIDING OF DROPS FROM SURFACES OF DIFFERENT ROUGHNESSES

J. J. Bikerman

Research Laboratories, Merck and Co., Inc., Rahway, New Jersey

Received January 13, 1950; revised March 15, 1950

The effect of surface roughness on rolling friction and on wetting has been studied earlier (1,2). The present work is concerned with the effect of surface roughness on sliding of water drops.

I. Materials

As surfaces differing in roughness, those of 18-8 stainless steel plates (7 × 5 × 0.08 cm.) of six different standard finishes were used. These plates served also for the measurements already reported (1,2) so that comparison between the effects of roughness on rolling of balls, on contact angles, and on sliding of drops was possible. Table I presents, for all the six finishes studied, the code numbers; the type of treatment of finish (3); the root-mean-square elevations (h_{rms}) on two spots of each sample, determined by means of a commercial tracer instrument[1]; and the "equilibrium" contact angles θ (through water) between laboratory air, distilled water drops, and plates (2).

TABLE I

18-8 Stainless Steel Plates of Different Finishes

Code no.	Type of finish or treatment	h_{rms} μ		θ
				degrees
1	Hot rolled, annealed, and pickled	3.1	3.1	89
2*D*	Cold rolled, annealed, and pickled	0.8	1.0	81
2*B*	Produced by final light cold-rolling	0.25	0.40	91
6	Produced by brushing a No. 4 surface with a rotating brush of tampico fiber loaded with fine abrasive and oil	0.084	0.10	60
4	Polished with No. 120-grit	0.033	0.045	70
7	Polished with No. 320-grit	0.020	0.030	89

In addition, some experiments have been carried out on stainless steel specimens representing consecutive stages of polishing; these specimens were obtained through courtesy of Mr. J. J. Heger, Carnegie-Illinois Steel corporation, Pittsburgh, Pa. Sample 1 was taken from a water still; it was ground on a Thompson Model A surface grinder using 46-grit wheel to give Sample No. 2; this was sanded by hand on 320-grit, then 400-grit, then 2/0, and finally 3/0 metallographic abrasive paper (thus producing Sample Nos. 3, 4, 5, and 6, respectively), and metallographically polished on a wet "Gamal" cloth wheel using "Gamal" (γ-Al_2O_3) abrasive. This resulted in Sample No. 7 which was a good mirror.

---

[1] Determinations kindly arranged by Dr. S. S. Kistler, Norton Company, Worcester, Mass.

II. Experimental Procedure

The above-mentioned specimens were placed on a brass plate provided, at two opposite ends, with flanges which prevented the specimens from moving when the brass plate was tilted. This brass plate was screwed to a horizontal brass shaft which could freely rotate within a brass sleeve, thus causing tilt of the plate. This tilt was read on a graduated circle to the nearest 0.5 of a degree [see Ref. (1)].

The specimens were washed with soap and hot water, rinsed with distilled water, rubbed with cotton soaked in acetone, rinsed with acetone, rubbed with cotton soaked in carbon tetrachloride, rinsed with carbon tetrachloride, placed on the brass plate freshly cleaned with cotton soaked in carbon tetrachloride, and allowed to dry for 10–15 min., protected from dust. Essentially identical treatment was used in the determination of θ on these specimens [see Ref. (2)].

Distilled water drops deposited on the steel plates had volumes of 0.400, 0.200, 0.100 and 0.050 cm.^{3}.

When a drop is placed on a steel plate, its base usually is nearly circular (Fig. 1*a*). When the plate is slowly tilted, the drop becomes elongated in the direction of the tilt. Simple visual observation was not sufficient to detect the minimum tilt at which this elongation starts. The rear part of the 3-phase line (along which gas, liquid, and solid meet) does not move during this stage. On further increase of tilt, the rear of the drop eventually starts moving (Fig. 1*b*). If, then, the tilt is not reduced at once, the drop slides down with considerable acceleration and reaches the lower edge of the steel plate before any measurement on it can be made. If the tilt is rapidly reduced, it can be seen that the drop gradually acquires a cylinder-like shape (Fig. 1*c*) and retains this shape along all its path to the lower edge of the plate. During this stage, a small increase of tilt produces sliding with acceleration and a small decrease of tilt stops the sliding. The angle of tilt in the middle between these points is denoted in the following by α.

Although the outline of a slowly moving drop usually is less perfect than that pictured in Fig. 1*c*, it is possible to measure the length l and the width w of the drop. The degree of elongation associated with sliding can

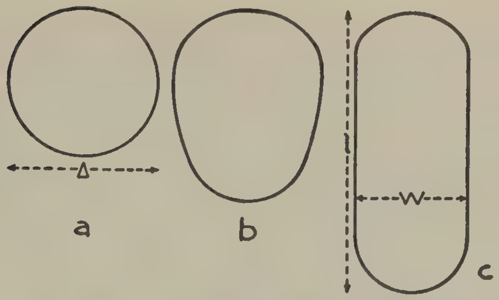

FIG. 1. Shape of drop (top view); *a* before tilting; *b* when the rear boundary starts moving; *c* during sliding without acceleration. The direction of the movement is from top to bottom of the figure.

be seen from comparison of these values with the diameter Δ (Fig. 1*a*) of the drop before tilting (see Table III).

The values of α, Δ, l, and w were all determined in the final series of experiments performed in a constant temperature room between 20.9–21.6°. In preliminary experiments, carried out at widely fluctuating room temperature, l had not been measured. In the final series the values of w were somewhat smaller on all plates, and the values of α were on Plates 2*D*, 2*B*, 6, and 4 greater than, and on Plates 1 and 7 equal to those of the preliminary series. In Tables II, III, and V only the results of the final series are listed although the "equilibrium" contact angles θ (see Table I) have been determined at varying temperatures.

III. EXPERIMENTAL RESULTS

The averages of the directly measured magnitudes α, Δ, l, and w are listed in Table III. The values of α, l and w are averages of from 4 to 24 single measurements, while some values of Δ represent only 2 measurements. On Plate No. 6 and especially on Plate No. 4, the drops are elongated along the polishing grooves even before tilting starts, and the Δ values are means of the longest and the shortest axes; thus, they are not directly comparable with the other Δ values referring to approximately circular drops.

The Δ values seem to be correct within ± 1%. The reproducibility of l and w may be estimated as ± 5%. The reproducibility of the α values is

TABLE II

Reproducibility of the Angle of Sliding α (in Degrees) for 0.100 cm.^{3} Drops

Plate	1	2*D*	2*B*	6	4	7
First expt.	30	29.5	30	24.5	21.5	17.5
Second expt.	34	29.5	30	26	20	18

TABLE III

Angles of Sliding (α) and the Dimensions of Water Drops Before (Δ cm.) and During (l cm., w cm.) Sliding along Steel Plates of Different Roughnesses

Drop volume	α	Δ	l	w	α	Δ	l	w
	Plate No. 1				Plate No. 2D			
cm.³	degrees				degrees			
0.400	13.5	1.23	2.63	0.905	11.5	1.225	2.61	0.895
0.200	19	0.915	2.08	0.65	17	0.95	1.775	0.72
0.100	32	0.715	1.395	0.535	29.5	0.725	1.30	0.57
0.050	59.5	0.545	0.98	0.42	50	0.565	0.995	0.455
	Plate No. 2B				Plate No. 6			
0.400	11	1.175	2.17	0.86	10	1.235	2.66	0.855
0.200	18	0.90	1.62	0.675	15	0.925	1.875	0.665
0.100	30	0.66	1.175	0.50	25	0.73	1.37	0.545
0.050	53	0.54	0.82	0.425	44	0.59	1.05	0.43
	Plate No. 4				Plate No. 7			
0.400	8.75	1.23	1.97	0.90	6.75	1.17	1.435	1.005
0.200	13	0.915	1.30	0.705	11.5	0.935	1.16	0.795
0.100	21	0.71	0.93	0.57	18	0.735	0.88	0.645
0.050	34	0.57	0.735	0.45	28	0.56	0.665	0.47

exemplified in Table II showing the angles α determined in the two most recent experiments on each plate (all done in the constant temperature room) with 0.100 cm.³ drops; each value in the table is an average of 6 single determinations.

Table IV presents the angles of sliding and the width of sliding drops (volume: 0.050 cm.³) on steel surfaces at 7 successive stages of polishing. Each value is the averaged result of at least 6 measurements. The temperature of the room was not controlled.

TABLE IV

Angles of Sliding (α) and Width (w cm.) of Sliding Water Drops on Steel at Different Stages of Polishing

Stage	1	2	3	4	5	6	7
α (degrees)	43	37	28	27	23	25	22
w (cm.)	0.50	0.46	0.50	0.48	0.50	0.50	0.50

IV. Resistance to Sliding and Surface Roughness

The diameters of the drop bases before sliding, *i.e.*, Δ in Table III, show that the contact angles were not greatly different from 90°; this was also so for Plate No. 6 and No. 4 which in the previous experiments with very small droplets at variable temperature (2) gave θ values of 60° and 70°, respectively (see Table I). In the absence of gravitation, if the contact angle is 90°, the drop is a hemisphere. The diameters of the hemispheres of 0.400, 0.200, 0.100, and 0.050 $cm.^3$ are 1.152, 0.914, 0.726, and 0.576 cm., respectively. The observed diameters are close to these values for all plates. Since the contact angles on different plates are equal or almost equal, the variation of α from plate to plate seems to demonstrate the effect of surface roughness only.

It is clear from Table III that the angle of sliding α increases with roughness, expressed as h_{rms} (Table I), except that Plates 2*D* and 2*B* are in wrong order.

TABLE V

The Ratio W sin α/w (g.sec.⁻²) for Different Drops on Different Surfaces

Drop volume	Plate No. 1	No. 2*D*	No. 2*B*	No. 6	No. 4	No. 7	Sum
cm.³							
0.400	101	87	87	79	66	46	466
0.200	98	79	90	74	62	49	452
0.100	97	85	98	76	61.5	47	464.5
0.050	100	82	92	79	61	49	468
Mean	99	83	92	77	63	48	

Increase of α with roughness is manifest also in Table IV, as long as α is 27° (for 0.050 $cm.^3$ drops) or greater. Presumably, α was not lowered by further polishing because casual impurities, such as dust particles always present in the laboratory air, took over the function of surface asperities (see Section V). The rolling friction of steel balls ceased to depend on roughness at even coarser finishes (1).

The effect of surface roughness on sliding of drops is made particularly clear by using, instead of α, a function independent of drop volume. It was observed that the ratio $W \sin \alpha / w$ is such a function. W is the weight of the drop and, consequently, $W \sin \alpha$ is the gravitational force just sufficient to maintain the drop in sliding. Table V, calculated from the α and w values of Table III, shows the invariability of the ratio $W \sin \alpha / w$ for each plate. W is expressed in dynes and w in centimeters. The ratio $W \sin \alpha / w$ increases with roughness, excepting again the step between Plate 2*D* and Plate 2*B*.

If the ratio $W \sin \alpha/w$ preserves its value up to $\sin \alpha = 1$, the volume of the smallest drop which is able to slide along a plate can be calculated; smaller drops would stick to the plate also when it is vertical. According to Table III, the width w is approximately proportional to $W^{1/3}$. Hence, $W^{2/3} \sin \alpha$ is approximately constant for each plate, and the minimum value of $W^{2/3}$ is equal to this constant. Thus computed, the volume of the smallest mobile drop is 0.040 cm.^{3} for Plate No. 1, and 0.017 cm.^{3} for Plate No. 7.

The importance of the microrelief of steel surfaces for sliding of drops is well revealed also by experiments in which drops moved across the ridges of Plate No. 4. This plate is covered with parallel grooves and ridges (see Section III) clearly visible at a magnification as low as 20 times. The data of Tables II and III refer to sliding along these grooves; also h_{rms} of Table I has been determined parallel to the direction of polishing. Sliding across the grooves was irregular, in jerks. The angles α were 12°, 21°, 31° and 49° for 0.400, 0.200, 0.100, and 0.050 cm.^{3} drops, respectively; the mean ratio $W \sin \alpha/w$ was 80, *i.e.*, 1.3 that of Plate No. 4 in Table V.

It may then be concluded that roughness affects resistance to sliding of water drops in the same manner as it does the sliding (4,5) and the rolling (1) friction between solids.

V. The Nature of the Resistance to Sliding

The dimension of the ratio $W \sin \alpha/w$ is identical with that of surface tension, and its range of magnitudes (48–99 g.sec.$^{-2}$) includes the value (72 g.sec.$^{-2}$) of the surface tension of water at the temperature of the experiments. This observation led to an attempt, presented in this section, of explaining, as far as possible, the sliding of drops by surface-tension effects (that is effects involving the liquid–air boundary only) as distinct from wetting phenomena. It should be remembered that $\theta = 90°$ according to the classical theory of wetting [see, *e. g.*, Ref. (6), p. 326] means that the tensions between solid and air and solid and liquid are equal; therefore, the energy of the solid surface should not change when liquid is displaced from it by air or air by liquid.

As long as the rear boundary of the drop remains stationary, tilting the plate causes elongation of the drop in the direction of the tilt. This elongation is associated with an increase in the water–air interface, and we may expect the work spent on this increase to be approximately equal to the decrease of the potential energy of gravitation caused by the lowering of the center of gravity of the drop. This expectation can be roughly tested using the values valid for the maximum elongation of the drop, *i.e.*, at the tilt α. An exact test is impossible as the shape of the drop is too intricate. If the length of the drop increases by dl, its center of gravity is lowered by approximately $\frac{1}{2}\, dl \sin \alpha$ and the work done by gravitation is $\frac{1}{2}\, W \sin \alpha\, dl$. Let the drop be approximated as half-cylinder with quarter-spherical ends (see Fig. 2). Its volume $V = \frac{\pi w^3}{12} + \frac{\pi w^2 x}{8}$ is constant, and its surface area $S = \frac{\pi w^2}{2} + \frac{\pi w x}{2}$ increases when the length $l\ (= w + x)$ of the drop increases. At constant V, $\frac{dS}{dl} = \frac{\pi w x}{2w + 4x}$ and the variation of the surface energy is $\frac{\pi w x}{2w + 4x} \gamma_{12}\, dl$, γ_{12} being the surface tension of water. Hence, $\frac{1}{2} W \sin \alpha = \frac{\pi w x}{2w + 4x} \gamma_{12}$ or, substituting $l - w$ for x,

$$\frac{W \sin \alpha}{w} = \frac{\pi(l - w)}{2l - w} \gamma_{12}. \qquad [1]$$

With $\gamma_{12} = 72$ g.sec.$^{-2}$, the right-hand side of eq. 1 is, on the average, 88 for Plate No. 1, 84 for No. 2*D*, 79 for No. 2*B*, 87 for No. 6, 69 for No. 4, and 51 g.sec.$^{-2}$ for No. 7. These values agree with those of $W \sin \alpha/w$ of Table V perhaps as well as can be expected from the crude approximations on which Eq. 1 is based. It has not been checked whether closer approximation to the real shape of the drop would result in better agreement.

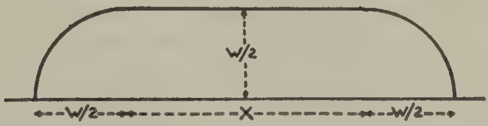

FIG. 2. Shape of drop (side view) approximating the real shape during sliding without acceleration.

When the drop slides down, its shape seems not to change. However, it is very probable (and in many instances certain) that the drops leave some water behind them along the track. The hypothesis seems reasonable that the resistance to sliding is essentially the stretching (or tearing) resistance of the water "ribbon" which persists for a time in the wake of the drop (and then breaks down to minute droplets). This "ribbon" cannot move at the speed of the drop because of the roughness of the solid which forces water to meander between the hills (see, *e. g.*, Ref. (6), p. 249]. When sliding at an observable rate occurs, this ribbon is either stretched or ruptured. Stretching or rupturing water surface of width w_1 requires force $\gamma_{12} w_1$. We should expect, therefore, that

$$W \sin \alpha = \gamma_{12} w_1. \qquad [2]$$

If the surface is very rough, the real width w_1 of the "ribbon," *i.e.* along all the hills and valleys wetted by a thin water film, is greater than the distance between the edges of the "ribbon," which is the w given in Table III. Therefore, $W \sin \alpha/w$ for rough surfaces is greater than γ_{12}. If the surface is relatively smooth, water is retarded by a smaller number of hills and only a fraction of the drop track is occupied by water "ribbons." In this instance, $w_1 < w$, and $W \sin \alpha/w$ for smooth surfaces is less than γ_{12}.

The progress of the drop front over the solid surface meets with little resistance presumably because the drop vibrates. In vibrating, the water surface touches the next row of hills without the 3-phase line sinking into the valley between; or the energy of vibration may be sufficient to push the 3-phase line over an energetically unfavorable position [see Ref. (2)]. As mentioned in Section IV, these vibrations are quite large when the drop moves across ridges, but they are sometimes noticeable also on isotropic sufraces.

VI. Comparison with Earlier Interpretations

1. The resistance R to movement of liquid "indexes" or "pellets" in capillary tubes has been investigated before the sliding of drops from flat surfaces. The pressure required to start or maintain movement of such pellets causes asymmetry of the pellet; its meniscus in contact with high-pressure air (pressure P_1) simulates a greater wettability than the other meniscus which is adjacent to air at low pressure (P_2) (7). The difference between the contact angles (or their cosines) at the rear (θ_1) and the front meniscus (θ_2) was repeatedly made responsible for the apparent friction between liquid pellets and capillary tubes (8,9) and also for that of drops sliding on flat surfaces (10); however, difference between θ_1 and θ_2 must exist *if* there is a resistance to the movement of the pellet and, therefore, a difference between P_1 and P_2; but it gives no information on why this difference between P_1 and P_2 is present or, in other words, why liquid in contact with solids does not move under the slightest stress.

2. It follows from West's measurements (8) that R of mercury pellets in glass tubes is proportional to the internal perimeter of the tube. This rule was extended to the perimeter of bubbles sliding on plates (11). However, experiment shows that drops having a more circular shape (and consequently a smaller perimeter) start moving at a greater tilt than more cylindrical drops (whose perimeter is greater) (see Section II above). Let α_0 be the angle at which the rear of the drops begins to slide. If, instead of a usual nearly circular drop, an elongated drop is deposited on a steel plate so that the longer axis of the drop is normal to the direction of sliding, α_0 proves to be greater. (The angle α observed after the drop has acquired its quasi-cylindrical shape is independent of the original outline of the drop.) This dependence of angle α_0 on the original outline of the drop may be one of the causes of the poor reproducibility of α_0 compared with that of α; see, *e.g.*, the data for α_0 published by Aron and Pavlova (12).

3. The resistance per centimeter of perimeter was in West's experiments 252 g.sec^{-2} (my calculation). For a similar system (mercury in

glass capillary), Yarnold (g) found it to be 96 g.sec.$^{-2}$. The difference may have been due to roughness difference; the effect of roughness on the movement of mercury in glass has been emphasized by Rosenberg (13) and de Turk and Lockenvitz (14). The values recorded by West and Yarnold are about 0.5 and 0.2 the surface tension of mercury; if the hypothesis of Section V is applicable to this system, only 0.5 or 0.2, respectively, of the pellet perimeter was hanging on mercury "ribbons."

4. Macdougall and Ockrent (10) noticed that, for a given system, the product $A \sin \alpha_0$ was independent of drop size. The angle α_0 is defined as "the value of the angle of tilt at which sliding first occurs." A is the area of the vertical longitudinal projection (elevation) of the drop; if h is the height of the drop, A is roughly proportional to hl. Since drop volume is roughly proportional to hlw, the ratio $W \sin \alpha/w$ varies approximately as $hl \sin \alpha$. It may well be that the product $A \sin \alpha_0$ appeared independent of drop size because the ratio $W \sin \alpha/w$ was independent of it.

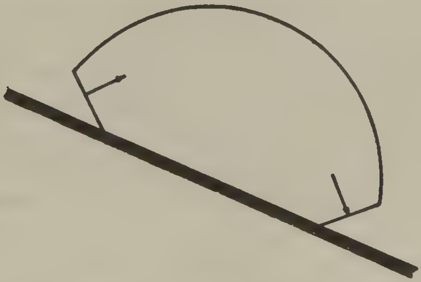

FIG. 3. "Rolling" of drops, according to Frenkel.

5. For water drops sliding on built-up multilayers, the product $W \tan \alpha$ seemed to be independent of drop volume V (15). It varied with V in the present work. The contact angle between air, water, and some multilayers also was about 90°, but the angle α was smaller than those found now; apparently, built-up films are rather smooth.

6. A theory of sliding of drops on flat surfaces has recently been published by Frenkel (16). Frenkel pays no attention to the alteration of drop shape before sliding starts, but his theory can readily be improved in this respect. If the drop moves dx cm. along the plate, the area $w\,dx$ (w = width of the drop) is "bared" by the drop. Frenkel assumes that in this process areas $w\,dx$ of solid–air and liquid–air interfaces form, and the area $w\,dx$ of the solid–liquid interface disappears; that is, the change of the free interfacial energy is $(\gamma_{13} + \gamma_{12} - \gamma_{23})w\,dx$, γ being the surface or interfacial tension, and subscripts 1, 2, and 3 referring to air, liquid, and solid, respectively. As a matter of fact, no new liquid–air interface forms during sliding (except along the trail), but Frenkel believes that the movement

proceeds via an intermediate stage which may be pictured as shown in Fig. 3. At the rear of the drop, liquid is supposed to rise thus forming a new liquid-air interface, and at the front, an equal area of the liquid-air interface vanishes. If this "rotation" of the drop occurs and the processes at the front of the drop are neglected, then the term γ_{12} is justified.

To test the mechanism suggested by Frenkel, the rear part of a drop—in its final shape—on a tilted plate was just tinted with $KMnO_4$ or $Na_2Cr_2O_7$ (if the concentration of the coloring solution is too high, the solution flows down along the bottom of the drop) or dusted with talc or paraffin wax. When the tilt was slightly increased and the drop started *slow* sliding, no movement similar to that represented in Fig. 3 was visible. Talc, *e.g.*, slid down chiefly along the 3-phase line, wax particles often moved at the same rate as the drop or stayed behind, and so on. West (8) and Yarnold (9) had previously pointed out the absence of slippage between the liquid and solid, but they did not claim that a liquid-air interface is produced.

Frenkel's theory, which in my opinion is not correct, leads to an equation which is disturbingly similar to Eq. 2 of this paper. If the energy change associated with "baring" the area $w\,dx$ behind the drop is $(\gamma_{13} + \gamma_{12} - \gamma_{23})w\,dx$, this change can be expressed also as $\gamma_{12}(1 + \cos\theta)w\,dx$, θ being the equilibrium contact angle [see, *e.g.*, Ref. (6), p. 326]. It may be set equal to the change of the gravitational energy, *i.e.*, $W \sin\alpha\,dx$. Hence, $W \sin\alpha = \gamma_{12}(1 + \cos\theta)w$. As θ is nearly 90° for most of the plates used in this work,

$$W \sin\alpha = \gamma_{12}\,w. \qquad [3]$$

Consideration of surface roughness (not mentioned by Frenkel) would account for the value of $W \sin\alpha/w$ being greater than γ_{12} (see section V). However, Eq. 3 seems to be incompatible with $W \sin\alpha/w$ being less than γ_{12}. The actual area cannot be less than the geometrical area, and the area "bared" by the drop must be at the least equal to $w\,dx$ also for best polished solids.

ACKNOWLEDGMENT

I thank Dr. P. K. Frolich, Vice President for Research and Development, for permission to carry out the work herein reported in the laboratories of Merck and Co., Inc.

SUMMARY

Water drops, from 0.05 to 0.4 cm.^{3} in volume, slide without acceleration along tilted plates of stainless steel at such an angle α that $W \sin\alpha = kw$, if W is the weight and w the width of the drop, and k is a constant. The value of k increases with surface roughness from 48 g.sec.$^{-2}$ for polished steel (average height of hills 0.02–0.03 μ) to 99 g.sec.$^{-2}$ for pickled steel (average height of hills 3.1 μ). These results are accounted for by

surface tension effects only, without regard to wetting. Some earlier work on friction between solids and liquids is examined.

REFERENCES

1. BIKERMAN, J. J., *J. Applied Phys.* **20**, 971 (1949).
2. BIKERMAN, J. J., *J. Phys. & Colloid Chem.* in press.
3. CARNEGIE-ILLINOIS STEEL CORP., Fabrication of U. S. S. Stainless and Heat Resisting Steels (1947).
4. BIKERMAN, J. J., *Revs. Modern Phys.* **16**, 53 (1944).
5. BIKERMAN, J. J., *Lubrication Eng.* **4**, 208 (1948).
6. BIKERMAN, J. J., Surface Chemistry for Industrial Research. Academic Press Inc., New York, 1947.
7. JAMIN, J., in "Société chimique de Paris, Leçons de chimie et de physique professées en 1861," pp. 1–55. Paris, 1862.
8. WEST, G. D., *Proc. Roy. Soc.* (*London*) **86A**, 20 (1911).
9. YARNOLD, G. D., *Proc. Phys. Soc.* (*London*) **50**, 540 (1938).
10. MACDOUGALL, G., AND OCKRENT, C., *Proc. Roy. Soc.* (*London*) **180A**, 151 (1942).
11. VESELOVSKII, V. S., AND PERTSOV, V. N., *J. Phys. Chem.* (*U. S. S. R.*) **8**, 245 (1936).
12. ARON, YA. B., AND PAVLOVA, M. V., *J. Phys. Chem.* (*U. S. S. R.*) **22**, 1251 (1948).
13. ROSENBERG, P., *Rev. Sci. Instruments* **9**, 258 (1938).
14. DE TURK, E. P., AND LOCKENVITZ, A. E., *Rev. Sci. Instruments* **13**, 295 (1942).
15. BIKERMAN, J. J., *Proc. Roy. Soc.* (*London*) **170A**, 130 (1939).
16. FRENKEL, YA. I., *J. Exptl. Theoret. Phys.* (*U. S. S. R.*) **18**, 659 (1948).

THE ACTION OF POLYOXYETHYLENE MONOSTEARATE UPON STARCH WITH REFERENCE TO ITS SOFTENING ACTION IN BREAD

D. D. Lord

From the Group Research Department, Scribbans-Kemp Limited, London, England

Received January 18, 1950; revised April 11, 1950

INTRODUCTION

The introduction into bread of substances known as "softeners" has recently aroused great interest, and much controversy has arisen as to whether these substances reduce the rate of staling of the bread. Most of the published evidence is concerned with one particular softener, polyoxyethylene stearate, and with the measurement of the firmness and compressibility of the bread crumb. Very few explanations have been offered to account for the results, and the present investigation was undertaken with the object of elucidating the mode of action of this ester when added to bread. Most of the experiments to be described are concerned with the effect of the ester upon the starch constituent of the bread and apart from its practical bearing, therefore, this work may be regarded as a contribution to the colloid chemistry of the starches.

Favor and Johnston (1) reported that the ester reduced the firmness of a prism of bread, measured as the stress in grams necessary to cause a constant depression, and also that it reduced the rate of increase of firmness of the bread on aging. These results were confirmed by a later communication (2) and by the work of Edelmann and Cathcart (3), Edelmann, Cathcart, and Berquist (4) and Skovholt and Dowdle (5). Freilich (6) measured the compressibility of the bread crumb as the depression resulting from a constant stress, and found that the ester increased the compressibility and reduced the rate of increase of compressibility on aging.

In addition to the increase in the firmness of the bread crumb which occurs on aging, other changes in the starch portion of the bread may be observed and provide further tests of the staling process. The usual chemical tests are modifications of those developed by Katz in his classical work upon the subject (7), and the two most suited for quantitative measurements are based on (*a*) the swelling power of the crumb when placed in an excess of water, or other related quantities such as the viscosity of an aqueous suspension of the crumb, and (*b*) the amount of soluble starch which may be leached from the bread by water. A development of this test is to determine the amylose content of the starch leached from the crumb. In all of these measurements, the stale bread gives a lower value than the fresh bread.

At the same time as his compressibility measurements, Freilich measured the consistency of a "dough" of bread crumb and water (of 60% moisture content), a quantity which is related to the swelling-power determinations. He found that the ester lowered the swelling power of the crumb compared with that of a standard and that it had a slight accelerating effect upon the rate of staling. These experiments show that the chemical tests and compressibility measurements may give completely opposite interpretations of the effect of a particular change on the rate of staling.

The changes which occur in bread on staling (apart from such factors as loss in aroma, flavor, or moisture which may be eliminated by sealing in cans) are due to alterations in the starch of the bread. Katz showed that such changes may be observed in a simple starch–water gel containing about 50% of starch. Earlier views that the amylose fraction of the starch is solely responsible for the staling have been discounted by the work of Noznick, Merritt, and Geddes (8) who showed that loaves made from a synthetic flour containing no amylose staled at about the same rate as a normal loaf.

Schoch and French (9) came to the conclusion that the amylopectin constituent of the starch was solely responsible for the staling process, and that most of the amylose was made insoluble by retrogradation immediately after baking, thus contributing nothing to the staling process. Their results were obtained from observations upon bread and upon 50% starch gels, but they also showed that the addition of 2% of oleic acid to the gel caused it to have a greatly reduced swelling power and soluble extract. Moreover, the latter contained no amylose and gave a wine-red color with iodine. Oleic acid is known from the work of Schoch and Williams (10) to associate with the linear (amylose) fraction of starch and to make it insoluble. It has no apparent effect upon the amylopectin fraction. This observation does not agree with the theory that the amylose plays no part in the staling process, especially as the gels containing oleic acid behaved in a similar manner to stale gels.

The important influence of fatty acids on the gelatinization of starch has been shown by Caesar (11). Measuring the resistance to shear of a 20% dispersion of corn starch in water, it was found that normal starch begins to gelatinize at a temperature almost 1.5°C. higher than defatted starch. Normal starch contains about 0.8% of adsorbed fatty acids, which may be removed only by extraction with a hydrophilic solvent such as 80% dioxane or 85% methanol [Schoch (12)].

Caesar also found that the 20% defatted starch pastes, when cooled, had a higher consistency and gave firmer and clearer gels than the normal starch. This was attributed to the interference by the adsorbed fatty acids in the normal starch with the associative forces through hydrogen bonds holding the gel together.

Favor and Johnston (1) reported the effect of polyoxyethylene stearate upon the viscosity of starch pastes as measured in the Brabender Amylograph. The temperature at which the viscosity commenced to rise was increased by the addition of the ester, and the authors attributed this to a wetting or lubricating action. The pastes prepared in the Amylograph were tested the next day for cold viscosity, and the ester was shown to have a pronounced effect in reducing the cold viscosity. Larger batches of paste were prepared which were tested for viscosity in the Amylograph, when it was shown that the polyoxyethylene stearate prevented the increase in viscosity obtained with the standard paste on aging.

A criticism of this last work may be advanced, however, as in the preparation of the large batches of the paste the temperature did not rise above 90°C. It will be shown later that the condition of the starch at this temperature in the presence of polyoxyethylene stearate is very different from that of starch when the ester is absent, so that comparison between the two cases is not possible.

EXPERIMENTAL METHODS AND RESULTS

In structure, polyoxyethylene glycol stearate bears a close resemblance to the α-monoglycerides which, like the fatty acids, have a pronounced effect upon the amylose fraction of starch and retard the gelatinization of starch. In concentrated starch gels they reduce the swelling power of the starch, reduce the quantity of soluble extract, and bring to zero the amylose content of the extract. It seemed likely, therefore, that polyoxyethylene stearate would have similar effects upon starch, and several different experimental techniques have been used to investigate these effects. Except in the experiments with bread a commercial sample of wheat starch was used, and this was defatted by five extractions with 85% methanol before use, as advised by Schoch (12).

(a) *Preparation of Polyoxyethylene Stearate*

The ester may be formed by reacting stearic acid and ethylene oxide together under pressure, under conditions such that the final product contains about eight ethylene oxide groups for each stearic acid radical. It is identical with the monoester of polyethylene glycol containing eight ethylene glycol residues.

Samples of commercially available polyethylene glycols were obtained from General Metallurgical and Chemical Ltd., the English distributors for the products of the Carbide and Carbon Chemicals Corporation. Each is described by a number indicating the average molecular weight of the product, and contains practically all the polymers of ethylene glycol from two upwards, normally distributed about the molecular weight in question. Polyethylene glycol 400, containing an average of between eight and nine ethylene oxide groups, was chosen.

The glycol was esterified by heating 30 g. (0.075 mole) with 21.3 g. (0.075 mole) of stearic acid (supplied by British Drug Houses, Limited) and 0.062 g. of concentrated sulfuric acid *in vacuo* (with stirring) for 3 hr. at 130°C. Titration of a sample indicated that the esterification was 95% complete, and the reaction was stopped at that point. The product was a light, fawn-colored, fatty type of solid which melted over a range 27–32°C., with most melting at 31°C.

The mono- and diesters of polyethylene glycol 600 were prepared by a similar technique and are referred to as "polyoxyethylene 13 stearate" and "polyoxyethylene 13 distearate" respectively. "Polyoxyethylene stearate" is used to imply the compound containing 8–9 ethylene oxide residues per stearate group.

(b) *The Effect of the Ester Upon the Starch–Iodine Reaction*

It is only in comparatively recent years that a clear picture of the reaction between starch and iodine which produces the intense blue color has been obtained. One of the most useful tools in the investigation of this reaction has been the technique originated by Bates, French, and Rundle (13) who titrated the starch with iodine potentiometrically. They found that under strictly controlled conditions of iodide concentration, the iodine was taken up by the amylose fraction of the starch to an extent of about 20% of the weight of amylose, and with increased quantities of iodine, adsorption occurred very much more slowly. The end point of the titration was marked by a point of inflection of the graph drawn between the amount of iodine added and the potential developed on a bright platinum electrode. The amylopectin fraction of starch was shown to adsorb less than 1% of iodine and gave a wine-red color. In the original method of carrying out the titration, the starch was dissolved in dilute alkali and this was neutralized with hydriodic acid before titration. A modification of this method by Wilson, Schoch, and Hudson (14) is somewhat more convenient and the neutralization of the alkali is carried out with hydrochloric acid, potassium iodide being added after neutralization.

In the potentiometric titrations reported here a slightly modified technique was used to determine the end point of the titration. About 0.04 g. of defatted wheat starch was dissolved in 10 ml. of 0.5 *N* potassium hydroxide and well stirred. After a complete dispersion of the starch had been obtained, the solution was diluted with distilled water and neutralized to methyl orange with 0.5 N hydrochloric acid. The potassium iodide was added as 10 ml. of 0.5 N solution and the liquid was then diluted to 100 ml. The iodine solution was 0.001 N in 0.05 N potassium chloride and 0.05 N potassium iodide. A Cambridge Instrument Co. electrotitration apparatus was used, with a bright platinum electrode as indicator (in conjunction with a saturated calomel electrode). This instrument consists of an uncalibrated potentiometer with a sensitive galvanometer in series with a 10,000-ohm resistance. The scale reading of the galvanometer is proportional to the out-of-balance current, and the sensitivity of the galvanometer is such that the change of 0.07 volt in the potential of the platinum electrode during the titration is just covered by the full scale of the galvanometer.

During a preliminary titration, the potentiometer was adjusted so that the end point of the titration coincided approximately with the galvanometer deflection in the center of the scale, and from that point the potentiometer settings were left unchanged. The titration was carried out by noting the galvanometer deflection after each addition of iodine to the reaction, and a graph was drawn plotting scale readings of the galvanometer against milliliters of iodine added. Any polarization of the electrodes was found to be too small to influence the titration.

The end point of the titration was taken to be the point of inflection of the curve, and a blank determination was carried out without starch to find the amount of iodine necessary to give the same galvanometer deflection. This small amount, 0.6 ml. of 0.001 N iodine solution, was subtracted from the titer to give the amount of iodine adsorbed by the starch.

This method gave results agreeing closely with the accepted values for the adsorption of iodine by amylose. A sample of wheat amylose prepared by butanol precipitation adsorbed 15.20, 18.60, and 19.30% of iodine after successive recrystallizations. A sample of potato amylose adsorbed 18.35, 20.70, and 20.80% of iodine after similar treatment. Wheat amylopectin, prepared by precipitation with methanol after removal of the amylose and reprecipitation, adsorbed 0.46% of iodine.

Mikus, Hixon, and Rundle (15) titrated amylose (containing approximately 10% of amylopectin) with iodine after the addition of successive quantities of oleic and other fatty acids, and found a linear relationship existed between the percentage of fatty acid added and the iodine affinity of the amylose.

In this study, titrations of defatted wheat starch with iodine were carried out after small amounts of stearic acid or polyoxyethylene stearate had been added to the starch. The acid was added to the dry starch as a solution in 85% methanol, which was then evaporated to dryness. The starch was then dissolved in alkali and the titration carried out as described above. The ester was added as a dispersion in water, and in the first experiment it was added (*a*) before gelatinization, (*b*) after gelatinization and before neutralization, and (*c*) after neutralization. Almost identical results were obtained by each treatment, and in subsequent experiments the ester dispersion was added after neutralization of the alkali.

The results of the experiments are shown in Fig. 1, where the ordinate represents the percentage of iodine adsorbed by the starch and the abscissa represents the amount of adjunct added, expressed as the weight percentage of the starch.

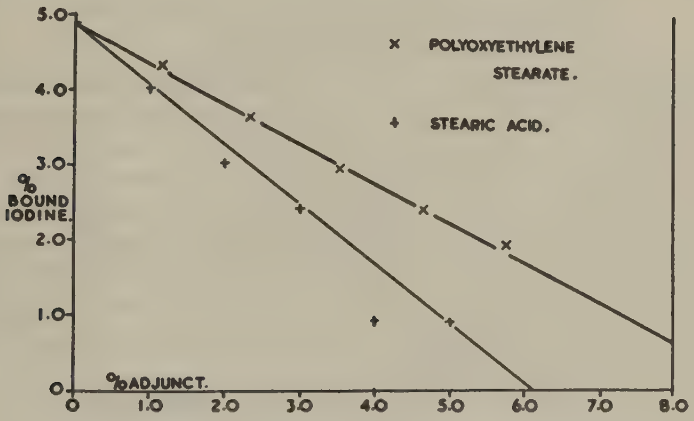

FIG. 1. The effect of adjuncts upon the iodine affinity of starch.

(*c*) *The Association of the Ester With the Amylose Fraction*

A large number of different compounds have been found to precipitate the amylose fraction of starch selectively, and among these may be mentioned butanol, amyl alcohols, nitro paraffins [Whistler and Hilbert (16)] and thymol [Haworth, Peat, and Sagrott (17)]. Schoch and Williams (10) found that oleic acid would precipitate a fraction which contained 78% of amylose from an autoclaved dispersion of corn starch.

A similar experiment was carried out, using polyoxyethylene stearate as the precipitant. Defatted wheat starch (3.0 g., dry) was creamed with water and poured into boiling water to give a total volume of 150 ml. This paste was autoclaved for 3 hr. at 16–18 p.s.i. pressure and then centrifuged in a Sharples Supercentrifuge for a few minutes to remove a small quantity of undispersed granules. The solution was then heated to boiling and 10 g. of polyoxyethylene stearate was added, after which the solution was allowed to cool slowly with stirring. After being left over a week end, the viscous paste was supercentrifuged for 10 min. at 47,000 r.p.m. in the batch bowl of the Supercentrifuge, giving a clot of precipitate and a thick liquid portion. The starch was recovered from both fractions, using an excess of methanol as precipitant, and dried with ethanol followed by heating at 80°C. The yields were 0.47 g. in the precipitated fraction and 1.58 g. in the soluble fraction.

After defatting by Soxhlet extraction with 85% methanol, the precipitated fraction had an iodine affinity of 8.52% (42.6% amylose) and the nonprecipitated fraction had an iodine affinity of 2.29% (11.4% amylose). The ester, therefore, does act as an amylose precipitant though it is not as efficient in this respect as oleic acid.

(d) *The Effect of Polyoxyethylene Stearate Upon the Gelatinization of Starch*

The effect of the naturally-occurring fatty acids in delaying the increase in the viscosity of concentrated starch pastes has been mentioned in the *Introduction*. It seemed likely that polyoxyethylene stearate would have a similar effect upon the gelatinization, in view of the results reported by Favor and Johnston. The Amylograph and other viscometric instruments working with fairly concentrated starch pastes are not very suitable for exact information upon the course of the gelatinization, as the viscosity measurements are complicated by the breakdown of the swollen granules during the gelatinization, and also they do not show the well-known effect of the two stages of gelatinization.

Harris and Jesperson (18) determined the swelling power of various starches at different temperatures by dispersing the starch in a large excess of water at the required temperature, leaving for 5 min., gently stirring during this time, and then centrifuging off the swollen granules. A modification of this method was used in the present experiments, and the effect of the addition of 1% of stearic acid or polyoxyethylene stearate was observed.

Defatted wheat starch was treated with the required adjunct dissolved in 85% methanol, which was then evaporated to dryness. The sieved starch was left overnight, uncovered, to reach equilibrium with the atmospheric humidity, and a moisture determination was then made. Samples of 0.100 g. (dry basis) were then weighed out into 5″ × ½″ test tubes and immersed in a thermostat at the required temperature (to within ±0.2°C.). Distilled water (10 ml.) from a flask which had been immersed in the thermostat for at least 15 min., was pipetted into the test tubes and the starch was gently stirred with small glass rods for 15 min. The tubes were then removed from the thermostat and rinsed into 50-ml. centrifuge tubes with 15 ml. of water. The centrifuge tubes were stood in a thermostat at 20°C. (±0.1°C.) for 15 min. and then centrifuged at 2,000 r.p.m. for 10 min. The liquid was decanted off and droplets removed from the tube with filter paper. The weight of swollen starch per gram of dry starch was taken as the swelling at that temperature. Measurements were made every 2°C. from 60°C. to 98°C. The standard deviation, estimated from all the results, was 0.39.

Results are shown graphically in Fig. 2, where the ordinate represents the swelling of the starch and the abscissa the temperature. The two stages of swelling in the gelatinization of starch are clearly shown, and it will be noticed that the stearic acid has a pronounced action upon the first stage of the gelatinization, whereas the polyoxyethylene stearate has a more pronounced action upon the second stage of gelatinization.

At 90°C., the swelling of defatted wheat starch is almost complete, whereas when 1% of stearic acid is present the second stage of gelatinization is about half completed. When the ester is present, however, the second stage of gelatinization is only just starting to increase with any rapidity.

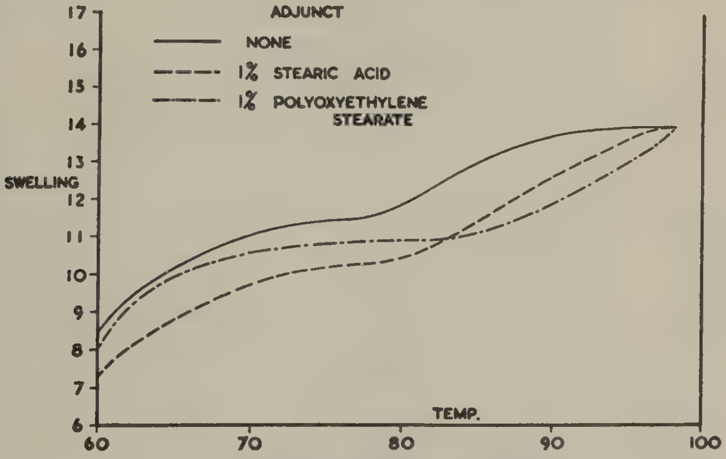

Fig. 2. The swelling of starch on heating.

The above method for investigating the gelatinization of the starch was also supplemented by an optical method where the change in the light transmission of a starch dispersion was observed as the temperature was increased. Such methods have been used by Cook and Axtmayer (19), Morgan (20), and Beckford and Sandstedt (21).

The apparatus of Beckford and Sandstedt was slightly modified to enable it to be used in conjunction with a "Spekker" Absorptiometer. The cell was filled with 110 ml. of a 0.1% dispersion of starch and readings were taken every 2°C. while the temperature was being raised at approximately 2°C./min. Several adjuncts were investigated, each being added in the proportion of 1% of the starch weight to defatted wheat starch, except where noted.

The light transmission of the dispersion fell gradually over the range from 30°C. to 58°C., owing to compound granules becoming dispersed, and then the transmission increased as the starch commenced to swell. The two stages of gelatinization are clearly seen in the specimen curves shown in Fig. 3. In Table I are collected the data obtained in the gelatinization of the starch. Here T_1 represents the start of the first stage of gelatinization, T_2 the end of this stage, and T_3 the commencement of the second stage. An estimate of the amount of swelling can only be made approximately, but it may be seen that in the period between the two stages of gelatinization, defatted wheat starch still continues to swell, whereas when stearic acid or polyoxyethylene stearate is present the rate of swelling is almost negligible.

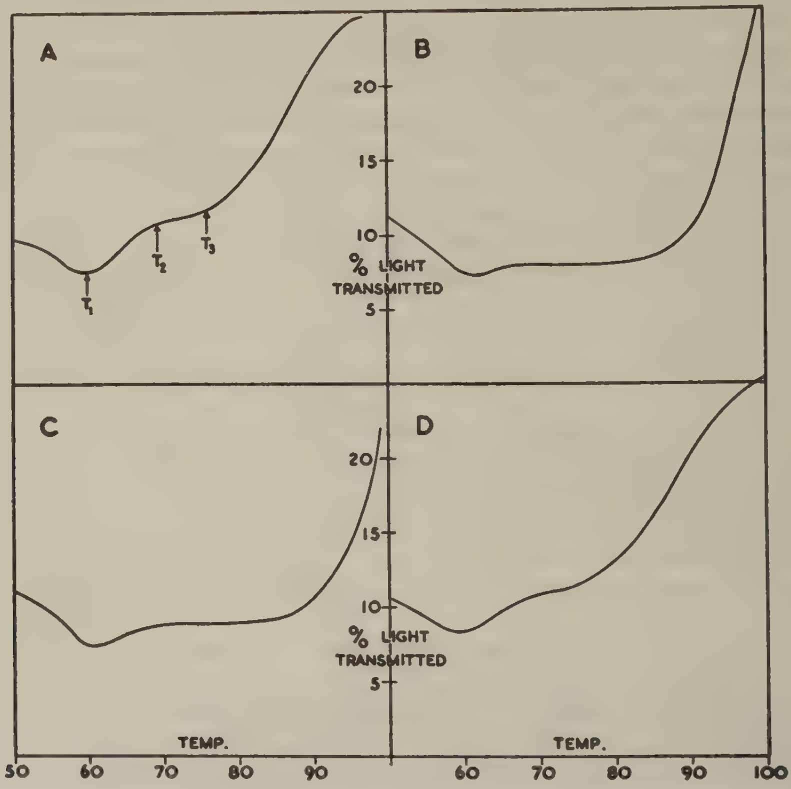

Fig. 3. The change in light transmission of 0.1% starch dispersions on heating. *A* No adjunct; *B* 1% stearic acid; *C* 1% polyoxyethylene stearate; *D* 1% vegetable shortening.

Compounds tested by this technique included the polyoxyethylene stearate containing approximately 13 ethylene oxide residues per stearic acid radical, and the distearate of this polymer. The vegetable shortening was a commercial bakery product.

It will be seen from Fig. 3 and Table I that the fatty acid and monoesters have a very definite retarding effect upon the gelatinization of the starch, and especially upon the second stage of the process. The fully esterified fats have little effect upon gelatinization except a slight depression of the swelling in the first stage of gelatinization. A mixture of polyoxyethylene stearate and vegetable shortening had an effect intermediate between that produced by the two substances used singly. Increasing the quantity of polyoxyethylene stearate decreased the first stage of gelatinization to a further extent.

The agreement between the temperatures of the stages of gelatinization found by the first, or static, method and the second, or dynamic, method is good and shows that the swelling of starch in a large excess of water is independent of time, or else that it is a very rapid process. If the swelling were to take an appreciable time, it would be expected that the dynamic method would give temperatures higher than those obtained from the static method.

TABLE I

The Gelatinization Temperatures of Wheat Starch in the Presence of Adjuncts

Adjuncts	T_1[a]	T_2[a]	T_3[a]
	°C.	°C.	°C.
None	60	69	76
1% Stearic acid	62	66	80
1% Polyoxyethylene stearate	61.5	69.5	83
2% Polyoxyethylene stearate	63	68	82
1% Polyoxyethylene-13-stearate	62	72	84
1% Polyoxyethylene-13-distearate	61	68.5	76
1% Vegetable shortening	61	70	76
1% Vegetable shortening + 1% polyoxyethylene stearate	61	70	81

[a] T_1 and T_2 represent the beginning and the end of the first stage of gelatinization, respectively. T_3 represents the beginning of the second stage.

(*e*) *The Effect of Polyoxyethylene Stearate Upon Gels of High Starch Content*

The experiments described above have all been concerned with the effect of the ester upon starch in dilute pastes. The problem of bread staling is concerned with starch gels of concentration approximately 50% starch. In a system of this type, there is insufficient water to gelatinize the starch completely, although it is very swollen and the characteristic polarization cross has been lost.

Katz (7) and Schoch and French (9) have shown that changes occurring in the quantity of soluble extract from starch and the changes in the swelling power of starch in bread could be paralleled by changes in 50%

starch gels, while the two latter workers also showed that the differences between starch gels and bread could be ascribed to the amylase action during the baking process.

Schoch and French found that oleic acid added to a 50% starch gel in 2% concentration (based on the starch weight) produced a considerable reduction in the soluble extract and the swelling power of the starch, and gave the effect of a gel already stale. Addition of hydrogenated shortening slightly decreased the figures obtained.

These experiments have been repeated using 5% (starch weight) of the adjuncts and extended to include the effect of the polyoxyethylene esters upon the swelling power of the starch. The technique employed followed that described by Schoch and French except that 2.00-g. (dry basis) samples of defatted wheat starch were used and all quantities were scaled down to one-fifth. The adjuncts were added as described in the experiments on the gelatinization of the starch.

TABLE II

Changes in the Swelling Power of Wheat Starch from 50 Per Cent Gels on Aging

Adjuncts	Swelling power		
	2 hr.	50 hr.	170 hr.
None	4.70	3.56	3.47
5% Stearic acid	3.64	3.21	3.04
5% Polyoxyethylene stearate	3.49	2.99	2.93
5% Polyoxyethylene-13-stearate	3.55	3.15	3.01
5% Polyoxyethylene-13-distearate	4.19	3.36	3.18
5% Vegetable shortening	4.74	3.88	3.64

The results are reported in Table II, where it will be noticed that the vegetable shortening had hardly any effect upon the swelling power of the starch, the polyoxyethylene distearate had a slight depressant effect, and the monoesters and stearic acid had a pronounced effect. The swelling power of starch from a fresh gel containing polyoxyethylene stearate was approximately equal to that from a standard gel which was 170 hr. old.

Two pieces of qualitative evidence may also be quoted. The starch extract obtained from the standard gel and the gel to which shortening had been added gave a blue color with iodine, but the monoesters and stearic acid resulted in the extract giving a wine-red color with iodine. In other words, the extracts either were wholly amylopectin or else contained so much adjunct that they could not adsorb iodine. The results of Schoch and French indicate that the former alternative is probably more correct.

The gels obtained from the defatted wheat starch were elastic when fresh and gradually became hard on staling. When the fat, esters, or stearic acid were added, however, the gels had a different "feel." They were not as elastic and broke up much more readily, being very much easier to force through a sieve. It is likely that the adjuncts surrounding the starch granules formed a film and retarded the cementing together of the granules on cooking.

(*f*) *The Softening Action of Polyoxyethylene Stearate in Bread*

Favor and Johnston (1) and Freilich (6) have shown that the ester has a pronounced softening action upon bread crumb. Both workers used recipes containing quantities of shortening which would be likely to complicate the staling of the bread, for it is well known that shortening gives a very much softer and tenderer loaf than one containing no fat.

Experiments were therefore done with a view to obtaining as simple a system as possible. The recipe used contained only flour, salt, skim milk powder, yeast, and water in addition to the adjuncts tested. It was:

Canadian flour	3 lb. 8 oz.
Salt	0.75 oz.
Skim milk powder	1.25 oz.
Yeast	1.25 oz.
Water	33 oz.
Adjuncts	Variable

The dry ingredients were sifted together and the adjuncts were added by melting, mixing with about three times their weight of flour, and stirring to give a powdery mass which was sieved with the other ingredients. The yeast was dispersed in water and the whole mixed in a laboratory-size "Peerless" planetary mixer for 7 min. The dough was then placed in a fermentation cabinet at 25.6°C. (78°F.) and approximately 90% relative humidity (R.H.). The dough was punched by remixing for 5 min. after 1.5 hr. and 2.5 hr. from the start. After 3.5 hr. the dough was weighed to 14 oz., balled up and sheeted in a "National" sheeter at 9/32 in. and then at $\frac{3}{16}$ in., with 5-min. rest periods between each operation. The dough was then hand-molded, tinned, and proved at 31.1°C. (88°F.), 90% R.H. for 45 min. It was baked at 221°C. (430°F.) for 30 min. and cooled for 1 hr. in moving air.

One loaf was taken for testing on the "Baker" compressimeter and the remainder were wrapped in moisture-proof cellophane and stored at laboratory temperature. For testing on the compressimeter, slices were cut of 2.0 cm. thickness in a miter box and placed on the instrument. The compressibility was recorded as the depression resulting from a stress of 8 g., using the circular plunger which was 36 mm. in diameter. It was noticeable that the two end slices were always much softer than the rest, a fact also reported by Platt and Powers (22), but no explanation of this can be offered. The compressibility recorded is the mean of the four remaining slices.

The adjuncts tested were vegetable shortening (1, 2, and 3% of the flour weight), polyoxyethylene stearate (1%), polyoxyethylene stearate (1%) with shortening (1%), and stearic acid (1%). The results are shown in Table III.

TABLE III

Changes in the Compressibility of Bread Occurring on Aging

Adjuncts	Compressibility		
	1 hr.	24 hr.	48 hr.
None	2.16	0.85	0.72
1% Vegetable shortening	4.04	0.97	0.84
2% Vegetable shortening	4.6	1.05	0.82
3% Vegetable shortening	4.22	1.13	0.99
1% Polyoxyethylene stearate	2.61	1.06	0.99
1% Vegetable shortening + 1% polyoxyethylene stearate	2.54	1.04	0.86
1% Stearic acid	1.84	0.84	0.55

DISCUSSION

The experiments described above have shown that the action of polyoxyethylene stearate upon starch is very similar to the action of fatty acids and other monoesters. The ester prevents the adsorption of iodine by amylose in the same manner as stearic acid, and a linear relationship is observed between the proportion of adjunct present and the iodine affinity of the starch. The effect of the stearic acid is greater than that of the ester if weight percentages are considered, but if account is taken of the difference in molecular weights of the two adjuncts then it will be seen that one mole of the ester prevents the adsorption of iodine to a greater extent than one mole of the acid.

Mikus, Hixon, and Rundle (15) showed that the fatty acid molecules are adsorbed into the helical structure of glucose units comprising the amylose molecule. If it is assumed that polyoxyethylene stearate is taken up in the same manner, the relative sizes of the two molecules would provide the explanation for this fact.

On the other hand, the ester is not as efficient as oleic acid when used as a fractionating agent for the amylose of starch, and the precipitated portion contained only 42.5% of amylose compared with the 78% of amylose precipitated by oleic acid.

The experiments in which were investigated the effects of the ester and other compounds upon the gelatinization of wheat starch and upon the aging of 50% starch gels have shown that the substances examined may be divided into two classes:

(*a*) The class including stearic acid and monoesters of polyethylene glycols, which retard the swelling of the starch and increase the temperatures at which the two stages of gelatinization occur. The amount of swelling finally obtained at 98°C. is, however, not affected by the adjunct. These compounds reduce the swelling power of the starch in 50% gels and reduce the amount of soluble extract which may be obtained from the gels. This extract is, moreover, almost wholly amylopectin and it gives a red color with iodine.

(*b*) The class of fully esterified compounds such as triglycerides and diesters of polyethylene glycols which have a very slight depressant action upon the swelling of the starch in the first stage of the gelatinization and do not increase the gelatinization temperatures. They have a negligible action upon the swelling power and solubility of starch in 50% gels.

It is thus seen that the action of polyoxyethylene stearate upon starch alone may be compared with the well-known action of the fatty acids, and the work of Freilich (6) has shown that the ester in bread reduces the swelling power of the crumb in the same way as it reduces the swelling power in starch gels.

The effect of stearic acid in bread, however, is to give a loaf which is very much harder than the standard, whereas the ester gives a softer loaf. It is evident that some other influence is being exerted in addition to the simple action of the ester upon the starch alone.

Similar differences in the effect of the ester are noted for very fresh bread in which there is a mixture of ester and shortening. Freilich found that, when bread but 1–2 hr. old was considered, the addition of 1% of ester to a loaf containing 3% of shortening produced a harder loaf than one containing only 0.5% of the ester and 3% of fat. Table III shows that 1% each of shortening and ester produces a harder loaf than 2% of shortening. The effect is not merely confined to polyoxyethylene stearate, for Edelmann, Cathcart, and Berquist (4) showed that in bread containing 3 or 8% of lard, the addition of 0.5% of glyceryl monostearate produced a harder loaf when it was 3 hr. old. A similar addition of polyoxyethylene stearate, however, produced a softer loaf, and after about 12 hr. the loaves containing the monoesters were softer than the control.

There is competititon between the shortening or softening action of the ester and the hardening action, and whichever is more pronounced will depend upon the age of the loaf and the ratio of shortening to ester.

It is well known that triglyceride fats have a great softening effect upon the bread crumb, and the results described above demonstrate this point. The action of these fats is still obscure and there are two theories which have been advanced to explain it, neither of which will fit all the facts. The first is the well known "lubrication" theory where the fat is supposed to act as a lubricant between the starch granules and also to be adsorbed upon the gluten and soften it. This is compared with the different characteristics of the heat-coagulable protein in a hard-boiled egg, the albumen of the white being tough while in the yolk the protein is softened by the fat. This theory is supported by the microscopic structure of bread doughs, as reported by Burhans and Clapp (23).

The second theory has been advanced by Baker and Mize (24), who found that liquid fats added to bread gave little or no increase in volume or crumb texture but that very hard or brittle fats, which were powdered and mixed with the dough, gave a large increase in volume. Plastic fats were intermediate in behavior and depended upon whether they were added in a liquid or a solid state. The theory advanced by Baker and Mize is that the finely dispersed solid fat plugs the small holes in the gluten structure through which the gas normally escapes, thus giving greater gas retention in the loaf and increased volume. The unusual behavior of the hard fats is certainly explained by this theory, but the increased volume of the loaf is almost all "oven spring" and is produced when the loaf is beginning to cook. The gas evolution which produces the "oven spring" only starts to be rapid above 32°C., at which temperature the plastic fats normally used in bakeries would be liquid, and should, according to this theory, give very little increase in volume.

The shortening action of fats is therefore very complex, but it is evidently related to the ability of the fat to spread over the flour particles in an even film. The polyoxyethylene stearate and glyceryl monoesters possess this property to a high degree because of the large hydrophilic group, and they would be expected to be better shortening agents than triglyceride fats. The ability of polyoxyethylene stearate to reduce greatly the cold viscosity of starch pastes is further evidence of this function.

Hence, a loaf containing polyoxyethylene stearate will be much softer than one containing stearic acid over the whole range of aging, because of the shortening action of the ester. When two shortening agents are compared, however, the fresh loaf containing the ester will be harder than the loaf containing the vegetable shortening because the ester has produced the effect on the starch of being partially stale even when it is freshly cooked. Because the starch is in effect partly stale, however, the loaf will not harden on aging to the same extent, and hence after one day the loaf containing the ester will be softer than the loaf containing the shortening.

It has been the tendency in recent publications to discount the chemical tests for bread staling and to focus attention upon measurements of the firmness of the bread crumb which, it is claimed, give a greater correlation with organoleptic tests. While the importance of this correlation is realized, the fact remains that the chemical tests do provide a direct measure of the changes taking place in the starch component of the bread, and they are not susceptible to interference from structural changes in the bread which profoundly influence the firmness of the crumb.

Experiments designed to measure the rate of staling bread should take cognizance of all manifestations of staling and, unless the rate of change of all factors is reduced, interpretation of the results should be made with caution.

Acknowledgments

The author wishes to thank the Directors of Messrs. Scribbans-Kemp Limited, for permission to publish this work, and Dr. C. G. Sumner (Director of Research) for helpful advice and criticism. The experimental baking described in this paper was carried out by Mr. M. G. Cooper, to whom thanks are also expressed.

Summary

The action of polyoxyethylene stearate in preventing the hardening of bread on aging is discussed and ascribed to two functions: (*a*) a very efficient "shortening" action which softens the bread crumb, and (*b*) a depression of the swelling and swelling power of starch gels which, in effect, causes the starch to be partially stale, the bread therefore does not change so rapidly with age.

The two functions may be observed separately by (*a*) the usual shortenings common to bakery practice which do not cause a hardening of the starch, and (*b*) stearic acid which has a depressant action on the swelling of starch but little or no shortening properties.

References

1. Favor, H. H., and Johnston, N. F., *Cereal Chem.* **24**, 346 (1947).
2. Favor, H. H., and Johnston, N. F., *Cereal Chem.* **25**, 424 (1948).
3. Edelmann, E. C., and Cathcart, W. H., *Cereal Chem.* **26**, 345 (1949).
4. Edelmann, E. C., Cathcart, W. H. and Berquist, C. B., *Cereal Chem.* **27**, 1 (1950).
5. Skovholt, O., and Dowdle, R. L., *Cereal Chem.* **27**, 26 (1950).
6. Freilich, J., *Cereal Chem.* **25**, 87 (1948).
7. Katz, J. R., in Walton, R. P., A Comprehensive Survey of Starch Chemistry. The Chemical Catalog Company Inc., New York, 1928.
8. Noznick, P. P., Merritt, P. P., and Geddes, W. F., *Cereal Chem.* **23**, 297 (1946).
9. Schoch, T. J., and French, D., *Cereal Chem.* **24**, 231 (1947).
10. Schoch, T. J., and Williams, C. B., *J. Am. Chem. Soc.* **66**, 1232 (1944).
11. Caesar, G. V., in Kerr, R. W., The Chemistry and Industry of Starch. Academic Press Inc., New York, 1944.
12. Schoch, T. J., *J. Am. Chem. Soc.* **64**, 2954 (1942).
13. Bates, F. L., French, D., and Rundle, R. E., *J. Am. Chem. Soc.* **65**, 142 (1943).
14. Wilson, E. J., Schoch, T. J., and Hudson, C. S., *J. Am. Chem. Soc.* **65**, 1380 (1943).
15. Mikus, F. F., Hixon, R. M., and Rundle, R. E., *J. Am. Chem. Soc.* **68**, 1115 (1946).
16. Whistler, R. L., and Hilbert, G. E., *J. Am. Chem. Soc.* **67**, 1161 (1945).
17. Haworth, W. N., Peat, S., and Sagrott, P. E., *Nature* **157**, 19 (1946).
18. Harris, R. H., and Jesperson, E., *J. Colloid Sci.* **1**, 479 (1946).
19. Cook, D. H., and Axtmayer, J. H., *Ind. Eng. Chem., Anal. Ed.* **9**, 226 (1937).
20. Morgan, W. L., *Ind. Eng. Chem., Anal. Ed.* **12**, 313 (1940).
21. Beckford, O. C., and Sandstedt, R. M., *Cereal Chem.* **24**, 250 (1947).
22. Platt, W., and Powers, R., *Cereal Chem.* **17**, 601 (1940).
23. Burhans, M. E., and Clapp, J., *Cereal Chem.* **19**, 213 (1942).
24. Baker, J. C., and Mize, M. D., *Cereal Chem.* **19**, 84 (1942).

THE USE OF ION EXCHANGERS FOR THE DETERMINATION OF PHYSICOCHEMICAL PROPERTIES OF SUBSTANCES, PARTICULARLY RADIOTRACERS, IN SOLUTION. III. THE RADIOCOLLOIDS OF ZIRCONIUM AND NIOBIUM [1]

Jack Schubert [2] and John W. Richter [3]

Oak Ridge National Laboratory, Oak Ridge, Tennessee and the
Argonne National Laboratory, Chicago, Illinois

Received April 26, 1950; revised June 8, 1950

INTRODUCTION

Numerous studies have demonstrated that the *absorption* of cations by organic cation-exchangers is governed by mass-action principles (3,4,22). An increase in the bulk or *supporting* electrolyte concentration results in a continuous decrease in the absorption of a tracer cation. The absorption of tracer amounts ($\sim 10^{-8}\ M$) of zirconium and niobium, however, generally increases with increasing concentration of bulk electrolyte. In the latter cases the tracers are not absorbed by the usual cation-exchange mechanism, and in addition, the absorption is generally of an irreversible nature.

The ubiquitous colloidal tendencies of subgroup elements IV and V are well known (5,11,23) and the anomalous absorption just mentioned is reminiscent of a physical *adsorption* process. In such a case the bulk electrolyte acts as a coagulating agent and the resin functions as an adsorbent by virtue of its surface area. In addition, the resin may act to coagulate colloidal particles because of its high concentration of ionic charges (2). The latter explanation was suggested by Bauman (2) to account for the marked reduction in turbidity in water which has been passed through a bed of an organic cation-exchanger.

Several radioelements have been shown to exhibit colloidal behavior (6,7,12,16). The phenomena of slow diffusion, inability to dialyze completely or at all, coagulation, *etc.*, are obtained with these radiocolloids. The intrinsic nature of radiocolloids is still debatable (16). Paneth (12) believes that they are true colloids. According to Hahn (6) the whole process is essentially an adsorption phenomenon. He states that "the radioactive ions are adsorbed upon solid impurities accidentally present in the solutions, thereby imitating a colloidal character. . . ."

---

[1] Much of the material in this paper was reported under Contract No. W-7405-eng-39 in documents CN-2197 and CN-1873 in December, 1944, and January, 1945, respectively. Most of the experiments were done in the Chemistry Division of Clinton Laboratories at Oak Ridge under the general direction of G. E. Boyd. See Refs. (13) and (14) for the first two papers of this series.

[2] Present address: Argonne National Laboratory, P. O. Box 5207, Chicago 80, Illinois.

[3] Present address: Merck and Company, Rahway, New Jersey.

A convenient index for differentiating cation-exchange adsorption on a cation exchanger from the colloidal type of adsorption is the equilibrium distribution coefficient K_d, which is given by the expression:

$$K_d = M_s/M_l \times \text{volume of solution/mass of resin} = M_s/M_l \times v/m, \quad [1]$$

where M_s and M_l are the fractions of the adsorbed substance, M, in the resin and liquid phases, respectively.

In the cation-exchange process it has been shown (15) that (*a*) K_d is constant when v/m is varied; (*b*) K_d decreases when the bulk electrolyte concentration is increased; (*c*) K_d is constant over a wide range of trace-ion concentration, though at a certain critical concentration of trace cation, a sharp drop in the value of K_d occurs. It is possible to calculate this critical concentration from a single experimental point; and (*d*) K_d decreases upon the addition to the solution of a complexing agent which forms an unadsorbed (*i.e.*, neutral or negatively charged) complex ion with the cation. The decrease in K_d is inversely proportional to the concentration of complexing agent added and offers a convenient and unique method for determining the composition and stability of complex ions (13,14,17).

In the present study the adsorption of Zr and Nb as reflected by changes in K_d will be reported.

EXPERIMENTAL METHODS

Adsorbent

The adsorbent used was the synthetic cation exchange resin Amberlite IR-1. After several conditioning cycles with alternate NaCl–HCl treatments the 60–80-mesh resin particles were converted to a given alkaline earth cation form, *e.g.*, Ca^{++}, Sr^{++}, or Ba^{++}, by slowly passing a 5% solution of the nitrate salt through a bed of the resin until the concentration of the effluent practically attained the concentration of the influent. The resin was washed free of adhering salts with distilled water. Finally, the resin was air-dried and stored in a glass-stoppered bottle.

The air-dried resins contained about 16% moisture on the average as determined by drying a sample to constant weight of 105°C. The resins contained about 2.5 mequiv. as M^{++}/g. as determined by analyses of the HNO_3 solutions from ashed samples.

Radiotracers

Zirconium ($Zr^{95} \underset{65\text{ days}}{\xrightarrow{\beta^-}} Nb^{95} \underset{35\text{ days}}{\xrightarrow{\beta^-}} Mo^{95}$). The Zr^{95} was isolated carrier-free from neutron-bombarded uranium and separated from its Nb daughter 24 hr. before use. The final carrier solution was contained in a ~ 1 *M* HCl solution.

Niobium. The Nb^{95} was carrier-free and contained in a 1 *M* HCl solution.

Solution Preparation

All solutions were prepared from analytical grade chemicals and distilled water. The amount of tracer solution used for "spiking" was sufficiently small so that it contributed a negligible part of the total ionic strength.

Radiochemical Measurements

All measurements were made with a mica end-window Geiger-Müller (G.-M.) tube. In assaying the solutions a measured volume was deposited on a 22-mm. watch glass supported on cardboard and covered with scotch tape. All samples were counted at 8% geometry. The gamma activities of the Zr^{95} and Nb^{95} samples were counted through an Al–Pb–Al sandwich of absorbers.

Equilibration Procedure

Known masses of the air-dried resin in a given cation form M^{++} were equilibrated in glass-stoppered flasks with measured volumes of solution at 25°C. The bulk cation in solution was usually the same type as that present in the resin. Three hours contact time was found sufficient to give constant adsorption values. After the resin had settled, aliquots of the supernatant solution were removed, deposited on the watch glasses, and evaporated to dryness by overhead heating with an infrared lamp.

RESULTS

Inasmuch as the particular bulk cation employed had no significant effect on the adsorption characteristics of Zr or Nb, we will merely refer to "alkaline earth nitrate" in recording the data.

Effect of Bulk Electrolyte Concentration

It has been reported (15,16) that an increase in the adsorption of tracer Zr and Nb was observed when the concentration of bulk electrolyte was increased. On the other hand, the adsorption of Sr^{++} which always proceeds by a typical cation-exchange mechanism at the pH's employed, decreased rapidly with increasing bulk salt concentration. In similar experiments we find that upon altering the mass of resin but keeping all other factors constant the value of K_d for Nb is found to be nearly independent of M_s/M_l but to vary in approximate direct proportion to the value of v/m. Such behavior is opposite to that observed when the adsorption involves cation exchange only (14,20). A study of the uptake of mixed fission products in solutions of different alkaline earth nitrates revealed that the uptake of all of the cations of the alkali metals, alkaline earths, and rare earths decreased with increasing concentration of the bulk electrolytes while that of Zr^{95} and Nb^{95} remained nearly constant or increased. The results are in keeping with the usual coagulation action of electrolytes upon colloids, disregarding peptization effects.

The fact that K_d for the adsorption of elements such as Zr and Nb varies in the manner described allows the separation of these elements from true cations to be made with great ease. Since their desorption is nearly independent of the cationic activity of an eluting solution, it is possible to desorb any cations that are simultaneously adsorbed without removing any appreciably colloidal material. One can also desorb the colloids with an eluting agent which forms strong complex ions with them and yet does not contain sufficient cationic activity to desorb any adsorbed cations (19).

Effect of Sulfuric Acid on Nb Adsorption

The per cent adsorption and hence, K_d, of a cation decreases markedly as the H^+ concentration of a solution is increased (3,4). However, in the case of Nb the addition of concentrations of H_2SO_4 up to 0.75 *M* has a relatively small effect on K_d when v/m is kept constant (Table I). Higher concentrations of sulfuric acid, *i.e.*, > 3 *M* probably result in much lower values of K_d since it appears that niobium eventually forms a stable complex with sulfate ion (8).

Effect of Nitric Acid on Zr Adsorption

The per cent adsorption of Zr^{95} in 0.15 *M* alkaline earth nitrate is found to increase upon the addition of nitric acid and to reach a maximum constant value at about 0.2 *M* nitric acid (Fig. 1). The fact that the per

TABLE I

Effect of Sulfuric Acid on the Adsorption of Carrier-Free Niobium by Amberlite IR-1
Solution: 25 ml., 0.4 *M* in alkaline earth nitrate, tracer Nb^{95},
0.423 g. of MR_2 (oven-dried basis)

Conc. of H_2SO_4 *moles/l.*	Tracer adsorbed %	Distribution coefficient, K_d
0	82	270
0.5	78	210
0.6	78	210
0.75	68	130

cent adsorption of the Zr^{95} remained nearly constant from 0.2–1.0 M HNO_3 rules out any possibility that any significant true cation exchange exists in such a system. This conclusion must follow from the fact that if, as might be postulated, the HNO_3 first acted to convert the Zr to a cation which itself was more strongly adsorbed than the colloid, then the per cent adsorption should, necessarily, undergo a sharp decrease instead of remaining constant or even increasing beyond 0.2 M HNO_3.

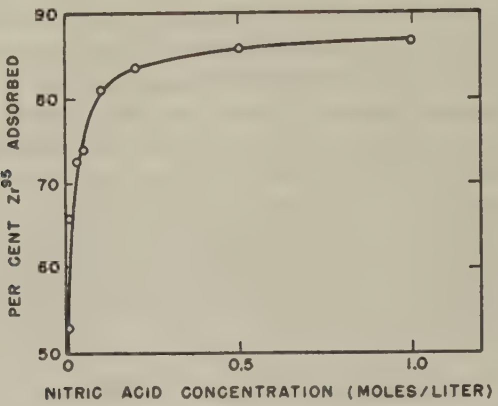

FIG. 1. Effect of varying nitric acid concentration on the adsorption of carrier-free Zr^{95} by the alkaline earth form of Amberlite IR-1 from a solution 0.153 M in alkaline earth nitrate. The ratio of the volume of solution to the mass of air-dried resin was 100:1.

An opposite result was observed in a similar experiment in which the tracer Zr^{95} used for "spiking" had been stored in 10 M HCl. In this case the adsorption of Zr^{95} decreased with increasing concentration of HNO_3, indicating that the conditions of storage had rendered the Zr^{95} cationic (16).

The Formation of Complex Ions of Zr and Nb

In a solution consisting of 0.5 M $M(NO_3)_2$ plus 0.5 M in fluosilicic acid, it is found that the adsorption of tracer Zr and Nb is greatly depressed (Table II). Inasmuch as solutions of equivalent ionic strength and hydrogen ion concentration have little or no effect on the adsorption of Zr and Nb, it must be concluded that these elements form complex fluoride ions probably similar to ZrF_6^{--} and NbF_7^{--}. Such complex ions, including the oxalates and citrates, are adsorbed by anion exchangers. As might be expected, protactinium is also complexed by fluorides in the same manner as Zr and Nb. The adsorption of Pa from HF solutions by an anion exchanger has been demonstrated and the composition PaF_7^{--} suggested (18).

In H_2SiF_6 solution, Nb is probably completely ionic. This is shown by the approximate constancy of K_d over a fivefold variation in the v/m ratio. Zirconium forms a much stronger complex fluoride ion than Nb inasmuch as no adsorption takes place under conditions in which considerable adsorption of the latter was observed.

A study of the variation of K_d with fluoride ion concentration and hydrogen ion concentration on a cation exchanger whose capacity is independent of pH such as Dowex 50 (3) should permit a determination of the composition and stability of the resulting complex ions. The procedure and calculations involved for such measurements are described in previous publications (13,17). The anion-exchange resin has also been utilized for such a measurement as was mentioned above (18).

TABLE II

Effect of Fluosilicic Acid in Alkaline Earth Nitrate on the Adsorption of Carrier-Free Niobium and Zirconium by Amberlite IR-1

Solution: 10 ml., 0.5 *M* H_2SiF_6, 0.5 *M* $M(NO_3)_2$, tracer

Tracer element	Weight of resin (oven-dried basis)	Tracer adsorbed	Distribution coefficient, K_d
	g.	%	
Nb^{95}	.423	40	16
Nb^{95}	.845	50	12
Nb^{95}	1.69	69	13
Zr^{95}	0.0845	0	0
Zr^{95}	.423	0	0
Zr^{95}	.845	0	0
Zr^{95}	1.69	0	0

Phosphoric and oxalic acids form complex ions with Zr and Nb in alkaline earth nitrate solutions which are 0.5 *M* in sulfuric acid (Table III). The strong complexing action of oxalic acid toward these elements is demonstrated by the marked decrease in K_d which occurs, especially in the case of Nb, with as little as 0.01 *M* oxalic acid. The distribution coefficient is strongly dependent upon the concentration of phosphoric or oxalic acid present even though the contribution of these acids to the ionic strength of the solution is very small, *i.e.*, as little as 1%. The ionic nature of Nb in the presence of phosphate is indicated by the relative constancy of K_d over an 18-fold variation of the v/m ratio.

As a result of these and other studies it was suggested (15) that elements such as zirconium and hafnium could be separated by converting them to the soluble anionic complex ions such as the fluoride, and subsequently adsorbing them on an anionic exchanger followed by chromatographic elution. Recently, it was demonstrated that such a procedure

TABLE III

Effect of Phosphoric and Oxalic Acids on the Adsorption of Carrier-Free Niobium and Zirconium by Amberlite IR-1

Solution: Includes $M(NO_3)_2$, 0.5 M H_2SO_4, tracer

Tracer element	Conc. of alkaline earth nitrate	Weight of resin (oven-dried basis)	Volume of solution	Composition of solution		Tracer adsorbed	Distribution coefficient, K_d
				H_3PO_4	$(COOH)_2$		
	moles/l.	*g.*	*ml.*	*moles/l.*	*moles/l.*	%	
Nb^{95}	0.5	0.0845	50.0	0	0	60	890
Nb^{95}	0.5	0.423	50.0	0	0	84	620
Nb^{95}	0.5	0.0845	10.0	0	0	87	790
Nb^{95}	0.5	0.423	50.0	0.094	0	34	61
Nb^{95}	0.5	0.0845	50.0	0.094	0	9.5	62
Nb^{95}	0.4	0.093	10.0	0.60	0	1.2	1.3
Nb^{95}	0.4	0.423	10.0	0.60	0	11	2.9
Nb^{95}	0.4	0.845	10.0	0.60	0	15	2.1
Nb^{95}	0.4	1.69	10.0	0.60	0	22	1.7
Nb^{95}	0.5	0.0845	10.0	0	0.01	39	76
Nb^{95}	0.5	0.0845	10.0	0	0.03	22	33
Zr^{95}	0.5	0.0845	10.0	0	0	61	190
Zr^{95}	0.5	0.0845	10.0	0.02	0	46	100
Zr^{95}	0.5	0.0845	10.0	0.05	0	24	37
Zr^{95}	0.5	0.0845	10.0	0.20	0	15	21
Zr^{95}	0.5	0.0845	10.0	0.60	0	0	0

results in excellent separation of Zr and Hf (8,10). The separation of Zr and Nb by anion exchange has also been accomplished by using oxalic acid to preferentially elute the oxalate complex ions (21).

In order to determine with certainty the composition and stability of the complex ions given above, more controlled experimental conditions than those given in Table III are necessary. This would involve keeping the ionic strength and hydrogen ion concentration constant. A preliminary calculation on the results of the interaction of Zr with H_3PO_4 (Table III) can be made by means of the equation (17):

$$K_c = \frac{(A^b)^n}{(K^0_d/K_d) - 1} \qquad [2]$$

where K_c is the dissociation constant of the complex ion, A^b is the concentration of the anion, n is the number of anion molecules per molecule of the cation, and K^0_d and K_d are the distribution coefficients (Eq. [1]) of the tracer in the absence and presence, respectively, of the given anion.

Using the data in Table III, $K^0_d = 190$, it is indicated that the complex ion formed between Zr^{95} and H_3PO_4 in a solution 0.5 M in $M(NO_3)_2$ and 0.5 M H_2SO_4 contains a 1:1 ratio of the two interacting components with a K_c of 0.02.

DISCUSSION

A summary of the experimentally observed adsorption characteristics of radiocolloids as compared with true cation exchange adsorption in terms of K_d is given in Table IV. There is little doubt that similar relationships will be found with the synthetic organic anion-exchangers. It would be of interest to extend these studies to include rates of adsorption.

TABLE IV

Summary of Some of the Variations in Adsorption of Tracer Cations and Radiocolloids by an Organic Cation Exchanger as Expressed by the Distribution Coefficient

Solution no.	Sol'n. composition relative to bulk electrolyte		Vol. of sol'n. / Mass of resin	Change in distribution coefficient, K_d, as related to adsorption process	
	Nature of bulk electrolyte	Concentration change		Cation-exchange adsorption	Radiocolloidal adsorption
			v/m	K_d	K_d
1	Noncomplexing salt	Increase	Constant	Decrease	Increase or nearly constant
2	Same as 1	Constant	Varied	Constant	Changes proportionately
3	Noncomplexing salt + noncomplexing acid	Constant salt, increasing acid	Constant	Decrease	Increase or nearly constant
4	Same as 3	Constant	Varied	Constant	Changes proportionately
5	Noncomplexing salt + noncomplexing acid + complexing agent[a]	Constant	Constant	Decrease	Decrease
6	Same as 5	Constant	Varied	Constant	Constant

[a] It is assumed that the complexing agent forms a neutral or anionic complex with the tracer.

In those cases where ion-exchange adsorption measurements indicated that a tracer was in the radiocolloidal state, confirmation was found in parallel studies involving diffusion rates, analysis, and ultrafiltration (16). The adsorption of normally cationic radioelements can often be rendered radiocolloidal by raising the pH of the solution to the region of the precipitation value for macroscopic concentrations of the cation, or by addition of anions which normally form insoluble compounds with the tracer. The application of such procedures to the separation or purification of substances is apparent.

It is reasonable to expect that the capacity of the cation exchanger for surface-adsorbed material would be much less than the cation-exchange capacity. That such is the case was shown in an experiment by Ayres (1) who found that the capacity of Amberlite IR 100 for zirconium from a 0.1 *M* solution of zirconyl nitrate was about 25 times less than the usual cation ion-exchange capacity (about 2 mequiv./g. anhydrous resin under the conditions given). Use was made of the colloidal state of zirconium to purify solutions of zirconyl nitrate by passing them through a cation-exchange column. Most of the $ZrO(NO_3)_2$ passed into the effluent while positive ions such as La, Fe, and Be were retained by the ion exchanger (1).

A qualitative indication of the relative strengths of some Nb and Zr complex ions can be obtained from the data in Tables II and III. In the case of Zr, the complexing strength of the different acids has the following order: fluosilicic > phosphoric > sulfuric. For Nb the order is: oxalic > phosphoric > sulfuric. Zirconium is much more strongly complexed by the fluoride ion than is niobium, as was mentioned previously.

Tracer Zr and Nb may not be entirely colloidal in any of the systems discussed. Qualitatively it can be assumed that the high adsorption of these tracers from relatively concentrated solutions indicates that these elements are predominantly colloidal in nature because no cation has been found to be as highly adsorbed under equivalent conditions. The relative proportion of the ionic to colloidal states, and the ranges of particle size will depend upon the previous treatment, manner of preparation, and conditions of storage of the tracers. All these and many other factors must be considered in interpreting radiocolloidal behavior (7,16).

Summary

The marked differences between cation-exchange adsorption and radiocolloidal adsorption by a synthetic cation-exchanger have been shown experimentally. The tracer elements studied were Zr^{95} and Nb^{95} in salt solutions of alkaline earth nitrates. It was shown that the differences between exchange adsorption and colloidal adsorption could be examined by means of the distribution coefficients. The composition of the alkaline earth nitrate solutions was varied by addition of nitric, sulfuric, phosphoric, fluosilicic, and oxalic acids. From the data, the relative strengths of some of the complex ions of Zr and Nb were deduced. The applications of radiocolloidal adsorption phenomena for the separation and purification of elements by an ion exchanger were discussed.

REFERENCES

1. AYRES, A. J., *J. Am. Chem. Soc.* **69**, 2879 (1947).
2. BAUMAN, W. C., *Ind. Eng. Chem.* **38**, 46 (1946).
3. BAUMAN, W. C., AND EICHHORN, J., *J. Am. Chem. Soc.* **69**, 2830 (1947).
4. BOYD, G. E., SCHUBERT, J., AND ADAMSON, A. W., *J. Am. Chem. Soc.* **69**, 2818 (1947).
5. BRITTON, H. T. S., Hydrogen Ions, Vol. II. D. Van Nostrand Company, New York, 1943.
6. HAHN, O., Applied Radiochemistry. Cornell University Press, Ithaca, New York, 1936.
7. HAISSINSKY, M., Les Radiocolloides. Hermann & Co., Paris, 1937.
8. HANSEN, R. S., AND GUNNAR, K., *J. Am. Chem. Soc.* **71**, 4158 (1949).
9. KIEHL, S. J., AND HART, D., *J. Am. Chem. Soc.* **50**, 2337 (1928).
10. KRAUS, K. A., AND MOORE, G. E., *J. Am. Chem. Soc.* **71**, 3263 (1949).
11. LATIMER, W. M., Oxidation Potentials. Prentice-Hall, New York, 1938.
12. PANETH, F., Radioelements as Indicators. McGraw-Hill Book Co., New York, 1928.
13. SCHUBERT, J., *J. Phys. & Coll. Chem.* **52**, 340 (1948).
14. SCHUBERT, J., AND RICHTER, J. W., *J. Phys. & Coll. Chem.* **52**, 350 (1948).
15. SCHUBERT, J., Ion Exchange: Theory and Application, Ed. by F. C. Nachod. Academic Press, New York, 1949.
16. SCHUBERT, J., AND CONN, E. E., *Nucleonics* **4**, 2 (1949).
17. SCHUBERT, J., RUSSELL, E. R., AND MYERS, L. S., JR., *J. Biol. Chem.*, in press.
18. THOMPSON, R., Studies on the Chemistry of Protactinium, Report No. AECD-1897. U. S. Atomic Energy Commission, February, 1948.
19. TOMPKINS, E. R., KHYM, J. X., AND COHN, W. E., *J. Am. Chem. Soc.* **69**, 2769 (1947).
20. TOMPKINS, E. R., AND MAYER, S. W., *J. Am. Chem. Soc.* **69**, 2859 (1947).
21. WACKER, R. E., AND BALDWIN, W. H., The Separation of Zr and Nb Oxalato Complexes by Anion Exchange, Report No. ORNL-637. U. S. Atomic Energy Commission, March, 1950.
22. WALTON, H. F., *J. Phys. Chem.* **47**, 371 (1943).
23. WEISER, H. B., Colloid Chemistry. John Wiley & Sons, New York, 1939.

THE CONCENTRATION DEPENDENCE OF VISCOSITIES IN DILUTE SOLUTIONS[1]

Robert Simha

National Bureau of Standards, Washington, D. C.

Received February 17, 1950

Several empirical expressions of the exponential of binomial type have been proposed to describe the variation of the viscosity with concentration, and fitted with more or less success to experimental data. One can write generally:

$$\eta_{sp}/c = [\eta] + a_2c + a_3c^2 + \ldots, \qquad [1]$$

where $[\eta]$ is the intrinsic viscosity. If any of the foregoing expressions hold, the coefficients a_i are related to each other and show some regularities. In other words one has:

$$a_2 = k_1[\eta]^2, \quad a_3 = k_2[\eta]^3. \ldots \qquad [2]$$

The k_i are numbers. For instance, in case the Arrhenius expression

$$\eta_{sp} = e^{[\eta]c} - 1$$

is obeyed, $k_1 = \frac{1}{2}$. On the other hand, for a polynomial expression of the Baker type, namely,

$$\eta_{sp} = \left(1 + \frac{[\eta]}{n}c\right)^n - 1,$$

one has $k_1 = (n - 1)/2n$. The coefficient k_1 has been measured for a number of systems and shown ordinarily to range between 0.3 and 0.7. These values are usually obtained at concentrations near 0.1 or 0.2% from a linear plot in η_{sp}/c. They should, therefore, not be compared with values which are frequently derived from measurements at much higher concentrations. The validity of [2] does, of course, not necessarily require the validity of an exponential or binomial equation.

In the following we shall briefly examine the effects which give rise to the appearance of the higher terms in Eq. [1]. For this purpose it is useful to consider the general features of the accepted treatment of intrinsic viscosity. Following Einstein, one assumes solute particles of a geometrically defined shape. On the basis of the hydrodynamic equations of motion one analyzes the flow disturbance and the resulting change in stress distribution and energy dissipation. The viscosity increase follows by adding up the individual effects of each molecule. This presupposes complete independence of all molecules in their action on the solvent flow, which in turn requires that the molecular dimensions be smaller than the intermolecular distances. This latter distance is proportional to $(M/c)^{1/3}$, where M is the molecular weight. For a rodlike molecule, therefore (length proportional to M), the critical ratio increases with increasing M and c as $M^{2/3} \times c^{1/3}$. For a coil we have proportionality with $M^{-(1/3-p)} \times c^{1/3}$, where p varies between $\frac{1}{2}$ and unity. As an example we take a polystyrene fraction, $M \doteq 10^6$, reported to have in benzene a radius of *ca.* 550 A (1). At $c = 0.1\%$, the ratio has a value of 0.4, which is already large.

---

[1] Presented at the Annual Meeting of the Society of Rheology, New York, N. Y., November 4–5, 1949.

Let us place the first molecule into the solution and then gradually approach with a second one. There will come a point, considerably before actual contact, where the flow patterns around the two particles begin to overlap, leading to what may be called interaction of the hydrodynamic type. At successively higher concentrations, there will appear interactions between clusters of increasing order, pairs, triplets, *etc.* This gives rise to quadratic, cubic, and higher terms in c, formally similar to the appearance of the higher virial coefficients in a gas or solution. In principle at least, one might think of describing in this way even concentrated solutions. However, under such conditions the physical picture loses its meaning. The original molecules rapidly approach closely, lose their identity, and form aggregates and nets until at high concentrations we are dealing with a swollen network. Mathematically expressed, the individual molecules with their individual flow patterns represent no longer a suitable starting point for a perturbation theory. However, here we shall be concerned only with dilute solutions in the sense indicated above and particularly with the coefficient a_2.

Under these conditions there are two possible effects to be considered, hydrodynamic interaction between pairs and the presence of double molecules in aggregation equilibrium. The concentration of aggregates depends on the square of the concentration. Hence, they contribute to the quadratic term by virtue of their intrinsic viscosity. More complex aggregates and the hydrodynamic interaction between them give rise to higher terms. For the pair aggregation we have:

$$K = c_2/c_1^2,$$

where c_2 and c_1 refer to double and single molecules, respectively. The contribution to a_2 can readily be shown to be (4):

$$a_2 \text{ (aggregation)} = K([\eta]_2 - [\eta]). \qquad [3]$$

K is the equilibrium constant and $[\eta]_2$ the intrinsic viscosity of an aggregate.

The question arises whether such a mechanism can lead to Eq. [2]. This can be answered by making an estimate of the molecular weight dependence. K is a ratio between rates of aggregation and disaggregation. If energy interactions were absent, the first quantity would simply be given by Smoluchowski's (2) well-known formula for rapid coagulation. It states that the rate of encounter of two particles is controlled purely by diffusion and proportional to the product $R \times D$, where R is the molecular radius and D the translational diffusion coefficient. The effect of energy interactions between the coagulating particles would be accounted for by a properly corrected diffusion constant. For the present argument, however (see below), this need not be considered. For a Gaussian coil, the product $R \times D$ varies between the limits $M^{-\frac{1}{2}}$ and M^0. Since K refers to weight by volume, this must furthermore be divided by M. The factor in the parentheses will, apart from the sign, be proportional to some power between 0.5 and 1.5 of the molecular weight. Thus in order for Eq. [2] to be valid, the ratio between the energy correction and the rate of dissociation must obey a rather special relationship. Without energy correction for instance, the rate of dissociation of double molecules would have to be proportional to M^{-2}–M^{-3}. While the inverse trend with molecular weight is in the expected direction, additional assumptions would be necessary to justify Eq. [2] on this basis.

It remains to investigate the hydrodynamic interaction. For spherical suspensions, the a_i are pure numbers and a_2 had been calculated some time ago (3). The resulting value for k_1 is much higher than is actually observed. The author has recently resumed the consideration of this problem for nonspherical molecules (4). The result confirms, with some restrictions, Eq. [2]. The details of the theory are somewhat involved. However, the general nature of the result can be seen by means of the following simple considerations. To make matters simple, we take a dumbbell-shaped particle (Fig. 1) which may be regarded as a model for a thin rodlike molecule, or as a section of a coil in which the line joining the two groups P and Q (each of radius a), passes through its center of gravity O. This particle is suspended in a solvent with a shearing motion of velocity gradient q relative to the center of the particle.

The rate of energy dissipation has the dimensions of force multiplied by a velocity and, hence, the contribution of one particle is

$$\left(\frac{dW}{dt}\right)_1 = \text{Force } (P) \times \text{velocity } (P) + \text{Force } (Q) \times \text{velocity } (Q).$$

It can be shown by exact methods that the velocities to be considered are those existing at the points P and Q in the absence of the particle. In other words, the effect of each of the two spheres on the solvent flow can be concentrated in its center. The corresponding force is the frictional force and given by Stokes's formula, if the two spheres do not influence each other. The velocities at P and Q are of equal magnitude and opposite sign. Hence, we can write, omitting numerical factors arising from the angular orientation, *etc.*, for the dissipation rate per unit volume the proportionality

$$\left(\frac{dW}{dt}\right)_N \propto \underbrace{\eta_0 aqL}_{\text{Force}} \times \underbrace{qL}_{\text{vel.}} \times N \propto \eta_0 q^2 a L^2 c/a^3, \qquad [4]$$

and for the intrinsic viscosity:

$$[\eta] \propto L^2/a^2. \qquad [4a]$$

N is the number of particles per unit volume. [4a] represents a familiar result, the intrinsic viscosity being proportional to the square of the length L.

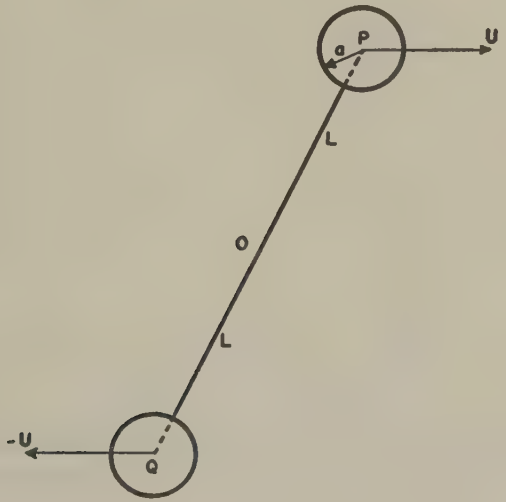

FIG. 1. Geometry of single molecule.

This result was obtained on the basis of Stokes's formula, which is valid only for a single sphere. When, with increasing concentration, two particles begin to approach each other (Fig. 2), this formula must be modified. It has been shown by Smoluchowski (5) that when two single spheres are moving with a velocity U and are a distance R_{12} apart ($a/R_{12} \ll 1$), the resistance of each is modified by an interaction term:

$$\text{Force} \propto \eta_0 aU(1 + a/R_{12}). \qquad [5]$$

Equation [5] merely gives the dimensional dependence on R_{12}, which is all that is needed here. It is seen that the interaction term in the force has dimensionally the same form as the coulomb potential exerted by a sphere on a second one very far away.

We now revert to the pair of particles (Fig. 2). Considering the signs of the velocities of the four centers P, Q, M, N, and remembering the $1/R_{12}$ formula, it is clear that the interaction problem in the viscous forces becomes analogous to the calculation of the interaction potential between two rigid dipoles. If $L/\rho \ll 1$ (Fig. 2), the term $1/\rho_{PM}$ and the other corresponding ones can be expanded. In analogy to the familiar result for the potential, *viz.*, μ^2/ρ^3 (μ-dipole moment) the interaction term becomes $\eta_0(a^2UL^2/\rho^3)$. Instead of Eq. [4], one finds now by substitution for U and summation over all particles acting on a primary one:

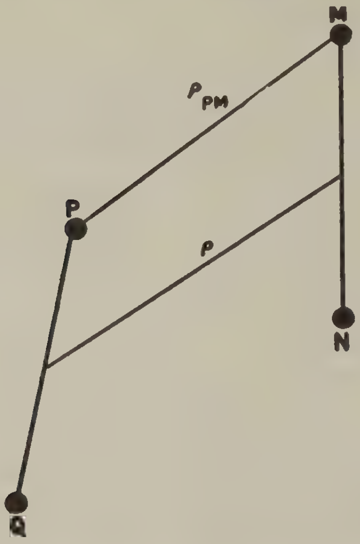

Fig. 2. Geometry of interacting molecules.

$$\frac{dW}{dt} \propto \eta_0 q^2 aL^2[1 + \sum_i (aL^2/\rho_i^3)] \times N \propto \eta_0 q^2 aL^2(1 + aL^2N)N. \quad [4b]$$

The second proportionality arises since the sum which extends over all n molecules in a volume V, will be proportional to $N = n/V$. Thus the interaction leads to a quadratic term in the concentration, and from [4*a*]:

$$a_2 \propto L^4/a^4 = k_1[\eta]^2. \quad [6]$$

While this conveys the general picture, and the intrinsic viscosity can actually be obtained in this way, the calculation of a_2 requires an explicit consideration of the field of flow. This was carried out under the following important assumptions:

1. Random orientation of particle axes, that is small shear rates.
2. Neglect of interaction between groups of the same molecule. This restricts the result to very thin ellipsoids or to open coils, for which Staudinger's rule is valid.
3. Uniform distribution of all particles in space.

In this connection it will be noted that some of the molecules around a given one will be so close that the expansion in powers of the reciprocal center-to-center distance breaks down. This fact has been disregarded. It will be particularly important at higher concentrations. The result then is (4):

$$k_1 = 0.77.$$

This is of the right order, but larger than the observed values except in poor solvents. Part of the discrepancy may reside in the approximations made. As far as the experiments are concerned, the question of extrapolation arises. The results so far obtained at extremely high dilution, *i.e.*, below 0.1%, do not seem to indicate a downward curvature in the curve of η_{sp}/c vs. c, (6), as found previously by some authors. This is still under investigation.

An extension of this work to intermediate cases between the extended coil in which there is no mutual shielding of groups, and the compact sphere previously analyzed is clearly desirable. Regardless of the question of exact numerical agreement, however, one may draw the following conclusions:

1. There are no reasons for expecting a binomial or exponential formula to be generally valid at low concentrations when hydrodynamic interaction is still important.
2. Orientation effects due to shear will be more pronounced at higher concentrations than at infinite dilution (intrinsic viscosity).
3. k_1 is larger for spherical particles than for asymmetric ones.

Possible confirmation for this may be found in the fact, that branched molecules seem to have higher k_1-values than linear ones and that globular proteins give large k_1's. Also in poor solvents in which flexible chain molecules assume more compact shapes, k_1 has been shown to have large values, even near or above unity. In such systems, however, aggregation effects assume increased importance and it would, therefore, be very desirable to examine the validity of Eq. [2] in extremely poor solvents. There, also, the hydrodynamic contribution to a_2 may depend on molecular weight. To obtain the dependence of this contribution on solvent power, it will be necessary to consider the change of the shape of the two interacting coils with changing solvent conditions.

It is of some interest that this increase of k_1 with decreasing solvent power or decreasing intrinsic viscosity (for a fixed molecular weight) can be made plausible by a quite different line of reasoning. On relating the viscosity of the solution to the free energy of mixing in a way somewhat similar to that of Powell, Roseveare, and Eyring (7) for low molecular mixtures, one finds a relation of the type

$$k_1 = \alpha + \beta/[\eta],$$

with $\alpha = \frac{1}{2}\cdot\beta$ varies slightly with solvent power and is nearly equal to the density of the polymer if the concentration is expressed in weight by volume. The numerical values are of the right order of magnitude. But, of course, this result should not be taken too literally.

Summary

At very low concentrations, at which the solute molecules either retain their identity and original shape or form low-order aggregates, the concentration dependence of the reduced specific viscosity η_{sp}/c results from two factors, hydrodynamic interaction, and aggregation. An expression for the latter and a simplified description of the former, which apply to the coefficient a_2 (Eq. [1]), are presented. On the basis of the complete theory previously given, the effect of particle shape and solvent on the coefficient k_1 (Eq. [2]) is discussed.

References

1. Bueche, A. M., *J. Am. Chem. Soc.* **71**, 1452 (1949).
2. Smoluchowski, M., *Z. physik. Chem.* **92**, 129 (1917).
3. Guth, E., and Simha, R., *Kolloid-Z.* **74**, 266 (1936); Gold, O., Thesis, Vienna, 1937.
4. Simha, R., Proc. Intern. Cong. of Rheology, Holland, 1948; *J. Research Natl. Bur. Standards* **42**, 409 (1949).
5. Smoluchowski, M., *Bul. Acad. Sci. de Cracovie* **1A**, 28 (1911); Oseen, C. W., Hydrodynamik, Akademische Verlagsgesellschaft, Leipzig, 1927.
6. Rothman, S., Simha, R., and Weissberg, S. G., *J. Polymer Sci.* **5**, 141 (1950).
7. Powell, R. E., Roseveare, W. E., and Eyring, H., *Ind. Eng. Chem.* **33**, 430 (1941); see also the author's discussion in connection with polymer solutions in "High Polymer Physics," Ed. H. A. Robinson, Chemical Publishing Co., Brooklyn, N. Y., 1948.

EXTINCTION ANGLES, INTRINSIC VISCOSITIES, AND MOLECULAR WEIGHTS OF POLYSTYRENE IN SOLUTION [1]

M. D. Schoenberg,[2] J. Riseman and F. R. Eirich

Institute of Polymer Research, Polytechnic Institute of Brooklyn, Brooklyn, N. Y.

Received February 17, 1950

ABSTRACT

Experimental measurements of the extinction angle of polystyrene fractions were made concurrently with intrinsic viscosity and sedimentation measurements. Data so obtained have been used to examine the Kuhn theory of streaming birefringence and also to calculate rotatory diffusion constants. A combination of intrinsic viscosity and rotatory diffusion constant was used to calculate molecular weights, and these were compared with previously calculated data from osmotic pressure, sedimentation, and intrinsic viscosity measurements on the same fractions. Furthermore, this pair measurement was used according to the Kirkwood-Riseman (K-R) theory to compute the fundamental molecular parameters b and ζ which were compared with the results from sedimentation measurements. The root mean square end-to-end distance is determined from the experimental values of b and compared with the analogous values from sedimentation and with the length obtained from a direct application of the Kuhn theory.

In addition the following information was obtained:

1. The changes in the extinction angle from solvent to solvent can be interpreted in a manner analogous to the intrinsic viscosity and sedimentation data as being connected with the average changes in shape (molecular dimensions). Thus the extinction angle is found to be lower in chloroform than in toluene, corresponding to the higher intrinsic viscosity in the former.
2. Molecular-weight measurements are readily made from the pair measurement of intrinsic viscosity and rotatory diffusion constant in direct analogy to the pair measurement of sedimentation constant and translational diffusion constant.
3. Sizes computed from the direct application of the Kuhn theory are several fold too low as compared with the values customarily found from light-scattering, sedimentation, and intrinsic viscosity.
4. Sedimentation constants calculated from the b and ζ values of extinction angle measurements are in satisfactory agreement with those previously reported for the same fractions.
5. Extinction angles near 45° were found up to gradients of 5×10^3 sec.$^{-1}$ for polystyrene molecular weights up to 8×10^5, in agreement with those calculated from the rotatory diffusion constant according to Riseman and Kirkwood.

---

[1] Presented at the Annual Meeting of the Society of Rheology, New York, N. Y., November 4–5, 1949.

[2] Taken in part from a dissertation presented by Melvin D. Schoenberg, June, 1949, to the Faculty of the Graduate School of the Polytechnic Institute of Brooklyn in partial fulfillment for the degree of Doctor of Philosophy in Chemistry.

Introduction

In order to obtain a fuller understanding of the hydrodynamic properties of macromolecules in solution, and to examine recently proposed theories, we have initiated a series of investigations wherein the same fractionated polystyrene samples were employed in sedimentation, viscosity, and streaming birefringence measurements. In a previous paper (1), the results of sedimentation studies of the polystyrene fractions in three solvents were presented and attempts were made to correlate these results with those of other hydrodynamic methods. This paper is a continuation wherein the method of streaming birefringence is used independently to obtain information about the properties of macromolecules in solution, to correlate these data with results of sedimentation and viscosity, and also to examine the current theories of streaming birefringence.

In the past, streaming birefringence measurements of solutions of flexible macromolecules have suffered from the use of unfractionated materials,[3] and from the absence of independent measurements such as sedimentation and light scattering on the same fractions. This situation is aggravated by the fact that current theories of the streaming birefringence of flexible molecules are not sufficiently well developed to interpret the results of experiment with confidence. Possessing intrinsic viscosity and sedimentation measurements (on the same fractions), the latter having been previously interpreted (1), we are now in a position to examine the results of Kuhn's theory (2) of flow birefringence; also, guided by these previous results, we shall propose a semiempirical method to interpret our experimental findings, the results of which will be found to be consistent with other methods. In particular, extinction angle measurements will be used to obtain the hydrodynamic parameters b and ζ of Kirkwood-Riseman (3,4). From these, the average end-to-end lengths and the rotatory diffusion constants of the several polystyrene fractions in toluene and chloroform will be calculated and compared with the theoretical values according to Riseman-Kirkwood (4). Finally, the rotatory diffusion constant will be used in conjunction with the intrinsic viscosity to obtain molecular weights.

Experimental

Polystyrene Samples and Solvents

Of the four polystyrene fractions used, the two lower-molecular-weight fractions were provided through the courtesy of Dr. E. Merz of the Monsanto Chemical Co. The raw polymer was prepared by polymerizing 100,000 g. of styrene with benzoyl peroxide as catalyst and some modifiers at 60°C. over a period of several days. Methyl alcohol was used to precipitate the polymer from butanone solution. Fractionation into more than 40 fractions of irregular quantity was effected, with fraction 1 M containing the most material (about 700 g.) being the highest-molecular-weight fraction. The samples used in this work were from raction samples 1 and 7 and are noted as 1 M and 7 M. They display some polydispersity, fraction 1 M somewhat more so than 7 M. On the other hand, the main peaks of the sedimentation diagrams of these fractions display single modes only, slight skewness, and, in general, retain their over-all shape after sedimenting a considerable distance through the cell even at low concentrations (1). These characteristics suggest appreciable homogeneity[4] of the main component.

---

[3] Signer and Gross' classical work was performed on fractions too low to assume highly coiled molecules.

The higher-molecular-weight fractions 3 G and 2 G were prepared by emulsion polymerization with persulfate catalyst. The polymerization was carried out in a closed container to low conversion for a period of 2 weeks at room temperature. The polymer was divided into two fractions of which one was discarded and the second refractionated into four parts. The second fraction of the latter series is 2 G. The third fraction was again refractionated into four parts, with 3 G being again the second fraction. The fractionations were made by solvent evaporation from ethyl methyl ketone–butanol solutions.

Viscosity measurements were made on the four fractions in ethyl methyl ketone, toluene, and chloroform at 27.2°C. using Ostwald viscosimeters. The solvents were of C.P. grade and were not further purified. All other measurements were made at 27°C.

Apparatus

The apparatus used is a modification of that described by Edsall (5). It consists of a rotating inner cylinder, a jacketed outer stator, and an optical bench with light source, lenses, polarizing elements, and compensator mounted on special riders. The driving mechanism is a ¼-horsepower d. c. motor operated by a General Electric Thymotrol control unit insuring constant speeds from 60 to 2500 r.p.m. and providing a full torque over the entire speed range. The speeds, as measured by a Strobotac, were found to be constant within the limits of the measuring device (10–12 revolutions/1000). The optical system patterned after that described by Snellman (6) was found to give satisfactory results. The previously annealed plane-surface windows were mounted by allowing them to rest with very slight pressure against polythene gaskets in snugly fitting seats. The brass cylinders were gold-plated, and another smooth, dull black copper oxide coating[5] was deposited electrolytically on the surface so as to eliminate reflections from the surfaces of the cylinders. The dimensions of the instrument are given in Table I.

---

[4] The existence of some unknown foreign material in all of the fractions of this series was noted by Dr. Merz, but they occur in very small amounts and their bearing on the measurements may be considered negligible.

CURRENT THEORIES OF STREAMING BIREFRINGENCE (EXTINCTION ANGLES)

In the case of rigid particles, rods, and ellipsoids, adequate treatment is available from the work of Boeder (8), Peterlin and Stuart (9), and others (10). For the extinction angle χ it is found that

$$\tan 2\chi = \frac{6D_r}{q}, \qquad [1]$$

where D_r is the rotatory diffusion constant, and q the velocity gradient. The same authors have also obtained expressions for the magnitude of the birefringence.

For flexible molecules the current state of the theory of flow birefringence is far from satisfactory. Probably the most explicit treatment is that of Kuhn (2), which we shall consider now.

TABLE I

Dimensions of the Instrument

Radius of outer cylinder	2.529 cm.
Radius of inner cylinder	2.479 cm.
Annular gap	0.050 cm.
Height of cylinders	6.98 cm.
Wavelength of light	5461 A
Critical gradient (7)	859,000 sec.$^{-1}$, η/ρ

The model chosen is such that the hydrodynamic forces act on the molecule as if one-fourth of the total chain were concentrated at each end. In this respect the model treated is effectively that of a dumbbell and does not represent the currently accepted model for a flexible molecule. (The introduction of a tension force would modify the model to that of an elastic dumbbell.) The rotation of this model is then treated in terms of the tangential motion of the ends, introducing a translational diffusion constant. It should be noted that, in the absence of the tensile force, keeping the length constant and introducing a rotatory motion instead of the translational motion would reduce Kuhn's expression for the density of distribution of the orientational angle θ to that of Boeder's two-dimensional case. We are, therefore, under the impression that the Kuhn treatment is not a satisfactory one, and we shall show from our data that dimensions obtained from the use of Kuhn's results are far out of line with those currently accepted.

---

[5] Ebinol C, by courtesy Philip Sievering Co., New York, N. Y.

Kuhn obtains from his model

$$\tan 2\chi = \frac{1}{\alpha h_0^2}; \text{ and } \alpha = \frac{q}{4D_t}, \qquad [2]$$

where D_t is the translational diffusion constant for an end containing one-fourth of the total chain length concentrated in it, and h_0^2 is the mean square end-to-end length.

$$D_t = \frac{4kT}{\lambda L \eta_0} \approx \frac{8kT}{3\pi\eta_0 L}, \qquad [3]$$

where, k = Boltzmann's constant,
T = Absolute temperature,
η_0 = Solvent viscosity,
$\lambda \approx 3\pi/2$, and L is the overall length of the chain. Finally, in terms of Kuhn's Eq. [3], one could define an "effective rotatory diffusion constant" D_{eff}, such that

$$D_{\text{eff}} = \frac{8kT}{3\pi\eta_0 L h_0^2}. \qquad [4]$$

As against this treatment, and in the absence of any other satisfactory theory of streaming birefringence, we propose to treat our data in terms of an empirical equation analogous to [1]

$$\tan 2\chi = \frac{mD_r}{q}, \qquad [1a]$$

where m is a number. For the extrapolated rotatory diffusion constants D_r we shall use $D_{\varphi\varphi}$ resulting from the theory of Riseman-Kirkwood (R-K).

In Eq. [1a] it is assumed that as a first approximation the flexible molecule behaves as a rigid particle. Kuhn's expression (Eq. [3]) falls into this form if, as in Eq. [4], one defines an "effective rotatory diffusion constant." It should be noted that this "effective rotatory diffusion constant," D_t/h_0^2, is purely artificial and is defined as such merely because of dimensionality requirements. Values of h_0 obtained using Eqs. [2] and [4] will be compared with our corresponding values $\langle R_0\rangle_{\text{Av}}$ calculated under the assumptions of Eq. [1a] and making use of the rotatory diffusion constant of R-K.

DISCUSSION OF RESULTS

Molecular Weights, Intrinsic Viscosity, and Rotatory Diffusion Constants

It has been known for a long time that the rotatory diffusion constant, intrinsic viscosity, and sedimentation constant should be related to each other. In the case of rigid particles the relationships follow from the work of Stokes and Einstein. We quote here the relationship between intrinsic viscosity and the rotatory diffusion constant for flexible molecules[6] which has been worked out by R-K (4):

$$M = \frac{NkT}{400\eta_0[\eta]D_{\varphi\varphi}}. \qquad [5]$$

In terms of the extinction angle we identify the extrapolated rotatory diffusion constant of Eq. [1*a*] with $D_{\varphi\varphi}$ as defined by R-K. This leads to the direct correlation of the extinction angle and intrinsic viscosity with the molecular weight M:

$$M = \frac{NkT}{400\eta_0[\eta]\left[\frac{q}{m}\tan 2\chi\right]_{\lim_{q=0}^{c=0}}} \qquad [6]$$

The extrapolation to zero concentration and vanishing gradient is necessary since $D_{\varphi\varphi}$ is calculated for infinite dilution and the absence of external deforming fields.

Kuhn (2) has also given a relationship between extinction angles, intrinsic viscosity, and molecular weights holding for small gradients and large values of χ

$$M = \frac{2RT[\omega]}{100[\eta]};\ [\omega] = \lim_{q=0}\frac{\omega}{\eta_0 q};\ \omega = \frac{\pi}{4} - \chi, \qquad [7a]$$

negligible internal viscosity

$$M = \frac{2}{3}\frac{RT[\omega]}{100[\eta]}. \qquad [7b]$$

large internal viscosity

It should be noted though that in obtaining these results Kuhn made use of his theory of intrinsic viscosity which omits internal interactions. Because of a similar neglect in his $[\omega]$ term, this omission is approximately compensated and the expressions reduce to a form close to that of K-R.

Figure 1 is a representation of the course of the extinction angles with gradient at various concentrations in toluene. The extrapolated rotatory diffusion constants were obtained from Eq. [1*a*] and were used together with the intrinsic viscosities to calculate the molecular weights. The results of the application of Eqs. [1*a*] and [6], using the factors $m = 2$ for our polystyrene in toluene, and $m = 1.75$ in chloroform, are given in Tables II and III. These values for m were chosen empirically with the help of the osmometrically-known molecular weight for fraction 1 M. The same values will then be seen to "fit," by reproducing the other molecular weights, or the $D_{\varphi\varphi}$, as determined by means of Eq. [5]. As stated above, this procedure is empirical in so far as the selection of a value for the constant m is concerned. It should be pointed out, though, that since Eq. [5] affords an absolute method for the determination of molecular weights, and inasmuch as Eq. [1a] represents an empirical attempt to correlate $D_{\varphi\varphi}$ and the extinction angle, the empirical nature of Eq. [6] arises from the substitution of [1a] into [5].

---

[6] In Eq. [8], reference (1), the numerical factor is misprinted as 200.

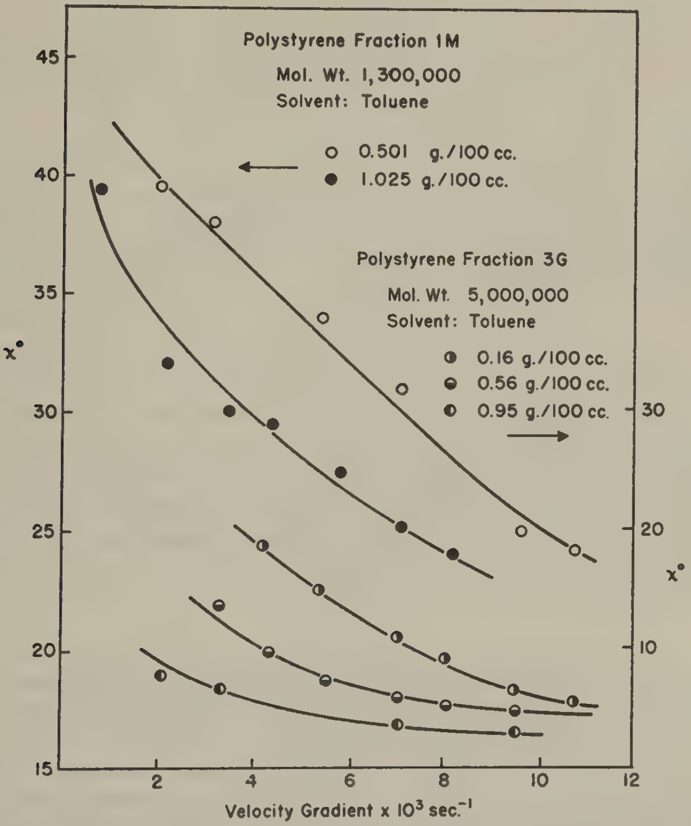

FIG. 1. Extinction angle χ *vs.* gradient. Polystyrene fraction 1 M (left-hand scale): mol. wt., 1,300,000; solvent, toluene; ○, 0.501 g./100 ml.; ●, 1.025 g./100 ml.; Polystyrene fraction 3 G (right-hand scale): mol. wt., 5,000,000; solvent, toluene; ◑, 0.16 g./100 ml.; ◒, 0.56 g./100 ml.; ◐, 0.95 g./100 ml.

The agreement shown by Tables II and III between the molecular weights obtained in this way in both solvents with those from other methods should be noted. The agreement of the results for fractions 7 M and 1 M with data obtained by osmotic pressure and sedimentation measurements appear to justify the assumptions made. The original value of the molecular weights of fractions 3 G and 2 G are questionable,

TABLE II

Comparison of Molecular Weights, Intrinsic Viscosities and Rotatory Diffusion Constants Obtained From Extinction Angles With Those From Direct Experiment, for Various Polystyrene Fractions in Toluene

Fraction	Molecular weight		Intrinsic viscosity		Rotatory diffusion constant	
	Exptl.[a]	Calcd.[b]	Exptl.	Calcd.[b]	Exptl.[c]	Calcd.[d]
	$\times 10^5$	$\times 10^5$				
7 M	8	9.7	2.3	2.7	5250	6250
1 M	13	15	2.8	3.2	2625	2885
3 G	(50)	45	6.2	5.5	412	400
2 G	(90)	65	9.6	—	225	—

[a] Experimental values for 7 M and 1 M from osmotic pressure data; values for 3 G and 2 G estimated from light-scattering and viscosity data.

[b] Calculated from Eq. [5] or [6], using $m = 2$, and $[\eta]$ exp. or M exp.

[c] From Eq. [1a], using $m = 2$.

[d] From Eq. [5], using M exp. and $[\eta]$ exp.

having been determined by viscosity measurements in a range far outside of the calibration range. We are, therefore, accepting the values that we have determined to be more correct.

In view of these results and of the relative ease of making birefringence measurements as contrasted with translational diffusion measurements, this method of obtaining molecular weights appears to be a valuable addition to the methods now commonly used.

TABLE III

Comparison of Molecular Weights, Intrinsic Viscosities and Rotatory Diffusion Constants Obtained From Extinction Angles With Those From Direct Experiment, for Various Polystyrene Fractions in Chloroform

Fraction	Molecular weight		Intrinsic viscosity		Rotatory diffusion constant	
	Exptl.[a]	Calcd.[b]	Exptl.	Calcd.[b]	Exptl.[c]	Calcd.[d]
	$\times 10^5$	$\times 10^5$				
7 M	8	10	2.8	2.9	3950	4950
1 M	13	16	3.3	4.2	2000	2580
3 G	(50)	51	9.6	10.9	225	255

[a] Experimental values for 7 M and 1 M from osmotic pressure data; values for 3 G estimated from light-scattering and viscosity data.

[b] Calculated from Eq. [5] or [6], using $m = 1.75$.

[c] From Eq. [1a], using $m = 1.75$.

[d] From Eq. [5].

The Basic Hydrodynamic Parameters b and ζ

According to the theories of K-R, the hydrodynamic behavior of flexible macromolecules depends on two parameters, b and ζ. A knowledge of these parameters and M suffices for the calculation of the sedimentation constant s_0, $[\eta]$, and $D_{\varphi\varphi}$. In the previous paper (1), sedimentation data were used to obtain b and ζ. Here, b was calculated by converting as above $D_{\varphi\varphi}$ to $[\eta]$, and then extrapolating $\frac{[\eta]}{Z^{\frac{1}{2}}}$ *vs.* $Z^{-\frac{1}{2}}$ to the limit[7] $Z \rightarrow \infty$ (3,4). ζ is determined by substitution into the expressions derived by R-K. These results are presented in Table IV along with the values from Refs. (1) and (3). The extrapolation involving the two fractions 3 G and 2 G, the molecular weights of which had not been previously accurately determined, yields values for b and ζ in reasonable agreement with previous independent methods.

TABLE IV

Basic Hydrodynamic Parameters for the Polystyrene Molecule

	b		$\zeta \times 10^{10}$ [b]	
	Toluene	CHCl$_3$	Toluene	CHCl$_3$
	Å	Å		
Birefringence	7.9	9.8	1.06	0.75
Sedimentation	9.2	11.0	1.5	0.96
Kirkwood-Riseman[a]	(8.1)		(1.3)	

[a] Calculated from data in benzene [see Ref. (3)].
[b] Dimension of $\zeta = m/t$.

TABLE V

Average End-to-End Lengths for Polystyrene Molecules

Fraction	Sedimentation		Extinction angle		Kuhn[a]	
	Toluene	CHCl$_3$	Toluene	CHCl$_3$	Toluene	CHCl$_3$
7 M	1100	1360	1080	1360	(250)	(300)
1 M	1400	1760	1340	1720	(330)	(400)
3 G	—	—	2300	3050	(900)	(1000)
2 G	—	—	2800	(3460)[b]	(1200)	

[a] Values approximate because of nature of extrapolation.
[b] Calculated assuming a molecular weight of 6.5×10^6.

---

[7] $Z \equiv$ number of carbons in the polymer chain.

Lengths and Sedimentation Constants from b and ζ

From the values of b and ζ it is now possible to calculate the average end-to-end length and also the sedimentation constants of the polystyrene molecule in the two solvents. These are presented in Tables V and VI. Agreement with the previously reported results of sedimentation measurements should be noted.

From our value of b, we would obtain for a molecular weight of 1×10^6 a length in toluene of 1100 Å which is comparable to that obtained by light-scattering (11) and by sedimentation.

The effect of the solvent on size is seen by comparing, in Table V, the corresponding values in toluene and chloroform. The change of size with solvent is in agreement with that of the previous paper (1). Thus the view expressed in this previous paper that chloroform is a "better" solvent for polystyrene than toluene is here confirmed.

TABLE VI

Sedimentation Constants

(Solvent: Toluene)

Fraction	s_0 Experimental (Sedimentation)	s_0 Calculated (Extinction angle)
7 M	9.3×10^{-13}	12.3×10^{-13}
1 M	11.2×10^{-13}	14.7×10^{-13}

The interrelationships between intrinsic viscosity, sedimentation, and extinction angle permit conversely the theoretical calculation of rotatory diffusion constants and extinction angles from intrinsic viscosity and molecular weight. We have found that for polystyrene of a molecular weight up to 8×10^5 in toluene the extinction angle differs only by a few degrees from 45° for gradients up to 5000 sec.$^{-1}$. This is in good agreement with the theoretical predictions.

SUMMARY

1. The empirical Eq. [1*a*] offers a way for the interpretation of the extinction angles found with flexible molecules. The rotatory diffusion constants obtained therefrom are in agreement with values of the theory of Riseman-Kirkwood if the required parameters b and ζ are taken from other methods, *e.g.*, intrinsic viscosity and sedimentation constant. This confirmation emphasizes the value of these fundamental parameters for the characterization of flexible molecules.

2. In consequence, the mean end-to-end lengths obtained agree with those deduced from light-scattering, intrinsic viscosity, and sedimentation measurements. In marked contrast, values calculated by means of Kuhn's theory of flow birefringence fall considerably below.

3. The pair measurement of intrinsic viscosity and rotatory diffusion constant (or extinction angle) as interpreted by the Kirkwood-Riseman theories offers in principle an absolute method for molecular-weight determination. In the absence of a theoretical relationship between $D_{\varphi\varphi}$ and experimentally measured quantities, molecular weights in good agreement with those from other methods are obtained by the semi-empirical procedure of introducing $[1a]$. This means of obtaining molecular weights should be most useful in the region of high molecular weights.

REFERENCES

1. NEWMAN, S., RISEMAN, J., AND EIRICH, F., The Shape of Macromolecules in Solution. Proc. International Colloq. on Macromolecules, Amsterdam, 1949.
2. KUHN, W., AND KUHN, H., *Helv. Chim. Acta* **26**, 1394 (1943).
3. KIRKWOOD, J. G., AND RISEMAN, J., *J. Chem. Phys.* **16**, 565 (1948).
4. RISEMAN, J., AND KIRKWOOD, J. G., *J. Chem. Phys.* **17**, 442 (1949).
5. EDSALL, J. T., AND FOSTER, J., *J. Am. Chem. Soc.* **70**, 1860 (1948); EDSALL, J. T., Advances in Colloid Science, Vol. 1. Interscience Publishers, New York, 1943.
6. SNELLMAN, O., *Arkiv Mineral Geol. Kemi*, **19A**, 1 (1945); SNELLMAN, O., AND BJORNSTAHL, Y., *Kolloid-Beihefte* **52**, 403 (1941).
7. TAYLOR, G. I., *Proc. Roy. Soc.* (*London*) **A157**, 546, 565 (1936); *Trans. Roy Soc.* (*London*) **A223**, 289 (1923).
8. BOEDER, P., *Z. Physik* **75**, 258 (1932).
9. PETERLIN, A., AND STUART, H. A., *Z. Physik* **112**, 1, 129 (1939).
10. SADRON, C., *J. phys., radium* **9**, 381 (1938).
11. DOTY, P. M., AFFENS, W. A., AND ZIMM, B. H., *Trans. Faraday Soc.* **42B**, 65 (1946).

THE FORMATION AND FLOW OF EMULSION

E. G. Richardson

King's College, Newcastle-upon-Tyne, England

Received January 20, 1950; revised April 4, 1950

INTRODUCTION

Although a considerable amount of work has been done on the properties and applications of emulsions, much of this work concerns the technical aspects, in particular, their relative stability, and there is less information on the fundamental aspects either of the common methods of their formation or of their behavior when subjected to shear. It is the purpose of this paper to survey this information and to put forward new data.

Emulsion Formation

The processes by which emulsions are manufactured may be reduced, in essentials, to two. Either (*1*) one liquid is squirted into another, whereby the former is atomized into the latter or, (*2*) the two liquids are allowed to mingle in turbulent motion, in order that portions of the one may be sheared off to form drops within the other.

Various mills are employed in making emulsions commercially. In most of these the two liquids are introduced in the desired proportions and agitated in contact. Each liquid is so broken into coarse threads and lamellae within the other. As Stamm and Kraemer (8) have pointed out, two processes are involved in such a mill; disruption into drops and recombination. The purpose of an emulsifying agent is to protect one phase against this coalescence.

Injection Process

The first process is essentially the problem of the breakup of a liquid jet under the combined action of the interfacial tension and the relative viscosity of the fluids.

In the main there are two types of breakup. In the first, interplay of inertia and surface tension results in the jet becoming varicose. Rayleigh (6) examined the conditions under which axial-symmetrical oscillations set up near the nozzle might increase in amplitude. He showed that in an inviscid jet a disturbance having a wavelength 4.4 times the diameter of the jet should grow fastest and eventually break up the jet into drops. Tyler and Richardson (11) have taken photographs of this type of breakup on capillary jets. Rayleigh modified his theory to take account of the viscosity of the liquid, which naturally reduces the rate of growth of the optimum disturbance, whose wavelength in relation to the diameter of the jet remains unchanged.

In the second type of disturbance, the jet becomes sinuous and the resistance to the passage of the humps becomes of more importance than surface tension. This type of breakup has been treated mathematically by Weber (14), but is only amenable to semiempirical analysis.

Since the air resistance to this type of motion increases rapidly with speed, breakup will occur at a faster rate as the speed of efflux rises, whereas the varicose form of disturbance has a rate of growth independent of the speed of efflux.

Hence it may be concluded that at high velocities in excess of a critical value, breakup is controlled by inertia and viscous forces. Any expression deduced for this breakup should involve the characteristic factors which enter into viscous flow, *i.e.*, velocity V, drop diameter d, interfacial tension σ, the densities ρ_1, ρ_0, and the viscosities η_1, η_0 (or their kinematic coefficients) of the two liquids. Ohnesorge (5) has given a criterion for the change of type, so too have Tyler and Watkin (12) who used jets of one liquid squirted into another. The former's formula for the critical velocity V_0 from a nozzle of diameter D is:

$$\frac{\eta_1}{\sqrt{(\rho_1 \sigma D)}} = 2000 \left(\frac{\eta_1}{V_0 \rho_1 D}\right)^{4/3}$$

but neither he nor Tyler and Watkin introduce the viscosity of the continuous medium into their formulas.

TABLE I

Ohnesorge's Critical V_0
(cm./sec.)

Liquids	$D = 0.1$ cm.	$D = 0.15$ cm.	$D = 0.275$ cm.
Aniline–water	70	50	19
Aniline–brine	89	70	26
Benzene–water	100	70	25
Paraffin–water	150	110	90

In the table are shown the critical velocities according to Ohnesorge's formula for the change from the varicose to the sinuous type of breakup for a number of pairs of liquids and nozzles which form the subject of an investigation by the present author.

A large tank 2 ft. high on a base 1 ft. square had a pair of opposite vertical sides glazed, one with frosted and one with clear glass, to permit the photographing of the jets when the frosted pane was illuminated from behind.

Nozzles in the form of drawn-out capillary tubes were arranged to squirt one or the other of the following liquids: aniline, benzene, paraffin, or fuel oil, into the water-filled tank. The nozzles were inclined at about 30° to the vertical in order to give a good spread of the droplets through the water for photography.

In one instance, aniline was injected into brine in the tank in order to vary the interfacial tension.

Flashlight photographs, by Arditron lamp, were taken of such jets and were projected, together with a superposed graticule, on a screen so that the different drop sizes could be sorted out and summation curves constructed. Speeds both above and below the critical values—which agreed qualitatively with the figures in the above table—up to a maximum of 8 m./sec. were employed.

In the varicose regime, breakup is governed by velocity, surface tension, and nozzle size. The drops also tend to be more uniform in size if the critical velocity is not exceeded. The difference can be seen on the specimen photographs reproduced. Figure 1 illustrates breakup of an oil into water jet just below the critical velocity. Figure 2 shows the spread of the same jet at a supercritical speed. The uniformity of size of drops at very low speeds is well seen in Tyler and Watkin's photographs of aniline–water jets, where the size is almost entirely governed by interfacial tension. When the speed of efflux is very slow, we have the well-known method of the "drop-weight" for measuring interfacial tension.

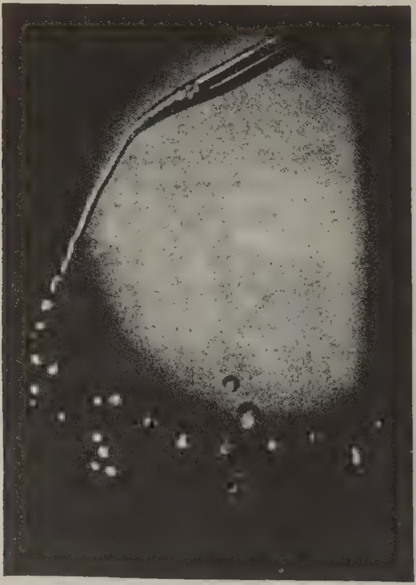

Fig. 1. Jet of oil entering water at subcritical speed.

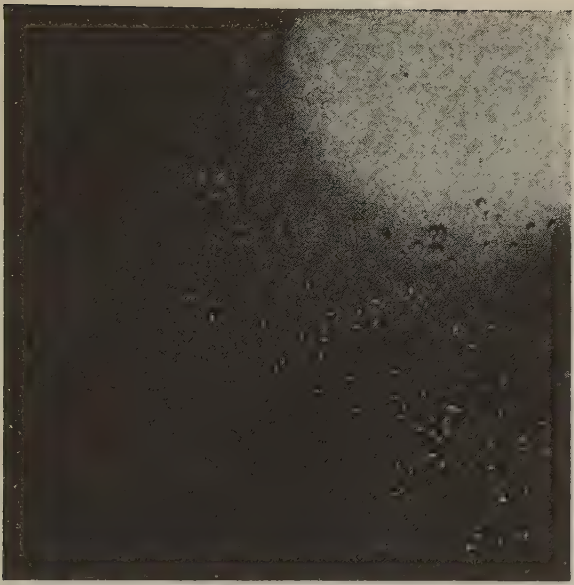

FIG. 2. Jet of oil entering water at supercritical speed.

As a further comparison, two typical summation curves, derived from photographs such as those of Figs. 1 and 2, are shown in Fig. 3 for oil into water dispersion, supercritical to left, subcritical to right.

When jets issue from large nozzles at low speeds, the drops are not found to be uniform in size for another reason. This is that drops of large diameter falling through a fluid are unstable, dividing up into smaller units to an extent dependent on the path of fall and therefore on the distance of the collecting apparatus from the nozzle.

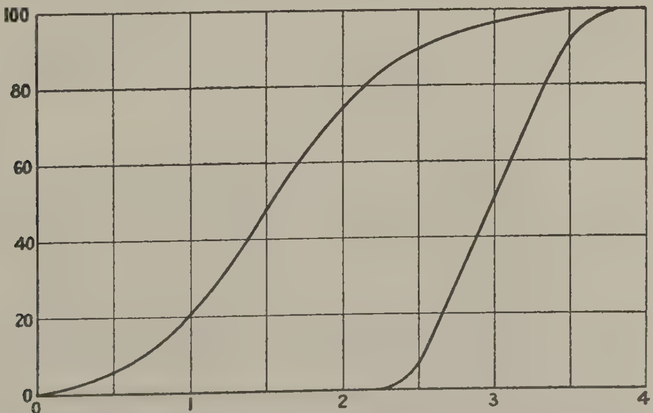

FIG. 3. Summation curves of drop size: oil–water jets: abscissae, diam. in mm.

A drop of liquid in motion through another fluid differs in behavior from a solid sphere in that it may (*a*) be deformed or (*b*) have a circulation set up within itself by the shearing effect of the relative motion of the two fluids. These effects upset the stability of the drop, causing it to oscillate about the spherical shape and eventually to burst into fragments or, at least, into smaller drops.

Before bursting, the effects of deformation and circulation become apparent as an increase in the resistance, compared to that of a rigid sphere of the same diameter. Bond and Newton (1) investigated this effect and showed that the parameter relevant to these changes was $(\rho_1 - \rho_0)d^2g/\sigma$ where ρ_1 and ρ_0 are the densities of drop (or bubble) and medium, respectively. The value of this "Bond number" (B) was of the order of unity when the rate of fall began to change. This value of B applied to air bubbles rising slowly in liquids: for liquid drops in a liquid medium it was higher—up to five in some cases.

Taylor (9) has obtained an expression for the upper limit to the size of the drop which can subsist while the fluid is being sheared. The conservative force is the interfacial tension between phases while the disruptive force is the pressure difference between the inside and the outside of the drop caused by the viscous forces: both of these depend on the radius of the drop. He has also carried out some illuminating experiments in which a drop of oil was poised in sirup, filling the space between four rollers rotating in such directions that the originally spherical drop was pulled out into an ellipsoid and finally burst under the action of the excessive shear.

The mean drop size is then read off from the 50% intercept of such figures and the Reynolds' number (*i.e.*, Vd/ν, where V is the efflux velocity, d the mean drop size and ν the kinematic viscosity of the liquid in the drop) plotted logarithmically against ν/ν_0, ν_0 being the viscosity of the continuous phase.

This has been done in Fig. 4, which comprises all the results obtained in the present research, plotted logarithmically. An empirical formula which fits the results is: $\left(\frac{Vd}{100\nu}\right)^{1.25} = 100\,\frac{\nu_0}{\nu}$.

If it is desired to produce an emulsion of given mean drop size by such a process, this graph or the formula can be used to find the velocity of injection which should be used, if the viscosities of the two constituents are known.

In most commercial injection processes the critical velocity is well exceeded, so that this formula should apply. It is also possible to influence drop size by acoustic agitation either directly on the nozzle or through the liquid. Capillary waves are then set up on the periphery whose wavelength is—in theory—uniquely determined by the quotient of the velocity

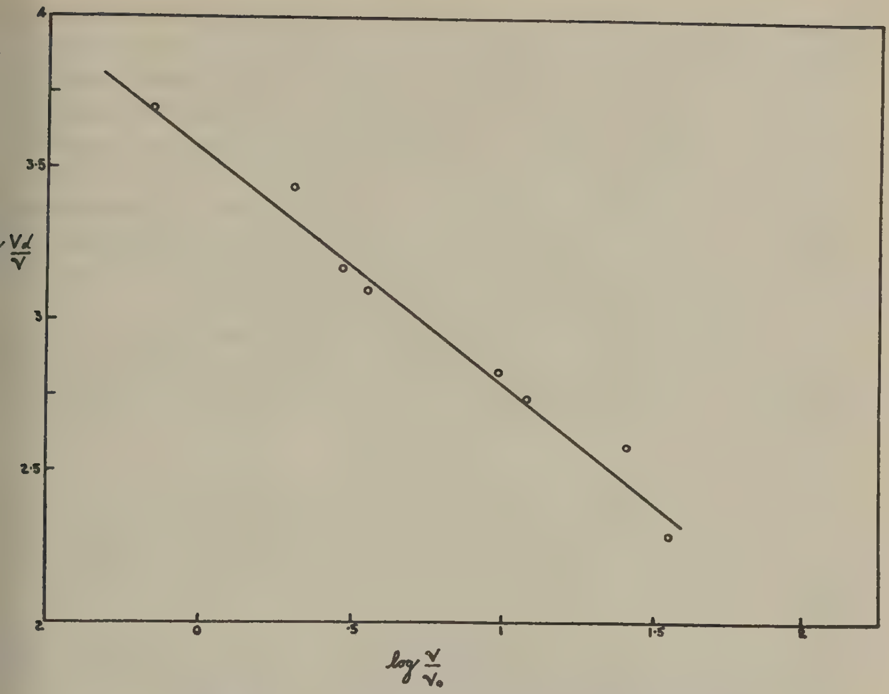

FIG. 4. Reynolds' number of mean drop size in jets of different relative viscosity.

of such waves by the frequency of agitation. The maker of an emulsion usually requires that the dispersion shall be both fine and moderately uniform. It should be possible to attain this object by ultrasonic agitation. The author has, in fact, found that at the speed corresponding to Fig. 1, the action of an ultrasonic magnetostriction generator on the nozzle is to cause a finer breakup like that of Fig. 2, without the necessity of increasing the velocity of efflux. There is, too, a greater uniformity in size of drop, but the author has not examined sufficient cases to give precise figures for this improvement.

Turbulent Flow Process

Clay (3) has done experiments on the refining of an emulsion by pumping it in turbulent motion through a pipe of 4-in. diameter at a Reynolds' number (for the pipe) of 10^5. His method was to introduce a coarse emulsion, suddenly to increase the speed, taking instantaneous photographs of the emulsion just before and after the impulse. In another apparatus, turbulence was set up in the space between two coaxial cylnders by rotating the inner one. He did find an improvement in the fineness, being able to produce a mean diameter of 10 μ from an emulsion nitially having drops of the order of ten times this size, but did not catch a glimpse of the actual partition process. All drops caught by the camera were, in fact, spherical in shape.

The Reynolds' number of the pipe ranged between 5×10^4 and 5×10^5 and was subjected to a sudden change while the effect on the dispersion was noted. A sudden increase favored further disruption but a decrease brought coalescence. Clay found, as in the present experiments, that a high equilibrium value of Reynolds' number promoted a homogeneous emulsion. In spite of apparent differences in different processes of emulsification, it seems that they reduced essentially to the one which has been here studied in what seems to be its simplest form.

Of course, in all these refining methods, care must be taken to prevent recoalescence of drops, inevitably becoming more difficult as the number population rises. This is, however, mainly the chemist's problem and I shall not discuss it here.

Flow Phenomena

The features of the flow of an emulsion, once formed, which interest the physicist are the effect on its viscosity of (*1*) concentration of the dispersed phase, (*2*) drop size distribution, and (*3*) rate at which it is sheared.

By thus glibly separating the effects into three classes, I do not imply that they can be separately and distinctly varied in experiments: far from it!

There is a well-known formula, due to Einstein (4), for the effect of the volume concentration (c) on the viscosity (η) of a suspension, *i.e.*, $\eta = \eta_0 (1 + kc)$, η_0 being the viscosity of the pure liquid (solvent).

Taylor (10) has modified the Einstein equation for variation of viscosity with concentration in an emulsion by allowing for the deformation of the droplets. Such deformation will be limited however by the Bond number of the motion and in most practical emulsions the drops are so small that when the emulsion is sheared they act as rigid spheres. They may not do so in very concentrated emulsions, but then the Einstein-Taylor formulas would not be expected to apply in such cases.

The author (7) made some measurements on the behavior of these systems when subjected to shear in a coaxial cylinder apparatus, using water and benzene as the two components. By adding a little sodium oleate to the water and shaking it up with the benzene the latter appeared in the emulsified form, whereas if magnesium oleate be added to the benzene and shaken up with water it is the latter which is dispersed in drops. Figure 5 shows how the torque communicated to the inner cylinder depends on the concentration in both types of emulsion, the speed of the outer cylinder remaining the same. Evidently the viscosity increases rapidly with the concentration of the disperse phase, although the water-in-benzene emulsion breaks up when the water predominates in quantity over the other constituent. The trend of the other curve (benzene-in-water) recalls that of solid suspensions and suggests an exponential relation between apparent viscosity and concentration. In fact, if one plots the logarithm of η/η_0 (where η is the viscosity of the emulsion and η_0 that of the "solvent") against concentration one obtains a straight line.

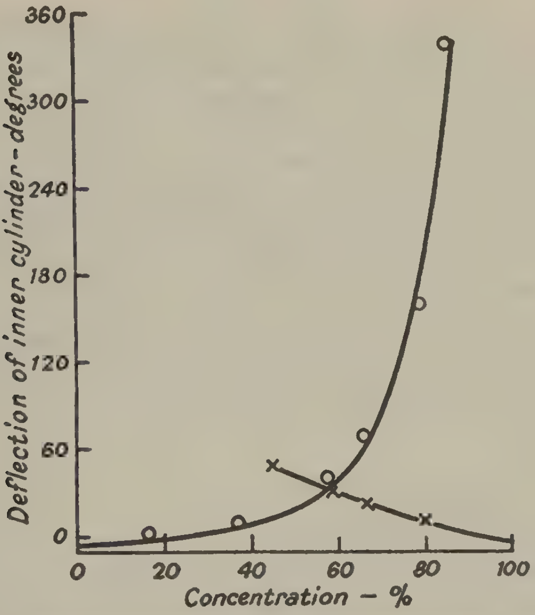

FIG. 5. Variation of apparent viscosity of emulsions with concentration. Circles: benzene in water; crosses: water in benzene.

If an increase of pressure δp acts on a substance of volume v to reduce it by δv, the compressibility is defined as $\delta v/v\,\delta p$. This is a constant for a given material as long as elastic laws are obeyed. In the same way we can think of an increase of the space occupied by the disperse phase by an amount δc as reducing the average separation of the discrete globules by the fraction $\delta l/l$, so that

$$\delta l/l\,\delta c = \chi,$$

where χ is a sort of "interphasal" compressibility, whose value depends on the relative compressibility of the two phases, or, in colloquial terms, on the overcrowding of the disperse phase, which is resisted by the continuous phase. When flow takes place we can think of the continuous medium having to move between obstacles of average separation l and in doing so being subject to a viscous resistance denoted by the coefficient η.

If overcrowding reduces the separation of the impedimenta to $l - \delta l$, the viscous resistance is supposed to increase in the proportion of η to $\eta + \delta\eta$, therefore

$$\frac{d\eta}{\eta} = -\frac{dl}{l} = \chi\, dc.$$

The solution of this equation is $\eta = \eta_0 e^{\chi c}$ or in logarithmic form, $\log (\eta/\eta_0) = \chi c$.

This formula, tested against the results of the author and those of other workers who measured the apparent viscosities of such emulsions as albumin and blood, gives good agreement with theory, having regard to the fact that most of the available data refer to apparent viscosity, derived from torque measurements in concentric cylinder-type viscometers.

Broughton and Squires (2) have made similar measurements in many types of emulsions. When, in fact the plot is made of $\log \eta/\eta_0$ against c, they find the straight line so obtained does not pass through the origin but has an intercept on the axis, indicating a "yield value." They write: $\log (\eta/\eta_0) = \kappa(c + c_0)$.

Another important conclusion from Broughton and Squires' work was that both the yield value and the coefficient κ depended on the emulsifying agent. The emulsions which are most stable are (for a given concentration) the least viscous.

A factor which has been much neglected is the effect of globule size distribution on viscosity.

Unfortunately, deductions on this point from experiments are difficult owing to the variation of viscosity with rate of shear. The viscosity does however tend to a limiting value at high rates of shear. Mr. Iskander and I are investigating this point and hope to publish details of the experiments later, but I should like to mention a few results here.

Taking the limiting values of the viscosity η_∞ at the highest rates of shear, these are shown below against mean particle size $\bar{d}$ and the product of these factors:

Emulsion	η_∞	$\bar{d}$	$\eta_\infty \cdot \bar{d}$
A	250	0.55	140
B	140	0.95	130
C	60	2.2	130
D	25	2.4	60

These products are in agreement for the three emulsions *A*, *B*, and *C*, which had the same shaped distribution curve about different means, but that of the last one, *D*, lies rather apart from the others. This is not surprising when one notes that this one had coarser droplets though its maximum lay at about the same diameter as *C*.

In this connection, I was very interested to observe the conclusions of Whitmore and Ward (13) in their paper presented at the May, 1949 discussion on suspensions at Exeter, *i.e.*, that the viscosity of suspension of rigid spheres depends on particle size distribution but not on the absolute size of the spheres. Mr. Iskander's results so far would indicate that both these factors intervene to determine the viscosity of a suspension of deformable particles.

References

1. Bond and Newton, *Phil. Mag.* **5**, 794 (1928).
2. Broughton and Squires, *J. Phys. Chem.* **42**, 253 (1938).
3. Clay, *Proc. Acad. Sci. Amsterdam* **43**, 852, 979 (1940).
4. Einstein, *Ann. Physik* **19**, 289 (1906).
5. Ohnesorge, *Z. angew. Math. u. Mech.* **16**, 355 (1936).
6. Rayleigh, *Proc. Math. Soc. (London)* **10**, 4 (1879).
7. Richardson, *Kolloid-Z.* **65**, 32 (1933).
8. Stamm and Kraemer, *J. Phys. Chem.* **30**, 992 (1926).
9. Taylor, *Proc. Roy. Soc. (London)* **A138**, 41 (1932).
10. Taylor, *Proc. Roy. Soc. (London)* **A146**, 501 (1934).
11. Tyler and Richardson, *Proc. Phys. Soc. (London)* **37**, 297 (1925).
12. Tyler and Watkin, *Phil. Mag.* **14**, 849 (1932).
13. Ward, *Nature* **164**, 220 (1949).
14. Weber, *Z. angew. Math. u. Mech.* **12**, 136 (1931).

LETTERS TO THE EDITORS

MIXED SOLVENT EFFECT IN SOLUBILIZATION

We refer to the article by Santi R. Palit, published in the *J. Colloid. Sci.* issue of October 1949, p. 523, "A Note on Mixed Solvent Effect in Solubilization." He reports that the solubilization of water by cetyldimethylammonium bromide is greater in mixtures of chloroform and benzene or of chloroform and carbon tetrachloride than in any of these solvents separately.

This phenomenon was also recorded by us [*Trans. Faraday Soc.* **54,** 391 (1948), Example III, Fig. 1] for the solubilization of water in mixtures of carbon tetrachloride and high-molecular-weight paraffin (Technical White Oil) by means of Aerosol OT. An explanation was advanced in terms of the general theory of solubilization proposed.

Suppose that gradual addition of water $\bar{W}$ to an organic liquid A containing a detergent C at a given concentration finally leads to the formation of a "Type II System" in which an excess aqueous phase separates that consists mainly of water with only minor amounts of A and C. Suppose further that addition of water to a second organic liquid B containing C at the above concentration leads to the formation of a "Type I system" in which the aqueous phase produced is relatively rich in both C and solubilized B while the excess B phase tends to be depleted in both C and $\bar{W}$ to the advantage of the aqueous phase. We have found that in such cases solutions of C in mixtures of A and B dissolve more water than solutions of C in either A or B separately.

The maximum solubility of water is to be expected for that mixture $\bar{O}$ of A and B which makes the ratio "R" — (mean solvent affinity of C for $\bar{O}$ saturated with $\bar{W}$)/(mean solvent affinity of C for $\bar{W}$ saturated with $\bar{O}$) — equal to unity. This is a special case of the principle of Bancroft (1) that if a third substance C is soluble in two partially miscible liquids $\bar{O}$ and $\bar{W}$ the miscibility of the two liquids is increased by addition of C; this occurs to a greater extent the more nearly the ratio of the comparative solubilities of C in $\bar{O}$ and in $\bar{W}$ approaches unity.

A frequently encountered example of the phenomenon under discussion is the much greater degree of miscibility of aqueous detergent solutions ($\bar{W} + C$) with suitable mixtures of n-alkanol (A) and hydrocarbon (B) than with either n-alkanol or hydrocarbon separately. This is observed with most detergents since, even with those of comparatively hydrophilic character, the *n*-alkanols function as A above and yield Type II systems($R > 1$) while the hydrocarbons function as B and yield Type I systems ($R < 1$).

Cases where the A function ($R > 1$) is shown by chloroform (Palit) or even by carbon tetrachloride or benzene (Winsor) are observed with less hydrophilic, and more "oil-soluble" detergents. An organic liquid (e.g. carbon tetrachloride or benzene) which behaves as B ($R < 1$) towards one detergent (e.g. undecane-3 sodium sulfate or cetyldimethylammonium bromide) may behave as A ($R > 1$) to a more lipophilic detergent (e.g. Aerosol OT). Also an organic liquid which with a particular detergent C behaves as B ($R < 1$) when $\bar{W}$ is water or (water + water-soluble organic liquid) may behave as A ($R > 1$) when $\bar{W}$ is (water + suitable quantity of inorganic salt).

Palit remarks that with cetyldimethylammonium bromide, chloroform-rich media show a positive temperature coefficient of solubilization, whereas carbon tetrachloride-rich media show the reverse behavior. We have noted (2) that this contrast in behavior is fairly general between Type II (in this case chloroform) and Type I (in this case benzene or carbon tetrachloride) systems, respectively. There are however numerous exceptions to this rule.

ACKNOWLEDGMENT

The writer wishes to thank the Directors of the "Shell" Refining and Marketing Co., Ltd., for permission to publish this note.

REFERENCES

1. BANCROFT, *J. Phys. Chem.* 1, 414 (1897).
2. WINSOR, P. A., *Trans. Faraday Soc.* 54, 455 (1948).

Thornton Research Centre,
Thornton-le-Moors,
Cheshire, England

P. A. WINSOR

Received February 1, 1950

REPLY TO LETTER OF P. A. WINSOR

Dr. Winsor's claim of priority of the above observation is undoubtedly correct. My failure to refer to this fact explicitly has happened through oversight of this part of his paper and is very much regretted. My observation is only a more remarkable demonstration of the same phenomenon, as the maximum in my case is about six times the weight of the detergent as against nearly equal weight in the case of Dr. Winsor.

The explanation given by Dr. Winsor on classical lines about this phenomenon seems to be quite reasonable. The important point that remains to be settled however is to relate this classical idea with the currently accepted picture about the role of micelles in solubilization.

Indian Association for the
Cultivation of Science,
Calcutta, India
Santi R. Palit

Received February 16, 1950

BOOK REVIEWS

Deformation and Flow. An Elementary Introduction to Theoretical Rheology By MARKUS REINER, Professor, Technical College, Haifa. H. K. Lewis & Co. Ltd., London, 1949. 346 pp. Price $6.50.

This book represents a very considerable revision and improvement of the author's "Ten Lectures on Theoretical Rheology," published in 1943, for physicists. The present book has been written primarily for chemists.

The author considers that Rheology belongs, together with classical mechanics (including relativity), thermodynamics, and Maxwellian electrodynamics, to the phenomenological side of physics. Hence, he does not advocate the more recent atomic–molecular approach to Rheology, and cites that "the unsatisfactory state [of this approach] in its relation to the problem of strength, where the atomic theory yields figures, a thousand-fold those of experience, is well known. The practice of investigators in material testing laboratories all over the world still largely follows the methods of phenomenological rheology."

The volume impresses the reviewer as a thorough and well-organized presentation of the subject from the viewpoint adapted.

VICTOR K. LA MER, New York, N. Y.

The Physical Chemistry of Electrolytic Solutions. By HERBERT S. HARNED, Professor of Chemistry, and BENTON B. OWEN, Professor of Chemistry, Yale University. 2nd Ed. Reinhold Publishing Corporation, New York, 1950. 645 pp. Price $10.00.

The second edition of this comprehensive well-known treatise differs from the first edition in the addition of thirty-six pages in the form of appendices. The authors state in their preface:

"While part of our original text was in press in 1941, revised tables of fundamental constants were published by Birge. At that time, it was decided to make no change in the numerical tables of physical constants, characteristic slopes and mathematical functions in Chapter (5). Had we decided to make this change, all of the numerical tables would have been inconsistent with the actual calculations in the book. In this edition we have not altered the tables in Chapter (5) for the same reason, but have incorporated in Appendix B revised values of those quantities affected by changes in the fundamental constants. This procedure leaves the original text representative of the calculations during the three decades preceding 1940, and we believe that this is the most unequivocal way of meeting this unfortunate complication.

"Appendix B is comparatively short, so no subject index for it has been included. Instead, a detailed Table of Contents and a separate Author Index are supplied. The sections in Appendix B are designated consecutively, (B-1), (B-2), etc., and the equations are numbered, (B-1-1), (B-10-4), etc., where (B-1-1) is the first equation in Section (1), (B-10-4) is the fourth equation in Section (10), etc. The Figures and Tables are similarly designated. Cross references between tables in the main body of the book and Appendix B have been introduced."

VICTOR K. LA MER, New York, N. Y.

Proceedings of the International Congress on Rheology. Holland, 1948. Edited by The Organizing Committee. North-Holland Publishing Company, Amsterdam, and Interscience Publishers, Inc., N. Y., 1949. Price $11.00.

Thirty-eight papers, all presented by well-known authors, are printed by the off-set process and collected into a large cloth-bound volume. Part I consists of *General Lectures;* Part II, of *Sectional Papers* dealing with a diversified range of subjects of importance not only to rheologists but to physical chemists interested in flow and Brownian movement.

The Organizing Committee has done a splendid job and the volume is a must for any practicing rheologist.

Victor K. La Mer, New York, N. Y.

The Scientist's Ready Reckoner. By W. Roman. Dr. W. Junk, Publishers, The Hague, Netherlands, 1950. 142 pp.

This handbook contains values and their logarithms for atomic weights and higher multiples, weights of molecules and radicals, gravimetric factors, titrimetric factors, specific gravity for liquids, temperature conversion tables, four-figure logarithms, and five-figure logarithms. These tables should be useful for all types of laboratory workers.

Victor K. La Mer, New York, N. Y.

The Chemistry and Physiology of Growth. Edited by Arthur K. Parpart. Princeton University Press, Princeton, New Jersey, 1949. 293 pp.

This stimulating book is the result of a series of conferences held at Princeton University where an attempt was made to bring together people interested in the various aspects of growth.

J. H. Northrup begins with a discussion of the mechanism of protein synthesis and favors a two-step hypothesis: a synthesis of a precursor (a proteinogen) from amino acids at the expense of an energy source; then a conversion of proteinogens into enzymes and special proteins by a reaction requiring no energy. He goes on to discuss the formation of viruses, adaptive enzymes, and antibodies, and suggests a mechanism for antibody formation from proteinogen.

F. O. Schmitt's section on *Molecular Morphology* summarizes our information about the physical characteristics of various fibrous proteins with emphasis on the keratins, myosins, nucleoproteins, and collagens. He discusses some ideas concerning the formation of fibers.

K. V. Thimann outlines briefly some recent developments in the field of plant growth hormones and proposes a tentative scheme for the mechanism of the action of auxin. The initial step is an acceleration of the rate of protoplasmic streaming. This leads to widespread changes resulting in the elongation of the cell.

In a rather provocative chapter on *Unidentified Vitamins and Growth Factors*, Karl Folkers analyzes a number of cases in which growth factors of unknown chemical composition are demonstrable. He tabulates a list of unidentified factors awaiting chemical analysis.

The general pattern of the growth process as exhibited in microörganisms is very ably treated by C. B. Van Niel. In the course of reviewing studies on the kinetics of growth, he points out that, while the total amount of growth is greater with increased concentration of nutriments, the *rate* of growth is independent of food supply. Factors such as the rate of diffusion of oxygen and the accumulation of excretory products limit growth.

E. S. Guzman Barron couples the growth process with cellular metabolism. Subjects discussed: Structure of the substrate in relation to the enzyme; the role of the mercapto group in enzyme activity; pyruvate oxidation: phosphorylation; synthesis of fats and proteins; the inhibition of cell growth.

The term "Molecular Ecology" is introduced by P. Weiss in a discussion of growth in relation to the chemical constituents of the cell. Various molecules must act together to produce synthesis, and the physical conditions in and around the cell will govern activity of these molecular aggregates. He discusses the role of surface tension and interfaces during growth. The physical orientation of the particles in the culture medium has a directional effect on the growth of nerve fibers.

With a discussion by J. S. Nicholas on *Problems of Organization*, the subject passes from a molecular level to a cellular level. For a colloid scientist interest will center about the role of the small granules of the cell with regard to development. These granules undergo extensive movements, and the mechanism as well as the significance of these granular migrations is discussed.

C. P. Rhoads treats with the problems of *Neoplastic Abnormal Growth*, coupling such phenomena as cancer and genes, viruses and mutation, intracellular granules and cancer. He discusses transmission by cell-free extracts and studies on cytoplasmic inheritance.

The volume ends with some new ideas on the role of the adrenal gland in growth by C. N. H. Long. Of special interest is the participation of adrenal hormones in protein metabolism and in the formation of antibodies.

L. G. Barth, New York, N. Y.

THE RATE OF SURFACE TENSION LOWERING AND ITS ROLE IN FOAMING

Emil J. Burcik

School of Petroleum Engineering, University of Oklahoma, Norman, Oklahoma

Received July 6, 1950

INTRODUCTION

Because of the widespread occurrence of foams a fundamental study of their properties is of practical interest. In the petroleum industry the foaming of crude oil in the well bore is of economic importance since its presence will result in a decrease in pumping efficiency. Furthermore because of the close structural similarity between foams and emulsions (3) a study of the fundamental mechanism of foaming may possibly lead to a clearer understanding of emulsions, and consequently an improvement in their treatment.

For this research it was considered advisable to employ, for the most part, pure surface-active agents whose physical and chemical properties were clearly characterized. Pure sodium laurate, sodium dodecyl sulfate, and sodium oleate were chosen for this study.

It will be shown that the rate of surface tension lowering is an important factor in determining the fundamental properties of a foam. This concept is not new since it was implied by J. Willard Gibbs (9) in his masterful discussion of liquid films. Donnan (5), in a theory which he attributes to Rayleigh, points out that for some surface-active agents the foam stability passes through a maximum with increasing concentration and that this fact can be explained by the high rate of surface tension equilibrium attainment in the concentrated solutions. However, in the past, no systematic study of the rate of surface tension lowering and its relation to foam stability has been described in the literature.

This is probably due to the fact that until the recent work of Addison (1), no method was available for measuring this rate with any degree of assurance. Addison's method is based on the classical experiments of Rayleigh (16) dealing with this mechanics of liquid jets issuing from noncircular orifices. The cross-sectional shape of such a jet will oscillate between that of the orifice and a circle, thus producing a series of standing waves along the jet. Rayleigh developed a mathematical relationship connecting the surface tension with the wavelength and other physical properties of the jet. Addison studied the rate of surface equilibrium establishment of water solutions of the C_5–C_8 aliphatic alcohols. He found that when a solution containing a surface-active agent is allowed to flow through a noncircular orifice the wavelength of successive waves increased as the jet moved outward. This increase is a manifestation of the decreasing surface tension of the liquid in the jet. Immediately after issuing from the orifice the newly formed surface will have a surface tension very nearly that of the pure solvent, and as the jet moves outward surface-active molecules contained in the liquid will diffuse into the interface and lower the surface tension. Obviously, if the velocity of the jet is known, the tension as a function of time can be calculated.

EXPERIMENTAL

Techniques

The technique employed to measure the rate of surface tension lowering was essentially that of Addison with a few modifications. A plate orifice was constructed by closing one end of a brass tube (9 cm. × 1.7 cm. I.D.) with a thin brass plate (.005 in. thick). An elliptical hole (1.70 mm. × 1.4 mm.) coaxial with the brass tube was pierced in the end plate. The orifice was enclosed in a glass-fronted box to eliminate air currents and to ensure constant temperature. Two rates of flow were employed in these experiments; 91.3 cc./min. and 100.0 cc./min. A constant rate of flow was maintained by the manostat arrangement described by Addison. The orifice tube was mounted in a nearly horizontal position so that corrections for the effect of gravity on the wavelength were unnecessary. A photograph of the jet was taken, making an accurate measurement of the wavelength possible. A gage wire of known diameter was always included in the photograph so that measurements could be made in standard units. Illumination for photography was provided by a fluorescent light placed over the jet and parallel with the direction of flow. A schematic diagram of the apparatus is shown in Fig. 1.

Rayleigh showed that for an ideal jet, that is, one in which no turbulence occurred and in which the effect of viscosity could be neglected, the surface tension is given by the following equation:

$$\gamma = K\rho\left(\frac{f}{\lambda}\right)^2,$$

where K is a constant whose value is determined by the size and shape of the orifice, ρ = the density of the liquid, f = the rate of flow, and λ = the wavelength. For a given orifice the value of K can be calculated from the rate of flow, density, and wavelength of a liquid whose surface tension is known. In these experiments pure water was used as the standard liquid, the value of K being checked at frequent intervals.

Addison found it necessary to use a more complicated equation in his work because, for some liquids, the rate of flow *vs.* wavelength curve was not linear. However, the departure from linearity for water was relatively small. In these experiments no departure from linearity was observed for rates of flow up to 100 cc./min., so that all calculations were carried out using the above equation.

In order to calculate the velocity of the jet from the volume of flow and hence the time elapsed for the passage of the jet from the orifice to a point midway between the particular pair of nodes which determines the wavelength, the equivalent circular jet diameter must be known. Since the cross section of the jet must become circular midway between a node and a trough, a measurement of the diameter at this point can be made.

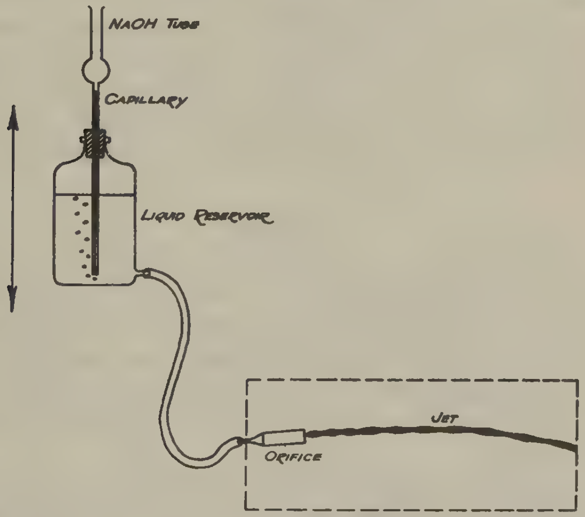

FIG. 1. Apparatus for measuring the rate of surface tension lowering.

All equilibrium surface tensions were measured with a du Noüy Interfacial Tensiometer. The Zuidema and Waters (20) corrections were applied.

To measure foam stability, the single bubble method (10) was employed. The technique consisted of forming single bubbles on the surface of the solution under carbon dioxide-free conditions and measuring the time elapsed before breakage occurred. The average life of 20–30 such uniformly sized bubbles of approximately 1 cm. diameter was taken as a measure of the foam stability.

To compare the behavior of a single bubble with that of a volume of foam consisting of a large number of bubbles of various sizes, the "pour foam" test, described by Ross and Miles (18), was used. One hundred ml. of solution was allowed to fall through a fixed height (70 cm.) from a separatory funnel into a graduated cylinder. The foam produced in this manner was loosely stoppered with a cotton plug and set aside. The initial volume of foam produced, and the time required for the foam to break down into half its original volume were recorded. For the latter, a plot of logarithm of volume *vs.* time (11) was found useful. However, a linear relationship was not always obtained.

An oscillating disk was used to measure the surface viscosity of sodium laurate solutions. The apparatus and technique employed were essentially those of Wilson and Ries (19) so that a detailed description is unwarranted. A weighted disk, suspended by a steel torsion wire, was arranged so that it could oscillate in the liquid surface. The depth of immersion of the disk was controlled by a screw arrangement which raised or lowered the entire solution. All experiments were conducted with the disk just touching the surface of the liquid. The disk proper was of brass, $1\frac{7}{8}$ in. in diameter and $\frac{3}{16}$ in. thick. The weighted disk had a natural period of oscillation of 4.16 sec. The amplitude of oscillation was measured in arbitrary units with the aid of a pointer rigidly attached to the disk and moving over a circular scale. Surface viscosity measurements were made at 20°C.

Materials

Sodium laurate. Eimer and Amend C.P. lauric acid was redistilled in vacuum. The constant-boiling fraction employed in the preparation of the soap had an equivalent weight of 201.5 (theory 200.3) and a melting point of 43.0–.5°C. (theory 43.8°C.). The fatty acid was neutralized in alcohol solution with saturated NaOH solution using phenolphthalein as indicator. The neutral solution was evaporated to dryness and subsequently dried under vacuum.

Sodium dodecyl sulfate. Eastman lauryl alcohol m. p. 23–4°C. was redistilled in vacuum. The middle fraction was sulfated with chlorosulfonic acid (7). The product after neutralization was recrystallized from butanol and then extracted with ethyl ether for 24 hr. in a Soxhlet apparatus. Water solutions of the product showed no minimum in surface tension when plotted as a function of concentration (see Fig. 9). Sulfur content by analysis was 11.0% (theory 11.10%).

Sodium oleate. Oleic acid was prepared by low-temperature crystallization of olive oil fatty acids from acetone (4). After repeated recrystallization at −20°C. and −60°C. the product was vacuum distilled. The product was a clear, colorless liquid whose equivalent weight was 281.5 (theory 282.4) and a m. p. of 11.5°–12.5°C. (theory 13.0°C.). The acid was neutralized with saturated sodium hydroxide and dried under vacuum.

Tween 20. A commercial sample of Tween 20 (Polyoxyethylene sorbitan monolaurate) was kindly supplied by the Atlas Powder Company and was used directly.

Inorganic reagents. All inorganic reagents employed were Eimer and Amend "tested purity" reagent-grade chemicals. All solutions were freshly prepared with distilled water.

RESULTS

The surface tension of sodium laurate solutions as a function of time at 20°C. is shown for various concentrations in Fig. 2. The rate of surface tension lowering increases as the concentration of sodium laurate is increased. The equilibrium surface tensions as determined with the tensiometer are also shown in this figure. It will be noted that for 0.050 *N* sodium laurate the equilibrium value of the surface tension is virtually attained after a few hundredths of a second, while for the more dilute solutions the tension is still far removed from the equilibrium value after the same time interval. The agreement, in the concentrated solutions, of the surface tension in the jet with the equilibrium tension as determined by the tensiometer confirms the assumption that the flow is streamlined.

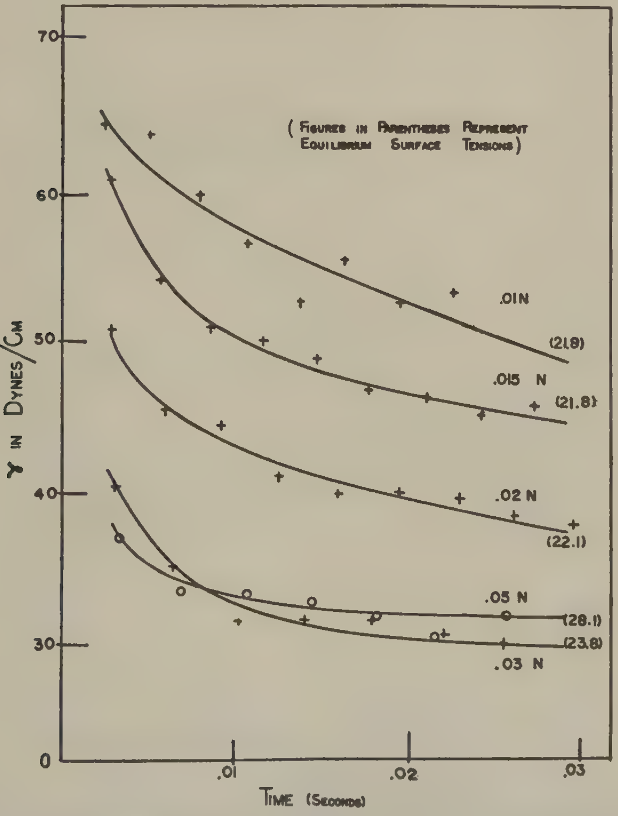

Fig. 2. Surface tension *vs.* time for sodium laurate. Temperature 20.0°C.

The surface tension as a function of time for sodium dodecyl sulfate is shown in Fig. 3. The rate of lowering for this substance is greater than that of sodium laurate. For example, the surface tension of 0.005 *N* sodium dodecyl sulfate after a given time interval is lower than that for the more concentrated 0.01 *N* sodium laurate.

The results for sodium oleate are of interest since in the more concentrated solutions a further addition of the surface-active agent results in only a small increase in the rate of surface tension lowering. As shown in Fig. 4 the rate for 0.04 *N* sodium oleate is only slightly higher than that for 0.02 *N*. Furthermore the surface tension after 0.03 sec. is still far removed from the equilibrium tension indicating that the rate of lowering is only moderate. A possible explanation of this behavior lies in the fact that the critical concentration for micelle formation is greatly exceeded in the solutions employed. Since the surface-active constituents of these solu-

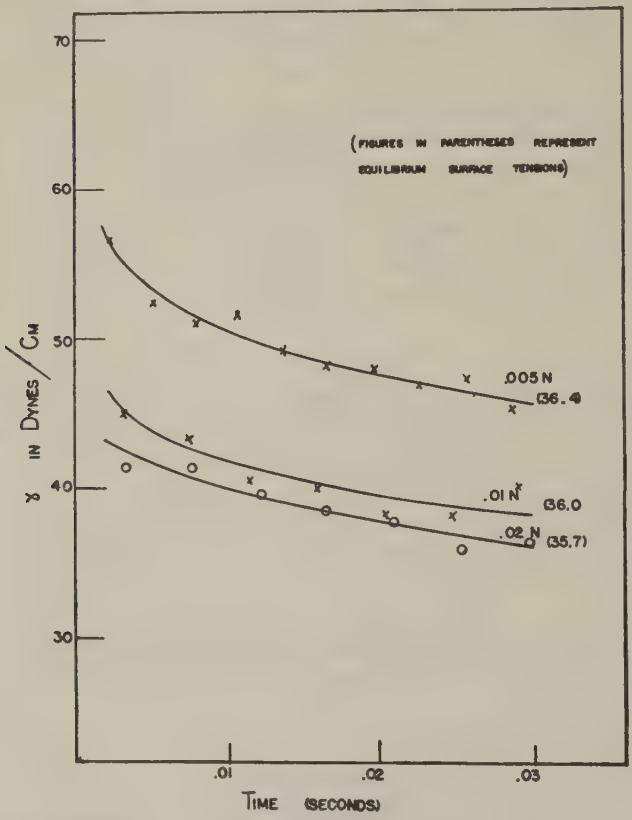

FIG. 3. Surface tension *vs.* time for sodium dodecyl sulfate. Temperature 20.0°C.

tions are probably single ions, acid soap, and, at best, small aggregates, an increase in concentration results in only a small increase in concentration of the surface-active component and conequently only a small increase in rate of surface tension lowering.

The effect of added sodium chloride on the rate of surface tension lowering of 0.015 *N* sodium laurate is shown in Fig. 5. The marked increase in rate due to added electrolyte is readily apparent, the effect becoming more pronounced as the concentration of additive is increased. Nutting, Long, Harkins (13), using the ring method in very dilute solution have also noted this effect of electrolytes on the rate. Note, however, that while an addition of electrolyte markedly increases the rate of surface tension lowering, it has little or no effect on the equilibrium surface tension.

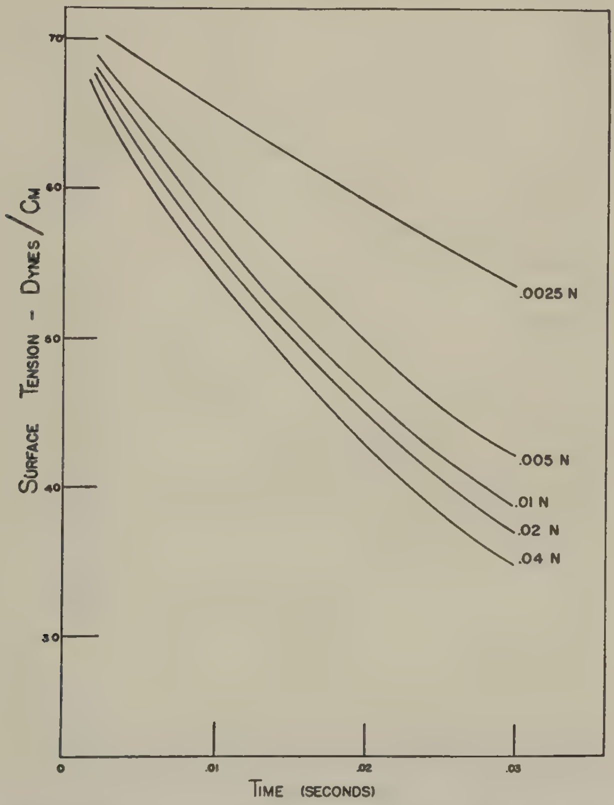

Fig. 4. Surface tension *vs.* time for sodium oleate solutions. Temperature 20.0°C.

The fact that salt addition increases the rate of surface tension lowering can be explained if one allows that the surface-active particles are charged. As those particles diffuse into the interface a charge will build up which will tend to repel the incoming ions and reduce the rate of surface tension equilibrium attainment (6). The effect of salt in decreasing the negative potential barrier at the surface follows at once from any theory of the diffuse double layer. The potential of any charged body is decreased by the presence of a neutral electrolyte in its environment since the charge will be effectively reduced by the presence of ions of opposite sign. This contention is strengthened by the experimental fact that neutral, nonionic surface-active agents do not show an electrolyte effect and their rate of surface tension lowering is not influenced by the addition of a salt. Three-hundredths normal sodium chloride has no effect on the rate of surface equilibrium attainment of 0.10% Tween 20 (nonionic polyoxyethylene sorbitan monolaurate) as is shown in Fig. 6.

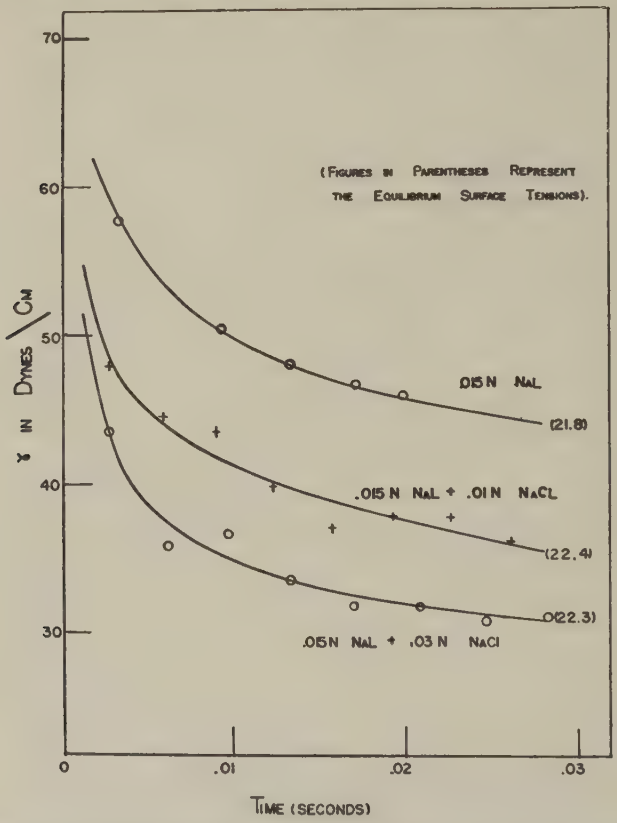

Fig. 5. Effect of added electrolyte (NaCl) on rate of surface tension lowering of 0.015 *N* sodium laurate (NaL). Temperature 20.0°C.

The foam stability of sodium laurate as a function of concentration as measured by the single bubble method and the "pour foam" test is shown in Fig. 7. The stability curve is characterized by a pronounced maximum in the 0.020–0.025 N concentration range when either the half-life of a volume of foam or the average life of a single bubble is taken as a measure of foam stability. On the other hand, when the initial volume of foam produced in the pour foam test is plotted as a function of concentration the resulting curve rises to a maximum with little or no falling off in the high concentration range. A possible explanation for this behavior will be discussed later.

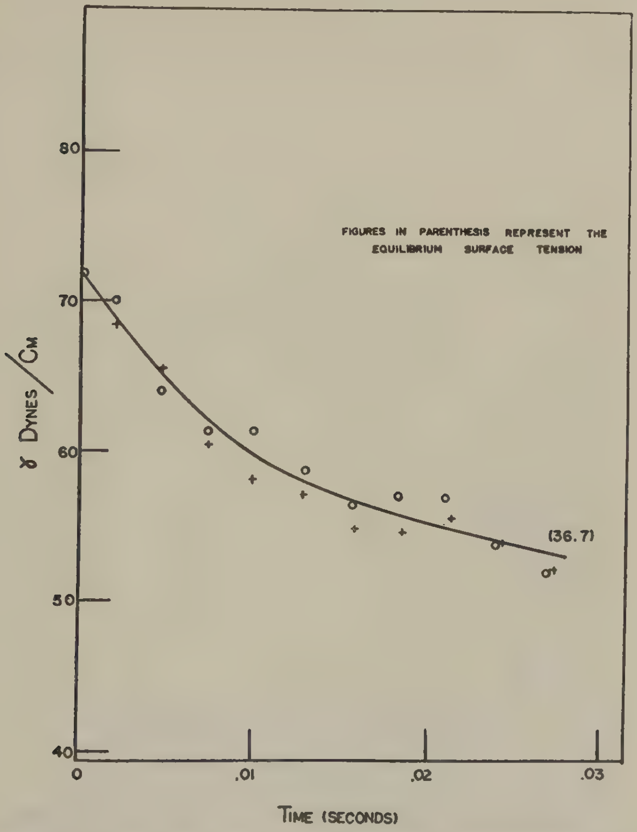

FIG. 6. Effect of added electrolyte on rate of surface tension lowering of a nonionic surface-active agent. + 0.1% Tween 20, ○ 0.1% Tween 20 + 0.03 N NaCl.

The foam stabilities of sodium laurate with and without added sodium chloride, sodium dodecyl sulfate, and sodium oleate as determined by the single bubble technique are shown in Fig. 8. As previously mentioned, the stability of sodium laurate as a function of concentration exhibits a pronounced maximum at about 0.020 *N*. With 0.010 *N* sodium chloride as solvent the stability curve is shifted toward the lower concentration range. The maximum occurs at a lower concentration so that in dilute sodium laurate solution the sodium chloride can be said to act as a foam stabilizer while in the more concentrated solution it acts as a foam inhibitor. As shown in this figure, sodium dodecyl sulfate foams are relatively unstable when compared to sodium laurate. The stability curve is characterized by a maximum which occurs at 0.010 *N*. The foam stability of sodium oleate is interesting since over the concentration range investigated the stability curve does not show a pronounced maximum that was so characteristic of the systems previously described. In this case the stability increased with increasing concentration and then remained essentially constant in the most concentrated solutions investigated.

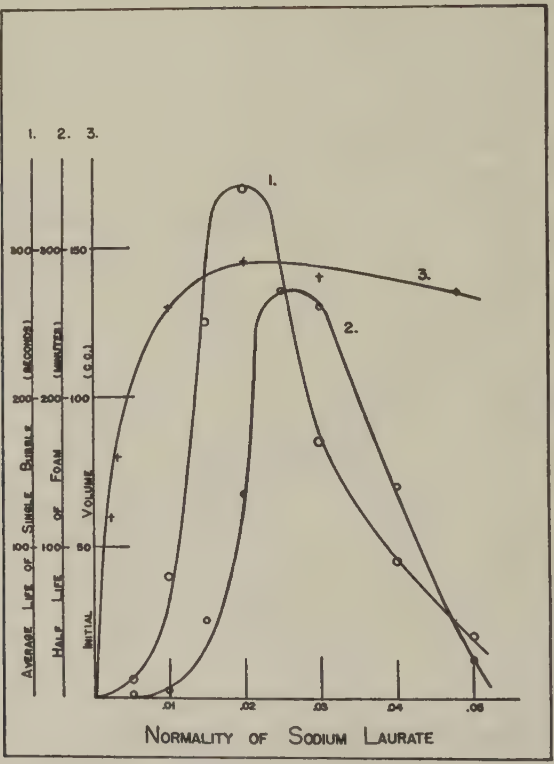

FIG. 7. Stability of sodium laurate foams. Temperature 20.0°C.

Equilibrium surface tensions as determined by the du Noüy tensiometer are shown in Fig. 9. Sodium laurate and sodium oleate show minima in the tension *vs.* concentration curve characteristic of surface-active agents which hydrolyze (14). On the other hand, sodium dodecyl sulfate shows no minimum (12). The addition of sodium chloride to sodium laurate has little or no effect on the static surface tension except in very dilute solution where a decrease is evident (15).

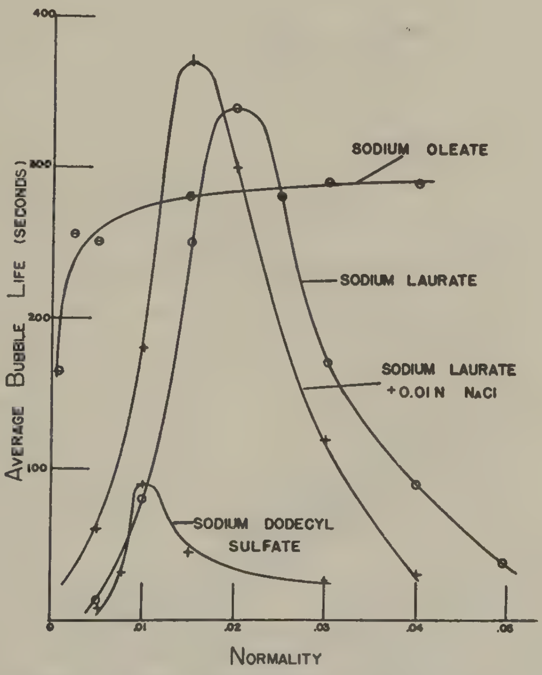

FIG. 8. Stability of single bubble. Temperature 20.0°C.

The results obtained with the oscillating disk are shown in Fig. 10 for sodium laurate. Here the logarithm of the amplitude is plotted as a function of the number of oscillations. As pointed out by Wilson and Ries (19), this should be a linear function for solution surfaces which show no plasticity. Furthermore, the surface viscosity is a function of the slope of this line. The straight, parallel lines obtained with sodium laurate of various concentrations indicate that no surface plasticity is evident and that the surface viscosity is essentially that of pure water.

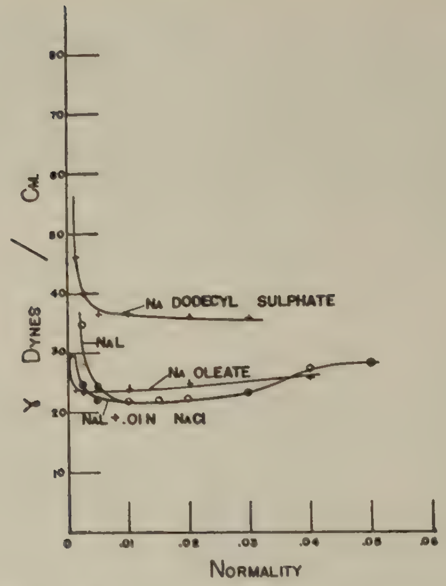

Fig. 9. Equilibrium surface tensions at 20°C.

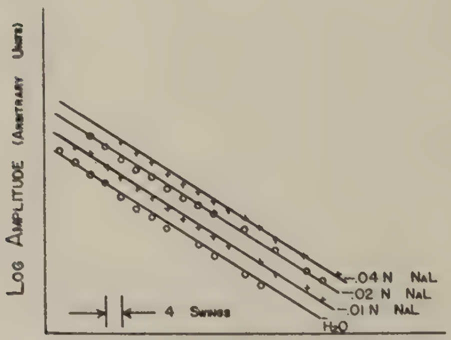

Fig. 10. Logarithm of amplitude *vs.* number of swings.

Discussion

Any theory of foaming must differentiate clearly between the ability of a solution to form foam and the stability of the foam once it is formed. It has been suggested in the past (2) that the ability of a solution to foam should be a function of the surface tension and the viscosity of the solution. This is entirely reasonable since the formation of foam by the usual method of agitation involves the introduction of gas bubbles into the solution with a large increase in surface area so that the production of foam requires the expenditure of energy against both the surface tension and viscosity forces. However, under the conditions of foam formation that usually prevail, the surface tension will not be the equilibrium tension but will be at some higher value which will depend on the degree of agitation and the rate of surface tension lowering. Obviously, the higher the rate of lowering the more closely will the tension approach its equilibrium value. In view of these facts, the requirements for a high degree of foaming ability are: (*1*) Low equilibrium surface tension, (*2*) low viscosity, (*3*) low rate of foam production, and (*4*) high rate of surface tension lowering.

Consequently, in a series of solutions in which the viscosity is essentially constant, the foaming ability should increase as the surface tension decreases. However, it should increase more slowly than the tension decreases since in dilute solution the effective surface tension would be appreciably higher than the equilibrium tension due to the low rate of equilibrium attainment. It is interesting to note that the initial volume produced in the "pour form" test (Fig. 7) has just these characteristics. It is obvious, however, that in this test, stability is also a factor since the foam already produced is subjected to the disrupting forces of the falling liquid. It is suggested, therefore, that the "pour foam" test is a measure of both foam stability and foam ability and consequently the discrepancy between the initial volume and half-life curves previously alluded to is to be expected.

A reasonable a priori assumption is that the stability of a foam arises from the ability of its component films to resist strains. As pointed out by Gibbs, one way for a film to do this is for the surface tension under deformation to always change in such a way as to resist the deforming force. Consider the film to be divided into small elements of area. The surface of each will be richer in the surface-active component than the central bulk liquid. Furthermore, it must be kept in mind that due to the forces of gravity, the liquid will be continually draining from each element so that considerable agitation can exist within the film. Under these conditions the surface tension will not be the equilibrium value but will be at some higher value determined by the rate of surface equilibrium attainment. Suppose such an element is subjected to a disturbance which causes, for example, an increase in surface area with a corresponding decrease in the area of the adjacent elements. The total area of the film, however, remains constant, for an increase in total area would imply film formation. It can readily be seen that the tension of this expanded element will increase since an expansion will effectively dilute the surface-active component in the interface. The effect of this increase in tension will be a tendency for the film to restore itself to its original condition. A film whose tension is lower than that of the pure solvent can, at best, exert a restoring force equal to the difference in tension between the pure solvent and that existing in the film. Consequently the lower the tension of the film is below that of the pure solvent, the greater the possible magnitude of the restoring force. However, in view of the fact that equilibrium does not exist in a draining film, a low tension requires not only a low equilibrium tension, but a high rate of equilibrium attainment as well.

Thus far the tendency of the expanded element to re-establish surface equilibrium by diffusion of the surface-active component from the bulk liquid within the film into the interface has been neglected. If the rate of surface tension lowering is very high there will be no effective restoring force since as fast as the element is expanded and the surface-active component diluted, more will diffuse into the interface and annul any increase in tension.

In order to have a large restoring force, and hence high resistance to deformations of the type considered, it is necessary to have not only a low surface tension relative to the pure solvent but a *moderate* rate of surface tension lowering as well. The rate must be high enough to produce a large lowering of the tension under the nonequilibrium conditions which exist in a film but not so rapid as to completely annul any increase in tension by rapid diffusion of the surface-active component from the interior liquid into the deformed surface. Thus, films which have the ability to exert large restoring forces can be said to be elastic to deforming forces which act for periods of time small in comparison to the time necessary for surface tension equilibrium to be attained. This time-dependent elasticity will tend to stabilize films with respect to transient shocks and deformations which occur. Deformations of the type considered are not uncommon in films, for, not only do they arise from air currents and external vibrations, but they can result from the drainage of the film as well. Observation of a film, particularly one showing interference colors, will show that the film elements are continually undergoing momentary expansions and contractions due to uneven drainage even though the total film area remains unchanged. These effects are particularly marked in portions of a film adjacent to a Gibbs ring where the liquid is actually being drawn from the film and consequently is subjected to particularly violent agitation.

A film which has an appreciable bulk viscosity, or which exhibits a high surface viscosity would tend to resist deforming forces (19). However, the sodium laurate surfaces studied showed no measurable surface viscosity or plasticity when tested by the oscillating disk technique (Fig. 10). Moreover, the bulk viscosity of the solutions employed in this research were essentially those of pure water. This would seem to indicate that the resistance to deformation resulting from the time-dependent elasticity is adequate to stabilize the film. It is probable, however, that a film not only elastic but viscous or plastic as well would be exceptionally stable.

To summarize, the conditions which favor high foam stability are: (*1*) Low surface tension relative to that of the pure solvent, (*2*) moderate rate of surface tension lowering, and (*3*) a high bulk or surface viscosity.

The stability curves shown in Fig. 8 can be explained in a qualitative manner on the basis of the theory proposed. For sodium laurate the reason for the stability maximum lies in the fact that at this concentration the tension is low and the rate of surface tension lowering is optimum. At lower concentrations the conditions for stability are not satisfied since both the surface tension reduction and the rate of tension lowering are low. At the high concentrations, on the other hand, the rate of tension lowering is too rapid for the film to exhibit an appreciable elasticity. Similarly sodium dodecyl sulfate films are relatively unstable because of the comparatively high surface tension. The stability maximum occurs at a lower concentration since the high rate of surface tension lowering would place the optimum rate at a lower concentration. Sodium oleate films do not exhibit a maximum in stability since in the concentration range investigated the rate of lowering is still moderate and does not exceed the optimum. Added confirmation of the theory is found in the effect of electrolyte on the stability. The effect of sodium chloride on the stability of sodium laurate is to shift the entire stability curve toward the lower concentration range. This is in agreement with theory since the effect of added electrolyte is to increase the rate of surface tension lowering with little or no effect on the equilibrium tensions so that the optimum rate for maximum stability occurs at a lower concentration.

The theory outlined above differs in one important respect from that of Gibbs (9) which implies that a slow rate of lowering is necessary for high stability. This would be correct if the film could be considered to be in equilibrium, but since this is not the case a moderate rate is required. An examination of Figs. 8 and 9 will make the need for this change apparent. If equilibrium existed in the film, the stability maximum would necessarily occur at the lowest concentration compatible with the surface tension minimum. However, this was not experimentally observed since the stability maximum always occurred at a higher concentration indicating that equilibrium does not exist and a moderate rate of surface tension is necessary.

It should be emphasized that this theory of foam stability does not apply to films which contain a second liquid present in discrete droplets. The effect of an insoluble foam inhibitor would therefore not be within the scope of the theory. It is probable that these agents influence the stability of foams through the production of heterogeneous films with unbalanced surface tensions which cause rupture (8,17).

ACKNOWLEDGMENTS

The author wishes to thank the University of Oklahoma for the opportunity to conduct this research. He also wishes to acknowledge, and express his appreciation for the suggestions, interest, and encouragement of his associates. In like manner he wishes to thank the Proctor and Gamble Company where some of the preliminary experiments for this research were undertaken by him.

Summary

1. The rate of surface tension lowering of solutions of sodium laurate, sodium dodecyl sulfate, and sodium oleate were determined by the oscillating jet technique.

2. The stabilities of foams containing these surface-active agents were measured by the single bubble technique.

3. The surface viscosity and surface plasticity were determined for sodium laurate solutions. No plasticity was observed and the viscosity was essentially that of pure water.

4. The rate of surface tension lowering of sodium laurate increases with increasing concentration. At a given concentration the rate of lowering for sodium dodecyl sulfate is appreciably greater than that for sodium laurate. In the higher concentration range the rate for sodium oleate does not increase appreciably.

5. Sodium chloride increases the rate of surface tension lowering of sodium laurate.

6. It is probable that the stability of a foam is due to the ability of its films to resist deformation. The conditions for high foam stability are: (*1*) Low surface tension relative to that of the pure solvent, (*2*) moderate rate of surface tension lowering, and (*3*) a high bulk or surface viscosity.

7. The foam stabilities determined in this research are in qualitative agreement with theory.

References

1. Addison, C. C., *J. Chem. Soc.* **1943**, 535; *ibid.* **1944**, 252, 477; *ibid.* **1945**, 98, 354.
2. Bartsch, O., *Kolloidchem. Beihefte* **20**, 1 (1924).
3. Bikerman, J. J., Surface Chemistry, p. 141. Academic Press, Inc., New York, N. Y., 1948.
4. Brown, J. B., and Shinowara, G. Y., *J. Am. Chem. Soc.* **59**, 3 (1937).
5. Donnan, F. G., *Chemistry & Industry* **42**, 902 (1923).
6. Doss, K. S. G., *Kolloid-Z.* **86**, 205 (1939).
7. Dreger, E. E., Keim, G. I., Miles, G. D., Shedlovsky, L., and Ross, J., *Ind. Eng. Chem.* **36**, 610 (1944).
8. Fisk, C. H., *J. Biol. Chem.* **35**, 411 (1918).
9. Gibbs, J. Willard, Collected Works, Vol. 1, p. 300 ff. London, 1906.
10. Hardy, *Proc. Roy. Soc.* (*London*) **A86**, 627 (1912).
11. Lederer, E. L., *Fettchem. Umschau* **40**, 69 (1933).
12. Miles, G. D., and Shedlovsky, L., *J. Phys. Chem.* **48**, 57 (1944).
13. Nutting, G. C., Long, F. A., and Harkins, W. D., *J. Am. Chem. Soc.* **62**, 1496 (1940).
14. Powney, J., *Trans. Faraday Soc.* **31**, 1510 (1935).
15. Powney, J., and Addison, C. C., *Trans. Faraday Soc.* **33**, 1253 (1937).
16. Rayleigh, *Proc. Roy. Soc.* (*London*) **29**, 71 (1879); *ibid.* **34**, 130 (1882).
17. Robinson and Wood, *J. Soc. Chem. Ind.* **67**, 361 (1948).
18. Ross, J., and Miles, G. D., *Oil & Soap* **18**, 99 (1941).
19. Wilson and Ries, *Colloid Symposium Monograph* **1**, 145 (1923).
20. Zuidema, H. H., and Waters, G. W., *Ind. Eng. Chem.* **13**, 312 (1941).

ENZYME–SUBSTRATE STABILIZATION WITH SURFACE-DENATURED PEPSIN–ALBUMIN

Teru Hayashi and George R. Edison

Department of Zoology, Columbia University, New York, New York

Received July 3, 1950

Introduction

The earlier studies on the autolytic activity of pepsin–albumin films rolled into fibers (1,2) demonstrated that the phenomenon was an actual proteolytic activity, due to the presence of pepsin in the fiber (or film) itself. The peptic nature of the action was shown in the heat-sensitivity of the autodigestion phenomenon, the pH dependence, and the formation of products soluble in trichloroacetic acid.

In the course of these earlier studies, it was recognized that there were two possible alternative roles of the pepsin molecules in the autodigestion process. These may be stated as follows:

a) The autodigestion of the rolled-up films was due to the action of pepsin molecules incorporated in the film itself. That is, the pepsin molecules responsible for the phenomenon had been actually "surface-denatured" in the sense that they had undergone certain physical changes at the air–water interface of the Langmuir trough, becoming part of the monomolecular film of pepsin and albumin molecules. These pepsin molecules, under certain rigid conditions of hydration and hydrogen-ion concentration, had acted proteolytically on the albumin molecules.

b) The autodigestion was due to the action of pepsin molecules which had not actually undergone "surface-denaturation"; rather, undenatured, native pepsin molecules had become adsorbed on the film and become entrapped in the fibers. Thus, the autodigestion of the fibers was due to the proteolytic activity of such native pepsin molecules present as contaminants in the fiber.

The results of a number of previous experiments devised to test these alternatives adduced evidence in favor of the first possibility and against the second (2).

The present investigation was undertaken for the purpose of throwing additional light on the above question and also to begin the elucidation of the mechanism of the autodigestion. It may be stated that the results provide additional evidence in favor of the first possibility given above, and indicate that the autodigestible pepsin–albumin film is a stabilized enzyme–substrate complex.

MATERIALS

The ovalbumin used was prepared from fresh hen's eggs according to the method of La Rosa (3). The albumin was thrice-recrystalized, then dialyzed overnight in several changes of distilled water, and finally frozen-dried. This lyophilized material was used in making up the experimental solutions, fresh, filtered solutions being used in each experiment.

The pepsin used was the crystalline Armour product, dialyzed overnight against distilled water rendered slightly acid with a drop of concentrated acetic acid, then frozen-dried. The frozen-dried pepsin was used in making fresh-filtered solutions for each experiment.

The ammonium sulfate and buffer solutions were all made of standard Merck products. Pyrex-distilled water was used throughout the experiments.

METHODS

The technique for making the pepsin–albumin film-fiber has been described in detail in a previous publication (2). Certain steps in the procedure are described below, since they bear on the present investigation.

1. Nine parts of a buffered albumin solution (5 mg./ml.) are mixed with 1 part of a buffered pepsin solution (5 mg./ml.). The pH of the resulting mixture is checked electrometrically ("mixture pH"). Either acetate buffer or phosphate–citrate buffer in the pH range 4.0–5.5 may be used without affecting the result; *i.e.*, the fibers formed from this mixture are readily autodigestible. Both types of buffer are used in the present investigation.
2. Drops of the mixture of proteins are placed at the air–water interface of a Langmuir trough in excess to form a monomolecular film. The trough is filled with 10 × diluted McIlvaine's buffer (checked electrometrically) at pH 4.0 ("trough pH").
3. The film is compressed by the use of suitable barriers (Devaux effect) giving a fiber, in reality a rolled-up monomolecular film of pepsin and albumin molecules. Autodigestion takes place when such a fiber is treated with dilute HCl at pH 1.5 ("digestion pH").

In the steps described above, it is to be noted that the "mixture pH" is that of the solution in which native pepsin and albumin molecules are mixed prior to their application to the air–water interface and the formation of the monomolecular film. The optimum "trough pH" for the formation of autodigestible complex fibers had been found experimentally to be 4.0–4.2, while the optimum "digestion pH" for digestion had been established sharply at 1.5 (2).

Observations of the autodigestion were made under the low-power magnification of the microscope to note only whether autodigestion occurred or not. In some cases, the time required for complete digestion was measured.

To precipitate the proteins, titration with a saturated, filtered solution of ammonium sulfate was employed. A measure of the precipitate thus formed was obtained by determining the optical density of a well-stirred sample of the precipitate suspension in a Coleman Junior spectrophotometer and also in a Klett-Summerson photoelectric colorimeter using monochromatic light of 420 mμ. Instead of blanks in the determinations, the instruments were set for zero optical density (100% transmission) in the clear protein solution containing the same reagents but before the formation of any precipitate (before the addition of the last increments of ammonium sulfate beginning the onset of precipitation).

Experiments and Results

From the foregoing descriptions, it may be assumed that, in the autodigestible fibers, both pepsin and albumin molecules are present. Since autodigestion involves a proteolytic action, some sort of association between the enzyme and substrate molecules would appear to be necessary. The question then may be asked whether this association is established at the time of mixture of the two proteins or at the time of application to the surface of the trough. The question was tested initially by making films and fibers incorporating both pepsin and albumin molecules but in such a way that mole-to-mole association of the enzyme and substrate molecules was prevented. This was done in two ways.

In the first method, paraffined threads were placed transversely across the surface of the trough dividing the trough surface into sectors in such a way that any protein film formed in any sector was effectively contained therein. Albumin and pepsin solutions were placed on the surface in alternate sectors to form respective films separated by the threads. With certain variations in procedure, the threads were then removed and the film compressed to form a pepsin–albumin fiber which was then tested for autodigestion. The procedural variations, after spreading the films and waiting 20 sec., were (*a*) remove threads and compress immediately; (*b*) remove threads, wait 5 min., then compress; (*c*) remove threads, wait 20 min., then compress; and (*d*) remove threads, compress immediately to 50% of the original area, wait 5 min., then compress.

In the second method, no separating threads were used. Instead, albumin and pepsin solutions were placed dropwise separately on the trough at varying distances apart, the films thus formed being compressed into fibers and tested for autodigestion.

In the foregoing experiments, it is necessary that each film and fiber tested be made on a clean trough containing fresh buffer solution. Anomalous results will be obtained if the same trough is used over and over for making the films and fibers. This is because in applying the drops of protein solution to the surface some of the protein molecules go into solution in the bulk of the trough. Such molecules in solution will make their way to the surface and become incorporated into films spread subsequently at the air–water interface.

From the results (see Table I) it was apparent that a necessary condition for making autodigestible fibers was the mixing of the enzyme and substrate prior to spreading on the trough; that is, an interaction between the pepsin and albumin occurred in the mixture. Attention was therefore directed to the effect of the mixture pH on autodigestion.

Protein mixtures of 9 parts of albumin to 1 part of pepsin in McIlvaine's buffer with final protein concentrations of 5 mg./ml., and final mixture pH's of 4.4, 5.0, 6.0, 6.6, and 7.2 were made. Fibers were formed from each mixture, and tested in the usual fashion. It was found that, at pH 7.2, the fibers were not autodigestible, whereas all the other mixtures formed autodigestible fibers.

The results of the foregoing experiments are summarized in Table I.

Since there seemed to be a definite difference in the behavior of pepsin and albumin molecules when mixed at pH 7.2 as contrasted to that when mixed at the lower pH's, some clue as to the nature of this behavior was

TABLE I

Observations on Autodigestion

Conditions for the formation of autodigestible (+) fibers as contrasted to non-autodigestible (−) fibers. Solutions for Expts. 1 and 2: pepsin 2 mg./ml.; albumin 10 mg./ml. For Expt. 3: final protein concentration of mixture 5 mg./ml.

Expt.	Conditions						Auto-digestion
	pH					Fiber formation	
	Alb.	Pep.	Mixt.	Trough	Dig.		
1	5.35	5.35		4.0	1.5	Alb. and pep. films Variation (*a*)	−
	5.35	5.35		4.0	1.5	separated on trough Variation (*b*)	−
	5.35	5.35		4.0	1.5	by threads, threads Variation (*c*)	−
	5.35	5.35		4.0	1.5	removed before compression. Variation (*d*)	−
	5.35	5.35	5.35	4.0	1.5	Control. Standard fibers, mixing pepsin and albumin prior to spreading.	+
2	5.35	5.35		4.0	1.5	Alb. and pep. films Placed 30 cm. apart	−
	5.35	5.35		4.0	1.5	placed dropwise separately Placed 10 cm. apart	−
	5.35	5.35		4.0	1.5	on trough. Placed 2 cm. apart	−
	5.35	5.35		4.0	1.5	Film then compressed. Placed 0 cm. apart	+
	5.35	5.35	5.35	4.0	1.5	Control. Standard fiber.	+
3	4.4	4.4	4.4	4.0	1.5	Standard fiber with the mixture pH varied.	+
	4.4	4.4	5.0	4.0	1.5	Standard fiber with the mixture pH varied.	+
	4.4	4.4	6.0	4.0	1.5	Standard fiber with the mixture pH varied.	+
	4.4	4.4	6.6	4.0	1.5	Standard fiber with the mixture pH varied.	+
	4.4	4.4	7.2	4.0	1.5	Standard fiber with the mixture pH varied.	−

sought by utilizing the differential susceptibility of the pepsin and albumin molecules to precipitation by saturated ammonium sulfate.

Figure 1 shows the curves obtained for pepsin and for albumin when titrated separately with saturated ammonium sulfate at pH 4.4. It is to be noted that these two molecular species have a clear-cut difference in their susceptibility to precipitation by ammonium sulfate, the pepsin responding to less reagent. The curves are smooth, indicating a homogeneity in the response of each protein to the precipitating action.

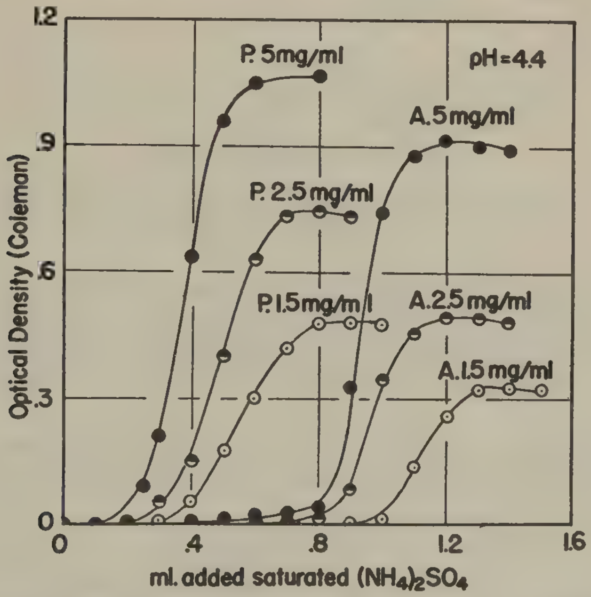

FIG. 1. Precipitation curves for various concentrations of pepsin (*P*) solutions, and albumin (*A*) solutions, showing differential susceptibility to $(NH_4)_2SO_4$. Phosphate–citrate buffer at pH 4.4.

When the pepsin and the albumin are mixed in a 1:1 ratio and then titrated, however, this difference in susceptibility is not reflected, as shown in Fig. 2. Instead, the two proteins are precipitated out together uniformly in a manner characteristic of the pepsin. It may be concluded that an interaction occurs between these molecules such that the pepsin and the albumin precipitate out together.

That the pepsin and the albumin may be precipitated independently out of the mixture can be shown readily by varying the mixture pH. Mixtures in a 1:1 proportion of the two proteins were made at final pH's of 4.4, 5.0, 6.0, 6.6, and 7.2. The lower mixture pH's gave precipitation curves similar to that observed in Fig. 2, but at the highest pH of

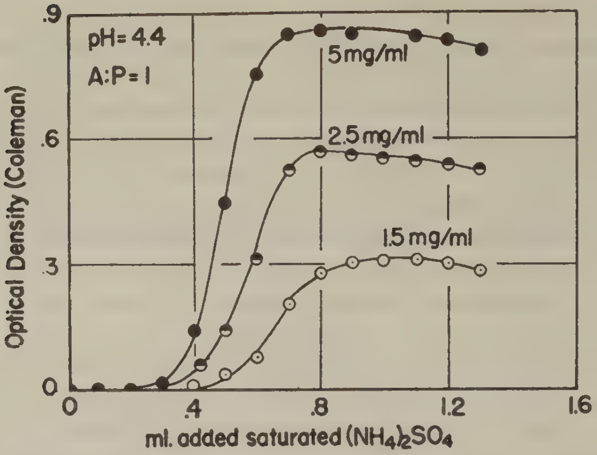

FIG. 2. Precipitation curves for various concentrations of albumin–pepsin mixture. $A/P = 1$, in phosphate–citrate buffer at pH 4.4.

7.2 the pepsin and the albumin precipitated out separately. Figure 3 shows the curve for a 1:1 mixture of pepsin and albumin at pH 7.2, along with the curves for pepsin alone and albumin alone at the same final pH. The shape of the curves shows clearly the separation of the pepsin and albumin.

The results give evidence for the belief that the pepsin and albumin in mixture between pH 4.4–6.6 form an enzyme–substrate complex. This

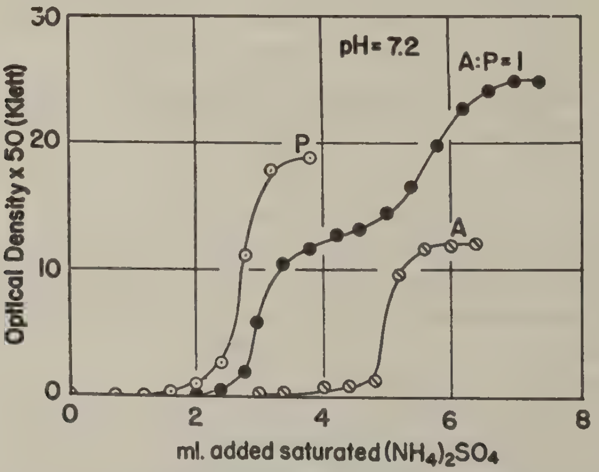

FIG. 3. Precipitation curves for pepsin (P), albumin (A) and albumin–pepsin ($A/P = 1$) mixture at pH 7.2. Protein concentration = 2.5 mg./ml. in phosphate–citrate buffer.

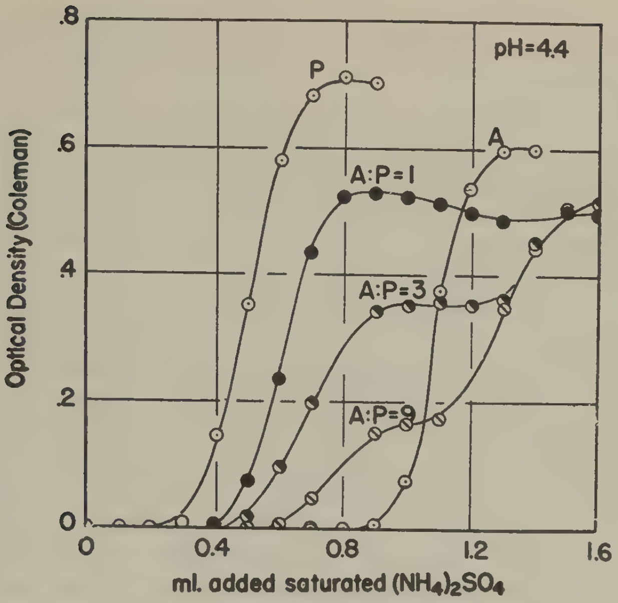

FIG. 4. Precipitation curves for pepsin (*P*), albumin (*A*) and mixture solutions at various albumin–pepsin ratios. Protein concentration = 2.5 mg./ml., buffered in phosphate–citrate at pH 4.4.

belief was further substantiated when mixtures with varying proportions of albumin and pepsin were titrated with saturated ammonium sulfate. As Fig. 4 shows, at the higher albumin to pepsin ratios, the albumin–pepsin complex precipitated out initially, to be followed by the subsequent precipitation of the excess albumin.

DISCUSSION

The first question to be considered in the light of the experimental results is whether an enzyme protein retains its specific activity after it has been subjected to the physical changes concomitant to the formation of a monomolecular film. The published information pertaining to this question does not give an unqualified answer because of technical considerations.

Thus, the question has been approached by using films deposited on slides. Using this technique various workers (4–7) have studied the enzymes catalase, saccharase, urease, pepsin (milk-clotting), and trypsin. In all of these with the exception of trypsin (7) positive activity of greater or less degree was reported. However, the point that could not be resolved was: Is the activity due to the spread protein film, or is it due to (*a*) adsorbed, unspread protein; (*b*) "incompletely spread" protein; or (*c*) adsorbed and subsequently desorbed protein? Because of this consideration, Rothen, in his review (7), points out that the belief in enzymatic activity of spread films is not substantiated.

The possibilities (*a*), (*b*), and (*c*) have been considered in some detail earlier (2). In addition, it may be pointed out that whether a protein molecule is completely spread or not, the fact that protein molecules in clear solution are transformed into a tangible, insoluble fiber is indicative of marked physical change in the protein molecules. Whether these molecules can be more completely spread is not the question; the point is that they are in a physically different state from the same molecules in solution.

The albumin–pepsin system of the present investigation differs from the work of other investigators in that the enzyme and substrate are both incorporated in the film. The results show that the pepsin and albumin molecules must be associated in a specific manner prior to (and probably during) the physical changes taking place at the air–water interface in order that the autodigestive capacity be maintained. The enzyme and substrate molecules, when mixed and then formed into a film, form autodigestible fibers. The molecules, if placed on the same interface separately but incorporated into the same film and fiber, do not form autodigestible fibers. The physical conditions for the adsorption of native pepsin molecules is the same in the two instances, yet with completely different results. The conclusion can be drawn that autodigestion is due to surface-spread pepsin molecules. This conclusion is supported by the work of Kaplan (8) who finds that surface-denatured catalase also retains its activity.

Parenthetically, it may be added here that autodigestible fibers may be formed on a trough filled with saturated ammonium sulfate.[1] In view of the work of Seastone (9) showing a minimal amount of protein going into solution in the underlying bulk of the trough under these conditions, it is difficult to see how adsorbed native pepsin can be responsible for the autodigestion.

As a tentative hypothesis, we may say that the establishment of intermolecular linkages between the pepsin and albumin molecules while in solution mixture is a necessary part of the formation of autodigestible fibers. The results given in Table I indicate then that such linkages are formed when the two proteins are mixed at pH 4.4, 5.0, 6.0, and 6.6. However, when mixed at pH 7.2, the necessary interaction of the pepsin and albumin does not occur, resulting in fibers that do not undergo autodigestion. It is probable that the pepsin–albumin complex formed in mixture is similar in nature to the pepsin–edestin complex demonstrated by Northrop (10). However, Northrop's work did not involve the subsequent surface-denaturation of the protein complex.

Data obtained in the precipitation of the proteins with saturated ammonium sulfate support the hypothesis. The results show that at the same mixture pH range of 4.4–6.6 for the formation of autodigestible fibers, pepsin and albumin precipitate out simultaneously, whereas independently they have completely different solubilities to the precipitating action of ammonium sulfate. At mixture pH 7.2, where no autodigestible fibers are formed, the two proteins show a lack of interaction by precipitating out separately. The notion, therefore, that within the pH range of 4.4–6.6, there is an intermolecular association of the pepsin and the albumin in mixture seems to be substantiated.

---

[1] Unpublished experiments.

The autodigestible fibers formed from the proper mixtures would then be the enzyme–substrate complex in the sense of Michaelis and Menten (11), but in a stabilized form. When this complex is placed in a medium of the proper hydrogen-ion concentration, it dissociates with the formation of digestion products of proteolytic activity.

The above scheme brings out the fact that the autodigestion of complex fibers is not an enzymatic activity of the pepsin as it is ordinarily considered. We may write the reaction in the standard form

$$E + S \rightleftharpoons ES, \qquad [1]$$

$$ES \rightleftharpoons E + P, \qquad [2]$$

where E and S represent enzyme and substrate, respectively, ES the complex, and P the products. In the mixture of pepsin and albumin at the pH range considered, reaction [1] predominates, while in the autodigestion of the complex fibers, reaction [2] occurs. Since the ordinary concept of enzyme action involves both [1] and [2], the autodigestion phenomenon cannot be considered as an enzymatic activity of the pepsin, but only the degradation of the enzyme–substrate complex. Thus, the autodigestible fiber becomes, according to this scheme, a stabilized complex.

A puzzling situation arises when the substrate to enzyme ratios are examined. As reported previously (2), there is an apparent complete digestion of the fibers at a substrate to enzyme ratio as high as 18:1. Yet, in the precipitation curves of Fig. 4 there is a sizable excess of uncombined substrate even at ratios as low as 3:1. It may be that the association of the enzyme and substrate molecules while in mixture is maintained but radically altered at the time of transformation from molecules in solution to molecules in a monomolecular film. On the other hand, the paradox may be only apparent, to be resolved by improved methods of analysis. Work is planned along these possibilities.

The nature of the bonds involved in the formation of the complex is as yet a matter of speculation. The dependence on the hydrogen-ion concentration for the establishment of the complex indicates that the complex binding is brought about by the opposite signs of electrical charges on the respective molecules. From the data of Tiselius (12) pepsin would have a net negative charge, whereas albumin, which has an isoelectric point of about 4.8 (13), would have a net positive charge at pH's below 4.8 and a net negative charge above this. This, of course, would fit in with Michaelis' proposal (14) for the mechanism of pepsin action. However, according to this, pepsin and albumin molecules would exhibit no attraction for each other at pH 5.0, 6.0, and 6.6; yet the data of the present investigations indicate that a complex forms in these pH ranges. Thus, if salt linkages are involved, some explanation, such as localization of charges on the molecular surface, would have to be invoked to explain complex formation at these higher pH's.

Summary

1. Pepsin and albumin molecules will form autodigestible fibers from a compressed monomolecular film if they are mixed in solution prior to application to an air–water interface.

2. When pepsin and albumin molecules in solution are placed separately on an air–water interface, the fibers formed are not autodigestible.

3. Autodigestible fibers are formed from pepsin–albumin mixtures in the pH range of 4.4–6.6. When the proteins are mixed at pH 7.2, the fibers formed are not autodigestible.

4. Curves obtained by precipitating these proteins with ammonium sulfate show that, although pepsin and albumin have distinctly different sensitivities to the action of this reagent, they precipitate out together when in mixture.

5. The two proteins precipitate out together in the same pH range (4.4–6.6) as found for autodigestible fibers. At pH 7.2 they come down out of solution separately, according to their different solubilities.

6. Mixtures containing albumin in excess show at pH 4.4 two separate precipitates.

7. A tentative scheme is proposed to explain the data. According to this scheme, pepsin and albumin mixed at pH 4.4–6.6 combine to form an enzyme–substrate complex, which is stabilized when spread at an air–water interface and compressed to a fiber. The autodigestion of this fiber at pH 1.5 is taken to be the degradation of this stabilized complex.

References

1. Mazia, D., Hayashi, T., and Yudowitch, K., *Cold Spring Harbor Symposia Quant. Biol.* **12**, 122 (1947).
2. Mazia, D., and Hayashi, T. (1950), in press.
3. La Rosa, W., *Chemist-Analyst* **12**, 2 (1927).
4. Langmuir, I., and Schaefer, V. J., *Chem. Revs.* **24**, 181 (1939).
5. Harkins, W. D., Fourt, L., and Fourt, P. C., *J. Biol. Chem.* **132**, 111 (1940).
6. Sobotka, H., and Bloch, E., *J. Phys. Chem.* **45**, 9 (1941).

7. Rothen, A., *Advances in Protein Chem.* **3**, 123 (1947).
8. Kaplan, J. G., *Federation Proc.* **9**, 69 (1950).
9. Seastone, C. V., *J. Gen. Physiol.* **21**, 621 (1938).
10. Northrop, J. H., *J. Gen. Physiol.* **17**, 165 (1933).
11. Michaelis, L., and Menten, M. L., *Biochem. Z.* **49**, 333 (1913).
12. Tiselius, A., Henschen, G. E., and Svensson, H., *Biochem. J.* **32**, 1814 (1938).
13. Moyer, L. S., *J. Phys. Chem.* **42**, 71 (1938).
14. Michaelis, L., Die Wasserstoffionen-Konzentration. Julius Springer, Berlin, 1914.

MICELLE FORMATION OF SULFONATES IN HYDROCARBONS

M. van der Waarden

Koninklijke/Shell-Laboratory, Amsterdam, Holland

Received May 18, 1950

INTRODUCTION

A good deal of insight into the structure of nonliquid soap–hydrocarbon mixtures was obtained from the work of, among others, Lawrence (1), Puddington *et al.* (2), McBain *et al.* (3), Vold *et al.* (4) and Pink *et al.* (5). These mixtures are microcrystalline pastes or gels. Gray and Alexander (6) investigated viscoelastic soap solutions in benzene. All these systems become liquid when the temperature is raised sufficiently. Lawrence (1) assumes that in this case serpentine soap micelles are formed with the hydrocarbon chains turned outside; Pink (5) supposes that these micelles are spherical.

Some recent data are available concerning *dilute* hydrocarbon–soap systems that are liquid at room temperature, leading to the conclusion that soaps associate or form micelles in hydrocarbons (5, 7–10).

Our object was to obtain a better understanding of the conditions of the dissolved soaps in *concentrated* hydrocarbon–soap solutions that are liquid at room temperature. Such systems appear to be possible only when the soap shows little tendency to crystallization as in the case of mixtures of homologous and isomer soaps. Recently Mattoon and Mathews (11) investigated concentrated liquid solutions of Aerosol OT in *n*-dodecane; these authors assume that the soap forms spherical micelles in the solution. We used a mixture of sodium naphtha sulfonates as soap; corresponding sulfonates with other cations were used in addition. From one per cent to 40 was dissolved in various hydrocarbons and mineral oils. The relative viscosities and in some cases the stream double refractions of these mixtures were determined.

In many cases the relative viscosity (η_r) of a colloidal system may give indications as to the condition of the colloidal particles. To this end the intrinsic viscosity is calculated:

$$[\eta] = \left(\frac{\eta_{sp}}{c}\right)_{c\to 0},$$

where $\eta_{sp} = \eta_r - 1$ = specific viscosity, and
c = concentration of colloidal material.

For a very dilute homodisperse system of rigid globules, which are large with respect to the molecules of the solvent, $[\eta] = 2.5$ according to Einstein's equation. Deviations from this value are in the first place attributed to deviations from the spherical shape and to the fixation of solvent by the particles, *i.e.*, to an increase of the active volume of the particles during flow. The ratio of the active volume to the real volume of the colloidally dissolved substance is called the voluminosity (V) of the dissolved substance.

To calculate $[\eta]$, η_r must be determined at low concentrations; here, the assumption is made that shape and dimensions of the colloidal particles are independent of the concentration and that the particles do not interfere with each other's movements. The former requirement is probably not met in the case of concentrated soap solutions in hydrocarbons: if there is aggregation of soap molecules, this may be expected to depend on the concentration; further, the movement of the particles will be interfered with. This interference is more or less taken into account in the equation developed by Eilers and Van Dijck (12), which has been tried out by Eilers (13) on viscosity data of colloidal systems partly measured by himself, partly derived from the literature. This empirical equation has a form analogous to that of Bredée and de Booys (14); it not only passes into Einstein's equation at very low concentrations, but also meets the requirement that the relative viscosity at the closest packing of homodisperse rigid globules ($c = 0.74$) becomes infinitely high. The equation has the following form:

$$\eta_r = \left(1 + \frac{2.5\ VC_v}{2(1 - 1.35\ VC_v)}\right)^2 = \left(\frac{1 - 0.1\ VC_v}{1 - 1.35\ VC_v}\right)^2, \qquad [1]$$

where η_r = relative viscosity,
V = voluminosity of dispersed substance in solution,
C_v = vol. concentration of dry dispersed substance in parts by volume, and
VC_v = rheologically active volume concentration in parts by volume.

If the solutions over the whole concentration range meet the requirements for the equation (rigid particles of equal size which are large with respect to the solvent molecules), the same value for V from η_r and C_v should be found in the whole range. Both the absolute value of V and possible changes of V with the concentration may therefore give indications as to the condition of the colloidally dissolved substance.

The stream double refraction may give indications as to the shape of the colloidally dissolved particles.

EXPERIMENTAL METHODS

The mixture of sodium naphtha sulfonates was obtained by treating an SO_2-extracted mineral oil with oleum and neutralizing the oil-soluble sulfonic acids formed. The technical product was freed from mineral oil and water by extracting a solution in 50% ethanol with a low-boiling hydrocarbon fraction. After evaporation of the solvent, the product was dried at 105°C. The white, powdery product contained about 0.5% of sodium sulfate and about 3% of sodium carboxylate (naphthenate). The sulfonates had an average molecular weight of about 450 [determined by titration with hexadecylpyridinium bromide (15)] and consist mainly of alkylbenzene (naphthene) sulfonates.

Lithium, potassium, and, for comparison, sodium sulfonates were prepared by separating the sulfonic acids from the purified sodium naphtha sulfonate by means of concentrated hydrochloric acid and neutralizing a solution of the acids in a low-boiling hydrocarbon fraction with alkali hydroxide solutions in ethanol or water–ethanol. For the preparation of magnesium, calcium, and barium sulfonates, sulfonic acid solutions in water of 90°C. were neutralized with the corresponding solid oxides or hydroxides. after which the soaps formed were extracted from the reaction mixture by means of ether. After evaporation of the solvents and drying at 105°C., all the soaps were obtained as hygroscopic white to yellowish powders.

The hydrocarbons were distilled before use. The average molecular weights of the mineral oils were determined ebullioscopically; the percentages of carbon in paraffinic, naphthenic, and aromatic structures were calculated according to the ring analysis of Vlugter, Waterman, and van Westen (16), which has been further developed in this laboratory, and which will shortly be published.

The sulfonates were dissolved in hydrocarbons or mineral oils by heating to about 95°C., the solutions being kept for about 24 hr. at the temperature of measurement before the viscosity was determined; the viscosity did not change after this period. The viscosities were measured in B.S.I. viscometers in which the rate of flow was so low that the Hagenbach correction could be neglected. That it is proper to speak of the viscosity of the solutions under such conditions was shown by experiments in which the shearing stress at the wall varied from 10 to 100 dynes/cm.^{2} and the calculated viscosities were the same; the rates of shear at the wall in those cases were from 7 to 70 sec.$^{-1}$

The stream double refractions of solutions of a sodium naphtha sulfonate in *n*-heptane and toluene were measured[1] in a Couette apparatus, the rates of shear varying from 2000 to 12,000 sec.$^{-1}$

---

[1] These measurements were made and used for calculations by Messrs. D. J. Coumou and W. Boog of this laboratory.

Results

1. *Viscosity Measurements*

Purified sodium naphtha sulfonate in various concentrations was dissolved in *n*-heptane, toluene, a white oil (aromatic-free, av. mol. wt. 320) and an aromatic extract[2] [acid-free, av. mol. wt. 250; percentage of carbon in aromatic structure 50; the dark compounds (resins) were removed by means of an excess of silica gel]. From the relative viscosities of the solutions at 20°C., the VC_v values were calculated by means of Eq. [1], and from these the V values. The V's were plotted against VC_v in various solvents (Fig. 1). V proves to be higher than 1 and even to rise to 4. V is constant in the VC_v range 0.10–0.15 to 0.45–0.60. Outside this range V decreases to both sides. In aromatic solvents V is lower than in nonaromatic solvents and higher in higher molecular hydrocarbons.

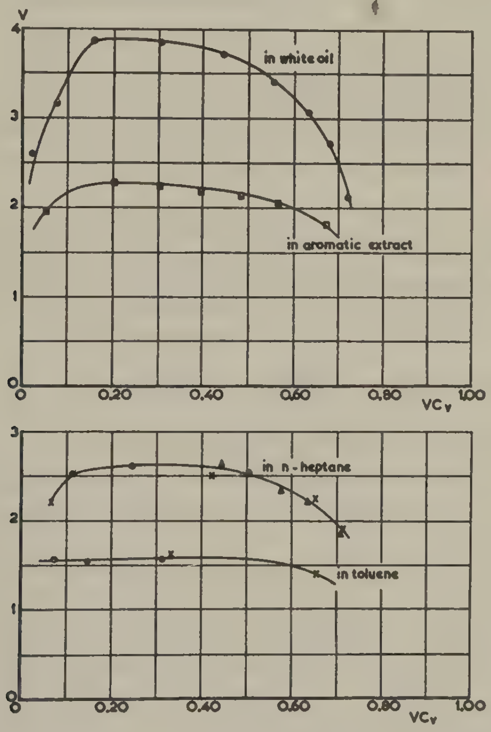

Fig. 1. Relation between voluminosity (V) of a sodium naphtha sulfonate in various hydrocarbons (mixtures), and the rheologically active volume concentration in the solutions (VC_v). Different marks in one and the same curve indicate solutions prepared separately.

---

[2] Obtained by extraction of a distillate fraction of a mineral oil (spindle oil) with SO_2.

This relation between *molecular weight* and *aromatic content* of the solvent on the one hand and V of the dissolved sulfonate on the other, was examined for a large number of hydrocarbons and mineral oils. In all cases 16.5% by vol. of sulfonate was dissolved, as a result of which VC_v lies within the range of constant V in all cases. The sulfonate used in these experiments contained 1.6% water. The results have been collected in Table I and Fig. 2. In Fig. 2, V has been plotted against the av. mol. wt. M of the solvent; smooth curves can be drawn through the points pertaining to oils of about the same aromatic content; V decreases with increasing aromatic content of the oil; this value first shows a considerable increase with rising molecular weight of the oil, until a maximum is reached for each aromatic content.

Measurements carried out at different temperatures on sodium naphtha sulfonate solutions of different concentrations in a white oil showed that V decreases with rising temperature. In the horizontal part of the V vs.

TABLE I

VC_v and V Values of 16.5 % by Vol. Solutions of a Sodium Naphtha Sulfonate in Hydrocarbons and Mineral Oils Calculated From the Relative Viscosities

Solvent	Mean molecular weight	Carbon in aromatic structure	VC_v	V
		%		
n-Hexane	86	0	0.296	1.79
n-Heptane	100	0	0.314	1.91
Isoöctane	114	0	0.346	2.09
Cyclohexane	84	0	0.274	1.66
White oil 1[a]	320	0	0.438	2.66
White oil 2	399	0	0.467	2.83
Raffinate 1	500	5	0.469	2.84
Distillate fraction 1	172	9	0.334	2.02
Distillate fraction 2	392	8	0.411	2.48
Residual oil	712	8	0.387	2.34
Raffinate 2	375	12	0.383	2.32
Distillate fraction 3	356	25	0.367	2.22
Distillate fraction 4	503	26	0.355	2.15
Extract 1	130	49	0.248	1.50
Extract 2	247	47	0.322	1.95
Extract 3	316	49	0.314	1.92
α-Methylnaphthalene	142	90	0.234	1.42
Benzene	78	100	0.198	1.20

[a] Mineral oil is separated into *distillate fractions* by distillation. Such a fraction is separated into a *raffinate* poor in aromatics and an aromatic *extract* by extraction with a selective solvent. By treating a raffinate with oleum, an aromatic-free *white oil* is formed. The *residual oil* is obtained as distillation residue of an asphaltene-free mineral oil.

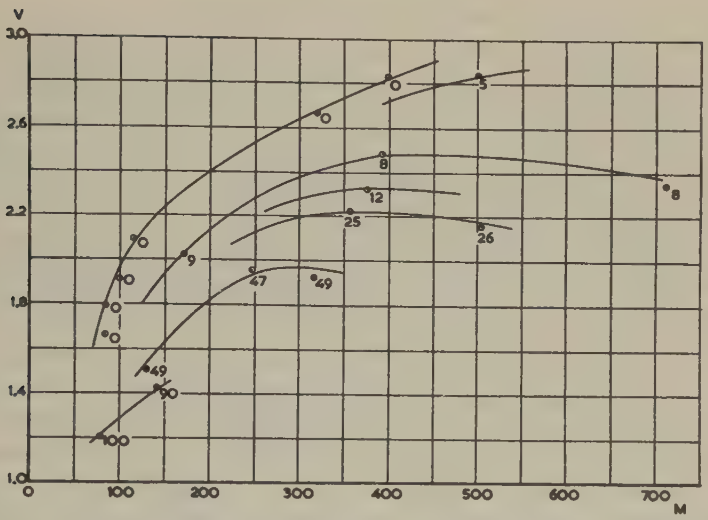

FIG. 2. Relation between voluminosity (V) of a sodium naphtha sulfonate dissolved in various hydrocarbons (mixtures), and mean molecular weight of the solvent.

The solutions contain 16.5% by vol. sulfonate. The figures at the points indicate the percentage of carbon in the aromatic structure of the solvent.

VC_v curve (cf. Fig. 1), V at 20, 50, and 90°C. was 3.85, 2.50, and 1.80, respectively.

Five and 10% by vol. of naphtha sulfonates with *different cations* were dissolved in a white oil. Table II shows that the V of the sulfonate largely depended on the cation. It increases with rising atomic weight and valency of the cation.

TABLE II

V Values of 5 and 10% by Vol. Solutions of Various Sulfonates (Prepared From the Same Sulfonic Acids) in a White Oil, Calculated From the Relative Viscosity

Cation	Atomic weight cation	Ion radius	V	
			at 20°C.	at 60°C.
		A		
H	1		1.85	—
Li	7	0.60	2.25	1.80
Na	23	0.95	2.83	2.00
K	39	1.33	high or gelated	4.70
Mg	24	0.65	4.1	—
Ca	40	0.99	7.4	—
Ba	137	1.35	10.2	—

2. Measurements of Stream Double Refraction

The relation between stream double refraction (Δ) and rate of shear (q), the Sadron constant, of sodium naphtha sulfonate solutions in *n*-heptane and toluene is almost constant for various rates of shear and, as shown by Table III, for various sulfonate concentrations. For solutions in heptane this constant is somewhat higher than for solutions in toluene; for a 20% solution in heptane it is much higher.

The major axis of the index-ellipse, by which the double refraction is characterized, makes an angle of some degrees with the direction of flow, except in the case of a 20% solution in heptane, where the angle is 35°.

TABLE III

Sadron Constants of Sodium Sulfonate Solutions at Various Rates of Shear

	$\frac{\Delta}{q} \times 10^{12}$					
Sulfonate concentration in solution	20	10	1.5	1	0.05	0
Solution in n-Heptane	(142)	32	27	25	28	*ca.* 2
Solution in toluene	27	27	24	23	24	*ca.* 1

An opinion about the sign of the double refraction can only be given when an assumption is made concerning the shape of the particles causing the double refraction. If the particles are assumed to be oblate rotation ellipsoids (discs, plates) the double refraction is positive; if they are conceived as greatly elongated rotation ellipsoids (bars, serpentines) the double refraction is negative.

DISCUSSION

Since in the case of solutions of molecules showing little or no aggregation (such as oleic acid and the higher hydrocarbons in a white oil) the calculated V values are far below 1 (in that case Eq. [1] may therefore not be applied), the results ($V > 1$) directly point to the presence of particles which are large with respect to the molecules of the solvent: they probably are relatively large aggregates of sulfonate molecules. As V is considerably higher than 1, the conclusion can further be drawn that the aggregates, which on the following pages will be referred to as micelles, either bind relatively large quantities of solvent, or are of a shape deviating considerably from the spherical one (17).

Now, it is obvious to assume in this case that the micelles have a plate-like shape, because solid soaps have a lamellar structure consisting of double layers with a two-dimensional ion lattice at the inside and hydrocarbon chains at the outside. Linking up with Lawrence's (1) line of thought we assume that the binding between these double layers is effected by the relatively weak van der Waals-London attraction of the hydrocarbon chains of various double layers. When mixtures of sulfonates are used consisting of components of divergent structure and length of these chains, this van der Waals-London attraction will be weaker on account of the lower degree of orientation, and the bonds between the double layers can easily be broken by a hydrocarbon medium. In that case independent double layers are left which have the shape of plates and are probably more or less flexible. The stream double refraction, too, indicates that the particles largely deviate from the spherical shape.

In this connection the influence of temperature, sulfonate concentration, sulfonate cation, molecular weight, and aromatic content of the solvent on V may be considered as an influence of these factors on the dimensions of the platelike micelles; assuming that the thickness of the plates remains the same, V increases with increasing extension of the plates. It may be assumed that the size of the plates is determined by the equilibrium between disintegrating and constructive factors. The disintegrating forces grow with increasing *temperatures*; at higher sulfonate *concentrations*, on the other hand, there is a greater chance of agglomeration.

The decrease in V with high VC_v values (about 0.5) can be attributed to the strong mutual interference of the platelike micelles with each other's movements. In an *aromatic* medium the disintegrating forces are stronger than in a nonaromatic medium, as a result of the stronger interaction between the polar group of the soap and the aromatic nucleus. This interaction manifests itself, for instance, when aromatics and nonaromatics are separated by polar solvents and is shown by the higher solubility of, *e.g.*, stearic acid in aromatic hydrocarbons. The rising V with higher *molecular weight* of the hydrocarbon would mean decreased disintegration. This is in accordance with our observation that the solubility of stearic acid in nonaromatic hydrocarbons decreases with higher molecular weight. The cause of the latter phenomenon will not be discussed here.

The influence of the *cation* of the sulfonate on the building-up–disintegration equilibrium may be understood if the disintegration is considered as sublimation from a two-dimensional lattice (by ignoring the medium, white oil, which in these cases has the same influence on the hydrocarbon part of the sulfonate molecules and is almost indifferent with respect to the sulfonate group). The heat of sublimation S of molecules from a three-dimensional ion lattice is determined by the charge of the ions, the distance between the ions, the polarization of the ions (particularly of the anions), and the lattice type. In the case of highly polarizable anions, such as the iodides, polarization dominates all the other factors (18), as a result of which S increases in the order H, Li, Na, and K salts. The polarization of the anion in sulfonate double layers is very probably higher than in a three-dimensional lattice, because the ions are arranged two-dimensionally. The cation will, therefore, certainly show the above-mentioned effect. The same reasoning probably holds good for the Mg, Ca, and Ba sulfonate series. A rising S may be expected in both series, *i.e.*, a decreasing tendency to disintegration of micelles in molecules and consequently an increasing V, as has been found.

If the univalent cations are replaced by divalent ones, S would be expected to increase on account of the higher charge of the cation and to decrease on account of the higher polarization of the anion. There is no clear indication as to the total effect to be expected, as in the case of the alkali sulfonates.

Although it is quite possible that the micelles retain hydrocarbon molecules of the solvent at the surface during flow, this is considered of secondary importance.

Starting from platelike micelles, the results enable us to make suppositions as regards the ratios of their dimensions. If, for instance, Burgers' equation (19) $\left(\frac{\eta_{sp}}{c} = 1.19 + \frac{4}{3\,\pi\,p}\right)$ for rigid discs (oblate rotation ellipsoids) with axis ratio $p \ll 1$ and so small that the Brownian movement is not interfered with by flow in viscosity measurements, is applied to our solutions, where $\frac{\eta_{sp}}{c}$ varies between 5 and 20 ($VC_v = 0.15$–0.50), the calculated p is 1/10–1/50.[3]

SUMMARY

1. The viscosities were determined of 1–40% solutions of a mixture of sodium naphtha sulfonates in various hydrocarbons and mineral oils. The voluminosity (V) of the sulfonate in the solutions was calculated from the relative viscosity of the solutions by means of Eilers' equation. The stream double refractions of some solutions were determined.

2. The voluminosity of the sulfonate in the solutions increases with rising sulfonate concentration; at high concentrations it decreases again. V decreases with rising temperature and with rising aromatic content of the hydrocarbon medium and increases with the molecular weight of this medium. V increases if the sulfonate cation changes in the sequence H, Li, Na, K, or in the sequence Mg, Ca, Ba, or from univalent to divalent cations.

3. The results are in agreement with the supposition that the sulfonates are present in hydrocarbons as platelike micelles consisting of a sulfonate double layer with the polar groups at the inside, the degree of disintegration in molecules being determined by the factors mentioned above under 2.

[3] According to Simha's equation (20), it follows from η_{sp}/c that $p = 1/5.5$–$1/30$.

REFERENCES

1. LAWRENCE, A. S. C., *Trans. Faraday Soc.* **34**, 660 (1938); *ibid.* **35**, 702 (1939); *J. Phys. & Colloid Chem.* **52**, 1504 (1948).
2. GALLAY, W., AND PUDDINGTON, I. E., *Can. J. Research* **21B**, 202, 211, 225 (1943); MOSES, G. B., AND PUDDINGTON, I. E., *Can. J. Research* **27B**, 616 (1949).
3. MCBAIN, J. W., MYSELS, K. J., AND SMITH, G. H., *Trans. Faraday Soc.* **42B**, 173 (1946); MARSDEN, S. S., MYSELS, K. J., AND SMITH, G. H., *J. Colloid Sci.* **2**, 265 (1947).
4. DOSCHER, T. M., AND VOLD, R. D., *J. Phys. & Colloid Chem.* **52**, 97 (1948); VOLD, R. D., AND VOLD, M. T., *ibid.* **52** 1424 (1948).
5. PINK, R. C., *Trans. Faraday Soc.* **37**, 180 (1941); MARTIN, E. P., AND PINK, R. C., *J. Chem. Soc.* **1948**, 750.
6. GRAY, V. R., AND ALEXANDER, A. E., *J. Phys. & Colloid Chem.* **53**, 9 (1949).
7. GONICK, E., *J. Colloid Sci.* **1**, 393 (1946).
8. MCBAIN, J. W., AND WORKING, F. B., *J. Phys. & Colloid Chem.* **51**, 974 (1947).
9. STROBEL, H. A., AND ECKSTROM, H. C., *J. Chem. Phys.* **16**, 817 (1948).
10. ARKIN, L., AND SINGLETERRY, C. R., *J. Am. Chem. Soc.* **70**, 3965 (1948); *J. Colloid Sci.* **4**, 537 (1949).
11. MATTOON, R. W., AND MATHEWS, M. B., *J. Chem. Phys.* **17**, 496 (1949).
12. EILERS, H., *Kolloid-Z.* **97**, 313 (1941).
13. EILERS, H., *Kolloid-Z.* **102**, 154 (1943).
14. BREDÉE, H. C., AND DE BOOYS, J., *Kolloid-Z.* **79**, 32 (1937); *ibid.* **91**, 39 (1940).
15. EPTON, S. R., *Trans. Faraday Soc.* **44**, 226 (1948).
16. VLUGTER, J. C., WATERMAN, H. J., AND VAN WESTEN, H. A., *J. Inst. Petroleum Technol.* **21**, 661, 701 (1935).
17. BURGERS, J. M., Second Report on Viscosity and Plasticity, pp. 153, 161. Acad. Sci. Amsterdam, 1938.
18. VAN ARKEL, A. E., AND DE BOER, J. H., La valence et l'électrostatique. Félix Alcan, Paris, 1936.
19. BURGERS, J. M., *Proc. Acad. Sci. Amsterdam* **43**, 307 (1941); PHILIPPOFF, W., Die Viskosität der Kolloide, 1942.
20. MEHL, J. W., ONCLEY, J. L., AND SIMHA, R., *Science* **92**, 132 (1940).

SOLUBILITY AND SWELLING OF ALKALI SOAPS IN ORGANIC SOLVENTS

A. Bondi

Shell Development Company, Emeryville, California

Received June 19, 1950; revised August 2, 1950

INTRODUCTION

The physical properties of soap–solvent systems are well known to depend upon the chemical structure of the solvent. The mechanical properties, particularly, of soap gels in viscous liquids are often strongly affected by the medium in which they have been prepared. Such effects are usually referred to very glibly as "solubility" or "swelling." A detailed study of the nature of the interaction between soap and solvent and the resultant properties of soap gels such as greases led to the conclusion that the chemical structure of the solvent affects not only the equilibrium states of the soap–solvent system but also the rate processes determining the number and shape of the soap crystallites (fibers). This paper will deal only with the equilibrium states of soap–solvent systems, namely the solubility of soap in solvents and the swelling of soaps by solvents.

The Solubility of Sodium Soaps in Organic Solvents

Calculation of the ideal solubility curve (2,6) from published heat of transition and fusion data of soaps (14) has shown that the level and slope of the observed solubility data fall into fairly definite patterns. The solubility in hydroxylic solvents, calculated from published data for sodium palmitate (7) as a typical example, follows the slope of the ideal curve rather closely especially in the more dilute region (as shown in Fig. 1). Except for *p*-cresol the level of the ideal solubility curve is approached the more closely the higher the cohesive energy density of the solvent. This is essentially what one should expect (6) and is in keeping with observations on other long-chain compounds (1). The excess free energy of mixing with alcohols is thus largely due to a markedly negative heat of mixing.

The solubility in hydrocarbon solvents (3,11,12,13) (shown in Fig. 2) on the other hand, is far removed from the ideal curve, indicating large negative enthalpy and entropy changes on mixing. The solubility in these solvents is so low at lower temperatures that the data are probably not very reliable. For this reason and because of the small number of results in regions where the curves do not pass through peculiar gyrations (11), correlation between solubility and the structure or properties of the solvent is not possible at present.

A paucity of data suitable for thermodynamic calculations persists in a field of considerable technical interest, namely soap solubility in (binary) solvent mixtures. The well known solubilizing effect of water in all of the presently known solvents may be accountable on the basis of the reduction in soap melting point and in heats of transition and fusion by the presence of the water in the soap, *i.e.*, soap + water have to be considered as a new compound, the solubility of which is determined by its melting point and total heat of fusion. Addition of small amounts of alcohols and fatty acids to the sodium soap system increases the solubility in hydrocarbons and other solvents, probably by the same mechanism.[1]

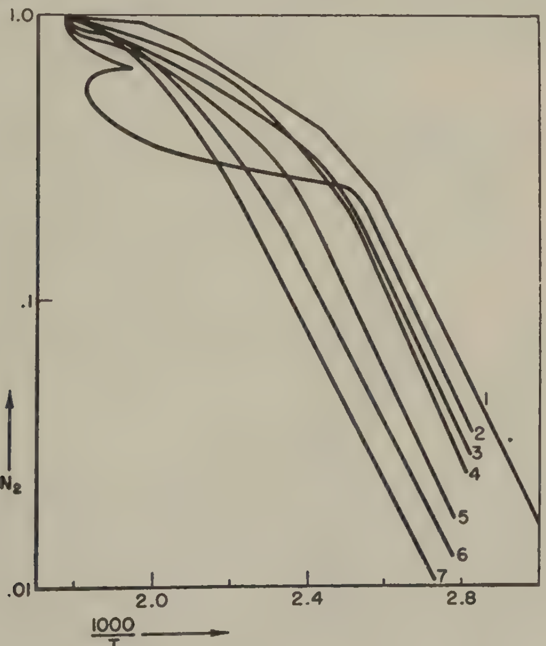

Fig. 1. Solubility of sodium palmitate in hydroxylic solvents (smoothed curves). 1. Ideal $(\Delta E/V)^{\frac{1}{2}}$. 2. Glycerol 15.3. 3. *p*-Cresol 10.7. 4. Diethylene glycol 12.7. 5. Ethyl alcohol 12.7. 6. *n*-Heptyl alcohol. 7. Cetyl alcohol.

From the point of view of the grease manufacturer it is important to note that in the temperature range of grease application (below 180°C.)

---

[1] This mechanism has been found valid also in the case of solubilization of fatty acids by each other (9).

the solubility of sodium soap in higher-molecular-weight hydrocarbon oils is negligible, namely below 0.1%.

Swelling of Soaps by Solvents

The swelling of soaps by solvents has become a generally accepted fact, and numerous data on swelling have recently been presented (4,8). Close inspection of these data reveals that not swelling but only the sedimentation volume of soap powder has been measured. The sedimentation volume, however, is essentially a measure of the strength with which particles stick together after collision and of the distance to which they can approach each other; whether or not changes in particle dimensions take place cannot be determined from sedimentation volumes.

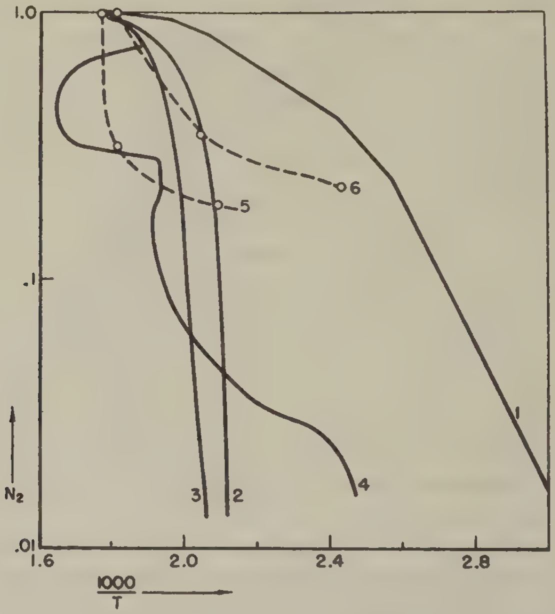

FIG. 2. Solubility of sodium palmitate in hydrocarbons (smoothed curves). 1. Ideal $(\Delta E/V)^{\frac{1}{2}}$. 2. Cetane 7.5. 3. Nujol 7.8. 4. Toluene (sodium stearate) 8.8. 5. Toluene (sodium stearate + 0.5% water). 6. Toluene (sodium stearate + 5.5% water).

The direct measurement of the swelling of soaps in organic solvents has not been undertaken before. A few exploratory experiments have therefore been carried out in which the swelling of individual soap crystals was observed microscopically.

The soaps employed in this work were prepared (by Mr. E. R. White) from highly purified fatty acids of the following characteristics:

Acid	Melting point °C.
Lauric	47.5
Myristic	54.15
Stearic	69.6
Behenic	82
Erucic	33.3
Brassidic	59.9
12-Hydroxystearic	80.35

The soaps were obtained by neutralization in alcoholic solution in the absence of CO_2. All soaps were tested for neutrality by titration. (The melting points and transition points of the soaps will be reported elsewhere.)

Two commercial soaps were also employed: potassium stearate, Kahlbaum; and sodium oleate, U.S.P. Merck.

The solvents used and their physical properties are:

Cetane (prepared by E. R. White): m.p., 18.8°C.
1,1-Diphenylethane (prepared by E. R. White): b.p., 269.5–270°C.
Bis(2-ethylhexyl)adipate (Du Pont): $V_{37.8°\text{C.}} = 8.21$ centistokes (cs.), $V_{98.9°\text{C.}} = 2.38$ cs.
Nonyl naphthalene (Sharples): $V_{37.8°\text{C.}} = 18.9$ cs., $V_{98.9°\text{C.}} = 2.83$ cs.
Nitrobenzene (Eastman): m.p., 7°C.
n-Octyl alcohol (Eastman).
Oleyl alcohol (Michel): m.p., 15°C.
Glycerol (Merck).
Polyethylene glycol (Carbide and Carbon): mol. wt., 600.
Paraffinum liquidum: $V_{37.8°\text{C.}} = 75.6$ cs., $V_{98.9°\text{C.}} = 8.78$ cs., $d_4^{20} = 0.8703$.
Aromatic lubricating oil: viscosity index, −53; specific dispersion $\times 10^4 = 155$.

PROCEDURE

The slightly ground soap crystals were introduced into small flattened glass capillaries which were nearly completely filled with solvent and sealed. The higher boiling solvents could also be used between microscope cover glasses on which a few soap crystals had been sprinkled. In either case the object was then placed on a hot stage and viewed with the microscope, which was also equipped with Nicol prisms for viewing by polarized light. The selection of magnification was governed primarily by the appearance of the soap crystals. Regular and noncomposite particles could often be found only in the smaller size ranges requiring 300 or even 700 magnifications. From the point of view of rapid establishment of swelling equilibrium, it is also desirable to use small particles, since the (probably governing) diffusion rate increases as the inverse square of the particle size.

The heating rate was adjusted at about 0.5–1°C./min. The temperatures given in the text are those of the hot-stage oven. Occasional direct measurements of the temperature obtaining in the capillary showed that the temperature of the sample is at least within 5°C. of the oven temperature, most of the time probably within 2°C. of the oven temperature.

The measurement of the soap crystals was performed with a Whipple Micrometer eyepiece. Due to proximity in refractive indices and the difference in refractivity–temperature curves between soap and oil, the particles become invisible at the temperature at which the respective refractive index curves cross. It is then often possible to make the measurements in the light of the crystalline particles between crossed Nicol prisms. Peculiarly enough, there are considerable differences in birefringence between the various fragments of the same soap lump, a considerable portion of fragments exhibiting frequently no birefringence at all.

At the indicated heating rate, swelling equilibrium is apparently established with sufficient speed so that the observed degrees of swelling can be taken as reversible equilibrium values, as has been checked at a few instances. The actual heating rate increased with temperature, 1°C./min. being only the average over 140°C.

TABLE I

Reproducibility of Swelling Measurements of Sodium Stearate in 1,1-Diphenylethane

	Relative swelling at				
	20°C.	80°C.	100°C.	120°C.	140°C.
Test A	1	—	1.35	1.7	2.2
Test B (1 year later)	1	1.06	1.3	1.6	2.1

The reproducibility of the method is evident from the data in Table I, which were obtained by repetition after a lapse of one year with different hot stages.

SWELLING MEASUREMENTS

General Observations

The swelling data in this work are expressed as the ratio of the visible area of the crystal or crystal fragment at the temperature of observation to the area at room temperature. The definition indicates the two basic limitations of our swelling measurements: (*a*) the impossibility of simultaneous measurement in three dimensions, and (*b*) the relativity of the swelling data, insofar as they express the degree of swelling only relative to that at room temperature. They have an absolute meaning only if one assumes that the swelling of our soaps in organic solvent at room temperature is negligible. For the sodium and lithium soaps examined, this may well be a reasonable assumption.

Occasionally a soap crystal will be turned around or twisted by convection currents. The thickness which one observes then is usually of the order of 5–10 μ, while the normally viewed dimensions are of the order of 50–500 μ, indicating that these soap crystals are essentially platelets or flat needles (ribbons). The particles of sodium oleate, sodium behenate, sodium erucate, and sodium brassidate were much less regularly shaped than those of the other soaps and had to be viewed at high magnifications in order to obtain the individual particles instead of spongy aggregates.

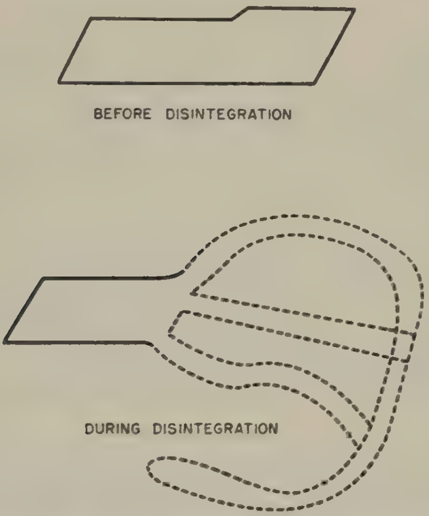

Fig. 3. Rough sketch of the disintegration of a sodium stearate crystal immersed in oil at high temperatures.

As one approaches the dissolution temperature in a hydrocarbon solvent, the soap crystal begins to disintegrate in the manner sketched in Fig. 3. This process can be arrested simply by reducing the temperature. The tendency to fibril formation in the course of thermal disintegration is a parallel to the characteristic crystallization of these soaps in needle or fiber form. Both processes are indicative of the fact that the weakest planes of the soap crystal run parallel to its length axis.

Swelling of Sodium Stearate in Various Solvents

The data in Table II show that this soap swells very little in saturated hydrocarbons, somewhat more in the aliphatic ester and in nitrobenzene, and very considerably in aromatic hydrocarbons. Mixtures of aromatic and aliphatic hydrocarbons act essentially as if only the aromatic component were present, leading to the notion that perhaps a selective removal of aromatic hydrocarbons could be effected by the swelling of soap. Examination of mixtures of aromatic and aliphatic hydrocarbons before and after stirring (for 15 hr.) with soap indicated

TABLE II

Swelling of Sodium Stearate in Organic Solvents

Solvents	Relative swelling at[a]							δ_1[b]
	20°C.	80°C.	100°C.	120°C.	130°C.	140°C.	150°C.	
A. Hydrocarbons								
1) Cetane	1.0	Unchanged to 120°C.						7.5
2) *Paraffin liq.*	1.0	1.0	1.0	1.0	1.1	1.2	1.5	7.8
3) Nonylnaphthalene	1.0	—	1.2	—	1.7			9.0
4) 1,1-Diphenylethane	1.0	1.06	1.3	1.6	—	2.1		9.7
5) 50% No. 1 + 50% No. 4	1.0	—	1.5	—	2.1			—
6) 5% No. 4 + 95% No. 2	1.0	1.0	1.35	1.75	1.9	2.1		—
7) Aromatic distillate	1.0	1.0	1.3	—	1.8			—
B. Non-Hydrocarbons								
1) Nitrobenzene	1.0	—	1.25	—	1.6			12
2) Bis(2-ethylhexyl)adipate	1.0	—	1.02	1.15	1.4			8.5
3) Oleyl alcohol	1.0	1.9 (75°C., disintegrates at 80°C.)						

[a] Relative swelling = area of crystal at t/area at 20°C.

[b] $\delta_1 = (\Delta E/V)^{\frac{1}{2}}$ = (cohesive energy density)$^{\frac{1}{2}}$ = solubility parameter of solvent at 20°C. (6).

that only a small portion of the aromatic hydrocarbon present was removed selectively (see Table III). It appears, therefore, that the swelling of soap in these mixtures is initiated by the aromatic component. The crystal lattice is then weakened or opened sufficiently to admit the nonswelling compounds into its interstices. The same observation has been made on swelling of crosslinked high polymers in aromatic oils (5). From heat of swelling measurements it is known that the sorption of the first 10% is accompanied by the absorption of about 90% of the total

TABLE III

Selective Swelling Effects

(after 16 hr. at 120°C.)

	Soap	Diphenylethane	Cetane	K[a]
Initial composition	10% NaSt[b]	3.9	96.1	—
Final composition	—	3.0	97.0	2.5
Initial composition	10% NaSt[b]	1.09	98.9	—
Final composition	—	0.44	99.5	12

[a] Estimated partition coefficient of diphenylethane between swollen sodium stearate and the liquid phase.

[b] Sodium stearate.

heat of swelling, indicating that the initial loosening of the lattice involves the determining changes in the potential energy of the system. The swelling of soaps in lubricating oils may thus be determined by the presence in the oil of small amounts of aromatic components.

While the solvents so far discussed have all been recruited from the group of "poor" solvents of Fig. 2, the "good" solvents of Fig. 1 behave rather differently. There is no swelling at all observed in glycerol or polyethylene glycol. On heating to 60–70°C. the soap crystal dissolves in the solvent about in the same fashion as a salt crystal dissolves in water, *i.e.*, first, the corners begin to round off, and, subsequently, the crystal decreases in size continuously until its complete disappearance. The previously claimed swelling of sodium stearate in glycerol (8), which had been inferred from sedimentation volume data, could thus not be verified by direct observation. The sedimentation volume must, therefore, be accounted for in the usual manner, namely, by saying that in glycerol suspensions the soap particles tend to stick to each other. This sticking may just be due to the difference in cohesive energy density between the hydrocarbon-like soap surface and the glycerol, *i.e.*, the soap particles prefer contact with each other to contact with the glycerol molecules.

The behavior in the higher alcohols differs from both that in the glycols and in the hydrocarbons. The soap swells in octyl alcohol and in oleyl alcohol at quite low temperatures. But, while the swelling in hydrocarbons was reversible, provided the dissolution temperature had not been reached, swelling in the alcohols was found to be irreversible. The apparent swelling in alcohols is just a manifestation of the disintegration which precedes dissolution. This conclusion is also borne out by the fact that in the alcohols investigated a steady state could not be reached at any temperature above the one at which swelling had commenced. The disintegration is also evident from the blurring of the crystal contours. True, *i.e.*, reversible, swelling does therefore probably not occur in "good" soap solvents.

Effect of Soap Composition on Swelling

(a) *Molecular Weight of Fatty Acid*

The swelling data of sodium soaps, ranging from laurate to behenate, in 1,1-diphenylethane, our most potent swelling agent, have been assembled in Table IV. As one might expect, the tendency to swell increases with increasing chain length of the fatty acid up to stearic acid. The 22-carbon-atom salt, the behenate, does not differ materially, however, from the stearate. This observation is in agreement with the fact that,

TABLE IV

Effect of Molecular Weight on Swelling of Sodium Soaps in 1,1-Diphenylethane

Soap	Relative swelling at				
	20°C.	80°C.	100°C.	120°C.	140°C.
Laurate	1.0	1.0	1.02	1.2	1.3
Myristate	1.0	—	1.1	1.2	1.8
Stearate	1.0	1.06	1.3	1.6	2.1
Behenate	1.0	1.1	1.2	1.6	2.15

except for the melting transition, the temperatures of phase transition of sodium stearate and sodium behenate are practically identical (17).

(b) *Effect of Double Bonds and Hydroxyl Groups*

A few soaps of fatty acids containing double bonds and hydroxyl groups were available so that an indication of the direction could be obtained in which these changes in molecular structure affect the swelling behavior. The resulting data are assembled in Table V. While the reduction of swelling by the hydroxyl group may be expected from the strengthening of the crystal lattice by the hydroxyl bonds, the strong reduction in swelling by the introduction of double bonds is somewhat surprising. Even more astonishing is the behavior of the *cis-trans* isomers. The degree of swelling of erucate and brassidate is just opposite in direction to that expected from the melting point of the acids. The thermal behavior of the soaps has not yet been investigated.

(c) *Effect of the Cation*

The change from sodium to lithium soap results uniformly in a reduction of swelling tendency, as is shown by the data in Table VI.

TABLE V

Effect of Double Bond and Hydroxyl Groups on Swelling of Sodium Soaps in 1,1-Diphenylethane

Soap	Relative swelling at				
	20°C.	80°C.	100°C.	120°C.	140°C.
Stearate	1.0	1.06	1.3	1.6	2.1
Oleate	1.0	1.07	1.1	1.2	1.4
12-Hydroxystearate	1.0	1.0	1.0	1.03	1.25
Behenate	1.0	1.1	1.2	1.6	2.1
Erucate	1.0	1.0	1.05	—	2.1
Brassidate	1.0	1.0	1.35	1.45	1.5

TABLE VI

Effect of Ion on Swelling of Alkali Soaps

Soap	Relative swelling at					
	20°C.	80°C.	100°C.	120°C.	140°C.	
Lithium stearate	1.0	1.0	1.0	1.1	1.23	In 1,1-diphenylethane
Sodium stearate	1.0	1.06	1.3	1.6	2.1	
Potassium stearate	1.0	1.03	1.1	1.13	1.2	
Lithium 12-hydroxystearate	1.0	1.0	1.0	1.0	1.0	
Sodium 12-hydroxystearate	1.0	1.0	1.0	1.03	1.25	
Lithium stearate	1.0	1.0	1.05	1.05	1.1	In bis(2-ethylhexyl) adipate
Sodium stearate	1.0	—	1.02	1.15	1.4	

The lithium 12-hydroxystearate is unique in that it does not show any swelling up to the dissolution temperature. The potassium stearate does not swell more than the sodium salt as one might have expected from the trend Li to Na, but rather less. This behavior corresponds, however, to what one can predict from the heat of transition.

Discussion

The swelling data reported are insufficient for the discussion of the thermodynamics of the swelling process, no means having been provided to measure the concurrent free energy change. This could conceivably be done by measuring the change in vapor pressure of the solvent during sorption. The published sorption isotherms of cyclohexane on sodium stearate (10) provide at least a rough indication of the energetics of the swelling process. One can estimate from the sorption isosteres that ΔH is about 1.5 ± 0.5 kcal./mole; ΔF being very small (since swelling occurs only at $P/P_0 > 0.5$), $T\Delta S$ is of the same order as ΔH. Similar measurements on the less volatile solvents of this investigation would be quite difficult.

We must, therefore, try to deduce the mechanism of the soap-swelling process from empirical correlations. The relatively steep temperature coefficient of swelling suggests that loosening of the crystal lattice is a prerequisite for soap swelling in contrast to most of the high polymers which swell in the proper solvent already at low temperatures. A good measure of the effect of temperature on the loosening of the crystal structure is the occurrence and extent of (*i.e.*, the heat of) phase transitions, compressibility measurements having shown that tristearin, for instance, at temperatures above a first-order phase transition approaches the liquid state rather closely in cohesion (16).

A plot of the percentage of swelling in 1,1-diphenylethane at 140°C. versus the sum of the heats of transition to that temperature provides indeed very good correlation, as is apparent from the curve of Fig. 4.[2] A similar curve is obtained by plotting per cent swelling against the ratio $\sum_{140°\text{C.}} \Delta H_i / \sum_{\text{m.p.}} \Delta H_i$, which might be called the degree of loosening of the crystal lattice at 140°C. Particularly striking is the fact that the lithium 12-hydroxystearate, which does not show any phase transitions up to 165°C. also does not swell below that temperature.

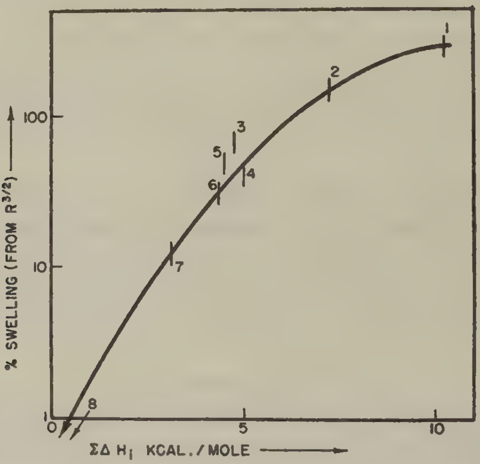

Fig. 4. Relation between swelling of soaps in 1,1-diphenylethane at 140°C. and the sum of their heats of transition to 140°C. 1. Sodium stearate. 2. Sodium myristate. 3. Sodium oleate. 4. Sodium 12-hydroxystearate. 5. Sodium laurate. 6. Potassium stearate. 7. Lithium stearate. 8. Lithium 12-hydroxystearate. R = relative swelling.

While the sorption of water vapors by sodium stearate takes place in discrete steps, which are related to the corresponding phase transitions (10), no such stepwise swelling could be observed either in cyclohexane vapors or in diphenylethane in this work. It appears that once the crystal structure is loosened (beginning at about 80–90°C. for most of the soaps studied), further loosening in subsequent transitions "smeared" by the effect of the solvent present, just as—isothermally—the loosening of the structure by small amounts of aromatic solvent will make it swellable by otherwise nonswelling solvents.

[2] The heat of transition data for sodium laurate, myristate, stearate, and oleate were taken from the paper by Vold (14); that of the sodium and lithium 12-hydroxystearate and potassium stearate from unpublished results obtained in this laboratory (17); that of lithium stearate was computed from Vold's data on lithium palmitate (15), assuming similar phase behavior for the two salts.

From the few data available so far, it appears that just as in the case of polymers (5), swelling ability of the solvent can be correlated largely to its cohesive energy density. Many more solvents have to be examined, however, before a similarly general rule can be established for soap swelling, even though the basic principle of such correlation is of sufficient generality to make its applicability outside the polymer field seem reasonable.

Anisotropy of swelling, *i.e.*, dependence of the degree of swelling upon the crystal axis, was observed primarily with the weaker swelling agents, but hardly when considerable swelling took place. Determination of the crystallographic axis of the observed crystal fragments not having been attempted, a report of the observed anisotropy data appears useless. The same applies to the observed birefringence.

ACKNOWLEDGMENT

It is a pleasure to acknowledge helpful discussions with Prof. James W. McBain, Messrs. O. Redlich, E. R. White, F. H. Stross, and S. T. Abrams. The latter two also kindly made available still unpublished data on the phase-transition temperatures and enthalpy changes of sodium and potassium stearate, sodium and lithium 12-hydroxystearate, and sodium behenate.

SUMMARY

1. The ideal solubility curve of sodium palmitate has been calculated from published heat of transition data. The solubility curves of sodium palmitate in hydroxylic solvents were then found to approach the ideal curve fairly closely, whereas the high degree of nonideality of the solution of soda soap in hydrocarbons became quite conspicuous.

2. The swelling of lithium, sodium, and potassium soap crystals in various organic solvents was measured microscopically. It was found that sodium stearate crystals dissolve or disintegrate but do not swell in hydroxylic solvents at temperatures above 80°C., swell slightly in aliphatic hydrocarbons and high-boiling aliphatic esters, and swell considerably in aromatic hydrocarbons. The degree of swelling at a given temperature and in 1,1-diphenylethane (the strongest swelling agent found) increases continuously from sodium laurate to stearate, decreases as double bonds and hydroxyl groups are introduced into the fatty acid radical, and is much smaller for lithium and potassium stearates than for sodium stearate. All of the observed swelling data could be correlated with the sum of the heats of transition up to the temperature at which the swelling is measured: the larger $\Sigma_i \Delta H_i$, the greater the extent of swelling. Swelling of soaps in solvents is thus due to the thermal loosening of the crystal lattice.

REFERENCES

1. Bondi, A., *J. Phys. Chem.* **51**, 891 (1947).
2. Bondi, A., *J. Chem. Phys.* **16**, 157 (1948).
3. Doscher, T. M., and Vold, R. D., *J. Colloid Sci.* **1**, 299 (1946).

4. Galley, W., and Puddington, I. E., *Can. J. Research* **B22**, 16 (1944).
5. Gee, G., *Advances in Colloid Sci.* **2**, 145 (1946).
6. Hildebrand, J. H., Solubility of Non-Electrolytes, New York, 1936.
7. Leggett, C. W., Jr., Vold, R. D., and McBain, J. W., *J. Phys. Chem.* **46**, 429 (1942).
8. Mardles, E. W. J., and Clarke, E. B., Faraday Society Discussion on Swelling and Emulsification, 1946.
9. Ralston, A. W., and Hoerr, C. W., *J. Org. Chem.* **10**, 170 (1945).
10. Shreve, G. W., Ph.D. Thesis, Stanford, 1946.
11. Smith, G. H., Ph.D. Thesis, Stanford, 1946.
12. Smith, G. H., and McBain, J. W., *J. Phys. Chem.* **51**, 1189 (1947).
13. Smith, G. H., *J. Am. Oil Chemists Soc.* **24**, 353 (1947).
14. Vold, R. D., *J. Am. Chem. Soc.* **63**, 2915 (1941).
15. Vold, R. D., and Vold, M. J., *J. Phys. Chem.* **49**, 32 (1945).
16. Kornfeld, M. O., and Shestikin, P., *Compt. rend. acad. sci. U. R. S. S.* **36**, 52 (1942).
17. Stross, F. H., and Abrams, S. T., private communication.

THE METHODS OF FORMING, DETECTING, AND MEASURING THE SIZE AND CONCENTRATION OF LIQUID AEROSOLS IN THE SIZE RANGE OF 0.01 TO 0.25 MICRONS DIAMETER[1]

Victor K. La Mer, Edward C. Y. Inn[2] and Irwin B. Wilson[3]

From the Department of Chemistry, Columbia University, New York, N. Y.

Received April 6, 1950

ABSTRACT

(*a*) The objective of this research was to develop methods of producing, detecting, and measuring rapidly and easily the size and concentration of liquid aerosol droplets in a range (0.01–0.08 μ) smaller than those at present available.

(*b*) The new contribution to the method of measurement of particle size consists in growing quantitatively exceedingly small aerosol droplets to a size range where they can be measured by established optical methods.

(*c*) Aerosol droplets with radii less than 0.08 μ are too small to be measured by any of the optical methods available. The electron microscope is not always suitable on account of the liquid character of the droplets and their volatility.

(*d*) The sizes of homogeneous aerosol droplets following controlled growth are easily measured by a variety of optical methods developed previously in the Columbia University Laboratories (under NDRC-OSRD contracts in 1940–45), for a size range terminating at the approximate lower limit of 0.08-μ radius, depending upon the index of refraction and the precision desired. The polarization of the scattered light furnishes the most sensitive measure in this range of size. As size is increased, measurement naturally becomes less difficult and more reliable. The various optical methods applicable in these upper ranges make contact with those of the ordinary light microscope.

(*e*) The homogeneous aerosol generator of La Mer and Sinclair can be used for the production of exceedingly small particles; 99% H_2SO_4 and dibutyl phthalate have proven to be suitable examples. The lower limit of size production appears to be the critical nucleus (radius $\sim 10^{-7}$ cm. or 0.001 μ); the smallest radius *measured* by the present growth is about 0.01 μ, although smaller sizes of the order 0.006 μ are detectable and these sizes can be estimated crudely.

(*f*) Aerosols of 99% H_2SO_4 when exposed to H_2SO_4 solutions of higher water content absorb water, and grow to a size such that the aqueous tension of the droplet equals that of the master solution to which it is exposed. Vapor pressure equilibrium is attained exceedingly rapidly.

(*g*) Similar behavior is exhibited by dibutyl phthalate aerosol droplets when exposed to the vapors of volatile solvents such as toluene, xylene, *etc.* Theory indicates, and there

---

[1] This paper is based upon a research project initiated by the Office of Naval Research and supported by Navy Contract N6onr-27116, Columbia University.

[2] Present address: Base Directorate, Geophysical Research, Watertown Arsenal, Mass.

[3] Present address: College of Physicians and Surgeons, Medical Center, Columbia University, New York, N. Y.

is no evidence to the contrary, that all liquid aerosols when exposed to the vapors of a miscible and volatile solvent can be grown under controlled conditions.

(*h*) In the case of 99% H_2SO_4, measurements can be made following growth by a factor as large as 8-fold in radius (512-fold in volume or an increase in the intensity of light scattering of roughly 4000- to 250,000-fold, depending upon initial radius). The control of the growth is more reliable the smaller the growth. Five-fold is recommended.

(*i*) The number and radii of the grown sulfuric acid droplets were determined by the optical transmission method. The mass of H_2SO_4 thus calculated was compared with the mass deposited upon a filter which was washed, and the pH of the wash liquid was determined with a glass electrode. Considering the minute amount of material collected, satisfactory agreement was secured.

(*j*) The range and reliability of the transmission method was improved by generating new functions of the type K/α^n, where K is the optical scattering area coefficient, and $\alpha = 2\pi r/\lambda$; n was varied from 1 to 3. These derived functions give characteristic maxima and minima in more desirable ranges of droplet radii.

INTRODUCTION

Although methods have been developed for measuring particle radii of liquid aerosols greater than 0.15 μ, very little investigation of smaller particles has been reported and none below 0.08 μ. Visual counting methods suitable for larger particles at least 0.8 μ in radius and only for fairly dilute aerosols ($n < 10^5$ particles/ml.) have been described by Zsigmondy (1), Whytlaw-Gray (2), and Green (3). Several optical and sedimentation methods especially applicable for smaller particles have been reported by La Mer and Sinclair and their co-workers (4,5). Gucker and O'Konski (6) have developed electronic devices for counting individual aerosol droplets based upon one of these methods; namely, the forward angle Tyndallmeter developed in 1941–2 by Sinclair (5) and by Hochberg in this laboratory for the measurement of the smoke penetration of improved filters.

Unfortunately when employed as a counter of individual particles, the radius must be 0.6 μ or larger. However, one of the other optical methods, namely, polarization of scattered light, is applicable to particle radii as small as 0.07 μ. It is the purpose of this research to extend these methods to still smaller radii by introducing a controlled growth before measuring the size.

PRODUCTION OF AEROSOLS OF EXCEEDINGLY SMALL PARTICLE SIZE

The homogeneous aerosol generator (5) (Fig. 1) used previously has proven satisfactory for the production of small particle aerosols of H_2SO_4. Particles can be produced which are so small that they fail to show a Tyndall beam in a bright beam of light (1600 ft.-c.). Aerosols for which $r \approx 0.05\ \mu$ and $n \approx 5 \times 10^6/\text{cm.}^3$ are just barely visible.

Sulfuric acid is placed in a flask called a boiler which is heated to temperatures ranging from 50 to 135°C. A stream of filtered air, dried over P_2O_5, which is blown over the surface of the acid (bubbling through the liquid produces spray), acquires H_2SO_4 vapor and passes into a second flask called a reheater which must be maintained at least a few degrees higher than the boiler. From the reheater, the vapor and air enter a double-walled chimney where the gases cool slowly and uniformly to room temperature, yielding both aerosol particles and a condensate of H_2SO_4 upon the chimney walls.

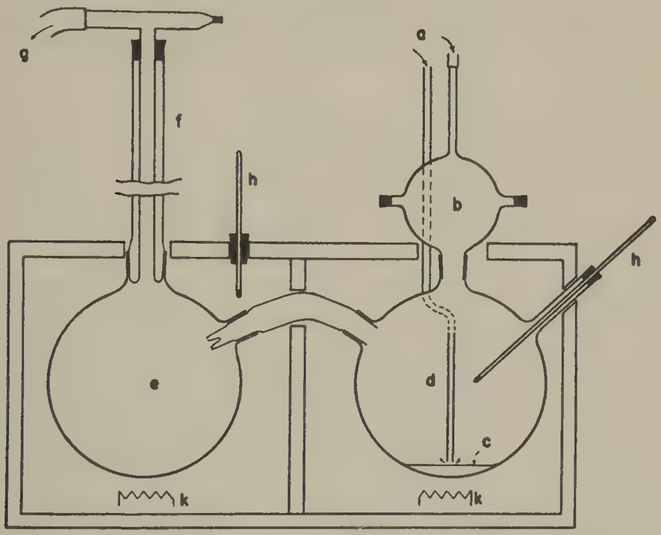

Fig. 1. Aerosol generator. *a* dry air; *b* (nuclei source placed here if necessary, *e.g.*, spark gap); *c* H_2SO_4, dibutyl phthalate, *etc.*; *d* boiler; *e* reheater; *f* double-walled chimney; *g* aerosol outlet; *h* thermometer; *k* heaters.

When liquids other than H_2SO_4 are used, nuclei from the spark gap shown in Fig. 1 or fine dusts have been introduced into the vapor to serve as condensation nuclei. If no nuclei are introduced, condensation occurs almost exclusively upon the chimney walls and very little aerosol s produced. *However, H_2SO_4 is unusual in that it requires no foreign nuclei; the vapor self-nucleates and forms a homogeneous aerosol.* Even when foreign nuclei are introduced, self-nucleation may still occur yielding so controlled nucleation only when the number introduced exceeds that which would form spontaneously.

Ninety-nine per cent H_2SO_4 was used since if there is more than 2 or 3% water in the acid, water will appear in the aerosol. If the water content is too low, the aerosol particle will contain an indefinite quantity of SO_3. The 99% acid was prepared by adding fuming H_2SO_4 (130%) to the concentrated acid (95%), and was assayed by titration.

In Fig. 2, the particle radius generated is plotted against the boiler temperature. Although the radius depends primarily upon boiler temperature, the points are scattered indicating that some other minor variables are involved. Boiler temperature is a very useful, but only an approximate determinant of particle size. The air flow was maintained at 2.1 l./min. and the reheater at 140°C.

The particle radius is controlled by the ratio of the mass of superheated vapor to the number of nuclei that form. The vapor pressure of the liquid would naturally be expected to be an important factor in determining the radius. This is borne out by the linear dependence of log nr^3 (proportional to mass) upon the reciprocal of the absolute temperature of the boiler (Fig. 3). However, the slope is much greater than for the corresponding vapor pressure curve for H_2SO_4. The latent heat of vaporization of H_2SO_4 at 326°C. is 1.2×10^4 cal./mole, but the slope in Fig. 3 corresponds to 3.2×10^4 cal./mole, which indicates that there are other important temperature-dependent variables controlling the mass of aerosol.

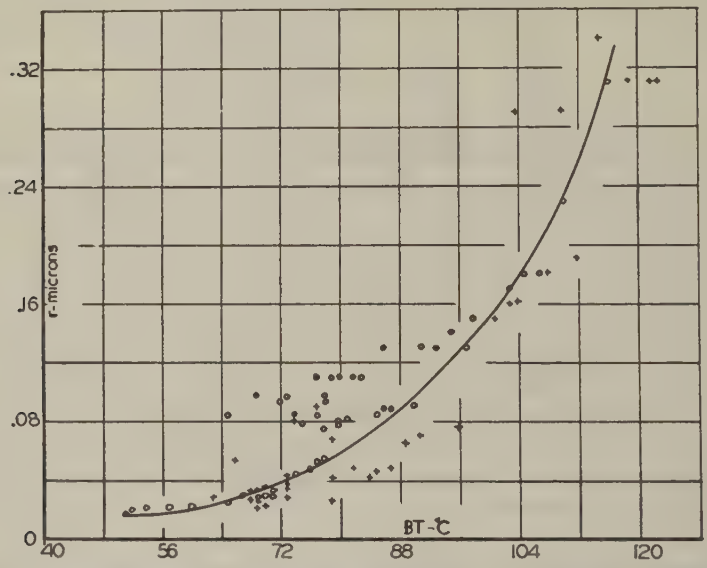

FIG. 2. Particle radius, r, vs. boiler temperature, °C. Reheater temperature = 140°C. Flow rate = 2.1 l/min. ○—Polarization measurements. +—Transmission measurements.

The air which blows over the surface of the liquid in the boiler does not become saturated with vapor. The vapor concentration is probably limited by the diffusion of H_2SO_4 molecules from the liquid surface through a thin film of stationary air. The thickness of this film and the diffusion coefficient will be temperature dependent.

A further complication occurs during the formation of aerosol. The condensation of vapor yields both aerosol and a condensate on the chimney walls. At low boiler temperatures, the vapor concentration will be low, and the mixture of air and vapor will have to move further up the chimney to reach lower temperatures before the critical supersaturation is reached. Consequently, condensation on the walls will be correspondingly greater. This may contribute quite significantly to the large slope in Fig. 3.

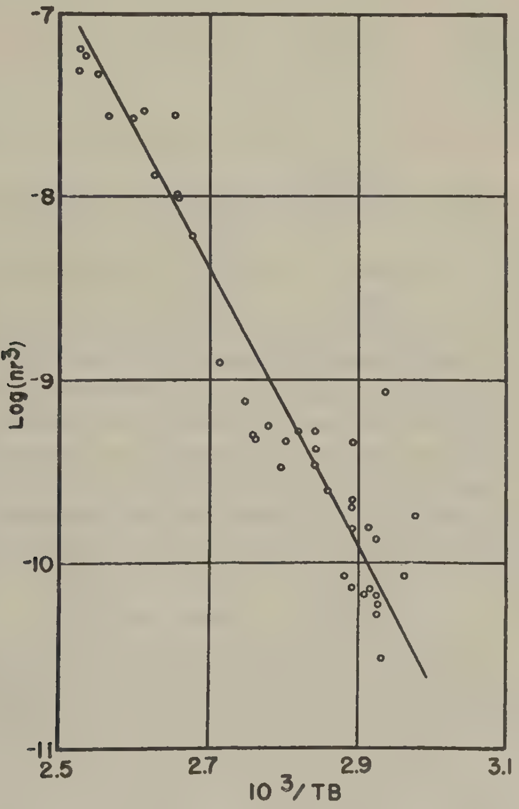

FIG. 3. Log (nr^3) vs. $\frac{1}{TB}$. $nr^3 \sim$ mass. TB = Boiler temperature in °K.

Theoretically, the rate of nucleation is extremely sensitive to the degree of supersaturation, varying on the order of 20-fold for a change of 2–3% in the supersaturation (7). This indicates that the number of particles formed by self-nucleation will be difficult if not impossible to

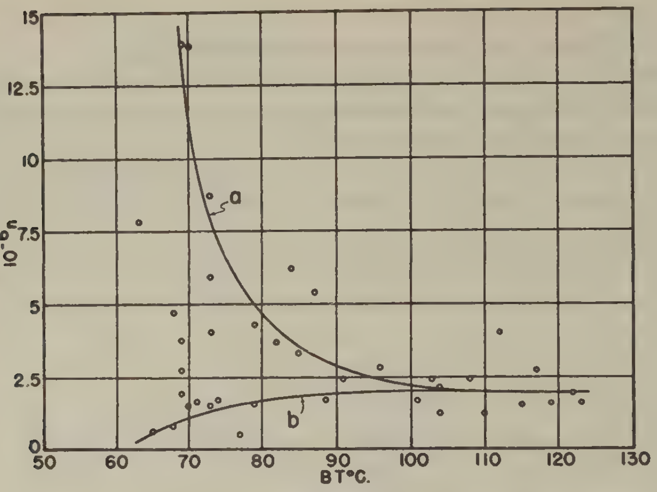

FIG. 4. n vs. BT. n = number of particles/cm.³. BT = Boiler temperature in °C.

reproduce (Fig. 4). Experimentally, it was found that above 90°C., n lies between 1–3 × 10^6/cm.³ (except for one point), but at lower temperatures there is a greater scatter of points which may arise in part from an additional source. The curve appears to break into two branches. At lower temperatures, the conditions for self-nucleation become poor. There may be some foreign nuclei in the filtered air which compete with self-nucleation giving rise to the upper branch and less control of particle number. This question of extraneous nuclei is common to all phase transition studies.

LIMITATIONS UPON n AND r

Aerosols of high number concentration undergo rapid coagulation (8). Making the customary assumption that every collision results in coalescence, the number concentration varies with time in accordance with the equation

$$\frac{1}{n} = \frac{1}{n_0} + k(t - t_0), \qquad [1]$$

where $k = \frac{4}{3}\frac{RT}{N\eta}\left(1 + A\frac{L}{r}\right)$,
T = absolute temperature,
η = viscosity of air,
N = Avogadro's number,
R = gas constant,
L = mean free path of air molecules,
r = radius of particle,
n = number concentration,
t = time,
A = constant ~ 0.9 for C.G.S. units.

Table I shows the time required for the number of particles to decrease by 50%; *i.e.*, the half-life.

TABLE I

Half-Life of Coagulation

n is initial number of particles/cc. The time in seconds tabulated for the radius r is the time necessary to reduce n to one-half of its value.

r	k (Eq. 1)	n			
		10^5	10^6	10^7	10^8
μ	$\times 10^{+10}$	*(sec.)*	*(sec.)*	*(sec.)*	*(sec.)*
1.0	3.3	3×10^4	3×10^3	3×10^2	3×10^1
0.1	5.7	1.8×10^4	1.8×10^3	1.8×10^2	1.8×10^1
0.05	9.9	1×10^4	1×10^3	1×10^2	1×10^1
0.01	30.	3×10^3	3×10^2	3×10^1	3

It is evident that $n = 10^6$–10^7 is the maximum number concentration for stable aerosols. On the basis ($n = 10^7$), a table of maximum mass concentrations for different radii has been constructed (Table II).

If a large fraction of the material is present as vapor, the aerosol will be unstable to temperature changes. For example, if the vapor pressure is 10^{-4} mm. Hg at room temperature, the mass of vapor is roughly 10^{-6} g./l., which is 20 times the maximum mass for a 0.01 μ aerosol. Thus an increase of 5% in vapor pressure which could be produced by a small temperature change ($\sim 2°$), would vaporize all particulate matter. With larger aerosols or less volatile material, this effect is not important.

Even at a fixed temperature, there is a lower limit on particle radius since aerosols of very small size are not stable. Exceedingly small droplets have a higher vapor pressure than the liquid in bulk. Consequently, there will be a continual transfer of liquid from the droplet to the walls of the container.

TABLE II

Maximum Mass Concentration as Function of Radius of Particle for $n = 10^7/cm.^3$

Density = 1

(For comparison 1 l. of air = 1.2 g.)

r_μ	Concentration *g./l.*
0.01	4×10^{-8}
0.02	3.2×10^{-7}
0.03	1.1×10^{-6}
0.04	2.6×10^{-6}
0.05	5.0×10^{-6}
0.06	8.6×10^{-6}
0.07	1.4×10^{-5}
0.08	2.0×10^{-5}
0.09	3.2×10^{-5}
0.10	4.0×10^{-5}
0.20	3.2×10^{-4}

The vapor pressure of a droplet of curvature $\frac{1}{r}$ is given by

$$\ln \frac{p}{p_0} = \frac{2\gamma}{r\rho} \cdot \frac{M}{RT}, \qquad [2]$$

where γ = surface tension,
ρ = density of droplet,
M = molecular weight of vapor,
p_0 = vapor pressure of flat surface, and
p = vapor pressure of droplet.

The rate of change of mass of an *isolated* droplet is given roughly by the following equation (9) (the problem has not been solved exactly):

$$-\frac{dm}{dt} = \frac{4\pi MD}{\rho RT}(p - p_0)r, \qquad [3]$$

where D = the diffusion coefficient of the vapor, and
p_0 = pressure of vapor at a large distance from drop and is here taken as the normal vapor pressure.

If $\frac{p}{p_0}$ is close to 1, Eq. [2] becomes

$$p - p_0 = \frac{2\gamma}{r\rho} \cdot \frac{M}{RT} p_0 \qquad [4]$$

and Eq. [3] becomes

$$-\frac{dm}{dt} = 8\pi\gamma D \left(\frac{M}{\rho RT}\right)^2 p_0. \qquad [5]$$

If the vapor pressure is about 10^{-6} mm. Hg, the rate of loss of mass of an isolated droplet is calculated to be of the order of 10^{-19} g./sec., and independent of r, or about 2% of the mass of a 0.01-μ particle/sec. However, the rate of evaporation of a droplet in a cloud is certainly very much less than an isolated droplet, so that $p_0 = 10^{-5}$ will probably yield rates sufficiently slow for stability. This effect clearly places a limit on smallness, which probably is of the order of 0.005 μ, depending of course on the volatility of the material.

The process of vapor condensation also places a limit on smallness. The particles cannot be smaller than the critical nucleation radius (7) which is about 10^{-3} μ(10 A).

ANALYSIS OF AEROSOLS

Detection

Aerosols may be detected with the aid of a bright beam of light. When the particle radius is less than 0.03 μ and the number concentration $< 10^7$/cm.^{3}, the aerosol may not exhibit a detectable Tyndall beam. Such aerosols may be rendered visible by subjecting the particles to growth with the vapors of a volatile solvent.

In particular, H_2SO_4 mists may easily be grown tenfold in radius by exposure to water vapor. For very small particles (Rayleigh's law valid), tenfold growth increases the light scattering by a factor of 10^6.

Homogeneity

The larger H_2SO_4 aerosols ($r > 0.2\ \mu$) produced with the generator exhibit higher-order Tyndall spectra (Fig. 5), and are therefore quite homogeneous (4,5), leading one to suspect that smaller size aerosols will also be monodisperse. Actually, the smaller aerosols are only fairly homogeneous as indicated by the fact that the water-grown aerosols show only broad and diffuse orders.

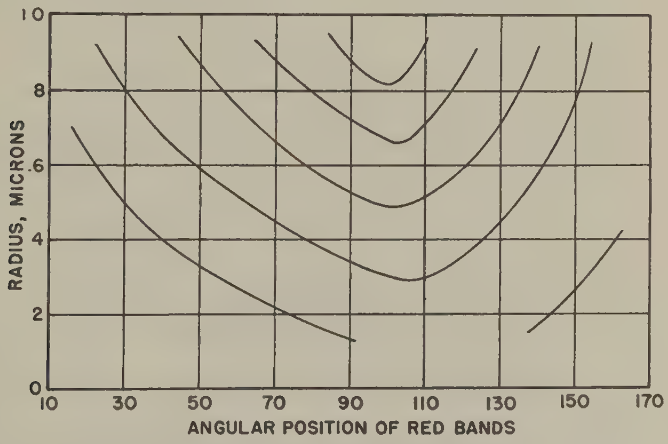

FIG. 5. Higher-order Tyndall spectra.

Consider an aerosol whose particles lie in the range 0.04–0.06 μ. Such an aerosol would be assigned an average radius, 0.05 μ, and would be described as moderately homogeneous. After growth by a factor of 5 to equilibrium with a volatile solvent, the range would be 0.2–0.3 μ. Such an aerosol would not exhibit distinguishable orders (4,5). This type of growth preserves the initial inhomogeneity in size, whereas growth within the cooling column of the generator is controlled by the rate of diffusion of vapor to the particle and follows the approximate law $r^2 = r_0^2 + kt$. In this latter case, the initial inhomogeneities in radii are obliterated by growth.

Particle Size

The particle-size measurement of such exceedingly small aerosols is difficult because of the extremely low mass concentration. A low mass concentration is actually beneficial where counting methods can be employed, but is a serious handicap for all other methods. Light-scattering techniques which are the most sensitive of all particle-size methods can be applied down to about 0.07 μ but cannot be extended much further since the intensity of the scattered light varies as r^6. For example, light passing through 1 m. of a 0.1-μ aerosol will be attenuated 15%, whereas a 0.01-μ aerosol requires 10^6 m. for the same attenuation.

An easy way around these difficulties is to grow the aerosol particles to 0.08 μ or larger, and then apply the usual light-scattering methods. Transmission and polarization measurements may be used.

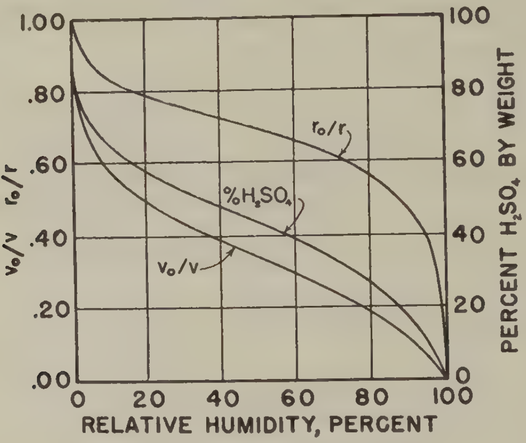

Fig. 6. Growth of H_2SO_4 smoke.

In Fig. 6,[4] curves are given showing the dependence of the radius and the volume of H_2SO_4 aerosol particles upon the relative humidity of H_2SO_4 master solutions. In this preliminary work, it was found that H_2SO_4 aerosols adjust themselves rapidly to the relative humidity of the gas phase. It is evident then that a particle will grow until its composition becomes equal to that of the master solution. Hence, calculation of the relative growth becomes exceedingly simple.

In the present research, the aerosol particles were frequently grown by a factor of 5, which is readily accomplished as follows: A master solution is prepared by diluting 1 vol. of concentrated H_2SO_4 to 125 vol. of aqueous solution. The aerosol is then brought into equilibrium by a countercurrent technique with the solution flowing down over a 12-in. column of large glass beads (5-mm. diameter) and the aerosol flowing up through the same bed. The water vapor condenses on the aerosol particles until their composition is the same as the master solution, *i.e.*, until their volume increases 125-fold and their radius 5-fold.

---

[4] Based upon unpublished experiments and calculations of S. Hochberg, I. B. Wilson, and V. K. La Mer (1942).

If the aerosol is removed from the master solution, the temperature must be maintained the same as that of the last equilibration. This is illustrated in Fig. 7, where it can be seen that a variation of 0.1°C. greatly alters the growth ratio, since with water solutions a variation of 0.1°C. changes the relative humidity by 0.4%. The greater the growth ratio, the more sensitive is the grown aerosol to temperature variations.

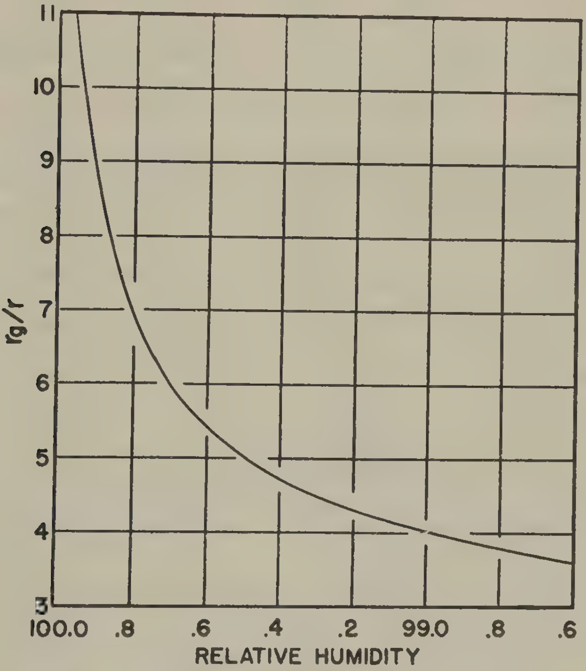

FIG. 7. Predicted growth r_g/r of sulfuric acid particles in a moist atmosphere as function of relative humidity (99.7 to 100.0%).

When all conduits and vessels are wetted with the master solution, normal precautions to prevent temperature change without thermostatic control are sufficient. All flow rates subsequent to formation of the aerosol should be low and jets eliminated to avoid adiabatic cooling and coagulation.

Although the aerosol will grow rapidly by simply passing it through a flask partially filled with the master solution, the countercurrent technique with beads has been adapted to insure perfect equilibration of vapor pressure. The amount of water vapor the original particles absorb is negligible compared with that necessary to saturate the dry gas phase.

Experiment showed that the beads exercised a negligible filtering action upon the aerosol; the mass of H_2SO_4 present in the aerosol before and after passage through the beads agreed within experimental error of 10%.

Transmission

The incident and transmitted light intensities, I_0 and I, respectively, are related by the equations (4,5):

$$I = I_0 e^{-K_s \pi r^2 nL};\ \log \frac{I_0}{I} = \frac{K_s \pi r^2 nL}{2.3}, \qquad [6a, b]$$

where L = length of path, and K_s is the scattering-area coefficient. K_s is a function of $\alpha = \frac{2\pi r}{\lambda}$ and of the index of refraction of the particle, where λ = wavelength in air. Complete tables and figures of K_s have been published (10). An abridged set of values is given in Table III. The quantity $K_s \pi r^2 n$ is called the turbidity by workers in the field of high-polymer solutions.

Measurements of I and I_0 are made as a function of wavelength and the results plotted in terms of log log $\frac{I_0}{I}$ *vs.* log $\frac{1}{\lambda}$. This curve is compared with the corresponding theoretical curve of log K_s *vs.* log α. The two

TABLE III*a*

Scattering Functions

$m = 1.33$

α	K	$\frac{K}{\alpha}$	$\frac{K}{\alpha^{3/2}}$	$\frac{K}{\alpha^2}$	$\frac{K}{\alpha^{5/2}}$	$\frac{K}{\alpha^3}$	$\frac{K}{\alpha^{7/2}}$	$\frac{K}{\alpha^4}$
0.5	0.00677	0.0135	0.0191	0.0270	0.0382	0.054	0.0765	*0.108*[a]
0.6	0.0138	0.0230	0.0297	0.0383	0.0495	0.064	0.0827	0.107
1.0	0.0938	0.0938	0.0938	0.0938	0.0938	0.0938	*0.0938*[a]	0.0938
1.2	0.171	0.142	0.130	0.118	0.108	*0.0984*[a]	0.0894	0.0819
1.5	0.322	0.215	0.176	0.143	0.117	0.0957	0.0782	0.0638
1.8	0.523	0.291	0.218	0.162	0.121	0.0901	0.0672	0.0501
2.0	0.710	0.355	0.252	0.178	*0.126*[a]	0.0890	0.0629	0.0445
2.4	1.123	0.469	0.302	*0.195*[a]	0.126	0.0814	0.0525	0.0339
2.5	1.212	0.485	0.308	0.194	0.123	0.0777	0.0492	0.0311
3.0	1.75	0.583	0.336	0.194	0.112	0.0623	0.0359	0.0208
3.6	2.38	0.661	0.350	0.184	0.0971	0.0511	0.0269	0.0142
4.0	2.825	0.706	*0.352*[a]	0.176	0.0880	0.0440	0.0220	0.0110
4.8	3.49	*0.727*[a]	0.331	0.151	0.0690	0.0315	0.0144	0.00656
5.0	3.59	0.718	0.322	0.144	0.0645	0.0288	0.0129	0.00576
6.0	*3.29*[a]	0.648	0.265	0.108	0.0442	0.0180	0.0074	0.0030
7.2	3.59	0.498		0.0691				

[a] Numbers in italics indicates near a maximum value.

TABLE III*b*

Scattering Functions

$m = 1.44$

α	K	$\frac{K}{\alpha}$	$\frac{K}{\alpha^{3/2}}$	$\frac{K}{\alpha^2}$	$\frac{K}{\alpha^{5/2}}$	$\frac{K}{\alpha^3}$
0.5	0.0115	0.0230	0.0325	0.0460	0.0650	0.0918
0.6	0.0238	0.0397	0.0512	0.0662	0.0853	0.110
1.0	0.167	0.167	0.167	0.167	0.167	0.167
1.2	0.306	0.255	0.232	0.212	0.193	*0.176*[a]
1.5	0.577	0.384	0.313	0.256	0.209	0.170
1.8	0.994	0.552	0.411	0.307	0.228	0.171
2.0	1.365	0.682	0.482	*0.341*[a]	*0.241*[a]	0.171
2.4	1.89	0.788	0.508	0.328	0.212	0.137
2.5	2.03	0.812	0.513	0.325	0.205	0.130
3.0	2.91	0.970	*0.559*[a]	0.323	0.187	0.108
3.6	3.63	*1.01*[a]	0.532	0.280	0.148	0.0778
4.0	3.85	0.962	0.481	0.240	0.120	0.0600
4.8	*4.04*[a]	0.843	0.384	0.175	0.0802	0.0366
5.0	3.98	0.796	0.356	0.159	0.0712	0.0318
6.0	3.61	0.602	0.246	0.100	0.0410	0.0167

[a] Near maximum values.

curves exhibit identical shapes (assuming constant index of refraction), but are displaced one from the other along the abscissa and ordinate. The identification of a corresponding characteristic point, *e.g.* a maximum, enables the calculation of both n and r. The maxima of the two curves correspond to the same α, the value of which is read from the theoretical curve, whereas $\frac{1}{\lambda}$ is read from the experimental curve. The radius is then given by

$$r = \frac{\lambda_{\text{exptl}}\,\alpha_{\text{theor}}}{2\pi}. \qquad [7]$$

Log $\frac{I_0}{I}$ is read from the experimental curve and K_s from the theoretical. These quantities obey the relationship

$$nr^2 = \frac{2.3}{\pi L}\frac{\left[\log \frac{I_0}{I}\right]_{\text{exptl}}}{[K_s]_{\text{theor}}} \qquad [8]$$

as can be seen from Eq. [6]. Since r is known, n may be calculated.

In practice, only a small range of wavelengths is available so that only a small portion of the experimental curve can be obtained for any one particle size. If this portion happens to lie in an α range corresponding to a maximum (or a minimum), corresponding points (same α) can be identified. With smaller particles, the α will be too small. However, this may be remedied by generating new functions, *i.e.* by multiplying Eq. [6] by λ.[5] Thus

$$nr^3 = \frac{\left[\lambda \log \frac{I_0}{I}\right]_{\text{exptl}}}{\left[\frac{K_s}{\alpha}\right]_{\text{theor}}} \times \frac{2.3}{2\pi^2 L}. \qquad [9]$$

This new function $\left[\frac{K_s}{\alpha}\right]$ has a maximum at $\alpha = 4.5$ for refractive index 1.33, while K_s has a maximum at $\alpha = 6$.

Further multiplication by λ yields

$$nr^4 = \frac{\left[\lambda^2 \log \frac{I_0}{I}\right]_{\text{exptl}}}{\left[\frac{K_s}{\alpha^2}\right]_{\text{theor}}} \times \frac{2.3}{4\pi^2 L}. \qquad [10]$$

$\frac{K_s}{\alpha^2}$ has a maximum at $\alpha = 2.5$. Repeated multiplication by λ broadens the maximum so that it becomes difficult to apply Eq. [7], *i.e.*, it becomes more dffiicult to identify the α and $\frac{1}{\lambda}$ corresponding to the maximum. However, this broadening enables one to identify more easily the ordinates at the same α for two functions and so both n and r can be evaluated. Thus, at $r = 0.14$ (water), plots of $\lambda^3 \log I_0/I$ and of $\lambda^{5/2} \log I_0/I$ yield maxima, and both nr^5 and $nr^{9/2}$ can thus be computed. Since this aerosol had been grown by a factor of 5, the original radius was 0.028 μ.

If the mass concentration, m, is known from other methods, r may be obtained with a measurement at only one wavelength from

$$\left[\frac{2 \times 2.3\rho}{3\pi L m} \lambda \log I_0/I\right]_{\text{exptl}} = \left[\frac{K_s}{\alpha}\right]_{\text{theor}} \qquad [11]$$

The value of α is read from the $\left[\frac{K_s}{\alpha}\right]$ curve and since λ is known, Eq. [7] can be applied. The various functions including some experimental results, are plotted in Figs. 8 and 9.

The double-grating monochromator of a Coleman spectrophotometer was used as the light source. A 1-m. glass absorption tube, which could be wetted with the master solution for measurements with grown aerosols, was used. A duplicate absorption tube could be moved into its place for the measurement of I_0. Shorter absorption tubes were used for larger aerosols. The light intensities were measured with a standard slide-back phototube circuit.

---

[5] This procedure was first used by Seymore Hochberg in this laboratory. See Refs. (5,10).

Polarization

The light scattered by these aerosols is partially polarized. The ratio of the intensity of the vertically polarized light, i_1, to that of the horizontally polarized light i_2, can be used as a measure of particle size in the range of $\alpha = 0.5$ to $\alpha = 3$. Tables of i_1 and i_2 as a function of refractive index, α, and scattering angle, θ, were prepared by Arnold Lowan's staff (10).

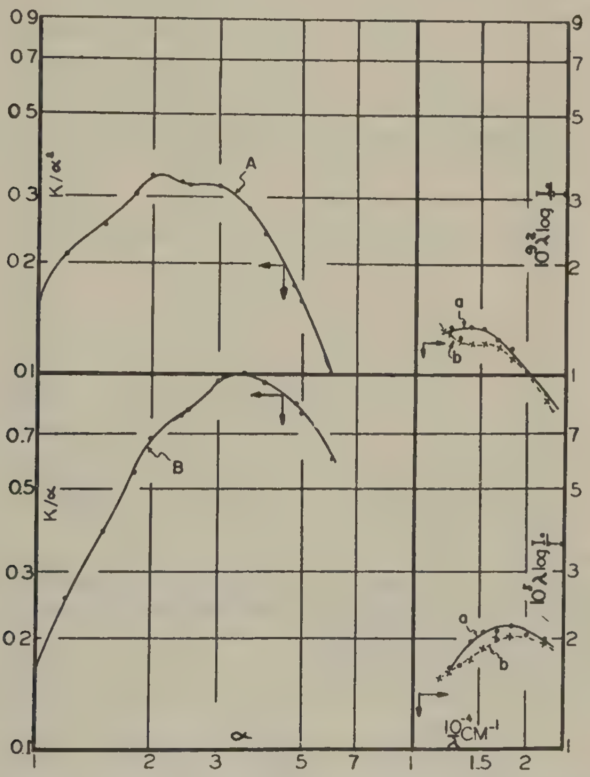

FIG. 8. $m = 1.44$. A, B: theoretical scattering curves. Experimental transmission curves: a Expt. 3, $r = 0.31\mu$; b Expt. 5, $r = 0.31\mu$.

Below $\alpha = 0.5$, Rayleigh's formula is valid and i_1/i_2 does not depend upon r but is given simply by

$$\frac{i_1}{i_2} = \frac{1}{\cos^2 \theta}. \qquad [12]$$

Figures 10, 11, and 12 show i_1/i_2 as a function of α for different angles of scattering and for different refractive indices. Other values can be obtained when needed from the Lowan computations.

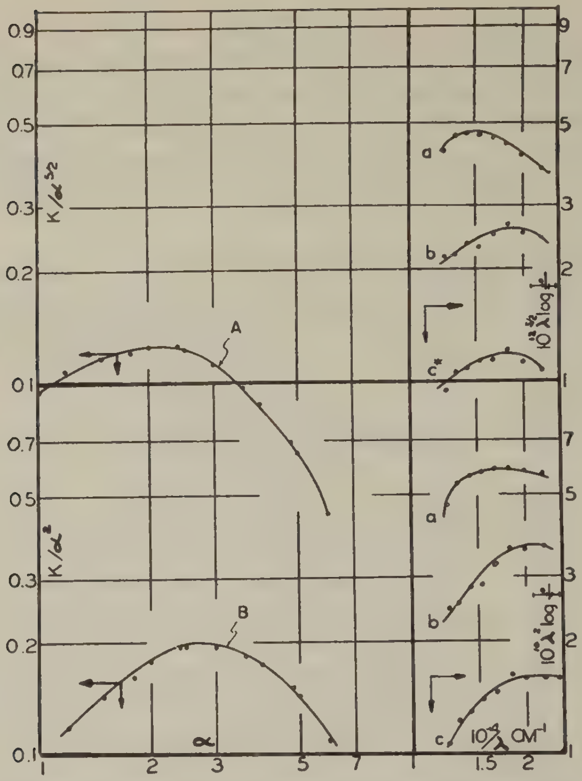

FIG. 9. $m = 1.33$. A, B: theoretical scattering curves. The circles represent accurately calculated points for a perfect monodisperse sol. A smooth curve has been drawn through the circles since, in practice, slight deviations from monodispersity smooth out the minor "wiggles" in the theoretical data.

Experimental transmission curves for grown particles ($r_g/r = 5$). *a* Expt. 28, $r_g = 0.24\mu$; *b* Expt. 41, $r_g = 0.17\mu$; *c* Expt. 49, $r_g = 0.18\mu$; *c** Expt. 49, multiply ordinate by ten.

The selection of the best scattering angle depends upon the particle radius; 110° (from backward direction) is a generally suitable direction. The following considerations enter into the selection of scattering angle.

1. Both i_1 and i_2 must be sufficiently large to be accurately measured.
2. i_1/i_2 must change rapidly with particle size.
3. i_1/i_2 must not be near an extremum because (a) the function is double valued near an extremum, and (b) unless monochromatic light is used, an aerosol will exhibit a range of α values even if monodisperse. The effect will be to lower i_1/i_2 in the neighborhood of a maximum and raise the ratio in the vicinity of a minimum.

4. i_1/i_2 should not change rapidly and unsymmetrically with the angle of scattering since the measured light is gathered from an angular range, say 110° ± 3°.

Measurements of i_1 and i_2 were made with the ONR photoelectric "Owl" (loaned to us by Dr. Ramskill), but with one arm blocked off and with the optical system altered so as to gather only the nearly parallel ($< \pm 3°$) scattered light, also with Nicol prisms replacing the polaroid disks. A Corning No. 5850 blue-light filter was used (Fig.13). The effective λ was determined as 0.410 μ by plotting the product of the intensity distribution function for a tungsten filament, the transmission function of the filter, and the response function of the 1P21 photomultiplier tube against λ. This arrangement does not use null-point readings but the microammeter deflections are proportional to the light intensities.

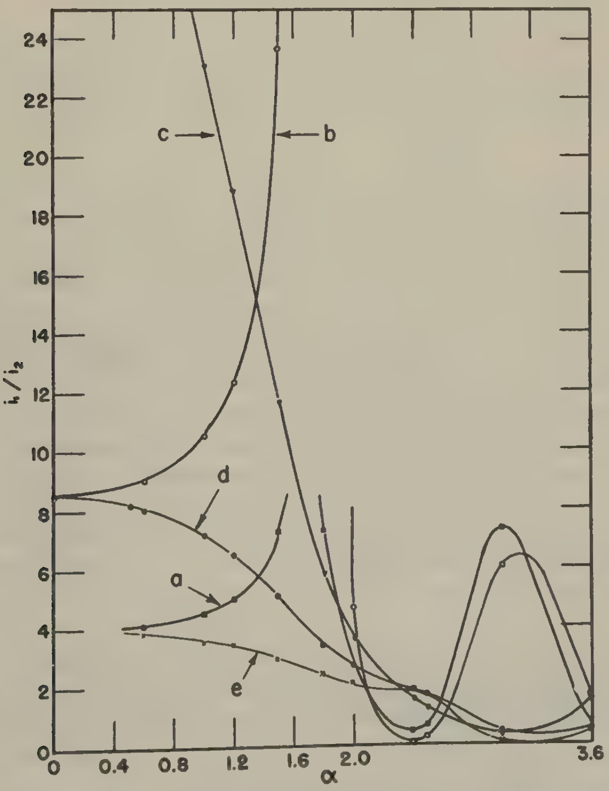

FIG. 10. Values of i_1 and i_2 obtained from the Mie theory. γ represents the supplement of the angle between the direction of the path of light and the direction of observation. $m = 1.33$. *a* $\gamma = 60°$; *b* $\gamma = 70°$; *c* $\gamma = 100°$; *d* $\gamma = 110°$; *e* $\gamma = 120°$.

When grown aerosols are being measured, a small watch glass containing the master solution is placed on the floor of the aerosol chamber to insure a humid atmosphere.

Mass Concentration

The mass concentration can be measured optically as indicated above, or more directly by filtering the aerosol and estimating the H_2SO_4. The most convenient method of analysis is to dissolve the acid from the filter in a known volume of water and measure the acidity with a pH meter.

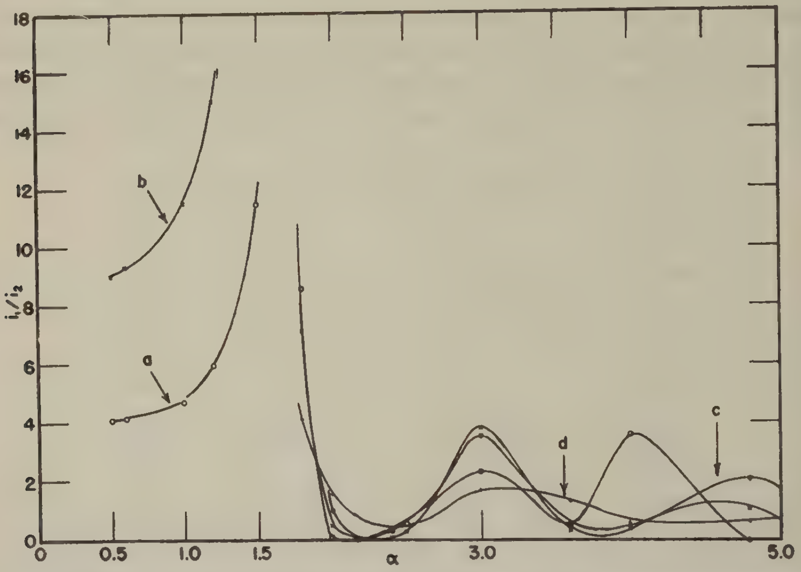

FIG. 11. Values of i_1 and i_2 obtained from the Mie theory. γ represents the supplement of the angle between the direction of the path of light and the direction of observation. $m = 1.44$; $a\ \gamma = 60°$; $b\ \gamma = 70°$; $c\ \gamma = 80°$; $d\ \gamma = 90°$.

Measurements of pH can be made to ± .02 units corresponding to ± 5% in concentration. A pH-concentration curve was prepared by diluting standardized H_2SO_4. The volume of aerosol was measured with a flowmeter.

The aerosol filtering medium must be selected with care since many natural and artificial filters commonly used introduce alkaline ingredients or react with the acid, thus spoiling the pH measurements. Glass wool, asbestos, and cotton are not satisfactory filters in this respect. A filtering medium should meet the following requirements:

(*a*) It should be in the form of fibers or needles.
(*b*) It should be insoluble in water.
(*c*) It should be neutral toward H_2SO_4.

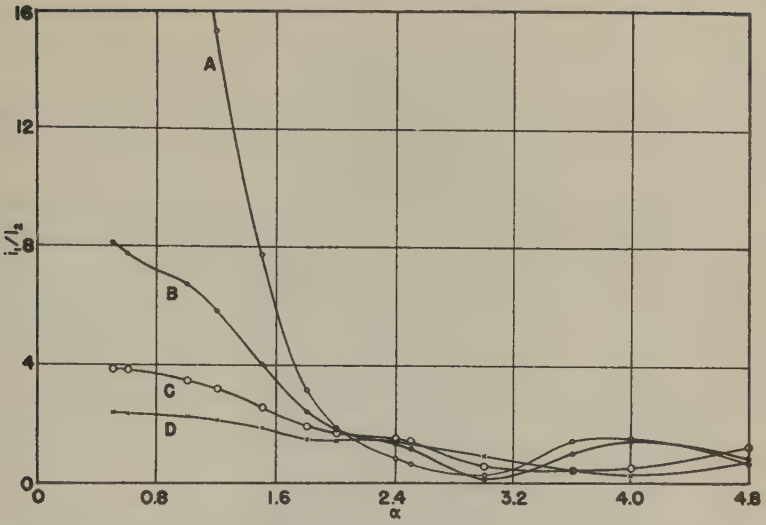

FIG. 12. Values of i_1 and i_2 obtained from the Mie theory. γ represents the supplement of the angle between the direction of the path of light and the direction of observation. $m = 1.44$; $A\ \gamma = 100°$; $B\ \gamma = 110°$; $C\ \gamma = 120°$; $D\ \gamma = 130°$.

Many organic solids will meet these requirements, but acenaphthenol was used since it was readily available in quantity. A tightly packed bed of 1–1.5 in. was used. The aerosol was drawn through by suction.

The acenaphthenol filters were tested for the recovery of varying amounts of acid by passing known quantities of H_2SO_4 into the filter and subsequently washing out the acid repeatedly with the same water. The pH of the extracted acid was measured and the total amount of acid calculated from the pH-meter calibration curve. It was generally found that satisfactory recovery (more than 90% which is within the experimental error of the pH meter at this pH) of acid was obtained when the pH of the recovered solution was 4.5 or less. The amount of aerosol, *i.e.*,

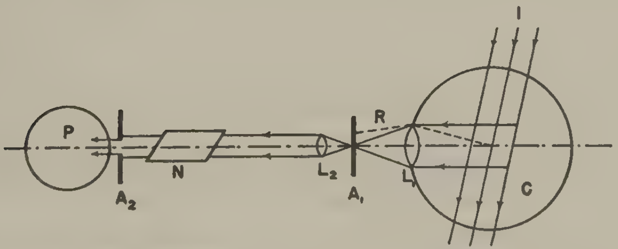

FIG. 13. Optical system for polarization measurements.
C = aerosol chamber; I = incident parallel light; L_1, L_2 = convex lenses; A_1, A_2 = apertures; N = Nicol prism; P = photomultiplier tube; R = nonparallel ray.

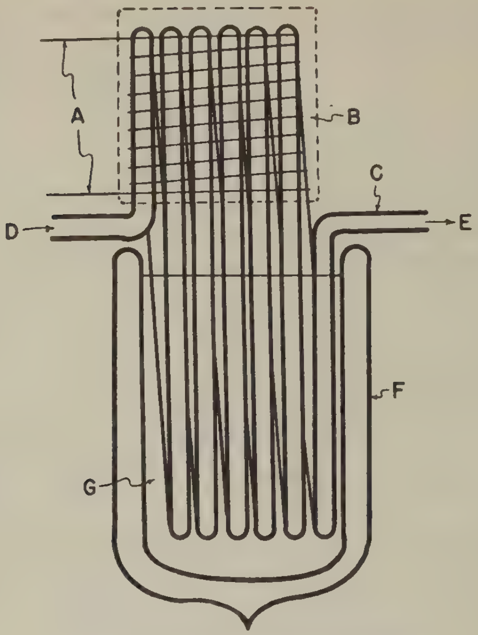

FIG. 14. Aerosol condensation collector.
A nichrome heating wire; *B* asbestos insulation; *C* 8-mm. tubing (quartz or glass); *D* aerosol inlet; *E* air exit; *F* Dewar flask; *G* Dry-Ice–acetone mixture.

acid, collected and also the amount of wash water used was therefore adjusted whenever possible to give an acidity greater than pH 4.5 for the acid-recovery solutions.

In cases where the amount of acid was very small, only 20 ml. of wash water were used but was passed through the filter several times. The aerosol is easily filtered if it is first grown further by bubbling through water; this water was retained and used as wash water.

A condensation-type collector was developed which requires no filtering medium (Fig. 14). A helical loop of pyrex glass or preferably quartz tubing (8 mm.) is formed with 4 or 5 rectangular loops. The upper bends are heated electrically and the lower bends are immersed in a Dry-Ice bath. The aerosol entering is vaporized on each upper bend and is cooled rapidly in each lower bend. Under these conditions, most of the vapor in each loop condenses on the walls. If each loop has an efficiency of 80%, after 5 loops only 0.03% will emerge. This collector requires no pump and introduces no appreciable pressure drop.

An attempt was made to measure n by following the rate of coagulation of the aerosol. From Eq. [1], it can be shown that

$$\frac{dr^3}{dt} = knr^3. \qquad [13]$$

Since sedimentation is negligible over short periods of time, the mass, which is proportional to nr^3 remains constant, and, therefore, r^3 should vary linearly with the time. A linear relation was actually obtained when r was computed from polarization measurements and plotted against time. The aerosols studied had been grown to an r value of about 0.1 μ. The value of n calculated in this manner was about 2×10^6. However, the values of n determined directly from pH measurements (3 cases) were about 5 times higher.

There are a number of possible reasons for this discrepancy. In the first place, the (Smoluchowski) k in Eq. [1] actually varies with different smokes depending upon the nature, shape, volatility, and concentration of the particle, heterogeneity of size, *etc.*, as pointed out by Whytlaw-Gray and Patterson (8). This important and intriguing approach merits further investigation. In particular, the question of whether or not two colliding particles always coalesce needs further independent study.

Vapor Pressure of H_2SO_4

The question arises as to whether an H_2SO_4 aerosol also contains significant amounts of acid as vapor at room temperature. This was tested by bubbling dry air through H_2SO_4 and passing the gases including a small amount of spray through a moist atmosphere. *No visible aerosol was produced!* This experiment was modified in that the spray was removed with a filter. Again no visible aerosol was produced. Since other hygroscopic vapors (HCl and chlorosulfonic acid) condense moisture to form a fume, it is concluded that the quantity of H_2SO_4 in the vapor state at room temperature is negligibly small.

These results are not in agreement with Abel's calculation which is based upon several difficult extrapolations that the vapor pressure of H_2SO_4 should be 10^{-4} mm. Hg at room temperature (11). This vapor pressure corresponds to 6×10^{-7} g./l., comparable to the particulate mass of a 0.03-μ aerosol. Our experience would indicate the vapor pressure of 99% H_2SO_4 to be of the order of 10^{-6} mm. Hg.

On the other hand, in the boiler of the homogeneous generator, 99% H_2SO_4 at 51°C. has sufficient vapor pressure to produce an aerosol having the characteristics $r = 0.02\ \mu$ and $n \approx 5 \times 10^6$. If the air were saturated, this corresponds to a vapor pressure of about 5×10^{-5} mm. Hg. If the air is $\frac{1}{5}$ saturated, the vapor pressure at 51°C. would be 2×10^{-4} mm. Hg.

These questions are being re-investigated at the present time (April 1950) under more carefully controlled conditions.

DISCUSSION OF PARTICLE-SIZE RESULTS

The transmission and polarization methods were compared with the higher-order Tyndall spectra method for particle radii of 0.18–0.31 μ. The agreement was better than 10%.

Values of nr^3 obtained from transmission can be compared with those determined more directly from pH measurement. The transmission values were higher by a factor of 1.63 ± 0.13. The reliability of nr^3 by transmission measurements is estimated to be ± 10%; those by pH are estimated to be of similar magnitude. These estimates account satisfactorily for the average deviation of ± 0.13 in the ratio (based upon 12 ratios), but still leaves a systematic error (factor 1.6). The reason for this difference is not known. A possible explanation may lie in the rather large molecular scattering of H_2SO_4. The problem of light scattering by spheres of such material has not been solved theoretically (or experimentally), but it is unlikely that the result would differ much from the predictions of the Mie theory, since the transmission of the bulk liquid is high.

Experimentally, this factor would be treated as a calibration to be used in measuring mass concentrations optically.

The value of nr^3 of a grown aerosol determined by transmission can be compared with the pH measurement to check the growth ratio r_0/r. For 28 cases (Table IV) in which the master solution was prepared for a growth factor of 5, the experimental average growth was 4.7 with an average deviation of ± 0.65 and a probable error of 0.08. We consider this agreement satisfactory evidence that the growth process can be controlled quantitatively.

Measurements of radii were made to slightly below 0.02 μ. Rough visual estimates can be made below this value since the experimenter learns to recognize the appearance of the Tyndall beam for sizes above 0.03 μ. For example, if a grown aerosol were just barely visible, the grown size would be estimated as 0.03 μ. If the growth factor were 5, the initial size would be estimated as 0.006 μ. In this connection it must be borne in mind that humidification may condense a vapor and produce an aerosol where none previously existed.

Dibutyl Phthalate Aerosols

When dibutyl phthalate was used, the nuclei were supplied in the form of fine dusts of NaCl, obtained by evaporation of NaCl from an electrically heated nichrome wire. Under these conditions, the temperature of the wire controls the number concentration and thus the particle radius.

The aerosol produced is more homogeneous than with H_2SO_4. This is shown by the presence of distinguishable orders in the higher-order Tyndall spectra when the aerosol is grown with xylene or toluene. The appearance of distinguishable orders in the grown aerosol renders the determination of particle size extremely simple. A sample is collected in a flask containing the master solution corresponding to a suitable

TABLE IV

Summary of Results

Transmission

BT = boiler temperature

r_u = radius of ungrown particles = $\left(\frac{nr^3(\text{pH})}{n}\right)^{1/3}$

r' = radius by higher-order Tyndall spectra

$nr^3(\text{pH}) \sim$ mass of aerosol/unit vol.

n = number of particles/cm.^{3}.

r_g = radius of grown particles

μ = microns

BT	r(trans)	r_g(trans)	r_u	r'	$\frac{r_g}{r_u}$	nr^3(trans)	nr^3(pH)	n
°C.	μ	μ	μ	μ		$\mu^3/cm.^3 \times 10^8$	$\mu^3/cm.^3 \times 10^8$	$\times 10^6$
63	(0.028)[a]	0.14	0.024		5.7		0.013	8.8
65	(0.054)	0.27	0.054		5.0		0.0088	0.58
68	(0.028)	0.14	0.022		6.5		0.0051	4.7
68	(0.033)	0.17	0.041		4.0		0.059	0.86
69	(0.031)	0.15	0.033		4.6		0.014	3.7
69	(0.022)	0.11	0.019		5.8		0.0091	14.0
69	(0.032)	0.16	0.038		4.3		0.010	1.8
69	(0.027)	0.14	0.027		5.0		0.0053	2.7
70	(0.023)	0.11	0.020		5.7		0.011	14.0
70	(0.036)	0.18	0.039		4.7		0.0089	1.5
71	(0.035)	0.18	0.042		4.3		0.011	1.6
73	(0.044)	0.22	0.035		6.2		0.024	5.9
73	(0.028)	0.14	0.030		4.9		0.024	8.6
73	(0.038)	0.19	0.050		3.7		0.018	1.5
73	(0.028)	0.14	0.026		5.4		0.016	8.8
73	(0.034)	0.17	0.037		4.6		0.020	4.0
74	(0.080)	0.40	0.092		4.4		0.013	1.7
77	(0.090)	0.36	0.086		4.2		0.034	0.53
79	(0.068)	0.34	0.054		6.3		0.026	1.6
79	(0.026)	0.13	0.027		4.7		0.051	26.0
79	(0.042)	0.21	0.045		4.7		0.041	4.3
82	(0.048)	0.24	0.055		4.4		0.0625	3.7
84	(0.042)	0.21	0.050		4.3		0.080	6.2
85	(0.046)	0.23	0.062		3.8		0.079	3.3
87	(0.048)	0.24	0.056		4.2		0.10	5.4
89	(0.066)	0.33	0.095		3.4		0.15	1.7
91	(0.070)	0.35	0.090		3.9		0.17	2.3
96	(0.076)	0.38	0.11		3.6		0.33	2.8
101	0.15					0.60	0.36	1.7
103	0.16					0.90	0.52	2.4
104	0.16					0.94	0.58	2.1
104	0.29			0.26		2.7	1.7	1.2
108	0.18					1.3	0.78	2.4
110	0.29			0.21		3.0	1.6	1.2
112	0.19			0.19		2.7	1.4	4.0
115	0.34			0.32		6.4	4.0	1.6
117	0.22			0.20		2.8	1.4	2.7
119	0.31			0.28		4.7	1.9	1.6
122	0.31			0.30		5.6	3.2	1.9
123	0.31			0.29		4.9	3.8	1.6

[a] Numbers in parenthesis calculated from $r = r_g/5$; *i.e.*, growth factor = 5.

growth ratio, the solution is swirled around for 10 sec., and the angular position of the orders is noted. The particle size of the grown aerosol is read from the graph (Fig. 5), and the initial aerosol size is obtained by dividing by the growth factor.

This procedure was checked with polarization measurements. The agreement (Table V) was excellent. Dibutyl phthalate has a refractive index of 1.5. Calculations of i_1 and i_2 are not available for this index but values of α obtained for the same i_1/i_2 for indices 1.55 and 1.44 differ by only 10% so that a good interpolation can be made.

Suggestions for Future Work

Dibutyl phthalate (or perhaps dioctyl phthalate) should be used as a standard aerosol in place of H_2SO_4 in the testing of filters since the particle

TABLE V

Summary of Results

Polarization

r_g = radius of grown particles
BT = boiler temperature
r' = radius by higher-order Tyndall spectra
μ = microns

BT	r	r_g	r'	BT	r	r_g	r'
°C.	μ	μ	μ	°C.	μ	μ	μ
51	(0.017)[a]	0.087		78	(0.073)[c]	0.15	
52	(0.020)[a]	0.099		80	(0.080)[c]	0.16	
54	(0.021)[a]	0.10		80	(0.078)[c]	0.16	
54	(0.022)[a]	0.11		81	(0.080)[c]	0.16	
57	(0.022)[a]	0.11		85	(0.085)[c]	0.17	
57	(0.022)[a]	0.11		86	(0.089)[c]	0.18	
60	(0.021)[a]	0.10		87	(0.088)[c]	0.18	
60	(0.023)[a]	0.11		90	(0.090)[c]	0.18	
60	(0.022)[a]	0.11		90	(0.091)[c]	0.18	
65	(0.025)[a]	0.12		90	(0.091)[c]	0.18	
67	(0.028)[a]	0.14		90	(0.090)[c]	0.18	
67	(0.030)[a]	0.15		91	0.13		
68	(0.029)[a]	0.14		91	0.13		
70	(0.030)[a]	0.15		93	0.13		
71	(0.030)[a]	0.15		95	0.14		
74	(0.043)[a]	0.13		97	0.13		
75	0.078			98	0.15		
76	(0.046)[b]	0.14		103	0.17		0.18
77	(0.084)			105	0.18		0.21
77	(0.053)[b]	0.16		107	0.18		0.21
78	0.095			110	0.23		0.25
78	(0.055)[b]	0.17		116	0.31		0.29
78	(0.055)[b]	0.16					

[a] Growth factor = 5.
[b] Growth factor = 3.
[c] Growth factor = 2.

TABLE VI

Dibutyl Phthalate Aerosol Particle Sizes

r = radius by polarization
r_g = radius of grown aerosal by higher-order Tyndall spectra
r' = calculated radius before growth
μ = microns
γ^0 = supplement of angle between direction of light and direction of observation

BT	γ^0	r	r_g	r'
°C.		μ	μ	μ
58	110	0.10		
59	100	0.10		
59.5	100	0.097		
59.5	110	0.10		
60	110	0.10		
60	110	0.10		
58	110	0.11	0.55	(0.11)[a]
59	110	0.11	0.30	(0.10)[b]
52			0.2	(0.04)[a]
54			0.3	(0.06)[a]
56			0.4	(0.08)[a]
56			0.25	(0.08)[b]

[a] Growth factor = 5, humidifying solution prepared by mixing 1 ml. of dibutyl phthalate with toluene to a final volume of 125 ml.

[b] Growth factor = 3, humidifying solution prepared by mixing 1 ml. of dibutyl phthalate with toluene to a final volume of 27 ml. Flow rate = 2.1 l./min. Reheater temperature = 80°C.

size of the exceedingly small ungrown particles can be determined very simply by the method just described. It is suggested that problem of determination of mass in this case be attempted by ultraviolet absorption.

Conclusions

1. The aerosol generator can produce mono-disperse aerosols in the very small particle size range from 0.15 μ downwards below 0.01 μ.
2. Aerosol particles may be grown by condensation of volatile solvents, increasing the radii tenfold or greater. Growth of the radius by a factor of 5 may be controlled quantitatively.
3. With the aid of quantitative growing techniques, the particle size can be measured to below 0.02 μ. Crude estimates can be made to about 0.006 μ.
4. The mass concentration may be measured optically.

References

1. Zsigmondy, R. *See* Thomas, A. W., Colloid Chemistry, Chap. 3. McGraw-Hill, New York, 1943.
2. Nonhebel, G., Calvin, J., Patterson, H. S., and Whytlaw-Gray, R., *Proc. Roy. Soc.* (*London*) **A116**, 540 (1927); Patterson, H. S., Whytlaw-Gray, R., and Cawood, W., *Proc. Roy. Soc.* (*London*) **A124**, 502 (1929).

3. Green, H. L., *Phil. Mag.* [7], **4**, 1046 (1927); *see* Ref. 8.
4. La Mer, V. K., and Barnes, M. D., *J. Colloid Sci.* **1**, 71, 79 (1946); Johnson, I., and La Mer, V. K., *J. Am. Chem. Soc.* **69**, 1184 (1947); Barnes, M. D., Kenyon, A. S., Zaiser, E. M., and La Mer, V. K., *J. Colloid Sci.* **3**, 571–98 (1948); Sinclair, D., *J. Optical Soc. Am.* **37**, 475 (1947); Kenyon, A. S., and La Mer, V. K., *J. Colloid Sci.* **4**, 163 (1949).
5. Sinclair, D., and La Mer, V. K., *Chem. Revs.* **44**, 245 (1949). (References to the earlier NDRC reports (1941–5) on aerosols are given here.)
6. Gucker, F. T., Jr., O'Konski, C. T., Pickard, H. B., Pitts, J. N., Jr., *J. Am. Chem. Soc.* **69**, 429, 2422 (1947).
7. Volmer, M., Kinetik der Phasenbildung, p. 137. T. Steinkopff, Dresden & Leipzig, 1939. Reprinted by Edward Bros., Ann Arbor.
8. Whytlaw-Gray, R., and Patterson, H. S., Smoke, Chaps. 5, 6. E. Arnold & Co., London, 1932.
9. Langmuir, I., *Phys. Rev.* **12**, 368 (1918).
10. La Mer, V. K., and Sinclair, D., OSRD report 1857 (1943), Report No. 944, Office of Publications Board, U. S. Dept. of Commerce. These and further computations by A. Lowan and staff have been published as National Bureau of Standards Applied Math. Series 4, Tables of Scattering Functions for Spherical Particles (119 pp.).
11. Abel, E., *J. Phys. Chem.* **50**, 260 (1946).

BOOK REVIEWS

Elastomers and Plastomers Vol. I. General Theory. Edited by R. Houwink. Elsevier Publishing Company, Inc. New York, 1950. 495 pp. Price $7.00.

This first volume of the series (which was last to appear in print) contains the following chapters: I. Economic Aspects by H. A. Frank. II. Organic Chemistry by C. Koningsberger. III. Reaction Kinetics and Mechanism of Polyreactions by H. Wechsler, W. P. Hohenstein, and H. Mark. IV. Molecular Constitution by G. J. van Amerangen. V. Mechanical Properties by G. J. van Amerangen. VI. Physics and Structure by G. J. van Amerangen. VII. Electrophysics by L. Hertshorn. VIII. Mechanical Operations by H. Gibello. IX. Polymer–Liquid Interaction by G. J. van Amerangen. X. Plasticizers by R. S. Colborne.

Unfortunately the very important first chapter is of limited value because of "the difficulty [which] arises that complete details are not available for most countries which produce and consume plastics." Accepting this serious shortcoming the chapter makes interesting reading. Fortunately the limitations to which Frank was subjected do not apply to the other authors and in the second chapter a very thorough discussion of the organic chemistry of macromolecules is given. The discussion of the structure of polymers, condensation and addition reactions, and the principal types of macromolecular compounds is thorough and up-to-date. Although very much information is given in a relatively short chapter it makes easy reading.

Mark's chapter on *Kinetics* is a most thorough treatment of the subject. Together with some paragraphs of the chapter by Koningsberger it gives all the information available on this subject.

Because of its completeness the concentration of the subject matter is, in spots, very great.

The brief chapter on *Molecular Constitution* can well be considered as an introduction to van Amerangen's subsequent chapter on *Mechanical Properties*. The thoroughness of treatment of this enormous field is as pleasantly surprising as it was in the preceding chemical chapters. Second-order transition effects, plasticity, elasticity and strength, theory of rubber elasticity, and, finally, viscous elastic phenomena are dealt with. In the chapter *Physics and Structure* the results obtained by various methods of structure investigation are given.

The chapter on *Electrophysics* is a critical survey of some of the results in this field.

The chapter on *Polymers–Liquid Interaction* covers two distinct subjects. On the one hand, solution of polymers in all the aspects of the problem are discussed, and then by using osmotic pressure as the connecting link, viscosity, lightscattering, and ultracentrifuging are presented. The treatment is again excellent, but even granting the logical sequence of the discussion, one has the feeling in reading this chapter that by an editorial mistake one was led to a point which one did not expect at the beginning. It would have been better to have split this chapter in two: one under the present title and another one on molecular weight determination. The last chapter, on *Plasticizers*, is somewhat less extensive than the earlier ones. This has been achieved, without loss of value, by giving relatively few experimental results.

Gibello's treatment on *Mechanical Operations* belongs in Vol. II of the series. It is a survey of the operation of manufacturing and processing macromolecular materials.

This first and most ambitious volume of Houwink's series is one of the major contributions to polymer literature. In the fields in which the reviewer specializes no omissions have been found. It is believed that the conclusion is justified that the other fields are equally completely treated. The contributors accomplished the literary feat of making complex and difficult subjects easily readable without resorting to the objectionable methods of so many authors of "introductory" texts.

A few words on the entire series "Elastomers and Plastomers" ought not be amiss. The series covers: I. *General Theory;* II. *Manufacture, Properties and Applications;* and III. *Testing and Analysis, Tabulation of Properties.* Despite some of the shortcomings inherent in this type of work it is a most valuable and an excellent contribution to the literature of this field. Dr. Houwink and his contributors deserve deep gratitude for the work they have accomplished.

George Goldfinger, Buffalo, N. Y.

Structure of Molecules and the Chemical Bond. By Y. K. Syrkin and M. E. Dyatkina. Translated and revised by M. A. Partridge and D. O. Jordan. Interscience Publishers, Inc., New York, N. Y., 1950. 509 pp. $8.75.

The text is a translation (1949) by Monica A. Partridge (University of Nottingham) and D. O. Jordan (Princeton University and Nottingham) of the Russian edition of 1946, and includes such revisions where appreciable advances have been made since the publication of the original which have necessitated a modification of the views put forward by the authors.

Thus many sections have been rewritten; e.g., Chapter 2, the synthesis of new elements; chapter 5, the section on cycloöctatetraene; chapter 7, molecular orbitals entirely rewritten on the basis of Coulson's new work; chapter 12, the hydrogen bond has been extended; chapter 15, boron hydride structures revised in the light of Pitzer's proposals.

The book is based on the Schrödinger wave equation, and treats in detail various types of bonds, resonance, spectra of molecules, intermolecular attraction, complex compounds, Slater's solution of three electron problems, etc.

There is a useful mathematical appendix (30 pp.) and extensive author, subject, and formula indexes (13 pp.).

Victor K. La Mer, New York, N. Y.

Physical Chemistry of High Polymeric Systems. High Polymers. Volume II. 2nd ed. By H. Mark and A. Tobolsky. Interscience Publishers, Inc., New York, 1950. 506 pp. $6.50.

Considerable progress has been made in the last decade since the appearance (1940) of the first edition of this well-known and authoritative monograph, and an expanded and amended edition is welcome. The purpose of the book is to present a condensed solution of the basic facts of the physical chemistry of macromolecules. Since limitation of space prohibits any lengthy treatment of the theoretical foundations of the fundamental methods of x-ray diffraction, infrared spectroscopy, light scattering, etc., the reader is referred to standard treatises, thereby reserving space for the applications and discussion of results.

The thermodynamic and kinetic behavior of polymer solutions and the mechanical properties of polymers, as well as the mechanism and kinetics of polymer formation and degradation are well presented in concise summaries of results and concepts. The authors are expert in presenting fundamental pictures and concepts in a clear and understanding manner.

The book is a "must" for workers in high polymers, but readers having an allied interest in this field will profit from reading about the important results that have accrued in a rapidly developing field which are fundamental to so many neighboring fields of science.

Victor K. La Mer, New York, N. Y.

DIFFUSION IN CHEMICAL REACTION PROCESSES AND IN THE GROWTH OF COLLOID PARTICLES

Frank C. Collins

Department of Chemistry, Polytechnic Institute of Brooklyn, Brooklyn, New York

Received August 28, 1950

INTRODUCTION

In an earlier paper (1) the validity of the Smoluchowski (2) diffusion equation when extended to bimolecular reaction processes was critically examined on the basis of random walk theory. It was there shown that a Fick's law treatment in bimolecular reactions in liquid solution is correct in the limiting case of small mean-square jump length of the diffusing molecules, providing Fick's law is solved with a new boundary condition. The new boundary condition was further shown to enable facile handling of problems wherein not all molecules arriving at the "reaction radius" react. The discussion in the above paper was largely confined to the role of diffusion in bimolecular chemical reaction rates. However, the theory is of general application in processes involving diffusion as, for example, in the growth and sedimentation of colloid particles.

In this paper, the previously developed flux equation is further examined, and simplified methods of calculation are presented. The theory is extended to general diffusion problems such as the rate of accumulation of material at phase boundaries. In particular, the effect upon the process of molecules diffusing up to the surface and having a probability of less than unity of being absorbed is studied. The results indicate a most interesting behavior of the rate of accumulation with time at the surfaces of both planar and spherical sinks.

The conclusions developed in the earlier paper may be summarized as follows: Fick's second law of diffusion

$$\frac{\partial c}{\partial t} = D\nabla^2 C \qquad [1]$$

is valid in the neighborhood of a sink in the limiting case of short mean-square diffusional jump length of the molecules and small gradient in c. Where the sink is a molecule or particle having the diffusion constant D_1, it is readily shown by a well-known argument (2) that the effective diffusion constant is

$$D = D_1 + D_2, \qquad [2]$$

where D_2 is the diffusion constant of the molecules diffusing up to the sink.

The proper boundary condition to be used in all diffusion problems where Fick's law applies is

$$c_s = \gamma(\nabla c)_s, \tag{3}$$

where the subscript indicates evaluation at the surface of the sink. This contrasts with the Smoluchowski boundary condition

$$c_s = 0 \tag{4}$$

generally used in the solution of diffusion problems. The transmission coefficient γ is related to the flux into the sink per unit area

$$\Phi = kc_s \tag{5}$$

and is readily found to be

$$\gamma = D/k. \tag{6}$$

Diffusion in One Dimension

Let us now investigate, in the one-dimensional case, the effect of the molecules impinging upon the sink having a probability α of being absorbed, where α may be less than unity. It was shown in the previous paper that where every particle entering the sink disappears from the system, the constant k is given by

$$k = \tfrac{1}{2}\nu\mu_1', \tag{7}$$

where ν is the mean jumping frequency and μ_1' is the mean magnitude of the x component of the displacements,

$$\mu_1' = 2\int_0^\infty x\varphi(x)dx, \tag{8}$$

$\varphi(x)dx$ being the probability of a jump having an x-component between x and $x + dx$.

In the case under investigation, Eq. [7] becomes

$$k = \tfrac{1}{2}\nu\mu_1'\alpha. \tag{9}$$

The diffusion constant is given by the well-known Einstein (3) equation

$$D = \tfrac{1}{2}\nu\mu_2, \tag{10}$$

where μ_2 is the mean-square jump length

$$\mu_2 = 2\int_0^\infty x^2\varphi(x)dx. \tag{11}$$

By combining Eqs. [5], [6], and [9] we obtain

$$\gamma = \frac{\mu_2}{\mu_1'\alpha} = \rho/\alpha, \tag{12}$$

where now ρ is simply the ratio of the mean-square and the mean jump length and hence is of the order of the mean jump length.

The solution of Eq. [1] with the boundary condition [3] and the initial condition

$$c(x,0) = c_0 \tag{13}$$

is well known (4) and is

$$\frac{c}{c_0} = \operatorname{erf}\left(\frac{x}{\sqrt{4Dt}}\right) + \exp\left(\frac{x}{\gamma} + \frac{Dt}{\gamma^2}\right) \operatorname{erfc}\left(\frac{x}{\sqrt{4Dt}} + \frac{\sqrt{Dt}}{\gamma}\right), \tag{14}$$

where

$$\operatorname{erf} y = \frac{2}{\sqrt{\pi}} \int_0^y e^{-z^2} dz$$

and

$$\operatorname{erfc} y = \frac{2}{\sqrt{\pi}} \int_y^\infty e^{-z^2} dz.$$

The flux into the sink per unit area is, by combining Eqs. [5], [6], [12], and [14]:

$$\Phi = \frac{c_0 D\alpha}{\rho} \exp\left(\frac{D\alpha^2 t}{\rho^2}\right) \operatorname{erfc}\left(\frac{\sqrt{D\alpha^2 t}}{\rho}\right). \tag{15}$$

Equation [15] and its integral are, however, unwieldy and approximate limiting forms are useful in practical calculations. For small values of $\alpha^2 t$, by expansion of the exponential and the error function in power series, we have

$$\Phi = \frac{c_0 D\alpha}{\rho}\left[1 - \left(\frac{D\alpha^2 t}{\rho^2}\right)^{\frac{1}{2}} + \frac{D\alpha^2 t}{\rho^2} - \ldots\right]. \tag{16}$$

The mean jump length in liquids is ordinarily considered to be of the order of 1×10^{-8} cm. Hence, where $D = 1 \times 10^{-5}$ cm.^{2} sec.$^{-1}$, Eq. [16] is valid for values of $\alpha^2 t$ less than 1×10^{-11} sec. Thus, even for small values of α, the flux is strongly time-dependent. The time during which [16] is convergent is negligible in most processes even should α have a value as small as 1×10^{-4}. This differs from the case of a small spherical sink where it has been shown elsewhere (5) the transient effect may be negligible.

For values of the time such that α^2/t is sufficiently larger than unity, the error function may be expanded in the well-known asymptotic series

$$\operatorname{erfc} y = \frac{1}{\sqrt{\pi}} e^{-y^2}\left(\frac{1}{y} - \frac{1}{2y^3} + \frac{3}{4y^5} - \ldots\right) \tag{17}$$

and Eq. [15] assumes the form

$$\Phi = \frac{c_0 D\alpha}{\rho} \frac{1}{\sqrt{\pi}}\left[\frac{\rho}{\sqrt{D\alpha^2 t}} - \frac{\rho^3}{2(D\alpha^2 t)^{\frac{3}{2}}} + \ldots\right] \tag{18}$$

which upon neglect of all but the first-order term becomes

$$\Phi = c_0\sqrt{\frac{D}{\pi t}}, \tag{19}$$

which is identical with the result obtained by solving Fick's law with the Smoluchowski boundary condition (3). Thus, we are led to the somewhat anomalous conclusion that, at sufficiently long times, the flux rate in the one-dimensional case is independent of the probability factor α. However, examination of Eq. [15] shows this to be a reasonable result. The effect of the probability factor being less than unity is twofold: (*a*) the flux of any instant is multiplied by α; and (*b*) the transient is retarded by multiplication of the time by α^2. At large values of the time, the two opposed effects cancel each other.

DIFFUSION IN THREE DIMENSIONS

For spherically uniform diffusion into a spherical sink of radius R, the solution of Eq. [1] with the boundary condition [3] and the initial condition

$$c(r, 0) = c_0 \tag{20}$$

is readily derived and is[1]

$$\frac{c}{c_0} = 1 + \frac{R-\beta}{r}\left\{\operatorname{erf}\left(\frac{r-R}{\sqrt{4Dt}}\right) + \exp\left(\frac{Dt}{\beta^2} + \frac{r-R}{\beta}\right)\operatorname{erfc}\left(\frac{\sqrt{Dt}}{\beta} + \frac{r-R}{\sqrt{4Dt}}\right)\right\}, \tag{21}$$

where β is related to γ as follows:

$$\beta = \frac{R\gamma}{R+\gamma}. \tag{22}$$

The transmission coefficient γ is related to the probability factor α by an expression formally similar to that in one dimension

$$\gamma = \frac{\rho}{\alpha} \tag{23}$$

except that here ρ has the significance

$$\rho = \langle s^2\rangle/\langle s\rangle, \tag{24}$$

where $\langle s\rangle$ and $\langle s^2\rangle$ are the first and second moments of the jump length

$$\langle s\rangle = \int_0^\infty s\varphi(s)ds, \tag{25}$$

$$\langle s^2\rangle = \int_0^\infty s^2\varphi(s)ds. \tag{26}$$

---

[1] The corresponding equation in Ref. (1) unfortunately had two typographical errors.

The total flux into the sink is

$$\Phi = k4\pi DR^2c(R),$$

$$\Phi = 4\pi Dc_0\left\{\left(\frac{\alpha R^2}{\alpha R + \rho}\right) + \frac{\alpha^2R^3}{\rho(\alpha R + \rho)}\exp\left[\frac{Dt(\alpha R + \rho)^2}{(R\rho)^2}\right]\operatorname{erfc}\left[\frac{\sqrt{Dt}(\alpha R + \rho)}{R\rho}\right]\right\}. \quad [27]$$

The limiting forms of Eq. [27] are of interest. When the values of α, t, and R are such that

$$\frac{\sqrt{Dt}(\alpha R + \rho)}{R\rho} < 1,$$

the exponential and error function may be explanded in power series and [27] takes the form

$$\Phi = 4\pi Dc_0\left\{\frac{\alpha R^2}{\alpha R + \rho} + \frac{\alpha^2R^3}{\rho(\alpha R + \rho)}\left[1 - \frac{\sqrt{Dt}(\alpha R + \rho)}{R\rho} + \frac{Dt(\alpha R + \rho)^2}{(R\rho)^2} - \cdots\right]\right\}. \quad [28]$$

For small values of α, unless R is very large, the second term in Eq. [28] may be neglected and the flux takes the limiting form

$$\Phi = 4\pi Dc_0\frac{\alpha R^2}{(\alpha R + \rho)}, \quad [29]$$

which is independent of the time. Where $\alpha R \ll \rho$, Eq. [28] may be further simplified as follows:

$$\Phi = 4\pi R^2c_0\alpha\tfrac{1}{4}v\langle s\rangle, \quad [30]$$

which represents the usual case in chemical reaction kinetics when steric effects other than diffusion are neglected.

However, for moderate values of α and large values of R, the transient term becomes increasingly important. In fact, if R is sufficiently large, Eq. [28], when expressed as flux per unit area, goes smoothly over into the one-dimensional flux equation [16].

For large values of the time, the expansion [17] may be used, and Eq. [27] simplifies as follows:

$$\Phi = 4\pi Dc_0\left\{\frac{\alpha R^2}{\alpha R + \rho} + \left(\frac{\alpha R^2}{\alpha R + \rho}\right)^2\frac{1}{\sqrt{\pi Dt}} + 0\left[\frac{1}{(\pi Dt)^{\frac{3}{2}}}\right]\right\}. \quad [31]$$

In the usual case of small R, the quantities α, R, and ρ are not separately determinable. Thus, without loss of observables, they may be lumped together, as follows

$$R' = \frac{\alpha R^2}{\alpha R + \rho}. \quad [32]$$

With neglect of higher-order terms, Eq. [31] then becomes formally identical with the Smoluchowski flux equation

$$\Phi = 4\pi DR'c_0\left[1 + \frac{R'}{\sqrt{\pi Dt}}\right]. \qquad [33]$$

Equation [33] will then represent the physical situation adequately unless the incoming flux causes R to vary relative to ρ. The latter case is of interest in connection with the growth of colloid particles.

The effect of the moving sink boundary upon the growth of colloid particles has been recently discussed by Reiss and La Mer (6) and by Frank (7) who, however, did not use the present boundary condition, Eq. [3]. The effect of an "accommodation coefficient" α, less than unity, upon the solution of the moving boundary problem will be the subject of a subsequent paper. For the present, let us examine the effect of α upon the effective flux Φ into spherical sinks of fixed radius of small and large R. In considering colloid particles, we follow Smoluchowski (2) in neglecting the transient term in the flux equation, and the effective flux becomes

$$\Phi = 4\pi Dc_0\frac{\alpha R^2}{\alpha R + \rho}. \qquad [34]$$

For values of R sufficiently small so that $\alpha R \ll \rho$, Eq. [34] becomes

$$\Phi = 4\pi Dc_0R\left(\frac{\alpha R}{\rho}\right) \qquad [35]$$

with the flux proportional to α as might be expected. However, for sufficiently large R, and $\alpha R \gg \rho$, [34] assumes the simple limiting form: $\Phi = 4\pi DRc_0$ with the flux independent of α. This behavior of the flux with respect to α and R indicates an acceleration of the flux into the growing colloid particle after R attains a certain critical value.

ACKNOWLEDGMENTS

The partial support of this research by the Office of Naval Research of the U. S. Navy is acknowledged gratefully. Thanks are also due to Mr. Stanley Grand and Mr. Harry Frisch who checked the calculations.

CONCLUSION

The effect of α (the probability of a molecule diffusing up to the sink being absorbed) upon the flux has been investigated in the case of both planar and spherical sinks. In the case of planar sinks at sufficiently long times, the effective flux becomes independent of α, that is, the flux behaves as if α were unity. This behavior has been confirmed experimentally in studies of the current transients of planar microelectrodes. This work is the subject of a paper to be presented elsewhere. For spherical sinks, the value of α appears to be immaterial if the radius of the sink is sufficiently large. The effect of this behavior upon the rate of growth of colloid particles will be discussed in a subsequent paper.

REFERENCES

1. COLLINS, F. C., AND KIMBALL, G. E., *J. Colloid Sci.* **4**, 425 (1949).
2. SMOLUCHOWSKI, M. v., *Z. physik. Chem.* **92**, 129 (1917).
3. EINSTEIN, A., *Ann. Physik* [4] **19**, 371 (1906).
4. CARSLAW AND JAEGER, Conduction of Heat in Solids, p. 53. Oxford Univ. Press, London, 1947.
5. COLLINS, F. C., AND KIMBALL, G. E., *Ind. Eng. Chem.* **41**, 2651 (1949).
6. REISS, H., AND LA MER, V. K., *J. Chem. Phys.* **18**, 1 (1950).
7. FRANK, F. C., *Proc. Roy. Soc.* (London) **A201**, 586 (1950).

THE APPLICATION OF THE MASS LAW TO THE AGGREGATION OF COLLOIDAL ELECTROLYTES[1]

Marjorie J. Vold

Department of Chemistry, University of Southern California, Los Angeles, California

Received March 28, 1950; revised October 3, 1950

INTRODUCTION

It is well known that the materials classed as colloidal electrolytes are fully dispersed in molecular subdivision in sufficiently dilute solution and are ionized in aqueous solution, but aggregate to clusters or micelles of colloidal dimensions as the concentration increases. There have been a number of attempts to describe this behavior in terms of the mass law for the formation from a 1–1 electrolyte GA of a single micellar species G_MA_N (2, 15). However, since the micelles are in equilibrium with single ions (or ion pairs in nonpolar solvents) it seems rational to assume that a distribution of micellar sizes exists. That is, reasoning kinetically, existence of a finite concentration of micelles of n simple ions implies that micelles of aggregation number $n - 1$, $n - 2$, $n - 3$, etc., have at least a short life and so are present at concentrations which are finite, however small, in order that the larger micelles may be formed mostly during binary collisions rather than by less probable multiple collisions. Meyer and Van der Wijk (14) have explored the properties of the equilibria between a monomer and its polymer in some detail for the case that all the association equilibria

$$A + A_n = A_{n+1}$$

have the same numerical value of the equilibrium constant, but this treatment cannot be used directly for colloidal electrolytes in aqueous solution if the counter ions (G) and long-chain ions (A) are contained in different proportions in the micelles.

Debye (4) has shown that an optimum size exists for a micelle consisting solely of long-chain ions with a surrounding atmosphere of counter ions. It seems possible, however, that other sorts of micellar structures such as the McBain lamellar micelle may exist to which that calculation is not applicable. A discussion of micellar structure is outside the scope of the present paper. However, provision is made for any size distribution including narrow dispersion around a most probable aggregation number in that the equilibrium constants are left as arbitrary functions of aggregation number for the most part.

---

[1] This work was undertaken as part of a project, "Phase Studies of Greases," sponsored by the Office of Naval Research, Contract NR057-057, N6onr-238-TO-2, under the supervision of Robert D. Vold.

The principal contribution of this paper is a demonstration of the extent to which experimental regularities which have been interpreted as resulting from the operation of the mass law on the assumption of a single species of micelle apply as well to a distribution of micelles G_mA_n in which n ranges from 2 to some very large number N, and m ranges from 0 to N but is never larger than n. To the extent that a particular result follows from a completely general distribution of this sort, it can no longer be accepted as implying the physically real existence of the particular micelle G_MA_N whose M and N values bring the experimental data into accord with the mass law predictions on the basis of a hypothesis of a monodisperse micellar system.

Among examples of such results are the following: Brady and Salley (1) find that plots of (gC) versus C (where g is the osmotic coefficient and C the stoichiometric concentration of colloidal electrolyte) are substantially linear above the critical concentration. McBain and Brady (12) find that the curves of g versus C for several colloidal electrolytes of a given class can be brought into coincidence by a simple manipulation of the concentration scale. Corrin (2) explains the dependence of the critical concentration for micelle formation upon added simple electrolyte as a common ion effect. Likewise the commonly accepted result (1, 6, 8) that the concentration of unaggregated long-chain ion reaches a maximum value in dilute solution has been derived on the basis of a single size of micelle but is here shown to follow also from a much more general treatment.

The most serious limitation upon the validity of the present work is the neglect of the activity coefficients, which have been taken as unity throughout.

FORMULATION OF THE MASS LAW PROBLEM

Nomenclature

Let C_{mn} be the concentration (moles per liter) of the species G_mA_n. Thus C_{10} is the counter-ion concentration derived from GA (*i.e.*, the potassium-ion concentration from potassium laurate, the chloride-ion concentration from cetyl pyridinium chloride, *etc.*). Similarly C_{01} is the concentration of unaggregated long-chain ion. Let C be the concentration of substance GA in solution and S the stoichiometric concentration of any added counter ion from simple salts. Define the equilibrium constant for the formation of a micelle G_mA_n from its ultimate constitutents as K_{mn}:

$$K_{mn} = \frac{C_{mn}}{(C_{10} + S)^m(C_{01})^n}, \text{ except } K_{10} = 1; K_{01} = 1. \qquad [1]$$

Conservation conditions are then:

for A, $$\sum_{m,n}{}^{*2} nC_{mn} = C, \qquad [2a]$$

for G, $$\sum_{m,n}{}^{*2} mC_{mn} = C. \qquad [2b]$$

Solution of the Mass Law Problem

Combination of Eqs. [1] and [2] leads to the fundamental relationship

$$\sum_{m,n}{}^{*} (n - m)K_{mn}(C_{10} + S)^m(C_{01})^n = 0. \qquad [3]$$

Numerical calculations can be made for a given selection of values of K_{mn} by assuming a value for C_{01}, calculating the corresponding value of C_{10} from [3], concentrations of other species from [1], and the pertinent total stoichiometric concentration from [2a] or [2b].

RESULTS

Maximum Concentration of Long-Chain Ion

Equation [3] is a polynomial equation of degree N in $(C_{10} + S)$ of which all the coefficients are guaranteed positive except that for which $m = 1$, which is given by: $-1 + \sum_{n=2}^{*} (n - 1)K_{1n}C_{01}{}^n$. If this term is positive there are no real positive roots of [3] and the selected value of C_{01} is physically unrealizable. If it is negative, there are either two or no real positive roots of [3]. This follows directly from Descartes' theorem (5). Starting at infinite dilution, the counter-ion concentration C_{10} increases with increasing total concentration, as does the concentration C_{01}. If subsequently there are to be two real positive values of C_{10} for a given C_{01}, it follows that between them C_{01} reaches a maximum value. While for special choices of K_{mn} it is conceivable that the two roots might be coincident for all choices of C_{01}, this is not generally likely.

The occurrence of a maximum value of the long-chain ion concentration is thus seen to be a general consequence of restriction of the micellar charge to zero or a single sign (less counter ions than long-chain ions), applying to any distribution of aggregation numbers. Equation [1] shows that the concentrations of all other fully ionic species (C_{0n}) simultaneously reach a maximum value.

For the general case the total concentration of colloidal electrolyte at which this maximum occurs cannot be calculated explicitly. For a single micellar species (aggregation numbers M, N) it occurs at a "degree of dissociation" (C_{01}/C) given by

---

[2] This symbol (*) is used throughout to signify a summation over all allowed values of m and n which are all values of N less than some finite upper limit and all $m \leqq n$, but including also $m = 1$, $n = 0$.

$$\frac{C_{01}}{C} = 1 - \frac{N}{M(N+1-M)}. \qquad [4]$$

This point lies, for intermediate ratios of M/N, somewhat beyond the observed critical concentration. If it is correct to assume with McBain that equivalent conductivity of fully ionic micelles is higher than for single ions, the occurrence of values of the measured conductivity above the Debye-Onsager values for 1–1 electrolytes in the neighborhood of the critical concentration for micelle formation (c.m.c.) would seem to be accounted for.

Calculation in this special case confirms that once its maximum value has been reached, the concentration of single long-chain ions declines only slowly, as was first shown by Hartley (8) and is now quite generally recognized and used (1, 6).

For a single micellar species, one can write an explicit expression for dC_{01}/dC as follows:

$$\frac{dC_{01}}{dC} = \alpha + C\frac{d\alpha}{dC}$$

where $\alpha = C_{01}/C$, the degree of dissociation, and

$$K_{MN} = \frac{\frac{1}{N}C(1-\alpha)}{C^M\left(1 - \frac{M}{N} + \frac{M}{N}\alpha\right)^M \alpha^N C^N}.$$

Differentiating yields

$$C\frac{d\alpha}{dC} = -\frac{M+N-1}{\frac{1}{1-\alpha} + \frac{N}{\alpha} + \frac{M^2/N}{1 - \frac{M}{N} + \frac{M}{N}\alpha}}$$

which yields [4] when dC_{01}/dC is set equal to zero (condition for an extremum).

Variation of Osmotic Coefficient with Concentration

The osmotic coefficient g may be defined as

$$g = \sum_{m,n}{}^{*} C_{mn}/2C. \qquad [5]$$

For the single micelle case this becomes

$$2gC = C_{10} + C_{01} + C_{MN}. \qquad [6]$$

Since $C_{10} + MC_{MN} = C_{01} + NC_{MN} = C$, it follows that at concentrations such that dC_{01}/dC is small (*i.e.*, beyond the maximum in C_{01}), $dC_{MN}/dC = 1/N$ and $dC_{10}/dC = -M/N$, whence

$$\frac{d(gC)}{dC} = \frac{1}{2}\left(1 - \frac{M}{N} + \frac{1}{N}\right) \qquad [7]$$

Plots of gC versus C for various colloidal electrolytes are assembled in Fig. 1 from which it is apparent that Eq. [7] is an excellent representation of the experimental data.

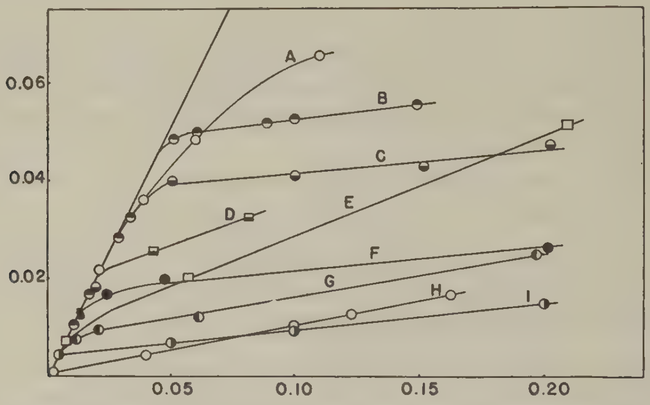

FIG. 1. Osmotic data for various colloidal electrolytes. The ordinate is proportional to the product of osmotic coefficient and concentration. The abscissa is proportional to the concentration. Different factors of proportionality have been used for different materials, to bring them onto the same diagram without distorting the slope of the curves. The scale factors are in parentheses. Curve *A*. Potassium oleate (× 50) (9). Curve *B*. Lauryl sulfonic acid (× 5) (9). Curve *C*. Potassium laurate (× 1) (10). Curve *D*. Sodium laurate (× 1) (7). Curve *E*. Sodium oleate (× 5) (7). Curve *F*. Cetylpyridium chloride (× 5) (7). Curve *G*. Potassium myristate (× 1) (7). Curve *H*. Potassium oleate (× 1) (9). Curve *I*. Cetyltrimethylammonium bromide (× 1) (7)

Whether this result implies that a single micellar species of the given M and N values predominates in the solution depends on whether any less specialized derivation of Eq. [7] can be given. Substituting [1] directly into [6] and using [2*a*] and [2*b*] yields

$$\frac{2d(gC)}{dC} = \frac{d \log C_{10}}{d \log C} + \frac{d \log C_{01}}{d \log C} \qquad [8]$$

$$\frac{2d(gC)}{dC} \cong \frac{d \log C_{10}}{d \log C}, \text{ for } \frac{dC_{01}}{dC} = 0. \qquad [8a]$$

Neither [8] nor [8*a*] yields the experimental result of constant dgC/dC without specialization. An alternative procedure is to differentiate [2*a*] and [2*b*] obtaining

$$\frac{dC_{01}}{dC} + \sum_{m,n}{}^{*} n \frac{dC_{mn}}{dC} = 1 \tag{9a}$$

$$\frac{dC_{10}}{dC} + \sum_{m,n}{}^{*} m \frac{dC_{mn}}{dC} = 1 \tag{9b}$$

whence it is apparent that if the micelles carry a fixed ratio of counter ions to long-chain ions ($m = nr$) and $dC_{01}/dC = 0$, the relation follows

$$\frac{2d(gC)}{dC} = 1 - r + \sum_{m,n}{}^{*} \frac{dC_{mn}}{dC}. \tag{10}$$

Since the last term is small, representing lowered particle concentration as the micelles increase in size, [10] is as satisfactory as [7] for describing the data of Fig. 1. The interpretation is that this relationship implies a fixed ratio of counter ion to long-chain ion in the micelles.

The McBain-Brady relation is entirely equivalent to [7] or [10]. These investigators plotted g as a function of log C^* where C^* was obtained by dividing the measured concentration by that at which $g = 0.5$ and found that curves for colloidal electrolytes of the same chemical type were coincident. Equation [10] may be written (if $\sum\sum dC_{mn}/dC \cong 0$) as

$$\frac{dg}{d \ln C} = \frac{1}{2}(1 - r) - g, \tag{10a}$$

whence if $r = m/n$ is constant for a given class of electrolytes, curves of g versus log C will be parallel and can be brought to coincidence by an appropriate change of scale.

McBain and Brady point out that their empirically discovered relationship would result from a mass law representation of the association process for a single micelle with the same M value and the same N value, independent of the numerical value of the equilibrium constant. Equation [10] shows that it is more general still, resulting from a distribution of micellar sizes for which the ratio m/n is constant.

Dependence of Critical Concentration for Micelle Formation on Salt Concentration

Corrin (2) has shown how the linear relationship between log c.m.c. and log ($C_{10} + S$) found by Corrin and Harkins (3) and satisfied also by the data of Merrill and Getty (13) can be derived from the mass law expression for a single micellar species, the slope of the line being identified with M/N. Their derivation is predicated upon the supposition that the same minimal concentration of sizeable aggregates of long-chain ions is required for the dye indicator method to exhibit a c.m.c. independent of salt concentration.

Equation [8a] shows that the Corrin relationship will obtain, provided a fixed value of $d(gC)/dC$ corresponds to a state of the solution capable of exhibiting a c.m.c. by the dye method. If this value is small enough to lie on the linear portion of the curves of Fig. 1, then the value of M/N calculated from the Corrin relation will be identical with that calculated from osmotic data. It is to be expected, however, that an experimental critical concentration will fall somewhere in the region in which $d(gC)/dC$ is changing from unity to its final value. Thus values of M/N calculated from the Corrin relation are expected to be lower than those calculated from osmotic data. Table I gives values of M/N for the substances whose osmotic behavior is plotted in Fig. 1. Of these, data on potassium laurate by the salt method is available for comparison. The salt method gives $M/N = 0.58$ which is smaller, as expected, than the 0.90 obtained from osmotic data.

TABLE I

Ratio of Counter Ions to Long-Chain Ions (M/N) for Various Colloidal Electrolytes from Osmotic Data

Substance	M/N	Substance	M/N
Sodium laurate	0.64	Potassium oleate	0.80
Potassium laurate	0.90	Lauryl sulfonic acid	0.87
Potassium myristate	0.82	Cetyltrimethylammonium bromide	0.89
Sodium oleate	0.59	Cetylpyridinium chloride	0.89

Influence of Salts on Micellar Size

The results from light-scattering experiments (4) indicate that the average size of the micelles in a colloidal electrolyte increases with increasing concentration of added salts. The same conclusion could be inferred from the circumstance that the separation of liquid crystalline phases from soap solutions occurs at progressively lower soap contents as the salt concentration is increased. It is clear that if counter ions are included in the micelle, the common ion effect will promote their increased incorporation as the salt concentration is increased. That the micelles also grow in physical size (aggregation number of long-chain ions) must mean that the equilibrium constant K_{mn} is much larger for large values of $n - m$ than for small values of $n - m$ for a given n.

Probable Values of K_{mn}

It seems likely that with $m + n$ values of hypothetical equilibrium constants to select arbitrarily, many alternative sorts of micellar distributions could be adjusted to derive a variation of osmotic coefficient with concentration which would be in accord with the experimental data. In order to allow for a dilute range in which association is almost negligible, all the K_{mn} must be numerically much smaller than $C_0^{-(m+n)}$, where C_0 is the observed critical concentration. On the other hand, in order to permit a rapid increase in degree of association over a narrow concentration range, K_{mn} for large n must be very much larger than those for small n. Thirdly, in order to account for the persistence of a considerable concentration of counter ions in solutions in which most of the long-chain ions are present in aggregated form, the K_{mn} for a given n must be negligibly small for small values of $n - m$.

ACKNOWLEDGMENT

The author wishes to acknowledge the helpful criticism of R. D. Vold throughout this work, and the assistance of Miss Dorothy Wallace in performing calculations.

SUMMARY

It has been shown that experimental data for colloidal electrolytes which are in accord with the predictions of the mass law for a single micellar species are capable also of an entirely similar description in terms of the mass law for a distribution of micellar species. The results also suggest that in this distribution large micelles are favored, and that as the concentration of colloidal electrolyte increases, the proportion of bound counter ion tends rapidly toward a constant value which is not very different for different colloidal electrolytes.

REFERENCES

1. Brady, A. P., and Salley, D. J., *J. Am. Chem. Soc.* **70**, 914 (1948).
2. Corrin, M. L., *J. Colloid Sci.* **3**, 333 (1948).
3. Corrin, M. L., and Harkins, M. D., *J. Am. Chem. Soc.* **69**, 638 (1947).
4. Debye, P., *J. Phys. & Colloid Chem.* **53**, 1 (1949).
5. Dickson, L. E., First Course in the Theory of Equations, John Wiley and Sons, Inc., New York, 1922.
6. Erikson, J. A., and Lingafelter, E. C., *J. Colloid Sci.* **4**, 591 (1949).
7. Fineman, M. N., and McBain, J. W., *J. Phys. & Colloid Chem.* **52**, 881 (1948).
8. Hartley, G. S., Aqueous Solutions of Paraffin Chain Salts, Hermann et Cie, Paris, 1936.
9. Johnson, S. A., and McBain, J. W., *Proc. Roy. Soc.* (London) **181A**, 119 (1942).
10. McBain, M. E. L., Dye, W. B., and Johnston, S. A., *J. Am. Chem. Soc.* **61**, 3210 (1939).
11. McBain, J. W., and Bolduan, O. E. A., *J. Phys. Chem.* **47**, 94 (1943).
12. McBain, J. W., and Brady, A. P., *J. Am. Chem. Soc.* **65**, 2072 (1943).
13. Merrill, R. C., and Getty, R., *J. Phys. & Colloid Chem.* **52**, 774 (1947).
14. Meyer, K. H., and Van der Wijk, A., *Helv. Chim. Acta* **20**, 1321 (1937).
15. Murray, R. C., and Hartley, G. S., *Trans. Faraday Soc.* **31**, 183 (1935).

THE SPREADING OF LIQUIDS ON LOW ENERGY SURFACES. I. POLYTETRAFLUOROETHYLENE [1]

H. W. Fox and W. A. Zisman

Naval Research Laboratory, Washington, D. C.

Received April 28, 1950; revised September 29, 1950

INTRODUCTION

When a drop of liquid on a solid surface does not spread but comes to some equilibrium state, it exhibits a finite contact angle θ toward the solid. Many authors have expressed this equilibrium by means of the Young equation (1)

$$\gamma_{SA} = \gamma_{SL} + \gamma_{LA} \cos \theta, \tag{1}$$

where γ_{SA}, γ_{SL}, and γ_{LA} are the free energies of the solid–air, solid–liquid, and liquid–air interfaces, respectively. Bangham and Razouk (2) and later Boyd and Livingston (3) have pointed out that Eq. [1] is incorrect since γ_{SA} can be altered by adsorption of vapor on the solid. If the free surface energy of a solid in a vacuum is γ_{SO}; in saturated vapor, γ_{SV°; and in vapor at pressure p, γ_{SV}; the correct statement of the Young equation for a solid in saturated vapor is

$$\gamma_{SV^\circ} = \gamma_{SL} + \gamma_{LV^\circ} \cos \theta_E. \tag{2}$$

In a vapor at partial pressure p, less than the saturation pressure, for systems where θ does not change with time,

$$\gamma_{SV} = \gamma_{SL} + \gamma_{LV} \cos \theta. \tag{3}$$

The correct form of the Young-Dupré relation for W_A, the work of adhesion of the solid and the liquid, can, therefore, be derived from [3] and the well-known Dupré relation

$$W_A = \gamma_{SO} - \gamma_{LV^\circ} - \gamma_{SL}. \tag{4}$$

Eliminating γ_{SL} from [3] and [4] and noting that

$$\gamma_{SO} - \gamma_{SV} = \pi, \tag{5}$$

where π is the spreading pressure of the adsorbed vapor on the solid, then

$$W_A = \pi + \gamma_{LV}\left(1 + \frac{\gamma_{LV}}{\gamma_{LV^\circ}} \cos \theta\right). \tag{6}$$

---

[1] The opinions or assertions contained in this paper are those of the authors and are not to be construed as official or reflecting the views of the Navy Department.

For liquids of low vapor pressure, γ_{LV} and γ_{LV° are essentially equal so that [6] to a good approximation becomes

$$W_A = \pi + \gamma_{LV}(1 + \cos \theta) \qquad [7]$$

and for systems in saturated vapor

$$W_A = \pi_E + \gamma_{LV^\circ}(1 + \cos \theta_E). \qquad [8]$$

Doss and Rao (4) derived from Eq. [2] and an application of Langmuir's principle of independent surface action, the following simple relation between the equilibrium contact angle θ_E and σ, the fraction of the solid furface covered with adsorbed molecules of the liquid:

$$\cos \theta_E = 2\sigma - 1. \qquad [9]$$

Livingston (5) after discussing the derivation of Eq. [9] examined available data to check the theory and concluded that no reliable data were available for which $\theta_E > 0$ or $\sigma < 1$.

In the past it has been difficult to measure W_A for solid–liquid interfaces because most pure liquids spread on most clean solids. The exceptions to this in the literature have been limited largely to water or aqueous solutions on hydrophobic surfaces and liquid metals on surfaces with which they do not alloy. By "spreading" will be meant the indefinite spreading of the bulk liquid, or a thin film but not a monolayer, *i.e.*, Hardy's "secondary spreading" (6) or Harkins' "duplex spreading" (7).

A more recent development of interest here has been the discovery of methods of modifying the wettability of solid surfaces by the adsorption from solution of oleophobic monolayers of oriented polar compounds. Many organic liquids as well as water will not spread on such surfaces (8, 9). The wettability of platinum coated with such films has been discussed and analyzed in a later publication (10) where it is shown that an oleophobic monolayer can reduce the free surface energy of a normally high-energy surface to a point at which there will be no net energy decrease resulting from the spreading of the given fluid. In this case a drop of liquid placed on the treated surface remains as a discrete droplet and exhibits a finite contact angle. The study of the wetting of such low energy surfaces is, however, limited to liquids which are not good solvents for the monolayers.

The remarkable inertness of polytetrafluoroethylene (TFE) has been described by Hanford and Joyce (11). Some preliminary observations by us (12) indicated that many varieties of organic liquids do not spread on TFE and that it is necessary to resort to liquids with surface tensions of less than about 20 dynes/cm. at 20°C. before spreading is found. The numerous new observations of this type given here have enabled us to plot the contact angle as a function of molecular weight and related properties, as well as to calculate the adhesion tension, work of adhesion, and the Doss and Rao surface condensation. In subsequent papers results will be presented from the study of the wetting behavior of partially fluorinated hydrocarbon solids and other low surface-energy solids.

Materials and Experimental Procedures

The liquids used in this study were derived from various sources as indicated in Tables I and II. The results obtained are in general insensitive to small amounts of impurities, provided the impurities are of the same molecular type and the same order of volatility as the nominal molecular species. But it was of major concern to avoid the presence in nonpolar liquids of small amounts of strongly adsorbable impurities such as highly polar molecules. Such molecules tend to form oriented arrays, thereby seriously modifying the underlying surfaces. To insure the absence of this type of impurity, every liquid was passed through a column of an appropriate adsorbent. The homologous series of *n*-alkanes was percolated through successive layers of activated alumina and silica gel. The resulting liquids (with the exception, of course, of the lowest members which normally have positive initial spreading coefficients) did not spread in a hydrophil tray on either acid or alkaline water. The di(*n*-alkyl)ethers were similarly treated. Each of the homologous series of polymethylsiloxanes was percolated through Florisil until the equilibrium spreading pressure was at a minimum (13). The alkyl benzenes were treated with alumina, and the miscellaneous group of liquids were treated variously with Florisil, alumina, and silica gel, always avoiding use of the latter when the liquid contained ring structures. In some cases several percolations were necessary, but in every instance but one the final percolate was crystal clear and colorless, although some of the starting materials were appreciably colored. Perchlorocyclopentadiene, never reported to be colorless, was pale yellow after percolation. It was of considerable importance too, that the high-boiling liquids contain no appreciable amounts of volatile impurities. Accordingly, such liquids were stripped of volatiles at 100°C. and about 5 mm. pressure using a countercurrent of CO_2 to carry off the vapor.

The surface tensions quoted in Tables I and II were taken from what seemed the most reliable sources. Where such data were not available, the surface tensions given were carefully measured in this laboratory using the ring method, except in the case of the fluorocarbons. The Harkins and Jordan correction tables for this method (14) are not extensive enough to cover the unique combination of low surface tension and high density characteristic of those materials if one uses rings of moderate size. The surface tensions of the fluorocarbons were therefore measured by the differential capillary rise method described by Sugden (15).

The TFE used in this study was obtained from the DuPont Company as a uniformly white 1-in. slab. Suitably small pieces (about 2.5 × 2.5 × 1 cm.) were cut from the slab and prepared as follows: A clean surface free from gross irregularities was obtained by removing a layer 1 or 2 mm. thick with a clean microtome. The resultant surface in general was dull and showed knife marks. A glossy surface showing no knife marks was obtained by taking advantage of the plastic properties of this polymer. The piece was placed between two thick blocks of clean plate glass free from scratches with the test surface against one of the blocks. This system was then squeezed in a press at about 300 pounds per square inch for 3 hr. during which period the press was heated to 150°C. and then allowed to cool to 50°C. or less. This treatment produced surfaces which showed, for a given liquid, relatively little variation in contact angle from specimen to specimen. Considerable difficulty in achieving reproducibility had been encountered in the early phases of this study because of differences in roughness of the TFE surfaces. The smoothed specimens were then cleaned by boiling them in nitric–sulfuric acid (1:2), and were rinsed free of acid by boiling successively in three changes of freshly distilled grease-free water. The few adhering droplets remaining after the last rinse were earily shaken off, and the dry specimens while still hot were placed in a covered dish to exclude dust but admit air, thus allowing the specimen to come to equilibrium with its surroundings. It is of interest to note that TFE which had been handled or allowed to stand uncovered for a few days exhibited contact angles of 90° or less against water, whereas freshly cleaned TFE gave a contact angle of 108–110° against water. This value is the same as that frequently found in the literature as the contact angle of water on paraffin.

All the measurements were made in a constant-temperature room held at 20.0 ± 0.1°C. and 50% relative humidity.

A number of contact angles were measured in an atmosphere saturated with the vapor of the liquid being measured. This was done by pouring a few milliliters of the liquid into a cylindrical glass cell having fused windows through which the specimen could be observed. The 50-ml. cell used was made for a Cenco "photelometer" and its dimensions were such that about one-half the specimen was immersed in the pool of liquid at the bottom of the cell, the surface to be observed remaining about 1 cm. above the liquid level. The cell was closed with a horizontal glass plate which had in it a 5-mm. hole for insertion of the platinum wire carrying the drops. The hole was covered while the specimen in the cell was allowed to equilibrate with the vapor for at least 1 hr. Prior to placing the specimen in the cell, all the components of the system were allowed to come to thermal equilibrium with the room, from 2 to 4 hr. generally being sufficient. The hole was then uncovered for the few seconds required to place two drops of fluid on the surface of the specimen. The drops were observed immediately and 1 hr. later. Only the few most volatile liquids showed a change in drop size or in contact angle during the hour.

A single experiment was performed with hexadecane in vacuum. The vacuum chamber had plane windows for observation, and manipulators which could transfer a drop of liquid from a reservoir to the specimen without breaking the vacuum. The experiment was done at a pressure of less than 10^{-4} mm. of mercury. The drop when placed was observed immediately and at 5-min. intervals thereafter.

The contact angles were conveniently measured with a refined version of the contact angle goniometer described earlier (8), which gave a magnified, high-contrast image of the drop profile. The main improvement in the newer instrument was that provision had been made for raising and lowering, and for tilting and translating the solid specimen positively. For the vacuum experiment, it was necessary to mount the system so that the goniometer telescope could be given the above degrees of freedom instead of the specimen.

The general procedure was to place a drop of the fluid on the specimen (in air or in the photelometer cell) by means of a flamed platinum wire, taking considerable care that the drop be placed so as to insure an advancing contact angle. The drops could be varied in size with no observable effect on the contact angle. Each reported value is an average of from four to twelve separate determinations made on different specimens on different days. With few exceptions the maximum deviation from the mean encountered for a given system was ± 2°. Most often, especially for the high-boiling liquids, the maximum deviation from the mean was ± 1°.

Considerable difficulty, however, was encountered in obtaining quantitative results with the few most volatile fluids, chiefly because of two effects. There was a region of volatility (exemplified by the behavior of heptane) in which the values tended to be low. The loss of material by evaporation from the drop made its periphery recede, thus producing some value of the contact angle less than the advancing angle. To overcome this effect, the specimen was positioned in the field of the goniometer as precisely as possible so that a minimum of manipulation was necessary to bring the drop into position for reading the angle. By this means a reading could be taken within 5 sec. after placement of the drop. This procedure minimized the effect, and the reported value is probably within a degree or two of the true value. The other effect was noted for the two most volatile materials (*n*-pentane and diisopropyl ether). Here the evaporation was so rapid that no reliable value was possible in the open air. The advancing edge of any spreading drop is in the form of a thin layer, a fact which can easily be observed with any nonvolatile liquid. The very volatile liquids evaporated so rapidly from the thin spreading edge that a finite boundary of the drop was observed, superficially resembling the case of a liquid which has a finite contact angle. The rapidly receding periphery could be observed in profile through the goniometer telescope. The contact angles observed under those conditions were invariably very small.

Experimental Results

Tables I and II summarize the values of the surface tension at 20°C. (γ_{LV}), the average values of the measured contact angle (θ), the calculated values of the adhesion tension ($\gamma_{LV} \cos \theta$), and the Doss and Rao condensation (σ) of all the liquids investigated. Homologous series of *n*-alkanes, di(*n*-alkyl)ethers, *n*-alkylbenzenes, and polymethylsiloxanes are given in Table I, while Table II includes a variety of liquids grouped as halogenated compounds, esters, and miscellaneous liquids.

Several features of these tables are noteworthy. In three of the homologous series of Table I the adhesion tension is apparently constant over a wide range of chain lengths in a single series. But the *n*-alkylbenzenes show a trend to increasing adhesion tension with decreasing surface tension, as do the liquids of Table II. The adhesion tensions of the hydrocarbon series and of the di(*n*-alkyl)ether series are close enough together so that the average deviation in either sense may cover the differences. For example, if the contact angles for the ethers and *n*-alkanes are plotted together against the number of carbon atoms, the points fall on the same

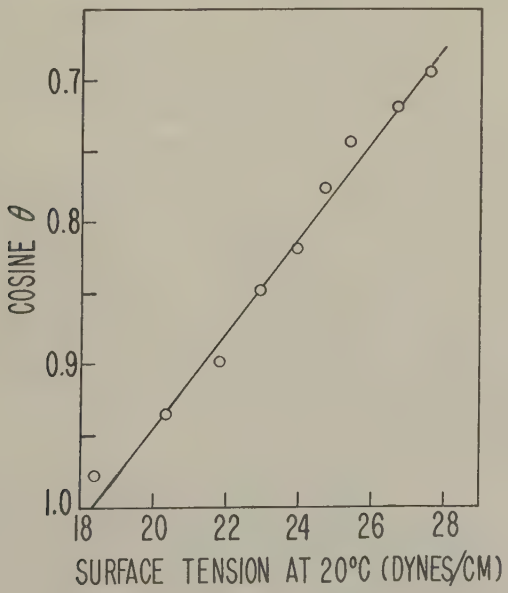

FIG. 1. Surface tension *vs.* cosine θ for the *n*-alkanes.

TABLE I

Surface Energy Relations of Four Homologous Series of Liquids and Polytetrafluoroethylene at 20°C.

Compound	Source of cpd.	γ_{LV}	Ref. γ_{LV}	θ	γ_{LV} cos θ	W_A	W_c	$W_A - W_c$	v
		dynes/cm.		*deg.*	*dynes/cm.*	*ergs/cm.*^{2}	*ergs/cm.*^{2}	*ergs/cm.*^{2}	
n-Alkanes									
Hexadecane	[a]	27.6	(19)	46	19.2	46.8	55.2	− 8.4	0.85
Tetradecane	[a]	26.7	(19)	44	19.2	45.9	53.4	− 7.5	0.86
Dodecane	[a]	25.4	(22)	42	18.9	44.3	50.8	− 6.5	0.87
Undecane	[a]	24.7	(22)	39	19.2	43.9	49.4	− 5.5	0.89
Decane	[a]	23.9	(22)	35	19.6	43.5	47.8	− 4.3	0.91
Nonane	[b]	22.9	(22)	32	19.4	42.3	45.8	− 3.5	0.92
Octane	[a]	21.8	(22)	26	19.6	41.4	43.6	− 2.2	0.95
Heptane	[a]	20.3	(22)	21	19.1	37.4	40.6	− 1.2	0.97
Hexane	[a]	18.4	(19)	12	18.0	36.4	36.8	− 0.4	0.99
Pentane	[a]	16.0	(22)	Spreads	—	>32.0	32.0	> 0.0	1.0
Di(*n*-alkyl)ethers									
Octyl	[e]	27.7	(20)	49	18.2	45.9	55.4	− 9.5	0.83
Heptyl	[f]	27.0	(20)	47	18.4	45.4	54.0	− 8.6	0.84
Amyl	[a]	24.9	(20)	40	19.1	44.0	49.8	− 5.4	0.88
Butyl	[a]	22.8	(20)	31	19.5	42.3	45.6	− 3.3	0.93
Propyl	[a]	20.5	(20)	19	19.4	39.9	41.0	− 1.1	0.97
Isopropyl	[a]	17.8	(20)	Spreads	—	>35.6	35.6	> 0.0	1.0
n-Alkylbenzenes									
Hexyl	[d]	30.0	(25)	52	18.5	48.5	60.0	−10.5	0.81
Butyl	[c]	29.2	(25)	49	19.2	48.4	58.4	−10.0	0.83
Propyl	[c]	29.0	(25)	49	19.0	48.0	58.0	−10.0	0.83
Ethyl	[c]	29.0	(25)	48	19.4	48.4	58.0	− 9.6	0.84
Methyl	[c]	28.5	(24)	43	20.9	49.4	57.0	− 7.6	0.87
Benzene	[c]	28.9	(24)	46	20.1	49.0	57.8	− 8.8	0.85
Linear polymethylsiloxanes									
Heptadecamer	(13)	19.9	(13)	30	17.2	37.1	39.8	− 2.7	0.93
Dodecamer	(13)	19.6	(13)	29	17.2	36.8	39.2	− 2.4	0.94
Nonamer	(13)	19.2	(13)	26	17.3	36.5	38.4	− 1.9	0.95
Heptamer	(13)	18.6	(13)	24	17.0	35.6	37.2	− 1.6	0.96
Hexamer	(13)	18.5	(13)	19	17.5	36.0	36.9	− 0.9	0.97
Pentamer	(13)	18.1	(13)	15	17.5	35.6	36.2	− 0.6	0.98
Tetramer	(13)	17.6	(13)	8	17.4	35.0	35.2	− 0.2	0.99
Trimer	(13)	17.0	(13)	Spreads	—	>34.0	34.0	> 0.0	1.0

[a] Eastman "white label" grade.

[b] Kaiser Wilhelm Institut ("Reinst" grade).

[c] American Petroleum Institute Spectrographic Standards (National Bureau of Standards).

[d] NDRC Preparation by Prof. Homer Adkins (University of Wisconsin).

[e] Connecticut Hard Rubber Company.

[f] Wallace and Tiernan Company.

curve if the ether oxygen is counted as equivalent to a carbon atom in making up the chain. The polymethylsiloxanes, on the other hand, give significantly lower values when plotted on the same coordinates counting each silicon and oxygen atom as equivalent to a carbon atom.

Among the liquids of Table II the adhesion tension varies with the surface tension. When these liquids are arranged in order of decreasing surface tension, they are in the order of increasing adhesion tension with a few exceptions. Adhesion tensions of the liquids that spread are of course indeterminate. Adhesion tensions of liquids whose surface tensions are above about 55 dynes/cm. are negative since the contact angles were greater than 90°.

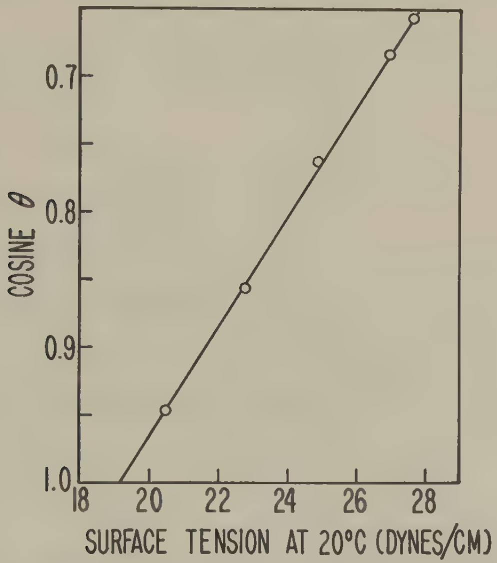

FIG. 2. Surface tension *vs.* cosine θ for the di(*n*-alkyl)ethers.

When surface tension is plotted against cos θ for the homologous series, in each case except the *n*-alkylbenzenes, a straight line fits the points better than the hyperbolas representing the relation $\gamma_{LV} \cos \theta$ = constant (Figs. 1–3). Straight lines also give a good approximation of the relationship between γ_{LV} and cos θ for the halogenated and miscellaneous liquids (Figs. 4 and 5). An insufficient spread in surface tension precludes drawing such lines for the *n*-alkylbenzenes and the esters, so that these fluids have been included in the plot of the miscellaneous group. The intercept of each line of Figs. 1–5 with the ordinate $\cos \theta = 1.0$ gives the surface tension of the liquid in the series which should just spread on TFE. The fact that *n*-hexane gives a finite angle although its surface tension is less than the value indicated by the intercept is anomalous and may be due to the evaporation effects noted earlier. The two fluorinated liquids with surface

TABLE II—*Surface Energy Relations of Some Miscellaneous Liquids and Polytetrafluoroethylene at 20°C.*

Compound	Source of cpd.	γ_{LV}	Ref. γ_{LV}	θ	$\gamma_{LV}\cos\theta$	W_A	W_c	$W_A - W_c$	σ
		dynes/cm.		*deg.*	*dynes/cm.*	*ergs/cm.²*	*ergs/cm.²*	*ergs/cm.²*	
Halogenated compounds									
Methylene iodide	*a*	50.8	(26)	88	0.8	51.6	101.6	− 50.0	0.52
sym-Tetrabromoethane	*c*	49.7	(26)	79	9.5	59.2	97.4	− 40.2	0.60
Aroclor 1242 (trichlorodiphenyl)	*i*	45.3	(23)	81	7.1	52.4	90.6	− 38.2	0.58
α-Bromonaphthalene	*a*	44.6	(26)	73	13.0	57.6	89.2	− 31.6	0.65
Aroclor 1248 (tetrachlorodiphenyl)	*i*	44.2	(23)	78	9.2	53.4	88.4	− 35.0	0.60
Hexachloropropylene	*j*	38.1	(23)	65	16.1	54.2	75.2	− 22.0	0.71
Perchlorocyclopentadiene	*d*	37.5	(23)	67	14.7	52.2	75.0	− 22.8	0.70
sym-Tetrachloroethane	*b*	36.3	(26)	56	20.3	56.6	72.6	− 16.0	0.78
Hexachlorobutadiene	*j*	36.0	(23)	60	18.0	54.0	72.0	− 18.0	0.75
Tetrachloroethylene	*e*	31.7	(26)	49	20.8	52.5	63.4	− 10.9	0.83
Carbon tetrachloride	*e*	26.8	(26)	36	21.7	48.5	53.6	− 5.1	0.91
Polymonochlorotrifluoroethylene (86.9 cs. at 100°F.)	*j*	25.1	(23)	Spreads	—	>50.2	50.2	> 0.0	1.0
Perfluorinated aliphatic hydrocarbon	*m*	24.6	(23)	<5	24.5	>49.1	49.2	(*ca.*) 0.0	>0.99
Perfluorotributylamine	*g*	16.2	(23)	Spreads	—	>32.4	32.4	> 0.0	1.0
Perfluorodibutylether	*g*	12.8	(23)	Spreads		>25.6	25.6	> 0.0	1.0
Esters									
Tricresyl phosphate	*i*	40.9	(23)	75	10.6	51.5	81.8	− 30.3	0.63
Benzyl phenylundecanoate	*d*	37.7	(23)	67	14.9	52.6	75.4	− 22.8	0.70
Di-(2-ethylhexyl)phthalate	*d*	31.2	(23)	63	14.2	45.4	62.4	− 17.0	0.73
Di-(2-ethylhexyl)sebacate	*d*	31.1	(23)	62	14.6	45.7	62.2	− 16.5	0.74
Pentaerythritol tetracaproate	*l*	30.4	(23)	64	13.3	43.7	60.8	− 17.1	0.72
1,6-Hexamethylene glycol di-2-ethylhexanoate	*d*	30.2	(23)	63	13.7	43.9	60.4	− 16.5	0.73
Di-(2-ethylhexyl)adipate	*d*	30.2	(23)	61	14.6	44.8	60.4	− 15.6	0.74
Tri-(2-ethylhexyl)tricarballylate	*d*	29.6	(23)	61	14.4	44.0	39.2	− 15.2	0.74

TABLE II—*Continued*

Compound	Source of cpd.	γ_{LV}	Ref. γ_{LV}	θ	$\gamma_{LV} \cos \theta$	W_A	W_c	$W_A - W_c$	σ
		dynes/cm.		*deg.*	*dynes/cm.*	*ergs/cm.²*	*ergs/cm.²*	*ergs/cm.²*	
Miscellaneous liquids									
Mercury		485.	(1)	150	−420	65.0	970	−905	0.07
Water	—	72.8	(1)	108	− 22.5	50.3	145.6	− 95.3	0.35
Glycerol	*f*	63.4	(26)	100	− 11.0	52.4	126.8	− 74.4	0.41
Formamide	*a*	58.2	(26)	92	− 2.0	52.6	116.4	− 60.2	0.49
Ethylene glycol	*a*	47.7	(26)	90	0.0	47.7	95.4	− 47.7	0.50
tert-Butyl naphthalene	*k*	33.7	(23)	65	14.3	48.0	67.4	− 19.4	0.71
Carbon disulfide	*e*	31.4	(26)	62	14.8	46.2	62.8	− 16.6	0.74
n-Heptylic acid	*a*	28.3	(26)	49	18.6	47.1	56.6	− 9.5	0.83
Polymethylphenylsiloxane (102 cs.)	*h*	26.1	(13)	55	15.0	41.1	52.2	− 11.1	0.79
Polymethylphenylsiloxane (dimer)	*h*	29.0	(23)	50	18.6	47.6	58.0	− 10.4	0.82
Polyethylsiloxane	*h*	23.3	(13)	43	17.0	40.3	46.6	− 6.3	0.87
Linear polymethylsiloxane (35 cs.)	*h*	19.9	(13)	38	15.7	35.6	39.8	− 4.2	0.89
Triptane	*e*	18.9	(24)	<5	—	>37.7	37.8	(*ca.*) 0.0	>0.99

[a] Eastman "white label" grade.
[b] Eastman "technical" grade.
[c] Eastman "practical" grade.
[d] Preparation of this laboratory.
[e] Commercial C.P. grade.
[f] U.S.P. grade.
[g] Minnesota Mining and Mfg. Co.
[h] Dow Corning Corp.
[i] Monsanto Chemical Company.
[j] Hooker Electrochemical Company.
[k] Sharples Chemicals Company.
[l] Hercules Powder Company.
[m] E. I. DuPont de Nemours & Company. (FCD-331, 49.0 cs. at 100°F.)

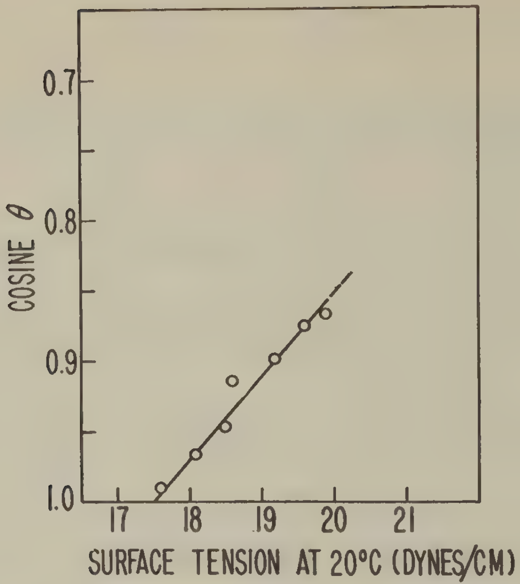

FIG. 3. Surface tension *vs.* cosine θ for the linear polymethylsiloxanes.

tensions over 20 dynes/cm., one of which exhibited a low angle and the other of which spread, seem to be an exception to the rule for all the other liquids. Properties other than the surface tension, such as molecular weight, boiling point, and density, yield no new information when plotted against θ or cos θ.

An interesting example of the dependency of the contact angle on surface tension is given by a group of six esters among the liquids of Table II.

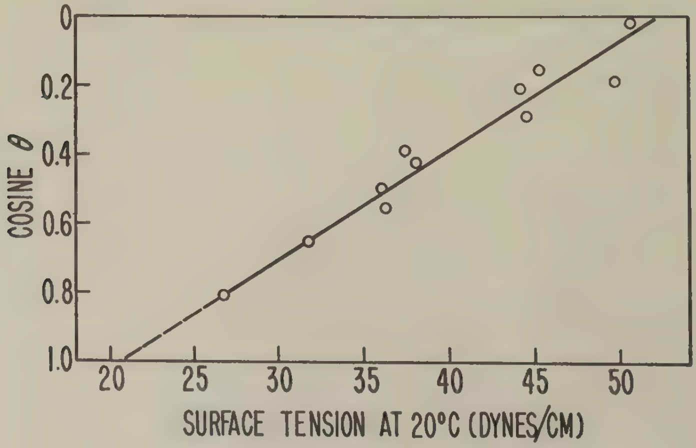

FIG. 4. Surface tension *vs.* cosine θ for the halocarbons.

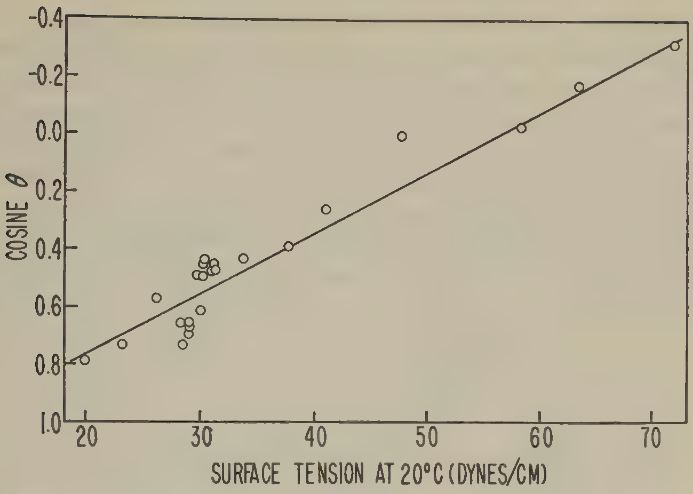

FIG. 5. Surface tension *vs.* cosine θ for some miscellaneous liquids.

Although di-, tri-, and tetraesters are represented in the group, the values of the contact angles are found to lie between 61° and 64°, presumably because the spread in the values of the surface tensions is only 1.6 dynes/cm.

The purpose of the single experiment in a vacuum was to show that the non-wettability of TFE is not due to a film of trapped or adsorbed air on the TFE surface. In this experiment the initial values of the contact angles made by *n*-hexadecane on TFE ranged from 35° to 42°; moreover, the contact angle decreased continuously with time. It was noted that simultaneously the size of the drop decreased. The low values and the continual decrease with time are undoubtedly due to evaporation of the

TABLE III

The Contact Angles of Volatile Liquids on Polytetrafluoroethylene in Air and in Air Saturated with the Liquid Vapor

Liquid	θ, in air	θ, in saturated air	σ, in air	σ, in saturated air
Di(*n*-butyl)ether	34	34	0.93	0.93
n-Octane	26	26	0.95	0.95
n-Heptane	21	22	0.97	0.96
n-Hexane	12	(*ca.*) 7	0.99	1.0
n-Pentane	(*ca.*) 0	Spreads	1.0	1.0
Silicone hexamer	19	22	0.97	0.96
Silicone pentamer	14	17	0.98	0.97
Silicone tetramer	(*ca.*) 8	(*ca.*) 12	0.99	0.99
Silicone trimer	Spreads	Spreads	1.0	1.0

hexadecane, which at pressures of less than 10^{-4} mm. is rapid enough to produce values characteristic of some state intermediate between the advancing and receding angle. Also, it should be pointed out that placement of the drop cannot be done as carefully with the vacuum manipulators as by hand in air, and that this also makes it difficult to insure the formation of the advancing angle. This accounts for the spread in the initial readings.

Another point of interest is the difference between the contact angles on rough and smooth surfaces. It was found that increasing roughness would lower the contact angle. With liquids of low surface tension, a finite angle would be observed on the smooth surface when the same liquid would spread on the rough surface. This observation is consistent with the conclusions from the work of Wenzel (16) and Cassie and Baxter (17) on roughness for liquids having contact angles of less than 90°.

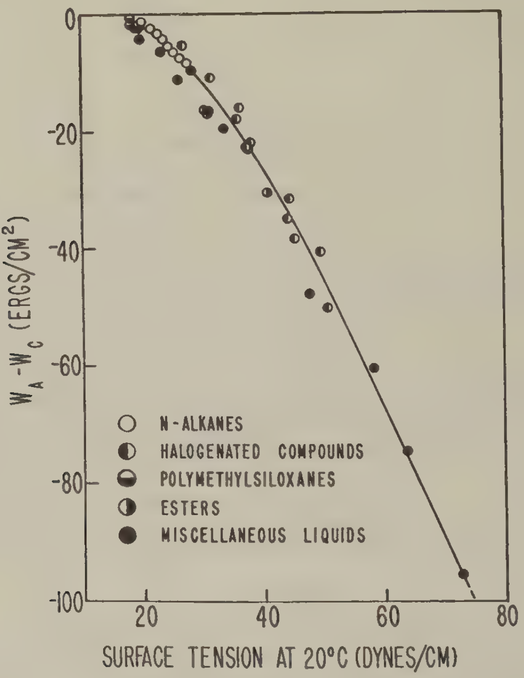

FIG. 6. Spreading coefficient *vs.* surface tension of various fluids on polytetrafluoroethylene.

Table III compares the contact angles of some of the volatile liquids in air, and in air saturated with the vapor of the liquid in question. It was intended by this means to arrive at an estimate of the importance here of the π_E term in Eq. [8] for the work of adhesion. As no difference was found between θ and θ_E for the less volatile liquids under both conditions, it was concluded that the term π_E was negligible for such liquids on TFE. As before, measuring the most volatile materials gave considerable difficulty, and the values are uncertain where the contact angle was very low. Some facts do, however, emerge from these data. Except for hexane, the value for which was a little uncertain both in air and in the saturated atmosphere, the hydrocarbons and di-*n*-butylether show no significant difference between the saturated and nonsaturated atmospheres. But every one of the polymethylsiloxanes gave angles which were about 3° higher in the saturated atmosphere than in air.

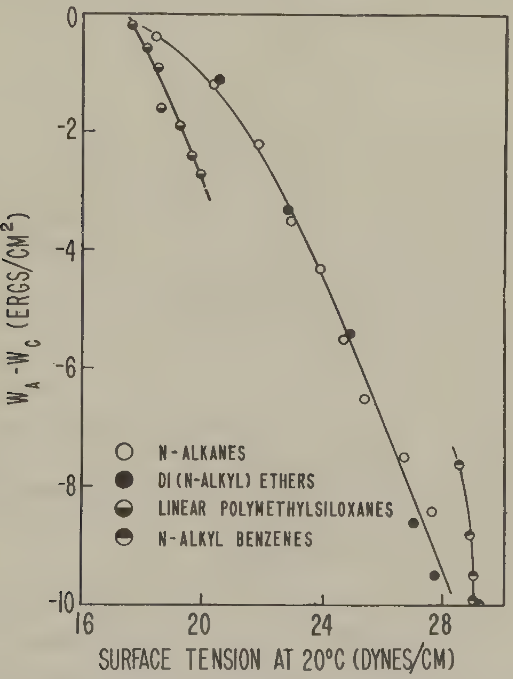

FIG. 7. Spreading coefficient *vs.* surface tension of four homologous series of fluids on polytetrafluoroethylene.

Since π_E was found to be negligible even for materials as condensable as heptane (but not for the polymethylsiloxanes), it can be concluded that $\gamma_{LV}(1 + \cos \theta)$ is a good approximation for W_A, the work of adhesion between TFE and those liquids which do not wet it. W_A, so calculated, is given in Tables I and II and is remarkably constant considering the variation in $\gamma_{LV} \cos \theta$ of the liquids reported here. Even the liquids with negative values of $\gamma_{LV} \cos \theta$ have values of W_A comparable to the others. Tables I and II also include the values of W_c, the work of cohesion ($W_c = 2\gamma_{LV}$) to permit the calculation of the spreading coefficient.

For all the liquids, the initial spreading coefficient $W_A - W_c$ is negative, of course, whenever θ is not zero. If the liquids are arranged in order of decreasing surface tension, with few exceptions they are also in the order of increasing spreading coefficient. This relationship is shown graphically in Fig. 6 where $W_A - W_c$ is plotted against surface tension. The ethers have been left out for the sake of clarity since the points nearly coincide with those of the alkanes. Mercury is also omitted because the compactness of the scale necessary to include it would hide the detailed positions of the points given by all the other liquids. A portion of the same plot is given in Fig. 7 on a magnified scale to show the details for the members of the homologous series of *n*-alkanes, di(*n*-alkyl)ethers, polymethylsiloxanes, and *n*-alkylbenzenes.

Discussion

From Figs. 1–4 it is obviously possible to estimate the surface tensions of the liquids represented in these figures by observing the contact angle against TFE. For the other liquids, a less accurate estimate can be made from Fig. 5. The implication of the observed regularities is, of course, that no other variables affecting spreading on TFE are present for the liquids of this study other than those in Eqs. [2] and [3].

$W_A - W_c$ can be calculated using the assumption made earlier that $\pi_E = 0$ and reduces to the simple relation

$$W_A - W_c = \gamma_{LV}(\cos\theta - 1). \qquad [10]$$

If θ can be expressed as a function of γ, it would permit the derivation from [10] of the relations graphed in Figs. 6 and 7. Since $\cos\theta$ has been shown to be a linear function of γ, it becomes easy to find the required relations by determining the equations of the straight lines $\cos\theta = a\gamma + c$ and substituting in [10]. Thus [10] becomes

$$W_A - W_c = \gamma_{LV}(a\gamma + c - 1) = \gamma_{LV}(a\gamma + b), \qquad [11]$$

where $c = b + 1$. The coefficients a and b, so calculated, are given in Table IV. The curves for $W_A - W_c$ plotted against surface tension are thus parabolic and cluster around the experimental curve for all the liquids when superimposed on Fig. 6, as would be expected. When superimposed on the magnified curves of Fig. 7, the calculated parabolas virtually coin-

TABLE IV

The Spreading Coefficient as a Function of Surface Tension in the Form $W_A - W_c = \gamma_{LV}(a\gamma_{LV} + b)$

Type liquid	*a*	*b*
n-Alkanes	−0.034	0.62
Di(*n*-alkyl)ethers	−0.040	0.77
Polymethylsiloxanes	−0.059	1.03
Halocarbons	−0.031	0.64
Miscellaneous liquids	−0.020	0.16

cide with the experimental curves. Extrapolation of the calculated parabolas to positive regions of $W_A - W_c$ is unwarranted since π_E presumably exerts a significant influence when θ approaches zero.

Equation [2] can be rearranged in the form

$$(\gamma_{\mathrm{SO}} - \gamma_{\mathrm{SL}}) - (\gamma_{\mathrm{SO}} - \gamma_{\mathrm{SV}^\circ}) = \gamma_{\mathrm{LV}^\circ} \cos \theta_E.$$

Since $\gamma_{\mathrm{SO}} - \gamma_{\mathrm{SV}^\circ} = \pi_E$ the above equation can be written

$$\gamma_{\mathrm{SO}} - \gamma_{\mathrm{SL}} = \pi_E + \gamma_{\mathrm{LV}^\circ} \cos \theta_E. \qquad [12]$$

The left hand side of [12] is the free energy of immersion of the solid in the liquid, and [12] permits π_E to be calculated from $\gamma_{\mathrm{LV}^\circ}$, θ_E and a measurement of the free energy of immersion. In the experiments described here $\theta_E = \theta$, so that to a good approximation $\pi_E = 0$ and $\gamma_{\mathrm{LV}^\circ} = \gamma_{\mathrm{LV}}$. Hence [12] can be written

$$\gamma_{\mathrm{SO}} - \gamma_{\mathrm{SL}} = \gamma_{\mathrm{LV}} \cos \theta. \qquad [13]$$

For those liquids for which $\pi_E = 0$ and $\gamma_{\mathrm{LV}} \cos \theta$ is a constant, [13] shows that the free energy of immersion is also constant. As γ_{SO} is a constant of the TFE, it follows that γ_{SL} must be nearly the same for all those liquids, a remarkable result considering the variety of liquids for which the adhesion tension was found to be between 18 and 20 dynes/cm.

There is apparently a range of "critical" surface tensions above which no liquid studied here spreads on TFE and below which every liquid spreads. This range has as a lower limit 17.5 dynes/cm. for the siloxanes and 20.5 dynes/cm. for halogenated compounds. A parallel study made in this laboratory (18) on the wetting of oleophobic monolayers on platinum gave a value between 23.0 and 23.6 dynes/cm. for $\gamma_{\mathrm{LV}} \cos \theta$ for the *n*-alkanes and di(*n*-alkyl)ethers, while all the polymethylsiloxanes spread. The critical surface tension below which all liquids spread on the monolayers was about 22 dynes/cm. Therefore, 23.0–23.6 ergs/cm.^{2} represents the free energy of immersion in the *n*-alkanes, say, of a solid covered with an exterior layer of methyl groups, whereas, 17.5–20.5 ergs/cm.^{2} represents that of a surface comprising perfluoromethylene and perfluoromethyl groups. The introduction of relatively small proportions of other substituents into TFE was found to modify the wettability considerably, and a study of the surfaces of modified polymers will be the subject of a subsequent paper. Although it is stimulating to try to relate the critical surface tensions to the free energies of the solid–liquid interface and of the solid surface itself, there is unfortunately no way of separating the two energies by this method.

No adequate explanation is at present available for the 3-degree increases in θ given by each of the siloxanes in its saturated vapor. It would be expected that with extensive adsorption of vapor the liquid droplets would tend to give smaller angles against what must be films of their parent substance. That the reverse is true cannot be accounted for by reduction of the apparent angle in air due to excessive volatility, because the differences noted were the same for three adjacent members of the homologous series with substantial differences in vapor pressure at 20°C.

The fraction (σ) of the surface area covered with condensed molecules from the liquid phase has been calculated using the Doss and Rao relation [9], and the results are given in the last columns of Tables I, II, and III. In general, the values of σ are surprisingly large for most of the liquids; for only a few like mercury and water is σ less than 0.50. It is not evident why such high-boiling liquids as Aroclor 1248, tricresyl phosphate, di-(2-ethylhexyl)sebacate, and the polymethylphenylsiloxane [102 centistokes (cs.) at 25°C.] should have values as large as 0.60, 0.63, 0.74, and 0.79, respectively, nor why so many alkanes, dialkyl ethers, and polymethylsiloxanes should give finite contact angles while σ is over 0.95. Since we have shown that $\cos \theta$ is a linear function of γ_{LV} for each group of homologous liquids, and since the Doss and Rao relation gives $\cos \theta$, as a linear function of σ, it is evident that σ can be expressed as a linear function of γ_{LV}. But from the physical definition of σ it is unexpected to find large values of σ determined by γ alone rather than by some expression containing parameters determined by the specific attractions or energies of the liquid–solid interface. It is therefore likely that σ is not correctly given by the simple theory of Doss and Rao.

The relative inertness of the TFE surface has been shown to result in values of W_A generally smaller than W_c for the fluids used in this study, so that the spreading coefficient is negative. Therefore most fluids do not spread on TFE. This inertness of TFE surfaces is consistent with the extraordinarily low surface tensions and high compressibilities of the perfluorinated hydrocarbon fluids. All these phenomena are apparently due to the low intermolecular forces which are in turn a result of the large size and extreme electronegativity of the fluorine atoms. In practice the low free energy of the surface of TFE has been reflected in the difficulty of finding adhesives for this material as well as the difficulty encountered in making TFE adhere to itself in the manufacture of solid TFE by sintering the powder. Plasticization will probably depend on the use of a fluid with a surface tension of around 20 dynes/cm. or less for nonfluorocarbon liquids.

ACKNOWLEDGMENT

The authors wish to acknowledge the assistance of Mrs. Dorothy Workman who measured many of the quoted surface tensions.

SUMMARY

1. Methods of preparing surfaces of polytetrafluoroethylene (TFE) are described which permit obtaining reproducible and reliable measure-

ments of contact angles with liquids. Polytetrafluoroethylene is found to be an ideal low energy surface for the study of the wetting relations of a solid with a wide variety of organic and inorganic liquids.

2. It is shown that all but the lowest-boiling liquids studied do not adsorb on TFE sufficiently from the vapor to produce a significant spreading pressure. Hence the π_E term in the expression for the work of adhesion (W_A) is negligible and $W_A = \gamma_{LV}(1 + \cos\theta)$. The calculated values of W_A are found to be consistent and reasonable.

3. It is found that for each homologous series of liquids $\cos\theta$ is a linear function of γ_{LV}. The constants of the resulting relations are given. From this $W_A - W_c$ can be expressed as a function of γ_{LV} alone.

4. The observations show that there is a critical surface tension (17.5–20.5 dynes/cm.) below which liquids wet TFE.

5. It is concluded that the corrected Young-Dupré relation coupled with the spreading coefficient permits a rational description of the results. The Doss and Rao relation for the surface condensation leads to such high values for high-boiling liquids as to make it unlikely that the theory is correct.

References

1. Adam, N. K., The Physics and Chemistry of Surfaces. Oxford Univ. Press, 1941.
2. Bangham, D. H., and Razouk, R. I., (*a*) *Trans. Faraday Soc.* **33**, 1459, 1463 (1937); (*b*) *Proc. Faraday Soc.* **A166**, 572 (1938).
3. Boyd, G. E., and Livingston, H. K., *J. Am. Chem. Soc.* **64**, 2383 (1942).
4. Doss, K. S., and Rao, B. S., *Proc. Indian Acad. Sci.* **7A**, 117 (1938).
5. Livingston, H. K., *J. Phys. Chem.* **48**, 120 (1944).
6. Hardy, W. B., *Proc. Roy. Soc.* (London) **A88**, 313 (1933).
7. Harkins, W. D., *Chem. Revs.* **29**, 385 (1941).
8. Bigelow, W. C., Pickett, D. L., and Zisman, W. A., *J. Colloid Sci.* **1**, 513 (1946).
9. Bigelow, W. C., Glass, E., and Zisman, W. A., *J. Colloid Sci.* **2**, 563 (1947).
10. Shafrin, E. G., and Zisman, W. A., *J. Colloid Sci.* **4**, 571 (1949).
11. Hanford, W. E., and Joyce, R. M., *J. Am. Chem. Soc.* **68**, 2082 (1946).
12. Fox, H. W., and Zisman, W. A., *Rev. Sci. Instruments* **19**, 274 (1948).
13. Fox, H. W., Taylor, P. W., and Zisman, W. A., *Ind. Eng. Chem.* **39**, 1401 (1947).
14. Harkins, W. D., and Jordan, H. F., *J. Am. Chem. Soc.* **52**, 1751 (1930).
15. Sugden, S., The Parachor and Valency. A. A. Knopf, New York, 1930.
16. Wenzel, R. N., *Ind. Eng. Chem.* **28**, 988 (1936).
17. Cassie, A. B., and Baxter, S., *Trans. Faraday Soc.* **40**, 546 (1944).
18. Shafrin, E. G., and Zisman, W. A., Oleophobic Monolayers III: Wetting Effects and Adhesional Energies, to be published.
19. Vogel, A. I., *J. Chem. Soc.* (London) **1946**, 133.
20. *Ibid.* **1948**, 616.
21. *Ibid.* **1948**, 607.
22. Quayle, O. R., Day, R. A., and Brown, G. M., *J. Am. Chem. Soc.* **66**, 938 (1944).
23. This laboratory.
24. Doss, M. P., Physical Constants of the Principal Hydrocarbons, 4th Ed. The Texas Co., (1943).
25. Quayle, O. R., Private communication.
26. *International Critical Tables.*

LOW TEMPERATURE STUDIES WITH COLLOIDAL SILICIC ACID[1]

J. Fred Hazel and Edgar Schipper

Department of Chemistry and Chemical Engineering, University of Pennsylvania, Philadelphia, Pennsylvania

Received September 13, 1950

In a recent brief communication (2) it was stated that the freezing temperature and the rate of thawing have a marked effect on the stability of silica sols and that their behavior, under certain conditions, appears to be related to the properties of ice. We present here the experimental detail upon which the statement was based. Data are included for the effect of electrolytes and of mineral acid used in the preparation of the systems.

EXPERIMENTAL

Silica Sols

Silica sols were prepared by two different methods. They were frozen within 1 hr. after preparation.

1. *Sols Prepared with Mineral Acids*

N-brand sodium silicate, a commercial grade silicate supplied by the Philadelphia Quartz Company, was diluted to eight times its volume with distilled water. The diluted silicate was mixed rapidly, by pouring back and forth, with an equal volume of mineral acid of suitable concentration to give the desired pH. The silica concentrations of the resulting systems were 2.5 ± 0.1%. Sols were prepared with hydrochloric, sulfuric, and phosphoric acids.

2. *Sols Prepared with Ion-Exchange Resins*

Silica sols containing 2.5 ± 0.1% silica were prepared by adding N-brand sodium silicate, diluted to 16 times its volume with distilled water, to weighed portions of ion-exchange resins in the hydrogen form (3). When pH values lower than about 2.8 were required, small volumes of hydrochloric or sulfuric acid were added.

Freezing Procedure

Temperatures ranging down to −65° were obtained with alcohol and Dry Ice. Five-ml. portions of the sols were frozen in test tubes for 20 min.

---

[1] This investigation was supported by a grant from the Committee on the Advancement of Research of the University of Pennsylvania.

In addition to the apparatus described previously (3), a large low-temperature bath was employed. The latter had a capacity of 13 l. and was equipped with a rack holding 14 test tubes.

The experiments with liquid air were conducted in a 4-l. Thermos vacuum jar covered with an asbestos plate. Holes in the cover permitted the insertion of the test tubes containing the sol. The test tubes were immersed in the liquid air for 5 min. The latter was selected as a convenient time after it was found that the time of freezing in liquid air had no bearing on the results.

Thawing was accomplished either by immersing the test tubes in water at room temperature, referred to as "rapid thawing," or by placing them in air at room temperature, indicated as "slow thawing."

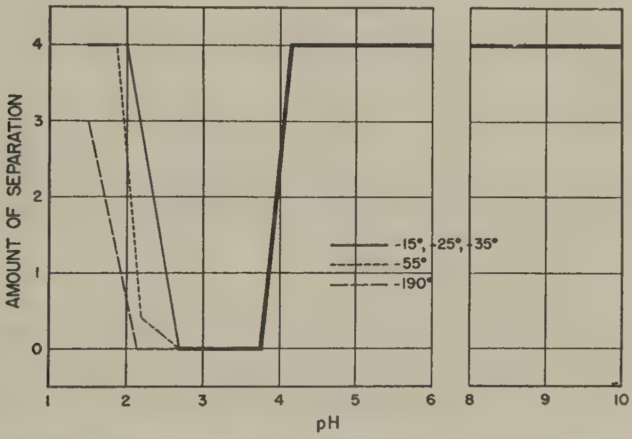

FIG. 1. Effects of pH and freezing temperature on the stability of a silica sol prepared with ion-exchange resins.

The pH values were determined with Leeds and Northrup pH meters.

The amount of flocculation as judged from the optical density was noted. This is recorded as a number in which the number 4 corresponds to maximum flocculation.

RESULTS

Electrolyte-Free Sol

Figure 1 shows the behavior of electrolyte-free sols of different hydrogen-ion concentrations when frozen at −15°, −25°, −35°, −55°, and −190° (estimated temperature of liquid air) and thawed rapidly. The minima in the amount of flocculation in the vicinity of pH 3 are in agreement with previous findings (3). A slight increase of the area of no separation with decreasing temperatures may be noted.

Sols Prepared with Mineral Acids

Figures 2, 3, and 4 show the behavior of silica sols which were prepared with sulfuric acid, hydrochloric acid and phosphoric acid, respectively. The systems were frozen at −15°, −25°, −35°, −45°, −55°, −65°, and −190°. Thawing was rapid in all cases.

Figures 1, 2, and 3 show clearly that there are two flocculation areas and that these are defined by the pH of the systems. The alkaline area, extending over the pH range 4 to 10.5, is affected very little by the freezing temperature or by the anion of the mineral acid. On the other hand, the acid flocculation area decreases with decreasing temperature. Figure

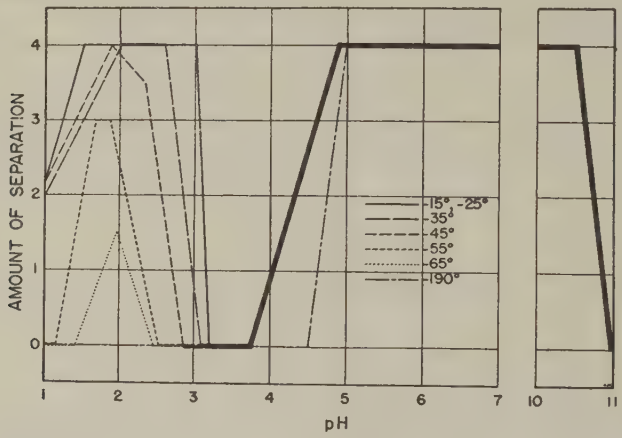

FIG. 2. Effects of pH and freezing temperature on the stability of a silica sol prepared with sulfuric acid.

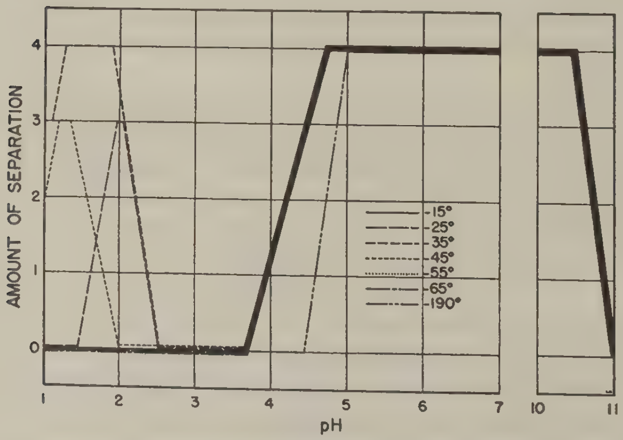

FIG. 3. Effects of pH and freezing temperature on the stability of a silica sol prepared with hydrochloric acid.

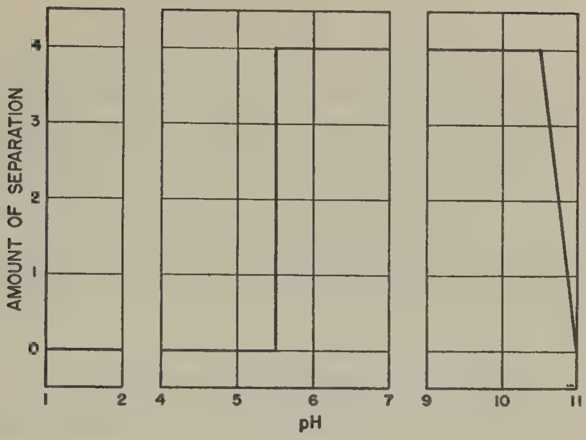

FIG. 4. Effects of pH and freezing temperature on the stability of a silica sol prepared with phosphoric acid.

2 shows that this area is eliminated completely at the temperature of liquid air for the system prepared with sulfuric acid.

The effect of freezing temperature on the stability of silica sols of low pH is illustrated more strikingly in Figs. 3 and 4. The system prepared with hydrochloric acid, Fig. 3, showed no separation at −15°. Flocculation was encountered at lower temperatures and reached a maximum at −35°. At still lower temperatures flocculation decreased and at −55° the acid zone of precipitation had disappeared. The sol prepared with phosphoric acid had the greatest stability. This system showed no flocculation in the acid zone at any of the freezing temperatures.

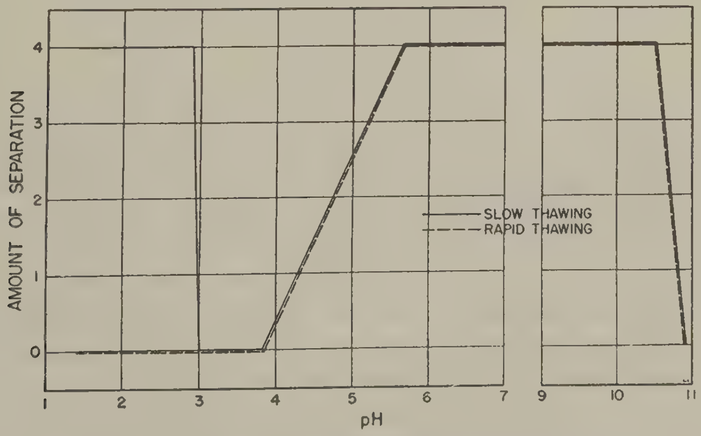

FIG. 5. Effect of rate of thawing on the stability of silica sols prepared with sulfuric acid and frozen in liquid air.

Effect of the Rate of Thawing

Silica sols were prepared with sulfuric acid and frozen in liquid air for 5 min. The frozen systems were divided into two groups and either placed in water at room temperature for the purpose of rapid thawing or were permitted to thaw slowly in the air. The effect of the rate of thawing is evident in the acid precipitation range of Fig. 5. Slow thawing caused complete separation of the silica while no separation occurred on rapid thawing. The rate of thawing was found to affect the behavior of these systems in a similar way when frozen at −65° and −55° but not when frozen at higher temperatures.

Changes Occurring in the Frozen State

Systems of pH 0.9 to 2.5, prepared with sulfuric acid, were frozen in liquid air for five minutes and then transferred to an alcohol–Dry Ice bath at −35° for 15 min. On thawing, complete separation occurred even though this operation was conducted rapidly, *i.e.*, by immersion in water at room temperature. Since the systems would have remained stable had the step at −35° been omitted (cf. Fig. 2), it is clear that a labilizing change occurred in the frozen systems between −190° and −35°.

TABLE I

Conditions of Transfer

Condition	Initial		Final	
	°C.	*min.*	*°C.*	*min.*
A	−190	5	− 35	15
B	−190	5	− 35	1
C	−190	5	− 55	15
D	−190	5	− 55	8
			− 35	7
E	− 15	15	−190	5
F	− 55	15	−190	5
G	− 15	10	− 35	15
			−190	5
H	− 15	10	− 35	10
I	− 15	10	− 35	20

The results of additional experiments in which systems prepared with sulfuric acid and hydrochloric acid were frozen at one temperature and then transferred to another temperature are given in Table II. In some cases this was extended to include two transfers but the final step in all procedures consisted of rapid thawing. Table I gives the experimental conditions. Exposure time corresponding to each temperature is indicated.

Results of Transfer Experiments

Comparing the results of the transfer experiments, Table II, with those involving no transfer, Figs. 2 and 3, it may be seen that a given system was flocculated upon being held for a sufficient length of time at one of the temperatures at which it ordinarily would be flocculated.

The principal results may be stated as follows:

1. The systems can be labilized readily (*e.g.*, by 15-min. exposure but not 1 min.) above −55° while still in the frozen state.
2. Flocculation produced by freezing is nonreversible.

The effects of temperature and of rate of thawing on a silica sol of pH 2, prepared with sulfuric acid are represented pictorially in Figs. 6 and 7. An explanation of the behavior has been offered (2) on the basis that the ice lattice is more disordered when formed below about −55° than it is when formed above this temperature. When frozen in liquid air and

TABLE II

Results of Transfer Experiments

Transfer condition	pH	A	B	C	D	E	F	G	H	I
Acid used in prepn. of sol		Amount of separation								
H_2SO_4	0.9	4				Trace				
	1.0	4				2				
	1.3	4				4				
	1.5	4				4				
	1.7	4				4				
	1.9	4				4				
	2.0	4				4				
	2.1	4	0			4				
	2.3	4	0			4				
	2.5	4		0	3	4				
	2.7	2		0	2	3				
	2.9	0		0		0				
HCl	0.8							4		4
	0.9	4				0	0	1		2
	1.1	4				0	0			
	1.3							4		4
	1.4	4				0		4		4
	1.6	4				0				3
	1.7			0						3
	1.8	3				2	0			
	1.9	3		0		1	0		0	2
	2.0	3		0		0	0			
	2.2			0					0	0
	2.3	0		0		0	0			

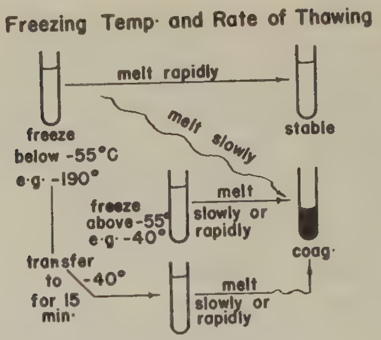
Freezing Temp· and Rate of Thawing
melt rapidly
melt slowly
freeze below -55°C e·g· -190°
stable
freeze above -55° e·g· -40°
melt slowly or rapidly
coag·
transfer to -40° for 15 min·
melt slowly or rapidly

FIG. 6. Effect of variables on the coagulation of silica sols.

thawed slowly, or held at a temperature above −55°, the solid state is retained long enough for well-defined crystals to form. This results in dehydration of the colloid particles and coagulation of the system. On the other hand, if the freezing temperature is below −55° and thawing is rapid, no coagulation occurs because the more stable lattice does not form. Freezing temperature and rate of thawing have been found to be important stability factors with hemoglobin and vanadium pentoxide suspensions (1) and synthetic rubber dispersions (4).

Effect of Electrolyte Concentration

The silicic acid sol prepared with phosphoric acid showed no separation in the acid precipitation range at any of the freezing temperatures (Fig. 4). Because it is a weak acid, a relatively high concentration of this acid was required in the preparation. As a result, the equivalent concentration of the phosphate was approximately seven times that of the chloride and sulfate in corresponding systems. In order to determine whether high concentrations of electrolytes enhanced the stability of the

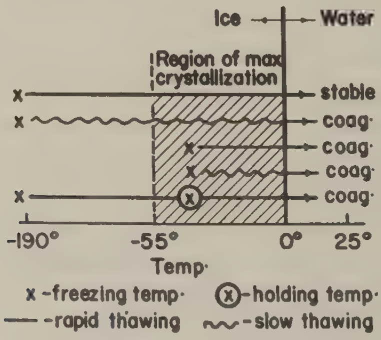

FIG. 7. Effect of freezing temperature, aging temperature, and rate of thawing on the coagulation of silica sols.

system, a study of the effect of added electrolytes on a resin-prepared system (adjusted to a pH of 1.5–2.1) was conducted. Two different concentrations of electrolytes were employed, the higher concentration corresponding to that of the phosphoric acid which was added to the stock solution of sodium silicate to prepare a silica sol of pH 2. The lower concentration corresponded to that of the other acids, hydrochloric and sulfuric, needed to prepare systems of the same pH. The results are given in Fig. 8.

Lithium chloride and calcium chloride had a strong stabilizing effect; coagulation was inhibited even at the lower concentration of these substances. The two sodium salts had weaker stabilizing effects, although at the higher concentration of the phosphate the system did not coagulate.

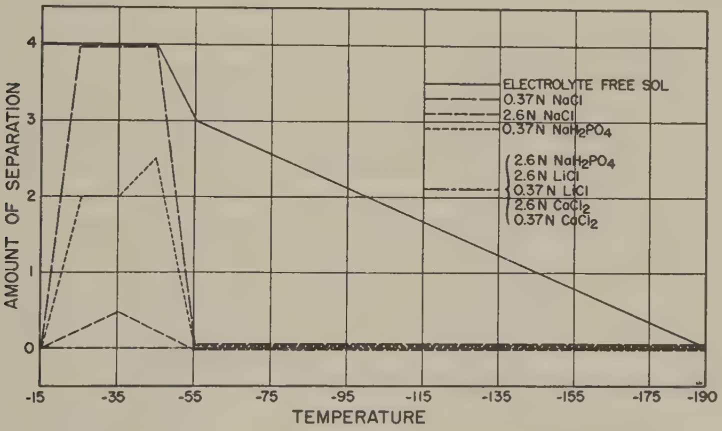

Fig. 8. Effect of electrolytes on the stability of silica sols prepared with ion-exchange resins.

This latter result is in agreement with the previous observation that silica sols prepared with phosphoric acid are stable under these conditions.

In explanation of the complex behavior represented by the above results, it may be suggested that the orientation of the dipoles of water by the small lithium and calcium ions retards the crystallization of water. Indeed, Walton and Braun (5) found that while the linear velocity of crystallization for water was 368 cm./min. at −9°C., that of 0.1 *M* solutions of calcium chloride, lithium chloride, and sodium chloride were 155, 170, and 247 cm./min. respectively.

SUMMARY

1. Silica sols prepared with mineral acids and with ion-exchange resins have been frozen at −15°, −25°, −35°, −45°, −55°, −65°, and −190°C.

2. The effects of hydrogen-ion concentration, rate of thawing, temperature of aging the frozen systems, and presence of electrolytes were investigated.

3. The following factors were found to increase the stability of the systems: (a) low temperature of freezing, (b) low temperature of aging, (c) rapid rate of thawing, and (d) presence of lithium chloride and calcium chloride.

REFERENCES

1. DJATSCHKOWSKY, *Kolloid-Z.* **59**, 76 (1932).
2. HAZEL, PARKER, AND SCHIPPER, *Science* **110**, 161 (1949).
3. HAZEL, *J. Phys. & Colloid Chem.* **51**, 415 (1947).
4. WALKER, *J. Phys. & Colloid Chem.* **51**, 451 (1947).
5. WALTON AND BRAUN, *J. Am. Chem. Soc.* **38**, 317 (1916).

PARTICLE SHAPE AND THE CONCENTRATION DEPENDENCE OF SEDIMENTATION AND DIFFUSION[1]

S. Newman[2] and F. Eirich

Institute of Polymer Research, Polytechnic Institute of Brooklyn,
Brooklyn, New York

Received August 4, 1950

INTRODUCTION

A macromolecule moving in an ultracentrifugal field is acted on by several distinct types of forces: a force from the external field producing a directed motion, frictional forces exerted by the medium on the particle in motion, and also random forces acting on the particle and its parts by the environment. For a spherical particle which is large relative to the size of the solvent molecules, the latter may be regarded as a continuum and Stokes's law may be used to represent the frictional force. When this condition does not hold, the frictional resistance must be regarded in the light of the interaction between the molecules of solvent and solute. For a particle moving with a small velocity relative to the surrounding medium, the assumption of a frictional resistance proportional to the first power of the velocity remains justified, but the proportionality constant is not necessarily that of Stokes.

In such a case, the motion of a particle in an ultracentrifugal field can be completely described by the Langevin equation (1), modified to include the field term:

$$m \frac{d\mathbf{v}}{dt} = -f\mathbf{v} + m\mathbf{w}^2\mathbf{x} + \mathbf{A}(t), \qquad [1]$$

where m is the mass of the particle, $\mathbf{v}$ its velocity relative to the medium, f a frictional resistance coefficient, $\mathbf{w}^2\mathbf{x}$ the centrifugal acceleration, and $\mathbf{A}(t)$ a fluctuating force characteristic of the Brownian motion of the particle. It can be assumed that the fluctuating forces change extremely rapidly ($> 10^{-13}$ sec.) and that they may be treated as independent of the steady forces so that $\mathbf{A}(t)$ may undergo several fluctuations during the time interval Δt while the variations in $\mathbf{v}$ are negligible.[3]

---

[1] The material herein presented is taken from the Ph.D. thesis of Seymour Newman, Polytechnic Institute of Brooklyn, June 1949.

[2] Present address: Southern Regional Research Laboratory, U. S. Department of Agriculture, New Orleans, Louisiana.

[3] This assumption is justified by the fact that it is possible to derive from the Langevin equation all of "the physically significant relations concerning the motions of the Brownian particles." See Ref. (1).

A solution of the Langevin equation has been given by Chandrasekhar. From his results it can be shown that for times which are relevant in ultracentrifuge action, i.e. $(f/m)t \gg 1$, the average value of the velocity of the particle is given to a very good approximation by the following equation:

$$\frac{\langle \mathbf{v} \rangle_{\text{av}}}{\langle \mathbf{w}^2 \mathbf{x} \rangle_{\text{av}}} = m/f. \qquad [2]$$

This leads to the usual Svedberg equation (2) for the sedimentation constant, s,

$$s = \frac{d\mathbf{x}/dt}{\mathbf{w}^2\mathbf{x}} = \frac{M(1 - \bar{V}\rho)}{F}, \qquad [3]$$

where s is the velocity of sedimentation in a unit centrifugal field, F the frictional coefficient per mole, M the molecular weight, $\bar{V}$ the partial specific volume of the solute and ρ the density of the solution. It is seen from the foregoing analysis that, if $\bar{V}\rho = \text{const.}$, the concentration dependence of the sedimentation constant should involve only the concentration dependence of the hydrodynamic frictional coefficient. It is also seen from Eq. [1] that the magnitude of the frictional coefficient which in a microscopic sense depends upon the intermolecular forces and the local distribution of molecules, will be the same in the presence or absence of the field as long as the field is not of such a magnitude as to influence the particle configuration or the equilibrium molecular distribution. The frictional coefficient in diffusion should therefore be the same as in sedimentation.

If we assume with other authors a concentration dependence of the frictional coefficient in the form of a power series in the concentration, C, we have

$$F = F_0(1 + KC + K_aC^2 + \dots), \qquad [4]$$

where F_0 is the frictional coefficient in the limit of infinite dilution. Using the first two terms of this expansion and noting that at infinite dilution Svedberg's equation is written as

$$s_0 = \frac{M(1 - \bar{V}\rho)}{F_0}; \; s_0 = s_{\lim C \to 0}, \qquad [5]$$

we obtain on substitution the following well-known approximate relation (3, 4, 5) for the concentration dependence of the sedimentation constant in solutions of moderate concentration:

$$s = s_0(1 + KC)^{-1}. \qquad [6]$$

The concentration dependence of diffusion has been treated by various authors (6–11) and has been shown to be related to the concentration dependence of sedimentation as follows:

$$K_d = (2BM/RT - K), \qquad [7]^{4}$$

$$D = \frac{RT}{F}\,(1 + \frac{2BM}{RT}\cdot C) = D_0(1 + K_dC),$$

where D_0 is the limiting value of the diffusion constant, D, at infinite dilution, T is the absolute temperature, R the gas constant and B is the second virial coefficient in the expression for the osmotic pressure, π:

$$\pi = (RT/M)C + BC^2 + \ldots. \qquad [8]$$

Equation [6] has received widespread experimental verification for a diverse variety of substances although, depending on the nature of the particles and solvent, deviations at higher concentrations are to be expected and have been observed. (See Fig. 1, for instance.) Equation [7] has received extensive experimental attention only recently (12).

Significant among the theoretical considerations of the concentration dependence of the frictional coefficient has been the work of Burgers who derived Eq. [6] for spheres and concluded that K is equal to 6.875 when the concentration is expressed as percentage volume concentration (13). His K is, of course, inapplicable to flexible macromolecules and it is our present purpose to show how K for linear flexible polymers is connected with the molecular weight and the average configurations of the solute particles. It is thus influenced by the solvent and may be related in principle to other parameters which depend on the molecular weight.

The dependence of the frictional coefficient and consequently of the sedimentation constant has also been frequently treated in terms of the effect of concentration upon the viscosity of the solution. This approach has proved to be of limited practical value, there being no strict hydrodynamic basis for the procedure (11, 14), but certain implications will be discussed in a future publication.

EXPERIMENTAL

Values of K have been obtained from sedimentation data on four fractions of polystyrene in chloroform, toluene, and methyl ethyl ketone (MEK). The apparatus, method of sample preparation, and sample characteristics have been discussed (15). (See also above.) The molecular weights were computed from measurements of the intrinsic viscosity in MEK and toluene and in part also from osmotic pressure data. The values for the molecular weights, reported in Table I, are believed to be reliable to 15%. Viscosity measurements were made in an Ostwald-type viscometer.

---

[4] This equation is also obtainable from the Langevin equation (Dr. J. Riseman, private communication).

Sedimentation data were obtained with an air-driven ultracentrifuge in the concentration range of 0.01–1.0%, and the reciprocal of s was plotted against C (expressed as g./100 ml. of solution) in accordance with Eq. [6]. In chloroform, where the fractions possessed a highly extended configuration, deviations from linearity necessitated a computation of K at concentrations below 0.5 g./100 ml. The correction for changes in concentration at the solvent–solution boundary during sedimentation and adjustment of the sedimentation constant to 20°C. were carried out in the customary manner.

TABLE I

Sedimentation–Concentration, Length, Molecular Weight and Intrinsic Viscosity Data on Four Fractions of Polystyrene in Several Solvents

Fraction	Solvent	Intrinsic viscosity, $[\eta]$	$10^{13}s_0$	K	$K/[\eta]$	$\langle R_0\rangle_{av}$
						Å
1. ($M = 13.0 \times 10^5$)	Chloroform	3.2	17.8	5.0	1.6	1700
	Toluene	2.8	11.2	4.0	1.4	1400
	MEK[a]	1.4	26.0	2.3	1.6	1000
7. ($M = 8.0 \times 10^5$)	Chloroform		15.4	4.0		1300
	Toluene		9.3	3.1		1100
	MEK[a]	1.1	21.3	1.7	1.5	780
19. ($M = 5.5 \times 10^5$)	Chloroform		13.1	3.2		1200
	Toluene		7.6	2.5		970
	MEK[a]	0.83	18.2	1.3	1.6	670
28. ($M = 2.5 \times 10^5$)	Chloroform		9.2	1.8		760
	Toluene		5.9	1.5		640
	MEK[a]	0.54	12.6	0.73	1.4	440

[a] Methyl ethyl ketone.

The particle dimensions expressed as the root-mean-square end-to-end distance, $\langle R_0\rangle_{av}$ have been previously calculated (15) according to the Kirkwood-Riseman theory (16) from the sedimentation constants at infinite dilution in conjunction with the molecular weight measurements. The accuracy of $\langle R_0\rangle_{av}$ is limited by the reliability of the molecular weights.

RESULTS AND DISCUSSION

Figure 1 presents representative data on the extrapolation of $1/s$ versus C for fractions 1, 7, and 19 in chloroform.

Values of s, M, K, and $\langle R_0\rangle_{av}$ of the four fractions in the three solvents mentioned are reported in Table I; and some intrinsic viscosity data are also included.

In examining the relation between K and the molecular weight in the three solvents, we notice over the range investigated a proportionality between K and $M^{\frac{1}{2}}$. (See Fig. 2.) In the light of the current theories a parallelism between K and s_0 is therefore evident. Further, in agreement with our previous conclusions from the Kirkwood-Riseman theory as regards the order of increasing molecular extensions in the solvents methyl ethyl ketone, toluene, and chloroform, we note that K is highest for chloroform and lowest for methyl ethyl ketone.

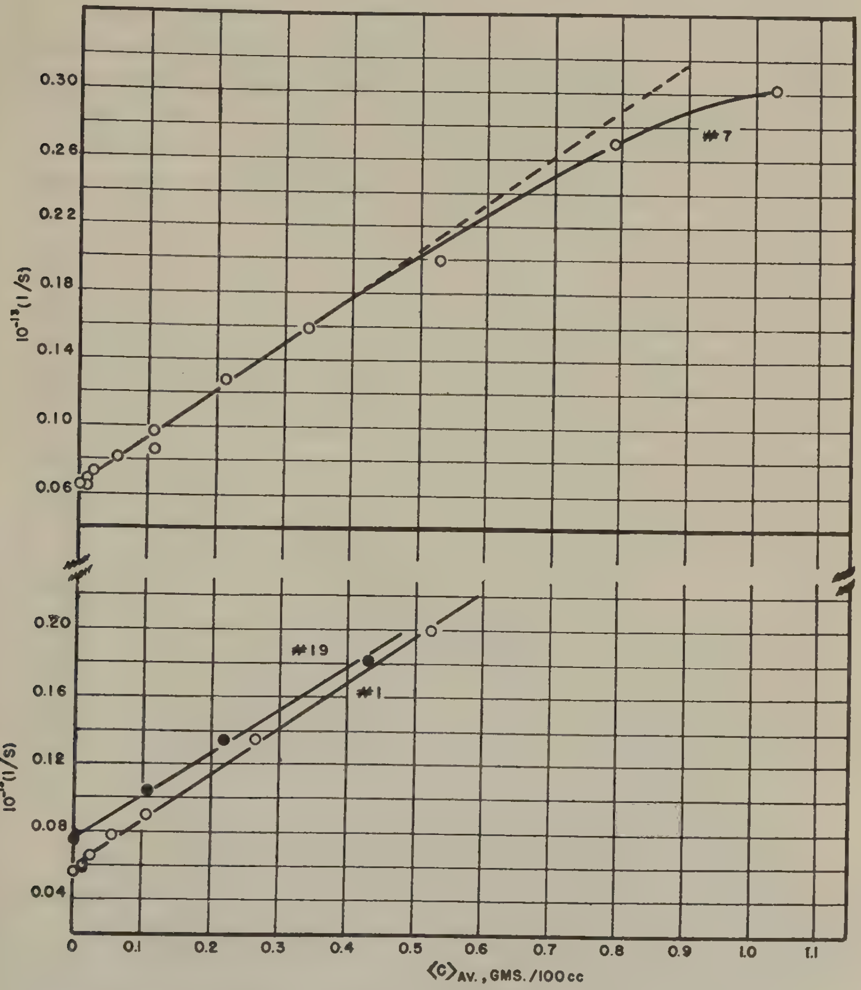

FIG. 1. Plot of the reciprocal sedimentation constant versus concentration for polystyrene fractions 1, 7, and 19 in chloroform.

By virtue of K being an interaction constant, this order was to be expected. For flexible macromolecules, the end-to-end extension of the particles in solution is given by the relation

$$\langle R_0\rangle_{\text{av}} = bZ^{\frac{1}{2}};\ Z = M/M_0, \qquad [9]$$

where M and M_0 are the polymer and monomer molecular weights, respectively, and b is the effective bond length. As such, the change in polymer chain configuration with solvent is described by the change with solvent of the average end-to-end distance or, perhaps more fundamentally, of the effective bond length b.

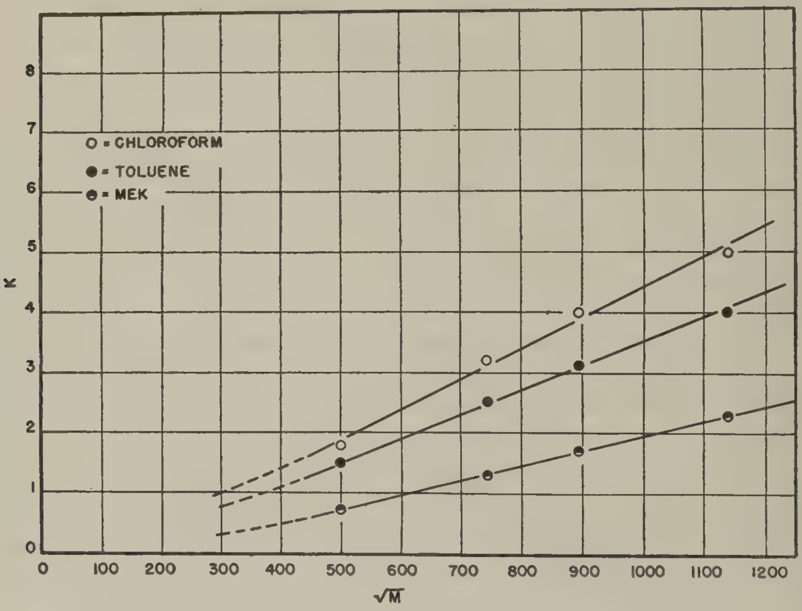

Fig. 2. Plot of K versus the square root of the molecular weight in methyl ethyl ketone, toluene, and chloroform.

Now, if the interaction constant were primarily a function of the molecular extension, then an even "better" proportionality ought to be expected between K and $\langle R_0\rangle_{\text{av}}$. This is shown in Fig. 3 where the individual curves from Fig. 2 are seen to almost coincide. On the other hand, it is not to be expected that they should actually coincide.

A flexible macromolecule such as polystyrene assumes an average configuration which depends upon the thermodynamic nature of the solute–solvent system. The hydrodynamic properties of the system, if the solute molecule is sufficiently large to apply classical hydrodynamics, will depend entirely on the effect such an average configuration has upon the original flow of the liquid. These hydrodynamic properties unlike $\langle R_0\rangle_{\text{av}}$

involve dynamic effects incapable of statistical thermodynamic representation; hence in describing K explicitly in terms of the hydrodynamic properties of the system the correlation of K and $\langle R_0 \rangle_{av}$ can be expected to be only a partial one. K may therefore be expected to show a further solvent dependence which, even for the same shape in a number of solvents, would result in different frictional properties. In this connection we have in mind the quantity, ζ, a frictional constant characteristic of the fluid and structure of the monomer unit as employed by Kirkwood-Riseman (16).

An inspection of Table I discloses a strong parallelism between K and the intrinsic viscosity, $[\eta]$; in fact, a plot of K vs. $[\eta]$ for the four fractions in MEK is a straight line extrapolating to the origin. A similar parallelism has been pointed out by Simha (8) and Lauffer (4). Simha pointed out the parallelism between the quantities $[\eta]$ and $2BM/RT$ in Eq. [7] as being measures of nonideal behavior in solutions and thus arrives at $K \propto [\eta]$ whenever $K_d \doteq 0$. It will be noted that this parallelism yields a proportionality between $[\eta]$ and BM. Simha's equality ought, therefore, be expected where Staudinger's law holds, except in cases of a dependence of B on M. (See e.g. Kunst (19).) Our relation, however, exhibits a condition nearer to $[\eta] \propto M^{\frac{1}{2}}$ and should apply, therefore, to tighter molecular configurations.

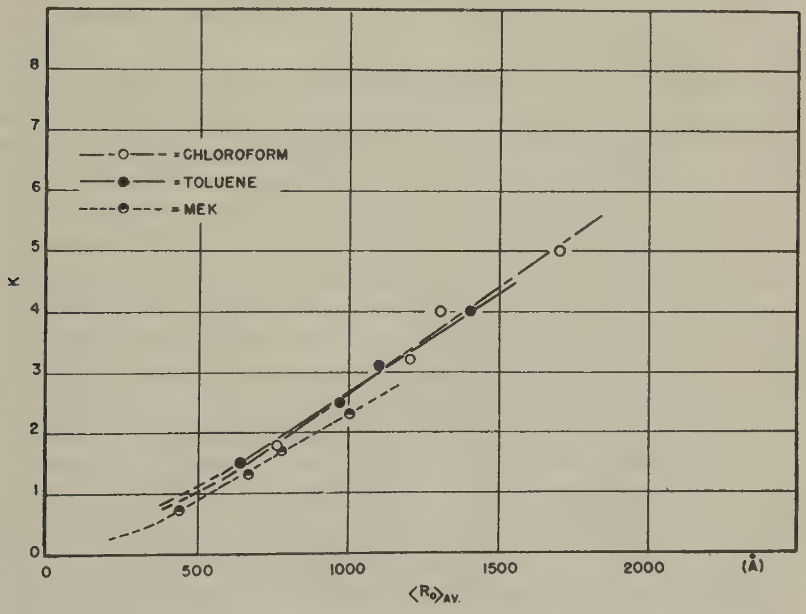

FIG. 3. Plot of K versus molecular end-to-end distance for polystyrene fractions in methyl ethyl ketone, toluene, and chloroform.

Any relation between K and $[\eta]$ for a homologous series in a given solvent is obviously of considerable practical value. The value and the interest in this relation are, however, increased by finding that for the same fraction in different solvents K again varies as $[\eta]$.[5] (See Table I.)

Although our relation is reminiscent of Lauffer's correction, a basic difference ought here to be pointed out. Lauffer's relation results from substituting into Eq. [6] the reduced viscosity of the solution in place of K. This is equivalent to saying that the individual particle is moving in a new liquid possessing the viscosity of the solution. This implicit assumption cannot be justified. Our results show, on the other hand, that there is a proportionality between K and the intrinsic viscosity, the proportionality constant being approximately 1.6. The conclusion to be drawn at this point is that K and $[\eta]$ both depend on the molecular structure in a closely similar fashion.

In connection with the concentration dependence of diffusion, it is of interest to consider the extent to which the term $2BM/RT$ increases more rapidly than K with molecular weight. This should make possible a prediction of the molecular weight region in which the slope of D/D_0 vs. concentration should change sign. See Eq. [7]. For fractions 1 and 19 of molecular weights $M_2 = 13 \times 10^5$ and $M_1 = 5.5 \times 10^5$, respectively, the ratio of $M_2/M_1 = 2.4$, whereas the ratio of $K_2/K_1 = 1.8$ in MEK. It is expected on this basis upon assuming an approximate value for B that K_d for polystyrene in MEK would be positive above molecular weights of the order of 5×10^5 and negative below. Evidence for the latter in the case of unfractionated polystyrene in a similar solvent, methyl isopropyl ketone, has been published (18). Similar results have been obtained by comparing the same fractions in chloroform and toluene, i.e., that the molecular weight ratio increases more rapidly than K in the molecular weight range involved. Thus while $M_2/M_1 = 2.4$, the corresponding values of K_2/K_1 are 1.25 and 1.3, respectively. Again, the actual molecular weight range in which $(2BM/RT - K)$ changes sign depends markedly on the solute-solvent system; although both the thermodynamic term B and the hydrodynamic term K increase from "poorer" to "better" solvents, they do so usually to a different degree.

The relation between the concentration dependence term in diffusion, K_d, and average molecular extensions as well as the influence of solvent and molecular weight on K_d may be inferred, according to Eq. [7], from our previous considerations of K as well as from properties of the thermodynamic term $2BM/RT$. A consideration of this latter quantity will be omitted here.

ACKNOWLEDGMENT

We are glad to acknowledge the assistance given to us by Dr. J. Riseman during many valuable discussions.

---

[5] Future publication, Eirich and Rosen.

SUMMARY

A consideration of the motion of a particle in an ultracentrifuge from the Langevin equation shows that the concentration dependence of sedimentation should involve only the concentration dependence of the frictional coefficient. The coefficient K appearing in the expansion of the frictional coefficient, $F = F_0(1 + KC + \ . \ . \ . \ +)$ has been evaluated from sedimentation data in the case of four fractions of polystyrene in methyl ethyl ketone, toluene, and chloroform. K was found to be proportional to the square root of the molecular weight over the range investigated in the three solvents mentioned. More fundamentally, K was found to be proportional to the average molecular extension in a manner nearly independent of solvent.

A parallelism noted for our fractions between K and the intrinsic viscosity is discussed.

The relationship between the concentration dependence of diffusion and K is briefly treated. The molecular weight region for polystyrene in methyl ethyl ketone in which the concentration dependence of diffusion should change from positive to negative is predicted.

REFERENCES

1. Chandrasekhar, S., *Revs. Modern Phys.* **15**, 1 (1943). Kirkwood, J. G., *J. Chem. Phys.* **14**, 180 (1946).
2. Svedberg, T., and Pedersen, K. O., The Ultracentrifuge. Oxford Univ. Press, 1940.
3. Signer, R., and Gross, H., *Helv. Chim. Acta* **17**, 59 (1934).
4. Lauffer, M. A., *J. Am. Chem. Soc.* **66**, 1195 (1944).
5. Gralen, N., Ph.D. Thesis, Uppsala, 1944.
6. Onsager, L., and Fuoss, R. M., *J. Phys. Chem.* **51**, 158 (1938).
7. Schulz, G. V., *Z. physik. Chem.* **193**, 168 (1944).
8. Beckmann, C. O., and Rosenberg, J. L., *Ann. N. Y. Acad. Sci.* **46**, 329 (1945).
9. Simha, R., *J. Applied Phys.* **17**, 406 (1946).
10. Singer, S. J., *J. Chem. Phys.* **15**, 341 (1947).
11. Simha, R., in High Polymer Physics, A Symposium. Edited by H. A. Robinson, Chem. Publishing Co., Inc., 1948.
12. Schick, A., Ph.D. Thesis, Polytechnic Institute of Brooklyn, 1948.
13. Burgers, J. M., *Proc. Koninkl. Nederland. Akad. Wetenschap.* **44**, 1045, 1177 (1941); **45**, 9, 126 (1942).
14. Schachman, H. K., and Kauzmann, W. J., *J. Phys. & Colloid Chem.* **53**, 150 (1949).
15. Newman, S., Riseman, J., and Eirich, F., *Rec. trav. chim.* **68**, 921 (1949).
16. Kirkwood, J. G., and Riseman, J., *J. Chem. Phys.* **16**, 565 (1948).
17. Schick, M., Ph.D. Thesis, Polytechnic Institute of Brooklyn, 1948.
18. Hengstenberg, J., and Schulz, G. V., *Makromolek. Chem.* **2**, 5, (1948).
19. Kunst, E. D., Proceed. Intern. Coll. Macromolecules Amsterdam 1949; D. B. Centen's, Amsterdam 1950.

CHEMISORBED OXYGEN ON CHARCOAL AND THE SORPTION OF STRONG INORGANIC BASES AND ACIDS

J. H. Wilson and T. R. Bolam

Chemistry Department, King's Buildings, University of Edinburgh
Edinburgh, Scotland

Received September 22, 1950

INTRODUCTION

The sorption, from aqueous solution, of strong inorganic bases by charcoal is usually regarded as due to the action of an acidic oxide formed on the surface of the charcoal by treatment with oxygen at temperatures below about 800°C., the optimum temperature being about 400°C. However, the precise state of oxygen chemisorbed on charcoal at 400°C. remains unsettled, as indeed does the question of what proportion of such oxygen is involved in the sorption of base. The present paper deals primarily with an attempt to throw light on these problems by a systematic study, hitherto lacking, of the effects produced by heating the oxidized charcoal in an inert atmosphere. In particular, the manner in which the sorption of base varies with the oxygen content of the charcoal has been investigated. At the same time we have measured the sorption of strong inorganic acid and that of iodine, to ascertain whether these indicate the presence of basic surface oxide or that the acid is physically adsorbed (1). An account is also given of experiments performed to determine what role, if any, chemisorbed water plays in the sorption of base (2).

EXPERIMENTAL

Preparation of Sugar Charcoal

"Analar" sucrose was charred in small open Pyrex basins with the Bunsen flame, and portions of the char which had not been in contact with the glass were further heated in silica basins (covered with Pyrex watch glasses) for 40 min. with the full Meker burner flame. The charcoal was finally thoroughly ground, in an agate mortar, and mixed. Two batches (*A* and *B*) were prepared. Each gave 0.04% ash, containing a very small trace of iron. Batch *A* was used for the *C* and *D* series of experiments, and batch *B* for the *J*, *K*, *L*, and *M* series.

In order to reduce the content of volatile matter, the charcoal was outgassed. The crude char, contained in silica boats, was placed in a horizontal silica tube, connected to the remainder of the apparatus by ground Pyrex joints. The middle portion of the tube, where the charcoal was positioned, was heated electrically, the vacuum grease of the end joints (about 1 ft. from the furnace) being kept firm by water cooling. The temperature, automatically controlled by a Sunvic regulator, was measured by a thermocouple (consisting of Ferry and Bright Ray nichrome wires), calibrated against a platinum: platinum–rhodium thermometer (Cambridge Instrument Co.). Outgassing, by means of a Cenco Hyvac pump, was carried out for 6 hr. at 825°C. The minimum pressure attained at this temperature was 0.2 mm., which fell to 0.001 mm. on cooling to room temperature.

Oxidation of Charcoal

In the case of series *C* and *D* the charcoal was treated with air, while oxygen (commercial) was used for the other series. Oxidation in most cases was carried out in the electric furnace described above, but the samples for the *K* and *M* series were heated in a second silica tube by means of Bunsen burners. Before entering the furnace tube the gases were passed through 10% NaOH and concentrated H_2SO_4, and then over $CaCl_2$ and P_2O_5 (75 cm.). The air or oxygen was passed, at the respective rates of 10 ml. and 5 ml., for 12–15 hr. in each direction. At temperatures in the neighborhood of 400°C. and treating about 4 g. charcoal (2 g. in each of two boats) at a time, good yields of fixed oxygen were obtained, with the loss of roughly half the material.

Thermal Treatment of Oxidized Charcoal

Portions of oxidized charcoal were heated, in the electric furnace, in a slow stream of nitrogen (*J*, *K*, *L*, and *M* series) or in vacuum (*D* series). The nitrogen (commercial) was purified by passage over heated Cu gauze (37 cm.), then through concentrated H_2SO_4 (and $CaCl_2$ in *L* and *M* series), and finally over P_2O_5 (75 cm.). Except in the *D* series, the charcoal was weighed before and after treatment, in order to ascertain the loss due to this.

Analysis of Gaseous Products

In the *L* and *M* series of experiments determinations were made of the amounts of the gaseous compounds evolved when the charcoal was heated in the stream of purified nitrogen. On emerging from the furnace tube (previously baked-out) the nitrogen was passed through the following, in the order given: (*a*) U-tube containing $CaCl_2$, to absorb water, (*b*) U-tube containing Sofnolite, to absorb CO_2, (*c*) U-tube containing I_2O_5 at 150°C., to convert CO to CO_2, (*d*) 10% KI, to remove iodine, (*e*) concentrated H_2SO_4 and $CaCl_2$, to remove water, and (*f*) U-tube containing Sofnolite, to absorb CO_2 formed from CO. At the end of the prescribed period of treatment the nitrogen stream was continued until the temperature had dropped by about 200°C., to ensure complete absorption of the gases. The change in weight of the U-tubes (*a*), (*b*), and (*c*) was then determined.

Complete Analysis of Oxidized Charcoal

The composition of samples of oxidized charcoal was investigated (Expts. *M*3 and *M*4) by determination of the H_2O, CO_2, and CO liberated by heating in nitrogen for 2.5 hr. at 855–865°C., followed by separate determination of the same substances yielded by complete combustion, in oxygen at 625°C., of the residual charcoal. The oxygen was freed from carbon dioxide by means of soda–lime and concentrated KOH, and dried with $CaCl_2$ and P_2O_5 (25 cm.).

Measurement of Sorption

In general a weighed sample (usually about 0.3 g.) of charcoal was shaken at room temperature for 24 hr. with 25 ml. of a standard solution of adsorbate. The charcoal was then sedimented by centrifuging and two 10-ml. portions of the solution titrated to determine the amount of substance unsorbed. HCl and HNO_3 were standardized with dried Na_2CO_3 and estimated with NaOH; NaOH was standardized and estimated with HCl; iodine was standardized with As_2O_3 and estimated with $Na_2S_2O_3$. Methyl red was used

TABLE I

Influence of Thermal Treatment on Sorption by Oxidized Charcoal

Expt.	Temp.	Period of heating	Loss in wt.	Sorption (mole × 10^{-5}/g. charcoal)		
				NaOH	HCl	Iodine
	°C.	*hr.*	*mg./g. charcoal*			
J_u	—	—	—	0	24.4	208
J_o	—	—	—	311	1.4	598
J1	600	0.083	64	222	3.4	562
J2	600	0.133	95	189	5.3	588
J3	600	0.25	124	157	6.8	608
J4	600	0.2	126	155	7.0	609
J5	600	1	177	103	11.6	680
J6	600	0.35	185	95	13.2	689
J7	600	0.5	191	92	13.2	707
J8	600–610	6	216	60	24.5	786
J9	600–615	41	255	29.8	27.9	846
J10[a]	825	6	277	12	40.5	846
K_o	—	—	—	359	1.0	582
K1	600	1	173	133	8.3	556
K2	600	6	210	97	14.1	613
K3	600	42	259	57	24.2	713
K4	840	5.5	304	22	31.8	744
K5	840	12	306	17	36.0	744
L_u	—	—	—	0	25.3	231
L_o	—	—	—	317	2.3	655
L_o	—	—	—	304	—	—
L1	550	Very short	41.3	249	4.4	633
L2	550	0.25	60.4	226	5.2	635
L3	550	1.5	100.9	176	7.4	631
L4	550	3.5	115.7	163	9.5	670
L5	585	1	138.1	139	11.1	698
L6	600	1.5	175.1	97	17.3	761
L7	600–610	26	209.9	49	56.2	837
L8	825	3	257.6	10.3	40.6	927
M_u	—	—	—	0	25.2	225
M_o	—	—	—	313	2.6	602
M1	510	Very short	18.9	278	3.2	593
M2	550	0.67	86.3	184	6.7	576
M3	855	2.5	265.0[b]	—	—	—
M4	865	2.5	266.3[b]	—	—	—

[a] Heated in N_2 to 825°C. and then in vacuum for 6 hr. at 825°C.

[b] Sum of weights of evolved CO_2 and CO.

for the acid–base titrations, CO_2 being eliminated by boiling. Pyrex vessels (except pipets and burets) were employed throughout. A special buret, capable of reproducing titers to 0.005 ml., was employed for small sorptions of acid and base. Each sorption value in the tables is the mean of two independent determinations, which seldom differed by more than 1% in the case of NaOH and iodine, and 3% in the case of the acids.

Hexaiodobenzene Charcoal

Hexaiodobenzene was prepared by Rupp's method (3), and purification of the large amount required was effected by crystallization from nitrobenzene or (preferably) *o*-dichlorobenzene. The charcoal was prepared by electrically heating the C_6I_6 in silica boats in a Pyrex tube, at first *in vacuo* at 200°C. (to remove adsorbed water), then in a stream of purified nitrogen at 450°C. (to decompose the C_6I_6), and finally *in vacuo* at 550–825°C. (to remove iodine). The nitrogen stream was freed from hydrogen, oxygen, CO_2, and H_2O by treatment with, successively, hot CuO (25 cm.), hot Cu gauze (30 cm.), 10% NaOH, concentrated H_2SO_4, and P_2O_5 (90 cm.). Two samples (*X* and *Y*) of charcoal were prepared.

RESULTS AND DISCUSSION

The Sorption of Base

The relevant sorption data are shown in Table I, where J_u, L_u, and M_u refer to the outgassed unoxidized charcoal, and J_o, K_o, L_o, and M_o to the charcoal after oxidation at 400°C. and before thermal treatment. It will be seen that whereas unoxidized charcoal sorbed appreciable amounts of acid but no base, after oxidation the sorption of base was very marked, while that of acid was reduced to very small proportions. The thermal treatment of the oxidized charcoal decreased the sorption of base and increased that of acid to an extent dependent upon the temperature and period of heating.

TABLE II

Composition of Gases Evolved During Thermal Treatment[a]

Expt.	H_2O	CO_2	CO	(H_2O + CO_2 + CO) − (loss in wt.)
*L*1	7.0	26.7	12.4	4.8
*L*2	8.4	33.5	26.1	7.6
*L*3	8.0	52.0	51.8	10.9
*L*4	9.6	54.9	59.8	8.6
*L*5	7.3	—	—	—
*L*6	6.5	80.3	96.7	8.4
*L*7	5.2	94.2	120.9	10.4
*L*8	9.5	93.4	161.7	7.0
*M*1	5.9	13.8	3.1	3.9
*M*2	6.6	47.4	38.9	6.6
*M*3	8.6	87.0	178.0	—
*M*4	14.7	87.4	178.9	—

[a] All quantities expressed as mg./g. charcoal.

Weller and Young (4) have produced evidence that the maximum uptake of NaOH by a highly oxidized charcoal is practically attained when the charcoal remains in contact with the solution for 24 hr., and the concentration of unsorbed base is not less than about 0.15 *N*. In the experiments of Table I, 0.2 *N* NaOH was used, which ensured that the final concentration was always greater than 0.15 *N*, and since the time of contact was uniformly 24 hr. throughout the investigation we have reason to believe that our figures are near the true saturation values.

Table II gives the quantities of H_2O, CO_2,, and CO evolved from the oxidized charcoal, during the thermal treatment, in the *L* and *M* series of experiments. The figures in the last column reveal that the observed loss in weight of the charcoal (Table I) was consistently less than the sum of the weights of the gases evolved, by an amount comparable with that of the liberated water. It appeared that the charcoal rapidly re-sorbed this amount of water during the interval of 15–20 min. which elapsed between the removal of the charcoal from the furnace tube, at the conclusion of the thermal treatment, and the determination of its weight. In support of this view it was found that if the charcoal was returned to the furnace tube (kept free from water vapor) at the end of the above interval and reheated, it yielded approximately the same quantity of water again. The re-sorption of water occurred despite the fact that for most of the 15–20 min. the charcoal was stored in a desiccator.

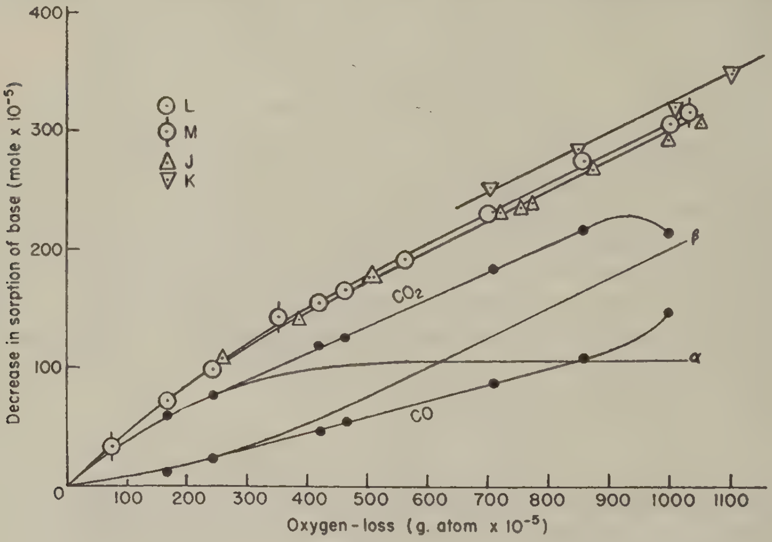

FIG. 1. Relationship between decrease in sorption of base and oxygen loss.

Figure 1 shows the relationship between the decrease in the sorption of base and the "oxygen loss" of the charcoal, produced by the thermal treatment. By "oxygen loss" is meant the oxygen evolved as CO_2 and CO. The decrease in sorption is calculated on 1 g. of the initial oxidized charcoal, i.e., is equal to

$$a - (1 - w)b,$$

where a = base sorbed by 1 g. initial charcoal, b = base sorbed by 1 g. final charcoal, and w = loss in weight (in grams) of 1 g. initial charcoal. For the L series, $a = 311 \times 10^{-5}$ mole, the mean of two values (see L_o in Table I), the one (= 317) obtained with a freshly oxidized charcoal and the other (= 304) with charcoal which had been stored for 3 months, during the second half of which period the experiments were carried out. For the M series, a = 313 (see M_o in Table I). In experiments $M3$ and $M4$ the charcoal, after heating in nitrogen, was subjected to complete combustion without removal from the furnace tube, and no sorption experiments were done. However it is certain that the drastic thermal treatment would reduce the sorption of base to very small proportions, and it is assumed that b in these experiments may be taken as zero without introducing serious error.

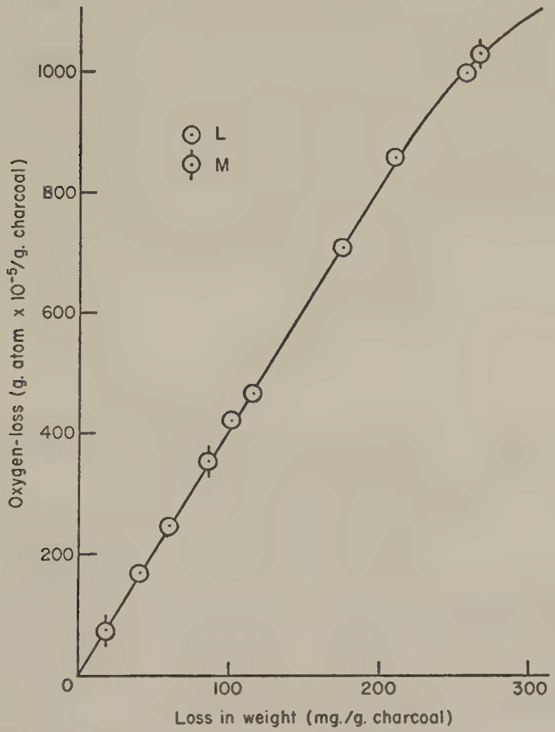

FIG. 2. Relationship between loss in weight and oxygen loss.

As will be seen from Fig. 2, the plots of oxygen loss against loss in weight of the charcoal for the L and M series give a common curve which is linear except at very high losses. In the case of experiment $L5$ and all the experiments of the J and K series, the oxygen loss is derived from the observed loss in weight by interpolation on this graph.

The points for the L series in Fig. 1 give a smooth curve of simple shape. As the oxygen loss increases from zero to about 600×10^{-5} g.-atom the slope continuously decreases from the value corresponding, in the limit, to the loss of 2 oxygen atoms for a decrease in sorption of 1 molecule of base. At oxygen losses greater than about 600 the graph is linear, with a gradient corresponding to 4 atoms of oxygen/molecule of NaOH. The simplest interpretation of these results seems to be that two types of surface oxygen-complex are involved in the sorption of base, the ratio "atoms of oxygen/molecules of base" being 2:1 in the case of the one ("α-complex"), and 4:1 in the case of the other ("β-complex"). Obviously in any given case the amounts of oxygen corresponding to those of the two complexes eliminated by the thermal treatment, and the respective decreases in the sorption of base can be calculated from the experimental data by means of the following expressions

$$x + y = \text{observed decrease in sorption of base}$$

and

$$2x + 4y = \text{observed oxygen loss.}$$

where x and y represent the decreases in sorption of base resulting from the destruction of α- and β-complexes, respectively.

The values of x and y deduced from the smooth curve for the L series are shown in Fig. 1. The oxygen loss corresponding to complete suppression of sorption of base, i.e., to a decrease of 311×10^{-5} mole, is 1034×10^{-5} g.-atom. Hence, as the x and y curves indicate, the maximum value of x is 105×10^{-5}, and that of y, 206×10^{-5} mole. We can therefore derive the sorption and oxygen content of each type of complex, at any stage of the thermal treatment, as set out below:

	α-Complex	β-Complex	Total
Sorption of base (mole $\times 10^{-5}$)	$105 - x$	$206 - y$	$311 - (x + y)$
Oxygen content (g.-atom $\times 10^{-5}$)	$210 - 2x$	$824 - 4y$	$1034 - (2x + 4y)$

In the J and K series the estimation of the loss in weight was probably somewhat less reliable than in the L series, and less care was taken to minimize reoxidation of the charcoal by exposure to the atmosphere after the thermal treatment. Actually, however, the points for the J series give a curve very close to that for the L series, which is to be expected, since the initial sorption of base was the same (311×10^{-5} mole). Similarly the M points (initial sorption $= 313 \times 10^{-5}$ mole) lie on or near the L curve. The K points give a straight line parallel to the linear portion of the L

curve but lying well above it. In this case the initial sorption (359×10^{-5}) is considerably greater than in the other series, and corresponds to the higher initial total oxygen content of 1160×10^{-5} g.-atom, as estimated from the K graph. These figures give 276×10^{-5} g.-atom of α- to 884×10^{-5} of β-oxygen, compared with 210 to 824 in the case of L_o. Hence the sorption due to the α-complex has been augmented by 33, and that due to the β-complex by only 15. The greater increase in the α-sorption readily accounts for the fact that the K curve lies above the L curve.

Weller and Young (4) found that their oxidized charcoal TUC-45, containing a total of 12.7% oxygen, sorbed 45×10^{-5} mole NaOH/g. from 0.03 N solution after 0.5 hr. contact. On heating in vacuum for 24 hr. at 900°C. the oxygen content was reduced to 4.6% and the sorption to 4×10^{-5} mole/g. The charcoal initially sorbed 220×10^{-5} mole from 0.5 N solution after at least 24 hr. contact, i.e., about five times the previous amount. No experimental figure is given for the sorption, under these (maximum) conditions, by the charcoal after the thermal treatment, but probably no serious error is entailed by taking it to be about five times the value obtained at the lower concentration, i.e., as 20×10^{-5} mole. Thus a decrease in sorption of about 200×10^{-5} mole was accompanied by an oxygen loss of 8.1%, i.e., 500×10^{-5} g.-atom. In the case of the L series this loss corresponds to a decrease in sorption of 175×10^{-5} mole, and between 175 and 200 for the K series. Hence the present results are comparable with those of Weller and Young, who used charcoal prepared from sawdust and activated with $ZnCl_2$.

TABLE III

Composition of Oxidized Charcoal

Analysis	Weight in mg./g. charcoal					Deficiency
	H_2O	O	C	H	Total	
						mg.
*M*3	8.6	165.0	807.0	4.6	985.2	14.8
*M*4	14.7	165.8	802.5	4.6	987.6	12.4
Mean	—	165.4	804.8	4.6	986.4	13.6

The composition of the oxidized charcoal M_o, as determined in the duplicate experiments $M3$ and $M4$, is recorded in Table III, where H_2O = water evolved during the heating in nitrogen, O = oxygen present in the CO_2 and CO evolved under the same conditions, C = total carbon = sum of carbon in CO_2 and CO obtained as above and from combustion of the residual charcoal, and H = hydrogen present in the water collected during the combustion. Allowing for an ash content of 0.04%, the mean deficiency is 13.2 mg./g. On the assumption that all of this is chemisorbed oxygen, the total amount of such oxygen is 179 mg. (or 1119 $\times$ 10^{-5} g.-atom)/g. As previously indicated, the sorption would be nearly, if not completely, reduced to zero by the thermal treatment, which produced an oxygen loss of 165 mg. (or 1034 $\times$ 10^{-5} g.-atom)/g. Hence at least 92% of the chemisorbed oxygen could be concerned in the sorption of base. However, it seems probable that part of the deficiency is not chemisorbed oxygen, and possible that none of it is. Some, or even all, could be oxygen present as water, since there is more than sufficient hydrogen for this. Again some oxygen and hydrogen might be present in products of partial decomposition of the sugar. It thus appears possible that complete liberation of the chemisorbed oxygen coincides with complete disappearance of the sorption, in which case it would be highly probable that the whole of the chemisorbed oxygen is involved, in some way or another, in the sorption. Weller and Young (4) quote analytical values varying from 2.9 to 4.6% for the oxygen in unoxidized outgassed charcoal (sorption of base = 0), and in oxidized charcoals after thermal treatment sufficient to reduce the sorption to small values. Since the oxygen was found by difference, the oxygen figures include any oxygen present as water, etc. Moreover, as with M_o, the hydrogen exceeds the amount required to account for all the oxygen as water. It is therefore possible that these charcoals, also, contained little chemisorbed oxygen.

Strickland-Constable (5) reports that of 25 cc. (or 223 $\times$ 10^{-5} g.-atom) of oxygen chemisorbed on 1 g. of a coconut charcoal oxidized by treatment with N_2O at 400°C., only 2 cc. (or 18 $\times$ 10^{-5} g.-atom), i.e., 8%, had acidic properties, the assumption being that 1 atom of chemisorbed oxygen is equivalent to 1 molecule of sorbed NaOH. On the same basis, 313 of 1034 $\times$ 10^{-5} g.-atom, or 30% of the oxygen on charcoal M_o would be acidic. However, Strickland-Constable's estimate must be far below the true value, since he used the very low alkali concentration of 0.02 N and his time of contact was only 0.5 hr. In addition, the grounds for the assumption that 1 molecule of NaOH is equivalent to not more than 1 atom of oxygen are not stated and are not obvious. We conclude that the evidence advanced by Strickland-Constable is insufficient either to justify his hypothesis of the formation of a great variety of surface oxides by oxidation at 400°C., or to invalidate our suggestion that there are only two types of complex produced, both of which are involved in the sorption of base.

Our results agree with those of Weller and Young (4) in showing that large quantities of oxygen can be chemisorbed at 400°C. For example, according to the analyses of M_o, the ratio "atoms of carbon/atoms of oxygen" in this case is 6.5 (or somewhat less):1. In contrast, Strickland-Constable (5) draws the "general conclusion" that "only very few points on the surface of the carbon are available at any one time for the attachment of O atoms for the formation of either stable or labile oxides." This view is based on the data for his charcoal Lot III, described as "fully charged with surface oxides," and containing but 1 atom of oxygen per 40 atoms of carbon.

At present little more can be said about the nature of the α- and β-complexes than that the former is much less stable than the latter. Reference to Table I reveals that heating for 1 hr. at 600°C. eliminated all the α-complex, the bulk disappearing in about 15 min., while appreciable quantities of the β-complex were still undecomposed after 40 hr. at 600–615°C.

The curves marked "CO_2" and "CO" in Fig. 1 are, respectively, the plots of (O evolved as CO_2)/2 and (O evolved as CO)/4 against the total loss of oxygen. Up to an oxygen loss of about 250×10^{-5} g.-atom these curves appear to coincide with those for the α- and β-sorptions. Between oxygen losses of about 250 and about 850×10^{-5} g.-atom the ratio of CO_2 to CO is constant, but decreases at higher losses, probably as the result of some reduction of the CO_2 at the high temperature employed. The partial coincidence with the sorption curves suggests that initially the α-complex gives only CO_2 and the β-complex only CO, but it is difficult to account for departure from this state of affairs at higher oxygen losses.

The Sorption of Acid

According to the careful work of Steenberg (1) the sorption of HCl and HNO_3 from 30 ml. of 0.0133 *N* solution by 1 g. of unoxidized charcoal requires about 48 hr. for completion, but is about 98% complete in 24 hr. Further, using 48 hr. contact, he obtained isotherms showing that the sorption is practically constant for equilibrium concentrations greater than 0.014 *N*. Hence, since 0.1 *N* solutions and 24 hr. contact were used in the present work, the sorption values must be very close to saturation. We determined the isotherm for iodine in the case of a well-oxidized charcoal, and found that the sorption became almost independent of the equilibrium concentration, for values of this greater than about 0.15 *N* after 24 hr. contact. The sorption values in Table I were obtained under these conditions, and are therefore comparable with one another and may serve, with certain reservations, as an approximate measure of the surface area of the charcoal.

In Fig. 3*a* the increase in sorption of acid is plotted against the decrease in sorption of alkali. The increase in sorption of acid is given by

$$d(1 - w) - c,$$

where c = acid sorbed by 1 g. of initial charcoal and d = acid sorbed by 1 g. final charcoal. Initially the *J* points are scattered about a straight line which starts at the origin and possesses a slope corresponding to a gain of 1 molecule of HCl for a decrease in NaOH of 40 molecules. When the decrease in NaOH reaches about 200 × 10^{-5} mole, the curve changes direction quite rapidly to give a second straight line of slope corresponding to 1 molecule of HCl increase per 4 molecules NaOH decrease. The *M* points and a majority of the *L* points fit the *J* curve, while the *K* points give a curve which has the same initial slope, but changes direction at about 250 × 10^{-5} mole NaOH and possesses a final slope such that HCl: NaOH = 1:5. Nitric acid is sorbed more strongly than HCl, but gives a curve of similar shape.

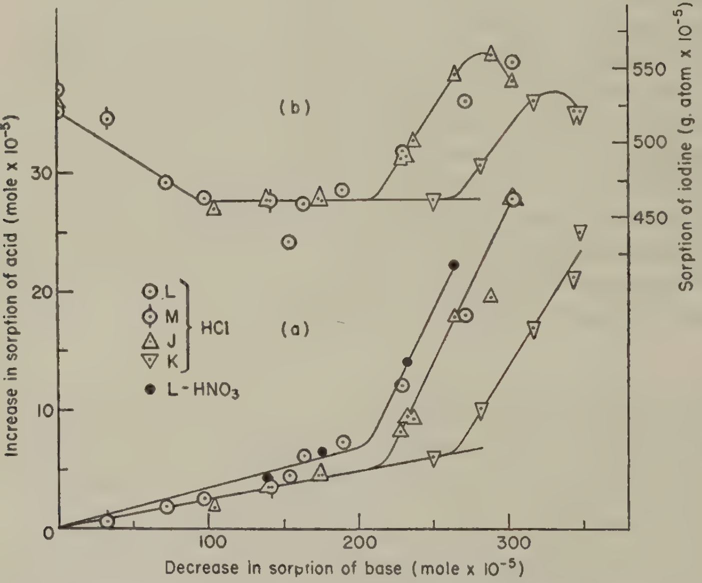

FIG. 3. Relationships between decrease in sorption of base, increase in sorption of acid (*a*), and sorption of iodine (*b*).

Steenberg (1) has advanced much evidence in favor of the view that the sorption of strong inorganic acids consists essentially in a van der Waals' adsorption of the hydrogen ions ("primary adsorption"), which then hold near the surface, by electrostatic attraction, an equivalent amount of the anions ("secondary adsorption"). It would appear that our results are more readily interpreted on this basis, than in terms of neutralization of the acid by basic surface oxides, as postulated by Schilov (6), King (7), and others [see Ref. (1) for full account]. If, as would be necessary to suppose, the increase in sorption of acid corresponding to the steep part of the curve, e.g., from about 6.0 to 27.5 × 10^{-5} mole for the *J* series, is brought about by the action of basic oxide produced by decomposition of the second half of the β-complex, it is difficult to understand why decomposition of the first half of the complex results in so much smaller an increase in the sorption (from 0.0 to 6.0×10^{-5} mole or less for *J* series).

The number of points on a carbon surface which are capable of adsorbing hydrogen ions is always small and, hence, in a well-oxidized charcoal so much of the surface is covered with oxygen that few, if any, sites are left. As the thermal treatment proceeds, sites become available at a rate which, if the sites are uniform in activity, is roughly proportional to the loss of oxygen or the decrease in sorption of base. The change in slope of the curves in Fig. 3*a* indicates that the rate of production of sites is greater in the later than in the earlier stages of the treatment.

This interpretation of the behavior of the acids is supported by the results obtained with iodine. In Fig. 3*b* the sorption of iodine for the *K* series is plotted against the decrease in sorption of base. The sorption with which we are here concerned is the amount of iodine taken up by the actual residue left from 1 g. of fully oxidized (i.e., initial) charcoal, at any given stage of the thermal treatment, i.e., sorption of iodine $= (1 - w)e$, where e = iodine sorbed by 1 g. of residual (i.e. final) charcoal. The points for the other series are the plots of $(1 - w)e - k$, where k = constant, having the values 71, 134, and 66 for the *K*, *L*, and *M* series, respectively. It will be seen that as the heating proceeds the sorption of iodine at first decreases, then becomes approximately constant, but later begins to rise rapidly in linear fashion at about the same stage as that at which the inflection occurs in the curve for the sorption of acid. This parallelism in the behavior of the acids and that of iodine is not easy to understand if the acid is fixed by a basic surface oxide, but is to be expected if the acid is physically adsorbed, since iodine is held on a carbon surface by van der Waals' forces.

Reference to Table I reveals that at the stage at which activation, as regards physical adsorption, of the carbon surface sets in, there is a marked decrease in the rate at which the sorption of base decreases. For example, in the case of the *J* series, heating at 600°C. reduces the sorption of base by 175 units in 15 min., but only 60 units more than this in 1 hr., while heating at 600–610°C. for 6 hr. produces a further reduction of still less, actually about 30. Thus the activation appears to accompany the removal of the highly stable complexes, and it is reasonable to suppose that it is due to the rupture of an exceptionally strong linkage between the carbon atoms which leave the surface as CO_2 and CO, and the neighboring atoms. It may well be that the numbers, relative positions, and degrees of saturation of these are such that they form a surface which adsorbs more strongly than that exposed at earlier stages of the thermal treatment.

The initial decrease in the sorption of iodine is obscure, but the possibility exists that it may be due to oxidation of the iodine by some portion of the chemisorbed oxygen, since experiments carried out in this laboratory by R. D. Easton and J. M. Lowenstein have shown that oxidation of quinol is brought about by the oxidized charcoal in the complete absence of gaseous oxygen. It may be added that this result is at variance with the conclusion of King (8) that the charcoal acts simply as a catalyst for oxidation by gaseous oxygen. We tentatively suggest that the final falling-off in the adsorption of the iodine is due to incipient graphitization of the charcoal (resulting from the drastic conditions required to remove the last portions of oxygen) and the consequent reduction in the surface area of the charcoal.

The Influence of Water

The results of his analyses of sugar charcoal treated with air at 500°C. led Ockrent (2) to state that the "acid oxide" or "acidic substance" which confers on charcoal activated at 500° the property of adsorbing alkali hydroxides is the "tightly bound unimolecular layer of adsorbed water which has been found to exist by the author." It was concluded from the analyses that the charcoal was composed exclusively (within the experimental error) of carbon and water, i.e., no chemisorbed oxygen was present. Ockrent observed that when the charcoal was heated in a stream of nitrogen, water was desorbed discontinuously at definite temperatures, the first considerable rush (apart from water adsorbed from the atmosphere at room temperature) occurring at about 580°C., and further amounts being evolved at approximately 650°, 780°, and 940°C. This behavior was thought to indicate that the water formed a very firmly bound adsorbed layer on the surface of the charcoal.

The results of the present investigation [also the analyses of Weller and Young (4), published during the course of our work] are clearly incompatible with Ockrent's hypothesis. On the one hand the charcoal after prolonged treatment with air or oxygen at 400° C. obviously contained large amounts of chemisorbed oxygen, and a decrease in the sorption of base produced by thermal treatment was accompanied by a corresponding loss of the oxygen. On the other hand the evolution of water bore no relation to the decrease in sorption of base. Whereas the sorption decreased continuously with increase in the temperature or period of the treatment over the range 550–825°C., the amount of water liberated was independent of these factors, undergoing only irregular and relatively small variations (see Table II). All the evidence suggests that little, if any, of this water was chemisorbed. The amounts were very much smaller than those obtained by Ockrent on heating to 850°C. (about 130–150 mg./g. charcoal), being even less than the quantities obtained at 250°C. and found by him to consist of water physically adsorbed from the atmosphere at room temperature. Visual observation strongly suggested that the bulk of the water in our experiments was released between 200° and 300°C., and mention has already been made of the rapidity with which the water was resorbed on exposure of the charcoal to the atmosphere.

The apparent absence of chemisorbed oxygen in the case of Ockrent's charcoal is not altogether surprising, since he heated a large mass (109 g.)

TABLE IV

Influence of Water on Sorption

Expt.	Procedure	Temp.	Period	Sorption[a] (mole × 10^{-5}/g. charcoal)		
				NaOH	HCl	Iodine
		°C.	*hr.*			
C_u1	Charcoal *A* outgassed	825	6	0	32.0	287
2	do	825	6	0	33.1	327
C_o1	C_u1 heated in dry air	370	24	216	5.6	517
2	do	370	24	226	5.3	517
3	C_u1 heated in moist air	370	24	223	4.1	512
4	do	370	24	240	3.0	526
5	C_u1 heated in dry air	440	24	263	2.5	531
6	do	440	24	266	3.5	531
7	do	475	24	214	6.4	578
8	do	525	24	66.5	12.7	522
9	do	520	24	50.5	18.5	498
10	do	750	24	7	42.5	762
1*C*	*A* outgassed as above, then heated in dry nitrogen	430	24	7.5	28.5	359
2*C*	As for 1*C*, but moist N_2 used	430	24	2.7	30.3	369
*D*1	*A* outgassed as above, heated in dry air for 24 hr. at 425–440°C., then heated in vacuum	425	24	228	5.8	554
2	do	520	3	202	7.3	565
3	do	495	20	180	9.0	583
4	do	520	24	166	9.8	606
5	do	515	48	143	13.1	626
6	do	535	24	122	13.6	653
7	do	555	48	108	16.5	660
8	do	750	Very short	78	25.2	725
9	do	750	1	56	31.1	742
10	do	825	1	26.2	45.3	884
H_u1	Charcoal *X* outgassed	825	6	38	84	—
H_u2	Charcoal *Y* heated in nitrogen	825	6	33	76	1455
H_o1	Charcoal *X* outgassed as above, then heated in dry air	430	6	279	32	—
H_o2	*Y* heated in nitrogen as above, then in dry oxygen	425	8	372	11	656

---

[a] From decinormal solution.

of the material for only 2 hr. in a very rapid stream of air at 500°C. (9). As is indicated by the data for experiments C_o5 to C_o10 in Table IV, treatment with air at 500°C. is much less efficient than at 400°C., in oxidizing the charcoal [see also King (7)], and our experience suggests that the other conditions employed were probably unfavorable. If the amount of chemisorbed oxygen was small the charcoal would sorb little base, but Ockrent gives no information with regard to the behavior of his charcoal in this vital respect.

Kolthoff (10) has reported that the presence of water vapor increases the rate of combustion of charcoal during treatment with air at 400°C., and also appears to "promote . . . formation of the acidic substance." Miller (11) likewise concluded that "For rapid formation of the complex acid it is necessary to heat the charcoal at 300–400° in the presence of air and water vapor." These results are regarded by Ockrent as support for his hypothesis. Our experiments (Table IV), however, showed no differences between the action of very carefully dried air (Expts. C_o1 and C_o2) and that of moist (saturated) air (Expts. C_o3 and C_o4) at 370°C. The sorptions of base, acid, and iodine by the resulting charcoals were the same in the two cases, as also were the losses in weight (25.1% for dry, and 26.3% for moist air) due to combustion. It seems possible that the more rapid combustion observed by Kolthoff, which may have had the effect of enlarging the surface area and thereby enhancing the sorption of base, was connected with the fact that he used a different charcoal, namely "carbon medicinalis Neu Merck." There is much evidence (12, 13, 14) that the degree of interaction between water vapor and charcoal depends upon the origin of the charcoal.

Another indication that the presence of moisture in the oxidizing gas has no influence on the properties of the resulting charcoal is afforded by the data obtained with samples of charcoal treated with intensively dried air at different temperatures (C series in Table IV). The plot of "sorption of base/sorption of iodine" against "sorption of acid/sorption of iodine" will be found to give a curve very similar to that given by the data of King (7), who employed moist oxygen.

From the results of experiments $1C$ and $2C$, in which nitrogen (probably containing a little oxygen), carefully dried in the one case and saturated with water in the other, was streamed at 430°C. over unoxidized outgassed charcoal, it will be seen that treatment with water vapor alone did not produce a material capable of sorbing base.

Since Ockrent found that when his charcoal was heated in nitrogen, the first considerable rush of water occurred at about 575°C., he attaches great importance to the observations made by Kolthoff (*loc. cit.*) that while 30 hr. heating in vacuum at 500°C. did not diminish the sorption of base by charcoal ("ash-free Nuchar") oxidized at 400°C., heating at 575°C. or 600°C. for 25 hr. produced a considerable decrease. Again, however, our results differ markedly from those of Kolthoff in that heating the charcoal, oxidized at 425°C., in vacuum for 24 hr. at 495°C. (Expt. *D*3) reduced the sorption of base by at least 24% (cf. Expt. *D*1). Heating for the same period at temperatures above 500°C. but below 575°C. resulted in still larger decrements (Expts. *D*4 and *D*6).

The experiments with hexaiodobenzene were undertaken with the object of ascertaining if a charcoal free from hydrogen, and therefore from water, was capable of sorbing base, after treatment with oxygen at 400°C. Analysis showed, however, that the unoxidized outgassed charcoal probably contained a little hydrogen, though much less than the sugar charcoal. As the data in Table IV show, the sorption of base after oxidation for a relatively short time was very marked.

Acknowledgments

We thank the Department of Scientific and Industrial Research for the grant of a maintenance allowance (to J. H. W.), and the Moray Fund of the University of Edinburgh and Imperial Chemical Industries Ltd. for grants for the purchase of apparatus.

Conclusions

1. The hypothesis that the sorption by charcoal of strong inorganic bases from aqueous solution is due to the presence of chemisorbed water is untenable.
2. Sorption of base is due to the presence of chemisorbed oxygen, which appears to form two types of complex. In the one type (α-complex) two atoms, and in the other (β-complex) four atoms of oxygen are equivalent to one molecule of sorbed sodium hydroxide.
3. At temperatures in the neighborhood of 400°C. sugar (and hexaiodobenzene) charcoal can fix large quantities of oxygen. The greater part, possibly the whole, of this oxygen is involved in the sorption of base.
4. Oxygen chemisorbed on sugar charcoal does not form basic complexes. Strong inorganic acids are physically adsorbed on the carbon surface.

References

1. Steenberg, B., Adsorption and Exchange of Ions on Activated Charcoal, Almqvist and Wiksells Botyckeri AB, Uppsala, 1944.
2. Ockrent, C., *J. Chem. Soc.* **1934**, 291.
3. Rupp, E., *Ber.* **29**, 1625 (1896).
4. Weller, S., and Young, T. F., *J. Am. Chem. Soc.* **70**, 4155 (1948).
5. Strickland–Constable, R. F., *Trans. Faraday Soc.* **34**, 1074, 1374 (1938).
6. Schilov, N., Schatunovskaja, H., and Tschmutov, K., *Z. physik. Chem.* **A149**, 211 (1930).

7. King, A., *J. Chem. Soc.* **1937**, 1489.
8. King, A., *J. Chem. Soc.* **1936**, 1688.
9. Ockrent, C., *J. Chem. Soc.* **1932**, 613.
10. Kolthoff, I. M., *J. Am. Chem. Soc.* **54**, 4473 (1932).
11. Miller, E. J., *J. Phys. Chem.* **36**, 2967 (1932).
12. Muller, S., and Cobb, J. W., *J. Chem. Soc.* **1940**, 177.
13. Gadsby, J., Hinshelwood, C. N., and Sykes, K. W., *Proc. Roy. Soc.* (London) **187A**, 129 (1946).
14. Taylor, H. S., and Neville, H. A., *J. Am. Chem. Soc.* **43**, 2055 (1921).

FILMS OF OMEGA-BRANCHED FATTY ACIDS[1]

Harry Sobotka, Shirley Rosenberg and Aina Birnbaum

Department of Chemistry, The Mount Sinai Hospital, New York, N. Y.

Received October 13, 1950

Abstract

This investigation deals with the effect of terminal branching upon the behavior of long-chain aliphatic acids. Monomolecular layers of these compounds, spread on buffer solutions, are characterized by determination of the force/area relationship. On the basis of their minimum molecular area in condensed films, the tilt of the molecule against the surface was computed and various possibilities for the conformation of the terminal groups were evaluated. The capability of building up polylayer films on a solid surface and the character of such films reflects the shape of the molecule and its deviations from the prismatic form. A number of surface phenomena such as contact angles, surface reflection, and skeletonization by dissolving the free fatty acids in the film are treated. Although films of branched fatty acids resemble those of normal fatty acids in several points, a striking difference is revealed by their enormous surface volatility. *Molecular Sublimation* of branched fatty acids across blankets of stearic acid, several hundred Angström units thick, is an important manifestation of the dynamic state prevailing in crystalline polymolecular films.

I. Materials

This is our first report on the investigation of long-chain aliphatic compounds of polar character with modification and variation of the terminal group. In order to learn the effect of the crowding of terminal methyl groups on surface properties (1,2), we have synthesized a series of *neo*-fatty acids with an even number of carbon atoms from neopalmitic acid, $(CH_3)_3C \cdot (CH_2)_{11}CO_2H$ to neolignoceric acid, $(CH_3)_3C \cdot (CH_2)_{19}CO_2H$ (3). In addition to these novel compounds we have prepared several *iso*-acids $(CH_3)_2CH \cdot (CH_2)_nCO_2H$. Members of the *iso*-series have been recognized as constituents of degras by Dr. A. W. Weitkamp (4) to whom we are greatly indebted for samples of these natural compounds. For purposes of further comparison, we have used one of Weitkamp's *anteiso*-acids, $(C_2H_5)(CH_3)CH \cdot (CH_2)_nCO_2H$; finally, we have prepared the triply branched 13,15,15-trimethylpalmitic acid (5).

II. Spreading on Aqueous Solutions: H-Films

The behavior of normal fatty acids, when spread on aqueous solutions as so-called *H*-films, has been extensively investigated by Langmuir,

---

[1] This investigation was in part supported by the Office of Naval Research, under contract N7onr-452, Task Order I, and by the Permanent Science Fund of the American Academy of Arts and Sciences.

Adam, and others. Measurement of the surface area occupied by a given number of molecules under various lateral pressures permits the construction of Force/Area (F/A) diagrams. From such curves one may learn at which pressures and temperatures fatty acids exist as two-dimensional gases, liquids, or solids. A comparison of the molecular area A_m with the cross section of the molecule perpendicular to its axis, obtained from other data, gives the tilt of the molecule under given conditions. The pH of the bath furnishes an additional variable. On this basis, we have studied *H*-films of the normal, *iso*- and *neo*-isomers of palmitic, stearic, arachidic, behenic, and lignoceric acids.

On a Langmuir trough (Cenco), provided with a torsion head, we spread 0.12 ml. of a 0.05% solution of the acid in benzene. The barrier consists of a mica float which is attached to the walls by two flexible Teflon strips (6) to keep the film confined. The bath contains 10^{-4} M barium acetate and 0.5×10^{-4} M potassium bicarbonate to bring the pH to 6.6. The measurements are recorded both during compression and decompression of the film. The identity of the two limbs of the graph serves as a control against leakage (see also below).

In another series of experiments, carried out by Miss Pat Lambert, we measured the volume of a 0.05% solution of a given acid in benzene which could completely cover the entire surface in a rectangular tray of 257.1 cm² area. In agreement with N. Miller (7), whose procedure we followed, the molecular area was found to correspond closely with that measured by the surface balance under a force of 9.5–10 dynes/cm.

Parallel experiments were carried out on a bath in which the equivalent amount of cadmium acetate was substituted for the barium salt. In a few representative cases, strontium chloride and zinc acetate of corresponding normality were used. The F/A curves with these other bivalent metal ions coincided within the limits of accuracy of the technique with those obtained on the barium bath. The nature of the bivalent metal is thus of no account for the molecular areas in the range of pressures studied. The averages of our measurements for two representative pressures, 25 and 10 dynes/cm., are summarized in Table I. This body of data may be discussed from two important viewpoints, the shape of the curves and the absolute value of the asymptotically approached minimum area.

The melting temperature of the normal acids under investigation ranges from 63° to 84°, at least 40°C. above the experimental temperature; the melting points of the *iso*-acids are 1–2° below those of their straight-chain isomers, but those of the *neo*-acids range from 44° to 64°, i.e., nearly 20° lower than those of the normal acids. The values for the normal acids at 25 and 10 dynes/cm. illustrate the steep gradient of the F/A curve, indicating compressibility of the films of *ca.* 5% or less between the selected pressures. The F/A curves of the *neo*-acids are considerably slanted with differences in area between 10 and 25 dynes/cm. of 15%, 20%, and more. The *iso*-acids take an intermediate position. The data for the palmitic and stearic acids reflect slightly greater compressibilities because of the smaller differences between the experimental temperature and the melting point which is known to affect the shape of the F/A curves (8). A comparison with the F/A curves for myristic acid indicates that all our curves down to 10 or even 5 dynes/cm. are within the condensed region and well towards the left side of the inflection points characterizing transition from gaseous to condensed films.

All curves were retraceable, i.e., their points on decompression coincided with those obtained during compression. With the branched acids certain irregularities were noticed in the nature of slow contraction under medium and high pressures. A film of neostearic acid did not contract when left for 10 min. under 5 and 10 dynes/cm. pressure, but under 15 dynes/cm. pressure its area contracted 4% and 1.5% respectively, during the first and second 5-minute period; then it became constant. We therefore measured all areas 5 min. after adjustment of the pressure. Such hysteresis phenomena have been treated by Adam (9), and in the case of proteins, where they are partially irreversible, by Langmuir and Waugh (10). Depending on the position, frequency, and duration of stops during compression and decompression, discontinuities in F/A curves may appear as artifacts and should be interpreted with caution, when looking for points of transformation (11) and for binary complexes of discrete integral proportions (12). In the case at hand, the hysteresis depends on the velocity with which the bulky terminal groups respond to the lateral pressure in forming a regular array. An investigation of this phenomenon with variation of the terminal groups may well serve as a simplified two-dimensional model for the study of crystallization phenomena.

TABLE I

Molecular Area A_m in A.^{2} of Fatty Acids with 16–24 C Atoms on Barium Bath of pH 6.6 at 18°C.

	Normal acid		*Iso*-acid		*Neo*-acid	
F (dynes/cm.)	25	10	25	10	25	10
Palmitic acids	25.6	26.4	33.6	41.8	32.0	38.0
Stearic acids[a]	19.7	22.3	26.9	31.3	31.3	36.6
Arachidic acids	20.7	21.2	22.6	25.0	25.7	29.8
Behenic acids	17.6	18.7	23.4	26.5	25.7	31.5
Lignoceric acids	17.5	19.0	18.5	22.0	22.5	30.3

[a] Measured at 26°C.

The two-dimensional pressure F under which an H-film collapses is a complex function of several factors and not too well reproducible, but the "crumple patterns" observable during collapse possess interesting features (13). For the normal fatty acid films on a barium bath, we can confirm the appearance of pleats, parallel to the compressing barrier and extending across the entire width of the tray. Easily distinguished from them are the spider-shaped patterns obtained on compression of *iso*-fatty acid films. The crumple patterns of *neo*-fatty acids are less distinct, but none the less of crystalline appearance. Films of 16-methylstearic acid, an *anteiso*-acid of m.p. 47° and of the multiply branched 13,15,15-trimethylpalmitic acid (5), m.p. 19°, are evidently liquid [cf. (Ref. 14)]; they show no patterns on collapse and, when gathering the completely collapsed film, a droplet rather than a crystalline scum is seen.

The limiting values for A_m, which the F/A curves approach asymptotically before reaching the collapse pressure, correspond to the cross-sectional area of the aliphatic chain divided by the cosine of its tilting angle. While the data for the two lowest members should be disregarded because of the aforementioned temperature relationships, one may discern a decreasing trend toward higher molecular weights not only in the normal, but also in the branched series. This we attribute to the increase of van der Waals' forces proportional to the length of the chain, but—in the case of the branched acids—also to the decrease in ratio of the incumbrance by the terminal group to the longitudinal extension of the molecule. Minimum A_m values and maximal chain length are predicated upon the assumption that the aliphatic chains form a zigzag in one plane. Joly (11) and Dervichian (15) envisage the rotation of individual C—C bonds outside this plane to form polygonal spiral forms and mixed forms in order to interpret F/A curves toward the larger A_m values; they correlate these forms with the known allomorphic forms of aliphatic compounds in the vicinity of the melting point. Whether this hypothesis is preferable to the assumption of varying tilting angles of a planar zigzag remains to be seen. But this theory may have to be adduced to explain the geometric conformation of the branched molecules in condensed films. An inspection of molecular models yields as the cross section, measured perpendicular to the bond of attachment, the values of 18.5 A.^{2} for the methyl group, 29 A.^{2} for the isopropyl group and 45 A.^{2} for the *tert*-butyl group. The cosine of the tilting angle of the entire molecule, assumed to consist of a planar zigzag, is obtained by dividing the thickness of the film (see Sec. III) by the computed length of the molecule, making allowance for the actual number of linear methylene groups which is one less for the *iso*-acids and two less for the *neo*-acids than for the isomeric normal acid. The cosine of the same angle is obtained by dividing the cross section of the aliphatic chain, 18 A.^{2}, by the observed cross section of the molecule under consideration, with the plausible assumption that the molecules are tightly packed. To this tilting angle α we add, with positive or negative sign, the angle formed between the bonds of the zigzag and the longitudinal axis of the molecule $(180 - 109)/2 =$ *ca.* 35°. Since the plane of the zigzag is not necessarily perpendicular to the surface of the film, the equator of the end group will form an angle between $(\alpha - 35°)$ and $(\alpha + 35°)$ with the surface of the film. Thus, the tilt of the *tert*-butyl may be as high as 75°, accepting tilting angles α of the chain of *ca.* 40° for the *neo*-acids, and 65° for the isopropyl group for an average molecular tilt of 30° for the *iso*-acids (Fig. 1). Evidently, these angles of 75° and 65° leave enough space for the projection of cross sections of 45 $A.^2$ (*tert*-butyl) and 29 A.^{2} (isopropyl) upon the molecular areas measured for the individual acids. While not inevitably required, the assumption of bond-rotation outside the plane of the molecule would further increase the flexibility of the end groups. With or without this alternative, the geometric possibility of close packing of omega-branched fatty acids seems established; one only has to assume a suitable tilting angle for the molecule and a larger tilting angle for the end group. It is significant for our further considerations that the end groups, especially the *tert*-butyl group, would be tilted *away* from the film surface; hence one only of the two or three terminal methyl groups would be situated in the surface itself. The branched groups must be visualized, as it were, nesting in each other in some definite steric relationship to the longitudinal axis of the titled chains.

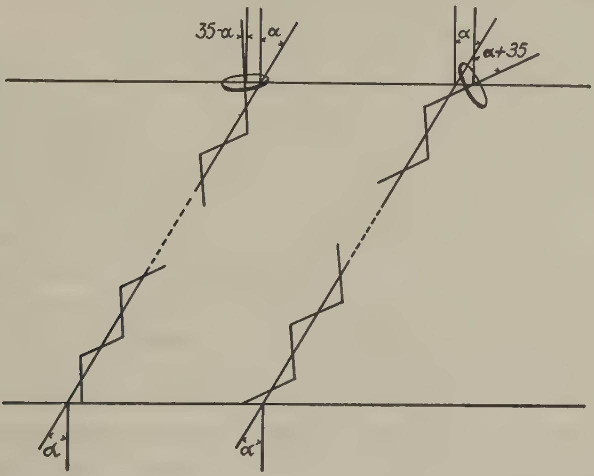

FIG. 1. Position of terminal group in relation to the aliphatic chain tilted α degrees. The two long horizontal lines indicate the upper and lower boundary of a monomolecular film. The disks, centering around the topmost limb of the zigzag, symbolize the equatorial plane of the terminal group.

Any alternative assumption, with the end groups pointing in an upward direction, requires distortion of the valence angles between the methyl groups. This point will be examined in Sec. VI, further below.

III. Built-Up Films

The technique of Blodgett and Langmuir of building up monomolecular layers on a solid base as monolayer and polylayer films has considerably widened the avenues for the study of this peculiar two-dimensional variety of the solid state. The technique of building *Y*-films by alternation of *A*-layers, formed on the down-trip, with *B*-layers, formed on the up-trip, and of *X*-films consisting of *A*-layers only, and the evaluation of film thickness by comparison of interference colors in white and in monochromatic polarized light has been repeatedly described (1,16).

We have used a buffer solution containing 10^{-4} *M* barium acetate and 2×10^{-4} *M* potassium bicarbonate with a pH of 7.35. According to Langmuir and Schaefer (17), stearic acid, spread on this bath, is converted to *ca.* 67% to a neutral soap as against 50% neutralization on a bath of pH 6.6. In the case of isostearic acid, slow and cautious operation permits the building of *Y*-layers on this bath. We have succeeded in building by 100 round trips a film consisting of 200 monolayers of barium isostearate on a chromium plate impregnated with a monomolecular layer of ferric stearate. This film displayed the bluish green of the second order when viewed from an angle of *ca.* 80° in light polarized perpendicular to the plane of incidence, and the corresponding yellow of the second order for the beam polarized parallel to the plane of incident light. The colors correspond to those seen with *ca.* 174–178 monolayers of normal barium stearate. The ratio 200:176 is definitely greater than the ratio of the chain lengths 18:17 and accounts for a greater tilt of the isostearic molecules resulting in an additional 7% decrease of thickness beyond that due to the difference in length, assuming identity of refractive index. Comparison of checkerboard patterns in white and in monochromatic D-light yielded similar figures.

Under similar conditions, *Y*-films of other *iso*-fatty acids can be obtained. The *neo*-acids, when spread on water, tend to collapse under the force of 29 dynes/cm., exerted by oleic acid as piston oil. At several occasions we were successful in obtaining *Y*-films from neolignoceric acid without achieving an exact definition of the conditions necessary for reproduction of the effect. In general, one may obtain from *neo*-acids *X*-films consisting of 20 and more *A*-layers. Not only because of their capriciousness in forming thicker films, but also because of the hazy appearance of the surface of *neo*-films, we covered them with several *AB*-layers of barium stearate which gave the usual surface with perfect reflection, best suited for optical measurements of thickness.

Under the conditions of our experiment, the standard barium stearate–stearic acid films came out about 5% thicker than the standard stearate films of Blodgett of $h = 24.4$ A. prepared at pH 6.6. The impression gained by inspection of the interference colors was confirmed by observation in the light of the sodium vapor lamp, where minimum reflection at 80° was given by a film of 44 monolayers. The average of many observations gave $h = 25.7$ A. according to the formula of Blodgett and Langmuir [Ref. (22), p. 973]. Direct comparison of interference colors on step-plates and the observation with monochromatic light yielded the following figures which take into account the aforementioned blanket layers of normal stearate:

	Thickness of monolayers on chromium	
	Comparison with normal stearic acid standard A.	Monochromatic minimum reflection method A.
Isostearic acid	22.0	22.4
Neobehenic acid	19.2	—
Normal lignoceric acid	41.9	39.1
Isolignoceric acid	33.1	32.0
Neolignoceric acid	20.6	19.7

The values show good agreement between the two methods. The decrease of thickness h from normal to iso- and neolignoceric acid is greater than the corresponding increase of molecular area A_m, given in Table I, indicating variations in "deposition ratio" (18,19).

We have also built up films of the various acids, especially of the C_{18}-set, with bivalent cations other than barium, namely, cadmium, strontium, and zinc. The spatial relationship between the two ends of the molecule finds expression in the ability to form *Y*-films and *X*-films. Excess in size of the terminal bulge at one end of the molecule over the cation at the other end limits the building-up of films to monolayers (*A*) instead of double layers (*AB*). Too great a deviation from the cylindrical or prismatic shape of the molecule completely prevents the building-up of films. Table II gives the cross section in A^2. of three cations and three end groups and the type of films obtainable by their combination on 10^{-4} M solutions of barium acetate, cadmium chloride, and zinc acetate of pH = 7.35.

Even the barium ion is smaller than the cross section of the normal fatty acids. One has, moreover, to consider that on a hypophase of pH 7.35, where as much as two-thirds of the anions are neutralized by barium, the interface between the *H*-layer and the bath is occupied by one bivalent barium atom plus one hydrogen atom in correspondence to an area of three stearic acid molecules. Our information is still incomplete with regard to the turning-around phenomena: we do not know whether, in the established form of a *Y*-layer upon emergence from the bath, the bivalent metal ion is shared by two stearic acid residues of the same layer or of adjacent layers, forming either a U or an open —.— structure, or whether the concept of such individual correspondence is altogether faulty. This question gains significance in the case of *X*-layers where the geometrically possible complete turning-around of individual stearic acid residues is likely to occur. The conditions for this inversion are not yet fully understood and fall outside the scope of the present investigation. The above purely geometric consideration is supported by the behavior of zinc stearate: the great cohesion and plaster-like character of these films must be mentioned; the symbol *Y-X* indicates that an *A*-layer is built up on the down-trip; on the up-trip, however, the deposition of a *B*-layer proceeds to a width of *ca.* 5 mm. only. At this point the film breaks along an irregular line across the slide and the lower part of the slide then emerges as a hydrophilic *A*-layer, which turns hydrophobic after it has dried. This phenomenon may be repeated twenty times on the same slide, leading to the formation of two irregularly demarcated fields, one with 40 layers of blue color, the other with 20 layers of straw-yellow color. It is plausible to assume that the *H*-layer is much more compressed on its surface than on its bottom with the small zinc ions. Thus, it breaks along the line where it is bent in the wrong direction, like a vault would break if one tried to bend it inside out.[2]

TABLE II

Cross Section of Anions and Cations and Formation of Films

	Cation..........	Barium	Cadmium	Zinc
Anion	cross section (A.^{2})	15.7	7.3	5.9
n-Stearic acid CH_3	18.5	*Y*	*Y*	*Y-X*
Isostearic acid $(CH_3)_2CH$	29	*Y-X*	*Y-X*	*X*
Neostearic acid $(CH_3)_3C$	45	(*Y*)*X*	*X*	0

In the case of the *iso*-acids a similar phenomenon, also symbolized by *Y-X*, was observed with some of the cations; but here the break occurs immediately upon the beginning of the up-trip. However, with sufficient lateral force, the deposition of the *B*-layer is resumed on the up-trip, leaving a naked *A*-film for a width of less than 1 mm., or often just a wavy and uneven line, at the top of the area.

Barium stearate–stearic acid *Y*-films of varying thickness, consisting of 30–60 monolayers, have been kept by us at room temperature, including the usual summer temperatures, for the last twelve years without showing any change in appearance with regard to the interference colors or to the brilliance of reflection. The appearance of barium isostearate–isostearic acid films of analogous specifications is equally beautiful upon emergence from the bath, but after 6 hr. a hazy appearance becomes noticeable which increases steadily. This opacity makes the checking of the colors impossible at the end of 2–3 weeks. The effect is not merely one of temperature; it occurs almost at an equal rate in the ice box. Contrariwise, in the case of normal stearic acid, melting one degree higher than isostearic acid, slides lose their luster only when heated to within 10° of the melting point of 69°, when the film seems to become totally disorganized. We assume that the lateral force during building-up produces a regular parallel organization of the isopropyl groups and that the subsequent hazing of the *iso*-acid films in the built-up state is due to a disturbance of the regular array of the terminal isopropyl groups by random thermic rotation around their binary axis or attachment, or by the rotation of valencies further down in the chain, as proposed by Dervichian (15). The opacity disappears upon skeletonization with benzene (see below).

---

[2] Gradual changes in thickness of calcium stearate films have been observed by Blodgett [Ref. (16), p. 1019] who attributed them to the length of time that the slide spends under water.

Films of *neo*-fatty acids, whether deposited as *Y*- or as *X*-films, appear hazy immediately upon formation. Whether the spatial relations, previously discussed, produce a pitted light-scattering surface, or whether the random position of the *tert*-butyl group is a necessary condition, cannot now be decided. The haziness of these films differs from opacities of similar outward appearance by its property temporarily to disappear when exposed to the human breath. This is also in striking contrast to optically perfect films of normal acids, which turn temporarily hazy from condensation of breath droplets. Quantitative measurement of light-scattering and possibly absorption or reflection spectroscopy with polarized infrared light may elucidate these points.

IV. Contact Angles

Among the unexpected observations made incidental to the study of monomolecular films of polar organic compounds has been the oleophobic nature of such films. The customary assumption has proved fallacious that hydrophilic and oleophobic behavior is associated one with another and, inversely, hydrophobic and oleophilic character. Films of one or several layers of barium stearate and stearic acid, built-up on solid slides, shed water at a contact angle of nearly 90°; films built-up of a hydroaromatic acid such as cholanic or abietic acid are equally hydrophobic. But their behavior toward a hydrocarbon like hexadecane shows a fundamental contrast: the drop of hydrocarbon flattens out completely with a contact angle of zero on the cholanic acid film, but sheds with a contact angle of about 42° at normal temperature on the stearic acid film. This difference between oleophilic and oleophobic character must be ascribed to the sequence of methylene groups on the surface of the hydroaromatic molecule as against the array of terminal methyl groups which form the surface of the normal fatty acid film (1,2). According to Bigelow, Pickett, and Zisman (20), monomolecular films of eicosyl alcohol and of octadecylamine, formed by adsorption from solution on metal surfaces, are simultaneously hydrophobic and oleophobic. According to these authors, contact angles of aliphatic hydrocarbons approach a maximum value of *ca.* 40° with increasing chain length, the individual values being a function of the surface tension of the liquid (21). In view of the striking differences between the behavior of liquid hydrocarbons on aliphatic as against hydroaromatic surfaces (2), it is noteworthy that the contact angles of hexadecane and tetradecane on built-up films of isostearic and neostearic acids were identical within the limits of error with those on normal stearic acid. This observation favors the assumption of a structure carrying a maximum number of methyl groups in its surface rather than keeping all of them tucked away.

V. SKELETONIZATION

Blodgett and Langmuir [Ref. (22), p. 980] have described the selective dissolving of fatty acid molecules out of a built-up film consisting of a mixture of the fatty acids and its soap.

While the skeletonized film displays interference colors that could be simply interpreted as a decrease in thickness, this "lowering" of the color is in fact due to a decrease in the refractive index for a film of original thickness, but which consists of a skeleton of soap molecules and interspaces of air. The latter may be refilled, e.g., with petrolatum or hexadecane, restoring the original refractive index and interference color. The amount of skeletonization increases with the percentage of free fatty acid, but at a certain limit the skeleton loses its vertical and horizontal coherence with resulting collapse. These limiting percentages have been correlated with the analytically ascertained content of metal ion, which, in turn, is a function of pH (17).

Factors besides analytical composition affect skeletonizability. The arrangement of free acid and soap molecules in built-up films is not static, but undergoes changes by turning around and migration of molecules. A film of barium stearate–stearic acid of approximate ratio 2 equiv. barium stearate to 1 equiv. stearic acid, obtained on a bath of pH 7.35, may be skeletonized in the fresh state with removal of 25–30% of its substance. But, when kept standing intact for 3 weeks, not more than what corresponds to one monolayer of a total of 40 layers (2.5%) may be removed with benzene. On the other hand, a film built on a bath of pH 6.6, when skeletonized to 50%, may be completely refilled, but after standing in the skeletonized state for 3 weeks, it has consolidated, if not actually collapsed, and can no longer be refilled. Similar studies of mixed hydrocarbon–fatty acid films, which will be reported separately (23), also point to the dynamic state of the molecules within built-up films.

In the skeletonization of *branched* fatty acid films two additional factors make themselves felt. The greater tilt and cross section of the individual molecule promotes channeling and penetrating into and from the lower layers of the films. The alkali salts of *neo*-fatty acids are considerably soluble in ether (3), but even the salts of bivalent metals, both of *neo*- and *iso*-fatty acids, are significantly more soluble than their straight-chain isomers, both in hot water and in nonpolar solvents. Polylayer films of normal and of isolignoceric acid, freshly built on a hypophase of pH 6.6 were skeletonized with benzene. The barium *n*-lignocerate skeleton could be refilled with hexadecane to match a non-skeletonized control strip on the same plate. The barium isolignocerate skeleton could not be restored to more than 75% of its original mass, because of partial removal of the barium salt skeleton by benzene.

VI. Surface Sublimation

In the course of these studies a phenomenon has been discovered which likewise leads to skeletonization.

The changes in thickness, described in Sections VI and VII, were so striking that they could be observed by direct comparison of the interference colors with a standard barium stearate–stearic acid gage, inspected under identical angles. The apparent thickness was checked, when in the suitable color range, by determination of the reflection minimum in monochromatic D-light. All films, unless otherwise noted, were built on chromium plates with a monolayer of ferric stearate on a hypophase of pH = 7.35, containing 10^{-4} mole barium acetate and 2×10^{-4} mole potassium bicarbonate.

Barium isostearate–isostearic acid films appear to lose thickness rather rapidly on standing; it will decrease over night by 2–4 monolayers out of 40 and after a few weeks it will be reduced to a residue of *ca.* 20 layers, which represents a final value. This apparent shrinkage is enhanced by a rise of temperature; it is always accompanied by the development of haziness. However, haziness per se cannot account for the profound changes in interference colors, since one can show that the standing of similar films at ice box temperature for 2 weeks results in strong hazing *without* shrinkage. Nor could the change of interference colors be due to any intermolecular rearrangement or transition into an allomorphic modification, since any decrease in volume on this count would be compensated for by a corresponding increase in refractive index. The phenomenon is actually due to volatilization of the free *iso*-fatty acid. The shrunk film is a regular skeleton film and may be restored at any stage of depletion to its original thickness by refilling with hexadecane. The refilled film remains hazy. Subsequent skeletonization by benzene removes not only the hexadecane, but enough of the barium isostearate to produce collapse of the skeleton. After several months' standing, the shrunk films have consolidated or collapsed and may no longer be refilled. Becausing of increasing difficulty of penetration with depth, sublimation of *iso*-fatty acids is limited to the upper 500–1000 A. of a film, as shown in the instance of an $(AB)_{100}$ film, where the loss of sublimation after 6 months did not exceed 10% of the total thickness. Short treatment of a shrunk film with benzene does not affect its apparent thickness, since it is the free fatty acid component of the film which has sublimated leaving behind the barium salt as skeleton.

A slide covered on both sides with a polyfilm of isostearic acid, kept in a horizontal position in a covered dish on a support a few millimeters from the bottom of the dish, showed loss on the top side, while the thickness of the film facing the bottom remained unchanged. Separate experiments with irradiation of one side of a doubly covered slide proved that the above observation is not caused by asymmetrical exposure to light, but by the relative position of the slide with respect to air currents. The effect was accelerated by placing the slides in a vacuum desiccator with 0.3 mm. Hg pressure.

VII. SUBLIMATION BY PENETRATION

Polymolecular films of barium isostearate–isostearic acid were covered with normal barium stearate–stearic acid *Y*-films in a step pattern, so that their combined thickness falls into the most sensitive color range. The number of isostearic acid monolayers was varied from 20 to 46, that of the normal stearic acid "blanket" inversely from 20 to 2 (N_{st}).

TABLE III

Percentage Loss of Isostearic Acid from a 42-Layer Y-Film

Thickness of barium stearate–stearic acid blanket	N_{st} . 0	2	4	6	8	10	12
	A... 0	55	110	165	220	285	330
Percentage loss after:							
2 days	20	20	20	20	17	13.5	11
4 days	28	28	28	25	22	22	20
5 weeks	39	39	39	33	33	31	28

Table III illustrates a test in which 42 monolayers of barium isostearate–isostearic acid were covered with a checkerboard of 2, 4, 6, 8, 10, and 12 layers of barium stearate–stearic acid. Measurement and color comparison in the fresh condition yielded $h = 22.0$ A. for the isostearic layers. The percentage losses after 2 days', 4 days' and the final losses after 5 weeks' standing at room temperature show that 2–6 layers of stearic acid were completely permeable to sublimation of isostearic acid; thicker blankets slow up the process. But in another experiment, even a barium stearate–stearic acid film of 24 layers still permitted the escape of the equivalent of 2 monolayers of isostearic acid in 3 days. The greater decrease below the thinner blankets leads, as can be gleaned from the numerical data in Table III, to a steadily increasing contrast between the steps of the interference "spectrum." The maximal loss of 39% corresponds approximately to the percentage of free isostearic acid in the film. An incidental advantage is gained in these experiments by the absence of haziness from the reflecting surface, which we have mentioned in Sec. III.

In contrast to the penetrability of barium stearate–stearic acid films, a blanket of 2–10 monolayers of pure barium stearate, deposited from a bath of pH 9.35, prevented sublimation of the underlying isostearic acid (deposited at pH 7.35), wherever it was thicker than 4 monolayers barium stearate. A similar effect of free stearic acid: strontium stearate ratio has been observed by Beischer (24) for the surface diffusion on carbon-14 tagged stearic acid.

The sublimation phenomenon was duplicated with neoisolignoceric acid; this acid also penetrates blankets of normal stearic or normal lignoceric acid of several molecules' thickness. Sublimation also occurs with films of neostearic acid, but here haziness develops so quickly as to make color comparisons soon impossible.

The enhancing effect of branching, especially of the *tert*-butyl group, upon the volatility of aliphatic hydrocarbons is known; this effect is much greater than one would anticipate from the differences in boiling points. The present manifestation of enormously increased volatility due to omega-branching is especially noteworthy as it pertains to the solid state. The thermic agitation of fatty acid molecules in a film will be about the same for straight chain and for branched molecules, but in the case of the straight chains the molecules encounter no obstacle that would prevent them from always falling back into the equilibrium position. On the other hand, the branched end groups, once they have been lifted by thermal motion above the surface, will freely rotate and thus assume conformations which will, in general, not fit back into their matrix. In addition to this geometric irreversibility, one must envisage the alternative or additional assumption (see Sec. II) that the bonds within the end groups are distorted and held in place by the van der Waals' forces between adjacent molecules. When they slip out above the surface, they will assume their normal valency angles and the diminished van der Waals' forces, acting on the straight-chain part of the molecule, will not suffice to overcome the resistance of the barb-like side groups and to squeeze them back into their hollow.

The sense of the thermic motion will in either case have become in part irreversible and will eventually lead to the molecule working itself loose and subsequently sublimating from the oleophobic surface. At the same time channels are formed for the emergence of other molecules from lower layers. Sublimation through superimposed blankets of a nonvolatile isomeric compound is an important proof for the dynamic state obtaining in crystals. The felicitous combination of film structure with the particular features of omega-branched acids, discussed in the preceding paragraph, permits this manifestation of continuous intermolecular change of position. It substantiates concepts of intramolecular changes of position such as the hypothesis of the facile "turning-around" of molecules, arrived at by indirect evidence. It also offers an explanation for some "long-range" effects such as the transmission of hydrophobic behavior through hydrophilic blankets, or vice versa (25). The effect may be termed "molecular sublimation" in analogy to "molecular distillation" which it parallels in many respects.

References

1. Sobotka, H., "Monomolecular Layers" in Medical Physics, Vol. I, p. 763. Yearbook Publishers, Chicago, 1944; *ibid.* Vol. II, pp. 550 and 561, 1950.
2. Sobotka, H., and Bloch, E., *J. Biol. Chem.* **124**, 559 (1938).
3. Sobotka, H., and Stynler, F. E., *J. Am. Chem. Soc.* **72**, 5139 (1950).
4. Weitkamp, A. W., *J. Am. Chem. Soc.* **67**, 447 (1945).
5. Sobotka, H., and Stynler, F. E., in preparation.
6. Fox, H. W., and Zisman, W. A., *Rev. Sci. Instruments* **19**, 274 (1948).
7. Miller, N. F., *J. Phys. Chem.* **45**, 289 (1941).
8. Langmuir, I., *Proc. Roy. Soc.* (London) **A170**, 1, esp. 12 (1939).
9. Adam, N. K., The Physics and Chemistry of Surfaces, 3rd Ed., p. 57. Oxford, 1941.
10. Langmuir, I., and Waugh, D. F., *J. Am. Chem. Soc.* **62**, 2771 (1940).
11. Joly, M., "Surface Chemistry," Discussion at Bordeaux Meeting of Soc. Chim. Phys. and Faraday Soc., p. 37. Butterworth, London, 1949.
12. Dervichian, D. G., and Joly, M., *Bull. soc. chim. biol.* **28**, 426 (1946).
13. Langmuir, I., and Schaefer, V. J., *J. Am. Chem. Soc.* **59**, 2400 (1937).
14. Stallberg, St., and Stenhagen, E., *Svensk Kem. Tid.* **53**, 44 (1941).
15. Dervichian, D. G., Surface Chemistry, p. 47. Butterworth, London, 1949.
16. Blodgett, K. B., *J. Am. Chem. Soc.* **57**, 1007 (1935).
17. Langmuir, I., and Schaefer, V. J., *J. Am. Chem. Soc.* **58**, 284 (1936).
18. Langmuir, I., Schaefer, V. J., and Sobotka, H., *J. Am. Chem. Soc.* **59**, 1751 (1937).
19. Stenhagen, E., *Arkiv Kemi, Mineral., Geol.* **14A**, No. 11 (1940).
20. Bigelow, W. C., Pickett, D. L., and Zisman, W. A., *J. Colloid Sci.* **1**, 513 (1946).
21. Fox, H. W., and Zisman, W. A., The Spreading of Liquids on Low-energy Surfaces. Naval Research Lab. Report 3651, March 15, 1950.
22. Blodgett, K. B., and Langmuir, I., *Phys. Rev.* **51**, 964 (1937).
23. Sobotka, H., and Rosenberg, S., *J. Colloid Sci.* **5**, 581 (1950).
24. Beischer, D. E., Beta Particle Standards for C^{14} and other Elements in the Form of Radioactive Monolayers. U. S. Naval School of Aviation Medicine, Project No. NM 001 059.16.03.
25. Sobotka, H., *Pub. Am. Assoc. Advance Sci.* No. **7**, 54 (1939).

FILMS OF HYDROCARBON–STEARIC ACID MIXTURES[1]

Harry Sobotka and Shirley Rosenberg

Department of Chemistry, The Mount Sinai Hospital, New York, N. Y.

Received October 13, 1950

Abstract

The formation of monomolecular layers on a barium buffer hypophase and of built-up Y-films is described for various mixtures of stearic acid with n-octadecane, n-octacosane, and n-hexatriacontane. The thickness of the resulting mixed films is interpreted with reference to their structure. The existence of a limiting proportion of 1 molecule of hydrocarbon to 2 molecules of stearic acid is explained by the crystal structure of the films. The relationship between three-dimensional and two-dimensional molecular compounds containing aliphatic acids is discussed.

Introduction

The study of monomolecular layers of mixtures is important for the recognition of structural principles, while polymolecular layers offer the additional possibility of investigating molecular migration and rearrangement in built-up films. Furthermore, one may induce the spreading of mixtures comprising a spreadable and a nonspreadable component and thus be enabled to observe the behavior in a two-dimensional array of substances which would not form monomolecular films by themselves.

As the least complicated examples for nonspreading compounds in the nonpolar group, we have selected some unbranched long-chain hydrocarbons: octadecane (m.p. 28°C.) octacosane (m.p. 56°C.) and hexatriacontane (m.p. 75°C., recrystallized from chloroform). As the spreading component for the mixtures we used stearic acid whose properties in the two-dimensional state are better known than those of any other substance.

Results

Langmuir (1), Mercer (2), and Zisman (3) have studied the spreading of petrolatum in which small amounts of stearic acid or other ionizable or unionized "spreaders" were dissolved. For our ends, we selected individual uniform hydrocarbons and used them in definite proportions to stearic acid, both compounds being jointly dissolved in benzene. The spreading of such solution on barium buffers results in the formation of H-layers, floating monomolecular layers, which may be compressed by oleic acid

---

[1] This investigation was in part supported by a Grant-in-Aid from the Permanent Science Fund of the American Academy of Arts and Sciences.

as piston oil with a lateral force of 29 dynes/cm. These layers consist of the hydrocarbon and stearic acid which is neutralized by barium in a proportion depending on the pH of the hypophase.

We used throughout these experiments a bath containing 10^{-4} mole barium acetate and 2×10^{-4} mole potassium bicarbonate. The pH was 7.35, the temperature 25–27°. Without admixture of hydrocarbons the ratio of barium stearate to stearic acid equivalents on this bath would be *ca.* 67:33.

We found for each hydrocarbon a limiting ratio of hydrocarbon to total stearic acid. Mixtures exceeding this ratio do not form uniform monomolecular *H*-layers, but at best films of a patchy appearance which collapse under a low lateral force. The stable *H*-layers may be built-up on metal slides as *Y*-films in a manner identical with pure stearic acid. The thickness of these built-up films varies with the molecular weight and the percentage of the hydrocarbon. Table I gives comparisons of the interference colors of such mixed films with those of pure barium stearate–stearic acid films, prepared under identical conditions.

TABLE I

Measurement of Thickness of Polymolecular Films by Comparison of Interference Colors

N_{St} = number of barium stearate-stearic acid monolayers in standard
N_m = number of monolayers of mixture

No.	Mixture of stearic acid and hydrocarbon		Matching values of $N_{St}:N_m$	Increment of thickness	
	Per cent hydrocarbon by weight	Molecular per cent of hydrocarbon		($N_{St} - N_m$)	Per cent
	Octadecane				
1*a*	20	21.85	38:38 to 46:46	0	0
1*b*	30	32.4	38:38 to 44:44	0	0
1*c*	40	42.7	No film		
	Octocosane				
2*a*	20	15.15	38:30 to 44:36	8	27 to 22
2*b*	30	23.45	38:26 to 44:32	12	46 to 38
2*c*	40	32.45	39:24 to 48:30	15–18	62 to 60
2*d*	50	41.7	No film		
	Hexatriacontane				
3*a*	20	12.3	36:30 to 45:38	6–7	20 to 18
3*b*	30	19.4	36:26 to 46:36	10	38 to 28
3*c*	40	27.25	40:28 to 51:38	12–13	43 to 35
3*d*	50	36.3	35:18 to 48:28	17–20	95 to 72
3*e*	60	45.7	No film		

In the case of *n*-octadecane which equals stearic acid in length, the admixture does not affect the apparent thickness of the film. This agrees have been postulated on the basis of discontinuities in Force/Area graphs of mixed monolayers (15).

Our above theory that a simple integral proportion, based on geometric considerations, is a limiting factor for the formation of mixed monolayers, containing one nonspreadable component, is fully compatible with the assumption of such molecular compounds in monolayers, but does not depend on the verification of their actual existence.

REFERENCES

1. LANGMUIR, I., *J. Franklin Inst.* **218**, 143 (1934).
2. MERCER, E. H., *Proc. Phys. Soc.* (London) **51**, 561 (1939).
3. ZISMAN, W. A., *J. Chem. Phys.* **9**, 534 (1941).
4. SOBOTKA, H., ROSENBERG, S., AND BIRNBAUM, A., *J. Colloid Sci.* **5**, 567 (1950).
5. CLOWES, G. H. A., *Pub. Am. Assoc. Advance. Sci.* No. **7**, 1 (1939).
6. LANGMUIR, I., SCHAEFER, V. J., AND SOBOTKA, H., *J. Am. Chem. Soc.* **59**, 1751 (1937).
7. STENHAGEN, E., *Arkiv Kemi, Mineral., Geol.* **14A**, No. 11 (1940).
8. HAVINGA, E., AND DE VAEL, J., *Chem. Weekblad* **34**, No. 43 (1943).
9. SOBOTKA, H., Chemistry of the Sterids, Chap. VII. Williams and Wilkins, Baltimore, 1938.
10. POWELL, H. M., *Endeavour* **9**, 154 (1950).
11. SMITH, J. W., *Science Progress* **38**, 698 (1950).
12. ANGLA, B., *Compt. rend.* **224**, 402 (1947).
13. REDLICH, O., GABLE, C. M., BEASON, L. R., AND MILLAR, R. W., *J. Am. Chem. Soc.* **72**, 4161 (1950).
14. SCHLENK, W., JR., *Experientia* **6**, 292 (1950).
15. DERVICHIAN, D. G., AND JOLY, M., *Bull. soc. chim. biol.* **28**, 426 (1946).

changed, only their distance from one another has been reduced exactly by the amount of the increment.

In order to reconcile all these results, we suggest that the deposition ratio (6,7) is substantially higher than unity; extra molecules of free stearic acid insert themselves during attachment of the *H*-layer to the slide to fill out the gaps between the protruding hydrocarbon chains. This reduces the ratio barium stearate to free stearic acid, and thus accounts for the observed increase in skeletonizability. X-ray diffraction measurements may decide the validity of these assumptions.

Limiting Molecular Ratios

The highest molecular percentage of hydrocarbon, permitting the formation of stable *H*-layers and subsequently *Y*-films in our experiments, was 32 for octadecane and octacosane and 36 for hexatriacontane. Thus, spreading of stable hydrocarbon–stearic acid layers seems to require a molecular ratio not exceeding one molecule hydrocarbon to two molecules stearic acid. In a two-dimensional hexagonal matrix the orderly removal of every third point leaves a beehive design. Havinga and de Vael (8) have shown by electron-diffraction measurements that stearic acid and stearyl alcohol films have hexagonal structure. If one-third of the stearic acid molecules were replaced by hydrocarbon molecules, there would still remain a contiguous network of stearic acid molecules surrounding each individual hydrocarbon molecule. Any higher percentage of hydrocarbon molecules would require interruption of the stearic acid network, the integrity of which appears to be vital for the stability of H-layers.[2]

The existence of a limiting ratio in these binary mixtures invites comparison with various types of molecular compounds which have been recently studied and discussed. Paraffin hydrocarbons, carboxylic acids, and related polar compounds (B) form molecular compounds with substance A of the formula A_nB. In the choleic acids (A = desoxycholic acid) n may assume the values 1, 2, 3, 4, 6, and 8 increasing as the length of the fatty acid chain increases (9). But in the case of urea (10–12), which coördinates with normal hydrocarbons and normal fatty acids, and of thiourea, which embraces in its crystal matrix hydroaromatic compounds (13) and branched aliphatics (14), n is not always integral, as some values approximating 2.5 and 3.5 have been reported. These ratios, whether integral or not, depend on the dovetailing of the two species of molecules in three-dimensional crystals. In the case of the two-dimensional aggregates with which we are dealing, complexes of discrete proportions have been postulated on the basis of discontinuities in Force/Area graphs of mixed monolayers (15).

---

[2] This ratio is the inverse of the limiting molecular ratio for skeletonization of built-up barium stearate–stearic acid films. There, occupation of every third point by the residual barium stearate seems to be the minimum requirement that assures reversibility by refilling.

Our above theory that a simple integral proportion, based on geometric considerations, is a limiting factor for the formation of mixed monolayers, containing one nonspreadable component, is fully compatible with the assumption of such molecular compounds in monolayers, but does not depend on the verification of their actual existence.

REFERENCES

1. LANGMUIR, I., *J. Franklin Inst.* **218**, 143 (1934).
2. MERCER, E. H., *Proc. Phys. Soc.* (London) **51**, 561 (1939).
3. ZISMAN, W. A., *J. Chem. Phys.* **9**, 534 (1941).
4. SOBOTKA, H., ROSENBERG, S., AND BIRNBAUM, A., *J. Colloid Sci.* **5**, 567 (1950).
5. CLOWES, G. H. A., *Pub. Am. Assoc. Advance. Sci.* No. **7**, 1 (1939).
6. LANGMUIR, I., SCHAEFER, V. J., AND SOBOTKA, H., *J. Am. Chem. Soc.* **59**, 1751 (1937).
7. STENHAGEN, E., *Arkiv Kemi, Mineral., Geol.* **14A**, No. 11 (1940).
8. HAVINGA, E., AND DE VAEL, J., *Chem. Weekblad* **34**, No. 43 (1943).
9. SOBOTKA, H., Chemistry of the Sterids, Chap. VII. Williams and Wilkins, Baltimore, 1938.
10. POWELL, H. M., *Endeavour* **9**, 154 (1950).
11. SMITH, J. W., *Science Progress* **38**, 698 (1950).
12. ANGLA, B., *Compt. rend.* **224**, 402 (1947).
13. REDLICH, O., GABLE, C. M., BEASON, L. R., AND MILLAR, R. W., *J. Am. Chem. Soc.* **72**, 4161 (1950).
14. SCHLENK, W., JR., *Experientia* **6**, 292 (1950).
15. DERVICHIAN, D. G., AND JOLY, M., *Bull. soc. chim. biol.* **28**, 426 (1946).

DIRECT OBSERVATION OF GEL STRUCTURE WITH THE ELECTRON MICROSCOPE[1]

The nature of the structure which enables gels of low solid content to immobilize enormous quantities of liquid, although a problem which has long interested colloid chemists (3), could previously be studied only by indirect methods of investigation. In connection with an intensive study of gels of calcium stearate monohydrate in cetane (5,6) it was desired to determine whether the structure responsible for the rigidity of these gels is merely a conglomeration of independent particles or whether there exists anything analogous to the three-dimensional network postulated in some polymers. Previous attempts (1,2) to utilize the electron microscope to study soap gels were complicated by the necessity of subjecting the sample to violent mechanical agitation, and extraction of the original oil with volatile solvent, before examination. In the present investigation, use was made of a modification of a recently developed technique (4) which permits cutting of sections 0.1-μ thick suitable for direct examination in the electron microscope. The sections were floated off on cold water and picked up on screens covered with a collodion film.

The results obtained are shown in the figure. Figure 1*A* is typical of many sections prepared and observed with minimum mechanical disturbance of the sample and with no contact with volatile solvents. The existence of a network is clearly evident, and it can be presumed that the mechanical properties of the bulk system may be in part attributed to the existence of this soap skeleton, and the immobilization of liquid to its entrapment in the small spaces formed by the crossed fibers. Most of the cetane has evidently been removed by the evacuation in the electron microscope.

Figure 1*B* is typical of the appearance of sections from which cetane was removed by extraction with benzene followed by lyophilization of the solvent before examination. Evidently this treatment results in destruction of the original network with formation of a mass of more or less independent particles. Another recently discovered example (7) of the possible weakness of structures existing in bulk systems is in the disintegration of bundles of fibers found in tobacco mosaic virus preparations merely on wetting with water.

---

[1] This work was undertaken as part of a project, "Phase Studies of Greases," sponsored by the Office of Naval Research, Contract No. N6onr-238-TO-2, NR 057 057.

Figure 1*C* is an electron micrograph of a smear preparation of a typical cup grease, and shows the apparently twisted, rope-like fibrils familiar from previous work on such systems. Consequently, if such structures had been present in the calcium stearate monohydrate–cetane gels they would have appeared with the present technique. The presence of many small particles, singly and in combinations of a few units, raises the possibility that the rope-like fibrils may not actually be twisted but merely aggregates of these segments.

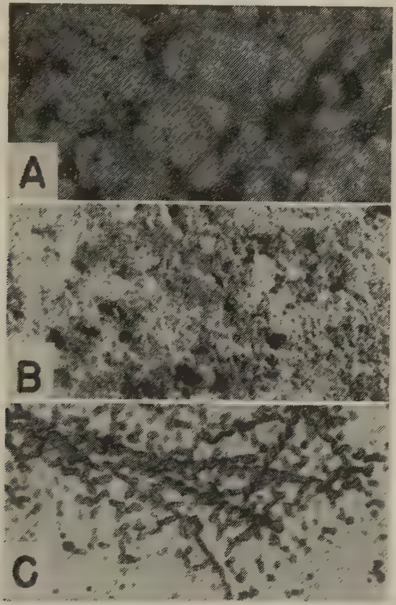

Fig. 1. Electron micrographs of soap gels. *A*. 25% calcium stearate monohydrate–cetane gel section; magnification 16,000. *B*. Same extracted with benzene, lyophilized, and shadowed with chromium; magnification 16,000. *C*. Smear preparation of commercial cup grease, shadowed with chromium; magnification 32,000.

The techniques employed to permit direct study of gel structure with the electron microscope will soon be reported more fully. Experiments are being continued to investigate the effect of varying mechanical, thermal, and aging treatments on the structures obtained, and to correlate the morphology with other properties of the gels.

References

1. Birdsall, D. H., and Farrington, B. B., *J. Phys. & Colloid Chem.* **52**, 1415 (1948).
2. Ellis, S. G., *Can. J. Research* **A25**, 119 (1947).
3. Lloyd, D. J., in Alexander, Colloid Chemistry, Vol. I, p. 767. Chemical Catalog Co., New York, 1926.

4. Pease, D. C., and Baker, R. F., *Proc. Soc. Exptl. Biol. Med.* **67**, 470 (1948).
5. Vold, R. D., and Vold, M. J., *J. Phys. & Colloid Chem.* **52**, 1424 (1948).
6. Vold, R. D., Phase Studies of Greases. Second Technical Report, Project NR 057 057, Library of Congress, 1949.
7. Williams, R. C., and Steere, R. L., *Science* **109**, 306 (1949).

Department of Chemistry and College of Medicine,
University of Southern California
Los Angeles, California

Robert D. Vold
Henry F. Coffer
Richard F. Baker

Received October 13, 1950

AUTHOR INDEX

A

Abe, Shigemi. See Kamiya, 149
Alfrey, Turner, Jr. See Guzzetti, 202
  Goldberg, A. I. and Price, John A. Dilute-solution viscosity of polymethyl methacrylate and a methyl methacrylate-styrene copolymer, 251
Arthur, Jett C., Jr., and Saik, Barbara H. Intrinsic viscosity of cottonseed globulin solutions, 326

B

Baker, Richard F. See Vold, Robert, 586
Bechtel, Welker G. Measurements of properties of corn starch gels, 260
Beeck, O., Givens, J. W., and Ritchie, A. W. The adsorption of hydrogen on nickel catalysts. II. Sorption isobars from 20°K. to room temperature, 141
Belcher, H. V. See Bestul, 303
Bestul, A. B., and Belcher, H. V. Flow behavior of concentrated GR-S rubber solutions, 303
Bikerman, J. J. Sliding of drops from surfaces of different roughnesses, 349
Birnbaum, Aina. See Sobotka, 567
Bondi, A., Solubility and swelling of alkali soaps in organic solvents, 458
Buchdahl, Rolf. See Nielsen, 282
Burcik, Emil J. The rate of surface tension lowering and its role in foaming, 421

C

Carroll, Benjamin. Solubilization in aqueous solutions of bovine serum albumin, 103
Coffer, Henry F. See Vold, Robert, 586
Collins, Frank C. Diffusion in chemical reaction processes and in the growth of colloid particles, 499

D

Davis, Lannes E. Ionic exchange and statistical thermodynamics. I. Equilibria in simple exchange systems, 71
  And Rible, John M. Monolayers containing polyvalent ions, 81
  Ionic exchange and statistical thermodynamics. II. Equilibria in irregular systems, 107
Dexter, F. D., and Dienes, G. G. Extrusion behavior of viscoelastic materials, 228
Dienes, G. G. See Guzzetti, 202
  See Dexter, 228
Doscher, Todd M. The electrophoretic mobility in relation to suspendability and detergency, 100
Drucker, D. C. See Stockton, 239

E

Edison, George R. See Hayashi, 437
Eirich, F. R. See Schoenberg, 393
  See Newman, 541
Eyring, Henry. Acceptance of Bingham Medal, 200

F

Fischer, Earl K. Rheological properties of commercial paints, 271
Fox, H. W., and Zisman, W. A. The spreading of liquids on low energy surfaces. I. Polytetrafluoroethylene, 514

G

Ginell, Robert. Association phenomena. II. Theories of chain molecules and their application to hydrogen bonding in gaseous hydrogen fluoride: *a correction*, 99
Givens, J. W. See Beeck, 141
Goldberg, A. I. See Alfrey, 251
Gralén, Nils, and Kärrholm, Marianne. The physicochemical properties of solutions of gum tragacanth, 21
Guzetti, A. J., Dienes, G. J., and Alfrey, Turner, Jr. Rheological properties of phenolic resins. Effect of reaction with hexamethylenetetramine on properties of a phenol-formaldehyde novolak, 202

H

Hayashi, Teru, and Edison, George R. Enzyme-substrate stabilization with surface-denatured pepsin-albumin, 437
Hazel, J. Fred, and Schipper, Edgar. Low temperature studies with colloidal silicic acid, 532
Hipp, N. J. See Hougen, 218
Hougen, Leif, and Hipp, N. J. Plastic flow properties of casein, 218

I

Inn, Edward C. I. See La Mer, 471

J

Joly, M. General theory of the structure, transformations and mechanical properties of monolayers, 49

K

Kamiya, Noburô, and Abe, Shigemi. Bioelectric phenomena in the myxomycete plasmodium and their relation to protoplasmic flow, 149
Kärrholm, Mariänne. See Gralén, 21
Kerker, Milton. The use of white light in determining particle radius by the polarization ratio of the scattered light, 165
Kimball, George E. See Markovitz, 115
Kuhn, Hans. Viscosity sedimentation, and diffusion of long-chain molecules in solution as determined by experiments on large-scale models, 331

L

La Mer, Victor K., Inn, Edward C. Y., and Wilson, Irwin B. The methods of forming, detecting, and measuring the size and concentration of liquid aerosols in the size range of 0.01 to 0.25 microns diameter, 471
Lord, D. D. The action of polyoxyethylene monostearate upon starch with reference to its softening action in bread, 360

M

Markovitz, Hershel, and Kimball, George E. The effects of salts on the viscosity of solutions of polyacrylic acid, 115

N

Newman, S., and Eirich, F. Particle shape and the concentration dependence of sedimentation and diffusion, 541
Nielsen, Lawrence E. and Buchdahl, Rolf. Viscoelastic and photoelastic properties of polystyrene above its softening temperature, 282

P

Palit, Santi R. Reply to letter of P. A. Winsor, 416
Philippoff, W. Micelles and x-rays, 169
Price, John A. See Alfrey, 251

R

Richardson, E. G. The formation and flow of emulsion, 404
Richter, John W. See Schubert, 376
Riseman, J. See Schoenberg, 393
Ritchie, A. W. See Beeck, 141
Rosenberg, Shirley. See Sobotka, 567, 581

S

Saik, Barbara H. See Arthur, 326
Schipper, Edgar. See Hazel, 532
Schoenberg, M. D., Riseman, J., and Eirich, F. R. Extinction angles, intrinsic viscosities, and molecular weights of polystyrene in solution, 393
Schubert, Jack, and Richter, John W. The use of ion exchangers for the determination of physicochemical properties of substances, particularly radiotracers, in solution. III. The radiocolloids of zirconium and niobium, 376
Simha, Robert. The concentration dependence of viscosities in dilute solutions, 386
Stockton, F. D., and Drucker, D. C. Fitting mathematical theories of plasticity to experimental results, 239

T

Taylor, Hugh S. Introduction of Henry Eyring, 197
Turner, C. F., and Van Hook, Andrew. The effect of ultrasonic irradiation on the formation of colloidal sulfur and ice, 315

V

VAN DER WAARDEN, M. Stabilization of carbon-black dispersions in hydrocarbons, 317
Micelle formation of sulfonates in hydrocarbons, 448
VAN HOOK, ANDREW. See Turner, 315
VOLD, MARJORIE J, AND VOLD, ROBERT D. The phase behavior of lithium stearate in cetane and in decalin 1
The application of the mass law to the aggregation of colloidal electrolytes, 506
VOLD, ROBERT D. See Vold, Marjorie J., 1
COFFER, HENRY F., AND BAKER, RICHARD F. Direct observation of gel structure with the electron microscope, 586
VONNEGUT, BERNARD. Techniques for generating silver iodide smoke, 37

W

WAGNER, CARL. Mathematical analysis of the formation of periodic precipitations, 85
WELTMANN, R. N. Instruments for the determination of rheological parameters of liquid bodies, 295
WILSON, IRWIN B. See La Mer, 471
WILSON, J. H., AND BALANI, T. R. Chemisorbed oxygen on charcoal and the sorption of strong inorganic bases and acids, 550
WINSOR, P. A. Mixed solvent effect in solubilization, 414

Z

ZISMAN, W. A. See Fox. 514

SUBJECT INDEX

A

Acids, inorganic, see *Charcoal*
Acrylic acid, see *Polyacrylic acid*
Aerosols, — of exceedingly small particle size, La Mer *et al.*, 471
Albumin, solutions of bovine serum —, Carroll, 103; pepsin- — and enzyme-substrate stabilization, Hayashi and Edison, 437
Aliphatic acids, effect of terminal upon the behavior of long-chain — —, Sobotka *et al.*, 567
Arachidic acids, *n*-, *iso*-, and *neo*- —, Sobotka *et al.*, 567
Association phenomena (II), a correction, Ginell, 99

B

Bases, inorganic, see *Charcoal*
Behenic acids, *n*-, *iso*-, and *neo*- —, Sobotka *et al.*, 567
Bingham medal, acceptance, Eyring, 200
Bovine serum albumin, solutions, Carroll, 103
Bread, action of polyoxyethylene stearate upon — crumb, Lord, 360

C

Carbon blacks, electrophoretic mobility of Malacco —, and Excelsior —, Doscher, 100; stabilization, van der Waarden, 317
Casein, — flow properties, Hougen and Hipp, 218
Cellulose acetate, properties, Kuhn, 331
Chain, properties of long- — molecules, Kuhn, 331
Charcoal, chemisorbed oxygen on — and the sorption of strong inorganic bases and acids, Wilson and Bolam, 550
Colloidal, mass law and the aggregation of — electrolytes, Vold, 506; low temperature studies with — silicic acid, Hazel and Schippper, 532
Colloids, see *Aerosols*, *Diffusion*, *Gel*
Corn starch, — — gels, Bechtel, 260
Cottonseed globulin, see *Globulin*

D

Dibutyl phthalate, — — aerosols, La Mer *et al.*, 471
Diffusion, — in chemical reaction processes and in the growth of colloid particles, Collins, 499; concentration dependence Newman and Eirich, 541

E

Electrolytes, see *Colloidal*
Electron microscope, micrographs of soap gels, Vold *et al.*, 586
Electrophoretic mobility, Doscher, 100
Emulsion, formation and flow, Richardson, 404
Enzyme, — -substrate stabilization with pepsin-albumin, Hayashi and Edison, 437
Exchange equilibria, ionic — —, Davis, 71, 107
Eyring, Henry, introduction of — —, Taylor, 197

F

Fatty acids, films of omega-branched — —, Sobotka *et al.*, 567
Films, see *Stearic acid*, *Surface*
Flow (see also *Protoplasmic flow*); — behavior of concentrated CR-S rubber solutions, Bestul and Belcher, 303
Foaming, surface tension lowering and —, Burcik, 421

G

Gels, corn starch —, Bechtel, 260; observation of — structure with the electron microscope, Vold *et al.*, 586
Globulin, viscosity of cottonseed —, Arthur and Saik, 326
Grease, electron micrograph, Vold *et al.*, 586

Gum tragacanth, solutions of — —, Gralén and Kärrholm, 21

H

Hexaiodobenzene charcoal, Wilson and Bolam, 550
Hexamethylenetetramine, effect of reaction with — on novolak, Guzzetti *et al.*, 202
Hydrocarbon(s), micelle formation of sulfonates in —, van der Waarden, 448; films of — -stearic acid mixtures, Sobotka and Rosenberg, 581
Hydrogen, adsorption of — on nickel catalysts (II), sorption isobars, Beeck *et al.*, 141
Hydrogen fluoride, hydrogen bonding in — (a correction), Ginell, 99

I

Ice, see *Ultrasonic*

L

Liesegang rings, Wagner, 85
Light (see also *X-rays*); particle radius determination, Kerker, 165
Lignoceric acids, *n*-, *iso*-, and *neo*- —, Sobotka *et al.*, 567

M

Macromolecules, properties, Kuhn, 331
Mass law, see *Colloidal*
Methacrylate, viscosity, Alfrey *et al.*, 251
Micelle(s), — and x-rays, Philippoff, 169; — formation of sulfonates in hydrocarbons, van der Waarden, 448; mass law and the aggregation of colloidal electrolytes, Vold, 506
Monolayers, theory of —, Joly, 49; polyvalent ions in —, Davis and Rible, 81; — of long-chain aliphatic acids, Sobotka *et al.*, 567; Sobotka and Rosenberg, 581
Myxomycete plasmodium, — — and protoplasmic flow, Kamiya and Abe, 149

N

Nickel, see *Hydrogen*
Niobium, radiocolloids of —, Schubert and Richter, 376
Novolak, hexamethylenetetramine and —, Guzzetti *et al.*, 202

O

Osmotic coefficient, colloidal electrolytes and — —, Vold, 506
Oxygen, see *Charcoal*

P

Paint rheology, Fischer, 271
Palmitic acids, *n*-, *iso*-, and *neo*- —, Sobotka *et al.*, 567
Particles, see *Aerosols*
Pepsin, — -albumin and enzyme-substrate stabilization, Hayashi and Edison, 437
Phenol, hexamethylenetetramine and — -formaldehyde novolak, Guzzetti *et al.*, 202
Phenolic resins, rheological properties, Guzzetti *et al.*, 202
Plastic flow, — — of caseins, Hougen and Hipp, 218
Plasticity, experiment and theory, Stockton and Drucker, 239
Polarization, optical system for — measurements, La Mer *et al.*, 471
Polyacrylic acid, salts and the viscosity of — — solutions, Markovitz and Kimball, 115
Polymethyl methacrylate, viscosity, Alfrey *et al.*, 251
Polyoxyethylene monostearate, action upon starch, Lord, 360
Polystyrene, viscoelastic and photoelastic properties, Nielsen and Buchdahl, 282; extinction, viscosity, and molecular weight of — in solution, Schoenberg *et al.*, 393
Polytetrafluoroethylene, spreading of liquids on low energy surfaces (I), — Fox and Zisman, 514
Precipitations, periodic —, Wagner, 85
Protoplasmic flow, bioelectric phenomena and — —, Kamiya and Abe, 149

R

Radiocolloids, — of zirconium and niobium, Schubert and Richter, 376
Rain making, see *Silver iodide*
Resins (see also *Phenolic resins*); extrusion of viscoelastic materials, Dexter and Dienes, 228
Rheology, Society of, — annual meeting, New York, Nov. *4–5, 1949*, 197; paint

—, FISCHER, 271; instrumentation, WELTMANN, 295
Rubber, flow of — solutions, BESTUL AND BELCHER, 303

S

Sedimentation, concentration dependence, NEWMAN AND EIRICH, 541
Silicic acid, colloidal — — at low temperature, HAZEL AND SCHIPPER, 532
Silver iodide, techniques for generating — — smoke, VONNEGUT, 37
Sliding, effect of surface roughness on — of water drops, BIKERMAN, 349
Soap(s), theory of monolayers, JOLY, 49; — -water systems, PHILIPPOFF, 169; surface tension and foaming, BURCIK, 421; solubility and swelling of alkali — in organic solvents, BONDI, 458; mass law and — aggregation, VOLD, 506; electron micrographs of — gels, VOLD *et al.*, 586
Sol, silica — at low temperatures, HAZEL AND SCHIPPER, 532
Solubility, see *Soaps*
Solvent, mixed — effect in solubilization, WINSOR, 414; PALIT 416
Sorption, see *Charcoal*
Starch, action of polyoxyethylene monostearate, LORD, 360
Stearate, phase behavior of lithium — in cetane and in decalin, VOLD AND VOLD, 1; electron micrograph of calcium —, VOLD, 586
Stearic acid(s), *n*-, *iso*-, and *neo*- —, SOBOTKA *et al.*, 567; films of hydrocarbon- — — mixtures, SOBOTKA AND ROSENBERG, 581
Stress, — -strain relations, experiment and theory, STOCKTON AND DRUCKER, 239; — relaxation of polystyrene, NIELSEN AND BUCHDAHL, 282
Sublimation, molecular —, SOBOTKA *et al.*, 567
Substrate, enzyme- — stabilization with pepsin-albumin, HAYASHI AND EDISON, 437
Sulfonates, micelle formation in hydrocarbons, VAN DER WAARDEN, 448
Sulfur, see *Ultrasonic*
Surface phenomena, films of omega-branched fatty acids, SOBOTKA *et al.*, 567
Surface roughness, effect on sliding of water drops, BIKERMAN, 349
Surface tension, the rate of — — lowering and its role in foaming, BURCIK, 421; — — of polytetrafluoroethylene, alkanes, dialkylethers, alkylbenzenes, polyalkylsiloxanes, halogen compounds, esters, and inorganic liquids, FOX AND ZISMAN, 514
Swelling, see SOAPS

T

Thermodynamics, ion exchange and —, DAVIS, 71, 107

U

Ultracentrifuge, motion of a particle in the —, NEWMAN AND EIRICH, 541
Ultrasonic irradiation, effect on the formation of colloidal sulfur and ice, TURNER AND VAN HOOK, 315

V

Viscoelastic materials, extrusion, DEXTER AND DIENES, 228
Viscosity, dilute-solution — of polymethyl methacrylate, ALFREY *et al.*, 251; intrinsic — of cottonseed globulin solutions, ARTHUR AND SAIK, 326; — and concentration in dilute solutions, SIMHA, 386; — and sulfonate micelle formation, VAN DER WAARDEN, 448

W

Water, see Sliding

X

X-rays, micelles and — —, PHILIPPOFF, 169

Z

Zirconium, radiocolloids of —, SCHUBERT AND RICHTER, 376

INDEX OF BOOK REVIEWS

Feigl, F., Chemistry of Specific, Selective, and Sensitive Reactions (transl. by Oesper, R. E.) (Neuberg, C.), 193

Harned, H. S., and Owen, B. B., The Physical Chemistry of Electrolytic Solutions. 2nd Ed. (La Mer, V. K.), 417

Houwink, R. (ed.), Elastomers and Plastomers, Their Chemistry, Physics and Technology, Vol. II: Manufacture, Properties and Applications (Goldfinger, G.), 195

Houwink, R. (ed.), Elastomers and Plastomers, Vol. I. General Theory (Goldfinger, G.), 497

International Congress on Rheology. The Organizing Committee, Proceedings of the International Congress on Rheology (La Mer, V. K.), 418

Mark, H., and Tobolsky, A., Physical Chemistry of High Polymeric Systems. High Polymers. Vol. II. 2nd Ed. (La Mer, V. K.), 498

Parpart, A. K. (ed.), The Chemistry and Physiology of Growth (Barth, L. G.), 418

Reiner, M., Deformation and flow. An Elementary Introduction to Theoretical Rheology (La Mer, V. K.), 417

Roman, W., The Scientist's Ready Reckoner (La Mer, V. K.), 418

Syrkin, Y. K., and Dyatkina, M. E. (translated and rev. by Partridge, M. A., and Jordan, D. O.), Structure of Molecules and the Chemical Bond (La Mer, V. K.), 498

Wyckoff, R. W. G., Electron Microscopy, Technique and Applications (Gordieyeff, V. A.), 193